The toxicity and potential pathogenicity of high-performance engineered multi-walled carbon nanotubes

Submitted by

Matthew S. P. Boyles

A thesis submitted in partial fulfilment of the

requirements of Edinburgh Napier University for the award of

Doctor of Philosophy

September 2012

School of Life, Sport and Social Sciences

Edinburgh Napier University

Edinburgh

Declaration

It is hereby declared that this thesis is the result of the author's original research. It has been composed by the author and has not been previously submitted for examination which has led to the award of a degree.

Signed:

Acknowledgements

Firstly I would like to thank my supervisor Prof. Vicki Stone for all the support, encouragement and belief she has shown me. She has seen me through from a Bachelors student to a Carnegie Fellow, on to a PhD and finally into a scientist. Her continued support and the enthusiasm she has for research truly is an inspiration, and I am whole-heartedly thankful.

There are many people in the department of Life Sciences at Edinburgh Napier University who I feel have supported me throughout my time there, including the other members of my supervisory team, Dr Lorna Proudfoot and Dr Paula Smith; particularly Lorna, who stepped in at the end with support and advice that was essential to my completing this thesis. I would also especially like to thank Dr David Brown and Dr Lesley Young, whose practical advice, support, patience and friendship have been invaluable during my project.

To close friends and colleagues at Napier, Heli, Martin, Wills, Elisa, Jen, Amy, Iain and Julia, thanks for keeping me sane…. and also many thanks to Kim Kellett, I really appreciate her help and support, not only during my PhD but also throughout my Bachelor's degree.

I would like to acknowledge the various collaborators who have had a helpful and positive impact on my research, including Prof. Alan Windle, Dr Fiona Smail, and Dr Anna Moisala at the University of Cambridge, particularly Anna for her friendship and support during the CNT synthesis; Dr Martie van Tongeren, Dr Lang Tran, Dr Rob Aitken, Dr Laura MacCalman, Hilary Cowie and Dr Yvette Christopher from the Institute of Occupational Medicine; Dr Craig Poland (previously of the University of Edinburgh); Dr Ian Kinloch (University of Manchester); and Barbara Rothen-Rutishauser (previously of the University of Bern).

To my family; my parents Sally and Alastair and my aunt Camilla, I want to thank you for supporting me and encouraging me throughout my (many!) years

of study; I'm sure they'll be glad that I'm finally through my education!!! And mum thanks for painstakingly correcting my bad grammar, I guess I may never manage to forget what an em dash is, or is it an en dash!!. And to my wife Angie, who truly gave me the inspiration and the dedication to undertake something like this; and (of course) to Freya, who really is the reason I have finally finished.

Finally, I would like to thank and acknowledge the Engineering and Physical Sciences Research Council (EPSRC) whose generous funding has made this research project possible.

"The trouble with having an open mind, of course, is that people will insist on coming along and trying to put things in it."

— Terry Pratchett

Publications

- Clift, M. J. D., Boyles, M. S. P., Brown, D. M. & Stone, V. (2010) An investigation into the potential for different surface-coated quantum dots to cause oxidative stress and affect macrophage cell signalling in vitro. Nanotoxicology, 4, 139-149.
- Gaiser, B. and Clift, M. and Johnston, H. and Boyles, M. and Fernandes, T.. (2011). Human and natural environment effects of nanomaterials. In: Sattler, K. *Handbook of nanophysics - nanomedicine and nanorobotics*. 7th ed. Florida: Taylor & Francis Group. 14.1-14.24.
- Rothen-Rutishauser, B., Brown, D. M., Piallier-Boyles, M., Kinloch, I. A., Windle, A. H., Gehr, P. & Stone, V. (2010) Relating the physicochemical characteristics and dispersion of multiwalled carbon nanotubes in different suspension media to their oxidative reactivity in vitro and inflammation in vivo. Nanotoxicology, 4, 331-342.

Conference presentations

Oral presentation: Boyles M., Rothen-Rutishauser B., Brown D.M., and Stone V. (2009) The oxidative potential of different carbon nanotubes *in vitro*, *in vivo*, and using a cell free system, and the effect different suspension media has on this reactive oxygen species generation. NanoImpactNet Conference, Lausanne, Switzerland, March 2009.

Poster presentation: Matthew S. P. Boyles, David M. Brown, and Vicki Stone (2010) The effect of carbon nanotubes, asbestos and carbon black on cell viability, growth, function and signalling. NanoImpactNet Conference, Lausanne, Switzerland, March 2010.

Poster presentation: Matthew S. P. Boyles, David M. Brown, Anton Wessels, Paula Smith and Vicki Stone (2010) The effect of carbon nanotubes on different cell lines displays a good correlation and reproducibility when using in vitro systems to measure of cell viability, growth and signalling. With slight limitations highlighted when accessing cell function. Nanotoxicology, Edinburgh, June 2010.

Abstract

The potential health consequences of carbon nanotube (CNT) exposure is often compared to asbestos and other fibre like materials due to their similar high aspect ratio and potential biopersistence; both are key in driving fibre toxicity and pathogenicity. With similar characteristics CNT are hypothesised to induce similar toxicity, and potentially similar pathogenicity. It is important to test this hypothesis in order to inform safe methods for production, handling and disposal of CNT.

The aim for this research was to employ a range of biological techniques to ascertain the cytotoxicity of different multi-walled (MW)CNT that are morphologically and compositionally distinct, and comparing these samples to toxicologically relevant materials such as asbestos and carbon black nanoparticles. The MWCNT used were either supplied by an industrial source, or were produced using controlled growth methods to allow investigation into certain size ranges, catalytic iron content, and sample purity (crystallinity).

Using cell free, *in vitro* and *in vivo* techniques for oxidative stress assessment, an early generation of ROS was found in response to entangled MWCNT, with greater observed responses to both short and long, straight MWCNT found as exposure times progressed. Also most prominent at the later exposure periods, substantial and significant cell death was observed in MM6 and J774A.1 cells in response to MWCNT samples, measured through reduced cellular viability and LDH release. The level of cell death induced by MWCNT was not matched by cell exposures to reference materials. Numerous markers of a pro-inflammatory responses and markers indicative of tissue damage and angiogenesis were assessed *in vitro* using MM6 and J774.A1 cell. Both cell types were found to secrete significantly elevated levels of MCP-1, TNF-α, TGF-β and VEGF in response to MWCNT. Although not as high as the CNT, LFA was also found to stimulate pronounced pro-inflammatory conditions, when compared to the other reference materials. Numerous techniques were employed to assess the ability of immortalised and primary cells to phagocytose particles. Frustrated phagocytosis was observed in response to the longer particles (both CNT and asbestos) and to agglomerates formed of shorter CNT. This frustrated phagocytosis induced by the long MWCNT samples was found to translate to

an exaggerated respiratory burst, and a dysfunction and inhibition in the ability of cells to phagocytose fluorescently labelled E. coli.

Taking all of the results of this study into consideration it was clear that the MWCNT samples tested display a greater toxicity than the reference materials in this panel. Above all, differences in the responses to the five MWCNT samples were considered to be induced by either a long individual length, or large agglomerate formation, and therefore the effects attributed to a high aspect ratio and frustrated phagocytosis. However, at times there was an inference that a high bioavailable iron content or high level of sample purity may intensify cellular response to MWCNT. The findings here, and throughout the current literature, demonstrate that CNT are certainly capable of inducing pathogenesis, but biological responses vary with differences in CNT morphology and composition.

Contents

Abbreviations

Ab	- antibody
AM	- alveolar macrophages
ATCC	- American Type Culture Collection
BAL	- bronchoalveolar lavage
BSA	- bovine serum albumin
CB	- carbon black
CBA	- cytometric bead array
CNT	- carbon nanotubes
CNTA	- short/straight / high iron(high release) / intermediate crystallinity / low alignment
CNTB	- short / straight / intermediate iron (low release) / intermediate crystallinity / low alignment
CNTC	- long / straight / low-intermediate iron (high release) / low crystallinity / well aligned
CNTD	- long / straight / low iron (low release) / high crystallinity / well aligned
CNTI	- short / straight / intermediate iron / high crystallinity
CPD	- critical point drying
CVD	- chemical vapour deposition
DCFH-DA	- 2',7'-dichlorofluorescein diacetate
DM	- disorder mode
DPPC	- dipalmitoylphosphatidylcholine
DWCNT	- double-walled CNT
ECACC	- European Collection of Cell Cultures
ELISA	- enzyme-linked immunosorbent assay
FCS	- foetal calf serum
FEGSEM	- field emission gun scanning electron microscope
FTIR	- fourier transform infrared
GSH	- reduced glutathione
HBSS	- Hank's balanced salt solution
HCl	- hydrochloric acid
HMM	- human monocyte-derived macrophages

HMOX1	- heme oxygenase-1
HO-1	- heme oxygenase-1
HRP	- horseradish peroxidase
ICP-AES	- inductively coupled plasma-atomic emission spectrometry
IL-8	- interleukin-8
J774A.1	- mouse monocytic cell line
LDH	- lactate dehydrogenase
LFA	- long fibre amosite
LPS	- lipopolysaccharide
MARCO	- macrophage receptor with collagenous structure
MCP-1	- monocyte chemoattractant protein-1
MDM	- monocyte derived macrophage
MIP-2	- macrophage inflammatory protein-2
MM6	- human monocytic cell line, Mono Mac-6
MWCNT	- multi-walled CNT
NIR	- near infra-red
nm	- nanometer
NM	- nanomaterial
NPCB	- nanoparticle, or ultrafine carbon black
NP	- nanoparticles
NT1	- long / straight / low-int. iron / well aligned /high surface area
NT2	- >10µm aggregates / straight / low-int. iron / low alignment / low surface area
NT3	- >10µm aggregates / entangled / low-int. iron/ high surface area
OGG1	- 8-oxoguanine DNA glycosylase
PBS	- phosphate buffered saline
PDGF	- platelet-derived growth factor
PMA	- phorbol-12-myristate-13-acetate
PMN	- polymorphonuclear
PS	- phosphatidylserine
RBM	- radial breathing mode
ROS	- reactive oxygen species
SD	- Sprague Dawley

SEM	- scanning electron microscope
SEM-EDS	- SEM-energy dispersive spectroscopy
SFA	- small fibre amosite
SN	- supernatant
SOD	- superoxide dismutase
SR	- scavenger receptor
SWCNT	- single-walled CNT
TEM	- transmission electron microscopy
TGA	- thermal gravimetric analysis
TGF-β	- transforming growth factor-beta
TM	- tangential vibration mode
TMB	- tetramethylbenzidine
TNF-α	- tumour necrosis factor-alpha
ufCB	- ultrafine, or nanoparticle carbon black
wt.%	- weight %

List of figures

Chapter 1

Chapter 2

Chapter 3

Chapter 6

Chapter 7

Chapter 8

List of tables

Chapter 2

Chapter 3

Chapter 7

Chapter 1

Introduction – nanoparticles, and the pathogenicity of asbestos and high aspect ratio nanoparticles

1.1 Nanoparticles, nanomaterials and nanotechnology

There is an incessant, enduring presence of nanomaterials (NM) in our atmosphere. NM have been generated naturally through forest fires, volcano eruptions, wind erosions and sea spray (Borm *et al.*, 2006), and more recently their generation can be attributed to the industrial revolution and advances in engineering technology. Anthropogenic NM formation is accidental through combustion, milling and mining, or intentional with the production of engineered NM. Research has identified combustion-derived nanoparticles as a potential pathological hazard, and the significant exposure of humans to air pollution and particulate matter have long been associated with respiratory disorders (Gardiner *et al.*, 2001) and abnormalities (van Tongeren *et al.*, 2002), mortality and cardiovascular disease (Dockery *et al.*, 1993, Schwartz and Morris, 1995), such as the induction of myocardial infarction (Peters *et al.*, 2001). Under laboratory conditions, both diesel soot and nanoparticle carbon black (NPCB; used as a surrogate for combustion derived NP have been shown to be carcinogenic, at least in rat inhalation studies (Heinrich *et al.*, 1995, Valberg and Watson, 1996). These exposures are potentially quite relevant to real human exposure scenarios. To induce carcinogenesis 2.5 mg/m^3 was needed for diesel exhaust, and over 7 mg/m^3 was needed in CB exposures, both over a period of several years (Heinrich *et al.*, 1995). Sampling within CB plants has given exposure levels of as little as 0.06–1.72 mg/m^3 (Valberg and Watson, 1996), but on other occasions as much as 13 mg/m^3 (Gardiner *et al.*, 1992).

With at least one dimension in the nanoscale (1–100nm) a material can be termed a NM, with all three dimensions under 100nm the NM is said to be a nanoparticle (NP) (BSI, 2007). NM may differ in size and shape, from spherical to rods or rings, and most will differ either slightly, considerably or completely in composition, from the very simple to very complex (Donaldson et al., 2004). This diversity generates many properties advantageous to many industries, and has opened a new field of technology termed nanotechnology, defined by BSI (2007) as the “design, characterization, production and application of structures, devices and systems by controlling shape and size in the nanoscale”. This diversity, however, also presents considerable and varied factors that may influence nanomaterial toxicity.

1.1.1 Nanotechnology and nanoparticle applications

The pattern of toxic behaviour displayed by some NM prompts the questions 'why actively pursue the formation and development of further NM?' This is a question that is easily answered as the benefits of many nanoscale materials are clear, and by isolating and highlighting toxic components and characteristics it is possible to provide safe development of these materials.

The worth of nanotechnology in this modern age is obvious. Being economically, industrially and medically advantageous nanotechnology is likely to impact globally in almost every walk of life and will encompass the use of both organic and inorganic materials (Bhushan, 2007). The provision of products within nanotechnology can be through atomic manipulation, or through the destruction or reconstruction of bulk material (Bhushan, 2007); and NM are being designed and exploited using numerous production techniques, such as wet chemical methods, solution methods, mechanical size reduction, and gas phase synthesis (Lee *et al.*, 2005).

The applications for NM are vast, and the use of such small materials is thought to reduce manufacturing costs, increase productivity, and in some cases vastly increase method effectiveness. With the specific manipulation of atoms allowed by nanotechnology it is possible to produce nanostructured materials that are lighter, stronger and more efficient than the existing analogous materials used in the many industries (El-Hag *et al.*, 2007, Mamalis, 2007). Nanotechnology has allowed advances in microelectronics, computer industries, robotics, fibre optic communication, aerospace technology, precision manufacturing, chemical engineering, environmental remediation and textile industries; and one particularly noteworthy use of nanotechnology is in medicine and biotechnology (Ashrafi *et al.*, 2007, Bhushan, 2007, Lee *et al.*, 2005, Mamalis, 2007, Parvinzadeh and Hajiraissi, 2007).

The use of nanomaterials in medicine can provide increased wear resistance and fracture toughness of prosthetic implants and surgical tools (Mamalis, 2007); or enhance diagnostic devices and drug delivery systems (Jahanshahi *et al.*, 2007, Pumera, 2007) through surface coating, or filling, of NP with protein ligands, oligonucleotides, antibodies (Bao and Suresh, 2003), or medicinal drugs (Berry *et al.*, 2004, Roy *et al.*, 2003, Wieder, 2006). This functionalisation may allow extended cardiovascular circulation, organ and tissue targeting,

phagocytic cell evasion, translocation through the blood–brain barrier, normally a decidedly selective barrier, and prolonged drug release (Donaldson *et al.*, 2004). Magnetic NP are shown to improve gene therapy, genetic screening, biochemical sensing, disease detection, targeted drug delivery, or toxicity cleansing, through the isolation and removal of toxic substances such as anthrax (Lee *et al.*, 2005). In terms of genetic screening, DNA-based nanostructures can be used to recognise DNA and RNA targets using optical, electrical, or magnetic signals, which aid many processes including polymerase chain reaction (PCR) and identification of RNA expression (Bao and Suresh, 2003). Improved drug efficacy can be achieved through the use of a magnetic field gradient to draw the coated NP to a desired location (Berry *et al.*, 2004), allowing the *in vivo* targeting of NP to markers of disease or infectious agents within the cell, thus permitting early detection by magnetic resonance imaging (Bao and Suresh, 2003); or through the generation of drug conjugates, such as the binding of gold NP to the photosensitiser drug phthalocyanine to form a conjugate used in photodynamic therapy (PDT) of cancer (Wieder *et al.*, 2006). With applications and construction techniques like this it is clear that it will often be the more complex, modified NM structures that are commonly used for therapeutic applications.

The extent of NM in medicine is widespread, and a full review here is not realistic. There are, however, numerous reviews demonstrating the scope of NP involvement in modern medicine, including reports by Azarmi *et al.* (2008), Koo *et al.* (2005) and Pison *et al.* (2006), who all describe the use of NP in drug delivery systems; a report by Jain (2005) gives a description of NP involvement in diagnostic techniques; and a more expansive overview of NP in medicine was given by Moghimi *et al.* (2005).

1.1.2 High aspect ratio nanomaterials (HARN)

High aspect ratio nanomaterials (HARN) have been proposed for use in many industries (Bauer *et al.*, 2004) and are defined as possessing a length to width aspect ratio of greater than 3:1 (Paradise and Goswami, 2007). The morphology of HARN has provided materials with new chemical, optical, magnetic and electronic properties. Using a number of production methods it is possible to generate a range of materials such as nanowires, nanotubes,

nanorods, nanobelts and nanosprings (Bauer *et al.*, 2004, Oberdorster *et al.*, 2007), composed of various materials such as nickel, gold, platinum, silver, cobalt, copper, carbon, and zinc, iron and titanium oxides, to name but a few (Bauer *et al.*, 2004). The potential biological applications of HARN are reviewed extensively by Bauer *et al.* (2004) and most notable include their use in analyte separation, as biological sensors for glucose sensors or protein recognition, and perhaps most obvious is the use of HARN as drug or gene delivery vectors. In respect to compatibility and practicality it is often fundamentally essential for HARN to be functionalised when used in biological applications (Bauer *et al.*, 2004).

The scope of research into proposed use of HARN is too much to cover in this report, and perhaps is not wholly relevant to this doctoral study. However, one high aspect ratio carbon-based material forms the basis of this research and is fast proving to be particularly important – perhaps even revolutionary. Carbon nanotubes (CNT) are receiving a particularly high level of interest in both the development of applications (Paradise and Goswami, 2007), and into methods to scale up production (Aitken *et al.*, 2006). This proposed increase in production and use, which could therefore lead to a potential increase in human exposure, together with potentially pathogenic characteristics (discussed later) dictates that research into this material is essential.

1.1.3 Carbon nanotubes

1.1.3.1 Structure

Carbon nanotubes have a similar basic structure. They are formed of continuous rolls of graphene sheets arranged as tubes (Novoselov *et al.*, 2004, Sinha and Yeow, 2005). These graphene sheets consist of hexagonal lattice carbon atom structures (Taeri and Eliasi, 2007), which can differ slightly in their topological indices generating slightly different forms, such as Zigzag, Armchair, or Chiral (Taeri and Eliasi, 2007), related to the spatial relationship between carbon atoms within a CNT (Taeri and Eliasi, 2007). Other physico-chemical characteristics of CNT can vary, and with variation there is a change in the particle properties.

CNT may be either single walled (SWCNT) with a single, continuous graphene sheet, or multi-walled (MWCNT), consisting of any number of graphene tubes held within each other along a common axis, with lengths up to micrometres and widths of hundreds to only a few nanometres (Popov, 2004, Wei *et al.*, 2007).

1.1.3.2 Proposed CNT use

With examples of crystalline and polycrystalline aggregated CNT found within a 10,000-year-old ice core it is evident that CNT have been present in our atmosphere for thousands of years (Esquivel and Murr, 2004). However, CNT have been accumulating and depositing in our environment over recent decades (Bang *et al.*, 2004, Murr *et al.*, 2004b). This is through vehicle combustion systems and break-lining degradation (Murr and Bang, 2003); and from the combustion of propane and natural gases in gas stoves and hot-water heaters, and on a larger scale from gas-powered power plants and industrial-sized gas furnaces (Bang *et al.*, 2004, Murr *et al.*, 2004b).

Moreover, after the realisation of intentional CNT production by direct current arc-discharge evaporation of carbon, reported by Iijima (Iijima, 1991) over a decade ago, the interest in CNT production, utilisation and subsequent toxicological investigation has risen considerably throughout the last two decades (figure 1.1).

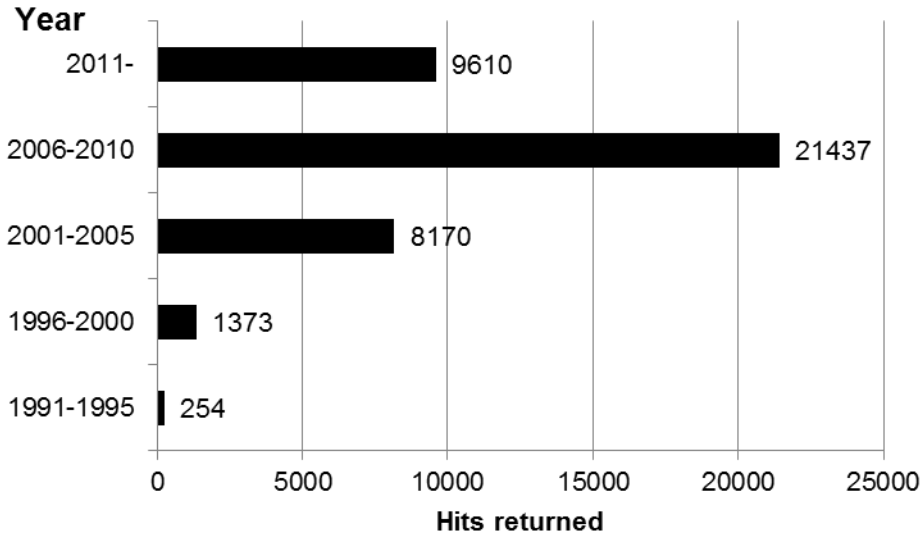

Figure 1.1 SciVerse® ScienceDirect journal search, hits returned using the search term "carbon nanotubes" – from different year ranges (information taken on 26/01/12)

The advantageous properties of CNT, including high tensile strength (Salvetat-Delmotte and Rubio, 2002), high electrical current carrying ability, and easy functionalisation (Wei *et al.*, 2007) allow an extensive range of applications in many industries (Esquivel and Murr, 2004).

In medicine, a scaffolding structure of CNT can be used to support tissue regeneration after injury or surgery (Abarrategi *et al.*, 2008, Popat *et al.*, 2007), and can be used to enhance cell adhesion and promote cell differentiation (Abarrategi *et al.*, 2008) and cell spanning between the pores of the CNT scaffolding structure (Edwards *et al.*, 2009). Delivery of drugs, such as antibiotics, bound to CNT enhances drug effectiveness and reduces side effects (Popat *et al.*, 2007), while photothermal properties of CNT, induced using near infra-red (NIR) light, can be used in the destruction of malignant tumours (Markovic *et al.*, 2011), with functionalisation with compounds such as folate allows for cancer cell specificity and cell death selectivity (Kam *et al.*, 2005). CNT functionalisation can also enhance drug solubility (Pantarotto *et al.*, 2004a, Pantarotto *et al.*, 2004b) or magnetic manipulation (Cai *et al.*, 2005), allowing easy and directed entry to mammalian cells, occurring even when the functional group creates a positive charge (Pantarotto *et al.*, 2004b), enabling the delivery of plasmid DNA for gene therapy, with greater efficiency than free DNA (Liu *et al.*, 2005, Pantarotto *et al.*, 2004b). With two independent functional groups there is the possible use for functionalised CNT (fCNT) as vectors for anti-bacterial, -fungal, -viral or cancer treatment, with one functional group allowing cell specificity and the other for drug treatments (Wu *et al.*, 2005). fCNT can also be used as diagnostic and imaging tools, with functional groups allowing identification of cellular location and uptake, with double functionality allowing a reduction in both CNT and nonspecific antibiotic toxicity (Wu *et al.*, 2005).

CNT applications are not solely isolated to medical. In fact their proposed use is incredibly diverse. For example, CNT have been found to remove potential tip damage and improve image resolution in scanning electron microscopy (SEM) techniques (Koo *et al.*, 2005), and with a large electron field emission capacity (Edwards *et al.*, 2009) their use has been proposed in field emission display units (Jain, 2005). The formation of mesopores and micropores by CNT aggregates (Hemraj-Benny *et al.*, 2008), and their high aspect ratio and large

surface area has allowed their use in techniques in water purification, through the removal of toxins and microorganisms (Brady-Estévez *et al.*, 2008, Li *et al.*, 2001). Their large surface area, along with an excellent electrical-current-carrying capacity, has also led to the proposed use of CNT in electrochemical biosensors and electrodes (Pumera, 2007), with a high electron transfer capacity (Pison *et al.*, 2006) proving useful in electrochemical reactions such as those found in batteries, and high surface adsorption properties proving valuable in the detection of harmful gases (Azarmi *et al.*, 2008). The tensile strength and high conductivity has led to the inclusion of CNT in numerous battery compositions (Endo *et al.*, 2001); and with their inclusion, CNT have been shown to improve the electrical properties of in metal, metal oxide or polymer composites (Liu and Gao, 2005), enhance the elasticity and abrasion resistance of rubber composites (Fan *et al.*, 2008), and reinforce metal composites (Fubini and Otero Arean, 1999), polymer resins (Schadler *et al.*, 1998) and alumina ceramics (Novoselov *et al.*, 2004). CNT could even potentially be used to scale-down the size of electrical circuits, allowing the production of nano-sized electrical devices (Paradise and Goswami, 2007).

The expectations for the role of CNT in many aspects of nanotechnology are very high, and rightly so, as the benefits in using these materials are clearly evident. Nevertheless, with this increased use there is obviously an increase in exposure. It is the more industrial related applications that are likely to provide much of the proposed exposure, possibly due to the sheer volume of CNT production that would be needed, 100 tons of CNT are produced each year for lithium-ion batteries alone (Sotowa *et al.*, 2008). With the use of CVD it has been possible to scale-up the production CNT to industrial size capacities, annually there is currently approximately 1000 tonnes produced (Endo, 2010). With companies such as Showa Denko producing 500 metric tons per year (Showa_Denko), there are concerns for occupational exposure. It is therefore vital that the risk of environmental, occupational and medical exposure is properly assessed. Currently the industrial production of MWCNT is much higher than SWCNT (Mitchell *et al.*, 2007), and therefore it is MWCNT that form the basis of the research presented in this study.

1.2 Nanotoxicology

The main emphasis of this report will be on the pathology of asbestos exposure, and the proposed pathology relating to CNT exposure. However, it is important to identify the basis of nanotoxicology. During the past decade there has periodically been a number of extensive nanotoxicology reviews published (Oberdörster *et al.*, 2005, Oberdörster *et al.*, 2007), relating to the toxic mechanisms of ultrafine particles (Donaldson and Stone, 2003), including the cellular and molecular interactions with ultrafine particles, NP and air pollution (Stone *et al.*, 2007), and the inhalation toxicity of combustion derived NP (Donaldson *et al.*, 2005). This section will therefore provide only a brief introduction to this discipline. As there has been such a rapid increase in the size of this field and the diversity of NM, this section will provide a historical perspective focussing on carbon based NP, and the earlier research done within my research group and our close collaborators. This will allow the main focus in the later section to largely concentrate on the literature concerning asbestos and CNT.

Historically it has been shown that in occasions of high pollution where there are high levels of particle-based smog, there is an increase in mortality (Schwartz, 1994), and research has suggested that ultrafine or nanoparticles play a role in driving these associated adverse health effects. In 1992 Ferin *et al.* first reported the health implications of nanoscale materials. In comparison to TiO_2 of a larger size, pulmonary exposure to nanoscale TiO_2 particles resulted in increased lung burden through diminished particle clearance and increased particle retention, and marked translocation of particles into the interstitium, with accompanying inflammatory response (Ferin *et al.*, 1992). The report highlighted the potential for greater pathogenicity from inhalation of nanomaterials compared to equivalent bulk material. Since this time air-pollution-associated pathogenicity (Dockery *et al.*, 1993) has been investigated with an emphasis placed upon nanoparticulate matter, and synergistic response to components of PM_{10} (Stone *et al.*, 1998, Stone *et al.*, 2000, Stone *et al.*, 2003, Wilson *et al.*, 2002). With research into normally innocuous material such as polystyrene, it was demonstrated that elevated inflammatory responses occur, both *in vivo* and *in vitro*, in response to nano-scale polystyrene particles (Brown *et al.*, 2001).

Occupational exposure to carbon black (CB) is shown to cause chest abnormalities associated with respiratory morbidity (Gardiner *et al.*, 2001, van Tongeren *et al.*, 2002), and *in vivo* studies have demonstrated lung inflammation (Brown *et al.*, 2000, Brown *et al.*, 2001, Gilmour *et al.*, 2004, Wilson *et al.*, 2002), and the development of fibrosis and tumourigenesis (Donaldson *et al.*, 2005) from exposure to combustion derived NP, can all be attributed to NP associated characteristics. Such characteristics include the potential of NP to generate reactive oxygen species (ROS) and induce oxidative stress when comparable bulk material does not (Stone *et al.*, 1998). *In vivo* pulmonary inflammation (Lee *et al.*, 2005) and *in vitro* stimulation of pro-inflammatory conditions (Oberdorster *et al.*, 2005) in response to NPCB were shown to occur as a consequence of oxidative stress induced cell signalling (Stone *et al.*, 2000) and gene expression (Brown *et al.*, 2004, Brown *et al.*, 2002). More specifically, nanoparticle carbon black (NPCB), coal dust, crystalline silica (quartz) and transition metal components found in particulate air pollution (PM10) (Donaldson and Borm, 1998, Donaldson *et al.*, 2002, Wilson *et al.*, 2002) are shown to cause excessive inflammation through redox activities.

This research has firmly implicated nanoscale materials with an increase in toxic behaviour and associated pathologies independently, but it has also been shown that NP exposure can intensify the health effects of pre-existing respiratory problems such as asthma (Peters *et al.*, 1997). Both these aspects of NP associated pathology, induced inflammatory responses and oxidative stress, are further reviewed in the following section. However, when assessing the potential of NP to cause harm it is important to evaluate a number of aspects, including particle characteristics and composition, as well as the route of exposure, as this will determine how they are deposited and cleared, and therefore the extent and longevity of particle-induced pathology.

1.2.1 Mechanisms of NP health effects

Many aspects that make NP attractive for potential industry materials are also often implicated in their toxicity. The small size is just one reason for NP utilisation in industry (Mamalis, 2007). However, it is the small size of normally innocuous substances that contributes to NP toxicity. Gold is normally

physiologically inactive, but when particle size is reduced to the nanoscale, biological pathways are disrupted, again largely through the generation of free radicals (Lee *et al.*, 2005). Additionally, much research has been used to establish the importance of this small size in air pollutant particles inducing reactions that do not occur to larger sized counterparts (Brown *et al.*, 2002, Brown *et al.*, 2000, Stone *et al.*, 2000).This change from innocuous to toxic is attributed to a number of factors: the small size of NP gives an increased surface area in relation to mass and volume, providing a greater surface reactivity. Moreover, this small size, increased surface area and greater surface reactivity may enable particles to gain access, through translocation into the blood flow, or crossing the blood-brain barrier (BBB), to locations within the body that larger particles cannot (Donaldson *et al.*, 2004). The association of NP with proteins is reported to be both advantageous, e.g. when used as a biocompatible scaffolding in tissue regeneration (Abarrategi *et al.*, 2008), but also detrimental, when found to potentially impede immune responsiveness within the lungs (Salvador-Morales *et al.*, 2007). An association with metals has also shown to potentially induce greater harmful systemic affects. With exposure of NPCB to a murine macrophage-like cell line the already significant generation of the pro-inflammatory cytokine tumour necrosis factor-alpha (TNF-α), was significantly and synergistically enhanced when particles and metals were incubated together (Wilson *et al.*, 2007).

1.2.1.1 Oxidative stress

ROS, such as superoxide anions or hydroxyl radicals, have an intrinsic volatile nature, and the ability to influence the redox state of a cell (MacNee, 2001); the fact that of many NP have the ability to induce oxidative stress (Oberdorster *et al.*, 2005) infers to the importance of NP generated ROS in NP toxicity. Although NP can be chemically and compositionally different, many appear to produce ROS, particularly when stimulated by natural light, ultraviolet light or transition metals (Oberdorster *et al.*, 2005).

The methods of ROS production are not always known but can be through the release of free electrons by photo excitation, the metabolism of NP into redox active intermediates, or the release of oxyradicals from macrophages during phagocytosis and inflammation (which is discussed later in section 1.3.2.3).

Extracellular release of ROS during a respiratory burst may damage tissue through enzyme activation inducing proteolysis, and is known to both encourage the inflammatory response, or indeed the healing process, dependent on the conditions, and can also induce apoptosis and reduce proliferation in surrounding cells as well as the cells producing the ROS (Halliwell and Gutteridge, 2007).

ROS, including superoxide anion and hydroxyl radicals, often contain unpaired electrons, and can therefore be highly reactive. The accumulation of these oxidants cause a redox imbalance. In most systems there is a balance between ROS generation and antioxidant defence mechanisms. However, through depletion or inhibition of antioxidants (Halliwell and Gutteridge, 2007), and therefore there is no longer the capacity to remove the reactive oxygen metabolites as they are being produced (Acworth *et al.*, 1997), a state of oxidative stress may occur (Halliwell and Gutteridge, 2007), which can lead to direct tissue injury or the generation of further ROS (MacNee, 2001). With oxidative stress there is the potential for cell proliferation and injury through oxidative damage to DNA (Halliwell and Gutteridge, 2007), predominantly from hydroxyl radical exposure (Acworth *et al.*, 1997). Oxidative stress can also cause extracellular matrix (ECM) remodelling (MacNee, 2001), a decrease in ATP production, through reduced functionality of the mitochondrial respiratory chain, and plasma membrane damage (Halliwell and Gutteridge, 2007), through lipid peroxidation (Acworth *et al.*, 1997). With ROS-initiated lipid peroxidation ROS will oxidise membrane phospholipids in the cell membrane; this causes membrane dysfunction, inactivation of membrane-bound enzymes and receptors, and an increase in tissue permeability, all of which can ultimately cause apoptosis or signalling pathway activation (MacNee, 2001). Indirectly, oxidative stress may cause injury through manipulation of ion channel proteins, resulting in concentration imbalances within the cell, cell senescence and even cell death (Halliwell and Gutteridge, 2007).

Subsequent release of pro-inflammatory cytokines will also occur in conditions of oxidative stress (Kannan and Jain, 2000). Transcription factor activation, such as nuclear factor-kappa B (NF-κB) or activator protein-1 (AP-1), and inflammatory responses will occur at low and high levels of oxidative stress and, at least at low levels, cells may adapt and survive (Halliwell and Gutteridge,

2007). The association between NP induced inflammatory responses and the prerequisite of oxidative stress has often been shown. For example it has been determined that one mechanism of NPCB (a nanoparticulate component of PM_{10}) induced TNF-α gene expression and protein secretion is through oxidative stress (Brown *et al.*, 2004, Brown *et al.*, 2002). This has been shown in alveolar macrophages and peripheral blood monocytes, and is thought to be dependent on an intracellular calcium signalling mechanism (Brown *et al.*, 2004, Brown *et al.*, 2002, Stone *et al.*, 2000) and activation of transcription factors such as AP-1 and NF-κB (Brown *et al.*, 2004). It appeared that these responses were reliant on the small particle size, as compositionally comparable bulk size particles were shown to have no effect (Brown *et al.*, 2004). Moreover, *in vivo*, this calcium dependent induction of inflammatory responses has been shown to not be determined by the transition metal components in PM_{10}, but other aspects such as surface area (Brown *et al.*, 2000), again highlighting particle size.

1.2.1.2 Inflammation

An excessive inflammatory response has been linked to the pathogenesis of many particle-associated complications. The recruitment of immune cells associated with particle inhalation is centred largely around the secretion of the pro-inflammatory cytokine TNF-α by alveolar macrophages, but also with further cytokine and chemokine release, such as interleukin-8 (IL-8), macrophage inflammatory protein-2 (MIP-2) and monocyte chemoattractant protein-1 (MCP-1), by epithelial cells and alveolar macrophages (Driscoll *et al.*, 1997). This may well determine, or at least contribute, to the potential pathology, as particularly cytotoxic material such as asbestos, coal dust and quartz are also shown to elicit a high release of TNF-α, while relatively inert substances such as titanium dioxide and latex beads have been shown to be less effective (Driscoll *et al.*, 1997). As with the literature inferring the oxidative potential of NP, corroboration of the impact nano-sized material has on inflammatory responses is also evident in previous studies. The secretion of TNF-α in response to NPCB and not bulk CB was demonstrated with particle exposure of alveolar macrophages (Brown *et al.*, 2002), an enhanced immune cell influx during lung instillation of particles such as titanium dioxide, carbon black and polystyrene was shown to

be influenced by the surface area of material (Duffin *et al.*, 2002), and the migration of immune cells was shown to be influenced by NP induced activation of serum components prior to cellular exposures, when mass equivalent doses of bulk particles induced no such responses (Barlow *et al.*, 2005b). An acute inflammatory response to NP has long thought to be determined by the increase in surface area of NP (Duffin *et al.*, 2002). However, *in vitro* studies that have highlighted the inflammatory potential of NPCB being greater than that of its bulk counterpart, also identified that NPCB had a greater inflammatory potential than TiO_2 and $NPTiO_2$ (Barlow *et al.*, 2005a); and moreover, *in vivo* inflammatory responses to nanosized CB, cobalt, nickel and TiO_2, were found to be quite different (Dick *et al.*, 2003). Both of these examples imply that the toxicity of NM is not as simplistic as surface area alone, but the reactivity of said surface area also plays a part, which again relates to the potential of some NP to induce the generation of ROS. The role of oxidants in the induction of inflammatory responses has been extensively researched and a number of intracellular signalling molecules involved in oxidant-induced inflammation have been well identified. These include cyclic AMP (cAMP), intracellular calcium and nuclear factor kappa B (NF-κB) (Brown *et al.*, 2004, Brown *et al.*, 2007a, Sen *et al.*, 1996).

1.2.1.3 Nanoparticle inhalation exposure

There is a large quantity of information available on the toxicity of ambient NP, including *in vivo*, *in vitro* and epidemiological investigations. In later sections the health effects, mechanisms and implications associated with a number of respirable fibres are discussed, and therefore here only a short introduction to the toxicity of respirable NP is provided.

Once inhaled, NP can be deposited along all regions of the respiratory tract, from the nasal region to the alveolar sacs. From here they differ from larger particles as they can migrate to other organs, including the brain, liver, heart, and spleen. In the case of radio-labelled iridium NP only a very small percentage were shown to translocate to extrapulmonary regions, but it was found to be higher with exposure to 15nm particles compared to those with 80nm diameter (Kreyling *et al.*, 2002). The inhalation of ^{13}C NP approximately 30nm in diameter resulted in considerable translocation of particles, particularly

into the liver (Oberdörster *et al.*, 2002), and uptake into the blood after inhalation of 10nm radio-labelled carbon NP (Nemmar *et al.*, 2002) was found to be particularly high and rapid. It has also been shown that not only will inhaled NP translocate into the circulatory system, but also into the lymphatics and sensory nerve endings, as carbon NP such as ^{13}C were found to enter the central nervous system (CNS), with significant levels found in the brain after inhalation (Oberdörster *et al.*, 2004). With the use of fluorescent, magnetic NP of approximately 50nm in diameter it has been shown that after nasal inhalation NP can translocate from the respiratory system and are found distributed throughout many organs, the highest proportion found within the liver and regions of the testes, determined by fluorescence intensity. These fluorescent particles were also found to accumulate in the lungs, heart, spleen, kidneys, ovaries and the brain, again showing the ability of NP to cross the BBB (Kwon *et al.*, 2008).

The removal of inhaled particles can be through physical or chemical clearance. The primary clearance mechanism in alveoli is through phagocytosis of particles by alveolar macrophages, which then exit via the mucociliary escalator. Although it has been shown that not all inhaled NP are taken up by the macrophages, probably due to the aforementioned translocation of the particles through or into epithelial cells, most are phagocytosed (Oberdorster *et al.*, 2005), as a defensive mechanism of the respiratory system.

1.3 The respiratory system

1.3.1 Lung structure

The respiratory tract consists of a series of branching tubes that terminate at millions of alveolar sacs (Alberts *et al.*, 2002). The uppermost part of the respiratory tract consists of structurally strong, keratin-dense, stratified squamous epithelium, while most of the rest of the tract is made up of respiratory epithelium, a tissue comprising of three main cell types specifically designed to aid the removal of inhaled debris, consisting of goblet cells for mucus secretion, ciliated cells that beat directionally to waft attached debris out of the respiratory tract and endocrine cells that secrete proteins to mediate the activity of the other two cell types. The combination of the beating cilia and the 5µm mucus layer creates a mechanism termed the mucociliary escalator (Alberts *et al.*, 2002).

The mucociliary escalator does not extend into the alveolar sacs; instead any removal of debris in this region is by patrolling alveolar macrophages. The function of the alveoli is gas exchange and therefore these alveoli are separated from a capillary bed by extremely thin walls. There are two epithelial cell types that make up the alveolar lining. Type I alveolar cells which permit gas exchange, and type II alveolar cells that secrete lung surfactant that relieves surface tension avoiding permanent alveolar collapse (Alberts *et al.*, 2002).

1.3.2 Lung defence

To avoid any deposition and necessity for clearance mechanisms, a first response to inhaled material is likely to be the cough reflex (Gerritsen, 2000). However, with deposition and deeper inhalation, other methods need to be employed. The innate immune system is considered the first line of defence within the respiratory system, and is key in controlling the impact inhaled particles have on the respiratory system. This system, within the respiratory system, consists of cellular components, numerous leukocytes and alveolar epithelial cells, as well as secreted hormonal and protein components (Chiang *et al.*, 2001). In the case of insoluble, inorganic inhaled material, there may be a number of components particularly important in respiratory defence.

1.3.2.1 Deposition

Inhaled particle deposition will occur along the whole respiratory tract, dependent on a number of factors. Particles greater than 10µm are likely to deposit in the upper respiratory tract (Gerritsen, 2000) where there are particularly high airflow velocities; many larger particles will deposit by inertial impaction, where they collide with the mucus lining of these regions through directional and turbulent changes (Acworth *et al.*, 1997). Inhaled particles that are less than 10µm can penetrate the inner lung regions (Acworth *et al.*, 1997); this value may relate to actual diameter or aerodynamic diameter. When the airflow is reduced, or particles reach a close vicinity to the mucus lining, deposition may occur by sedimentation (Acworth *et al.*, 1997, Gerritsen, 2000) or interception (Acworth *et al.*, 1997). The Brownian motion of gas molecules in the respiratory tract, particularly the alveoli, will also influence particle deposition (Acworth *et al.*, 1997), while inhaled particles associating with gas molecules may deposit via diffusion alone (Gerritsen, 2000). It is likely that diffusion is responsible for nanoparticle and perhaps nanotube deposition, depending upon the agglomerate size.

1.3.2.2 Clearance

Upon deposition, clearance of inhaled toxicants is vital to avoid prolonged exposure, which would encourage local injury and possible translocation, leading to more systemic issues. Anything trapped or deposited in the nasal vestibular is removed by mechanical methods (Schlesinger, 1985), while elsewhere in the nasal cavity, and in fact the rest of the upper respiratory tract, most particle clearance is by the action of the mucociliary escalator where deposited particles are removed through the action of goblet cell cilia on one of two mucus layers secreted by these cells (Acworth *et al.*, 1997, Schlesinger, 1985). The bronchial epithelial cells which, besides producing mucus secretions and using ciliated cells to drive attached material out of the lungs, will initiate an inflammatory response, and clearance methods through the release of immunoglobulins, defensins, pro-inflammatory cytokines, chemokines (Gerritsen, 2000), and collectins such as surfactant proteins A and D. Collectins are employed as an inflammatory control, through enhancement of phagocytosis and ROS production (LeVine and Whitsett, 2001), but also aid in

the formation and stability of lung surfactant (Kingma and Whitsett, 2006). In the alveolar region removal is by macrophages, which are also found throughout the airways, and within the interstitium and the pleura, and are responsible for not only removal of particles, but also for instigating inflammatory reactions (Acworth *et al.*, 1997).

1.3.2.3 Macrophages

Macrophages are resident in a number of tissues, and are therefore often the first defensive innate immune response to be encountered by invading pathogens or inhaled particles (Alberts *et al.*, 2002). Site specificity of macrophages may determine their responses, but ultimately all are focused on the same outcome, which is to eradicate invading material using the release of cytokines, chemokines and proteolytic enzymes, and the production of ROS, all during their main function as active phagocytes (Dörger *et al.*, 2001). The key function of phagocytic cells such as macrophages is the engulfment and destruction of microorganisms by phagocytosis; one mechanism during this defensive process involves the secretion of digestive enzymes, others include the action of ROS (Halliwell and Gutteridge, 2007) and other reactive oxidising metabolites (Chanock *et al.*, 1994).

If not removed by these methods, particles may translocate the alveolar epithelium, where they may occupy subpleural spaces or encounter peritoneal macrophages; or particularly small particles may enter the blood or lymphatic system directly (Schlesinger, 1985).

1.3.2.4 Uptake

The route and level of particle uptake is a particularly important aspect in particle and fibre toxicology, as it is often shown that an increase in uptake corresponds to an increase in cytotoxicity (Brown *et al.*, 1994b). The engulfment of large particles such as microorganisms, dead cells, or inanimate material is an active energy-dependent process which can be divided into two forms of endocytosis: phagocytosis and pinocytosis, divisible by the size of material being engulfed. Often this is governed by cell surface receptor binding (Alberts *et al.*, 2002), as membrane-bound proteins are used to aid the recognition of

invading pathogens or to engage in the phagocytosis of opsonised material, either organic or inorganic. Alveolar macrophages have in place a number of different surface receptors, including Fc-receptors, complement receptors, and pattern recognition receptors such as scavenger receptors, Toll-like receptors, and NOD-like receptors (Valdivia-Arenas *et al.*, 2007). In both instances of endocytosis, structural changes occur that allow the plasma membrane to form pseudopods that envelop around attached material, finally budding off within the cell as endocytic vesicles (Alberts *et al.*, 2002). The endocytic vesicles formed here, called phagosomes, will eventually combine with a lysosome to form a phagolysosome, where engulfed particles are degraded by lysosomal enzymes and through ROS and reactive nitrogen species (RNS) production. Once digested, peptides of the digested material may be presented at the surface of the cell, to stimulate the adaptive immune system. If the engulfed material is not degradable it will remain within the phagocyte, and in the case of alveolar macrophages, the whole cell is removed from the system by its movement, through the projection of lamellipodia, out of the alveolar sac and onto the mucociliary escalator (Alberts *et al.*, 2002), or into the lymphatic system (Evans *et al.*, 1973, Fubini and Otero Arean, 1999). Phagocytosis is only one outcome of particle binding, as this may also be used as an instigator of responses such as inflammation (Alberts *et al.*, 2002).

Due to the level of exposure found at the site of alveolar macrophages, the normal functioning and activation state is an anti-inflammatory one. Upon exposure to inhaled inorganic material these cells should control the removal of such particles with minimal ROS production and minimal inflammatory response, through uninterrupted phagocytosis and the release of anti-inflammatory mediators (Valdivia-Arenas *et al.*, 2007).

1.3.2.5 Oxidants and antioxidants

During the respiratory burst of phagocytosis the formation of phagocytic vacuoles leads to production of ROS (Alberts *et al.*, 2002) when O_2 is consumed from the surrounding tissue and catalysed, by the NADPH oxidase enzyme complex, to form O_2^- (Halliwell and Gutteridge, 2007). The respiratory oxidase enzyme catalyses the reduction of O_2 to O_2^-, using NADPH as an electron donor (Chanock *et al.*, 1994). For the destruction of microorganisms,

O_2^- may be transformed into H_2O_2 which will directly cause damage to biological organisms, or their destruction may be through subsequent formation of $OH^\bullet$ (Halliwell and Gutteridge, 2007). Other ROS/ RNS produced, and likely to be involved in bactericidal activity, are the formation of singlet oxygen from hypochlorous acid, and peroxynitrite from nitric oxide (NO) (Halliwell and Gutteridge, 2007). The release of these reactive metabolites is potentially very damaging, therefore the NADPH oxidase enzyme complex is strictly regulated, and only activated in response to certain stimuli (Chanock *et al.*, 1994).

This release of ROS/RNS during an inflammatory response can and does cause tissue damage, but if the stimulating factor does not instigate a chronic condition and inflammation subsides, then damage is kept at a minimum and damaged tissue can be repaired (Halliwell and Gutteridge, 2007). The apparent role of oxidative stress in the toxicity of many inhaled particles and fibres indicates the importance in a host's ability to control this redox activity, relieving and reducing the quantity of oxidants, as the consequences of oxidative stress is not always absolute. As discussed in section 1.2.1, an accumulation of oxidants can lead to numerous responses. These responses are outlined in figure 1.2 which demonstrates that at low level ROS generation activation of antioxidant defence mechanisms is often enough to maintain the redox balance (Nel *et al.*, 2006). An increase in ROS production in response to particle exposure may be sufficient to induce inflammatory responses (Kannan and Jain, 2000, Nel *et al.*, 2006), coupled with the activation of nuclear transcription factors such as Nrf1 and Nrf2, which with transcribe genes encoding antioxidant defence mechanisms, such as GST (Venugopal and Jaiswal, 1998); still further ROS production may lead to cell proliferation, oxidative damage to DNA, decrease in ATP, lipid peroxidation, cell senescence (Acworth *et al.*, 1997, Halliwell and Gutteridge, 2007, MacNee, 2001) and ultimately cell death (Nel *et al.*, 2006). This DNA damage may be induced by ROS generated by exposure to air pollutants, such as PM_{10}, or DEP for example, or from the subsequent activity of activated phagocytes, during phagocytosis and the action of the NADPH oxidase complex (Risom *et al.*, 2005). The association of OGG1 expression and repair of the oxidation induced DNA lesion 8-oxodG is well established, and an accumulation of 8-oxodG DNA lesions is found to be associated with numerous site specific cancers, including cancers of the lungs

(Dhénaut *et al.*, 2000). It is suggested that the OGG1 gene may be perpetually switched on, but expression can also be triggered and enhanced through the induction of transcription factor Nrf2 during episodes of stress, such as in response to an increase in ROS (Dhénaut *et al.*, 2000).

With DNA damage that has resulted in unsuccessful repair, cells may enter either apoptosis, initiated by the activity of p53 (Lakin and Jackson, 1999, Roos and Kaina, 2006), or programmed necrosis, via PARP activation (Edinger and Thompson, 2004, Zong *et al.*, 2004). Additionally, if either apoptosis or successful DNA repair are not completed there is the risk of perpetual, mutated cell generation, and therefore cancer formation (Norbury and Zhivotovsky, 2004). However, if cells do enter necrosis there is the potential for the release of intracellular components (Elmore, 2007, Mevorach et al., 2010, Proskuryakov et al., 2003). The release of these components can cause direct injury to surrounding areas but also induce the release of pro-inflammatory cytokines and activation of T-cells and dendritic cells, meaning that necrosis stimulates a much greater inflammatory response than apoptosis (Proskuryakov et al., 2003). Some of this may be reversible if the redox state of the cell is controlled and it is therefore vital that cells and tissues produce and utilise antioxidant defence mechanisms.

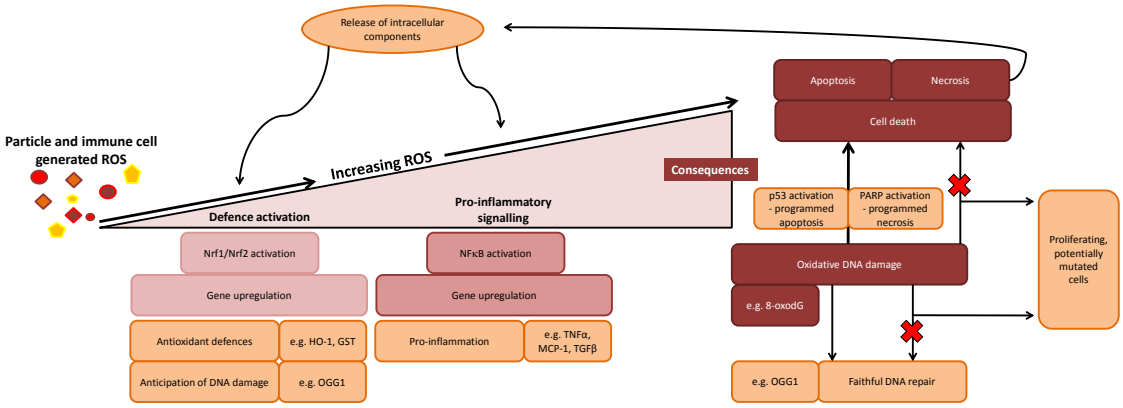

Figure 1.2 Consequences of oxidative stress in response to NP exposure. Diagram adapted from Nel et al. (2006), using data obtained during this PhD and other literature sources (Dhénaut *et al.*, 2000, Edinger and Thompson, 2004, Norbury and Zhivotovsky, 2004, Proskuryakov *et al.*, 2003, Risom *et al.*, 2005, Roos and Kaina, 2006, Venugopal and Jaiswal, 1998, Zong *et al.*, 2004).

With an imbalance of oxidants and antioxidants the potential increase in direct damage and inflammatory response is known to cause a number of problems and this pathology is certainly associated with a number of existing diseases, such as asthma and chronic obstructive pulmonary disease (MacNee, 2001). Antioxidants may be present within cells but also in extracellular fluid (Kelly, 1999). These may take the form of DNA repair enzymes, such as 8-oxoguanine-DNA glycosylase (OGG1), the presence of which are indicative of oxidative-induced damage to DNA upon exposure to diesel exhaust particles (Risom *et al.*, 2003a), or catalytic enzymes involved in antioxidant defence, such as haeme oxygenase-1 (HO-1) (Risom *et al.*, 2003a), or molecules such as glutathione, which is involved in direct ROS scavenging by acting as an electron donor, and subsequent ROS reduction into non-reactive compounds (Kelly, 1999).

1.4 Asbestos

1.4.1 Historic fibre pathogenicity

The first documented use of asbestos is reported to be in clothing as far back as 456 BC, and then again in 120–46 BC in lamp wicks (Martínez *et al.*, 2004). Although now banned in many countries, primarily in Western Europe (Mossman *et al.*, 2007), asbestos was once considered a “wonder” material. Its prevalence and heat-resistant properties provided clear benefits, and its use quickly spread throughout many industrial avenues leading to approximately 3000 applications of asbestos utilised in the pharmaceutical, textile, aeronautics, transport (nautical, aeronautical and land) and power industries, particularly nuclear power (Martínez *et al.*, 2004). The extensive use of asbestos, particularly as an insulation material was due to the crystalline structure providing a high tensile strength and high resistance to heat and chemical stress (Manning *et al.*, 2002). It is still found to be used in less developed countries, but also is still encountered globally as a component of existing structures (Mossman *et al.*, 2007).

The vast, global processing of asbestos led to huge asbestos exposure, with its easy fracture and fragmentation, leading to ready and stable aerosolisation during the intentional or deteriorative destruction of material containing asbestos (Martínez *et al.*, 2004). The severe health implications of this exposure have been studied for most of the last century, but due to its valuable industrial impact, many were opposed to regulating its use (Martínez *et al.*, 2004). There had been a considerable lag time of approximately six decades between the first documented association of asbestos with pulmonary fibrosis and carcinogenesis and asbestos prohibition (Martínez *et al.*, 2004). This is likely in part due to the latent period associated with disease progression, but also the huge economic impact caused by the removal of the asbestos industry. It was not until the late 1980s that a decline in its use was seen, but as asbestos was incorporated into many manufactured and construction materials, exposure, particularly to people working within the industries of demolition and waste removal, is still occurring (Martínez *et al.*, 2004). Presentation of respiratory disorders attributed to asbestos exposure, although now reduced, are still observed, due to the commonly long latent period after initial exposure.

Treatment is often difficult as the normal methods for treatment of fibrotic lung diseases, such as corticosteroids or immunosuppressants, are rarely successful (Mossman and Churg, 1998). Diseases associated with asbestos exposure are numerous and include asbestosis, pulmonary fibrosis, pleural fibrosis, pleural plaques, bronchogenic carcinoma and mesothelioma (Manning *et al.*, 2002, Shukla *et al.*, 2003b).

The vast global impact caused by asbestos exposure has led to continued interest in its pathogenicity, with an enormous output of literature dating from the early 1900s, and still prevalent today. In part this continued interest arises from the potential pathogenicity of materials such as CNT that is likened to that of asbestos. It is not possible in this report to fully report on the scope of asbestos research, but there are numerous excellent reviews on all aspects of asbestos exposure. These include reports by Manning *et al.* (2002), Martinez *et al.* (2004), and Robledo and Mossman (1999) who provide a history of asbestos exposure and an account of the causative factors and progression of asbestos associated fibrogenesis. Shukla *et al.* (2003a, 2003b) report on both the oxidant dependent and cell signalling determined pathogenicity of asbestos exposure, and Donaldson and Tran (2004) provide a short review focusing on the fibre paradigm, where respirable fibre length is associated with pathogenicity.

It is, however, important to identify a number of key aspects of asbestos exposure to verify the importance of the research done during this PhD. The epidemiological and clinical study of pathogenic fibre inhalation has raised much concern about exposure to airborne fibres, with, historically, asbestos being the most pronounced; and this study will highlight the dangers of ignoring potential hazards associated with CNT exposure.

1.4.2 Types of asbestos

The collective term asbestos is attributed to a group of naturally occurring silicate mineral fibres. They have a sub-micron width, and a length to diameter ratio of greater than 3:1 (Shukla *et al.*, 2003b), providing a high aspect ratio. Asbestos fibres are divided into two distinct groups that are chemically and morphologically different. The serpentine classification consists of just one asbestos example known as chrysotile asbestos, which is flexible and twisted (Shukla *et al.*, 2003b), and is constructed of a two-fold sheet, one composed of

silica and the other brucite, forming a spiralled structure (Light and Wei, 1977). The second classification is the amphibole group, which contains the other five asbestos forms: crocidolite, amosite, anthophyllite, actinolite and tremolite (Shukla *et al.*, 2003b). The main constituent of amphibole asbestos is silicon dioxide tetrahedron which forms corresponding chains linked by cationic layers (Light and Wei, 1977, Manning *et al.*, 2002) consisting of iron or magnesium (Manning *et al.*, 2002). All amphiboles are straight, inflexible and less soluble than serpentine asbestos (Shukla *et al.*, 2003b), partially due to instability of chrysotile in acidic conditions – environments where amphiboles are relatively resistant and stable (Manning *et al.*, 2002).

Serpentine asbestos can be attributed to 90% of the global usage (Martínez *et al.*, 2004), and therefore clearly is the most common and most utilised form of asbestos (Manning *et al.*, 2002). However, it is the iron content and the high aspect ratio of the amphibole group that are attributed as the main causal factors in asbestos toxicity (Manning *et al.*, 2002), which are often directly associated with asbestosis and asbestos related deaths (Wagner *et al.*, 1982). Within the amphibole group it is crocidolite (blue asbestos) and amosite (brown asbestos) that are most commonly used (Manning *et al.*, 2002). Toxicity may also be determined by durability, clearance, morphology and surface chemistry. With the leaching of cationic elements from the surface of asbestos, there is a change in overall charge. In the case of chrysotile, this change to negative charge is considered partially responsible for the lack of pathogenicity of this asbestos type (Manning *et al.*, 2002).

1.4.3 Asbestos pathogenicity

1.4.3.1 Asbestos associated respiratory disorders

Directly or indirectly a number of different disorders and disease developments are associated with asbestos exposure, and although there are a number of relatively benign disorders associated with asbestos exposure, the pathology of prolonged asbestos exposure is typified by pulmonary fibrosis, pleural fibrosis, pleural plaques, bronchogenic carcinoma, mesothelioma and asbestosis (Manning *et al.*, 2002, Shukla *et al.*, 2003b); incidentally, only a small proportion of asbestos-induced fibrosis is thought to develop into asbestosis (Mossman and Churg, 1998).

Pleural plaques are lesions formed predominately of collagen strands within the pleural space in response to many fibrous materials (Manning *et al.*, 2002). The fibres are likely to enter the pleural space through the lymphatic system, where, when deposited, will initiate mechanical irritation leading to an inflammatory response and subsequently fibrosis (Martínez *et al.*, 2004). An increase in deposition and plaque formation is then likely to hamper normal lung function (Manning *et al.*, 2002). The fibrosis induced by asbestos exposure will often be a prerequisite to a number of cancers, including mesothelioma and bronchogenic carcinoma.

Asbestosis is a form of interstitial pulmonary fibrosis, which will develop with a progression of fibrotic lesions in response to asbestos exposure as a result of chronic inflammation (Mossman and Churg, 1998), and is normally observed in the lower lung regions (Manning *et al.*, 2002). For tangible diagnosis, observed evidence of fibrotic site-associated asbestos fibres is needed (Manning *et al.*, 2002) in the form of either fibres or asbestos bodies (Martínez *et al.*, 2004), and preferably evidence of the work-related exposure location (Manning *et al.*, 2002). Asbestosis is clinically similar to idiopathic pulmonary fibrosis (IPF), and is characterised by a dry cough, shortness of breath and dry crepitations at the end of inspiration (Mossman and Churg, 1998). Internal examination reveals signs similar to interstitial pneumonia, with peripheral bands, lines, interlobular septa thickening and honeycombing, with fibrosis mostly seen towards the lower lung zones and worse-case disease nearer the pleura (Mossman and Churg, 1998). The initiation of asbestosis will often start with the attempted and failed phagocytosis of fibres, leading to apoptosis in macrophage and epithelial cells, which in turn stimulates the release of mediators for pro-inflammatory conditions and promotion of mesenchymal cell growth. This in turn will stimulate recruitment of further immune cells, activation of fibroblasts and prolonged release of ROS, which all will prolong and sustain the inflammatory responses, lipid peroxidation, collagen deposition and general pro-fibrotic conditions (Martínez *et al.*, 2004). Upon progression of this disease a shortness of breath will develop through a mechanical restriction and a reduction of oxygen diffusion capabilities (Manning *et al.*, 2002).

In addition to these two fibrosis-associated disorders, malignancies are also associated with asbestos pathology throughout the respiratory system (Davis

and Cowie, 1990), including the peripheral and lower lung regions, and the mesothelium of the pleura and peritoneum (Manning *et al.*, 2002). At least in animal models, these malignancies have at times been reported in association with the initial fibrotic lesions (Davis and Cowie, 1990). Although amphiboles are more likely to cause malignant mesotheliomas (Manning *et al.*, 2002), it is documented that chrysotile exposure is also potentially carcinogenic (Martínez *et al.*, 2004).

Investigation into the pathology of asbestos exposure incorporates toxicological, pathological and mechanistic studies, as well as incorporating epidemiology trends (Stayner *et al.*, 1996). Research into the cellular and systemic response to asbestos has predominately used chrysotile and crocidolite exposure. This is due to the former being the most widely used in industry and the most common type found (Mossman and Churg, 1998), particularly in the USA and Canada (Mossman and Churg, 1998, Shukla *et al.*, 2003b). The latter (crocidolite) has a particularly high iron content and is thought to be the most reactive and pathogenic of the amphibole group (Shukla *et al.*, 2003b). It is important to note that in terms of the epidemiological studies and etiological conclusions based on these studies, it is not prudent to place full emphasis on asbestos exposure, as often the exposure coincides with exposure to other known toxic agents, such as crystalline silica dust (Mossman and Churg, 1998). Therefore, progression of symptoms may be dependent on additional factors.

1.4.3.2 Fibre deposition and clearance

The deposition pattern of asbestos within the lungs will depend upon its length, diameter and rigidity (Martínez *et al.*, 2004), with the size and shape of many fibres allowing deep penetration and deposition throughout the lung, providing interactions with a wide range of cell types including alveolar macrophages, epithelial cells (in bronchi and alveoli) and fibroblasts (Mossman and Churg, 1998). Amphibole asbestos is cleared at a far slower rate compared to chrysotile (Mossman and Churg, 1998), and additionally it is the longer fibres that display considerable biopersistence. There are, however, additional factors that will influence asbestos clearance rates. For example, low-dose or short-term exposure to asbestos has not often been seen to cause development of fibrosis or asbestosis, and the latent period before presentation of disease is in

direct correlation with level of exposure, indicating the natural defences in the respiratory system can, under certain conditions, be quite adept at controlling these fibres (Mossman and Churg, 1998). Smoking may also influence clearance rates as it has been shown to not only hinder clearance but also cause the accumulation of the shorter fibres that would normally be cleared relatively effectively (Mossman and Churg, 1998), and the incidence of smoking in asbestos exposes people is sometimes found to correlate with asbestos attributed deaths (Dement *et al.*, 1982).

Once deposited, asbestos fibres are known to attract macrophages that accumulate at fibre deposition sites (Brody *et al.*, 1981), some will form asbestos bodies, or ferruginous bodies (Martínez *et al.*, 2004). These asbestos bodies are a result of the fibres becoming covered by iron and proteins (Manning *et al.*, 2002) and although a useful tool in diagnosis, their formation occurs approximately with only 1% of inhaled fibres (Martínez *et al.*, 2004).

Clearance of inhaled asbestos fibres depends largely on length and durability. The successful phagocytosis of long fibres by macrophages relies on them being easily degraded, which is the case for chrysotile and some other fibrous mineral material, such as wollastonite (Martínez *et al.*, 2004, Muhle *et al.*, 1991). Fibres may be broken down into manageable lengths and removed by normal mechanisms such as transportation within macrophages out of the respiratory system. However, if not easily degraded, which amphibole asbestos is not, the inhaled fibres may remain and accumulate within the lungs for years, even decades (Martínez *et al.*, 2004, Muhle *et al.*, 1991), which would also increase opportunities for translocation to pleural spaces. This has been shown with the inhalation exposure of rats to both chrysotile and crocidolite (Choe *et al.*, 1997). An influx of immune cells, increased TNF-α and elevated nitric oxide (NO) was demonstrated with exposure to both asbestos forms in comparison to inhalation of filtered room air. This is indicative of active phagocytosis and an inflammatory response occurring in the pleural space after translocation from the lungs (Choe *et al.*, 1997).

1.4.3.3 Fibre characteristics

The straight, inflexible and insoluble properties of amphibole asbestos prevents their safe removal from the lungs and pleura, making clearance more difficult and considerably slower than serpentine asbestos (Mossman and Churg, 1998, Shukla *et al.*, 2003b). This accumulation of amphibole asbestos will increase the exposure dose and prolong the exposure period, therefore adding to the pathogenic influence on tissues and cells (Mossman *et al.*, 1997). These factors, combined with the considerable iron content of amphibole asbestos (Mossman *et al.*, 1997) contribute to the toxic effect, and have given rise to the "amphibole hypothesis". There are, however, other characteristics that may influence biopersistence and pathogenicity that are found in both asbestos forms (Mossman and Churg, 1998); these can include small fibre dimensions, physical and chemical composition, surface charge (Mossman and Churg, 1998, Shukla *et al.*, 2003b) and surface reactivity, with abundant redox activity (Mossman and Churg, 1998).

The amphibole hypothesis refers to the proposed theory that amphibole asbestos samples are intrinsically more pathogenic than serpentine asbestos (Kamp and Weitzman, 1999); in fact, amphibole asbestos is shown to be associated, proportionally, with more cases of occupational-exposure-induced pleural mesothelioma than chrysotile (Mossman *et al.*, 1990). This is as a result of a number of characteristic differences such as a particularly durable structural integrity resulting in a greater accumulation of biopersistent fibres over time from inhalation of amphibole asbestos (Kamp and Weitzman, 1999), with a deeper penetration potential to the lung periphery (Mossman *et al.*, 1990). In fact, some researchers state that much of the chrysotile pathology could be attributed to sample contamination by tremolite (Kamp and Weitzman, 1999). This hypothesis, however, is not the inherent belief of all. As reviewed by Stayner *et al.* (1996), it is often shown that although less toxic and less carcinogenic than its counterparts, chrysotile asbestos is still associated with lung and mesothelium malignancies. With mortalities due to malignancies and non-malignant respiratory disorders in chrysotile textile workers also highlight the potential for all asbestos types to cause harm (Dement *et al.*, 1982). This was highlighted in a study by Bolton *et al.* (1982) where Wistar rats were exposed to both high aspect ratio amosite and chrysotile, via intraperitoneal

cavity injection. All treatments, were associated with 94% of exposured animals developing mesotheliomas, with the exception of heated chrysotile which induced mesotheliomas in only 41% of the animals studied. With such a high prevalence of tumour development samples were indistinguishable by this factor. Therefore, using assessments of mortality rate it was determined that chrysotile was the more detrimental of the two asbestos types. Although Bolton *et al.* (1982) did not rule out a length-dependency causative factor in their results, they did propose that this response may be due to a higher number of chrysotile fibres per unit mass, and therefore a greater number of fibres per exposure (Bolton *et al.*, 1982). Incidentally, the lower response seen from exposure to heated chrysotile is thought to originate from the heat treatment causing a reduction in fibrous morphology within the sample (Bolton *et al.*, 1982). Chrysotile is also shown to elicit greater erythrocyte haemolysis than crocidolite (Light and Wei, 1977), and in acute *in vitro* studies using alveolar macrophages, chrysotile has been shown to have a greater cytotoxicity than amphibole asbestos (Myrvik *et al.*, 1985).

1.4.3..4 Length

In vitro and *in vivo* studies involving asbestos and other fibrous material such as glass and rock wool, have identified length as a decisive factor in cytotoxicity and immune responses (Donaldson *et al.*, 1991, Tilkes and Beck, 1983). In fact, the assessment of short and long fibre amosite has demonstrated the induction of lung fibrosis, pulmonary tumours and mesotheliomas in rats exposed to long fibre amosite (LFA), when none were found in response to short fibre amosite (SFA) (Davis *et al.*, 1986). This is thought to be, in part, an outcome of an enhanced *in vivo* inflammatory response to the LFA (Donaldson *et al.*, 1989). A critical length for complete phagocytosis of fibres by alveolar macrophages is approximately 20µm (Dörger *et al.*, 2001). Miller *et al.* (1999) have shown, via injection, that mesothelioma development in response to fibres within the peritoneal cavity is largely dependent on fibre length. Using respirable-sized samples of amosite and other fibre-like material such as glass, stone, ceramic wool and silicon carbon whiskers, Miller *et al.* (1999) presented length dependency in the development of neoplastic mesothelial cells and lethal

mesothelial malignancies, again the significant length of fibres being greater than 20µm.

It is possible, however, that length is not the only factor responsible for asbestos pathology. LFA is indeed longer than SFA, but it is also associated with higher bioavailable iron and greater free radical activity, the two asbestos samples also differ in cationic sites and LFA has the potential to bind more protein. All of which indicates a difference in surface chemistry and oxidation state, both of which may induce potentially pathogenic environments (Graham *et al.*, 1999).

1.4.3.5 Bioavailable iron

The focal occurrence induced by a high-level bioavailable iron is the potential to induce oxidative stress through Fenton chemistry and the Haber-Weiss reaction involving iron species (Halliwell and Gutteridge, 2007). Therefore the importance of iron present in an asbestos sample relates to its bioavailability, and subsequently the generation of free radicals, and perhaps more particularly ROS, which may or may not be free radicals. The release of iron is likely to be dependent on the biological conditions that inhaled particles are exposed to. At a pH indicative to lysosomal fluid far more iron is released from a range of fibres, including silicate amosite, vitreous and ceramic, than from fibres that are suspended in fluid indicative of lung lining fluid (Gilmour *et al.*, 1997).

A free radical will have one or more unpaired electrons which are potentially very reactive. Iron is a transition-metal and as such has unpaired electrons, and can itself be classified as a free radical. There are two common species of iron, which are ferrous iron (Fe^{2+}) and ferric iron (Fe^{3+}). Fe^{3+} certainly has the capability to generate damaging oxygen metabolites, but Fe^{2+} has greater oxidising potential. Fe^{2+}, for example, can catalyse the formation of hydroxyl radicals from hydrogen peroxide, while Fe^{3+} will form superoxide from hydrogen peroxide (Halliwell and Gutteridge, 2007). Transition metals, including iron, play a crucial role in the Fenton reaction, which refers to a number of reactions that involve iron species and oxygen metabolites, and result in the formation of potentially damaging ROS. ROS can be formed through redox reactions, or catalysed by enzymes, and can include superoxide, hydroxyl radicals, singlet oxygen, hydrogen peroxide and peroxynitrite, to name but a few (Halliwell and Gutteridge, 2007). The composition of a number of asbestos types, including

amosite and crocidolite, incorporates iron forms capable of inducing oxidative damage through hydroxyl radical generation (Halliwell and Gutteridge, 2007). It has been shown that asbestos exposure can result in the inactivation and dephosphorylation of the epidermal growth factor receptor (EGFR) in a range of primary and immortalised epithelial and mesothelial human cell types. Once bound and activated this receptor may aid the survival of the cells undergoing exposure (Baldys and Aust, 2005), therefore this deactivation may instigate apoptotic pathways and ameliorate cytotoxicity during asbestos exposure. It was shown that this deactivation is due to the action of bioavailable iron within the asbestos samples (Baldys and Aust, 2005).

The influence of bioavailable iron in an asbestos sample is, however, difficult to elucidate. Although it has been shown, with iron chelation and the use of antioxidants, that bioavailable iron from pathogenic asbestos samples is implicated in the production of ROS such as hydroxyl radicals, and therefore is implicated in direct DNA damage (Gilmour *et al.*, 1995); it is also evident that asbestos and man-made vitreous fibres of a different morphology or composition that release an equal or higher level of Fe are found not to cause this same damage to DNA (Gilmour *et al.*, 1995). Additionally, cell signalling cascades resulting from activation of transcription factors AP-1 and NF-κB, through an increase in free radical-associated damage to DNA, are seen in response to LFA at a greater extent than for other fibrous material which in fact release greater levels of iron (both Fe^{2+} and Fe^{3+}) (Gilmour *et al.*, 1997). However, again, it is not quite as simple as this. It is often shown that the cytotoxicity in primary and immortalised macrophages induced by asbestos exposure, such as crocidolite, can be reduced through iron chelation or the addition of antioxidants (Goodglick and Kane, 1986), indicating the role that iron release, with subsequent oxidative stress, plays in asbestos cytotoxicity. Additionally, the inclusion of the iron based oxidant ferric chloride to treatments of innocuous material such as titanium dioxide results in toxicity not shown previously (Goodglick and Kane, 1986), which also substantiates the belief that iron content plays at least a partial role in fibre/particle toxicity. What is clear, however, is that the increase in bioavailable iron is implicated in the production of ROS (Manning *et al.*, 2002), which certainly has its own implications.

1.4.3.6 Oxidative potential

In vitro analysis has shown that the behaviour of rat and human mesothelial cells may differ in response to crocidolite exposure: both show signs of oxidative stress through a rise in defence mechanisms, while only exposure to rat cells results in oxidative DNA damage (in the form of 8-hydroxydeoxyguanosine (8-OHdG) accumulation). This may be responsible for the subsequent increase in cytotoxicity seen in rat mesothelial cells, which was not as prominent in human cell exposure, and is likely due to the difference in antioxidant activity which was more pronounced within the human MET5A cells (Fung *et al.*, 1997). Incidentally, the oxidative response was unaffected whether iron chelation was performed or not (Fung *et al.*, 1997), indicating that in this case the response was not through iron redox activity. However, others have found that other markers of oxidative DNA damage – in the form of 8-oxo-2'-deoxyguanosine (oxo^8dG), 8-oxoguanine (oxo^8G), and 8-oxoguanosine (oxo^8Gua) – increase in MET5A crocidolite exposure in identical conditions (Chen *et al.*, 1996). Here, Chen *et al.* (1996) used a non-fibrous but compositionally similar comparison, riebeckite, which provided no such response, indicating factors other than iron content may be responsible for asbestos induced DNA damage, possibly length. This result was reflected in a study by Hansen and Mossman (1987), who identified that production of superoxide can be consistently and exclusively reliant on fibrous dimensions, by using compositionally comparable material. This morphologically relevant tendency was also shown by Hill *et al.* (1995) when using opsonised short and long fibre amosite. Oxidative stress found in mesothelial and fibroblast cell lines in response to crocidolite and synthetic vitreous fibres (SVF) of the same length, however, is found to increase in response to iron-rich crocidolite asbestos (Cardinali *et al.*, 2006). This in part is attributed to a difference in surface binding and method of internalisation, indicating a difference in surface chemistry may be responsible. The asbestos fibres are found free within the cytoplasm while the SVF remain encapsulated within vesicles. This binding and endocytotic mechanism prompts an increase in markers indicative of oxidative stress and an increase in cell mortality after 24-hour exposure, but also an increase in proliferative signals in response to the crocidolite sample (Cardinali *et al.*, 2006). It has, however, also been shown that the induction of apoptosis

and MAP kinase-associated signalling pathways with crocidolite exposure is dependent on oxidant production and the release of bioavailable iron from asbestos samples (Jimenez *et al.*, 1997). *In vivo*, an important component in the ROS production during respiratory burst is the enzyme myeloperoxidase, which has not only been shown to exacerbate the oxidative potential of asbestos exposure, but also that of cell proliferation and inflammatory responses (Haegens *et al.*, 2005); both indicate the involvement of iron in oxidative stress, and oxidative stress in proceeding inflammatory responses.

1.4.3.7 Gene expression and cell signalling cascade related to pathology

With asbestos exposure there is an increase in gene expression for antioxidants and cell proliferation; this coincides with both acute and chronic inflammatory responses, leading to reversible or irreversible inflammatory lesions, and deposition of extracellular matrix components, including collagen. There is additional stimulation of fibrosis with an influx of neutrophils, mast cells and T-lymphocytes into asbestos-exposed lungs (Mossman and Churg, 1998). The release of TNF-α by alveolar macrophages plays a significant role in the progression of respiratory inflammatory responses to inhaled asbestos fibres by prompting the release of cytokines, chemokines and adhesion molecules, establishing chronic inflammatory reactions and inciting the recruitment of further inflammatory cells (Driscoll, 2000). Chronic activation of phagocytic cells encourages the development of cancerous cells (Halliwell and Gutteridge, 2007). The influx and prolonged activity of immune cells are thought to cause injury to lung epithelial cells resulting in destruction of alveolar type I epithelial cells and generation of alveolar type II epithelial cells. Type II cells may then proliferate, often through hyperplasia, and enlarge through hypertrophy, often resulting in fibrogenesis or carcinogenesis (Mossman and Churg, 1998).

This inflammatory response to asbestos exposure is related to the activation of transcription factors NF-κB (Janssen *et al.*, 1995) and AP-1, which are not only involved in inflammatory mediation but also with the cell proliferation associated with asbestos pathogenicity (Faux *et al.*, 2000). This mediation of cell proliferation can be initiated not only through the action of NF-κB and AP-1, but through a number of different methods in response to asbestos fibres. These include up-regulation of expression of growth factor receptors, increased growth

factor production, or the activation of intracellular signalling pathways – including the transcription factors NF-κB and AP-1, but also the intracellular signalling molecule calcium, and activation of isomers of protein kinase C (PKC) and other kinase enzymes such as mitogen-activated protein kinase (MAPK) (Shukla *et al.*, 2003b). Incidentally, many of these factors are found to be activated during reactions to NP (Shukla *et al.*, 2003b). AP-1 induction may be largely dependent on growth factor receptor expression, particularly EGFR, which is known to increase in cases of *in vitro* fibrous crocidolite exposure of mesothelial cells, but not to the non-fibrous crocidolite equivalent, or to chrysotile (Faux *et al.*, 2000). This again places emphasis back onto fibre length as the main factor responsible in toxic potential. However, subsequent to EGFR-mediated uptake of crocidolite fibres, the decision of the cell whether to enter proliferation or apoptosis appears to be associated with the nuclear localisation time of extracellular signal-regulated kinases (ERK), where prolonged localisation will result in apoptosis instead of proliferation (Yuan *et al.*, 2004). This ERK-induced apoptosis is also connected to the oxidative potential and surface iron content of the asbestos fibres, where a reduction of available iron, or a neutralisation of oxidants will result in the placating of apoptotic effects (Jimenez *et al.*, 1997). The avoidance of apoptosis with preincubation of cells with antioxidants or iron chelators was also demonstrated by Panduri *et al.* (2003), confirming the role of bioavailable iron in the intrinsic mitochondrial-mediated DNA damage and death of epithelial cells in response to asbestos exposure. In this case the signalling cascade is mediated by p53 activation (Panduri *et al.*, 2006).

Remodelling of cells in lung tissue and within the pleural space is vital during the development of fibrotic lesions or malignant tumours, and is provoked through a number of phases. *In vitro,* both crocidolite and chrysotile asbestos are shown to promote the expression of urokinase-type plasminogen activator (uPA) receptor (uPAR) on mesothelial cells, and therefore encourage the action of uPA, which is responsible for cell migration, proliferation and differentiation, as well as promoting angiogenesis and proteolysis (Perkins *et al.*, 1999). This is seen through direct exposure, or in response to signalling molecules such as IL-1, TGF-β, or dFGF, produced during exposure of asbestos to other cell types (Perkins *et al.*, 1999). IL-1β (Griffith *et al.*, 1994, Hasegawa *et al.*, 1997b) and

TNF-α release (Griffith *et al.*, 1994) by monocytic cells, for example, may be of particular importance as they are known to elicit uPAR expression and IL-8 release in epithelial and mesothelial cells. While TGF-β and not TNF-α will upregulate uPAR expression on mesothelial cells (Perkins *et al.*, 1999), TGF-β and TNF-α will both upregulate the expression of glycoproteins fibronectin and tenascin, which are considered to contribute to lung fibrosis and carcinogenesis (Kinnula *et al.*, 1998). Uptake of asbestos by mesothelial cells may be encouraged through asbestos opsonisation with various glycoproteins, such as vitronectin (Boylan *et al.*, 1995). A sugar-binding protein, intelectin, has previously been considered to act during immune responses to parasitic infections and allergic responses (Peebles, 2009), and now expression is also found to be prevalent in many tumours, including asbestos-associated mesotheliomas (Wali *et al.*, 2005).

The gene expression related to asbestos exposure can infer many outcomes, including inflammation, apoptosis (through initiation of apoptotic pathways, or through intracellular calcium imbalance), tumour suppression, oxidative stress and ROS release, or the identification of fragile/vulnerable DNA locations (Nymark *et al.*, 2007). It seems evident that the promotion of both inflammatory conditions and apoptosis can be initiated by asbestos through a number of pathways, including the use of p53, NF-κB, AP-1, ERK and MAPK; it is also apparent that these effects are diminished on treatment with antioxidants (Mossman *et al.*, 1997, Panduri *et al.*, 2006).

Above all, it appears that fibre biopersistence within the lung is the main factor influencing pathogenicity. The persistence of fibres within the respiratory system relies on certain fibre characteristics permitting the avoidance of natural lung defences (Davis, 1994). The first defence made redundant is the ability of phagocytic cells to engulf and remove long fibres. Length, however, is not the only issue. A change in fibre chemistry through metal leaching or direct destruction by lung surfactant components, macrophage digestive enzymes, or pH, will result in fracturing and formation of shorter fibres that are more easily removed, or completely dissolved, while particularly durable fibres which will oppose these destructive processes, are left intact and become biopersistent. This is indeed seen with asbestos exposures as whether fibres are long or

short, amphibole asbestos will accumulate in the lung at a greater rate than chrysotile, indicating that the chrysotile fibres are removed, and a structural or compositional difference relating to durability is responsible (Davis, 1994). Incidentally, the degradation, measured by leaching of magnesium from chrysotile is relatively fast in macrophage exposures, and is associated with an initial uptake into phagolysosomes, while exposure to mesothelial cells is shown to be much slower (Jaurand *et al.*, 1984).

There appear to be numerous factors associated with asbestos pathogenicity, although, even now, they are not all fully elucidated. It is certainly important to be mindful of the aforementioned factors when addressing the toxicity of fibre-like material, and aspects relating to lung deposition (aerodynamic diameter), fibre retention (durability, fibre length), fibre length (frustrated phagocytosis), surface charge and chemistry, which are all important when investigating fibre-induced toxicity.

1.5 High aspect ratio nanoparticles

As has been seen with other NP, the properties that make HARN attractive to many industries are also the properties that are causing a great deal of concern with respect to their pathogenicity. These properties have already been linked with the toxicity of other NM and of asbestos, including highly reactive surfaces and components, poor solubility, and a high aspect ratio. This all generates great concern to the biocompatibility and reactivity of HARN (Mitchell *et al.*, 2007). The delayed response to asbestos exposure, and subsequent severe worldwide health implications, is something that must be avoided if HARN are to be utilised to their full potential. Thus there is a lesson to be learned and an increasing body of literature into the toxic effects of HARN is becoming available, although often with conflicting suppositions. CNT are currently the most exciting HARN as they are the first with high volume production and clear operational commercial applications (Tran *et al.*, 2008), and therefore are given more attention than others.

1.5.1 Deposition and clearance of CNT

1.5.1.1 In vivo deposition and clearance from aspiration and instillation

The deposition and clearance of CNT from biological systems is a contentious subject, but what is obvious is that it will vary depending on exposure route, particle size, shape, electrostatic behaviour and functionalisation. The deposition of aerosolised CNT throughout the pulmonary system is a subject in itself that causes much controversy: the agglomeration of CNT by electrostatic or van der Waals forces (Porter *et al.*, 2008) may govern their accumulation into agglomerate sizes which are not permitted into the far-reaching areas of the lung that other NP can reach (Muller *et al.*, 2005). This, initially, was believed to make inhalation studies problematic and respiratory investigations would involve instillation or aspiration techniques. However, inhalation of CNT is indeed possible, and the effects of inhalation studies are discussed later.

Using methods of CNT instillation and aspiration it has been shown that 80% of a MWCNT sample can remain within a rat lung for at least 60 days; this concentration is reduced to 36% with physical grinding – therefore shortening of

tubes – prior to exposure (Muller *et al.*, 2005). This is the first indication that an important factor in determining biopersistence is length. Another possible factor that would influence pulmonary toxicity is dispersion. With the use of well-dispersed suspensions of both MWCNT and SWCNT prior to administration there is enhanced distribution within lung tissue (Mercer *et al.*, 2008, Muller *et al.*, 2005), while agglomerates formed from a less dispersed CNT samples will remain localised (Muller *et al.*, 2005, Shvedova *et al.*, 2005), and will predominately not reach the smaller airways (Muller *et al.*, 2005). It would therefore be assumed that an increase in dispersion would always be associated with an increase in toxicity, but this is not always the case: Murr *et al.* (2005) and Shvedova *et al.* (2005) have shown that agglomerated samples can, at times, result in a higher toxicity.

With presentation of oxidative stress and DNA damage within the lungs and aortic tissue and a tendency for increased atherosclerosis in SWCNT-exposed mice, it appears that there is either passage of CNT out of the lungs after administration by instillation or aspiration, or an indirect systemic response is initiated (Li *et al.*, 2007). After intratracheal instillation a large proportion of MWCNT are often rapidly removed, remaining in the lung for only one day, with no evidence of transfer into the blood (Deng *et al.*, 2007). This clearance is likely through action of alveolar macrophages attaching and readily phagocytosing CNT (Pulskamp *et al.*, 2007a); for this to occur in a short time period the fibres must be of a length that macrophages can easily engulf, which raises a question of length and biopersistence and introduces the “fibre paradigm”. The maximum length for successful phagocytosis by alveolar macrophages is believed to be 20µm (Dörger *et al.*, 2001), therefore fibre-like material, such as CNT, are believed to be particularly pathogenic when they have a length of over 20µm, width of less than 3µm, are durable and biopersistent (Donaldson and Tran, 2004). Under these conditions phagocytic cells will attempt but fail full phagocytosis, ultimately undergoing frustrated phagocytosis (figure 1.3). Instances of frustrated phagocytosis would lead to prolonged deposition, biopersistence and the induction of oxidative stress, acute and chronic inflammation, enhanced cell proliferation (Brown *et al.*, 2007b, Dörger *et al.*, 2001, Poland *et al.*, 2008, Ye *et al.*, 1999b) and formation

of foreign body giant cells (FBGC) (Poland *et al.*, 2008), which could potentially elevate to more aggressive disease development, as seen with some asbestos exposures.

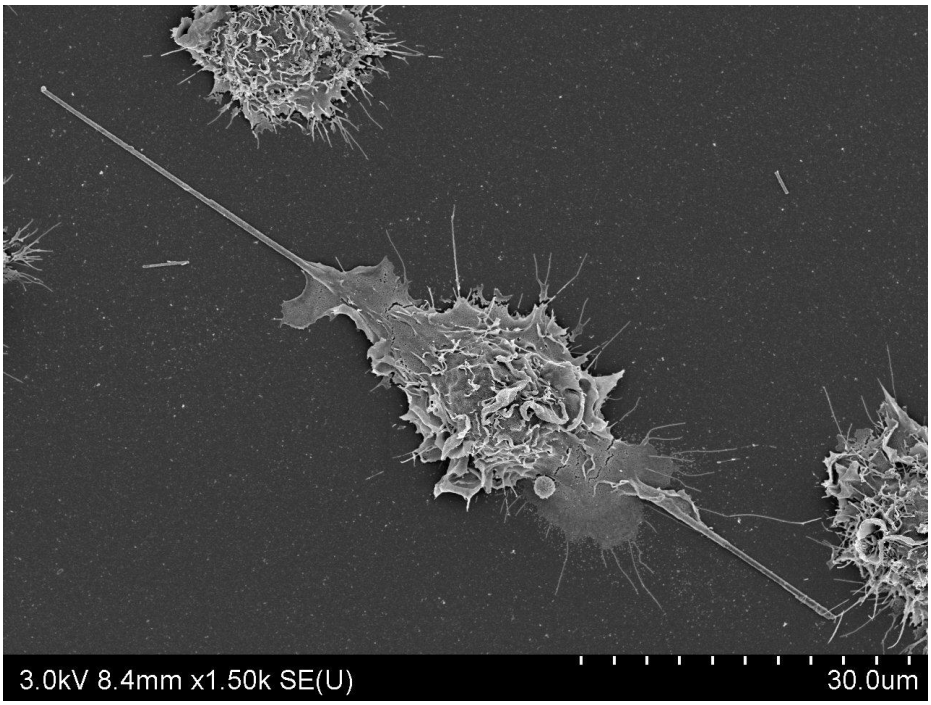

Figure 1.3 Attempted phagocytosis of long-fibre amosite (LFA) by murine macrophage-like cell, ultimately leading to frustrated phagocytosis. Scanning electron microscope images of J774A.1 cells exposed to 2.1µg/cm^2 for 4 hours prior to SEM preparation, and imaged using a Hitachi S-4800 FEG SEM scanning electron microscope.

For the development of more pathological outcomes the durability of CNT within the lung will be very important, and recently it has been highlighted that the degradation of CNT by natural defence systems of the lungs may be possible under certain conditions. For example, the degradation of SWCNT is shown to occur when samples are incubated in a solution containing hypochlorite and human neutrophil enzyme myeloperoxidase catalyse, but also with direct exposure to neutrophils (Kagan *et al.*, 2010). Degradation occurs within 12 hours with neutrophil exposure, and within 48 hours for macrophages. Additionally and potentially more significant observation is that this degraded material does not elicit an inflammatory response when compared to the original pristine SWCNT sample (Kagan *et al.*, 2010). This degradation, however, is likely to be dependent on CNT structure; it has been shown that carboxylated SWCNT are degraded within a simulated phagolysosome, while unfunctionalised CNT are left intact (Liu *et al.*, 2010).

1.5.1.2 Passage after alternative exposure routes

The passage CNT take through biological systems when administered through other routes of exposure is understandably quite different. When administered by intravenous injection CNT functionalised with diethylentriaminepentaacetic (DTPA) and indium (^{111}In), which aids water solubility and detection, are distributed throughout many organs and tissues within 30 minutes, irrespective of surface charge, with no organ specific tendencies. They were then rapidly excreted through the urinary tract, again relatively unchanged by surface charge (Singh *et al.*, 2006). However, taurine (a naturally occurring amino acid derivative) functionalised fMWCNT also administered by intravenous injection were quickly transferred to the liver, heart, lung and spleen, and remained unchanged in the liver for at least 28 days (Deng *et al.*, 2007). Intraperitoneal injection of SWCNT, functionalised for radiotracing and to enhance solubility, were extensively distributed throughout the body, predominately depositing in the stomach, kidneys and bone, remaining at relatively high levels within bone for 11 days (Wang *et al.*, 2004). With direct stomach intubation there appeared to be no entry of taurine functionalised MWCNT into the blood, but rather entry into the intestinal tract to be excreted in faeces (Deng *et al.*, 2007). This relatively innocuous behaviour of CNT shown by Deng *et al*. (2007), Singh *et al*. (2006) and Wang *et al.* (2004) may or may not be attributed to functionalisation. It does, however, provide some answer to the durability of CNT and again raises the question of biopersistence. TEM images of tissue and urine samples show CNT to be unchanged and intact (Deng *et al.*, 2007, Singh *et al.*, 2006), as does the previously mentioned work by Abarrategi *et al*. (2008) and Popat *et al*. (2007). Although proving to be advantageous, the exit route of the MWCNT scaffolding structures was not fully investigated, and Abarrategi *et al.* (2008) found that upon scaffolding disassembly most CNT were believed to be transported away through blood circulation, but some were found to have translocated to surrounding tissue.

1.5.2 In vivo pulmonary toxicology of CNT

Within the lung CNT have been found to initiate fibrosis using rodent models (Muller *et al.*, 2005, Shvedova *et al.*, 2005, Shvedova *et al.*, 2007). This was demonstrated through granuloma formation, alveolar wall thickening (Lam *et al.*,

2004b, Mercer *et al.*, 2008, Shvedova *et al.*, 2005, Shvedova *et al.*, 2007), increased cellular proliferation and significant increase in the profibrotic growth factors such as platelet-derived growth factor –B and –C (Mangum *et al.*, 2006). With evidence of collagen deposition established after two weeks in mice exposures of 0.02µg dispersed SWCNT per cm^2 lung surface. This was not evident in relative treatments of NPCB (Wang *et al.*, 2010b). Additional cell injury has apparent in the form of increased lactate dehydrogenase (LDH), total protein (Muller *et al.*, 2005, Shvedova *et al.*, 2005), particularly γ-glutamyl transferase (GGT), oxidative stress and alveolar type I (AT-I) cell death – indicated by an increase in alveolar type II (AT-II) cells (Shvedova *et al.*, 2005). An increase in granuloma formation and enhanced inflammatory response associated with the mesothelium was also evident with the injection of particularly high aspect ratio CNT into the peritoneal and pleural cavities, particularly when compared to negative controls and shorter CNT samples, but also when compared to a long asbestos sample (LFA) (Murphy *et al.*, 2011, Poland *et al.*, 2008). MWCNT of up to 50µm in length were also shown to increase LDH and total protein levels, and induce fibrogenesis when administered to rats by intratracheal instillation, with LPS co-exposure (Cesta *et al.*, 2010).

1.5.2.1 Reduced lung function

Dose-dependent deterioration of mouse lung function and lung defence systems has also been observed following SWCNT exposure, illustrated respectively by an increase in expiratory time and a decrease in clearance of infectious agents, such as bacteria (Shvedova *et al.*, 2005), but also with the appropriation of key pulmonary defence proteins by CNT (Salvador-Morales *et al.*, 2007, Shvedova *et al.*, 2007). Through the induction of calcium-signalling-dependent phagocytosis (Ohmer-Schrock *et al.*, 1995), two proteins found within pulmonary surfactant (SP-A and SP-D) play a key role in the pulmonary defence against allergens and microorganisms (Salvador-Morales *et al.*, 2007). It was found by Salvador-Morales *et al.* (2007) that calcium ion-dependent binding occurs between fDWCNT and these two surfactant proteins. This highlights two possible outcomes. Firstly, the proteins are not available for defence against pathogen infection and, secondly, SP-A and SP-D enhance

phagocytosis of CNT by alveolar macrophages (Salvador-Morales *et al.*, 2007), with the possible outcome of frustrated phagocytosis, if CNT lengths were sufficient.

1.5.2.2 In vivo inflammatory responses

In terms of an inflammatory response, irrespective of exposure route, an influx of various immune cells was found in response to a range of CNT in a variety of studies using exposures of both mice and rats (Mercer *et al.*, 2008, Muller *et al.*, 2005, Poland *et al.*, 2008, Rothen-Rutishauser *et al.*, 2010, Shvedova *et al.*, 2005), with an accompanying rise in pro-inflammatory cytokines (Muller *et al.*, 2005, Poland *et al.*, 2008, Shvedova *et al.*, 2005). Comparatively, SWCNT were shown to have a greater inflammatory potential than other particles, such as NPCB, QD or AuNP, during an acute three-hour instillation study, with a higher immune cell influx and inflammatory cytokine release (MIP-2, MCP-1, and IL-6), and coinciding DNA damage. As the exposure time continued to 24 hours NPCB was shown to elicit a greater inflammatory response than SWCNT, although a high level of inflammation was still on-going with SWCNT exposure (Jacobsen *et al.*, 2009).

Intranasal exposure into mice of approximately 100µm aggregates of DWCNT has also been shown to elicit an inflammatory response with a release of IL-6 and leptin, although not an increase in ROS production (Crouzier *et al.*, 2010). If CNT exposure is to be likened to asbestos, ROS production would be expected, and in fact, the redox potential of CNT has been demonstrated by Rothen-Rutishauser *et al.* (2010) in a cell-free system, in cultured macrophages, and in BAL cells isolated after intratracheal instillation. The lack of ROS found by Crouzier *et al.* (2010) may be due to ROS scavenging by CNT and not the lack of ability to elicit this form of response (Crouzier *et al.*, 2010).

1.5.3 In vitro responses

In vitro, SWCNT have been shown to cause the release of high levels of TGF-β1 from macrophages (Shvedova *et al.*, 2005), indicating the potential need for tissue regeneration after CNT exposure. Both MWCNT and SWCNT were shown to cause a marked increase in the pro-inflammatory cytokine TNF-α

when exposed to lipopolysaccharide (LPS) activated macrophages (Pulskamp *et al.*, 2007a). While MWCNT have been seen to induce TNF-α production, TNF-α mRNA expression and LDH release, when well dispersed (Muller *et al.*, 2005) but not when aggregated (Murr *et al.*, 2005), while little cytokine release (TNF-α, IL-1β, IL-12, IL-10, IL-8) was observed in response to SWCNT alone (Murr *et al.*, 2005, Pulskamp *et al.*, 2007a, Shvedova *et al.*, 2005). At realistic doses CNT have not been shown to cause significant increases in cell death, either by apoptosis or necrosis in alveolar macrophages (Pulskamp *et al.*, 2007a, Pulskamp *et al.*, 2007b), but were found to reduce mitochondrial membrane potential (Pulskamp *et al.*, 2007a). However, in a comparative study, MWCNT of undisclosed length were shown to be considerably more cytotoxic than crocidolite on the human bronchial epithelial cell line BEAS-2B. An IC_{50} was obtained with treatment of low density BEAS-2B cells to 12μg/ml MWCNT, with 100% cell death seen in response to 50μg/ml BEAS-2B, this was in cells shown to tightly associate with or take up only 12.5% of CNT during a five hour exposure period. An equivalent response to crocidolite-treated cells was only obtained with an IC_{50} of 678μg/ml, and viable cell populations did not drop much below this level with up to 1000μg/ml (Hirano *et al.*, 2010). This observation was somewhat reversed in a study using the epithelial cell line A549 by Thurnherr *et al.* (2010), who demonstrated that, although MWCNT can cause significant cell death at concentrations of 3.2-30μg/ml, crocidolite asbestos exposure resulted in substantially greater cell death at relative concentrations. In these acute exposure conditions, neither material was shown to elicit DNA damage; however, considerable ROS production was shown in response to MWCNT (Thurnherr *et al.*, 2010). Long-term low-level exposure to MWCNT was also used, and no adverse effects were found, nor any adaptive protection developed (Thurnherr *et al.*, 2010). At low single doses (0.02μg/cm^2), well-dispersed SWCNT were shown to increase collagen formation by fibroblast cells and induce significant proliferation of the epithelial cell line BEAS-2B, while the opposite occurred at higher doses (0.6μg/cm^2) (Wang *et al.*, 2010b).

Also at a relatively low dose of ≤10μg/ml, MWCNT were shown to increase protein and mRNA levels of many pro-inflammatory mediators, including IL-1, IL-6, IL-8, MIP-2, VEGF, activin, inhibin and TNFα; this was potentially through membrane interaction and deterioration, or through oxidative mechanisms, and

induction of NF-κB activation and MAP kinase phosphorylation (Hirano *et al.*, 2010). With the use of PCR gene array analysis of primary epithelial cells exposed to SWCNT, much higher doses of 100µg/ml revealed that CNT exposure can simultaneously upregulate genes associated with apoptosis, signal transduction and transcription factor activation, while down-regulating genes for survival, proliferation and adhesion (Alazzam *et al.*, 2010).

1.5.4 ROS and oxidative stress

The ability of CNT to cause oxidative stress is potentially an important aspect of their toxicity and is therefore well documented, and as indicated the literature is not always in agreement; but it does seem apparent that in certain circumstances CNT can directly and indirectly influence the redox state of a cell and cause oxidative stress.

The presence of ROS in response to CNT exposure is clear in both *in vitro* and *in vivo* studies (Ravichandran *et al.*, 2009, Srivastava *et al.*, 2011). There was an ensuing state of oxidative stress in response to SWCNT and MWCNT, with increased lipid peroxidation, extracellular superoxide dismutase cleavage, decreased antioxidants glutathione and ascorbic acid (Ravichandran *et al.*, 2009, Shvedova *et al.*, 2007, Srivastava *et al.*, 2011) and the conversion of superoxide radicals to hydroxyl radicals (Kagan *et al.*, 2006). Additionally, the ability of SWCNT to cause oxidative burst and direct generation of ROS was clearly demonstrated by Pulskamp *et al.* (2007b) *in vitro*. The aforementioned studies raise the issue of which CNT characteristics – potentially the iron content or level of amorphous carbon – are responsible for this oxidative potential. Iron is known to be potentially toxic with a high redox potential (Papanikolaou and Pantopoulos, 2005), the presence of which in the amphibole group of asbestos is believed, in part, to contribute to asbestos toxicity (Shukla *et al.*, 2003b). As iron may also be present in CNT samples through metal catalyst remnants of the production process (Oberdorster *et al.*, 2005), it is certainly feasible that iron redox activity may be playing a part in CNT toxicity, and may even control which ROS are produced. The specificity of ROS produced appeared dependent on CNT composition. Peroxynitrite ($ONOO^-$) can be generated in samples with a high metal content, while superoxide anion (O_2^-) production can be rapid and sustained in response to CNT samples with

high metal and amorphous carbon content, while a period of up to 24 hours was needed to generate the same response when amorphous carbon is removed (Pulskamp *et al.*, 2007b). It was shown by Pulskamp *et al.* (2007b) that purified (reduced metal content) CNT samples lacked the ability to an oxidative burst in lung epithelial cells, or produce ROS at all. Non-purified samples with a high metal content were shown to display a greater ability in generating hydroxyl radicals in activated macrophages (Kagan *et al.*, 2006), and not only cause oxidative burst, but did so in only 10 minutes, and dose-dependently after 24 hours (Pulskamp *et al.*, 2007b). Interestingly, CNT samples with reduced levels of amorphous carbon caused a relatively delayed increase in ROS, irrespective of iron content (Pulskamp *et al.*, 2007b). This behaviour was substantiated by Pulskamp *et al.* (2007a) where pristine SWCNT and MWCNT were found to induce ROS production in alveolar macrophages, and SWCNT with a reduced metal content had no ROS increase compared to controls. The difference in response to purified and non-purified CNT samples has been shown by Kagan *et al*. (2006) and Pulskamp *et al*. (2007b), but more importantly, it has been shown, using measurements of iron mobilisation and redox activity, that although most iron remains enclosed and inaccessible within the CNT, a small quantity can be released into suspension fluids, which was sufficient to cause redox reactions, subsequently causing single strand breaks in DNA (Guo *et al.*, 2007b). Additionally, increases in iron availability can result from stresses CNT are exposed to post-production, such as oxidation, mechanical grinding and sonication (Guo *et al.*, 2007b).

The leaching of metal ions from CNT samples has not been confirmed, but it is often shown that where toxic behaviour, such as reduced viability and increased DNA damage is observed in response to MWCNT, the same cannot be said for parallel experiments using relatively soluble metal ions (Karlsson *et al.*, 2008).

There has also at times been no evidence of oxidative stress shown in response to CNT exposure. For example no HO-1 expression was induced in either epithelial or endothelial cell lines (Pulskamp *et al.*, 2007b), and similarly both Kagan *et al.* (2006) and Shvedova *et al*. (2005) found no evidence of SWCNT-exposed macrophages initiating either an oxidative burst or production of nitric oxide (NO), nor active attempt to phagocytose the fibres. Through the measure of nitrite concentrations it was also shown by Pulskamp *et al.* (2007a)

that NO is not produced in response to SWCNT or MWCNT. Additionally it was shown that LPS-induced formation of NO is dampened with the inclusion of MWCNT. This is possibly due to CNT binding to the protein inducible nitric oxide synthase (iNOS) (Pulskamp *et al.*, 2007a), which again raises questions to the host's ability to react to inhaled pathogens with previous CNT exposure.

As mentioned in previous sections, some responses to a redox imbalance within a cell may be reversible, with no long-term concerns. However, the consequences of CNT induced oxidative stress may be severe, since oxidative stress is associated with the development of a number of diseases, including numerous inflammatory disorders (Rahman, 2002), and cancer (Valko *et al.*, 2006). There are extensive ways in which NP, including CNT, can induce oxidative DNA damage; both the direct and indirect methods of these mechanisms are well reviewed by Donaldson *et al.* (2010). Although thus far it has not been fully addressed, it is worth noting that potential for CNT, as with other NP, to induce DNA damage may not be fully dependent on oxidative mechanisms, and can be through the a physical interruption of cell division, or even direct contact with DNA (Donaldson *et al.*, 2010). In respect to CNT this would certainly be feasible, they can enter a cell through numerous mechanisms, other than phagocytosis (Doak *et al.*, 2009), where they have been shown to bind to cellular components including the cytoskeleton and to DNA (Li *et al.*, 2006, Porter *et al.*, 2007b), with the potential for physical spindle disruption during mitosis (Cveticanin *et al.*, 2010).

1.5.4 CNT toxic components

In the previous sections in both CNT and asbestos assessment there are a number of factors that may influence toxicity and potentially pathogenicity; these may include iron components, its availability and ability to initiate oxidative stress, a high aspect ratio and a low aerodynamic diameter, structural defects and extent of dispersion. With all these factors it becomes evident that the most effective method for identifying potential hazards of CNT exposure is to address these factors in tightly controlled investigations.

In a combination study design by Fenoglio *et al.* (2008) and Muller *et al.* (2008b) it was suggested that important factors in the pathogenicity of MWCNT can include the presence of amorphous carbons, or metal contaminants, an

increase in aspect ratio, changes to surface chemistry, and possibly the introduction of structural defects. Combination and alternate treatments of mechanical grinding and heating of CNT samples were used to identify and distinguish many of these potential causative factors. Grinding of a pristine CNT sample produced CNT that were <1μm in length, still contained metal production remnants and were relatively high in surface oxygen, due to the metal contaminants and/or oxygenated functional surface groups. Progressive heating gave temperature dependent decreases in surface oxygen and metal content, while post-heating additional grinding introduced further surface oxygenated functional groups (Fenoglio *et al.*, 2008). Incidentally, treatments to reintroduce structural defects also increased the surface area and decreased the proportional crystalline structure (Fenoglio *et al.*, 2008). While heating, and eventual annealing encouraged hydrophobic characteristics, and reduced the ability to scavenge ROS, hydrophilicity and ROS scavenging potential was introduced and reintroduced with grinding, therefore creating oxidised functional groups (Fenoglio *et al.*, 2008).

In this controlled study it was found that the main causative factor in MWCNT genotoxicity in rat epithelial cells, measured by micronuclei formation, was actually structural defects, and not as a result of metal contaminants (Muller *et al.*, 2008b). This sample manipulation has provided evidence that MWCNT with an increased surface area that contain structural defects and oxidised functional groups, aiding water solubility, are all potentially important factors in CNT induced cytotoxicity (through LDH release) and inflammation through immune cell influx and secretion of TNF-α and IL-1β (Muller *et al.*, 2008b). CNT length, however, cannot be excluded as, although length was not an obvious toxic factor in the study by Muller *et al.* (2008b), there was no effort to vary length and the CNT used by Muller *et al.* (2008b) were significantly shortened by the study design modifications (Fenoglio *et al.*, 2008).

As is often demonstrated in asbestos exposure, the length of a fibre is likely to play a crucial role in disease progression. It is therefore a clear focus when assessing the toxic effects of other high aspect ratio materials. Glass fibres that are easily phagocytosed – with a length of 7μm – have been shown to be far less effective than glass fibres of length 17μm in inducing oxidative and NF-κB-

dependent gene expression and production of TNF-α, through the frustrated phagocytosis in a mouse macrophage cell line (Ye *et al.*, 1999a). With exposure of stable THP-1 cell line and primary monocytes to a range of morphologically distinct CNT and carbon nanofibres the importance of length and dispersion was further clarified by Brown *et al.* (2007b). Long, straight and well-dispersed CNT were found to potentiate the greatest inflammatory response in the form of TNF-α release, and the greatest ROS production, which was attributed to their ability to cause frustrated phagocytosis (Brown *et al.*, 2007b). This response was also seen in the treatment of the A549 epithelial cell line, where an oxidant-induced activation of NF-κB in response to MWCNT and not NPCB resulted in IL-8 production (Han *et al.*, 2010). Similarly with THP-1 cells, long straight MWCNT were shown to cause an increase in TNF-α and IL-1β accompanied by markers of oxidative stress (Brown *et al.*, 2010), while short, well-dispersed MWCNT of approximately 1.5μm in length were shown to elicit almost no response upon intratracheal instillation into the rat lung (Kobayashi *et al.*, 2010). A single exposure dose of 0.04-1mg/kg with a post-exposure period of 3 days to 6 months elicited a small, acute inflammatory response in the form of neutrophil recruitment into the lungs, and a slight degree of cytotoxicity as demonstrated by LDH present in the BALF. This, however, was only at the higher dose of 1mg/kg and at the 3 day post-exposure measurement point. Animals exposed for longer periods displayed no such response, and no elevation in pro-inflammatory cytokines, while both inflammation and cell death was evident in exposure to relative treatments of crystalline silica. It was therefore apparent that the defence mechanisms in place in the body adequately controlled exposures to these short MWCNT, as seen by laden alveolar macrophages present in the alveolar region, and no inflammation (Kobayashi *et al.*, 2010).

1.5.5 In vivo inhalation

CNT inhalation studies provide a similar response to those using aspiration and instillation techniques and also often appear quite varied in their conclusions. The initial theory that CNT would not be inhaled to distal lung regions, due to electrostatic behaviour resulting in large agglomerates, has been disparaged by a number of studies. CNT dust samples were shown to generate aggregates with an aerodynamic diameter of predominately <3μm, which were certainly

respirable into the alveolar region (Ma-Hock *et al.*, 2009), and adverse pulmonary effects were established as a result. It was initially found by Mitchell *et al.* (2007) that both dispersed and agglomerated MWCNT are dose-dependently deposited throughout the lungs of exposed mice. CNT were readily taken up by resident cells, with the appearance of alveolar macrophages laden with particles. This interaction was not seen in conjunction with any further evidence of pulmonary toxicity; however, systemically the mice appeared to have a reduced and inadequate immune response which may indicate an evasion of the respiratory system defence systems by MWCNT (Mitchell *et al.*, 2007). MWCNT 0.5-40µm in length were also found throughout the lungs – including distal regions, upon inhalation and were also taken up by alveolar macrophages and epithelial cells. This however, was paralleled by an immune response in the form of PDGF and MCP-1 production (Ryman-Rasmussen *et al.*, 2009b). Furthermore, with sensitisation, MWCNT exposure was shown to elicit conditions that may promote fibrogenesis, with secretions of IL-13, TGF-β1, IL-5 and collagen deposition, through PDGF-induced fibroblast proliferation and subsequent collagen release stimulated in fibroblasts by TGF-β1 (Ryman-Rasmussen *et al.*, 2009b).

Using a well-ordered structured inhalation study of rats, an exposure period of 13 weeks to 0.1, 0.5 or 2.5 mg/m^3 MWCNT caused a dose-dependent increase in particle deposition. This was through measurement of lung weight, tissue discolouration and macrophage accumulation. It was also noted that granulous lesions were formed in the lungs, lymph nodes and upper respiratory tract (Ma-Hock *et al.*, 2009). There were clear associated inflammatory responses with this exposure, in the form of granuloma formation, and alveolar macrophages and epithelial cells were seen to contain particles. However, during the 13-week study, no fibrosis appeared, although the giant cell components of the granulomas did contain fibroblasts (Ma-Hock *et al.*, 2009). Additionally, the higher dose of 2.5mg/m^3 was enough to cause a slight systemic inflammatory response (Ma-Hock *et al.*, 2009). With the potential pathology likened to asbestos it is important to identify the passage and effect of MWCNT through the lungs, as CNT inhalation is now evident. Both Mitchell *et al.* (2007) and Ma-Hock *et al.* (2009) did not clarify if any translocation of MWCNT out of the lungs had occurred, but have presented the systemic impact, potentially indirect, of

MWCNT upon inhalation. It has, however, been shown that after just one six hour inhalation of 30mg/m^3 by mice, the uptake by alveolar macrophages and subsequent migration of MWCNT to the sub- pleura was accompanied with formation of giant cells which subsequently resulted in fibrogenesis in this area. This was in response to the high dose of 30mg/m^3 and not to the lower dose of 1mg/m^3, and also not in response to aerodynamic diameter and mass relevant exposures to NPCB (Ryman-Rasmussen *et al.*, 2009a). Using pharyngeal aspiration administration of MWCNT to mice, Mercer *et al.* (2010) further confirm the ability of MWCNT to readily cross barriers leading to the penetration of subpleural tissue and intrapleural spaces.

It must be noted that an airborne density value of under 53µg/m^3 has been identified in facilities producing MWCNT, which at present puts these inhalation values potentially very high (Lam *et al.*, 2006); however, the full extent of industrial accidental exposure has not yet been assessed.

1.5.6 Other aspects of CNT toxicity - routes of exposure and coexposure

Alternative routes of exposure

The large proportion of this review has concentrated on the respiratory toxicity of CNT, as this is the most likely common exposure route, but other routes of exposure including dermal, intestinal and intravenous are probable and therefore these are mentioned briefly here.

MWCNT exposed to human epidermal keratinocytes (HEK) were found to be readily taken up, where they appeared free in the cytoplasm, held within vacuoles, and also within close proximity and possibly scoring the nuclear membrane (Monteiro-Riviere *et al.*, 2005). SWCNT were shown to induce free radical production and cause oxidative stress when exposed to HEK, resulting in morphological changes (Shvedova *et al.*, 2003) and reduced viability (Monteiro-Riviere *et al.*, 2005, Shvedova *et al.*, 2003), with dose- and time-dependent increase in a pro-inflammatory reactions (Monteiro-Riviere *et al.*, 2005). When human dermal fibroblasts were exposed to purified (iron removed) SWCNT, there was considerable reduction in cell survival and cell adhesion, more so than when treated with other carbon nanomaterials, such as MWCNT, active carbon, carbon black (CB) or carbon graphite (all purified) (Tian *et al.*,

2006). This was accompanied with reduced expression of adhesion and cell-cycle-related proteins upon SWCNT exposure, in comparison to untreated cells, and an increase in cell death in response to a purified SWCNT sample that was not seen in the sample still containing its catalytic iron content (Tian *et al.*, 2006).

As previously mentioned, intravenous administration of CNT is likely to involve some form of functionalisation to enhance hydrophilicity. This will change their behaviour and interactions considerably, often reducing toxicity, as discussed in section 1.5.1. However, research into this exposure route has shown that relatively pure SWCNT can cause a reduction in the cell number of human peripheral blood lymphocytes, not through measurements of apoptosis or necrosis, but as a measure of reduced metabolic activity (Zeni *et al.*, 2008), while MWCNT have been shown to reduce the viability of human T-lymphocytes, significantly more so when samples are oxidised, compared to pristine samples. This decrease in viable cells was found to be dose- and time-dependent for both MWCNT samples and was through the initiation of apoptosis (Bottini *et al.*, 2006), and ending in programmed cell death. With functionalisation, the lack of response upon fMWCNT intravenous administration reported by Deng *et al.* (2007) and Singh *et al.* (2006) is likely related to the type of functionalisation. For example, ammonium functionalised SWCNT were found to elicit no activation or cytotoxicity of primary T-cells, B-cells or macrophages, while poly-ethylene-glycol (PEG) functionalised SWCNT, although not causing significant cytotoxicity or T-cell and B-cell activation, were readily taken up by primary immune cells and caused the activation of macrophages, which was not seen in response to PEG alone (Dumortier *et al.*, 2006). Although not widely researched, neuronal cells have been found to be sensitive to both short and long SWCNT, which dose-dependently decreased viability and increased oxidative stress in the PC12 cell line PC12 – incidentally this response was more pronounced in response to long SWCNT (Wang *et al.*, 2010a).

Co-exposure with other environmental factors

As HARN are a relatively new group of materials there is little available information addressing historical perspectives, or epidemiology with subsequent

etiological studies. However, some studies have already provided a correlation between CNT and associated respiratory problems (Murr *et al.*, 2005), and laboratory-based analysis has given insights into the effect of CNT exposure when it coincides with a predisposition to other respiratory issues or secondary exposures. Correlations between cases of asthma and exposure to sources of gas combustion have been found, with an increase in asthma deaths associated with an increase in the use of natural gas (Murr *et al.*, 2005). This is particularly relevant as CNT are present in our environment, both indoors and outdoors, through combustion of propane, methane and natural gases (Murr *et al.*, 2004a), and around gas cookers (Murr *et al.*, 2005). In a laboratory setting the risk of increasing the severity of fibrosis in asthma sufferers has been introduced by Ryman-Rasmussen *et al.* (2009b) using a mouse model. Individual responses to inhalation of MWCNT or ovalbumin were both found to induce an immune reaction, but together there was clear synergism resulting in pro-fibrotic conditions. MWCNT alone elicited PDGF and MCP-1 production, but not TGF-β1 or IL-13 (Ryman-Rasmussen *et al.*, 2009b); ovalbumin-exposed animals produced IL-13 and TGF-β1, but not PDGF or MCP-1; whereas the combination of MWCNT exposure and ovalbumin sensitisation resulted in the release of all these mediators, leading to considerable collagen deposition and expression of IL-5 (Ryman-Rasmussen *et al.*, 2009b). In a model to simulate elevated cholesterol levels (Apo-/- mice model) it was shown that in a comparison between carbon-based NM, QD, and AuNP, it was SWCNT and CB that consistently produced a greater inflammatory potential than the other particles (Jacobsen *et al.*, 2009). Another situation in which co-exposure was shown to enhance inflammatory and fibrogenic potential is with the environmentally available inflammatory agent lipopolysaccharide (LPS). In a rat study by Cesta *et al.* (2010) nasal aspiration of LPS produced no fibrosis, while intratracheal instillation of MWCNT stimulated significant levels of fibrogenesis; however, when LPS and MWCNT are combined the generation of fibrotic lesions was increased (Cesta *et al.*, 2010). This cumulative effect was also seen in respect to an increase in LDH and total protein levels, which only occurred with treatments of MWCNT plus LPS. The pronounced fibrotic effect was attributed to synergistic elevation of PDGF secretion with duel exposure and, to a lesser extent, the increased expression of PDGF-R on fibroblasts (Cesta *et al.*, 2010).

1.6 Project aims and objectives

Aims

The preceding literature review highlights a number of concerns with respect to the health consequences that could be associated with exposure to CNT. The research into CNT toxicity to date has at times clearly demonstrated the ability of CNT to follow, not only the intrinsic toxicity and pathogenicity of other NM, but also that of pathogenic fibres such as asbestos. The production and utilisation of CNT is already very high, and applications are certainly wide-spread, and are only set to rise, increasing the potential for exposure. It is therefore vital that as the production and utilisation of CNT increases, the investigation into CNT toxicity continues.

There is a clear need to fill the gaps and elucidate the contradictions found within the literature, particularly those relating to the effects of sample purity, such as metal contamination, and additional carbon forms found within CNT samples. There is also the need to establish the importance of CNT length, biopersistence and frustrated phagocytosis. All of these points need to be considered and clarified to aid the progression of safe CNT production and use.

To do this a number of techniques can be employed to evaluate the effects that CNT of different lengths and iron content have on a variety of cell types found within the pulmonary system, *in vivo* and *in vitro*; all in comparison to a number of reference materials, including NPCB and asbestos.

Research questions

The following research is designed to answer a number of specific questions:

1. Will a reduction of iron contaminants in a MWCNT sample reduce its toxic potential?
2. Is an increase in sample purity (reduction in amorphous carbons) likely to reduce MWCNT toxicity?
3. Do longer (>20µm) MWCNT cause an increased level of cytotoxicity compared to shorter (<20µm) MWCNT? Is this increase a result of frustrated phagocytosis?
4. Will a difference in MWCNT alignment (entangled or uniform) and shape affect cytotoxicity?
5. What are the cell signalling pathways initiated upon MWCNT exposure, and how will this signalling affect other cells and biological systems?
6. How does the toxicity of MWCNT compare to that of known toxic materials, such as NPCB and asbestos?

Hypotheses

Long MWCNT will be more potent than short MWNCT in terms of impacts on macrophages including cytotoxicity, ROS production/phagocytic burst, pro-inflammatory cytokine production and inhibition of phagocytosis. An increase in bioavailable iron will intensify these responses. An increase in sample purity will decrease the MWCNT induced impacts on macrophages

Chapter 2

General materials and method

2.1 Particle under investigation

2.1.1 Particle panel A

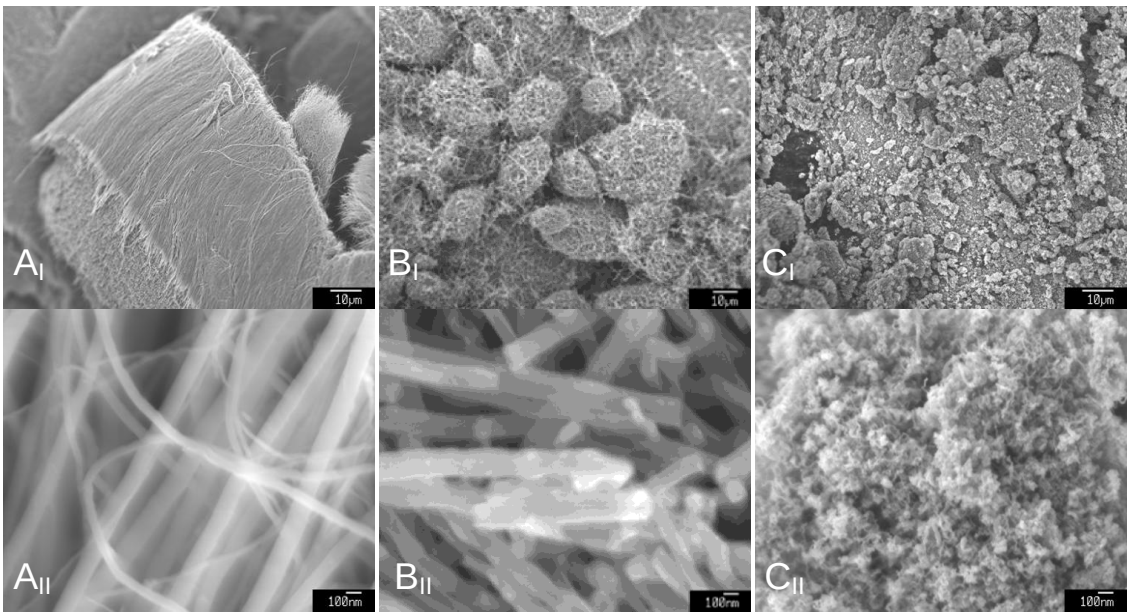

Figure 2.1 Scanning electron microscopy images of particle panel A. NT1 (University of Cambridge), NT2 (Applied Sciences Incorporated (ASI)), NT3 (Nottingham University) (A, B, and C respectively), displayed and characterised in Brown *et al.* (2007b).

The CNT used in figure 2.1 (NT1, NT2 and NT3) contribute to particle panel A, and were used in a study contained in chapter 4 only. This panel of CNT are described in Brown *et al.* (2007b); but briefly, NT1 are long (50µm, with a diameter of 20-100nm), straight, well aligned, contain 5.1 wt% iron, and have a surface area of 180 m^2/g. NT2 are also straight but less aligned, contain 1.3 wt% iron, with a diameter of 150nm and surface area of 25 m^2/g, and form >10 µm aggregates/agglomerates. NT3 are entangled, contain 2.7 wt% iron, have a diameter of 20nm, a surface area of 183 m^2/g, and also form >10 µm aggregates/agglomerates.

2.1.2 Particle panel B

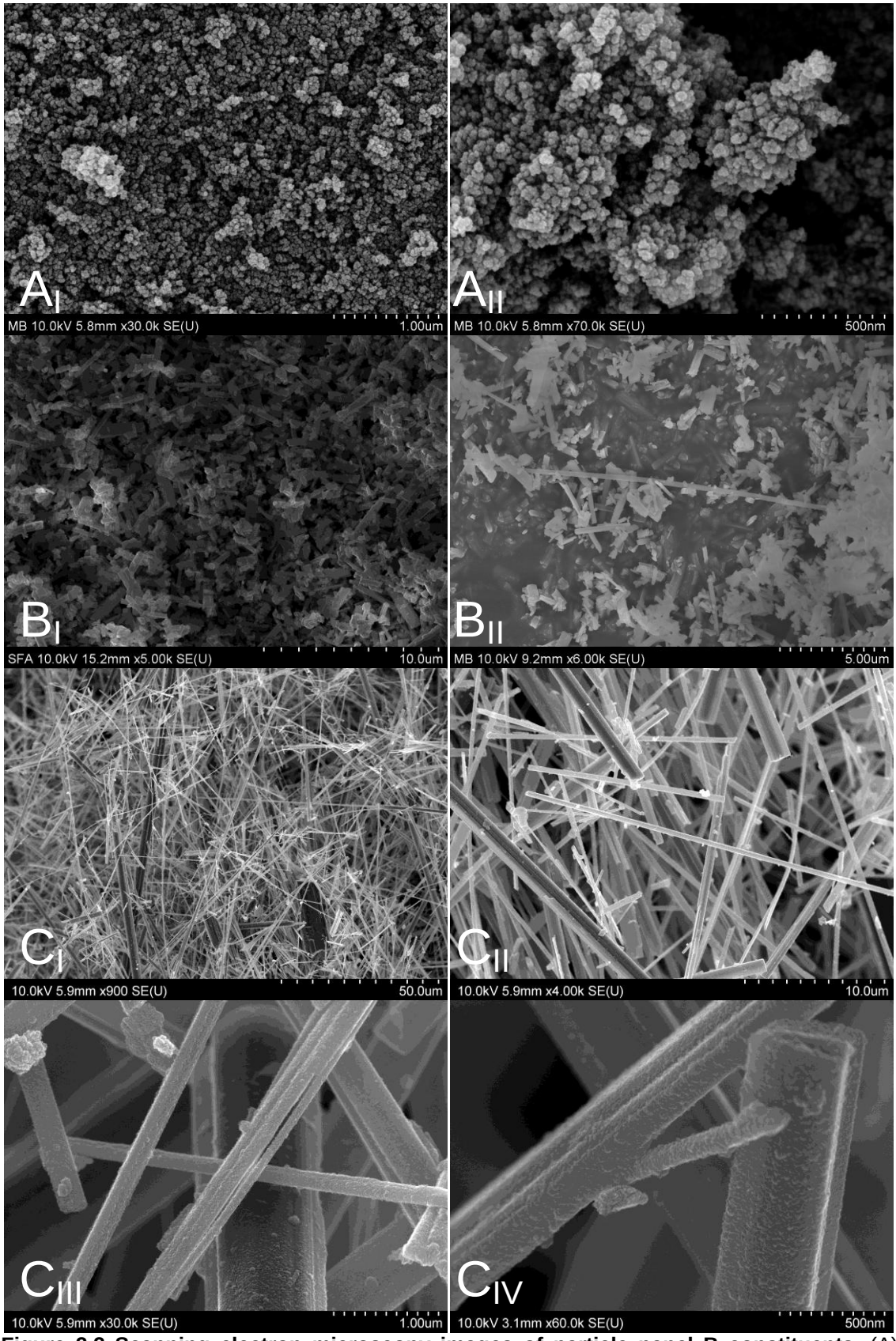

Figure 2.2 Scanning electron microscopy images of particle panel B constituents. (A) NPCB, (B) SFA and (C) LFA.

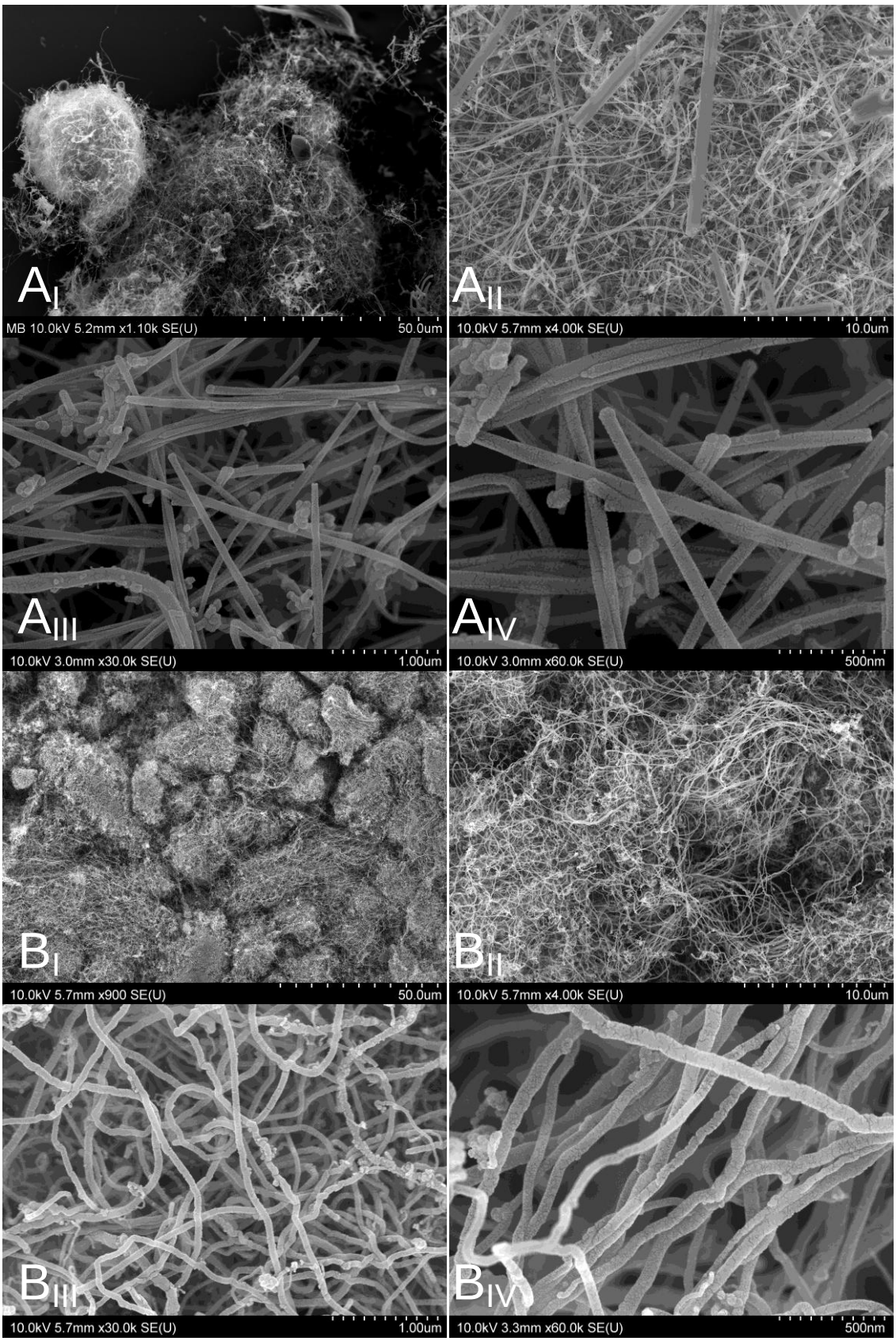

Figure 2.3 Scanning electron microscopy images of particle panel B constituents. (A) CNTI and (B) CNTA.

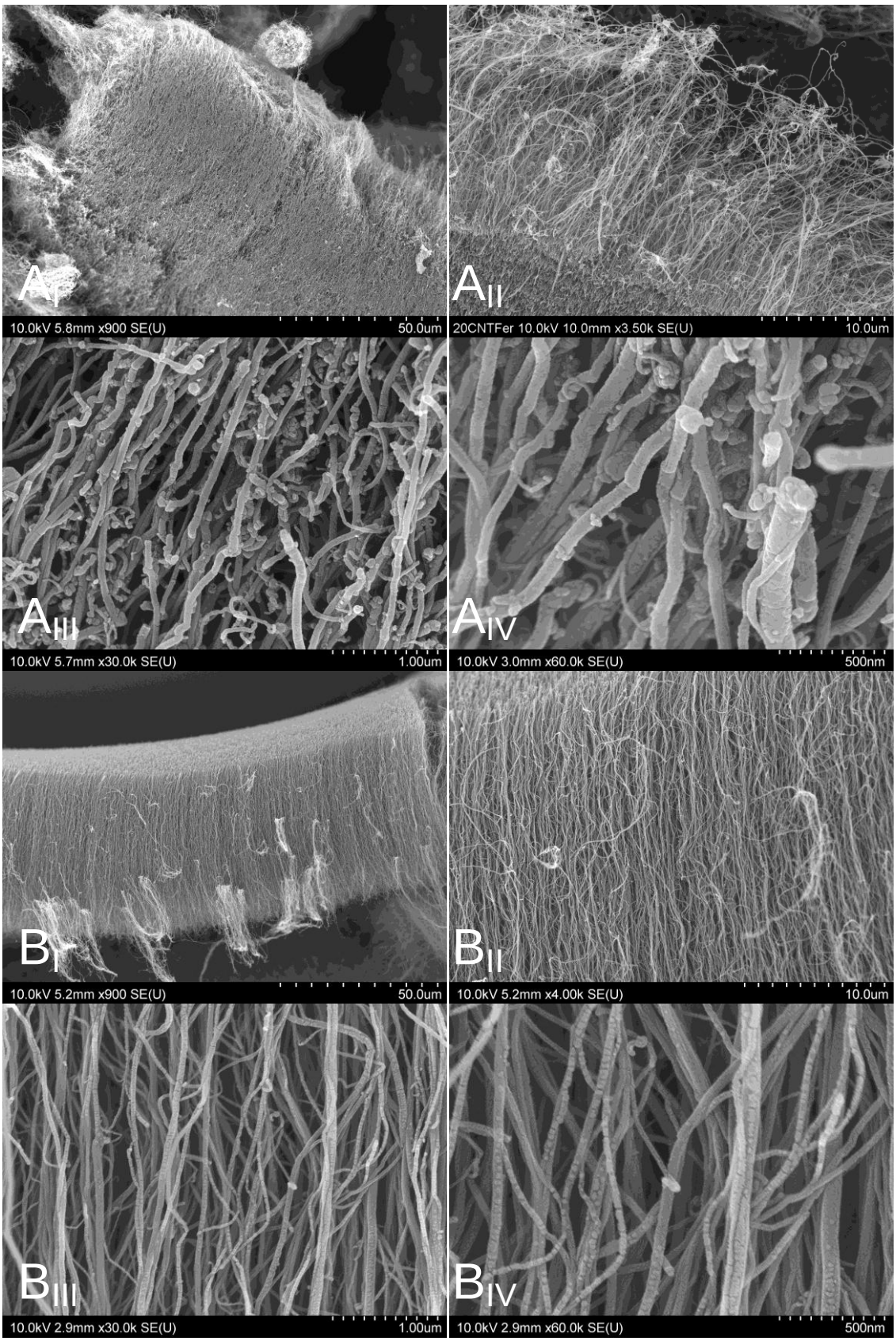

Figure 2.4 Scanning electron microscopy images of particle panel B constituents. (A) CNTB and (B) CNTC.

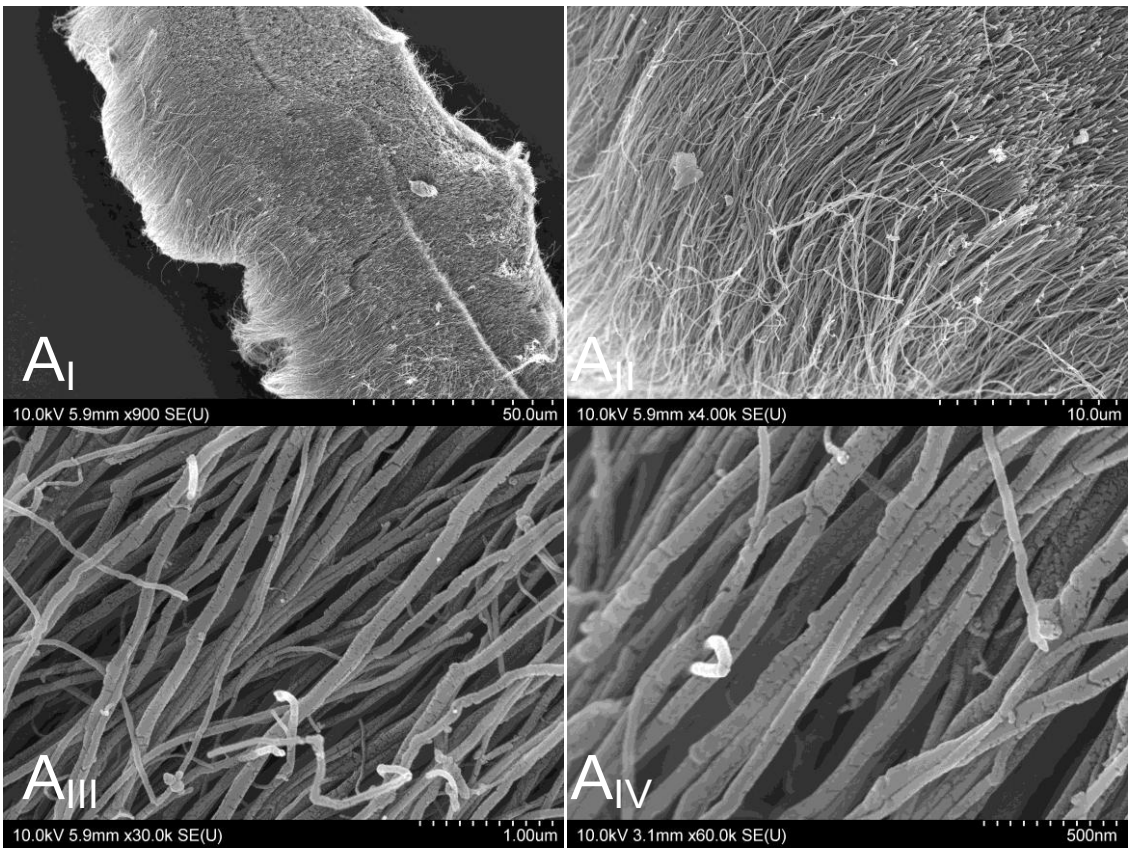

Figure 2.5 Scanning electron microscopy images of particle panel B constituents. (A) CNTD.

MWCNT	Fe content	Bioavailable Fe (μM)				Crystallinity	Length	Hydrophobicity
		Neutral pH		Acidic pH				
		Fe^{++}	Fe^{+++}	Fe^{++}	Fe^{+++}			
CNTI	++	++	+++++	+++	+++	+++++	Short	High
CNTA	+++++	+	+++	+++++	+++++	++	Short	Medium
CNTB	++++	+	+	+	+	+++	Short	High
CNTC	+++	+++++	++++	++++	++++	+	Long	Medium
CNTD	+	++	+++	++	++	++++	Long	High

Table 2.1 Characteristics of MWCNT in particle panel B. Allocated symbols to indicate low (+) to high (+++++) values for: dry iron content, bioavailable iron (in biologically relevant media), sample purity, CNT length, and a speculative assumption of hydrophobicity, based on crystalline structure and dispersion assay.

In figures 2.2–2.5 the material that contributes to particle panel B can be seen by scanning electron microscopy (SEM). This particle panel was used during the majority of this study. Much of the characterisation of the MWCNT shown in figures 2.3–2.5 is described in chapter 3. However, in table 2.1 the five MWCNT samples of particle panel B are briefly classified, allowing identification of CNT characteristics.

2.2 Tissue culture and particle treatment

2.2.1 Tissue culture

The human monocytic, monomac-6 (MM6), and mouse macrophage (J774A.1) cell lines were obtained from the European Collection of Cell Cultures (ECACC). Cell lines were maintained under sterile conditions in 75cm^2 (250ml) tissue culture flasks at 37°C and 5% CO_2. The adherent J774A.1 cells were sub-cultured using a scraping method under sterile conditions once a flask reached 95% confluency, using growth medium that consisted of RPMI 1640 general culture medium, supplemented with 2mM L-glutamine (Gibco Invitrogen), 100µg/ml streptomycin (Gibco Invitrogen), 100IU/ml penicillin (Gibco Invitrogen) and 10% foetal calf serum (FCS) (Gibco Invitrogen). The suspension MM6 cell line used the same medium, with higher percentage of FCS (20%) and additional supplementation of 0.1mM non-essential amino acid (MEM NEAA), 1mM sodium pyruvate solution, 1µg/ml holotransferrin, 1mM oxaloacetic acid and 10µg/ml bovine insulin.

Bronchoalveolar lavage (BAL) cells were obtained from 3-month-old Sprague-Dawley (SD) rats. The animals were euthanised using a 2ml single intraperitoneal injection of Euthatal (sodium pentobarbital). The lungs were isolated, cannulated, removed, and lavaged using 3 x 10ml sterile saline. Once pelleted and counted the BAL cells were suspended in assay relative medium.

Particle instillation and BAL for results in chapter 4 were performed by Dr D. Brown, Edinburgh Napier University. NT1, NT2 and NT3, were suspended in saline (0.9% NaCl) alone or saline with 0.1% BSA, and briefly sonicated. Adult male SD rats were exposed, via intratracheal injection, to 62.5µg/animal of each NT for 18 hours, after which animals were sacrificed and lavaged as above.

This variation in cell type was employed as each cell used has a phagocytic function, but are of a different lineage stage, and are from different biological locations. For example, MM6 cells are a good representation of mature peripheral blood monocytes (Ziegler-Heitbroc *et al.*, 1988), J774.A1 are a macrophage-like cell line that have been shown to behave in a similar fashion to peritoneal macrophages (Snyderman *et al.*, 1977), and the use of BAL cells allows the evaluation of phagocytes within lung alveoli. This may result in a slightly different response to particle exposures, and therefore the use of

multiple phagocytes gives a broader demonstration of biological responses to CNT.

2.2.2 Particle treatment

Due to the continued changing of treatment vessel throughout the *in vitro* components of this study it was necessary to standardise both cell density and particle concentrations that settle to the flat exposure area. By assessing other studies, such as the exposure of primary alveolar macrophages to long and short fibre amosite (Dogra and Donaldson, 1995), apparent sub-lethal concentrations of 3.75, 7.5, 15, 31, 62, and 125µg/ml (1.88, 3.75, 7.5, 15.5, 31µg/well of a 24-well plate) were chosen. Using exposure values expressed in this manner would lead to a disproportionate increase in exposure dose as volumes were increased when vessel size was increased; therefore particle treatments of 1.1, 2.1, 4.2, 8.5, and 17.5µg/cm^2 (calculated using the original planned 24-well-plate exposures) and cell densities of 1.7x10^5 cells/cm^2 were used allowing comparable exposures of cell treatments in 96 well plates (0.32cm^2), 24 well plates (1.8cm^2), and 6 well plates (8.6cm^2).

Cells were counted are viable cell populations established using a Neubauer haemocytometer, and 0.5% Trypan Blue (in PBS) exclusion. Specific cell densities were calculated and re-suspended dependent on assay.

Unless the assay required a specific optimal cell density the cells were seeded to a density of 1.7x10^5 cells/cm^2. J774A.1 cells were detached using a scraping method of removing adhered cells before they were counted and seeded. This was done one day prior to particle treatments, allowing for a 17-hour doubling time (ATCC recommended). On the day of exposure the supernatant was removed and cells washed once with PBS before the addition of relative treatment to culture wells. MM6 and BAL cells were counted and suspended in relevant treatment media on the day of exposure.

All particles were weighed and suspended in relevant media at 1mg/ml, briefly vortexed, followed by 10 minutes ultrasonication, in a bath sonicator. All samples were then progressively diluted to required exposure concentrations, with further ultrasonication of 5 minutes between dilution steps.

After treatment periods of 4, 24, and 48 hours (unless otherwise stated), to concentrations of 1.1, 2.1, 4.2, 8.5, or 17.5µg/cm^2 (unless otherwise stated), cells were used for relative endpoint assessment (cytotoxicity or PCR) and the supernatant collected, spun at 14,000g to pellet and dispose of any remaining particles, and then frozen at −80°C until required for cytokine or cytotoxicity assays.

2.3 Characterisation

2.3.1 Scanning electron microscopy - material preparation for SEM

Each sample was mounted on an aluminium SEM stub using adhesive carbon tabs, and sputter coated with gold or platinum for 3 minutes in a Emitech–K550X sputter coater using a coating current of 20mA, under an argon gas flow. The samples were then observed using a Jeol 6340 or Hitachi S-4800 field emission gun scanning electron microscope (FEG SEM).

2.3.2 Iron dissolution

The determination of iron dissolution from particle panel B in biologically relevant media (pH 4.5 and pH 7.4) was achieved using standards for Fe^{2+} and Fe^{3+}, and chelators for these two iron compounds. The protocol was adapted from Gilmour *et al.* (1995) and Graham *et al.* (1999).

Particles were weighed and suspended at 125µg/ml in 6ml citrate/phosphate buffer at pH 4.5 and pH 7.4. The buffer consisted of 42.4mM citric acid and 75.2mM disodium hydrogen phosphate (Na_2HPO_4), combined proportionately and then adjusted to relative pH with NaOH or citric acid. All particle suspensions were then ultrasonicated for 15 minutes and incubated on an orbital shaker at 37°C and 300rpm, for 48 and 96 hours.

On the day of iron measurements two sets of standards were made. For the determination of iron(II): ferrous sulphate (iron(II) sulfate heptahydrate, $FeSO_4 \cdot 7H_2O$), and for iron(III): ferric chloride (Iron(III) chloride hexahydrate, $FeCl_3 \cdot 6H_2O$). Chelators for these iron compounds were: for iron(II), 3-(2-Pyridyl)-5,6-diphenyl-1,2,4-triazine-4′,4″-disulfonic acid sodium salt (ferrozine), and for

iron(III): deferoxamine mesylate (desferrioxamine); both were made up in dH_2O to a concentration of 40mM.

For the standards, ferrous sulphate was dissolved in dH_2O at 10mM, with further dilutions in dH_2O to give a standard range of 0.25-16µM, with 2ml of each concentration; ferric chloride was dissolved in 1M HCl at 741mM, then diluted to 10mM in dH_2O, with further dilutions in dH_2O to give a 2ml standard range of 4-250µM. A blank of dH_2O was used for each iron compound standard.

Once the designated incubation period was complete, particles were removed from the orbital shaker, and after brief vortexing 1.5ml aliquots were taken from each particle suspension and centrifuged at 18620g for 10 minutes to pellet particles. Without disturbing the pellet 2x500µl of the supernatant (one for each iron chelator) from each particle were aliquoted into separate eppendorf tubes. Iron chelators were then added to the respective supernatant samples and standards; 12.5µl chelator was used for samples, and 50µl for standards, to give a final concentration of 1mM. All solutions were incubated for 5 minutes. After incubation all samples and standards were transferred, in duplicates of 200µl, to a 96 well plate and measured spectrophotometrically, at 562nm for Fe^{++}, and 430nm for Fe^{+++}; sample concentrations were calculated using standard curves.

2.3.3 Particle dispersion

Different culture media were assessed for their ability to disperse particle panel B. All particles, except CNTA and CNTB (due to limited sample available), were weighed and suspended at 1mg/ml in: RPMI 1640 (L-glutamine and pen/strep supplemented), RPMI 1640 plus 10% foetal calf serum (FCS), or RPMI 1640 plus 1% bovine serum albumin (BSA). Suspensions were ultrasonicated for 15 minutes, diluted to 125µg/ml in relevant media, sonicated again for 15 minutes, and vortexed. All vessels were then left undisturbed for 0-14 hours, with images taken at 0, 10 minutes, 30 minutes, and 14 hours.

Also included, and can be found in chapter 3, relevant to CNT production and characterisation, are:

- Chemical vapour deposition, for CNT production
- High temperature annealing
- CNT acid wash
- Thermal gravimetric analysis
- Raman spectroscopy (Raman analysis was performed by Dr Anna Moisala, University of Cambridge)

2.4 Oxidative stress

2.4.1 Cell-free assay

All CNT were initially suspended in RPMI 1640, RPMI 1640 with 10% FCS, or NaCl with 1% BSA (BDH Biochemical) and 0.025% dipalmitoylphosphatidylcholine (DPPC), to a final concentration of 60µg/ml, with two five-minute periods of sonication during dilution steps. CNT suspensions were then left for four hours at room temperature. During this time a number of solutions were made up: Hank's balanced salt solution (HBSS) with calcium and magnesium (Gibco), kept at 37°C; 0.1M PBS at pH 7.4; 4 IU/ml horseradish peroxidase (HRP) in sterile H_2O; a blank solution containing 20% 0.01N NaOH, 5% methanol and 75% 0.1M PBS; and 1mM 2',7'-dichlorofluoresin diacetate (DCFH-DA) in 500µl methanol which was kept on ice. Later, on ice, DCFH-DA was hydrolysed in 100µl 0.01M NaOH for 30 minutes (to form DCFH), then neutralised with 375µl PBS (at this stage the DCFH solution needs to be used rapidly). After the four-hour incubation time the reaction solution (1.4ml HBSS, either in the presence or absence of HRP and 400µl DCFH solution – final DCFH concentration once particle suspensions were added: 10µM) was added to a cuvette and then fluorescent readings were started. HRP was used in these assays as previous work into NP generated ROS production highlighted the requirement of this enzyme for detectable measurements (Foucaud *et al.*, 2007). Readings were taken continuously for 500 seconds with excitation and emission wavelengths of 485 and 530nm, respectively, and a slit width of 5nm. After the initial 100 seconds 200µl of the relative particle suspension was added with fluorescence read for the remaining 400 seconds. Each particle suspension

was measured in tandem, using the blank solution to replace the DCFH solution, also for 500 seconds – to enable the removal of any basal fluorescent levels upon data analysis. Additionally, medium-only controls were measured, again in the presence and absence of both HRP and DCFH.

To analyse the data the fluorescence trace at 120 seconds was subtracted from the trace at 500 seconds (for both DCFH and blank measurements); and the blank fluorescent reading was subtracted from the DCFH measurements.

2.4.2 ROS measurement in bronchoalveolar lavage cells

BAL cells were counted and adjusted to a final concentration of $0.125x10^6$cells/ml in 2ml of warm HBSS. There were two cell suspensions for each treatment, kept on ice until needed, alongside a 2mM DCFH-DA stock solution (in methanol) and methanol alone. Each 2ml cell suspension was given either 10µl of 2mM DCFH-DA (to give a final DCFH concentration of 10µM) or 10µl methanol; cell suspensions were then wrapped in foil and incubated for 10 minutes at 37°C. After incubation the samples were read by fluorimetry with a continuous trace for 2,000 seconds, excitation wavelength of 485nm, emission of 530nm, and slit width of 5nm. During replicates, the order that particle treatment cells were analysed was varied, to ensure the assay remains indiscriminate of cell storage time.

Similarly to the cell-free system, the suspensions containing methanol alone (without DCFH-DA) were used to remove the basal fluorescence of the samples, with the actual fluorescence intensity coming from the trace level at 5 seconds subtracted from fluorescence at 2,000 seconds.

2.4.3 RNA isolation

After exposure of MM6 cells to particle panel B, approximately $1.4x10^6$ cells were centrifuged, resuspended in 1ml Roche TriPure isolation reagent, sonicated to encourage cell lysis and stored at -80°C prior to RNA extraction.

RNA isolation was obtained following the manufacturer's guidelines, but briefly: chloroform was added (200µl/1ml TriPure) and the tubes briefly sonicated and incubated at room temperature for 5 minutes prior to centrifugation at 12,000xg for 15 minutes at 4°C. Following centrifugation, three phases were formed:

aqueous, interphase and organic. The aqueous phase was used for RNA isolation and therefore transferred to a new centrifuge tube for RNA precipitation. After the addition of 500µl isopropanol the tube was gently mixed and incubated at room temperature for 10 minutes before further centrifugation at 12,000xg for 10 minutes at 4°C, to pellet precipitated RNA. The pellet was then washed by removing the supernatant, replacing it with 1ml 75% ethanol and sonicating, prior to centrifugation at 7500xg for 5 minutes at 4°C, again to pellet the RNA. The supernatant was discarded and the tube allowed to air dry before resuspending the RNA in diethypyrocarbonate (DEPC)-treated RNase-free water. RNA was quantified using an optical density value of OD_{260} and further diluted in DEPC water to standardise RNA content for all samples.

2.4.4 cDNA synthesis

The synthesis of first strand cDNA for two-step real-time quantitative-PCR (qPCR) was carried out using the Roche Transcriptor High Fidelity cDNA Synthesis Kit. Manufacturer's guidelines were followed. Briefly, RNA was denatured and primed at 65°C for 10 minutes in a thermal block cycler, using a template-primer mix containing 2µg RNA, 60µM random hexamer primer and PCR-grade water to a total volume of 11.4µl. After this denaturation step reverse transcription (RT) was performed by adding (to a total volume of 20µl) a RT mix containing 8mM $MgCl_2$, 20 IU RNase inhibitor, 1mM of each deoxynucleotide (dATP, dCTP, dGTP, dTTP), 5mM DTT and 10 IU reverse transcriptase, prior to 30 minutes incubation at 45°C in the thermal block cycler. The reverse transcriptase was deactivated by heating to 85°C for 5 minutes, and the reaction stopped by placing the samples directly on ice prior to storage at -20°C.

2.4.5 Multiplex real-time qPCR

Real-time qPCR analysis of MM6 cells treated with particle panel B was performed with TaqMan® (Applied Biosystems) gene expression assays, using a TaqMan® duplex real-time PCR system, on an Applied Biosystems StepOnePlus™ Real-Time PCR System. Genes of interest were heme oxygenase 1 (HO-1), evaluated in the 4-hour exposure periods, and 8-

oxoguanine DNA glycosylase (OGG1), from 48-hour exposures. Analysis of the housekeeping genes used probes labelled with a VIC® dye, while all genes of interest used FAM™ labelled probes. The housekeeping gene chosen was human 18S ribosomal RNA (18S). It was presumed that 18S would be far more abundant than the genes of interest; therefore the amount of 18S specific primer was limited, allowing a sufficient amount of dNTPs for all reactions. Validation of primer-limiting had already been performed by Applied Biosystems and their gene expression kits use a primer concentration of 75nM; this is optimal as it reduces the fluorescent signal but does not change the C_t value when compared to higher primer concentrations. The volume of cDNA used was determined using observations of an increasing amplification step of the housekeeping gene (table 2.2), and 2µl was chosen. Validation of duplex assays was performed by comparing the amplification step of each gene individually and identifying if there was any interference when gene analysis was combined (table 2.2); in the case of the genes used in this study no interference was found. Additional controls included RNA- and DNA-negative control samples.

	C_t _ 18S	**C_t _ HO-1**	**C_t _ OGG1**
cDNA 0.5µl	20.4		
cDNA 1.0µl	17.8		
cDNA 2.0µl	15.5		
cDNA 4.0µl	14.3		
18S	15.9		
HO-1		32.5	
OGG1			32.8
18S + HO-1	15.9	32.9	
18S + OGG1	16.0		32.9

Table 2.2 Determination of cDNA volume for qRT-PCR, and validation of duplex materials.

The quantification of HO-1 and OGG1 was performed as per the manufacturer's guidelines. A PCR master mix was made consisting of (per sample number) 1µl 20x diluted TaqMan® Gene Expression Assay Mix (consisting of unlabelled forward and reverse primers, and fluorescently labelled probes) for both 18S and the gene of interest, 10µl 2x diluted TaqMan® Universal PCR Master Mix gene expression master mix and 6µl DEPC-treated H_2O. This PCR master mix was added in triplicate to a 96-well reaction plate. Prior to sealing, 2µl of respective cDNA was added in triplicate, to give a total volume of 20µl per sample replicate. The plate was briefly centrifuged and transferred to StepOnePlus™ Real-Time PCR System. PCR was performed using thermal cycling conditions of two holding stages of 2 minutes at 50°C and 10 minutes at 95°C, followed by 40 cycles of 15 seconds at 95°C and 1 minute at 60°C. StepOne software v2.2.2 was used for measurements and analysis, which included normalisation to the fluorescence of the reference ROX™ dye, and to the 18S endogenous control, and displayed as a fold change relative to medium-only treated cells.

2.5 Cytotoxicity and cell signalling

2.5.1 Enzyme-linked immunosorbent assay

An enzyme-linked immunosorbent assay (ELISA) (figure 2.6) was used to determine the concentration of TNF-α and TGF-β in supernatants collected post-exposure of particle panel B to MM6 (TNF-α) or J774A.1 (TGF-β). Kits were purchased from Invitrogen Biosource, and quantification of cytokines was made following the manufacturer's guidelines. Assay sensitivity was <15pg/ml for TGF-β, and <3pg/ml for TNF-α.

A coating (capture) antibody (Ab) was diluted in PBS and added to a 96-well plate at a volume of 100µl per well, plates were covered and sealed with a lid and parafilm and incubated overnight for 12–18 hours at 4°C. After incubation the plates were washed in wash buffer (saline (NaCl) with 1% Tween 20), which was removed by inversion of plates and tapping on absorbent paper. Blocking buffer (PBS with 0.5% BSA) was then added to each well, 300µl per well, for one hour, to block the rest of the available well space with non-specific protein. Assay buffer (PBS with 0.5% BSA and 0.1% Tween 20) was used for the

dilution of standards, samples and detection antibody. After removal of blocking buffer by the tapping method, 100µl of standards (prepared to manufacturer's guidelines, with concentration specific to kit) and samples were added to respective wells in duplicate. The samples for TNF-α were added directly from thawing; however, supernatant for TGF-β analysis underwent acidification to convert the latent TGF-β1 into its bioactive form; biologically this may be achieved by acidic conditions or more often through the application of enzymes. It is thought that acidic conditions within intracellular vesicles, such as in activated macrophages, can induce the activation of the latent TGF; but also that an acidic extracellular environment created by these activated cells during periods of chronic inflammation can activate secreted proteases, which will in turn cleave latent TGF into its active form (Alfranca *et al.*, 2008, Lawrence, 2001). Here it was achieved by addition of hydrochloric acid (HCl) to achieve sample pH 3; after 15 minutes neutralisation was achieved with NaOH (sample dilution here was taken into account when determining final values as the standards needed no such activation). Immediately after addition of samples and standards, 50µl of biotinylated detection antibody was added to all wells, and the plates were left with continual shaking at 300rpm for 2 hours at room temperature. After this time the plates were washed 5 times, again using a tapping method between washes, and 100µl streptavidin-HRP solution added to each well and plates incubated for 30 minutes, again at room temperature and continual shaking. All wells were then washed 5 times with wash buffer and 100µl per well tetramethyl benzidine (TMB) substrate added. Plates were then incubated for 30 minutes at room temperature with continual shaking, after which 100µl stop solution (sulphuric acid) was added and plates were analysed using a Dynex Biosciences MRX Revelation plate reader with absorbance wavelength of 450nm, and reference wavelength of 650nm. Cytokine concentrations were determined using a comparison to standards plotted on a log-log curve fit standard curve. An additional sample measured in TGF-β1 quantification was a sample of the original cell culture medium, as it may contain levels of TGF-β1, only in small amounts if the culture medium serum has been effectively inactivated, but possibly still present. The absorbance reading from this is used to remove any background values from all treatment values. For TNF-α, 1ng/ml lipopolysaccharide (LPS) was used as a positive control.

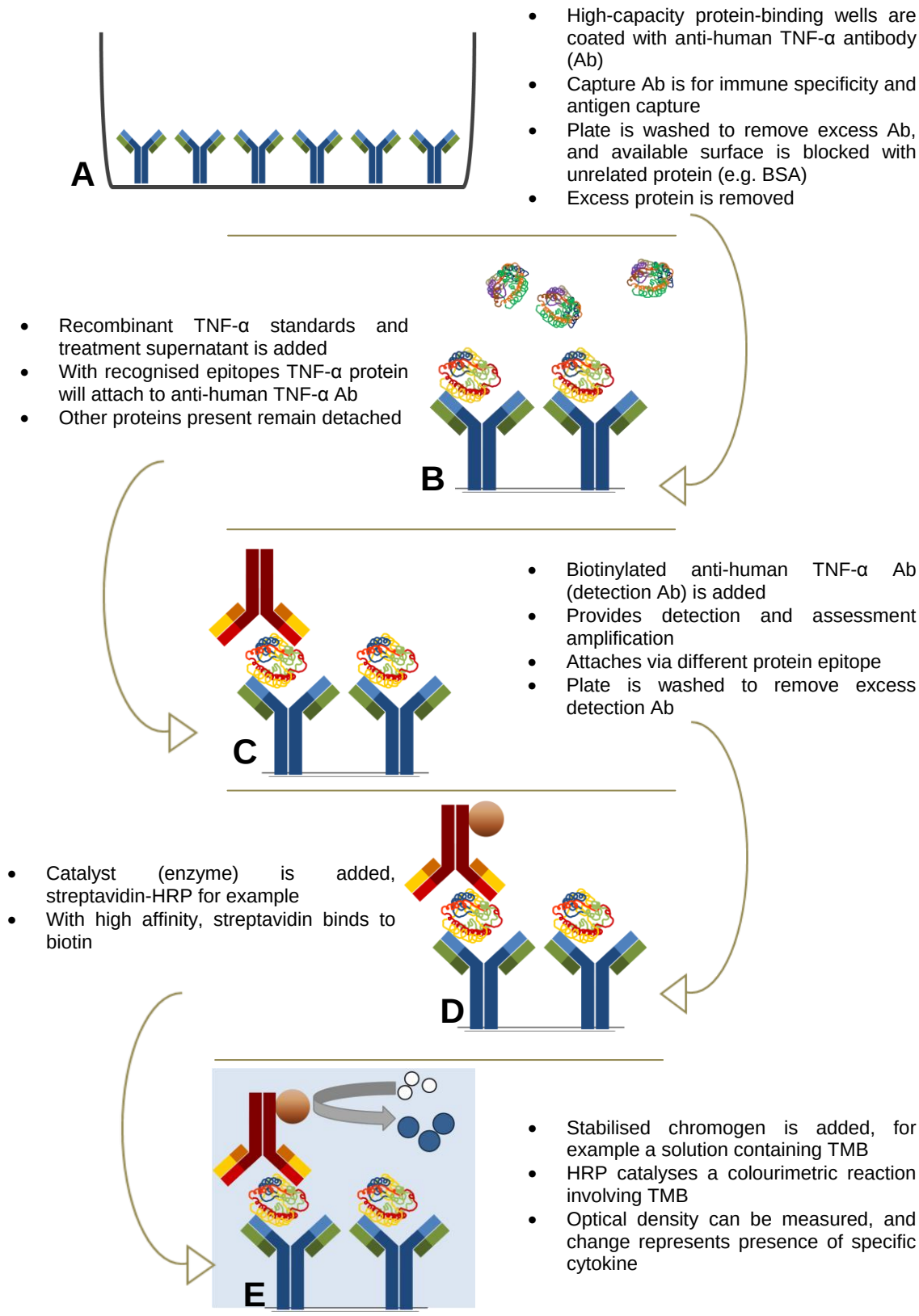

Figure 2.6 Schematic of basic sandwich enzyme-linked immunosorbent assay. An ELISA allows the determination and quantification of protein present in serum and supernatant. It involves the binding of protein to protein-specific capture antibodies, with additional enzyme bound protein antibodies used for detection.

2.5.2 Cytometric bead array

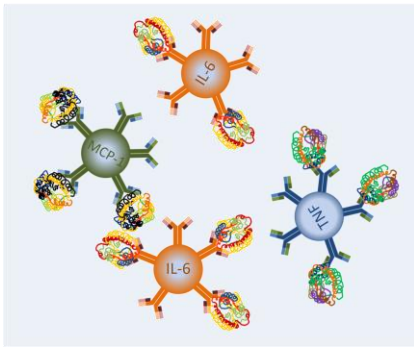

- Protein specific antibody-conjugated capture beads are incubated with exposure supernatant (SN)
- SN contains any number of signalling molecules
- Capture beads bind specific protein

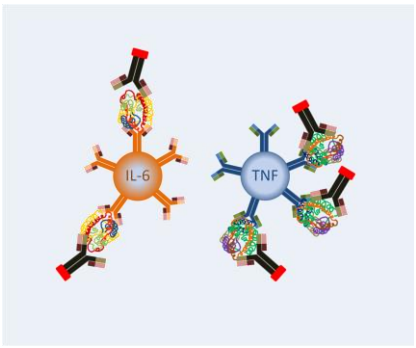

- Add phycoerythrin (PE)-conjugated antibodies (Ab)
- Ab bind specific protein
- Creates a sandwich complex (similar to sandwich ELISA)

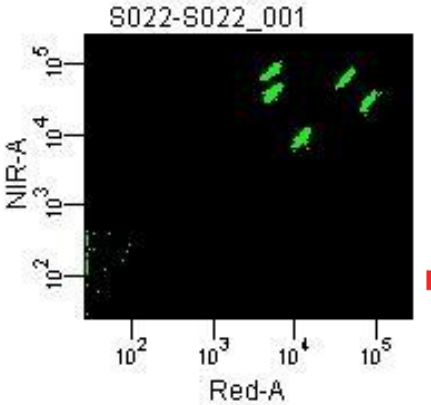

- Each bead's unique fluorescent intensity is located and distinguished (therefore cytokines are distinguished) using red (653–669nm) and near infra-red (750–810nm) laser

- Suspension is passed through optical cuvette in flow cytometer
- Individual bead complexes are located and gated using FSC and SSC of visible light

- The amount of bound protein (cytokine) is quantified by the fluorescent intensity emitted when the conjugated PE is excited by yellow laser (564–606nm)

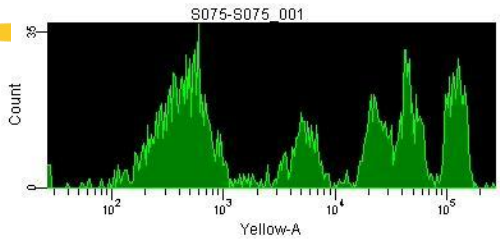

Figure 2.7 Schematic of cytometric bead array. CBA is a form of multiplex bead analysis that uses flow cytometry to detect, distinguish and quantify multiple proteins within serum or supernatant.

The cytometric bead array (CBA) (figure 2.7) uses a multiplex bead system that is principally the same as an ELISA: they both exploit the binding of antibodies to specific protein structures to acquire particular cytokines, with a further Ab used for detection. Detection in CBA, however, is via fluorescence of a phycoerythrin (PE)-conjugate, not an enzyme-induced absorbance change in the assay culture medium. In CBA up to 30 analytes can be examined in one sample at one time; and there is no need for plate coating in CBA.

After cellular exposure of particle panel B at designated time points and particle concentrations, release of GM-CSF, IL-1α, IL-1β, IL-6, MCP-1, TGF-β1, TNF-α, and VEGF from MM6, and IL-1β, IL-6, IL-10, MCP-1, TNF-α from J774A.1, were established using CBA and a BD FACSArray flow cytometer. A new assay template was created at monthly intervals based of new instrument calibration, with settings checked for continuity prior to each experiment using the experimental capture beads, and a 30 plex bead mixture. Buffer kits and flex sets were purchased from BD Biosciences; each CBA assay consisted of protein specific capture beads and detection beads, recombinant protein standards for all analytes, an assay buffer, wash buffer, and bead specific diluents for both capture and detection beads. For MM6 exposure all cytokines were examined simultaneously except for TGF-β1, which due to sample acidification had to be examined individually. In supernatant obtained from J774A.1 exposure all cytokines were examined simultaneously except MCP-1; the baseline release of MCP-1 here was particularly high at the later exposure times, therefore the sample had to be diluted. As it was likely that dilution would conceal the release of other cytokines it was necessary to examine MCP-1 alone with 1 in 10 dilution for 24- and 48-hour J774A.1 exposures.

On the day of analysis, samples were removed from the −80°C freezer and allowed to defrost. During this time recombinant protein standards were reconstituted in 4ml assay buffer, for 15 minutes. All lyophilised standard spheres were added to one falcon tube (except in the cases of the afore-mentioned TGF-β1 and MCP-1, which had to be treated individually, and will be the case in all future terming of “all”). After 15 minutes, serial dilutions were performed to obtain a working standard concentration range of 10–2500pg/ml, with assay buffer alone as 0pg/ml. During the standard reconstitution period both capture bead and detection reagent dilutions were performed. The volume

of each used was determined by the number of analytes under investigation and the number of samples to be analysed. For example, for 46 supernatant samples and 5 cytokines the total volume needed of capture or detection dilution (these were prepared separately as they were added separately, but volumes were the same) was 25µl per well (sample) – this is half the BD recommended volume but is quite sufficient for detection – so for 46 test samples and 10 standards 1500µl (60 x 25µl) was needed in total (this allows for a few extra tests). The volume of concentrated capture and detection solutions is 0.5µl/analyte/well, therefore for each of the 5 cytokines 30µl (60 x 0.5µl) of capture/detection solution was needed, therefore 150µl (5 x 30µl) in total, which was added to 1350µl (1500 – 150) of respective diluents, to give a total of 1500µl. The diluted detection reagent was protected from light and stored at 4°C until needed. The capture beads were used immediately; 25µl of each standard and test sample was added to separate wells of a round-bottomed 96-well plate, followed by 25µl of diluted capture bead to each well; this was left at room temperature protected from light, for 1 hour continually shaking at 150rpm. After this time 25µl of detection reagent was added to each well and again the plate was left at room temperature protected from light, with continual shaking (150rpm) for 1 hour for J774A.1 samples and 2 hours for MM6 samples (discernable by source species). After this time 150µl wash buffer was added to each well and the plate centrifuged at 717g for 5 minutes, to pellet assay complexes. The supernatant was removed with one firm invert instead of the tapping method used in ELISA techniques, and bead complexes re-suspended in 200µl wash buffer. Data was then obtained on each sample, one well at a time, using BD FACSArray software on a BD FACSArray, taking approximately 300 events for each analyte in a sample volume of 70µl; and analysed using “FCS Filter” and “FCAP Array” software programmes.

Data collected using both ELISA and CBA from the same experimental supernatant can be seen in figure 2.8; the values are not always identical, but they are comparable, therefore switching between these two detection methods adequately allows comparative analysis.

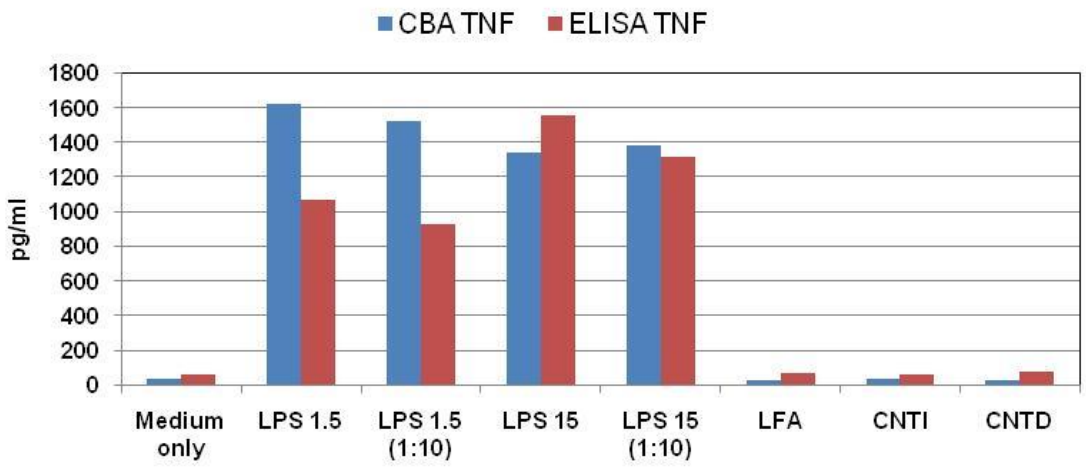

Figure 2.8 TNF-α release, measured by ELISA and CBA. MM6 cells were treated with medium only, 1.5 and 15µg/ml LPS, or 8.5µg/cm^2 LFA, CNTI and CNTD, for 4 hours. Data is expressed as TNF-α release in pg/ml (n=1).

2.5.3 Lactate dehydrogenase

Lactate dehydrogenase (LDH) release into culture medium is used as a measure of membrane permeability and therefore of cell death. This form of assessment is commonly used in cytotoxic assessments as it is an enzyme present in the cytosol of all eukaryotes (Raffray and Cohen, 1997). With a loss of membrane integrity there is a release of LDH into the surrounding medium, which when expressed in relation to either negative or positive control cells can be used as an indicator of particle induced cytotoxicity. Release of LDH from MM6 and J774A.1 into culture medium was determined after cellular exposure to particle panel B at designated time points and particle concentrations. Medium only and Triton X-100 treatments were used as negative and positive controls, respectively. Standardisation of the data collected was achieved by expressing all results in comparison to the 100% viable population, i.e. medium-only treated cells.

A range of standards were produced, to generate a standard curve of decreasing concentrations of pyruvate to signify increasing LDH activity, from 0–2000 IU/ml. In a 96-well plate 60µl of full standard range and 10µl of each sample were added in triplicate. To analyse actual LDH activity in treatment samples, 50µl of a 0.75mM sodium pyruvate solution (containing 1mg/ml NADH) was added to each sample well; the plates were then incubated for 30 minutes at 37°C. The LDH present in the sample supernatants will catalyse the formation of lactate from pyruvate, depleting the concentration of pyruvate. After

the 30-minute incubation period 50µl of 200µg/ml 2,4-dinitrophenylhydrazine was added to each well (standards and samples) and incubated at room temperature for 20 minutes. During this incubation the remaining pyruvate forms a complex with the 2,4-dinitrophenylhydrazine changing the optical density (at 540nm) proportionately to pyruvate concentration, which was seen as a strong brown colour with a high pyruvate level, and therefore low LDH content. After 20 minutes 50µl of 4M NaOH (stop solution) was added to all wells, and left at room temperature for 5 minutes, before being read at 540nm on a Dynex Biosciences MRX Revelation plate reader, using 160µl H_2O as a blank.

2.5.4 WST-1

A common measure of cellular metabolism which is representative of viable cell populations involves the reduction of tetrazolium salts, by cellular enzymes, to form formazans, where an increase in formazan formation is directly proportional to metabolically active cells. Most common of these colorimetric assays, established by Mosmann (2010), uses the reduction of 3-(4,5-Dimethyl-2-thiazolyl)-2,5-diphenyl-2H tetrazolium bromide (MTT). MTT reduction leads to formation of a particularly insoluble formazan (Mevorach *et al.*, 2010) which is extracted using 2-propanol prior to absorbance measurements (Worle-Knirsch *et al.*, 2006). The use of this assay in cytotoxicity assessment of CNT has demonstrated particle interference – where binding occurs between CNT and the insoluble formazan crystals – leading to an underestimation of population viability (Worle-Knirsch *et al.*, 2006). An alternative to the MTT assay, which utilises the same mitochondrial dehydrogenase enzymes (Ishiyama *et al.*, 1995, Worle-Knirsch *et al.*, 2006), is the reduction of 2-(4-iodophenyl)-3-(4-nitrophenyl)-5-(2,4-disulfophenyl)-2H tetrazolium monosodium salt (WST-1), to water soluble formazan. There are no intermediate insoluble products and this assay has not been shown to interfere with cytotoxic assessment of CNT (Ishiyama *et al.*, 1995, Worle-Knirsch *et al.*, 2006), therefore assessment of WST-1 reduction was chosen above that of MTT.

MM6 and J774A.1 cell cultures were assessed for formazan dye formation after exposure to particle panel B for designated time points and particle concentrations. Medium-only treatments were used as a negative control. After particle treatments, the supernatants and particles were removed, and cells

were incubated (in triplicate) in fresh culture medium containing 10% WST-1 reagent (purchased from Roche Applied Science) for a predetermined time period at 37°C, after which the absorbance was read at 450nm on a Dynex Biosciences MRX Revelation plate reader, using culture medium with 10% WST-1 as a blank, and using cells in culture medium alone as the 100% viable cell population.

Prior to full particle exposures, two quality control assays had to be performed. One was to ascertain the optimal incubation period of each cell line (at its designated cell density) with the 10% WST-1 reagent. Cells were incubated in WST-1 containing medium and the optical density read at regular intervals between 15 minutes and 4 hours, during which time there should be a relatively linear increase in absorbance as the time increases, until it begins to plateau. The time chosen for future incubation periods needs to be within this linear time period and before the plateau. A second quality control assay involves the assessment of any particle interference. Cells were incubated in the presence of medium-only, camptothecin (to induce apoptosis), particles, particles suspensions and no cells, and cells with particles and camptothecin. This would identify if any particles interfered with the optical density of the solution, or if they interfered with any components in the WST-1 reagent. No interference was found.

Also included, and can be found in:

- chapter 5 – viability assessment using annexin-V and propidium iodide staining.
- appendix I – response of cell signalling cascade on angiogenesis.

2.6 Particle uptake

2.6.1 Scanning electron microscopy - organic sample preparation

The preparation of J774A.1 cells prior to examination by SEM involved particle treatment, chemical fixation, sample dehydration, critical point drying (CPD), mounting and sputter coating. Until samples underwent CPD it was essential to keep them submerged within liquid throughout the procedure to avoid cell shrinkage, thereby causing shrinking artefacts, which would be visible as cracks on the cell surface.

J774A.1 cells were seeded at 1.7 x 10^4 cells/cm^2 into 24 well plates containing sterilised 10mm glass coverslips, using normal J774A.1 cell growth medium, and incubated for 24 hours at 37°C, 5% CO_2. After incubation the medium was removed and cells were washed once with sterile PBS. All of the particles in panel B were diluted as previously described (section 2.2.2), and then added at a concentration of 2.1µg/cm^2. The cells were then incubated for a further 4 hours at 37°C, 5% CO_2. After particle exposures the treatment media was removed and cells were washed once with 0.1M sodium cacodylate buffer, pH 7.3 (21.4g sodium cacodylate (MW 214.03) in 1L dH_2O), which was replaced with 500µl of fixing agent 2% glutaraldehyde (25% glutaraldehyde in H_2O, diluted to 2% in 0.1M sodium cacodylate buffer). Plates were transferred to 4°C for 2 hours. After this period the 2% glutaraldehyde was removed and wells were washed 3 times (10 minutes per wash cycle) using 0.1M sodium cacodylate buffer. After the final wash, 500µl 0.1M sodium cacodylate buffer was added to each well and plates were stored at 4°C until required.

Directly prior to CPD, the samples were dehydrated using organic solvents as follows. The glass coverslips to which the J774A.1 cells were attached were removed from the 24 well plates and rapidly transferred to a CPD cover slip housing boat and submerged in 10% acetone (diluted using dH_2O) for 5 minutes. The CPD boat (holding up to 6 coverslips at one time) was sequentially transferred to increasing concentrations of acetone (30, 50, 70, 90 and 100%), remaining submerged for 5 minutes in each. Care was taken not to air-dry the samples between baths, to avoid sample/cell shrinkage. The final method of drying/dehydration used for SEM preparation was critical point drying. This involves manufacturing a “critical point” when liquid is converted to gas without a liquid/gas interface developing. This is achieved by passing liquid

CO_2 through a “critical point” of temperature and pressure where liquid and gas have equal densities (Pathan *et al.*, 2010), resulting in samples devoid of surface tension effects, and therefore less likely to shrink, crack and disfigure. The chamber for CPD was attached to a mains water supply with hot and cold options on the same tap, and to a cylinder containing liquid CO_2. During the organic solvent dehydration procedure, the apparatus for CPD was cooled to <10°C by continually circulating cold water from the mains water supply throughout a CPD chamber feeding system. When the chamber temperature had sufficiently dropped, the boat containing cover slips and loaded with 100% acetone was transferred into the CPD chamber and the chamber was sealed. The liquid CO_2 cylinder was then opened, and the chamber was vented prior to rapid filling with liquid CO_2. At this stage the organic solvent that was still present in the transfer boat was removed from the chamber. To maintain the liquid level within the chamber there was continuous feed of liquid CO_2 from the cylinder while a drain valve was opened at the bottom. This allowed drainage of the solvent as, due to difference in substance density, the two liquids would separate and CO_2 was found to sit on top. Any gas generated was vented through a valve at the top of the system. The replacement of solvent with liquid CO_2 was seen to be complete when the visible interface between these two liquids had disappeared from the chamber viewing screen. With the liquid CO_2 level just above that of the transfer boat all valves were closed and the water supply changed from cold to hot. As the chamber temperature increased so did the pressure, until the CO_2 passes the “critical point” of 31.5°C and 1100psi. Once past this stage, and before reaching 36°C and 1200psi, the water was turned off. The chamber was then gradually (to avoid re-condensation of CO_2) vented and fully dehydrated samples removed.

Each coverslip was then mounted on an aluminium SEM stub using aqueous conductive silver, and sputter coated with platinum for 3 minutes in a Emitech–K550X sputter coater using a coating current of 20mA, under an argon gas flow. The samples were then observed using a Hitachi S-4800 field emission gun scanning electron microscope (FEG SEM).

2.6.2 Phagocytic burst

It is possible to measure the respiratory burst of particle-cell interactions using the chemiluminescence of lucigenin, which is a measure of superoxide production (Li *et al.*, 1999), or the chemiluminescence of luminol. Luminol is thought to be a direct measurement of peroxynitrite, hydrogen peroxide, hydroxyl radicals and superoxide (Rinaldi *et al.*, 2007), or of the myeloperoxidase-mediated formation of hypochlorous acid from hydrogen peroxide (Hasegawa *et al.*, 1997a). Alternatively, the change in light absorption from cytochrome C reduction can also be used to measure this oxidative burst (Johnston *et al.*, 1978).

Superoxide dismutase was used in the following experiments as a method of reducing the level of ROS available for interaction with the various assay components. Just prior to phagocytosis there is a consumption of oxygen and the release of superoxide anions, triggered by the NADPH oxidase complex; this is called a respiratory burst (Park, 2003). Superoxide dismutase, an enzyme present in both the cytoplasm and mitochondria of eukaryotic cells, is capable of causing a reaction of superoxide with itself, to form oxygen and hydrogen peroxide (Babior, 2000). This allows the use of this enzyme as a suitable negative control for both the lucigenin and cytochrome C assays; it may not, however, be quite so suitable for the luminol assay as luminol is thought to react with both superoxide and hydrogen peroxide.

2.6.2.1 Chemiluminescence

For chemiluminescence assays MM6 and J774A.1 cells were used at a density of $1.7x10^5$cells/cm^2. BAL cells were used at a density of $9x10^3$–$1.7x10^5$cells/cm^2 ($5.625x10^5$–$1x10^7$cells/ml). MM6 and BAL cells were counted, suspended in Hanks' balanced salt solution (HBSS) on the day of experiments, and kept on ice until needed. J774A.1 cells were seeded onto 96 well plates on the previous day to analysis.

Luminol and lucigenin

Luminol was only used briefly as lucigenin was found to be more suitable, but the assays for each were identical, allowing for substitution of luminol and lucigenin at 0.5mM.

All reagents were made up in advance and kept on ice. Luminol (MW 177.16) was dissolved in DMSO to a concentration of 50mM, and then further diluted in HBSS to 0.5mM. Lucigenin (MW 510.5) was dissolved in HBSS at a concentration of 0.5mM. A stock solution (1mg/ml, stored at −20°C) of phorbol 12-myristate 13-acetate (PMA) was thawed and diluted in HBSS to 0.4µg/ml (for a final concentration of 0.1µg/ml), PMA compound was used as a positive control. A stock solution of 6000 IU/ml (kept at −20°C, in H_2O) superoxide dismutase (SOD) was thawed and then diluted to 600 IU/ml in HBSS for a final concentration of 150 IU/ml. SOD was used as a negative control. All particles were suspended at 1mg/ml in HBSS, briefly vortexed and sonicated for 10 minutes. Then particle suspensions were diluted to 500µg/ml in HBSS (to give a final density of 8µg/cm^2), followed by another 10-minute ultra-sonication. In a 96 well plate a 50µl cell suspension was added (in the case of J774A.1 the cells were already present due to overnight culture, therefore culture medium was removed and replaced with 50µl HBSS), followed by 50µl of the respective stimulus, either SOD, PMA, medium alone, or particle treatments. This was followed by the addition of 100µl luminol or lucigenin. Once all components were added the plates were inserted into a BMG Labtech FLUOstar OPTIMA plate reader, and the light emitted recorded continuously over a period of 1–2 hours, with the instrument set to 37°C.

Luciferase

The luminescence assay for detection of ROS produced during respiratory burst requires the measurement to occur in the presence of particles. It was therefore necessary to perform an assay to investigate the occurrence of any luminescent quenching with different particle treatments. This was determined most suitable in the absence of cell interference, and an enzyme-induced luminescent assay was used. The firefly luciferase enzyme (Sigma L1792) was used to catalyse the oxidation of luciferin; the associated light emitted during this reaction was used to test for particle interference of luminescence. In a 96 well plate the

following components were added: 10µl 1ng/ml luciferase, 10µl particle suspensions; this gave a 0.4-1.6µg/cm^2 (125-500µg/ml) and 100µl reaction mixture (made up of luciferase substrate and assay buffer). The light emitted is considered stable for 1 minute, but the plate was added to a BMG Labtech FLUOstar OPTIMA plate reader and measurements taken immediately.

2.6.2.2 Cytochrome C reduction

An assay based on the reduction of cytochrome C (Johnston *et al.*, 1978) was used as a measure of superoxide anion (O_2^-) release during the phagocytic oxidative burst. By using superoxide dismutase to remove any response, the reduction of cytochrome C is shown to be specifically from the action of O_2^- (Babior *et al.*, 1973). A clear difference in light absorption between reduced and oxidised cytochrome C is seen at approximately 420, 520 and 550nm, and has approximately no change at 450nm (Babior *et al.*, 1973); this provides the opportunity to measure a progressive change in oxidative state of cytochrome C at 550nm from the generation of O_2^-.

Prior to BAL cell isolation all reagents were prepared and kept on ice. A "reaction mixture" was made up containing 50mg cytochrome C and 100mg dextrose (BDH, Glasgow) dissolved in 50ml PBS. A stock solution of 6000 IU/ml (kept at −20°C, in H_2O) SOD was diluted in the reaction mixture to a final concentration of 150 IU/ml. A stock solution (1mg/ml, stored at −20°C) of PMA was thawed and serial dilutions prepared in PBS to a concentration of 1.15µg/ml (assay final concentration is 0.1µg/ml). Once all reagents were ready BAL cells were isolated using the method previously described, suspended at 5x10^{6}cells/ml in sterile PBS, and also kept on ice.

In duplicate 24 well plates, 900µl reaction mixture was added to each well. An additional well was used for the ROS negative control of reaction mixture containing SOD. Added to each respective well were 100µl of 180µg/ml (final concentration: 10µg/cm^2) particle suspensions (nanoparticle CB, SFA, LFA, CNTI, CNTA, CNTB, CNTC and CNTD), or 100µl PBS for SOD and medium-only controls. This was followed by 50µl cell suspension. Plates were incubated for 4 hours at 37°C, 5% CO_2. After a 4-hour incubation period the plates were removed; in one 100µl PBS was added to each well, in the second 100µl PMA (1.15µg/ml) was added, to a final concentration of 0.1µg/ml. Both plates were

incubated for a further 1 hour, again at 37°C, 5% CO_2. After this period the plates were removed and centrifuged at 3000g for 5 minutes, to pellet cells and particles. In a 96 well plate 100µl of each treatment was transferred in triplicate and the plate read at 550nm and 450nm on a Dynex Biosciences MRX Revelation plate reader, using a blank of reaction mixture alone. The absorbance taken with a 450nm wavelength was subtracted from that of 550nm, and multiplied by 47.6, to allow the expression of data in nmoles.

To test for any particle interference, the procedure described above was used in full except the reaction mixture used contained SOD for every treatment. This should remove products of the oxidative burst and therefore prevent cytochrome c reduction in all cases; these data were directly compared to data obtained using the reaction mixture without SOD.

2.6.3 BAL cell staining

BAL cells were incubated in 96 well plates at a density of $8.8x10^4$cells/cm^2 with 10µg/cm^2 nanoparticle CB, SFA, LFA, CNTI, CNTA, CNTB, CNTC, CNTD, or medium alone, for 4 hours at 37°C, 5% CO_2. After particle exposure BAL cell cytocentrifuge smears were prepared using 100µl of each particle-exposed cell suspension. Glass slides, filters and funnels were placed in the appropriate cytospin slots, 100µl of cell suspensions were added to each respective funnel, and samples were centrifuged at 1500rpm for 2 minutes. The slides were then removed and left to air dry for 1 minute, then dipped (x10) in IMS to fix the cells, and stained with eosinophilic and basophilic dyes of the commercially available Romanowsky staining kit: Diffquik (Raymond A. Lamb, London, UK). Once dry, glass cover slips were mounted using DPX and slides were imaged by light microscopy.

2.6.4 Phagocytosis impairment

The impairment of phagocytic function of J774A.1 cells through exposure of particle panel B was measured using the manufacturer's guidelines of the Vybrant™ Phagocytosis Assay Kit (Molecular Probes). J774A.1 cells were seeded, using the method previously described, into 96 well plates at a density of $1.7x10^5$cells/cm^2. On the day of analysis the culture medium was removed

and cells washed once with PBS; following this either culture medium or particles (nanoparticle CB, SFA, LFA, CNTI, CNTA, CNTB, CNTC or CNTD) suspended in culture medium were added to each respective well, in triplicate, at a density of 10µg/cm^2. The medium-only treated cells were to be used as a positive control and represented 100% phagocytic ability. Additionally there were cell-free preparations that would be given medium plus all subsequent treatments (*E. coli* and trypan blue). These wells represent negative controls and were used to remove any background fluorescence. During the particle exposure time of 1 and 4 hours, the fluorescein-labelled *Escherichia coli* K-12 Bioparticles and trypan blue dilutions were prepared. One vial each of 5mg *E. coli* Bioparticles and 500µl 10x concentrated HBSS, were thawed, combined and briefly sonicated. This suspension was added to 4.5ml dH_2O and again sonicated until particles were homogenised. Trypan blue (1ml) at 1.25mg/ml was also thawed and diluted in 4ml dH_2O.

After respective treatment periods (1 or 4 hours), the exposure medium was removed and wells were washed once with PBS. To each well 100µl *E. coli* Bioparticle suspension was added and plates were again incubated at 37°C, 5% CO_2 for 2 hours, protected from light. After this incubation the *E. coli* suspension was removed, replaced with 100µl diluted trypan blue, to quench any fluorescent particles that have not been phagocytosed, and left for 1 minute. The trypan blue was then removed and wells washed with PBS directly prior to fluorescence intensity measurements using a BMG Labtech FLUOstar OPTIMA plate reader with excitation 480nm and emission of 520nm. The measure of phagocytosis was then expressed as % phagocytosis by subtracting the negative control reading from all sample readings, dividing the value for any experimental samples by that of the positive control, and multiplying by 100.

To test for fluorescence quenching through particle interference with the optical properties of this assay, fluorescein diacetate was used. Fluorescein diacetate was dissolved in DMSO to 10mM, aliquoted, and frozen at −20°C, until needed. J774A.1 cells were cultured and exposed to the full particle panel by the method described above. During the incubation period 40µl 10mM fluorescein diacetate was thawed and hydrolysed in 1.6ml 0.01M NaOH and 360µl methanol for 30 minutes, then neutralised with 6ml PBS. This solution was then diluted to a fluorescence intensity equivalent to that of the *E. coli* particles used in the

previous assay. After the particle exposure, the exposure medium was removed from all wells, replaced with the fluorescein dye, and read on a BMG Labtech FLUOstar OPTIMA plate reader with excitation 480nm and emission of 520nm.

2.7 Statistical analysis

Statistical significance was determined using the Minitab® 15.1.0.0. (Minitab Inc.) software. Data was accessed with a confidence interval of 95%, using a general linear module test for analysis of variance and post-hoc Tukey multiple comparisons. Observations were made of differences between particle treatments and control treatments, but also between particle treatments. The null hypothesis (the means of different treatment groups were equal) when the p-value < 0.05, with more specific p-values given throughout.

NB. Some methodology has not been included in this section, such as the annexin-V/PI lethality assay, the assays investigating angiogenesis, and much of the CNT production and characterisation. This is because these aspects needed substantial progression, optimisation and validation, therefore appear with the relevant results chapters.

Chapter 3

Production, purification, and characterisation of multi-walled carbon nanotubes

3.1 Introduction

3.1.1 Design outline

The factors that contribute to CNT pathogenicity have been previously discussed in section 1.5. Briefly, they include aspect ratio, biopersistence, aggregation, metal contaminants, crystallinity, and surface and/or structural defects. Samples with a lower relative purity (Pulskamp *et al.*, 2007b), a higher relative biologically available metal (particularly iron) content (Kagan *et al.*, 2006, Kim *et al.*, 2010a, Pulskamp *et al.*, 2007a), a high aspect ratio (Brown *et al.*, 2007b, Donaldson and Tran, 2004, Kim *et al.*, 2010a, Poland *et al.*, 2008), with length greater than 20µm (Dörger *et al.*, 2001), increased structural defects (Muller *et al.*, 2008b), and increased dispersal (Brown *et al.*, 2007b, Rothen-Rutishauser *et al.*, 2010) will all result in an increased toxicity. These may not be the only contributing factors, but all were used to design and manufacture the purpose-grown MWCNT used throughout this study.

CNT vary in length and width, depending on production method and reagents used; synthesis also results in the appearance of various sample impurities, such as catalytic metal particles, or unwanted carbon varieties, i.e. amorphous carbon and carbon particles. Due to the design and goals of this study it is important to obtain the values of these different factors, in order to ascertain which aspects of CNT morphology and composition are related to detrimental effects. This chapter will outline the methods used to produce a series of MWCNT with distinct characteristics, which will allow the examination of the aforementioned CNT properties and their effect on toxicity.

3.1.2 Carbon nanotube production

There are a number of methods commonly used to produce CNT such as catalytic growth through chemical vapour deposition (CVD) (Li *et al.*, 2004b, Motta *et al.*, 2005, Singh *et al.*, 2003b), arc-discharge (Iijima, 1991, Qiu *et al.*, 2010, Wang *et al.*, 2009), laser-ablation (Arepalli and Scott, 1999, Kusaba and Tsunawaki, 2006, Scott *et al.*, 2001, Thess *et al.*, 1996), and electrolysis with erosion of graphite cathode and anode (Kinloch *et al.*, 2003).

CVD is a particularly useful method for CNT synthesis; it can be used to produce both SWCNT and MWCNT by altering the size of catalytic metal NP

components (Li *et al.*, 2004a), both with very uniform growth alignment, nanotube characteristics such as length and diameter can be controlled, and under relatively low temperatures a high yield and sample purity is possible (Andrews *et al.*, 1999, Singh *et al.*, 2003b). These factors provide a method of CNT production that is extremely promising for industrial scale-up.

3.1.3 Chemical vapour deposition

Chemical vapour deposition (CVD) involves the addition of a metal catalyst, either on a furnace lining (a “fixed bed”) prior to carbon precursor administration at temperature (Moisala *et al.*, 2004), or, now more commonly, as a “floating catalyst”, where a feedstock containing both catalyst and carbon source are added to the furnace simultaneously, again at temperature (Li *et al.*, 2004a). When using the “floating catalyst” method CNT can be free-formed directly in the vapour phase reaction zone within a furnace (Li *et al.*, 2004b, Motta *et al.*, 2005, Singh *et al.*, 2002), or fixed on a substrate. In most cases a quartz (SiO_2) substrate is used (Singh *et al.*, 2003b), the use of other materials such as fumed silica has been attempted, but often results in unaligned, entangled CNT growth (Singh *et al.*, 2003a).

When using a substrate during CVD CNT production, the substrate is heated to a specific temperature within a furnace, at which point a feedstock containing hydrocarbons, such as benzene, xylene, toluene, ethylene, methane, or acetylene (Cassell *et al.*, 1999, Popov, 2004, Singh *et al.*, 2003b), and a dissolved metal catalyst, most often iron (Singh *et al.*, 2003b), but also nickel or cobalt (Popov, 2004), are injected through a pre-heater. For the production of SWCNT, but not MWCNT, it is essential to use transition metal catalysts (Popov, 2004). The ordered structure of CNT heavily relies on assembly around the metal catalyst, which is dependent on the carbon atoms attaching to, and diffusing through the metal at the correct temperature and concentration gradients. This means that the choice and combination of carbon precursor, metal catalyst, and furnace temperature and pressure are particularly important (Andrews *et al.*, 1999).

The metal catalyst source is shown to decompose within the feedstock (Singh *et al.*, 2003b), providing individual NP that, at relatively low temperatures attach to the substrate, and cause the chemical decomposition of hydrocarbons

(Moisala *et al.*, 2004), resulting in single carbon atoms. These atoms will then attach to the catalyst and then to each other to form tube-shaped continuous graphene sheets, CNT, with the length extending up from the substrate base, with continued growth from the root (Andrews *et al.*, 1999). Although good quality MWCNT can be grown at temperatures as low as 650°C (Andrews *et al.*, 1999), when using a feed stock of ferrocene in toluene the highest nanotube yield was found at 760°C. An increase in temperature (up to 940°C) or ferrocene concentration (up to 10 wt.%), was shown to cause an increase in tube diameter, and vary sample purity, with the highest quality produced at 800°C. Variations to ferrocene concentration was shown to affect tube alignment and diameter, and an increase in cycle time increased tube length (Singh *et al.*, 2003b). However, for good quality well-aligned CNT, a cycle time of 60 minutes was demonstrated as an approximate maximum, with outgrowths of carbon nanotubes, nanofibres and particles forming on top of already established CNT carpet growths at longer cycle times (Singh *et al.*, 2003b). All these provisions were taken into account with the design of CNT synthesis cycles.

3.1.4 CNT purification and characterisation

Impurities will always be present in conjunction with CVD, but they can be removed, or at least substantially depleted. The oxidation of metal catalysts has been shown with the use of strong acids, high temperatures, microwaves, filtration, or annealing (Chiang *et al.*, 2001, Cho *et al.*, 2009, Huang *et al.*, 2002, Vazquez *et al.*, 2002). Amorphous carbon can be reduced during tube formation with the presence of oxygen in the feedstock, where it has been used to form carbon monoxide when no catalyst particles are left to form new CNT (Li *et al.*, 2004b), or through the use of methane as a carbon source, shown to have a high thermal stability, which allowed an increase in furnace temperatures and therefore reduced formation of amorphous carbon (Cassell *et al.*, 1999). By adding hydrogen to the systems' gas flow (proportionally to argon) during a growth cycle, tube length has been controlled, and by reducing the catalyst source in the feedstock, it has been possible to reduce tube diameter (Singh *et al.*, 2003b). All of which allows the production of tailored CNT samples.

There are a number of techniques available for CNT characterisation. For measurements of tube lengths, widths, alignment, and number of CNT layers, SEM and TEM can be used (Arepalli *et al.*, 2004, Kinloch *et al.*, 2003, Kusaba and Tsunawaki, 2006, Qiu *et al.*, 2010). Surface area can be measured via the Brunauer Emmet Teller (BET) method of nitrogen absorption–desorption (Shvedova *et al.*, 2008b). The popular NP sizing technique of measuring dynamic light scattering (DLS) is designed to give a size depiction of spherical particles (Bootz *et al.*, 2004, Porter *et al.*, 2008), and not fibrous, so it is not often used for CNT size estimates. DLS has, however, been shown to allow identification of length to diameter ratios (Branca *et al.*, 2005).

The iron held within and around a CNT sample can be measured using thermal gravimetric analysis (TGA), SEM-energy dispersive spectroscopy (SEM-EDS) (Arepalli *et al.*, 2004, Cho *et al.*, 2009, Li *et al.*, 2004a), atomic absorption analysis (Vazquez *et al.*, 2002), nitric acid dissolution, or inductively coupled plasma-atomic emission spectrometry (ICP-AES) (Shvedova *et al.*, 2008b) to name but a few. Although noteworthy and certainly important, the iron production remnants may not be of as great significance in the interaction with biological systems, as its influence may rely upon it becoming bioavailable (Guo *et al.*, 2007a), and therefore it may be more prudent to measure the leaching of iron from these samples.

The quality of the carbon present, and the form that it takes, i.e. graphite, amorphous carbon, or carbon particles, can be measured by Raman spectroscopy (Arepalli *et al.*, 2004, Chou *et al.*, 2004, Koziol *et al.*, 2007, Kusaba and Tsunawaki, 2006, Qiu *et al.*, 2010). While using infrared spectroscopy, such as fourier transform infrared (FTIR), it is possible to assess structural defects of the nanotubes as well as impurities (Belin and Epron, 2005, Misra *et al.*, 2006, Stobinski *et al.*, 2010).

3.2 Production method and characterisation – of CNTA/B/C/D

3.2.1 Chemical vapour deposition & SEM

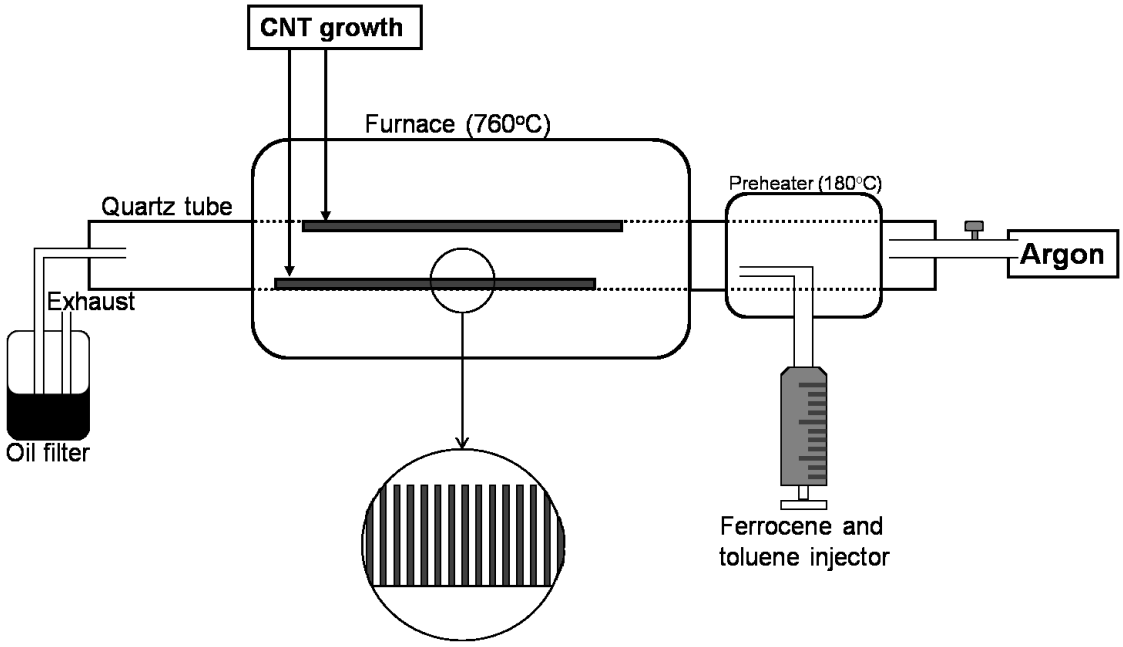

Figure 3.1 Schematic of the reactor used for CNT production. A mechanical syringe pump is used to inject the ferrocene–toluene solution into the preheated area. A flow-rate-controlled argon gas flow is used to move reactants through quartz tube housed within a furnace, where MWCNT carpet growth is achieved along most of the quartz substrate within the furnace boundaries. The gas flow is taken through an oil filter before reaching exhaust exit.

The method used here is a “floating catalyst” synthesis of MWCNT on substrate by chemical vapour deposition, where the feedstock (or reaction mixture) contained both catalyst and carbon precursor. The apparatus for MWCNT growth (figure 3.1) was a closed system allowing an argon gas flow at a controlled rate, and included a quartz (SiO_2) tube as substrate, and a reaction mixture of toluene and ferrocene providing the hydrocarbons and an iron catalyst. In this particular study the furnace housing the quartz substrate was heated and kept at 760°C for all CNT production cycles, and always under a sealed argon gas flow of 2.4 litres per minute, to prevent any loss of carbon, with a gas cylinder at the air flow initialising end and an oil filter at the gas flow exit end. The aforementioned constituents of the production process were kept constant for all growth cycles. However, to allow the growth of MWCNT of different lengths, the toluene/ferrocene solution ratio, injection time and injection rate were adjusted.

Initially a concentration of 5.6 weight% ferrocene in toluene was used. This was drawn into a syringe and injected, through a leak-proof septum and independent pre-heater (set at 180°C) at a rate of 5.6 ml/hour. After a specified growth time the hydrocarbon/catalyst injection was stopped and the furnace and pre-heater were turned off to allow cooling.

During cooling the argon flow was maintained and only removed when the temperature had substantially dropped. Once cooled, all connections were removed from the quartz tube and the “carpet” of MWCNT growth was manually scraped from all sides and deposited within a sealed glass jar. The quartz tube was then cleaned with ethanol and heated, with an atmospheric air flow, to 800°C for two hours, to remove residual carbon deposits, with subsequent ethanol cleaning to remove residual iron oxide; all in preparation for the next growth cycle.

3.2.1.1 Long MWCNT

After each growth cycle, CNT lengths were determined visually using a JEOL 6340 field emission gun scanning electron microscope (FEGSEM). The initial cycles allowed deposition times of between 10 and 60 minutes (figure 3.2), with a reaction mixture injection rate of 5.6ml/hour. The parameters used were adequate to provide well-aligned, uniform growth of the greater lengths (>20µm) needed for the long MWCNT sample.

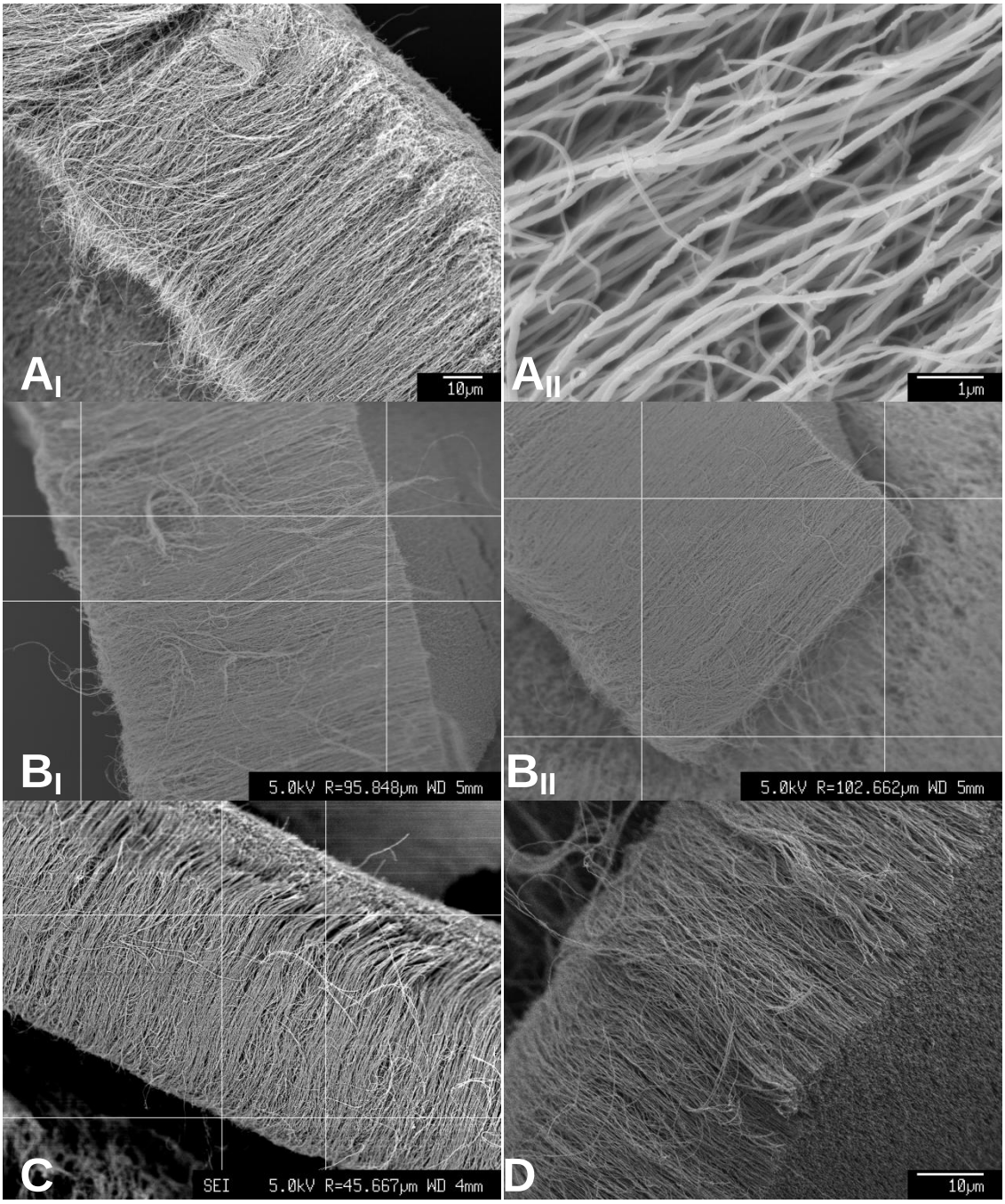

Figure 3.2 Scanning electron microscopy images of long CNT samples produced by CVD. Samples grown with 5.6 weight% ferrocene in toluene, with an injection rate of 5.6ml/hour for (A) 60 minutes, (B) 30 minutes, (C) 15 minutes, and (D) 10 minutes.

3.2.1.2 Short MWCNT

To obtain the shorter MWCNT (<20µm), a number of methods were attempted, including further reductions in cycle time, physical and mechanical breakdown of longer tubes, and a reduction in reaction mix injection time.

The growth cycles for the longer MWCNT provided a relatively high yield; therefore it was assumed that the best method to provide a similar quantity of the smaller length would be to physically break down the long MWCNT into smaller lengths. This was attempted using a ball mill (figure 3.3 A), acid washes with 4.7M hydrochloric acid (HCl), sonication in acetate, and sonication in 4.7M HCl (figure 3.3 B). All of these methods resulted in almost insignificant, and certainly not consistent, CNT breakages. These were not adequate for the parameters needed and therefore it was necessary to use control during the growth process to obtain the shorter lengths needed.

Using shorter injection times of the 5.6 weight% ferrocene in toluene still at 5.6ml/hour injection, 4–5 minutes did produce shorter MWCNT (figure 3.4), but not consistently. Often tubes would range well above the needed cut-off point of 20µm. It was therefore necessary to modify the injection rate of the reaction mixture (keeping a 5.6 weight%), a rate of 4ml/hour was then used. With this new rate of injection, growth periods of 4–20 minutes were used (figure 3.5) with 10 minutes giving the optimal yield of MWCNT <20µm in length. The parameters used in these final growth cycles did not allow clear uniform carpet growth of the shorter CNT (figure 3.5 B), therefore samples were dispersed with a short period (to avoid CNT disruption) of sonication in acetate, which then were filtered onto a TEM grid for SEM analysis to determine CNT length (figure 3.6).

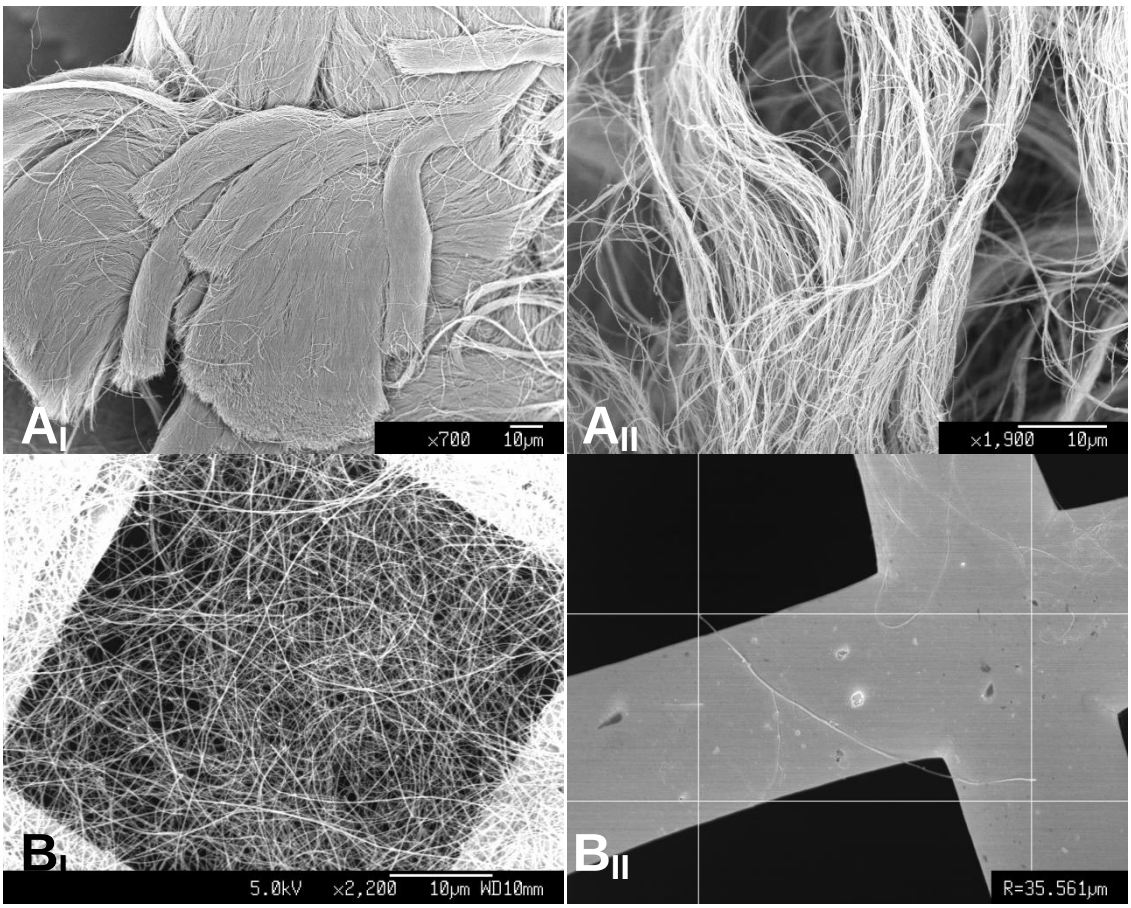

Figure 3.3 Scanning electron microscopy images of CNT break down attempts. Samples grown with 5.6 weight% ferrocene in toluene, with an injection rate of 5.6ml/hour for 60 minutes, with subsequent (A) ball milling, or (B) acid ultrasonication.

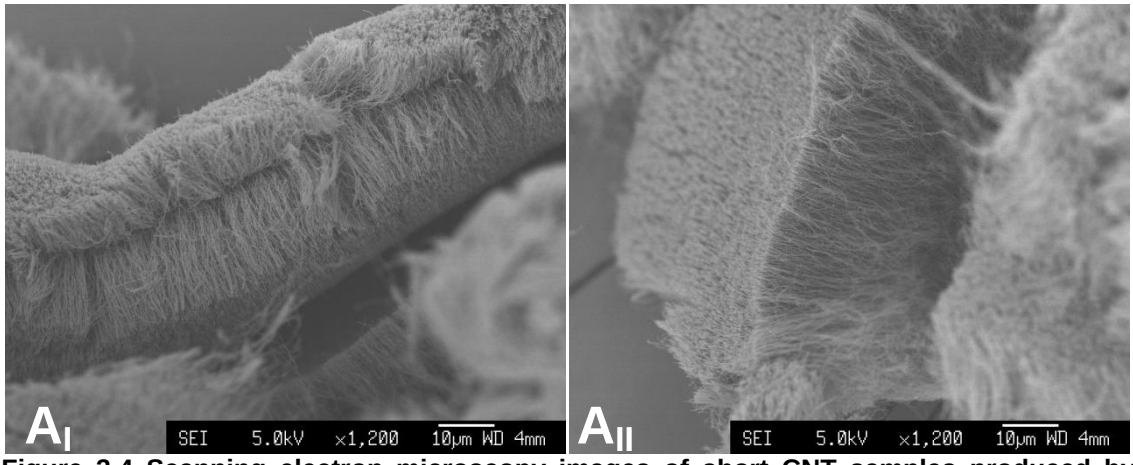

Figure 3.4 Scanning electron microscopy images of short CNT samples produced by reducing cycle time. Samples grown for 5 minutes with 5.6 weight% ferrocene in toluene, and an injection rate of 5.6ml/hour.

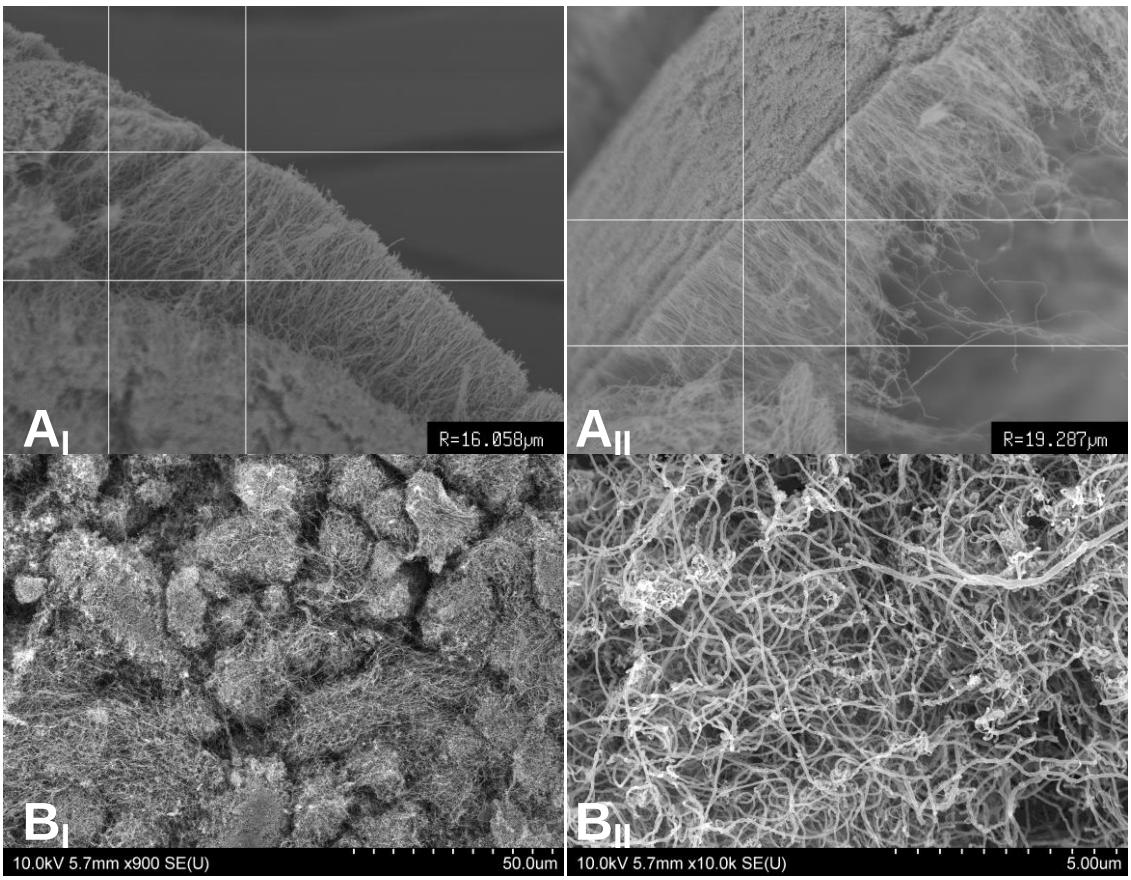

Figure 3.5 Scanning electron microscopy images of short CNT samples produced by reducing injection rate. Samples were grown with 5.6 weight% ferrocene in toluene, an injection rate of 4.0ml/hour for (A) 20 minutes, and (B) 10 minutes.

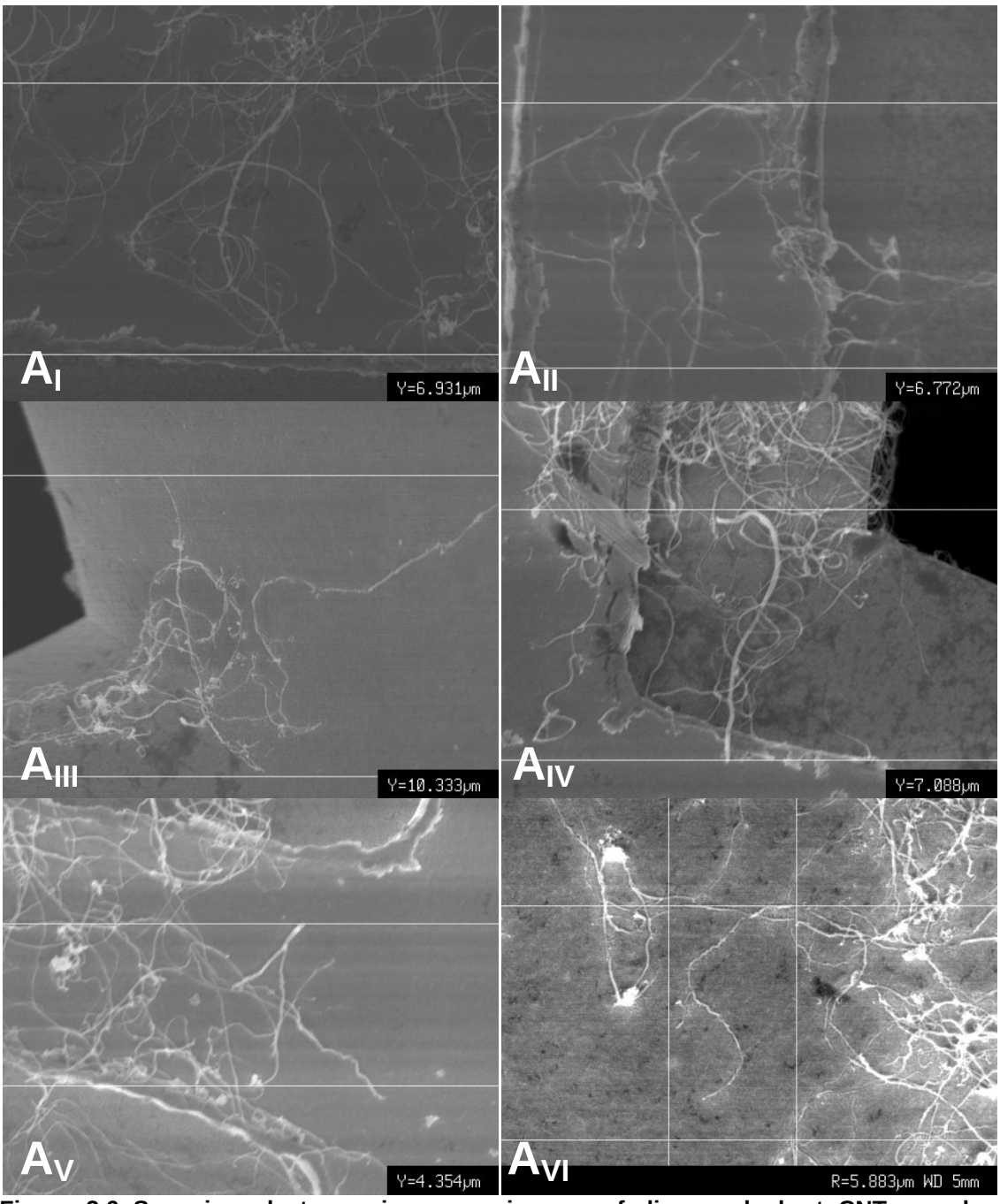

Figure 3.6 Scanning electron microscopy images of dispersed short CNT samples. Samples were grown with 5.6 weight% ferrocene in toluene, an injection rate of 4.0ml/hour for 10 minutes. Samples were sonicated in acetate for dispersal and mounted on TEM grids prior to SEM imaging.

3.2.2 Iron removal – high temperature annealing and acid wash

The iron catalyst within the reaction mixture can be left in quite considerable amounts, housed either within MWCNT layers or between the MWCNT themselves (Andrews *et al.*, 1999). To remove or at least deplete this production remnant, a number of techniques can be used. Two methods that were employed here were high temperature annealing and acid wash. An Astro

furnace was used to heat the long pristine MWCNT samples to a temperature of 2000°C for 6 hours, again with an argon gas flow to prevent loss of crystalline carbon. Alternatively, long pristine MWCNT were given a relatively gentle acid treatment of a 2 hour acid wash in 1M or 4.7M HCl, these conditions had previously been shown to not substantially reduce tube length.

The results of each can be seen in figure 3.7. It was shown that in the case of the long MWCNT sample, pristine MWCNT contained 7.4% iron oxide; the acid treatment only reduced this to 6.6% with 1M HCl treatment and 6.1% with 4.7M HCl. High temperature annealing reduced the iron content to 0.4%. Therefore, high temperature annealing was used for iron depletion in both the long and short MWCNT samples.

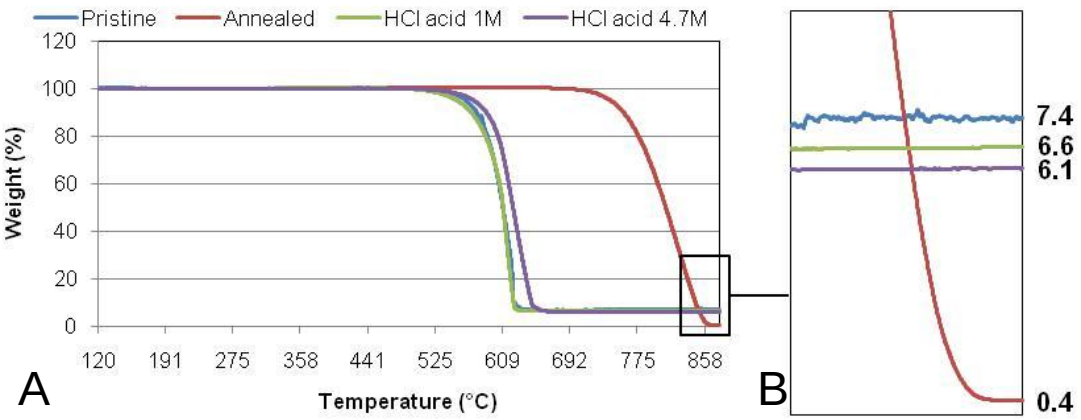

Figure 3.7 Iron determination by TGA analysis of pristine, annealed, and acid-treated CNT. The data is expressed as weight loss, by percentage, as MWCNT samples (pristine, annealed, 1M HCl wash, and 4.7M HCl wash) are heated to 900°C. (A) shows full TGA ramping period, while (B) is an enlargement of the final values, to clarify the final iron content (weight%).

3.2.3 Thermal gravimetric analysis

A Perkin-Elmer Thermal Analysis Series 7 System was used for thermal gravimetric analysis (TGA) to determine the iron content of the long and short, pristine and annealed MWCNT samples. Small volumes of CNT were held on a scale within a chamber with an atmospheric air flow. The sample was left to equilibrate at 120°C for 60 minutes, at which point it was ramped up to 900°C, as both CNT and amorphous carbon would be destroyed at this temperature (Misra *et al.*, 2006), at a rate of 10°C per minute and held for 10 minutes before cooling.

The high temperature annealing of MWCNT samples resulted in substantial loss of iron from both MWCNT samples, and can be seen from the TGA results displayed in figure 3.8 as weight percentage (3.8 A. short CNT, and 3.8 B. long CNT), and as a weight in mg (3.8 C. short CNT, and 3.8 D. long CNT). The iron present here was in the form of iron oxide therefore the use of percentage values can be used to compare samples. However, under the assumption that the iron contained within these samples is in the form of Fe_2O_3 the actual iron content was calculated.

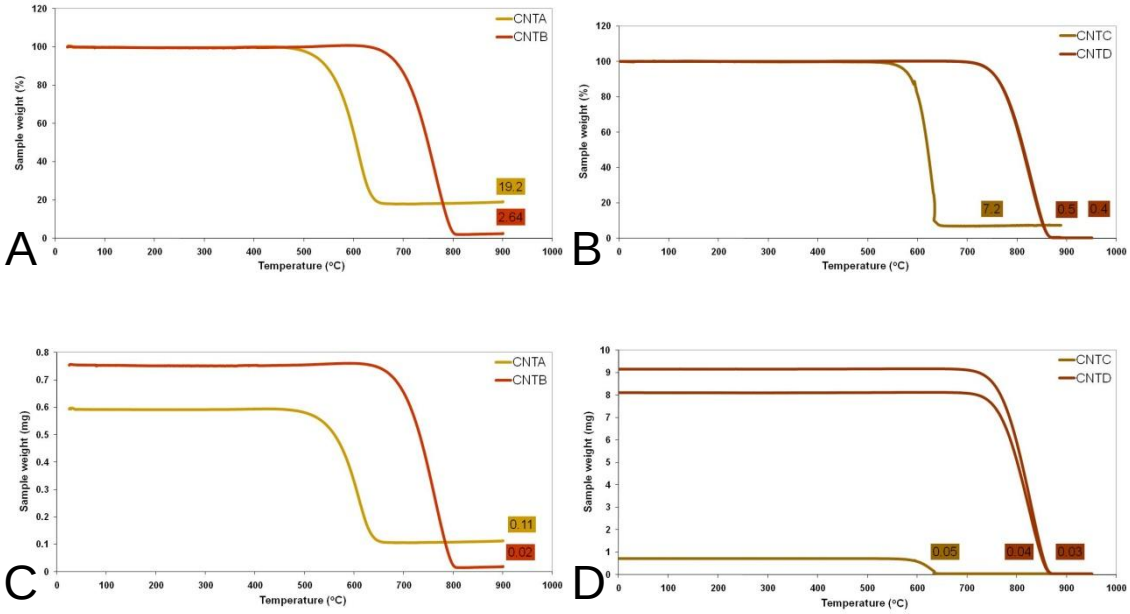

Figure 3.8 Iron determination by TGA analysis of pristine and annealed, short and long MWCNT. The data is expressed as weight loss, by percentage, of (A) short and (B) long CNT, and as weight, in mg, of (C) short and (D) long CNT; as samples are heated to 900°C under atmospheric conditions.

The molecular weight of iron is 55.847g/mol, and oxygen is 15.999g/mol, therefore Fe_2O_3 = 159.691g/mol. Consequently, the actual quantity of iron in each sample was calculated as follows:

$$n(Fe_2O_3) = m(residue) / M(Fe_2O_3)$$

$$n(Fe) = 2.n(Fe_2O_3)$$

$$m(Fe) = n(Fe).M(Fe)$$

where “m” is sample mass post TGA, “n” in number of mols, and “M” is molecular weight. Alternatively, the proportion of iron in each sample can be calculated using the assumption that 70% of the Fe_2O_3 left post TGA is Fe, as this is the proportion of iron in Fe_2O_3 by MW.

Using this calculation for Fe quantification, the iron present in each MWCNT sample can be viewed in table 1. The iron content of short pristine CNTA was by far the highest, and depleted from 133.9 mg/g in CNTA, to 50.3 mg/g in CNTB. The long pristine CNTC had a lower iron content than both of these short samples with 18.5 mg/g, but was also depleted by the annealing process, in this case to 3.0 mg/g (CNTD). Analysis of the other CNT sample used throughout this study, an industrially produced sample (CNTI), is shown in table 3.3. This was performed externally courtesy of Craig Poland of University of Edinburgh, who gave a value of 3.4 mg/g dry CNT using inductively coupled plasma by optical emission spectroscopy (ICP-OES), and Fiona Smail of the University of Cambridge who provided a slightly higher value of 8.5 mg/g dry CNT sample using TGA, these values indicate a Fe content of CNTI is between that of CNTC and CNTD.

MWCNT	CNTA	CNTB	CNTC	CNTD
Fe (mg/g sample)	133.9	50.3	18.5	3.0

Table 3.1 Representative Fe content of purpose-grown/treated MWCNT.

3.2.4 *Raman spectroscopy*

Raman spectrometry, using a Renishaw 1000 micro-Raman spectrometer, was employed to evaluate the relative purity of the MWCNT samples, by assessing carbon crystalline structure, and the presence of impurities such as amorphous carbon and carbon particles. Samples were placed on a quartz slide and, using 10% intensity of a red laser with 633nm excitation, data was collected for 60 seconds at three different locations for CNTA, CNTB, CNTC, and CNTD.

The individual Raman spectra of each CNT sample can be seen in figure 3.9; all CNT were shown to have clear D-band (1350cm^{-1}) (disorder) and G-band (1580cm^{-1}) peaks. D-band and G-band intensities for each sample were as follows: CNTA, 1181 and 2528 respectively; CNTB, 1646 and 3418; CNTC, 1342 and 2218; and CNTD, 1153 and 3006. The second disorder peak, D'-band (at 1620cm^{-1}), appeared only as a shoulder on the G-band of the pre-annealed CNTA and CNTC, while it was more pronounced and clearly a peak after the

annealing process; for CNTB the D'-band intensity was 1184 (figure 3.9B) and for CNTD was 896 (figure 3.9D).

An overlay of all relevant CNT peaks (figure 3.10. A) highlights the differences between these samples, while figure 3.10 B particularly highlights the difference in D'-band caused by the annealing process.

The ratios between sample defects (D- and D' – peaks) and pure graphite (G-peaks) of a Raman spectrum can be used to determine relative sample purity and disorder within CNT (Li *et al.*, 2004a, Ouyang *et al.*, 2008, Singh *et al.*, 2003b, Steplewska and Borowiak-Palen, 2009), where a higher G/D (or G/D') ratio is indicative of fewer sample defects, and a higher crystallinity (Singh *et al.*, 2003a). The ratios of all the CNT samples produced here are shown in table 3.2. The quality of the long CNT was greatly changed upon high temperature annealing, the pristine CNTC had the lowest graphite to defects ratio of all four samples, while the annealed CNTD had the highest of all four, with increases of 0.9 in the G/D ratio and 1.3 for G/D' ratio. The short CNT were relatively unchanged, the same value for G/D ratio, and only an increase of 0.5 in the G/D' ratio.

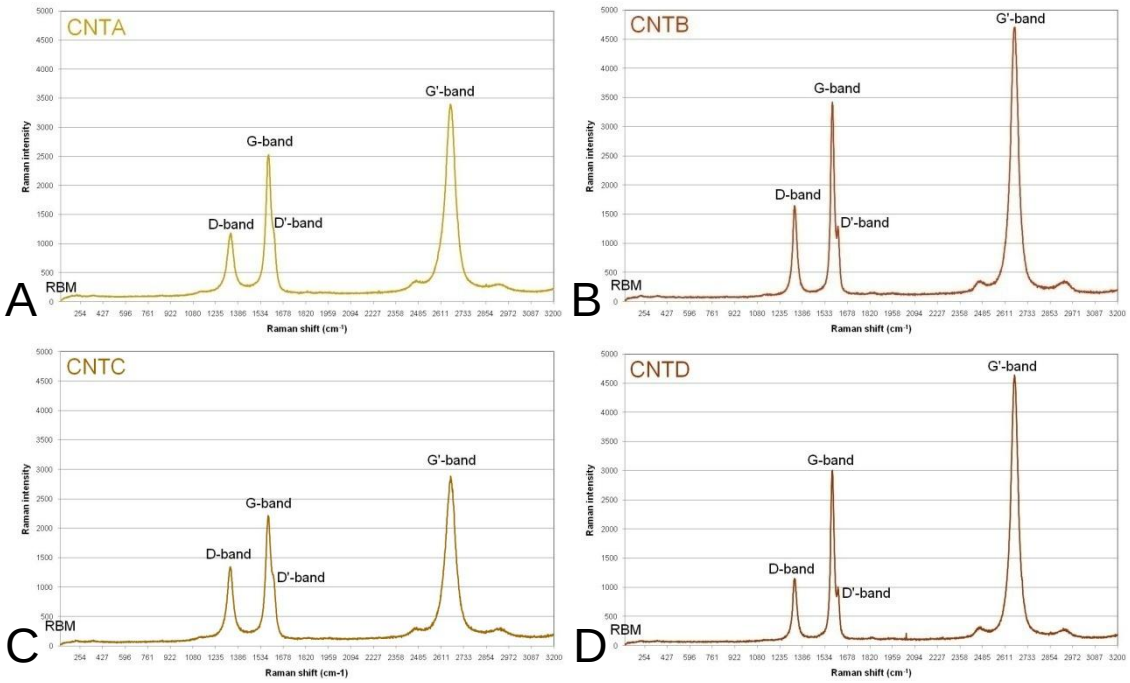

Figure 3.9 Raman spectrum of all short and long purpose-grown/treated MWCNT. (A) short/pristine CNTA, (B) short/annealed CNTB, (C) long/pristine CNTC, and (D) long/annealed CNTD. Data is expressed as intensity of Raman shift as samples are excited with a red laser at 633nm. Data is the average of at least 3 locations.

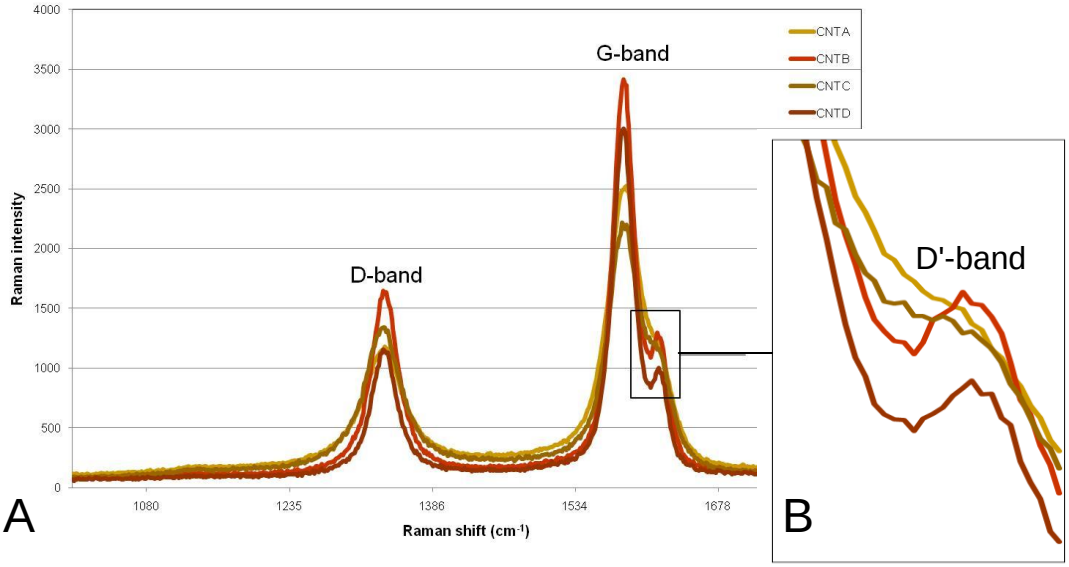

Figure 3.10 Highlighting the differences of Raman spectrum of all short and long purpose-grown/treated MWCNT. (A) represents an overlay of all relevant peaks, while (B) highlights the changes in D'-band. Data is expressed as intensity of Raman shift as samples are excited with a red laser at 633nm. Data is the average of at least 3 locations.

MWCNT	CNTA	CNTB	CNTC	CNTD
Crystallinity (by D-band, $R = I_G/I_D$)	2.1	2.1	1.7	2.6
Crystallinity (by D'-band, $R = I_G/I_{D'}$)	2.4	2.9	2.1	3.4

Table 3.2 Representative crystallinity of purpose-grown/treated MWCNT.

3.3 Further characterisation – involving all of particle panel B

3.3.1 Iron dissolution

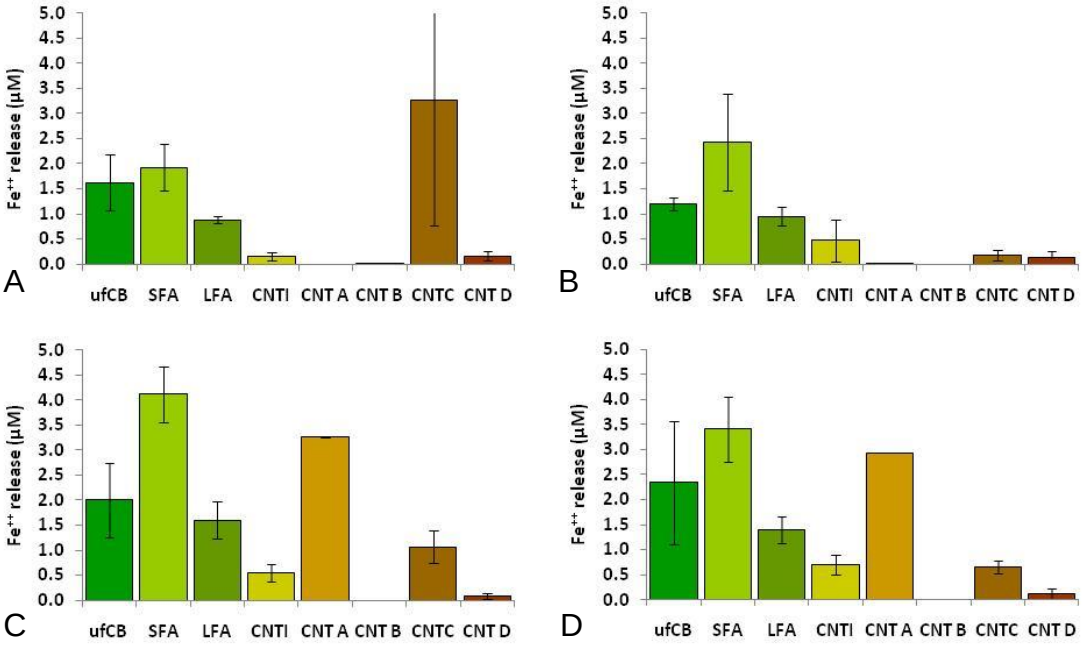

Figure 3.11 Iron (Fe^{2+}) dissolution in particle suspensions. Data represents Fe^{2+} release (µM) from all of particle panel B when suspended at 37°C under different conditions: (A) 48 hours pH 7.4 (B) 96 hours pH 7.4 (C) 48 hours pH 4.5 (D) 96 hours pH 4.5. Data is expressed as mean±SEM (n=3) (except CNTA and CNTB, where n=1, due to limited sample available).

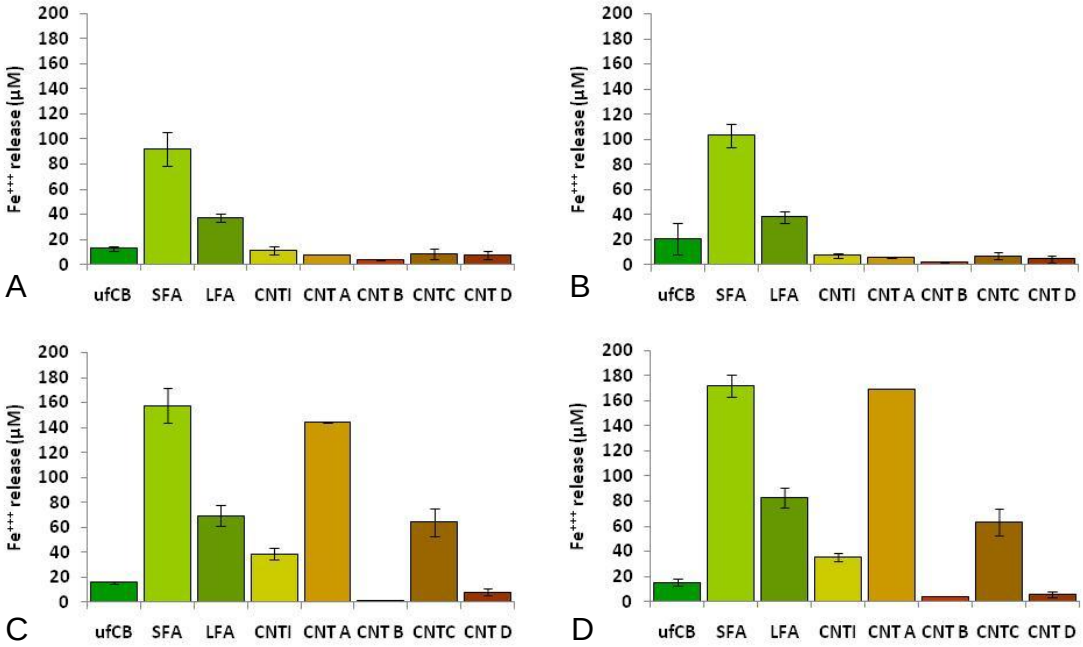

Figure 3.12 Iron (Fe^{3+}) dissolution in particle suspensions. Data represents Fe^{3+} release (µM) from all of particle panel B when suspended at 37°C under different conditions: (A) 48 hours pH 7.4 (B) 96 hours pH 7.4 (C) 48 hours pH 4.5 (D) 96 hours pH 4.5. Data is expressed as mean± SEM (n=3) (except CNTA and CNTB, where n=1, due to limited sample available).

The study of iron dissolution from suspended samples was conducted to show which samples can release the highest proportion of iron. The iron contained on and within the dry CNT samples was attained for all five of the MWCNT, but it cannot necessarily be presumed that this will all become available upon exposure to biological systems. So under biologically relevant conditions both Fe^{2+} and Fe^{3+} were measured after incubation at 37°C on an orbital shaker (300rpm) for 48−96 hours, in suspension buffers of pH 4.5 and pH 7.4.

A small release of Fe^{2+} (figure 3.11) was detectable, slightly more at pH 4.5 than at pH 7.4, and if any particles were consistently higher it was SFA and CNTA at pH 4.5. Pristine MWCNT (CNTA and CNTC) were shown to release a greater quantity of Fe^{2+} than their respective annealed samples (CNTB and CNTD), which displayed practically no Fe^{2+} release. The release of Fe^{3+} (figure 3.12) was much greater than Fe^{2+}, but as seen in respect to Fe^{2+}, the release of Fe^{3+} was greater at pH 4.5 than at pH 7.4, particularly in the case of the CNT samples. In a solution of pH 7.4 there was substantial iron dissolution from the SFA suspension, some release from LFA suspensions, but insignificant release from other particles, including all MWCNT. At pH 4.5 (figure 3.12 C and 3.12 D) the most iron dissolution was still seen from SFA, with LFA also having some release, but at this pH both pristine MWCNT (CNTA and CNTC) were shown to have substantial Fe^{3+} release, particularly the short pristine CNTA, and both far greater than their relative annealed samples, which again released practically no detectable Fe^{3+}. Interestingly, CNTI, which has a similar dry weight iron content as CNTD, was shown to leach far more iron than CNTD at pH 4.5. NPCB did not have any noteworthy iron dissolution.

3.3.2 CNTI outsourced characterisation

CNTI, an industrially produced MWCNT provided by Mitsui & Co Ltd., has in part been characterised by Dr Craig Poland (University of Edinburgh) and Dr Fiona Smail (University of Cambridge) (table 3). CNTI was shown to have a dry iron content of 3.4–8.5 mg/g, an average diameter of 85nm, and an average length of 13µm. Its Raman spectra consisted of a clear D-band, G-band, and G'-band, with the D'-band appearing as a shoulder on the G-band. G/disorder ratio values are: G/D = 5.7, and G/D' = 5.3, representing a relatively high crystallinity value (figure 3.13).

MWCNT	Fe content by ICP-OES (mg/g)	Fe content by TGA (mg/g)	Diameter (nm)	Length (µm)	Length (% above 20µm)
CNTI	3.4	8.5	85±2	13	11.5

Table 3.3 CNTI outsourced characterisation – iron content and CNT size. Courtesy of Craig Poland (University of Edinburgh) and Fiona Smail (University of Cambridge).

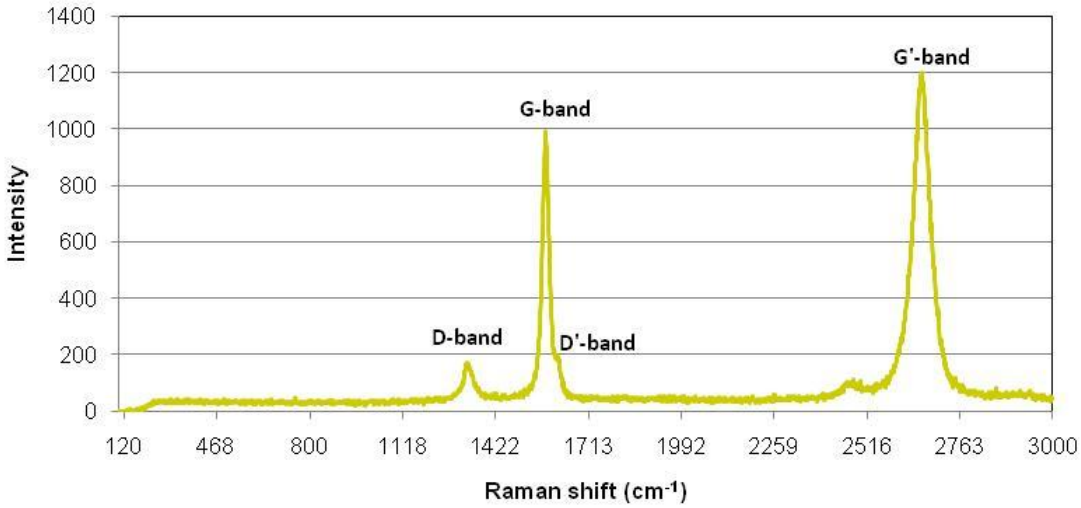

Figure 3.13 CNTI outsourced characterisation – Raman spectrum. *R = G/D* = 5.7, *R = G/D'* = 5.3. Courtesy of Dr. Fiona Smail (University of Cambridge).

3.3.3 Particle dispersion

CNT are notoriously difficult to disperse, but ideally a good dispersion was desired for the *in vitro* assessment that was to be performed. Three culture media were assessed for their ability to create and maintain a relatively stable particle suspension. RPMI 1640 was used as a popular and recommended culture medium. RPMI 1640 was used on its own, and to demonstrate the importance of a protein additive on dispersion (Foucaud *et al.*, 2007), with 10% FCS (the desired culture combination), and with 1% BSA (previously used with interesting toxicological effects by Rothen-Rutishhauser *et al.* (2010), and in chapter 4, section I).

Figure 3.14 shows the dispersion of nanoparticle CB, SFA, and LFA suspended in the three culture media, for 0, 30 minutes, and 14 hours. Due to spectral properties it was difficult to clearly see the dispersion of either asbestos sample.

However, upon close examination there were far more deposits at the bottom of the tube at a faster rate when suspended in RPMI 1640 alone. NPCB clearly had come out of suspension after 30 minutes when RPMI was used alone, but suspensions were still fairly stable with the inclusion of both protein additives even at 14 hours.

The dispersion of CNTI, CNTC, and CNTD is shown in figure 3.15. It was clearly evident, even at time zero, that none of the CNT samples (CNTI, CNTC, and CNTD) remained in suspension when no protein additive was used. After 30 minutes suspension in solutions containing FCS and BSA CNT samples did remain stable. However, when left for 14 hours the inclusion of BSA was not adequate to keep a stable suspension, while the addition of FCS appeared to allow CNT suspensions to remain stable.

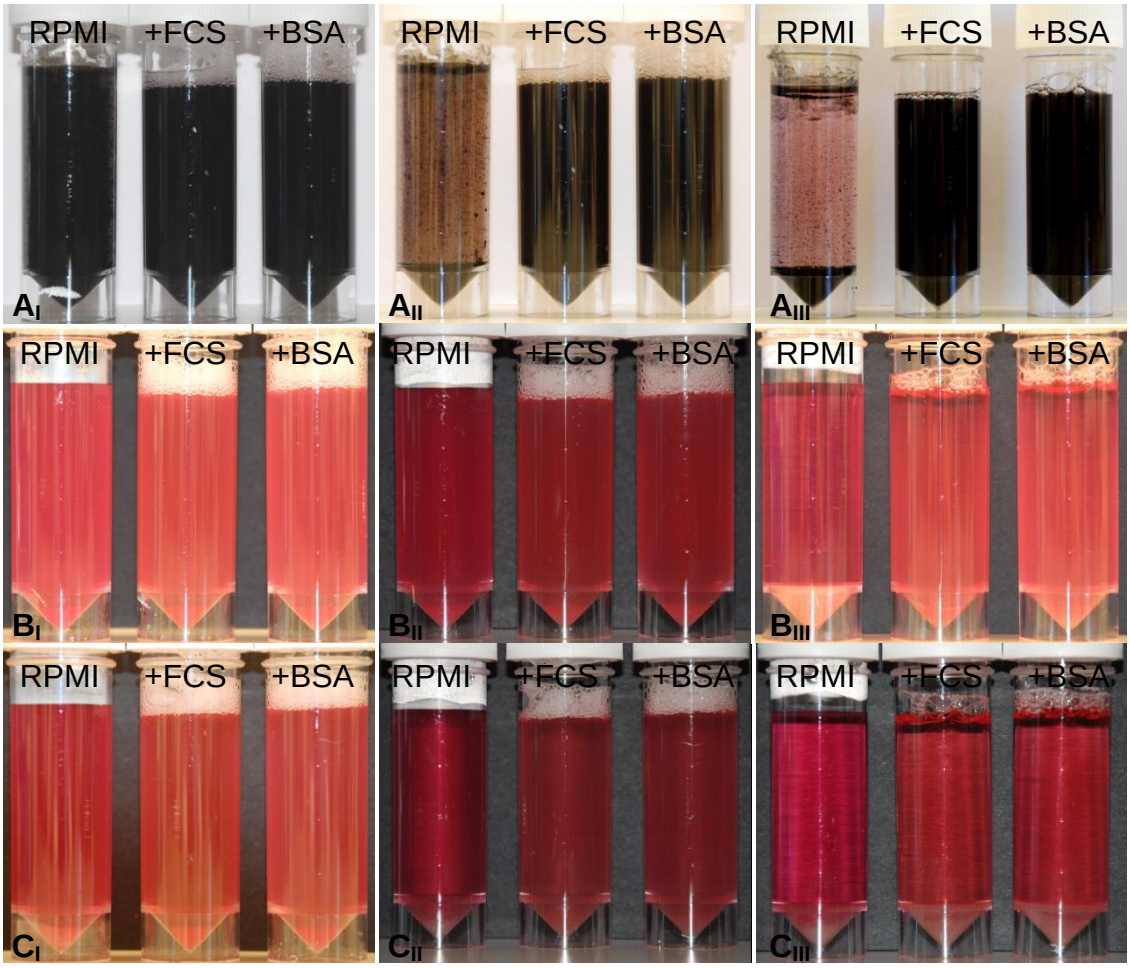

Figure 3.14 Dispersion of nanoparticle CB, SFA, and LFA in different media. (A) nanoparticle CB, (B) SFA, and (C) LFA were suspended in RPMI 1640, RPMI + 10%FCS, or RPMI + 1%BSA, for (I) zero minutes, (II) 30 minutes, or (III) 14 hours.

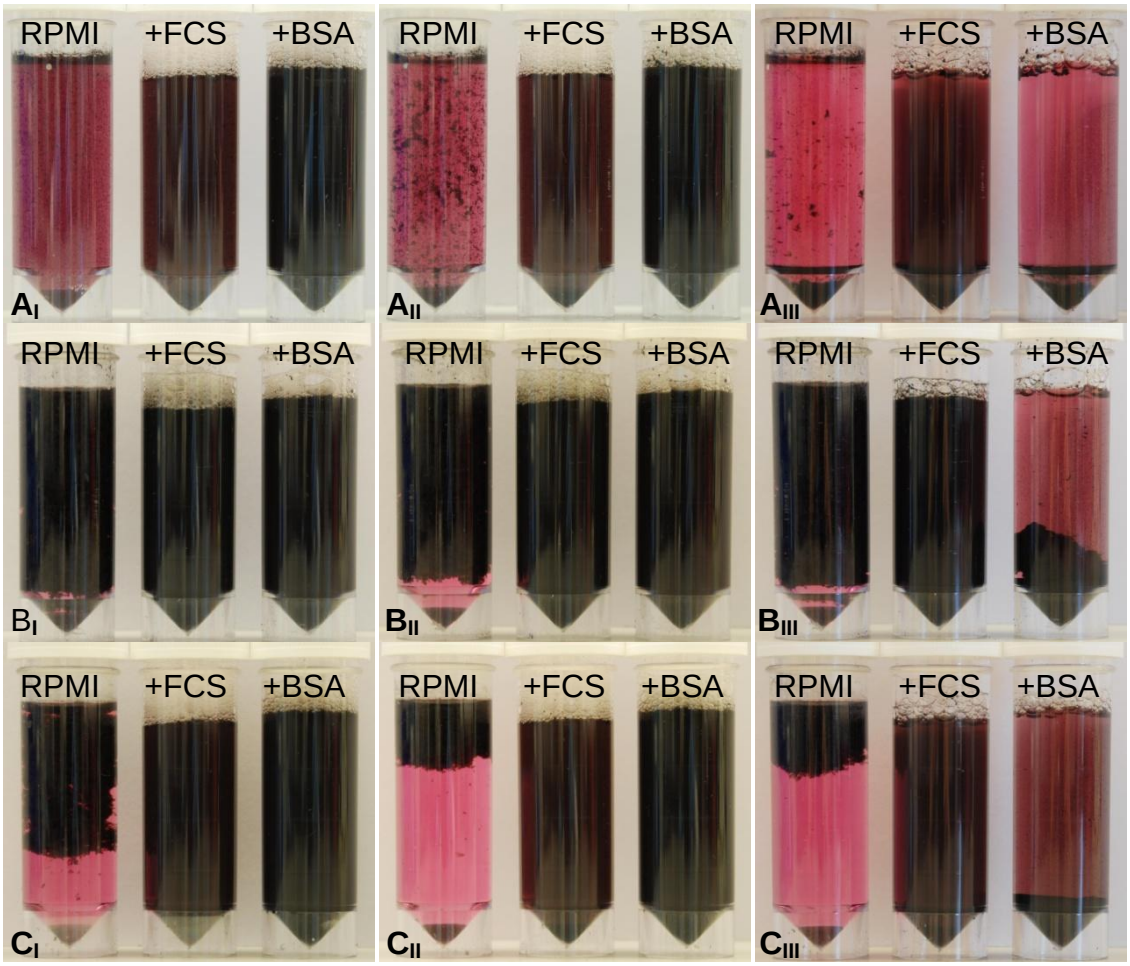

Figure 3.15 Dispersion of CNTI, CNTC, and CNTD in different media. (A) CNTI, (B) CNTC, and (C) CNTD were suspended in RPMI 1640, RPMI + 10%FCS, or RPMI + 1%BSA, for (I) zero minutes, (II) 30 minutes, or (III) 14 hours.

3.4 Discussion

Four specifically designed MWCNT have been synthesised to vary length, iron content, and crystallinity. The four MWCNT samples include two long, 30–80µm (CNTC and CNTD), and two short, <20µm (CNTA and CNTB); with a range of high to low iron content, and graphene quality. For dry weight the order of iron content, in high to low is: A-B-C-D; for dissolution the order is, in high to low order: A-C-D-B; and for sample quality, in the order high quality CNT structure to lower quality CNT structure is D-B-A-C. All characteristics are also outlined in chapter 2, table 1. A fifth MWCNT sample (CNTI) was industrially produced by free-forming “floating catalyst” CVD. CNTI has a length similar to CNTA and CNTB, a dry weight iron content similar to that of CNTD, while iron dissolution was found to be closer to CNTC, and its relative structural quality appeared much higher than the other four MWCNT.

The production of four MWCNT samples, and inclusion of CNTI, has allowed the differential analysis of three factors believed to influence CNT toxicity: particle length, iron content, and structural condition. With the inclusion of nanoparticle CB and asbestos it was possible to relate any findings regarding MWCNT toxicity to material with known pathogenic behaviour.

Length

The generation of MWCNT that are between 30µm and 80µm in length (CNTC and CNTD), with a high aspect ratio, will allow the assessment of these CNT in relation to the fibre paradigm, which has previously been outlined. Briefly, the role that fibre length plays in their pathogenicity is thought to be critical for many fibre-like particles, including asbestos (Donaldson *et al.*, 1989, Donaldson *et al.*, 1992), glass fibres (Ye *et al.*, 1999a), and of course CNT. Particles with lengths greater than 20µm (Dörger *et al.*, 2001) will result in frustrated phagocytosis, with subsequent enhancement of toxicity both *in vitro* and *in vivo* (Brown *et al.*, 2007b, Dörger *et al.*, 2001, Kim *et al.*, 2010a, Poland *et al.*, 2008). With MWCNT of different lengths (CNTI, CNTA, and CNTB) of below 20µm, it was possible to directly assess the effect that length has on biological systems.

Iron content

Samples that are morphologically similar but vary in iron content and iron dissolution will allow the evaluation of how bioavailable iron from MWCNT can impact on their toxicity. A higher bioavailable iron content has been shown to be instrumental in the formation of hydroxyl radicals in asbestos samples (Gilmour *et al.*, 1995), causing an increase in the potential oxidative stress (Kagan *et al.*, 2006) and increased inflammatory response (Kim *et al.*, 2010a, Muller *et al.*, 2008b).

The different techniques employed for iron removal had very different effects. The long pristine CNTC consisted of 7.4 weight% iron oxide, and upon high temperature annealing this iron content was almost completely eliminated, with a value of only 0.4% remaining; while the relatively gentle acid wash that was utilised did little to deplete iron content, with values dropping only to 6.6% with 1M HCl, and 6.1% with 4.7M HCl. This certainly shows that the method of annealing is the most suitable, but not only in respect to iron depletion. Although acid treatments are supposed to reduce sample impurities (not seen here), the process should also decrease the quality of the carbon form (Huang *et al.*, 2002, Jeong *et al.*, 2001, Stobinski *et al.*, 2010), as acid treatments would create functional groups, i.e. carboxyl, hydroxyl, carbonyl, ether, and ester groups (Stobinski *et al.*, 2010) (to name but a few) on the CNT surface, affecting the quality of the graphite structure. Ultrasonication would also commonly be employed during the acid washing of samples and this has been shown to cause breaks to occur within the nanotubes themselves (Jeong *et al.*, 2001). High temperature annealing, on the other hand, maintains the CNT structure and has been shown to remove these functional groups and other impurities (Huang *et al.*, 2002, Misra *et al.*, 2006).

The quantity of iron in the dry samples is known for all five of the CNT, and was expected to be high for the asbestos samples (Gilmour *et al.*, 1997, Graham *et al.*, 1999). So in the dissolution study it was expected that both asbestos samples would leach a relatively large quantity of iron, while the MWCNT would release an amount proportional to that of their dry iron weight, and would therefore be in the iron content descending order of: CNTA:CNTB:CNTC:CNTI-CNTD. This exact pattern was not seen. The order, in fact, was as follows: the short pristine CNTA released the highest amount of iron, then the long pristine

CNTC and the short CNTI. CNTB and CNTD released practically no iron. So CNTB, although having a substantial iron content (compared to CNTC, CNTD, and CNTI) does not leach any discernable quantities; this reveals that the annealing process has primarily stripped CNTB of its more accessible iron and left other areas intact. Additionally, the amount leached from CNTI and CNTD was expected to be similar, but for the CNTI suspension it was far greater, again pointing to the location of the iron within CNTD restricting its release.

The pH used to suspend the particles was chosen to represent conditions found within alveolar macrophage lysosomes (pH 4.5–5.0), and alveolar or interstitial fluid (pH 7.4) (Stopford *et al.*, 2003). This feature is not the only aspect of these biological regions that may impact on iron dissolution, but pH is a critical aspect in particle iron leaching (Gilmour *et al.*, 1997), and therefore this method was deemed appropriate. This would suggest that the release of iron in or around cells of the respiratory system would occur in exposure to a number of these samples.

Crystallinity

The structural differences in MWCNT samples may impact heavily on their influence on biological systems upon exposure, as nanofibre structure has been shown to influence their toxicity (Brown *et al.*, 2007b, Muller *et al.*, 2008b), and forms of amorphous carbon have a history of pathogenic behaviour (Barlow *et al.*, 2005b, Brown *et al.*, 2004, Brown *et al.*, 2000, Stone *et al.*, 1998); therefore Raman spectroscopy was used to quantify the relative graphite quality in the MWCNT samples.

Raman spectroscopy is a useful tool for the analysis of CNT sample purity, as it is fast, non-destructive (Ouyang *et al.*, 2008), and displays indicators of purity and sample quality that are unique to CNT (Dresselhaus *et al.*, 2007). There are five key features of the Raman trace that are found when assessing CNT: the radial breathing mode (RBM), D-band, G-band, D'-band, and G'-band.

The radial breathing mode (RBM), found at the low frequency region of the Raman spectrum (100-300 cm^{-1}), is normally only present when analysing SWCNT and not MWCNT, and is representative of diameter (Baltog *et al.*, 2008, Bandow *et al.*, 1998, Li *et al.*, 2004a); where the equation $d = (238/F)^{1.075}$

can be used to determine tube diameter, where *d* = diameter in nm, and F = Raman shift frequency, in cm^{-1} (Li *et al.*, 2004a). Both D-band (disorder mode (DM) (Ouyang *et al.*, 2008)) and D'-band, found at 1350cm^{-1} and 1620cm^{-1} respectively, are indicative of defects: amorphous carbon and carbon particle defects, disordered graphite, surface defects or bending of nanotubes (Dresselhaus *et al.*, 2010, Li *et al.*, 2004a, Ouyang *et al.*, 2008, Singh *et al.*, 2003b, Steplewska and Borowiak-Palen, 2009, Stobinski *et al.*, 2010). The G-band (1580 cm^{-1}), termed tangential vibration mode (TM), is representative of pure graphene sheets; it is caused through the optical vibration of flanking carbon atoms (Dresselhaus *et al.*, 2007, Li *et al.*, 2004a, Singh *et al.*, 2003b), and corresponds to the stretching mode of carbon-carbon bonds. The ratios between these peaks on a Raman spectrum can be used to quantify sample purity and disorder within CNT samples (Li *et al.*, 2004a, Ouyang *et al.*, 2008, Singh *et al.*, 2003b, Steplewska and Borowiak-Palen, 2009). A higher G/D or G/D' ratio is indicative of fewer sample defects, and a higher crystallinity (Singh *et al.*, 2003a).

According to the G/D ratio there appeared to be no change in carbon defect/disorder to crystalline ratio after the high temperature annealing treatment of CNTA, creating CNTB, while for G/D' ratio there was a slight increase in proportional crystallinity after annealing, with the ratio increasing by 0.5. This seems to indicate that, although metal impurities are depleted, the carbon forms present are hardly changed by the process. It was, however, clear that when the long pristine CNTC is annealed to form CNTD there was an observable increase in sample purity, by both ratio values, with an increase in G/D of 0.9 and G/D' of 1.3. The purity of the long pristine CNTC started below that of both short MWCNT samples, and was higher than both after the annealing process (CNTD). Crystallinity values of CNTA and CNTC (2.1 and 1.7 respectively, by $R = I_G/I_D$; and 2.4 and 2.1, by $R = I_G/I_{D'}$) clearly show a higher quality MWCNT sample was obtained through the shorter growth cycle, in respect to pre-annealed samples; however, CNTD values (2.6 by $R = I_G/I_D$, and 3.4 by $R = I_G/I_{D'}$) clearly show a better quality MWCNT after the annealing of a longer growth cycle. This is likely due to a greater initial presence of amorphous carbon in the long pristine MWCNT sample (CNTC), as when a longer growth/reaction time is used, there can be formation of other, disordered carbon

structures occurring when the metal catalyst has become used up (Singh *et al.*, 2003b), with removal of these impurities during the annealing process.

Upon close examination of the four purpose-grown MWCNT sample D'-peaks, a second carbon disorder indicator (Dresselhaus *et al.*, 2010, Stobinski *et al.*, 2010), two further consequences of the high temperature annealing become evident. The G-peaks had become tighter and therefore more pronounced in the annealed samples (CNTB and CNTD); and, while the D'-peaks of CNTA and CNTC only appeared as a shoulder, for CNTB and CNTD there was a clear generation of a distinct peak. This tighter more pronounced G-peak indicates a more ordered and crystalline structure (Eck *et al.*, 2011). The second detail is the clear drop in D'-peak with the annealing treatment of long MWCNT, not seen for the short, again indicating the formation of a purer sample for the long MWCNT after high temperature annealing, while the short CNT remained relatively the same.

The G/D and G/D' ratio values for CNTI were 5.7 and 5.3 respectively, these data plus evaluation of iron content, and SEM images, imply that the industrially produced MWCNT (CNTI), although not well aligned, is actually a good quality CNT sample with very high purity and relatively low iron content. However, peaks on the Raman spectra can be affected by the laser conditions used: as the laser intensity increases so do the carbon disorder peaks (D and D'), while the graphite peak (G-band) will remain the same (Kastner *et al.*, 1994, Ouyang *et al.*, 2008).

Dispersion

The influence that particle dispersal has on the response of biological systems upon treatment is ambiguous. Pathogenic effects of both well dispersed and aggregated CNT deposits in the lung are shown in the form of fibrosis and granuloma formation (Muller *et al.*, 2005, Shvedova *et al.*, 2005). There is evidence that an entangled CNT sample can cause a greater ROS production than a straight sample upon good dispersal (Rothen-Rutishauser *et al.*, 2010), but also that a well-aligned and well-dispersed straight CNT sample can provide a greater response than an entangled sample, in respect to phagocytic ability and ROS production (Brown *et al.*, 2007b). It therefore seems important to at least know the dispersal state of the material upon exposure.

To provide stable suspensions of CNT often the best dispersant would be a solvent, such as dimethyl formamide (Arepalli *et al.*, 2004); this, however, is not suitable for tissue culture experiments due to the level of toxicity of most solvents. Therefore protein additives are the best option to achieve relatively stable suspensions. Visual identification of sample dispersal is certainly not quantitative, and possibly cannot identify if a sample is “nano-dispersed” or “macro-dispersed”; a quantitative method would be UV-VIS-NIR spectrometry (Arepalli *et al.*, 2004). However, the images taken here do allow the comparison of biologically suitable media and point towards the use of RPMI 1640 with 10% FCS being optimal for the treatment of cells, as it holds the MWCNT suspensions adequately for at least 14 hours. It is also worth noting that when CNT were suspended in cell culture medium without the addition of any protein components there appeared to be a distinct separation of the sample. Some agglomerates would sink, while others would float. This phenomenon was not investigated, and without analysis to determine the differences between these samples an explanation for its occurrence cannot be given. It is worth noting that the terms agglomeration and aggregation are often used during assessment of NP characteristics. The two phenomena are distinguishable by the strength of their bonds, with aggregated containing far stronger bonding between primary particles (Jiang *et al.*, 2009). It is thought that ultra-sonication can be used to separate agglomerates (Jiang *et al.*, 2009) and therefore distinguish between agglomerates and aggregates. During this study sonication was consistently used to aid dispersion of the particles, and differences in dispersion were certainly found, particularly among the CNT samples. However, it cannot be assumed that CNT samples which dispersed less were aggregated and those which dispersed more were agglomerated; mainly as it has been shown that a more suitable method of agglomerate separation is by probe sonicator, and here a bath sonicator was used. Secondly, the other methods used for characterisation, such as SEM are not able to discern between these phenomena.

In summary, the methods employed in this chapter generated four MWCNT samples; two long (CNTC and CNTD) and two short (CNTA and CNTB). For each length, samples had either low or high Fe content, and either high or a

lesser crystal structure. In addition we characterised an industrial MWCNT sample (CNTI), and numerous control particles. CNTI was found to have lengths similar to CNTA and CNTB, dry Fe content similar to CNTD, but Fe dissolution levels closer to CNTC, and a greater crystallinity than all other MWCNT used here. The control particles included LFA, an asbestos sample with lengths greater than all samples used here and relatively high Fe dissolution; and also SFA, a short asbestos sample with high Fe release, and NPCB, a small carbon based NP with practically no bioavailable Fe.

Chapter 4

Reactive oxygen species elicited carbon nanotubes

4.1 Introduction – reactive oxygen species and oxidative stress

In this chapter the ability of CNT to stimulate oxidative stress was addressed. In Section I 'particle panel A' was used to access the capacity for CNT to directly produce ROS in a cell-free system, to stimulate the production of ROS, *in vitro*, and to initiate an oxidative and inflammatory response *in vivo*. Additionally, the effect of particle dispersion on these factors was also assessed. In Section II oxidative stress in response to 'particle panel B' was considered using the gene expression of antioxidant defence mechanisms, and markers of oxidative DNA damage.

The ability of any NP to produce ROS and other free radicals has been shown to be a particularly important issue in nanotoxicology. The literature describing the formation of ROS and subsequent oxidative stress caused by NP, transition metals, asbestos and CNT was provided in chapter 1. So, briefly, oxidative stress can result in enhanced pro-inflammatory conditions (Brown *et al.*, 2004, Donaldson *et al.*, 2002, Wilson *et al.*, 2002) through the activation of pro-inflammatory gene expression and alterations in cell signalling (Kannan and Jain, 2000, Oberdörster *et al.*, 2005); this is known to cause local tissue injury and cell death (MacNee, 2001). The whole process becomes enhanced and sustained through further ROS production (MacNee, 2001). The mechanism of ROS generation, and stimuli necessary to induce it, is relatively well documented, with light, ultraviolet light and transition metals shown to induce the production of ROS by NP through the release of free electrons, production of redox active intermediates or direct release of oxyradicals from cells (Oberdörster *et al.*, 2005).

As with the toxicity of other NM, much consideration has been given to the ability of CNT to cause oxidative stress. The presence of ROS and subsequent oxidative stress was clearly evident in response to CNT, *in vivo*, and in the exposure of epithelial cells and macrophages *in vitro* (Kagan *et al.*, 2006, Shvedova *et al.*, 2007, Srivastava *et al.*, 2010, Thurnherr *et al.*, 2010). It has been shown that CNT can cause a phagocytic burst and direct generation of ROS (Pulskamp *et al.*, 2007b), often higher than asbestos (Thurnherr *et al.*, 2010), and that pro-inflammatory conditions can be directly stimulated and intensified in the presence of ROS generated through CNT exposure (Han *et al.*, 2010). So as a key aspect of NP activity/reactivity (Oberdörster *et al.*, 2005)

the ability of CNT to generate or stimulate the production of ROS certainly needs attention.

4.2 Section I – particle panel A

4.2.1 Aim

The aim of this study was to assess the ability of morphologically and compositionally distinct CNT to generate ROS *in vitro*, *in vivo*, and using a cell-free system, and to measure the subsequent oxidative stress and inflammatory response *in vivo*.

The data for this investigation was collected in collaboration between the Biomedical Research Group (BRG) at Edinburgh Napier University, by M. Boyles and Dr D. Brown, and the University of Bern, by Dr B. Rothen-Rutishauser (for the full set of results see *Appendix II: Publications* (Rothen-Rutishauser *et al.*, 2010)).

4.2.2 Results

4.2.2.1 ROS production, cell-free assay – four-hour particle incubation

In the absence of HRP the entangled CNT sample (NT3) was consistently found to increase DCFH oxidation, irrespective of suspension medium. A significant increase in ROS production was seen by NT3 compared to medium-only controls (figure 4.1), and compared to both straight samples (NT1 and NT2) when suspended in medium containing FCS (figure 4.1 B) and saline containing BSA and DPPC (figure 4.1 C). NT3 was also significantly higher than the long straight NT1 when suspended in RPMI alone.

The addition of HRP significantly raised the level of ROS production in all assays including particle treatments and controls, except when the suspension medium was RPMI alone. With respect to particle differences, NT3 only produced significantly higher levels of ROS compared to medium-only controls when the suspension media was RPMI 1640 alone (figure 4.1 A); but levels were still significantly higher than the other CNT in all suspension media. Interestingly, with protein and surfactant additives, both NT1 and NT2 were shown to decrease oxidative capacity compared to the medium-only control (figure 4.1 B and C).

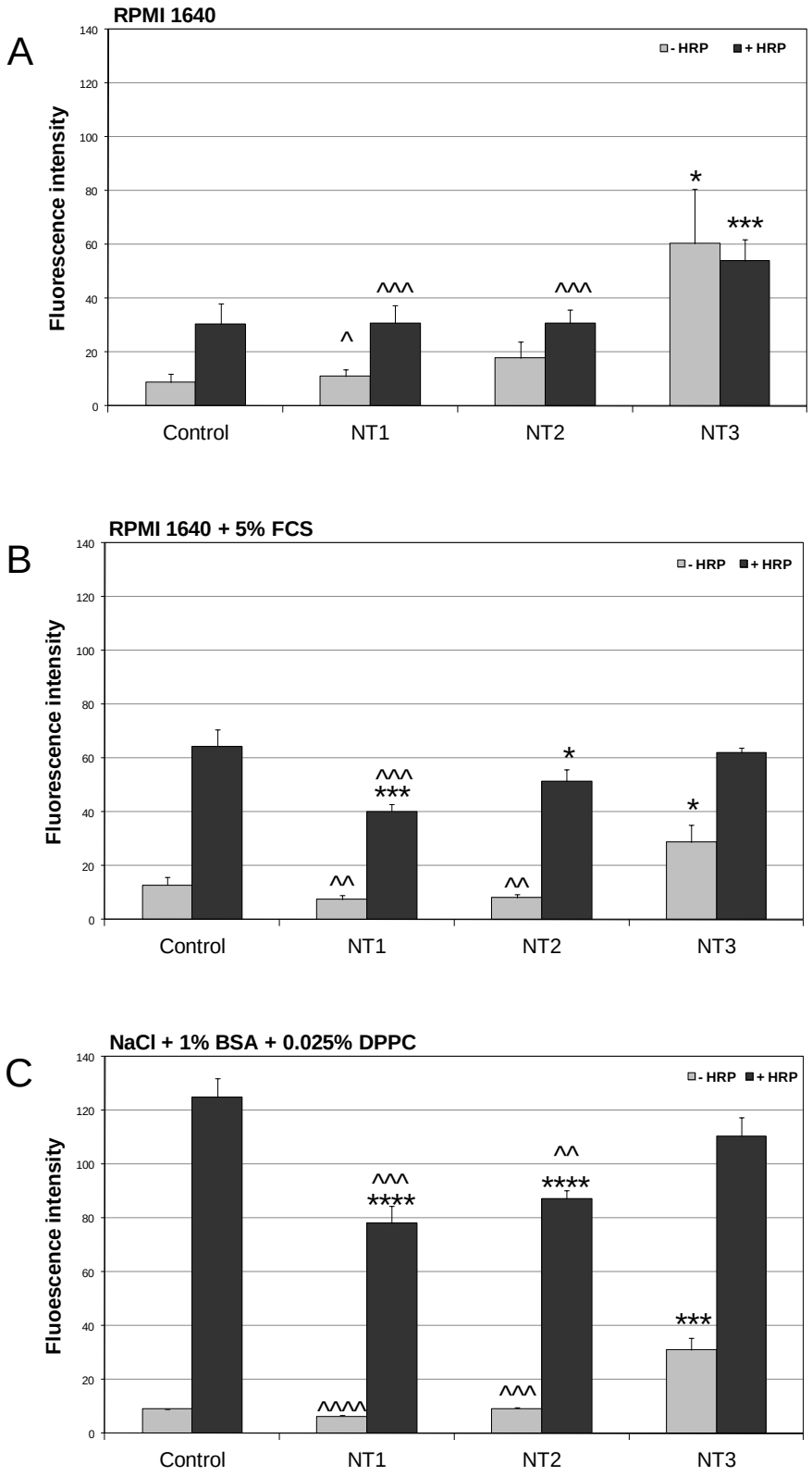

Figure 4.1 ROS released from CNT in a cell-free system. CNT were suspended in different media for four hours prior to addition of fluorescent probe and fluorescent measurements; (A) RPMI 1640 (B) RPMI 1640 + 5% FCS (C) NaCl + 1% BSA + 0.025% DPPC. Results are expressed as fluorescence intensity caused by DCFH oxidation, and each data point is representative of mean±SEM (n=3). Statistical significance is shown by *=p<0.05, ***=p<0.005, ****=p<0.001, compared to medium only control, and ^ = p<0.05, ^^ = p<0.01, ^^^ = p<0.005, ^^^^ = p<0.001, compared to NT3.

4.2.2.2 ROS production by bronchoalveolar lavage cells

ROS production in cells, obtained through BAL of Sprague-Dawley male rats, was assayed after an 18-hour instillation of 62.5µg/ml of each respective CNT (NT1, NT2, and NT3) into the rat lung. Prior to instillation CNT were suspended in saline only (figure 4.2 A) or saline plus 0.1% BSA (figure 4.2 B), with control animals administered with the relevant vehicle only. At this dose and time BAL cells from animals exposed to NT2 and NT3 suspended in saline with BSA exhibited a significantly higher level of DCFH oxidation (figure 4.2 B) compared to cells obtained from vehicle-only administrated animals. When particles were suspended in saline alone no significant differences were found.

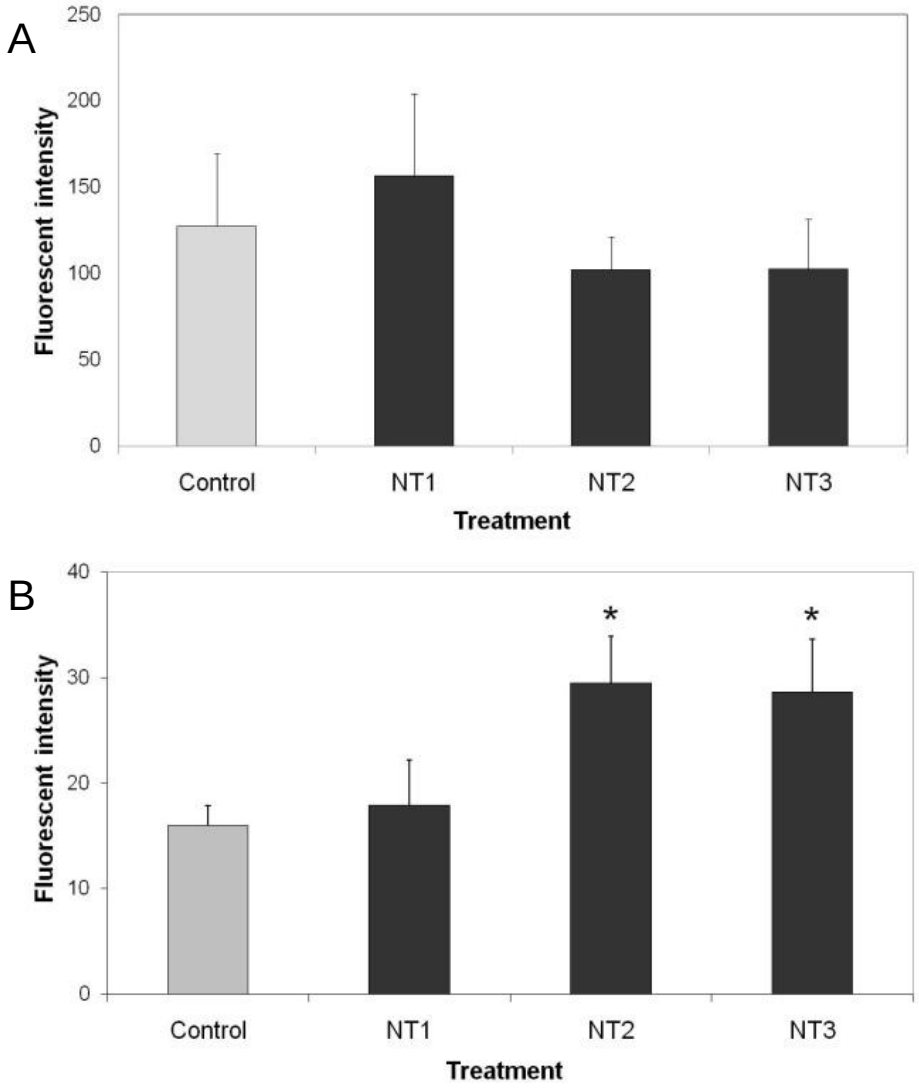

Figure 4.2 ROS generation in BAL cells, using different suspension media (A) saline and (B) saline + 0.1% BSA. Results are expressed as fluorescence intensity caused by DCFH oxidation, and each data point is representative of mean±SEM (n=4). Statistical significance is shown by * = $p<0.05$. N.B. (A) uses a slit width of 10, (B) a slit width of 5.

4.2.3 Results obtained by collaborators – full results in appendix II 'publications'

Cell-free assay – with 30-minute particle incubation

With HRP absent from the assay, the long, straight CNT (NT1) did not display any increase in DCFH oxidation compared to the medium-only control, irrespective of suspension medium. The entangled CNT (NT3) induced a significantly high rate of DCFH oxidation, compared to medium only, when suspended in RPMI alone and in the saline containing BSA and DPPC; NT3 was also significantly higher than both NT1 and NT2 when suspended in the saline solution. The short, straight NT2 only showed an increase in ROS production, compared to control, when suspended in the saline solution.

In the presence of HRP no statistically significant differences were found between any of the NT treatments and negative controls, in any of the suspension media.

Cellular uptake of CNT by J774.A1 – by light microscopy

In all culture media the murine macrophage-like cell line, J774.A1, attached themselves to the straight CNT samples (NT1 and NT2), but cellular uptake was not complete. The entangled CNT (NT3) were readily taken up by the cells; they were found aggregated in the medium, but were predominately observed within the cells.

Cellular uptake of CNT by BAL cells – by light microscopy

The long straight CNT (NT1) were better dispersed when administered in saline containing BSA than in saline alone, but did not appear to be entirely taken up by the cells in either instance. The entangled sample (NT3) was readily taken up by the BAL cells in both media types; and uptake of short straight CNT (NT2) appeared to improve when suspended and instilled in the saline solution containing 0.1% BSA.

Generation of ROS in J774.A1 cells in response to CNT

Positive control treatments of tert-butyl hydroperoxide (TBHP) provided clear ROS generation. There was a significant increase in the number of fluorescent cells when compared to medium-only negative control cells, with 19% in response to TBHP and 6% in response to medium-only (data not shown). When exposed to the entangled CNT (NT3) suspended in RPMI 1640 alone there was a rapid and statistically significant increase in the proportion of J774.A1 cells producing ROS which was sustained from the initial reading at 30 minutes through to the 4-hour measurement. The straight samples, both long and short, did not increase ROS production compared to negative controls after 30 minutes, but over time the proportion of cells expressing fluorescence increased and was statistically significant in both cases at the final measurement at four hours. This exact pattern was observed when CNT were suspended in RPMI 1640 with 5% FCS. When suspended in the saline solution the CNT induced a similar pattern again, with exposure of NT1 and NT2 causing the gradual and eventually statistically significant increase of ROS production at four hours; NT3, again, caused a rapid increase in ROS production, which in this case was not sustained and dropped close to the level of medium-only control at the four-hour time point.

Data obtained from BAL

Measurements of oxidative stress and an inflammatory response were taken from BAL fluid obtained after intratracheal injection and 18-hour exposure of 62.5µg CNT suspended in saline alone or saline containing 0.1% BSA, by quantifying neutrophil influx, and concentrations of LDH, protein and GSH. No statistical significance was found between either CNT-treated animals or the control animals, except for neutrophil influx into the lung of the rats exposed to the long straight CNT (NT1) when suspended in saline containing 0.1% BSA (Rothen-Rutishauser *et al.*, 2010).

4.2.4 Discussion

In summary, the entangled CNT (NT3) displayed a high, but short-term oxidative potential, both *in vitro* and in a cell-free system. The aggregates of NT3 formed were easily engulfed, and with no increase, and sometimes a decrease, in ROS signal over time. This suggests that the NT3 was readily taken up by the macrophages leading to accomplished phagocytosis rather than frustrated phagocytosis so that the ROS response was relatively short. Straight CNT did not increase ROS at an early stage, but did demonstrate a gradual and possibly more sustained response *in vitro.* They were not easily or fully engulfed by the cell line or BAL cells, and with the *in vivo* inflammatory response to NT1 it appeared that frustrated phagocytosis was occurring. This would support the hypothesis that long straight CNT are more pathogenic than short or entangled CNT. However, without full characterisation of the three samples, for level of carbon purity and structural integrity, and of metal catalyst dissolution, it is difficult to unequivocally lay responsibility on fibre length and morphology alone.

One key aspect in the proposed pathogenicity of any fibre is its ability to evade removal from the alveolar region, which is largely due to fibre length and durability, where fibres of over 10-15µm are not cleared by alveolar macrophages, causing frustrated phagocytosis, interaction with epithelial cells, and possible translocation to the pleural space (Bernstein *et al.*, 2005). It has been shown that frustrated phagocytosis and enhanced pro-inflammatory conditions are MWCNT length and shape dependent *in vitro* (Brown *et al.*, 2007b); and that inflammation and granuloma formation, *in vivo*, is also fibre length and shape dependent, for both MWCNT and asbestos (Poland *et al.*, 2008). Here, using the same panel of MWCNT as Brown *et al.* (2007b), it was possible to relate these aspects of CNT toxicity to their ability to cause oxidative stress.

From asbestos fibres (Chen *et al.*, 1996, Fung *et al.*, 1997, Gilmour *et al.*, 1995) to NP (Brown *et al.*, 2004, Foucaud *et al.*, 2007, Li *et al.*, 2008, Stone *et al.*, 1998), the generation of ROS, free radicals and resultant oxidative stress has been implicated in their toxicity – from oxidative damage to DNA by asbestos (Gilmour *et al.*, 1995) to an enhanced inflammatory response from NP exposure

(Brown *et al.*, 2004). Both SWCNT and MWCNT are shown to directly and indirectly influence the redox state of a cell and cause oxidative stress. The presence of ROS and subsequent oxidative stress was clearly evident in response to SWCNT, with increased lipid peroxidation, cleavage of extracellular superoxide dismutase, decreased antioxidants glutathione and ascorbic acid (Shvedova *et al.*, 2007), and conversion of superoxide radicals to hydroxyl radicals (Kagan *et al.*, 2006), with the ability of CNT to cause oxidative burst and direct generation of ROS clearly demonstrated by Pulskamp *et al.* (2007b). The production of ROS (Han *et al.*, 2010, Thurnherr *et al.*, 2010) and the induction of antioxidant defence mechanisms suggesting the production of ROS (Brown *et al.*, 2010) in response to MWCNT have led to enhanced pro-inflammatory conditions; these can be alleviated using administration of additional antioxidants (Brown *et al.*, 2010) and ROS scavengers (Han *et al.*, 2010).

Although CNT length is clearly important, and with frustrated phagocytosis any effects are likely to be prolonged, metal impurities are also likely to impact on oxidative potential. With exposure periods of 10 minutes to 24 hours, CNT induced elevated ROS in both alveolar macrophages and epithelial cells at concentrations of 5–100µg/ml, which appeared to be dependent on the presence of sample impurities (Pulskamp *et al.*, 2007a). The role of iron was further illustrated in macrophage responses to CNT as high iron (26wt.%) CNT generated more ROS and depleted a greater proportion of antioxidant reserves compared to low iron (0.23wt.%) CNT (Kagan *et al.*, 2006); and a depletion of antioxidants in rats was found with the four day exposure to 5mg/m^3 short (<1µm) high iron content (17wt%) SWCNT. Measurements were taken 1, 7 and 28 days post exposure, but results were evident from only one day post-exposure (Shvedova *et al.*, 2008a).

In this study the potential for CNT to generate ROS was demonstrated in a cell-free system. An entangled sample (NT3) with a large surface area generated considerably more ROS than a short CNT with relatively small surface area (NT2); however, this same entangled sample also generated more ROS than the long, straight, well-aligned MWCNT (NT1) that has the same relative surface area. One explanation could be a difference in dispersal between these

two CNT samples. This was investigated, and described in the experimental design (section 8.3) (Rothen-Rutishauser *et al.*, 2010), through the addition of media components, but the level of dispersion was not quantified. From these findings it seems unlikely that surface area alone is responsible. The amount of iron leaching or surface available iron may also be responsible, but again this was not quantified. There is not any great difference in iron content between the CNT samples, with quantities ranging from 1.3–5.1 wt.% (incidentally, the lowest iron proportionally is in NT2), but it is the biologically and chemically available iron that is likely to impact on ROS generation, and with production remnants being encased within the nanotubes and within the graphite lattice the availability cannot be presumed. So the release/availability may be higher in NT3, but this is only speculative as iron dissolution was not assessed. Chapter 3, figure 3.12, demonstrates that the dry weight of iron within a CNT sample does not convey the availability of iron. Amongst the CNT described in chapter 3, CNTB, which contained 50.3 mg Fe/g sample iron was shown to release considerably less iron than CNTC and CNTI, which contained 18.5 mg/g and 3.4–8.5 mg/g, respectively.

In this study, it was observed that the phagocytic cell line J774.A1 quickly and promptly phagocytosed the entangled CNT sample (NT3). This was evident as dark aggregates of material were visible within the cells; but also from the rapid ROS response, which after 30 minutes was found to deplete to levels comparable to medium-only treated cells, at least when the particles were suspended in saline containing BSA and DPPC.

It has been shown that attachment to macrophages will initiate a phagocytic burst and start the formation of ROS (Chanock *et al.*, 1994, Goodglick and Kane, 1986, Valko *et al.*, 2007). This is through activation of NF-κB which will in turn initiate an inflammatory response, shown for both ultrafine particles (Brown *et al.*, 2004) and MWCNT (Han *et al.*, 2010) exposure, and with this continued inflammatory response there is likely to be continued release of ROS (Goodglick and Kane, 1986). The release of ROS during phagocytosis is known to be intensified during exposure to particles with fibre-like dimensions (Hansen and Mossman, 1987, Hill *et al.*, 1995). This has been explained as frustrated phagocytosis where the production of ROS is maintained (Dörger *et al.*, 2001,

Ye *et al.*, 1999c) as the cells are not able to completely engulf the fibre (Poland *et al.*, 2008), leading to elevated inflammatory responses which are dependent on this sustained accumulation of ROS (Ye *et al.*, 1999a). This appeared to be evident with J774.A1 exposure to both straight CNT samples as they were shown to attach themselves to the phagocytes, but were not wholly taken in; there was no apparent ROS production after 30 minutes but after four-hours the response was clearly stronger than both the control cells and those treated with NT3. The ROS production and proposed frustrated phagocytosis seen here in response to NT1 and NT2, but not NT3, were reflected in Brown *et al.* (2007b), using superoxide anion produced during phagocytic burst as a measure of ROS production, and inhibited phagocytosis, sustained pro-inflammatory conditions, and visualisation as indicators of frustrated phagocytosis.

The oxidative response in BAL cells removed 18 hours post instillation did not clearly follow any pattern previously identified, with the short (NT2) and entangled (NT3) CNT expressing a significantly higher level of DCFH oxidation compared to control cells, not seen with treatments of the long CNT sample. NT2 and NT3 both form 10µm aggregates, which may indicate that they could have similar effects *in vivo*; it is therefore possible that any effect we observed here is the normal and successful phagocytosis of these two CNT samples. Any effect from NT1 is time dependent (as seen in the *in vitro* experiments) and a long enough exposure period may not have been included in this study. Alternatively, the long CNT sample may have hindered the successful remove of cells during the lavage process.

Other factors examined in BAL fluid were neutrophil influx, and concentrations of LDH, total protein and GSH. With the 18-hour exposure period there were no increases in LDH, protein or antioxidant defence when particles were delivered in saline containing BSA. It has been shown that 3 and 15 days post exposure of short MWCNT instillation can induce an increase in LDH release and protein content in BAL fluid (Muller *et al.*, 2005), so possibly the time point employed in this study was not sufficient to demonstrate this behaviour.

There was, however, a clear neutrophil recruitment that took place during the 18-hour exposure to the long straight NT1; the study by Muller *et al.* (2005) also demonstrated a neutrophil influx during their longer exposures. Much of this

thesis involves the effect of particle exposures to monocytes and monocyte derived cells, therefore it is monocytic cell responses which are highlighted. Macrophages are considered to undergo considerable active endocytosis, neutrophils are not, neutrophils are often considered relatively passive (Lee *et al.*, 2003). However, when activated neutrophils are effective phagocytes, and to produce considerable ROS, and although site specific macrophages may be the first immune cells to encounter inhaled material, it is the neutrophils that accumulate much faster than monocytes at sites of inflammation (Dale *et al.*, 2008), and as shown here (Rothen-Rutishauser *et al.*, 2010), a clear influx of neutrophils does occur with the appearance of long MWCNT in the rat lung. It is therefore important to highlight a number of similarities and differences in the REDOX products formed by macrophages and neutrophils. Both neutrophils and macrophages are professional phagocytes (Lee *et al.*, 2003), therefore neutrophils engulf non-self material in much the same manner as was described in section 1.2 and 1.3 on macrophage phagocytosis (Hampton *et al.*, 1998).

As with macrophages, neutrophils also generate an oxidative burst during phagocytosis generating superoxide ($O_2^{\bullet-}$), through the action of a NADPH oxidase complex (Hampton *et al.*, 1998), also using the one electron donation from NADPH to O_2 (Lee *et al.*, 2003), this respiratory burst, however, is found to be far greater in neutrophils than in recruited monocytes (Dale *et al.*, 2008), and, indeed, neutrophils are known to express higher levels of NADPH oxidase than macrophages (Lee *et al.*, 2003). In the case of neutrophils, only small quantities of $O_2^{\bullet-}$ or its derivative, hydrogen peroxide (H_2O_2), are released during phagocytosis, however, considerable amounts are released within the phagosome and in response to cytokine stimulus (Hampton *et al.*, 1998). The conversion of $O_2^{\bullet-}$ into H_2O_2 will occur in exposures of both macrophages and neutrophils, and at high concentrations H_2O_2 is bactericidal; but H_2O_2 can give rise to potentially more destructive oxidants, such as hydroxyl radicals ($^{\bullet}OH$) or hypochlorous acid (HOCl). The formation and subsequent reduction of $O_2^{\bullet-}$ allows the formation of H_2O_2 by superoxide dismutase (Babior, 2000). In the presence of iron or copper this H_2O_2 may be converted into the highly reactive hydroxyl radicals ($OH^{\bullet}$), or, in neutrophils at least, the H_2O_2 may be further converted to hypochlorous acid (HOCl) by the action of myeloperoxidases (Babior, 2000, Winterbourn, 2002). This is because the formation of $^{\bullet}OH$ relies

heavily on Fenton chemistry and as neutrophils do not contain transition metals (Hampton *et al.*, 1998) $^{\bullet}OH$ formation is more likely to naturally occur during phagocytosis by macrophages; unless transition metals such as iron are available from another source, which is the case in these MWCNT exposures. In neutrophil exposures it is potentially most likely that more HOCl would be produced than $^{\bullet}OH$, as the myeloperoxidase enzyme in neutrophils consumes H_2O_2, with one outcome being HOCl. In fact, the pathway generating HOCl is considered one of the most bactericidal processes used by neutrophils. (Hampton *et al.*, 1998).

The toxicity of inhaled particles is thought to be partially attributed to the generation of ROS by both macrophages and neutrophils, with each type of phagocyte having a discretely different contribution (Aam and Fonnum, 2007). For example, peroxynitrite ($ONOO^-$) is considered attributable to the phagocyte induced inflammatory responses to many inhaled particles, such as DEP, asbestos, silica, and titanium dioxide (Ito *et al.*, 2000). This reactive compound can be formed in a number of reactions, which may be dependent of cell type. One method is through the combination of nitric oxide (NO) and $O_2^{\bullet-}$ (Al-Ali and Howarth, 1998, Ito *et al.*, 2000). NO generation is through the action of iNOS, using O_2 and NADPH, which, in humans at least, is shown predominately by macrophages in response to stress signals such as cytokines, or exposure to bacterial products such as LPS (Babior, 2000, Ito *et al.*, 2000); incidentally, in rodents NO produced by both macrophages and neutrophils is found to be substantial (Fialkow *et al.*, 2007). Although considered important in the function of macrophages, the NO reaction with $O_2^{\bullet-}$ forming $ONOO^-$ is not considered in neutrophil responses. Instead, the RNS $ONOO^-$ may be generated through the oxidation of nitrite by myeloperoxidase and HOCl (Hampton *et al.*, 1998).

As previously mentioned, it is plausible that the long NT1 CNT sample used here somewhat impeded the isolation of the cells undergoing oxidative stress, which would in part explain why there is a strong inflammatory response with no extraction of ROS producing cells. It has been demonstrated, albeit in the pleural cavity, that long CNT samples almost identical to NT1 are retained, while shorter fibres were cleared (Murphy *et al.*, 2011). The measure of other inflammatory responses has also been shown at very short exposure periods, starting at just six hours post instillation of 1.5mg/kg DWCNT into the rat lung.

Crouzier *et al.* (2010) have shown elevated markers such as leptin and IL-6, while no increase in TNF-α or IL-1 was measured, nor was there any evidence of ROS generation. The authors speculate that this could be due to the purity of their CNT sample, having a lack of metal impurities, or through the appropriation of ROS by the CNT (Crouzier *et al.*, 2010). After inhalation of short, high Fe (<1µm, 17wt%) SWCNT, for four consecutive days, an increase in PMN cells, LDH, TNF-α, IL-6, TGF-β and total protein was found only one day post exposure, and an increase in alveolar macrophages and total cell numbers seven days post exposure (Shvedova *et al.*, 2008a). A rapid and sustained oxidative response (10 minutes to 24 hours) has been demonstrated by Pulskamp *et al.* (2007b) *in vitro*. An alveolar epithelial cell line was exposed to CNT that contained relatively high levels of both metal impurities and amorphous carbons; the removal of both of these components also alleviated the oxidative potential of the CNT. However, with the removal of amorphous carbons but with metal impurities remaining, there was a slow but eventual ROS response. It therefore seems evident that amorphous carbons may be responsible for a rapid induction of ROS generation while metal impurities can produce a slower but possibly more sustained ROS response (Pulskamp *et al.*, 2007b).

The use of different suspension media used here has brought up the importance of using the most appropriate particle suspension medium for CNT toxicology studies. If factors are to be used to aid dispersal it is important to keep any dispersant biologically relevant. It is considered that once inhaled, particles within the alveolar will encounter various proteins and pulmonary surfactant, helping to aid their dispersion (Sager *et al.*, 2007). Sager *et al.* (2007) investigated dispersal effects using different relative media. Suspension medium alone resulted in considerable agglomeration, as did the use of protein or DPPC, while a combination of the two increased dispersion. The most effective dispersant used was BAL fluid, either from mouse or rat, which resulted in a far better dispersal of NP. *In vivo* and *in vitro* assessment of toxicity revealed that although particles displayed a level of toxicity in all suspension media, the effects were greater and seen at a lower dose when suspended in BAL fluid (Sager *et al.*, 2007). The use of BAL fluid in toxicological

studies is, however, not always economically feasible or appropriate, or experimentally comparable (Porter *et al.*, 2008). To alleviate these issues Porter *et al.* (2008) reported the use of a BAL fluid imitation consisting of a calcium and magnesium free buffer containing D-glucose, protein and DPPC additives. This suspension provided a far better dispersion of particles, including MWCNT, than the use of PBS alone. The use of DPPC in toxicological studies, however, should be questioned. Although DPPC has no inherent toxic effect itself, it may actually attenuate toxicity. This has previously been seen with the use of DPPC, which can cause the inhibition of ROS and TNF-α in a monocytic cell line stimulated with zymosan or phorbol-12-myristate-13-acetate (PMA) (Tonks *et al.*, 2001), and a reduction in the cytotoxicity of quartz on a macrophage cell line (Gao *et al.*, 2001). The use of 10% FCS in particle suspension media can also enhance particle dispersion, but may also reduce cytotoxicity (Davoren *et al.*, 2007). Incidentally, the inclusion of 5% FCS in this study did not demonstrate any such attenuation. Conversely, the use of dispersant additives may indirectly increase sample toxicity, as upon greater dispersal CNT samples may sequester medium constituents that are vital to healthy cell growth (Casey *et al.*, 2007, Casey *et al.*, 2008).

Variation to particle toxicity is often apparent with varied degrees of dispersion (Foucaud *et al.*, 2007, Shvedova *et al.*, 2005). The addition of BSA and DPPC in culture medium was used by Foucaud *et al.* (2007), where particle dispersal was improved with the inclusion of both additives, which led to greater ROS generation by 14nm carbon black particles. An increase in dispersion will cause an increased available surface area, therefore increasing surface reactivity which not only may induce a higher response (Oberdörster *et al.*, 2007), but may also allow NP to cross cell membranes (Oberdörster *et al.*, 2007) or translocate into the pleural space (Mercer *et al.*, 2010). It certainly is an important factor to consider when planning particle exposures, both *in vivo* and *in vitro*, and if we are to assess the intrinsic toxicity of CNT it is important to achieve suitable dispersions. Large aggregates have been shown to cause granuloma formation (Shvedova *et al.*, 2005), but this may not be a realistic response to respirable fibres, and has actually resulted in asphyxiation during instillation of too large aggregates (Warheit *et al.*, 2004). This study clearly demonstrates the importance of an aid to particle dispersion, with no

inflammatory or oxidative response found *in vivo* without the inclusion of a protein additive, in this case BSA; and a greater acute ROS signal in the cell-free system when CNT are suspended in solution containing both BSA and DPPC. So it is clear that the addition of protein and surfactants can increase CNT dispersal; however, suitable controls must be included to avoid any underestimation of CNT toxicity.

The use of 2'-7'-dichlorodihydrofluorescin diacetate (DCFH-DA) is a popular choice for the measure of ROS within a cell. Its action is through easy membrane penetration by diacetate, which is subsequently hydrolysed by intracellular esterases (or by controlling pH in the cell-free system), leaving DCFH, which upon contact with certain ROS forms the highly fluorescent 2'-7'-dichlorofluorescein (DCF) (Bilski *et al.*, 2002). Its first use was as a detector of hydrogen peroxide (Keston and Brandt, 1965) and it is now shown to be capable of giving a more universal view of oxidants present (Wang and Joseph, 1999). This is valuable as the specificity of ROS produced can be dependent on CNT composition and exposure period. Peroxynitrite ($ONOO^-$) can be generated in samples with a high metal content, as can a rapid and sustained generation of O_2^- in response to CNT samples with high metal and high amorphous carbon content; with the removal of amorphous carbon the generation of O_2^- is limited to 24-hour post exposure (Pulskamp *et al.*, 2007b).

The use of DCFH-DA here allowed accurate measurements of cell-free and BAL-cell ROS production; while the use of a similar alternative (5-6-carboxy 2',7'- dichlorodihydrofluorescein diacetate (carboxy-H_2DCFDA)) in the *in vitro* study was to aid cellular retention, and gave accurate measurements of oxidative signals within J774.A1 cells during exposure to CNT. The use of HRP, however, hindered or hid the ability of these CNT (NT1, NT2 and NT3) to produce ROS when it was included in the cell-free assay. With HRP absent there was a clear pattern of DCFH oxidation upon exposure to the entangled NT3, which was seen in all suspension media and nearly all time points. The inclusion of HRP resulted in a clear increase in DCF formation when comparing the two relative negative control populations. However, there appeared to be a dousing of the particle responses relative to medium-only cultures, with NT3 only significantly higher in one instance and NT1 and NT2 actually significantly

lower in a number of suspensions. The inclusion of HRP here was based on its ability – and actual necessity – to amplify the ROS signal from chemically inert particles (Foucaud *et al.*, 2007). It has certainly amplified the background signal, but this in turn has masked detection of any possible particle specific effect. It seems CNT do not need this amplification from HRP, and with possible interference, it probably should be left out of future experiments investigating CNT.

A number of compounds have been implicated in the control of DCFH oxidation including: hydrogen peroxide (H_2O_2), peroxynitrite ($ONOO^-$), hydroxyl radicals ($^{\bullet}OH$), iron and singlet oxygen ($O^{\bullet}$) (Bilski *et al.*, 2002, Myhre *et al.*, 2003, Possel *et al.*, 1997). However, each can be consequentially different and have need of different requirements for any reaction to occur. $ONOO^-$ is a potent oxidant formed from the nitric oxide (NO) and superoxide ($O_2^{\bullet-}$) generated by activated macrophages (Ischiropoulos *et al.*, 1992). Fe and $^{\bullet}OH$ have all been shown to substantially, rapidly and independently cause the oxidation of DCFH to DCF (Myhre *et al.*, 2003, Possel *et al.*, 1997). $ONOO^-$ was shown to be a very strong DCFH oxidation-inducing agent in a cell system, as was peroxyl radicals, through induction by 2,2'-Azobios (2-amidino-propane) dihydrochloride (AAPH) (Wang and Joseph, 1999). Independent DCFH oxidation does not occur on exposure to nitric oxide (NO), hypochlorous acid (HClO), or $O_2^{\bullet-}$ (Myhre *et al.*, 2003), and in a cellular system NO appeared to be only a weak oxidant of DCFH (Wang and Joseph, 1999). However, the carboxy-H_2DCFDA used in the *in vitro* analysis of ROS production by J774.A1 cells can be oxidised by $O_2^{\bullet-}$, adding to the importance of using carboxy-H_2DCFDA instead of DCFH-DA in the *in vitro* experiments. $^{\bullet}OH$ has also been shown to mediate DCFH oxidation through Fe, in the presence of peroxides (Myhre *et al.*, 2003). These are all factors that are likely to impact on the DCFH oxidation seen in this study when HRP is not present in the assay.

In a cell system (Wang and Joseph, 1999), or in the presence of HRP (or other cellular peroxidases), H_2O_2 will oxidise DCFH (Myhre *et al.*, 2003, Rota *et al.*, 1999a), which is likely to be one explanation for the amplification seen with inclusion of HRP. However, the problems arise due to the fact that HRP will alone oxidise DCFH (Myhre *et al.*, 2003, Rota *et al.*, 1999a); this is very likely to

be responsible for the high background effects seen. There are also other issues that may arise even in the absence of HRP, including the possible attenuation by certain ROS, as $O^{\bullet}$ cannot independently generate DCF from DCFH, but can in fact lower this reaction when directly exposed to DCFH – the only influence of $O^{\bullet}$ in causing DCFH oxidation seems to be circuitously through cellular singlet oxygen substrates (Bilski *et al.*, 2002); or a chain reaction may occur resulting in continued DCFH oxidation with no participation from particles at all. H_2O_2 is shown to be generated during the cleavage of the diacetate compound from DCFH-DA (Rota *et al.*, 1999a), and DCFH oxidation through the action of HRP alone can cause the production of $O_2^{\bullet-}$ and $^{\bullet}OH$ (Rota *et al.*, 1999a). This initiation with no particle interference can all contribute to a chain reaction causing continued DCFH oxidation, since in aerobic conditions, in the presence of an electron donor such as GSH, and visible light or intracellular enzymes such as peroxidases, the oxidised DCF can become reduced and $O_2^{\bullet-}$ can be generated; this can in turn go on to form H_2O_2, and DCFH oxidation will continue irrespective of particle induced ROS production (Marchesi *et al.*, 1999, Rota *et al.*, 1999b).

4.3 Section II – particle panel B

4.3.1 Aim

To further explore the role and extent of ROS production seen in section I, particle panel B was used to ascertain if MWCNT exposure can initiate the gene expression of antioxidant defence mechanisms, and if the ROS produced by MWCNT and the ensuing oxidative stress is sufficient to cause oxidative damage to DNA.

4.3.2 Results

After a four-hour exposure to particle panel B MM6 cells were assessed for gene expression of the antioxidant haemoxygenase-1 (figure 4.3). There appeared to be a slight increase in HO-1 gene expression in response to all treatments, only one, however, was significant. The treatment of MM6 cells with 17.5µg/cm^2 CNTB caused a 1.4-fold increase in HO-1 gene expression ($p<0.05$) (figure 4.3 B). Other MWCNT treatments also generated this level of gene expression or higher. A treatment of 4.2µg/cm^2 CNTB induced a border line significant increase in HO-1 expression ($p=0.052$), and all concentrations of CNTI had a p-value = 0.1.

The later exposure time period of 48 hours was used to assess if oxidative DNA damage had occurred in MM6 cells after exposure to particle panel B, with concentrations ranged from 4.2–17.5µg/cm^2. This was assessed using the gene expression of OGG1 (figure 4.4). Elevations in gene expression were observed with treatments of LFA, CNTI, CNTB and CNTD; none, however, were significantly higher than control cells.

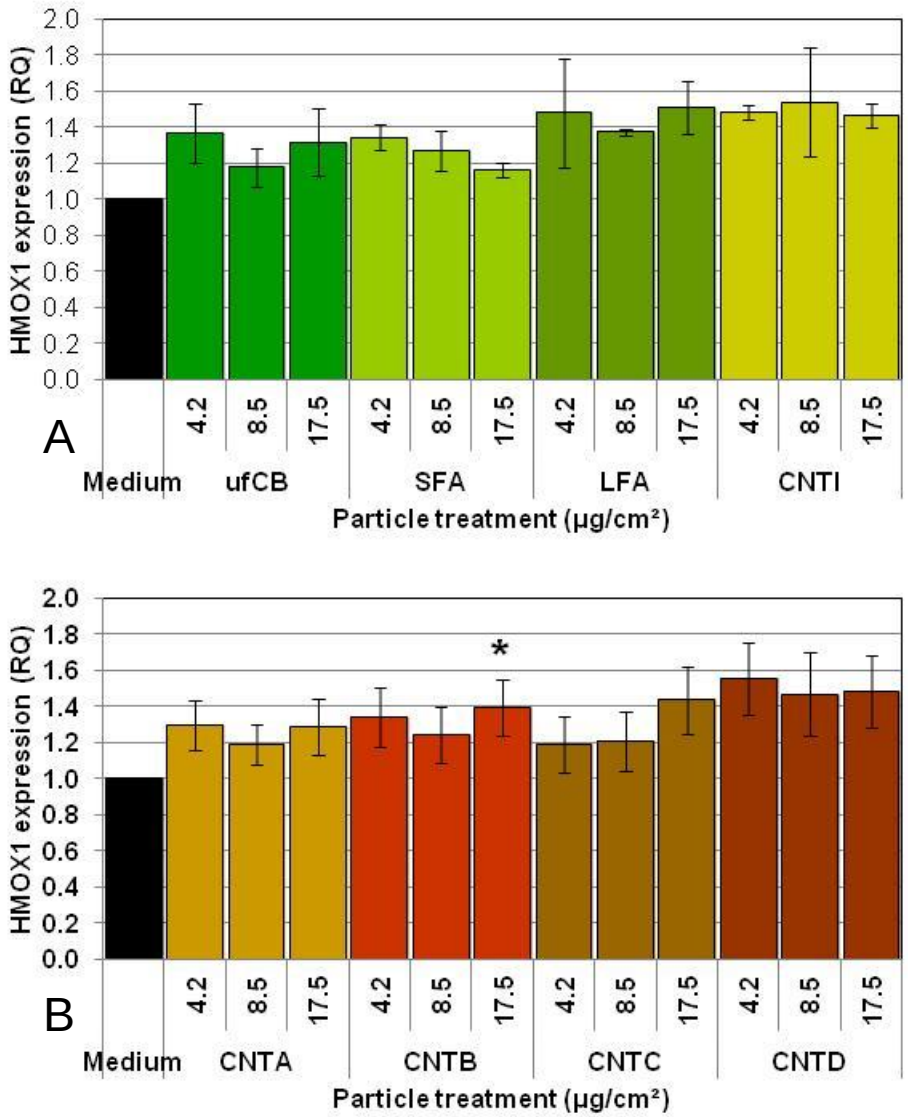

Figure 4.3 The effect of particle panel B on HO-1 mRNA expression in MM6 cells. (A) In response to ufCB, SFA, LFA and CNTI, and (B) in response to CNTA, CNTB, CNTC and CNTD. The mean fold change in expression of HO-1 for each treatment was calculated using the $2^{-\Delta\Delta Ct}$ method and results are shown as mean ±SEM (n=3). Statistical significance is shown by *=p<0.05.

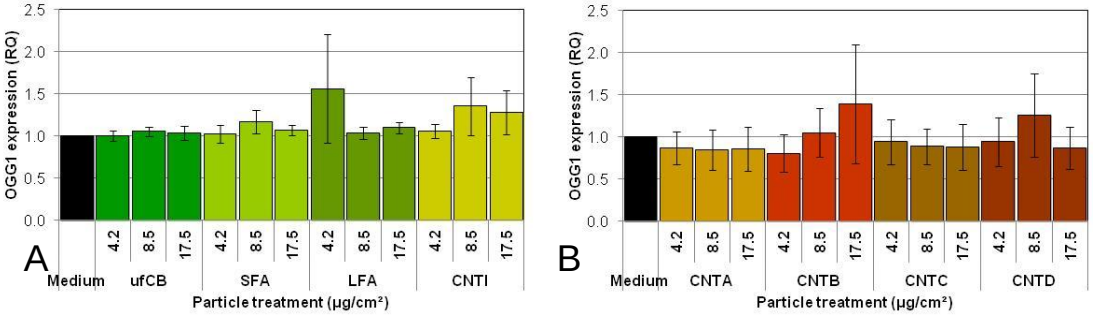

Figure 4.4 The effect of particle panel B on OGG1 mRNA expression in MM6 cells. (A) In response to ufCB, SFA, LFA and CNTI, and (B) in response to CNTA, CNTB, CNTC and CNTD. The mean fold change in expression of OGG1 for each treatment was calculated using the $2^{-\Delta\Delta Ct}$ method and results are shown as mean ±SEM (n=3).

4.3.3 Discussion

As discussed in chapter one, the cause of much particle-induced toxicity and genotoxicity may be attributed to oxidative stress and oxidative-induced DNA damage. In section I of this chapter the potential for CNT to generate ROS and potentially induce oxidative stress was addressed and confirmed. Here, in section II, the gene expression of HO-1 and OGG1 in response to MWCNT and reference materials was evaluated, to ascertain the cellular response to an increase in ROS, and to determine if this particle panel has the potential to cause oxidative DNA damage.

There are a number of antioxidant defensive mechanisms that were discussed in chapter one. One such defensive system involves the enzyme HO-1 (Bräuner *et al.*, 2007), which is a stress-induced enzyme used in the catabolism of haem, and is expressed in association with both oxidative stress and inflammation (Orozco *et al.*, 2007). HO-1 is expressed potentially in response to redox activity of glutathione (Kutty *et al.*, 1994). Glutathione has been shown to deplete in numerous cell types, in response to NPCB (Stone *et al.*, 1998), quantum dots (Clift *et al.*, 2010b) and NP polystyrene (Clift *et al.*, 2010a). Here it has been demonstrated that MWCNT can induce the upregulation of the antioxidant HO-1; in this case in response to the short MWCNT sample, CNTB. This sample has relatively low iron content; therefore redox activity of metal contaminants is unlikely to be responsible for this upregulation. CNTB has a particularly high sample purity which encourages its agglomeration into larger forms. Incidentally, the CNT samples greater in length (CNTC and CNTD), or higher in potential hydrophobicity (CNTI), actually display a slightly greater induction of HO-1 expression, as does LFA, these data, however, were not significant.

The *in vitro* exposure of other particles such as diesel exhaust NP has been shown to upregulate HO-1 expression in association with O_2^- generation in endothelial cells (Folkmann *et al.*, 2009); titanium dioxide can induce activation of antioxidant defence mechanisms that is also associated with oxidative DNA damage (Jugan *et al.*, 2011), and long MWCNT similar to those used here are shown to increase HO-1 expression in THP-1 cells (Brown *et al.*, 2010).

If antioxidant defences are not successful in modulating oxidant levels, one consequence may be oxidative-induced DNA mutations and lesions, which appear in numerous tumours, and can include 7,8-dihydro-8-oxoguanine (8-

oxoG), 8-hydroxydeoxyguanosine (8-OHdG), and 8-Oxo-7,8-dihydro-2´-deoxyguanosine (8-oxodG) (Folkmann *et al.*, 2009, Potts *et al.*, 2003). A common repair mechanism of this form of damage, and therefore a good marker for oxidative DNA damage is through the work of DNA glycosylase enzymes, particularly 8-oxoguanine DNA glycosylase (OGG1) (Bräuner *et al.*, 2007, Potts *et al.*, 2003). Therefore, the upregulation of OGG1 can be indicative of oxidant induced DNA that has undergone attempted repair, and down-regulation may contribute to carcinogenesis (Potts *et al.*, 2003).

These lesions are found in response to various materials such as cadmium (Potts *et al.*, 2003) and asbestos (Unfried *et al.*, 2002), and *in vivo* SWCNT have been shown to cause oxidative DNA damage, in the form of an increase in 8-oxodG mutations. This, however, was not associated with the expression of either HO-1 or of OGG1 (Folkmann *et al.*, 2009). Diesel exhaust particles are also shown to cause DNA damage in the form of 8-oxodG and 8-hydroxyguanine (8-OH-Gua), and in this case the DNA mutation is associated with both an increase in antioxidant defences (HO-1) and DNA repair mechanisms (OGG1) (Risom *et al.*, 2003a, Tsurudome *et al.*, 1999), and at times with tumour development (Iwai *et al.*, 2000). The exposure of healthy participants to ambient ultrafine particles was shown to cause significant DNA damage in peripheral blood monocytes, with no measurable increases in HO-1 or OGG1 (Bräuner *et al.*, 2007). While respirable quartz was shown to induce generation of ROS but not in association with oxidative DNA damage, in the form of 8-OHdG (Albrecht *et al.*, 2005).

There was no increased expression of OGG1 in response to any of the particles investigated here; therefore the upregulation of HO-1 that was demonstrated is potentially not in association with damage to DNA, at least not in response to the exposure conditions used here. However, the time point used here for OGG1 mRNA expression may not have been the most suitable, therefore no great conclusions can be made concerning oxidative DNA damage in response to these particles. It appears that OGG1 is continually expressed in all mammalian tissues, but is enhanced significantly in response to oxidant stimuli (Dhénaut *et al.*, 2000), this, however, may be very early in the signalling response (Dhénaut *et al.*, 2000), with it being shown to be expressed after four hours in response to MWCNT (Zhu *et al.*, 2007) for up to only six hours in

response to X-ray irradiation (Risom *et al.*, 2003b), but has also been shown to progressively increase for up to 27 hours in response to crocidolite (Kim *et al.*, 2001).

CNT-induced oxidative DNA damage is not well documented but has been shown to occur, including the previously mentioned study by Folkmann *et al.* (2009). Zhu *et al.* (2007) have also shown that MWCNT can cause the DNA damage and expression of OGG1 in embryonic stem cells. However, DNA damage by CNT is consistently shown by different methods of detection than those used here, including DNA strand breaks detected by the comet assay and micronuclei formation (Jacobsen *et al.*, 2009, Kisin *et al.*, 2007, Lindberg *et al.*, 2009, Migliore *et al.*, 2010, Muller *et al.*, 2008a).

It is clear during this investigation that MWCNT can consistently cause the generation of ROS in many circumstances, and in many morphological and compositional forms, and that this production of ROS may lead to the activation of antioxidant defence mechanisms. However, the extent of oxidative stress initiated in this study was not enough to elicit oxidative DNA damage, or defensive mechanisms were accomplished in their protective roles.

Chapter 5

Viability, cytokine responses and cell signalling

5.1 Introduction

5.1.1 Outline

The panel of materials exclusively used from this point onwards consists of nanoparticle CB, two asbestos samples: small fibre amosite (SFA) and long fibre amosite (LFA), and five multi-walled carbon nanotubes. CNTI is industrially sourced, and CNT-A/B/C/D were produced in a manner to allow the comparison of certain parameters, including length, iron content, and sample purity. The details of these characteristics can be viewed in detail in chapter 3, and are briefly tabulated in chapter 2; but here the MWCNT have been ranked by physicochemical characteristic parameters:

- Length: CNTC = CNTD > CNTI = CNTA = CNTB
- Crystallinity: CNTI > CNTD > CNTB > CNTA > CNTC
- Iron content – dry: CNTA > CNTB > CNTC > CNTI > CNTD
- Iron release – neutral pH: CNTI > CNTC > CNTD > CNTA > CNTB
- Iron release – acidic pH: CNTA > CNTC > CNTI > CNTD > CNTB

SFA was shown to leach iron at levels equivalent to CNTA, LFA equivalent to CNTC, and NPCB only slightly greater than CNTB and CNTD. By length, LFA was designated to be equivalent to CNTC and CNTD, while SFA and nanoparticle CB can be classed as smaller than all other particles.

5.1.2 Aims and Hypotheses

The link between the potential pathogenicity of asbestos, NPCB, and CNT and the induction of pro-inflammatory and pro-fibrotic conditions, and cytotoxicity has been described in chapter one. The aim of the study described in this chapter is to ascertain *(1)* the extent of MWCNT cytotoxicity and inflammatory potential, *(2)* how this relates to known pathogenic materials, and *(3)* what characteristics of MWCNT are responsible for the cytotoxicity and inflammatory potential. This work will focus on macrophages as they are likely to be the first defensive component that these particles would encounter once inhaled, and when doing so would instigate an inflammatory response, with potential ensuing complications.

Based upon the published literature outlined in chapter 1, we hypothesise that particle characteristics influence their ability to induce an inflammatory

response, including characteristics of increased length and aspect ratio due to their ability to cause physical stress and frustrated phagocytosis. This would indicate that the largest inflammatory and cytotoxic reaction would be from CNTC, CNTD and LFA, which are likely to demonstrate a sustained, chronic response. Within this group the redox potential of the high iron release CNTC is likely to exacerbate its effects, making it relatively toxic. The smaller/shorter particles may have an early inflammatory response, but are likely to diminish over time as it is believed that the phagocytic cells used here would successfully phagocytose these shorter particles; any subsequent differences would be seen by a decrease in iron content and/or an increase in crystallinity reducing toxic effects.

5.1.2 Mechanisms of cell death

The mechanisms that cells undergo that may result in their death can be divided into three clear, but transposable, processes: apoptosis, necrosis and autophagy (Mevorach *et al.*, 2010).

The classical form of programmed cell death is apoptosis, and is an essential process in tissue development, tissue regeneration and defence against pathogens. Basically apoptosis is a method for cell population control removing damaged, infected, or old cells without causing an inflammatory response (De Saint-Hubert *et al.*, 2009, Elmore, 2007). However, when dysregulated, apoptosis has the potential for considerable pathogenicity, including autoimmune disease and cancer (Elmore, 2007). Apoptosis may be initiated by different internal or external factors (De Saint-Hubert *et al.*, 2009, Mevorach *et al.*, 2010), and different stimuli will cause the induction of different apoptotic pathways (Mevorach *et al.*, 2010), using slightly different intracellular signalling pathways (Elmore, 2007). This may result in the conclusion of cell death with slightly different patterns; nevertheless, apoptosis is programmed cell death that can be exemplified by certain morphological modifications and observations including pyknosis, followed by fragmentation of the nucleus, and membrane blebbing leading to release of apoptotic bodies (De Saint-Hubert *et al.*, 2009, Elmore, 2007, Mevorach *et al.*, 2010). These bodies can be recognised and consumed by phagocytes, preventing unwanted inflammatory conditions (Zimmermann *et al.*, 2001). Apoptosis is predominately an active process and

often energy-dependent (Mevorach *et al.*, 2010), relying on a complicated succession of intracellular signalling, with early activation of caspase enzymes (De Saint-Hubert *et al.*, 2009, Elmore, 2007). Necrosis, on the other hand, is primarily neither active or energy dependent; the process leading up to the actual spilling of intracellular components is termed oncosis and may in some cases be an active process, but necrosis is not. During periods of duress a cell may enter a state of autophagy, where it actively digests elements of itself in the pursuit of energy. This may go unnoticed and a full recovery is made when the period of duress is over; alternately it may reach an irreversible state and enter programmed cell death (Mevorach *et al.*, 2010).

Necrosis is less common than apoptosis (Raffray and Cohen, 1997), and is often due to direct toxic or physical insult to the cell (Edinger and Thompson, 2004, Elmore, 2007) causing rapid loss of homeostasis (Raffray and Cohen, 1997), resulting in immediate lysis of the cell. Necrosis can, however, also be through programmed cell death (Elmore, 2007), and can be initiated through the exposure to numerous infections, removal of cytokines or energy sources, such as in cases of ischaemia, or exposure to certain cytokines and ROS during inflammatory responses (Proskuryakov *et al.*, 2003). Necrosis is typified by certain morphological changes. These changes differ from apoptosis and include karyolysis: instead of chromatin condensing, cell swelling instead of shrinking, and membrane impairment instead of blebbing and production of apoptotic bodies, resulting in permeability and the release of intracellular components (Elmore, 2007, Mevorach *et al.*, 2010, Proskuryakov *et al.*, 2003). The release of these components can cause direct injury to surrounding areas but also induce the release of pro-inflammatory cytokines and activation of T-cells and dendritic cells, meaning that necrosis stimulates a much greater inflammatory response than apoptosis (Proskuryakov *et al.*, 2003). Necrosis is as a result of extreme abrupt injury and is less common than apoptosis, which is typified by a programmed cell death, and is associated with a number of disease progressions (Raffray and Cohen, 1997).

The transformation of apoptosis to necrosis can occur from a number of circumstances. One function, or outcome, of apoptotic cell signalling is to allow the early recognition of these cells by phagocytes (Mevorach *et al.*, 2010), through the appearance of phosphatidylserine on the cell surface (De Saint-

Hubert *et al.*, 2009). Upon recognition phagocytes will engulf, destroy and remove them from the system, to avoid unwanted release of cellular components. However, in the absence of phagocytic cells, or the impairment or over-exertion of the immune system, these apoptotic cells will not be processed and will eventually enter secondary necrosis and release their components (Mevorach *et al.*, 2010). In addition, without the necessary ATP (De Saint-Hubert *et al.*, 2009, Elmore, 2007) or caspase cascade (Elmore, 2007) needed for the active apoptotic process, cells will also quickly enter secondary necrosis, spilling their components, instigating an inflammatory response (De Saint-Hubert *et al.*, 2009). The extent of the stimulus inducing cell death can also determine whether a cell undergoes apoptosis or necrosis (Elmore, 2007).

5.1.3 Fibre and NP cytotoxicity

The evidence of cytotoxicity elicited by NP, CNT and other fibre-like material is clear and cannot be characterised by any one aspect. However fibre cytotoxicity is often epitomised by the "fibre paradigm", which relates the toxicity of a fibre to its length and durability in the lungs (Donaldson and Tran, 2004), and is exemplified by many forms of asbestos. The *in vivo* cytotoxicity of CNT and other fibres, including asbestos, is discussed in detail in sections 1.4 and 1.5. Here, due to the *in vitro* design of this study, most cytotoxicity data will be related to *in vitro* studies.

In the literature, particle exposure to other cell types, at doses relevant to this study, is shown to have varying degrees of cytotoxicity, and is not always complementary. Glass wool and rock wool will, for example, cause no discernable mortality in mesothelial cells and fibroblasts with exposures of up to 48 hours and 25µg/cm^2 (Cardinali *et al.*, 2006); while on other occasions 24-hour exposure of 20µg/cm^2 glass wool is shown to be considerably toxic to mesothelial cells (Pelin *et al.*, 1992). Exposure of peripheral blood monocyte-derived macrophage (MDM) to concentrations, similar to this study, of SWCNT (length unknown) has been shown to cause no cytotoxicity, while a reference material of graphite is shown to cause 25% cell death after 48 hours at the same concentrations (Fiorito *et al.*, 2006). The particularly aggressive crocidolite asbestos will cause iron-induced oxidative stimulation of apoptosis at only 5µg/cm^2 on rat pleural mesothelial cells (Jimenez *et al.*, 1997), and 11–

15% cell death with 24-hour exposure of 5–25µg/cm^2 to fibroblast and mesothelial cell lines (Cardinali *et al.*, 2006). On exposure to A549 epithelial cells, crocidolite at 0.78 and 1.56 µg/cm^2 is shown to reduce mitochondrial function by approximately 35% and 60%, respectively, after 3 days; this response is approximately matched by MWCNT (<15µm in length), which dose-dependently reduced mitochondrial function from 30–45% at 0.33, 0.65, 1.3, and 2.6µg/cm^2 (Thurnherr *et al.*, 2010). Measured by enhanced membrane permeability and by reduced cellular respiration it has been shown that crocidolite asbestos will reduce J774A.1 cell viability at 24-, 48- and 72 hours, with treatments of 1, 11, and 21µg/cm^2 (Cardile *et al.*, 2004). Non-dividing alveolar macrophages are induced to produce both TNF-α and IL-1β with 24- and 48-hour exposure of 25µg/ml crocidolite but not chrysotile; however, neither were shown to reduce viable cell numbers in comparison to untreated cells, during the 14 day exposure periods, considerably more by chrysotile (Mongan *et al.*, 2000). Hirano et al. (2010) have shown that short MWCNT display substantially higher cytotoxicity to bronchial epithelial cells *in vitro* than crocidolite asbestos; the IC_{50} of crocidolite was only reached with exposure to 678µg/ml while only 12µg/ml MWCNT was needed (incidently, this dose was considerably reduced with a reduction in cell density). Amosite asbestos (length unknown) has no Met5A cytotoxicity after 4-hour treatments of up to 100µg/cm^2 (Kinnula *et al.*, 1994). At much lower doses than those used here (maximum of 0.2µg/ml) Magrez *et al.* (2006) found that MWCNT cytotoxicity was substantially lower than that of carbon nanofibres and carbon nanoparticles of much lower aspect ratios, when exposed to lung epithelial cells. However, the lengths of MWCNT were still considerably lower than those needed to inhibit effective phagocytosis. Exposure of a MWCNT sample similar to the CNTI used here is shown to elicit a slight reduction of fibroblast-like cells with concentrations up to 100µg/ml, with more significant cell death when exposure dose is increased up to 400µg/ml; this, however, is dwarfed by the cytotoxicity observed in response to chrysotile asbestos, which appears to reduce viability by almost 100% with only 10µg/ml exposure (Asakura *et al.*, 2010). While MWCNT aggregates are shown to elicit greater or at least relevant cytotoxicity to that of both chrysotile and crocidolite asbestos in lung epithelial cells *in vitro*, measured as mitochondrial function (Tabet *et al.*, 2009), no response was found with exposure of nanoparticle CB at 100µg/ml, even though it was internalised

(Tabet *et al.*, 2009). Exposure of A549 cells to short MWCNT (0.3–2μm) is not seen to cause much cell death by membrane impairment or mitochondrial function at conditions equivalent to the data presented in this chapter (Srivastava *et al.*, 2010).

This concludes much of the *in vitro* assessment of CNT cytotoxicity consisting of epithelial, mesothelial, and fibroblast cell assessment. Where CNT are found to be often potentially as cytotoxic as the various asbestos samples they have been compared to, and certainly more cytotoxic than material such as nanoparticle CB, with length-dependent toxicity often highlighted. The length dependent effects of SWCNT has also been investigated on the nervous system, where long SWCNT are shown to cause greater cytotoxicity than short SWCNT (Wang *et al.*, 2010a).

This study, however, assesses macrophage cell lines: although the first likely contact upon inhalation would be epithelial cells, the first defensive contact would be with alveolar macrophages, and immune cells are shown to be more sensitive than fibroblasts or keratinocytes to CNT exposure (Hu *et al.*, 2010). SWCNT (100μm in length) have been shown to elicit a strong cytotoxic response on THP-1 cells at 6.25 and 7.8μg/cm^2, with viability reduced by up to 30%, with a greater response observed in exposure to the much longer carbon fibre. Incidentally, this is dependent on cell density, in that a decrease in particle response is proportional to an increase in cell density (Kalbacova *et al.*, 2006). Exposure of the J774A.1 macrophage cell line to MWCNT with varying length (3–30μm) also displays considerable cytotoxicity. The IC_{50} after 24 and 32 hours was shown to be 26μg/ml and 22μg/ml, respectively (Hirano *et al.*, 2008). Much smaller CNT (220nm and 825nm in length) are taken up by macrophages; this is shown to induce an acute but controlled inflammatory response, but it was not shown to be cytotoxic *in vitro* or *in vivo* at the low doses used by Sato *et al.* (2005). In a study using two MWCNT that differ in iron content and both likely to cause frustrated phagocytosis, and therefore were similar to CNTC and CNTD used in this study, human monocyte-derived macrophages (HMM) were shown to dose-dependently decrease in viability, mainly by necrosis, in response to 0–20μg/ml of both pristine and purified MWCNT during a 4-day exposure (Cheng *et al.*, 2009). Incidentally, exposures of HMM (Cheng *et al.*, 2009) and A549 cell (Karlsson *et al.*, 2008) have revealed no such cytotoxic

effects in response to free iron oxides. Additionally, A549 epithelial cells are also shown to have no reduced viability in response to SWCNT exposure, irrespective of metal contaminant (Pulskamp *et al.*, 2007b). Kim *et al.* (2010b) also demonstrated that iron contaminants have little influence on MWCNT cytotoxicity; human embryonic stem cells were exposed to high aspect ratio MWCNT, low aspect ratio MWCNT, and iron oxide. Both MWCNT samples consistently caused a reduction in viability after 24-, 48-, and 72-hour exposures, in a dose-dependent fashion using 12.5-200µg/ml, with the high aspect ratio MWCNT often demonstrating a greater cytotoxicity than the low aspect ratio. Iron oxide displayed no such cytotoxicity (Kim *et al.*, 2010b).

The studies described above collectively suggest the most important factor in CNT toxicity is length, and that their toxicity is greater than that of popular reference materials. However, not all the literature coincides with this theory. Sometimes shorter length induces the greater response – SWCNT of length 1µm display substantial cytotoxicity on isolated alveolar macrophages, with over 20% reduced viability in response to 1.41µg/cm^2, increasing dose-dependently to 60% at 28.25µg/cm^2; this was greater than both C_{60}, and MWCNT (0.5-40µm) (Jia *et al.*, 2005). Aggregated MWCNT, nanoparticle CB, and chrysotile asbestos have been shown to elicit comparable levels of cell death in RAW 264.7, THP-1, and A549 cell lines, with significant death at concentrations as little as 5µg/ml for 48 hours (Soto *et al.*, 2008). Toxicity may be discernible by composition and not length, for example, *in vitro*, alveolar macrophages display slight cytotoxicity to pristine SWCNT; this response is lost with removal of metal contaminants, while nanoparticle CB is shown to cause considerable cell death (Pulskamp *et al.*, 2007a), indicating again the possible detrimental impact of iron and amorphous carbon content within some CNT samples. Diameter and not length may prove significant, for example, it was observed that MWCNT obtain entry into HMM cells by active and passive means, with 4-hour and 4-day exposures. They were found within vacuoles, free within the cytoplasm, and inserted into the nucleus and through the cell plasma membrane (Cheng *et al.*, 2009), with implications of translocation dependent on diameter. At similar doses SWCNT induced cell death in HMM cells (Porter *et al.*, 2007b). The SWCNT were also seen to translocate and localise within the cell's nucleus and the authors raised the issue of diameter, stating the small width would allow

easy translocation into and within the cell's constituents, raising concern for toxicity (Porter *et al.*, 2007b).

5.1.4 Beneficial and detrimental cytokine responses

5.1.4.1 Inflammation

The induction of pro-inflammatory conditions is a vital defensive mechanism, which is used for the removal of foreign material, organic or inorganic, and subsequent essential tissue repair (Driscoll *et al.*, 1997). An inflammatory response to foreign material will include the release of chemical messengers, ROS, and an influx and activation of leukocytes (Driscoll *et al.*, 1997). IL-8 is specifically responsible for neutrophil and lymphocyte recruitment and MCP-1 is primarily responsible for recruitment of monocytic cells (Driscoll *et al.*, 1997). Activated leukocytes are further stimulated into secreting pro-inflammatory cytokines such as TNF-α, IL-1, IL-6, and IL-8 (Baud and Karin, 2001, Gretzer *et al.*, 2003, Pfeffer, 2003). TNF-α is well-established and extensively reviewed (Baud and Karin, 2001, Pfeffer, 2003) as an important and often initiating factor for an inflammatory response, with its control over inflammation being determined by its ability to either induce apoptosis or inflammation (Baud and Karin, 2001). Release of TNF-α from alveolar macrophages is responsible for recruitment of other leukocytes, and secretion is evident on exposure to both inhaled particles and asbestos fibres (Driscoll *et al.*, 1997). Incidentally, phospholipids present in lung surfactant may help to modulate any occurring inflammatory response and actually prevent TNF-α release (Morris *et al.*, 2000).

If allowed or encouraged to continue or become severe, the results of inflammation may be far from supportive (Driscoll *et al.*, 1997), and can have quite severe consequences. Therefore, for an inflammatory response to be effective it needs to be controlled and limited, so release of anti-inflammatory mediators is needed. When stimulated by IL-4, macrophages enter their alternative activation, into M2 cells, and secrete IL-10 (Tan *et al.*, 2006), as do other recruited leukocytes (Gretzer *et al.*, 2003), to encourage tissue repair without an enhanced inflammatory response (Tan *et al.*, 2006). When secreted IL-10 is shown to significantly subdue an inflammatory response by inhibition of pro-inflammatory cytokines and chemokines (Shanley *et al.*, 2000). The next

stage would be the repair of any damaged tissue. In this process TGF-β plays a particular role in tissue repair after injury (Kloen *et al.*, 1997).

5.1.4.2 Fibrosis

Pulmonary fibrosis is acknowledged as one possible succession to chronic pulmonary inflammation (Coker and Laurent, 1998). With tissue injury and inflammation, there will undoubtedly be an initiation of pro-fibrotic conditions to ensure tissue repair, with the release of cytokines and growth factors such as IL-1, TNF-α, PDGF, IFN-γ, and TGF-β from macrophages, lymphocytes, and parenchymal cells, which at this stage will function as anti-inflammatory and pro-fibrotic mediators (Mangum *et al.*, 2006, Shaw, 1991, Shvedova *et al.*, 2008b, Szpaderska *et al.*, 2003). The express purpose of these mediators is tissue repair, and will cause fibrosis through the synthesis of numerous extracellular matrix proteins (such as collagen), down-regulation of matrix degradation enzymes (Branton and Kopp, 1999, Coker and Laurent, 1998, Sime *et al.*, 1997), increased activation and proliferation of fibroblasts (Gauldie *et al.*, 1993, Shaw, 1991, Sime *et al.*, 1997). Pathogenically this process is implicated in the formation of fibrotic plaques (Branton and Kopp, 1999), pathogenic pulmonary fibrosis in both the lungs and pleura (Coker and Laurent, 1998, Sime *et al.*, 1997), and is associated with idiopathic pulmonary fibrosis (IPF) through alveolar macrophage secreted TGF-β (Broekelmann *et al.*, 1991), and bronchopulmonary dysplasia (BPD) (Kwong *et al.*, 2006). For a reduction in these pro-fibrotic and scarring conditions there would usually be a down-regulation of macrophage activity by IL-10 (Szpaderska *et al.*, 2003). Particularly important in the formation of fibrotic lesions is the generation of TGF-β, PDGF, and GM-CSF (Gauldie *et al.*, 1993), and there is evidence that TGF-β-induced pathogenicity is reliant on TGF-β secretion by alveolar macrophages (Murray *et al.*, 2011). There is also evidence implicating the role of the chemoattractant MCP-1 in pulmonary fibrosis, where it is likely to encourage the infiltration and accumulation of macrophages within the lungs (Antoniades *et al.*, 1992, Hasegawa *et al.*, 1999). High levels of MCP-1 are found to be present in BAL fluid obtained during cases of pulmonary fibrosis (Emad and Emad, 2007), and a correlation between high serum levels of MCP-1 and pulmonary fibrosis has been identified (Hasegawa *et al.*, 1999).

An eventual outcome of a continued fibrotic and inflammatory response is the development of tumours. The association of MCP-1 induced macrophage infiltration is found with many tumours, including those of the ovaries, prostate, breasts and lungs (Arenberg *et al.*, 2000, Ghilardi *et al.*, 2005, Lu *et al.*, 2006, Negus *et al.*, 1995); however, the development of these tumours is a complex procedure, but for further relevance to this study the link between the production of many cytokines during an inflammatory response and tumourigenesis can be viewed in reports by Germano *et al.* (2008) and Lin and Karin (2007). The main cytokines highlighted by these articles are TNF-α, IL-1, IL-6, IL-10 and TGF-β (Germano *et al.*, 2008, Lin and Karin, 2007), with molecules such as IL-1, PDGF, and VEGF being involved in cancer- associated angiogenesis (Germano *et al.*, 2008).

5.1.4.3 Angiogenesis

For tumour growth to be successful there is the need for growth of new blood vessels; angiogenesis. For this to occur there are a number of steps involved which require considerable communication. Basement membrane must be degraded, cells must migrate, proliferate, reform, and reassembly of matrix, and assembly of lumen must all occur before blood flow can begin (Ma *et al.*, 2007). The abundance of VEGF in human malignant pleural mesotheliomas is associated with a reduction in patient survival rate, which is hypothesised to be due to VEGF angiogenic properties (Cacciotti *et al.*, 2002). During angiogenesis VEGF plays a role in cell proliferation and migration for integration in lumen formation (Ma *et al.*, 2007). TGF-β is a growth factor for cell differentiation found to be prevalent in cancers, and implicated in tumourigenesis (Kloen *et al.*, 1997, Marzo *et al.*, 1997); its importance in blood vessel growth has been demonstrated in embryonic angiogenic studies (Ma *et al.*, 2007), and blood vessel growth in tumours by its prevalence in small blood vessels supplying osteosarcomas (Kloen *et al.*, 1997). TGF-β stimulates the secretion of other angiogenic mediators, including VEGF (Alfranca *et al.*, 2008, Lee *et al.*, 2002, Ma *et al.*, 2007), and additionally helps to stabilise endothelial cell growth, anchor vessels, and encourages communication between vessel component cells (endothelial and smooth muscle cells) (Ma *et al.*, 2007). VEGF (Cacciotti *et al.*, 2002, Ferrara and Davis-Smyth, 1997) and TGF-β (Marzo *et al.*, 1997) are

found to be prevalent in pleural malignancies and other tumours. MCP-1 plays a crucial role during an inflammatory reaction through the recruitment of monocytes and leukocytes, but is also found to independently encourage angiogenesis through recruitment, migration and proliferation of endothelial cells, and is also found to strengthen the effects of VEGF, and collaborates with TGF-β in gathering endothelial and smooth muscle cells at angiogenic sites (Ma *et al.*, 2007).

5.1.4.4 Fibre and NP mediated cytokine responses and cell signalling

The inflammatory response to inhaled pathogenic particles and fibres is often typified by certain regulatory mediators, including TNF-α, IL-8, MIP-2 (the rat homologue of IL-8), and MCP-1, all of which are released from alveolar macrophages and epithelial cells (Driscoll *et al.*, 1997). This response is often associated with the activation of certain intracellular signalling molecules and transcription factors. Nuclear factor-kappa B (NF-κB) and activator protein-1 (AP-1) are often key and may be activated through a number of stimuli including oxidative and physical stress, causing the expression of pro-inflammatory genes and subsequent release of pro-inflammatory cytokines (Kannan and Jain, 2000, Sen *et al.*, 1996). Cyclic AMP (cAMP), intracellular calcium and NF-κB have also been implicated in the oxidant-induced release of the pro-inflammatory cytokine tumour necrosis factor alpha (TNF-α) from J774A.1 macrophage cells (Brown *et al.*, 2007a). These transcription factors are highlighted in NP and fibre-induced toxicity. Asbestos and NP-induced cell proliferation can be through up-regulation of growth factor and growth factor receptors, and activation of transcription factors such as nuclear factor-kappa B (NF-κB) or activator protein-1 (AP-1) (Shukla *et al.*, 2003b). MWCNT exposure is seen to induce activation of NF-κB and not AP-1 (Hirano *et al.*, 2010), which can initiate an inflammatory response through oxidative stress stimulated activation of NF-κB, causing a release of IL-8 from MWCNT exposure, not seen in response to nanoparticle CB exposure (Han *et al.*, 2010). However, nanoparticle CB is shown to induce activation of both NF-κB and AP-1 through calcium signalling and oxidative mechanisms, leading to induction of an inflammatory response with the release of TNF-α (Brown *et al.*, 2004). NF-κB is likely to contribute in the pathogenicity of asbestos-induced pulmonary disorders; it is responsive to

oxidative stress and is responsible for transcription of genes for TNF-α, MIP-2, IL-6, and IL-8 (Driscoll *et al.*, 1997, Janssen *et al.*, 1995, Luster and Simeonova, 1998). Additionally, the redox activity of metals, including iron, is known to induce activation of NF-κB, AP-1 and p53 (Valko *et al.*, 2005). The importance of iron induced oxidative stress in particle and fibre cytotoxicity is shown when the ability of crocidolite asbestos to induce a signalling cascade that results in apoptosis is blocked with the addition of antioxidants or iron chelators (Jimenez *et al.*, 1997).

The *in vivo* response from these pro-inflammatory and pro-fibrotic conditions stimulated by exposure to CNT and pathogenic fibres is well documented. With asbestos exposure an increase in gene expression for cell proliferation (Mossman and Churg, 1998, Shukla *et al.*, 2003b) and antioxidants is found, with acute to chronic inflammation (dependent on dose), leading to reversible or irreversible inflammatory lesions, and deposition of extracellular matrix components including collagen. Additional stimulation of fibrosis is found with an influx of neutrophils, mast cells, and T-lymphocytes into asbestos-treated lungs seen using *in vivo* animal models. This influx and extended activity of immune cells are thought to cause injury to lung epithelial cells resulting in destruction of alveolar type I epithelial cells and generation of alveolar type II epithelial cells, which proliferate, often through hyperplasia, and enlarge through hypertrophy, often resulting in fibrogenesis or carcinogenesis (Mossman and Churg, 1998). An increase in cellular proliferation and recruitment, and pro-fibrotic growth factors is also seen in response to CNT (Mangum *et al.*, 2006, Poland *et al.*, 2008), with substantial granuloma formation, alveolar wall thickening and fibrosis (Lam *et al.*, 2004a, Mercer *et al.*, 2008, Muller *et al.*, 2005, Poland *et al.*, 2008, Shvedova *et al.*, 2008a, Shvedova *et al.*, 2005, Shvedova *et al.*, 2007). In terms of an inflammatory response, an influx of various immune cells is found (Mercer *et al.*, 2008, Muller *et al.*, 2005, Poland *et al.*, 2008, Shvedova *et al.*, 2008a, Shvedova *et al.*, 2005) in response to CNT, with an accompanying rise in pro-inflammatory and pro-fibrotic cytokines TNF-α *in vivo*; and *in vitro*, IL-1β, IL-6, MCP-1, and TGF-β are expressed (Muller *et al.*, 2005, Shvedova *et al.*, 2008a, Shvedova *et al.*, 2005, Shvedova *et al.*, 2007, Shvedova *et al.*, 2008b). Incidentally, the induction of a pro-fibrotic environment

where a rise in TGF-β is found, may be dependent on the resolution of the inflammatory response and removal of invading immune cells (Shvedova *et al.*, 2008b).

5.2 Results

5.2.1 Viability

5.2.1.1 Annexin-V and propidium iodide

The protocol using the fluorescent dyes annexin-V and propidium iodide (PI) is designed to report the occurrence of both apoptosis and necrosis. During apoptosis the negatively charged phosphatidylserine (PS) is reversed within the phospholipid cell membrane and is bound, with high specificity, by annexin-V-fluorescein (Aubry *et al.*, 1999). However, during necrosis PS will also become available and bound, therefore the inclusion of PI is used to differentiate between apoptotic and necrotic cells. Due to increased membrane permeability during necrosis PI will penetrate cells and bind to nucleic acids, which would only be available during this process. Therefore, there are three possible cell populations, healthy (no stain), apoptotic (annexin-V only) and necrotic (double staining of annexin-V-fluorescein and PI). Controls used during this investigation include two positive controls of camptothecin-treated cells, to induce apoptosis, and Triton X100 treated cells, to represent necrosis; and a negative control of cells suspended in medium alone. This assay required substantial development and optimisation from the original protocol outlined by the manufacturer. Ultimately the resulting data provided a false negative impression of CNT cytotoxicity, with none found; therefore it was decided that either assay interference was occurring, or the assay was not sensitive enough to detect the small changes in viability that was demonstrated in later assays.

Here, a brief outline of the protocol adaptations is provided to show the requirements for accurate measurements, followed by the initial results obtained and a short discussion in relation to the use of this method for CNT viability assessment.

Original protocol and adaptations

Initially, J774A.1 cells were treated with 32µg/ml camptothecin for 30 minutes, 0.1% TritonX100 for 5 minutes, or medium only. Cells were washed, scraped and re-suspended in 1ml of the Annexin-V-FLUOS Staining Kit incubation buffer (Roche) containing relative staining solution of either 20µl annexin-V-fluorescein (0.1µg/µl), 20µl PI (50µg/ml), 20µl of both annexin-V and PI, or containing neither dye. These suspensions were left at room temperature, in the dark, for 15 minutes; after which 400µl incubation buffer was added, tubes were agitated to re-suspend cells, and suspensions were analysed via flow cytometry; with excitation wavelengths of 488nm for fluorescein and 488–540nm for PI; and emissions measured at 518nm (fluorescein) and 617nm (PI). Initial readings at this point demonstrated substantial cell death by necrosis, even in cells that had not received any positive control treatments (figure 5.1 A), and cells that had undergone treatment with camptothecin (figure 5.1 B), which could not be eliminated by any amount of compensation.

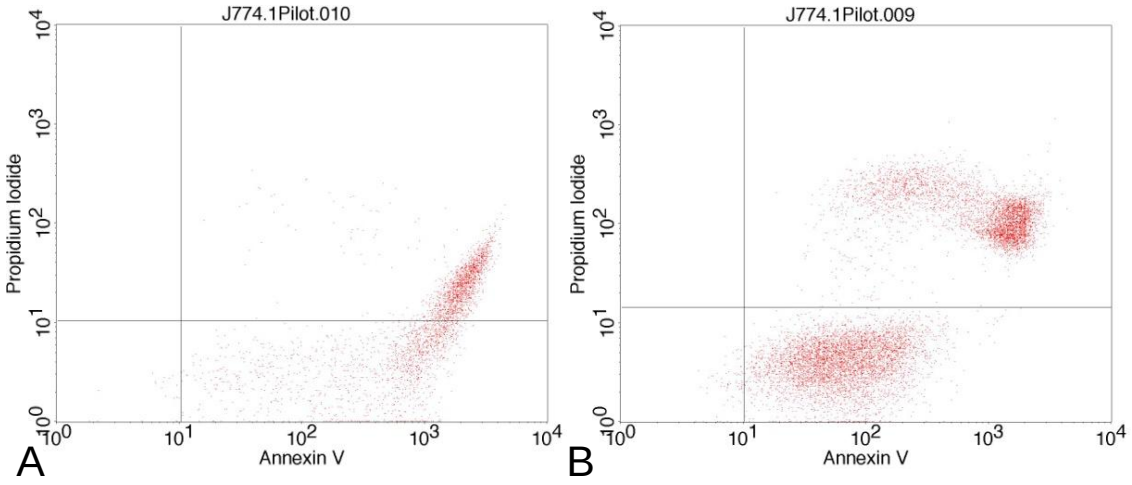

Figure 5.1 Analysis of J774A.1 cells via flow cytometry using the fluorescent dyes annexin-V and propidium iodide. (A) J774A.1 cells incubated in medium alone and (B) J774A.1 cells incubated in medium containing 32µg/ml camptothecin.

One possible reason for the necrotic cell population was thought to be through the method of removing adhered J774A.1 cells from the flask, causing undue stress. Therefore the human macrophage suspension cell line monomac-6 (MM6) was used as a replacement. Again, no particle exposures were used, only treatments of control conditions, with the same four dye combinations as before. Again substantial cell death was evident. It was established that the

necrotic cell populations were due to two factors: one, an over-fluorescence of annexin-V; observed when only annexin-V and no PI staining was used (Figure 5.2 A) with annexin-V fluorescent cell populations appearing in a zone gated for PI positive populations only; and secondly, a 15-minute incubation at this PI concentration was causing some toxicity to cells.

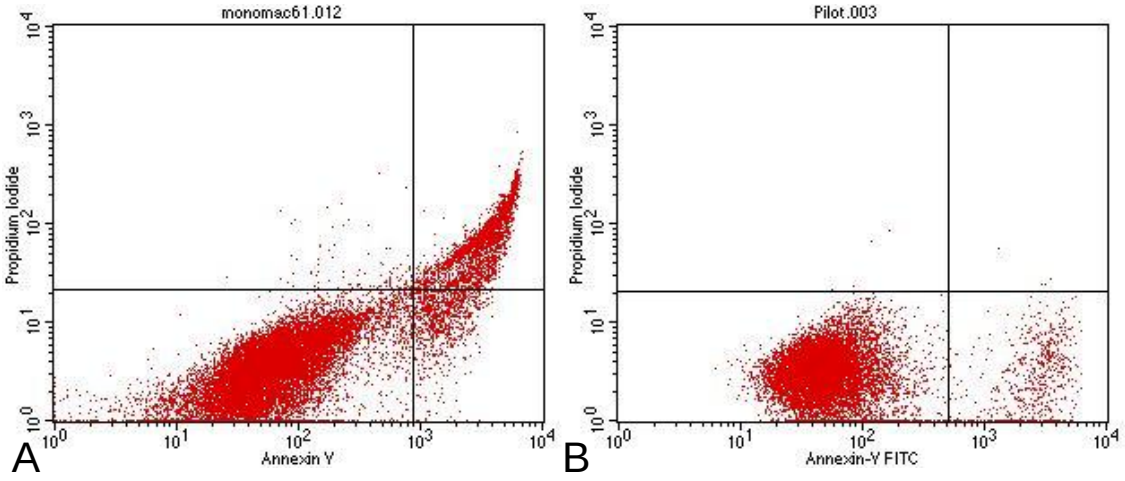

Figure 5.2 Analysis of MM6 cells via flow cytometry using the fluorescent dyes annexin-V and propidium iodide. (A) Analysis of untreated MM6 cells stained with annexin-V only, demonstrating over fluorescence of annexin-V; (B) analysis of untreated MM6 cells stained with annexin-V and propidium iodide after protocol adaption.

The protocol was followed as previously described, with changes to the staining solution. PI was removed, to be added directly prior to analysis at 33.3, 3.3, 2, and 1µg/ml, and annexin-V was diluted. The original method uses an annexin-V concentration of 2mg/ml, which was diluted 4X, 10X and 20X, giving final annexin-V concentrations of 500µg/ml, 200µg/ml and 100µg/ml. The combination of 200µg/ml annexin-V staining solution, with PI added directly prior to analysis at 2µg/ml improved both the problems of PI toxicity and annexin-V over-fluorescence (Figure 5.2 B).

With all adaptations in place analysis of particle panel B was started, with the exposure of MM6 cells, using concentrations of 4.2-17.5µg/cm^2, for 4, 24, and 48 hours. Under these conditions there was no evidence of any cytotoxicity, except in response to positive controls (figure 5.3). However, a discrepancy was revealed through analysis of the supernatant (SN) collected during these exposures. An increase of LDH in the SN of some particle exposures, most

notably 48-hour exposure of MWCNT, indicated clear evidence of cytotoxicity (figure 5.4), when no change was detected by annexin-V and PI staining.

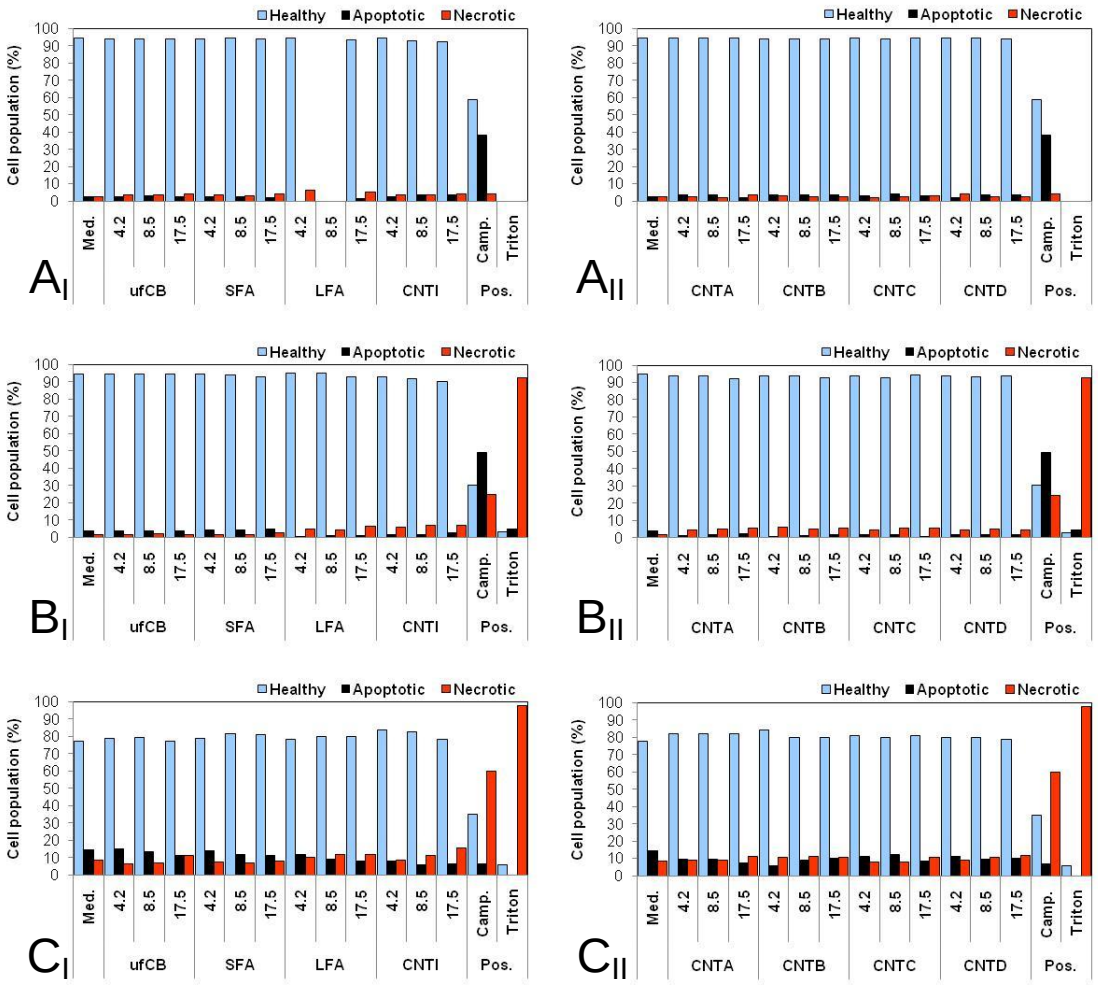

Figure 5.3 Analysis of MM6 cells via flow cytometry using the fluorescent dyes annexin-V and propidium iodide, in response to various particulate treatments (µg/cm^2) for (A) 4 hours, (B) 24 hours and (C) 48 hours; to show healthy, apoptotic and necrotic populations; measured by flow cytometry and the fluorescent dyes annexin-V-fluorescein, at 200µg/ml, and PI at 2µg/ml. With controls of medium alone, triton at 0.1% for 5 minutes and camptothesin at 5µg/ml.

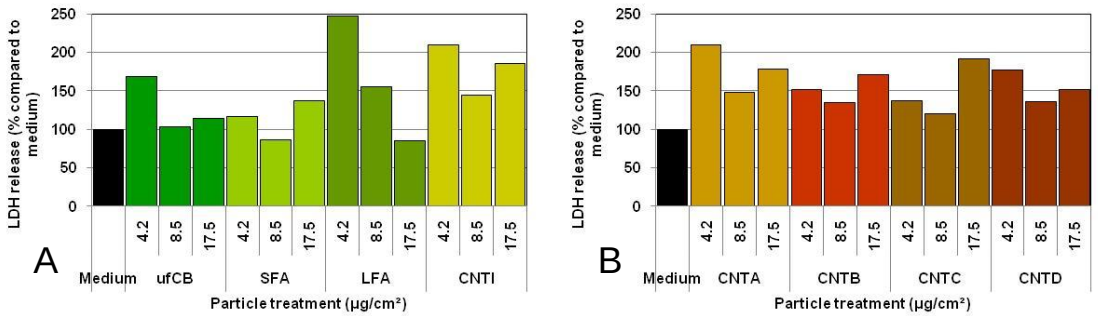

Figure 5.4 LDH release from MM6 – comparison to annexin-V PI assay. Cells were treated with medium only, 4.2, 8.5, and 17.5 µg/cm^2 (A) ufCB, SFA, LFA, CNTI, and (B) CNTA, CNTB, CNTC, and CNTD for 48 hours. Results are expressed as a percentage increase compared to medium only control (n=1).

To test if this discrepancy was due to an assay sensitivity issue in the flow cytometry technique, different treatments of camptothecin and Triton-X100 were used to give proportional increases in apoptotic and necrotic cell populations. For camptothecin, treatments included 0µg/ml, 32µg/ml for 4 and 5 hours, and 5µg/ml for 16 hours (figure 5.5); and for triton-X100 cell populations were exposed to 0.1% for 5 minutes (figure 5.6). In both cases, the shifts in viable cell populations were easy to distinguish using the annexin-V-fluorescein and propidium iodide staining method of FACS analysis, and assay sensitivity was not a concern.

It was therefore likely that one of two complications may be occurring; either particle interference or the removal of dead and dying cells in the longer exposure periods by phagocytosis conducted by remaining viable cells.

One aspect of flow cytometry is to use the forward and side scatter of projected light through the cells to isolate and “gate” around single cell populations, this provides accurate cell counts. If cells have accumulated into “giant cells” they may be excluded by this gating method, and therefore if cell suspensions are not adequately dispersed, the majority of dead cells may pass through unrecorded. CNT have been shown to induce this phenomenon. A549 (Bergamaschi, 2009, Worle-Knirsch *et al.*, 2006) and ECV (Worle-Knirsch *et al.*, 2006) cell lines have been shown to accumulate around sites of aggregated CNT. Cells actively migrate to these sites creating “giant” cells, which are shown to consist of many apoptotic cells (Bergamaschi, 2009). Giant cell formation, through macrophage fusion, is also evident with *in vivo* exposures to CNT and asbestos, and was shown to be dependent on particle length (Poland *et al.*, 2008). An example of this can be seen in figure 5.7, in response to BAL cell exposure to 10 µg/cm^2 long MWCNT.

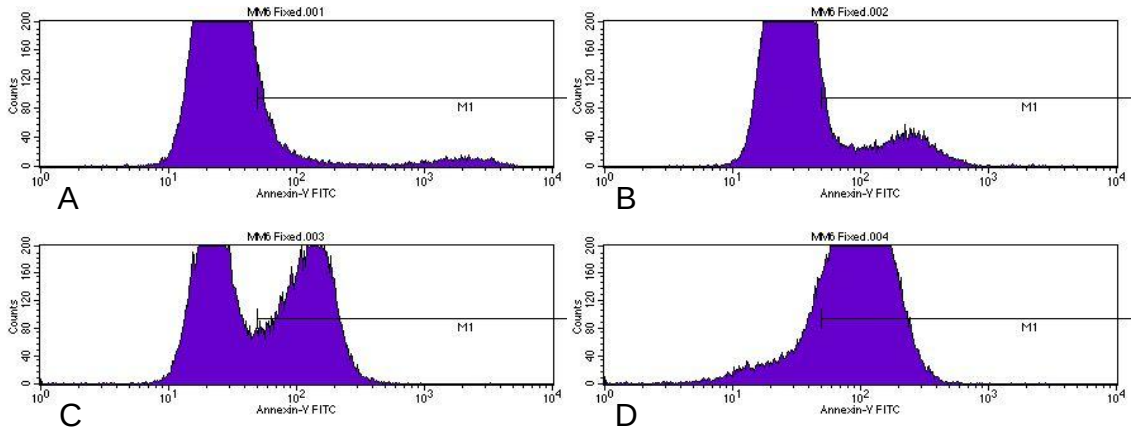

Figure 5.5 Analysis of MM6 apoptosis, measured by flow cytometry and the fluorescent dye annexin-V-fluorescein at 200µg/ml, and using variations of camptothecin concentration and exposure time: (A) 0µg/ml, (B) 32µg/ml for 4 hours, (C) 32µg/ml for 5 hours and (D) 5µg/ml for 16 hours.

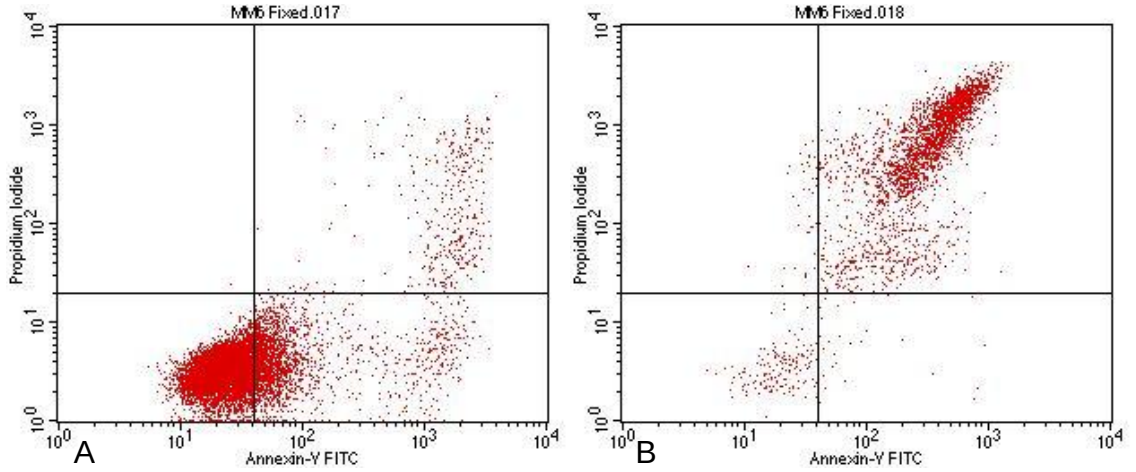

Figure 5.6 Analysis of MM6 necrosis, measured by flow cytometry and the fluorescent dyes annexin-V-fluorescein, at 200µg/ml, and propidium iodide, at 2µg/ml; with triton treatments of (A) 0% and (B) 0.1% for 5 minutes.

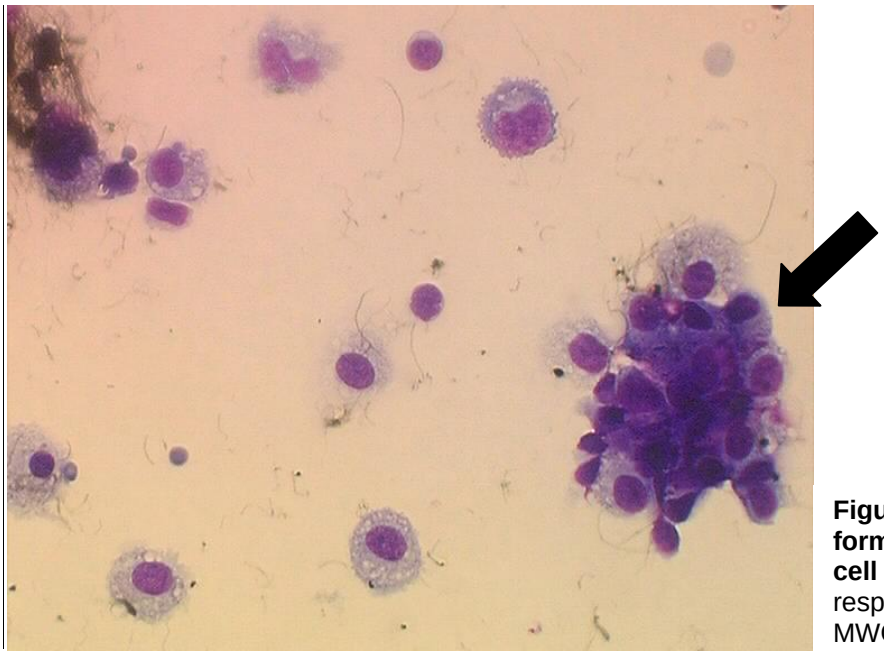

Figure 5.7 BAL cell formation of giant cell (black arrow) in response to long MWCNT treatment.

The second potential cause for under estimation of particle cytotoxicity relates to the cell type used here. One function of phagocytes is to recognise and remove cells that are undergoing any form of cell death (Mevorach *et al.*, 2010). An early indication of apoptosis is the appearance of PS on the cell surface (De Saint-Hubert *et al.*, 2009). As previously mentioned, PS is bound by annexin-V in this assay and is attributed to cell death (Aubry *et al.*, 1999); however, this is also a signal for phagocytes, including macrophages, to dispose of these dying cells (Aubry *et al.*, 1999, De Saint-Hubert *et al.*, 2009). Both cell types used here are phagocytes and therefore have the ability to remove many of the cells that are undergoing apoptosis. Any substantial cell death found through other cytotoxicity assays (LDH and WST-1) was seen only during 48-hour exposures; the test assays using camptothecin were performed for a maximum of 16 hours. It is therefore possible that dead cell removal by other cells may occur at these later time points. The measurement of LDH and WST-1 reduction is of either the presence of viable cells, or presence of necrotic cell death markers in the culture medium; both would be unaffected by this cell removal phenomenon, and would give more accurate results.

The underestimation of cytotoxicity by flow cytometry techniques that has been demonstrated here may have also been observed by Thurnherr *et al.* (2010). MWCNT exposures of 6.25µg/cm^2 were shown to provoke an approximate 12% reduction in viable cells using annexin-V PI staining and flow cytometry. However, the mitochondrial activity of MWCNT treated cells was reduced dose-dependently from 30% to 45% with all MWCNT treatments of 0.33-2.6µg/cm^2 (Thurnherr *et al.*, 2010); these data seem to corroborate the findings of this study. It is evident that the evaluation of cytotoxicity induced by MWCNT is possibly restricted, but certainly hidden when using annexin-V PI staining, while mitochondrial function, or detection of intracellular components released into the SN, may give a more reliable indication of cytotoxicity. Any interference of particles in the mitochondrial activity assay used here (WST-1), and that utilised by Thurnherr *et al.* (2010), was tested and none was found.

5.2.1.2 Lactate dehydrogenase – monomac-6

The human monocytic cell line MM6 was exposed to the full particle panel B range, for 4, 24, and 48 hours, at concentrations of 4.2, 8.5, or 17.5µg/cm^2. After exposure the SN was removed, aliquoted, and frozen at −80°C for cell signalling and cytotoxicity assays. Here the SN was removed, thawed and evaluated for the presence of LDH, a recognised indicator of cell membrane impairment and therefore of cell death. A positive control of treatment with Triton X-100 was used to fully lyse the cells and give the total possible presence of LDH. This is often used to give 100% LDH release, with particle treatments made comparable to this. Here the negative control has been used to normalise the data for particulate treatments, and was expressed as a ratio value compared to medium-only control. This was to allow a clear comparison of the two cytotoxicity assays, as the WST-1 assay uses medium-only treated cells as a marker of a 100% viable population.

In figure 5.8 the dose response of all particle treatments can be seen for all exposure time points. There is no significant increase in LDH release from any of the reference materials (figure 5.8 A, B, and C); neither is there any cytotoxicity in response to the long CNT (CNTC and CNTD) (figure 5.8 G and H). However, exposure to all short CNT samples (CNTI, CNTA and CNTB) for 48 hours induced significant cell mortality, CNTI (figure 5.8 D) and CNTB (figure 5.8 F) at the highest concentration, CNTA at the lowest concentration (figure 5.8 E); all with a p-value <0.05.

Figure 5.8 contains all data for all particles, doses and time points. In order to allow comparisons between particles a proportion of this data, one dose and one time point, has been replotted in a summary graph (figure 5.9) to highlight further comparisons between particle exposures (this has been done throughout this chapter). The industrially produced CNTI was found to be significantly more cytotoxic than all of the reference materials, at the highest concentration and longest exposure period (figure 5.9) ($p<0.05$).

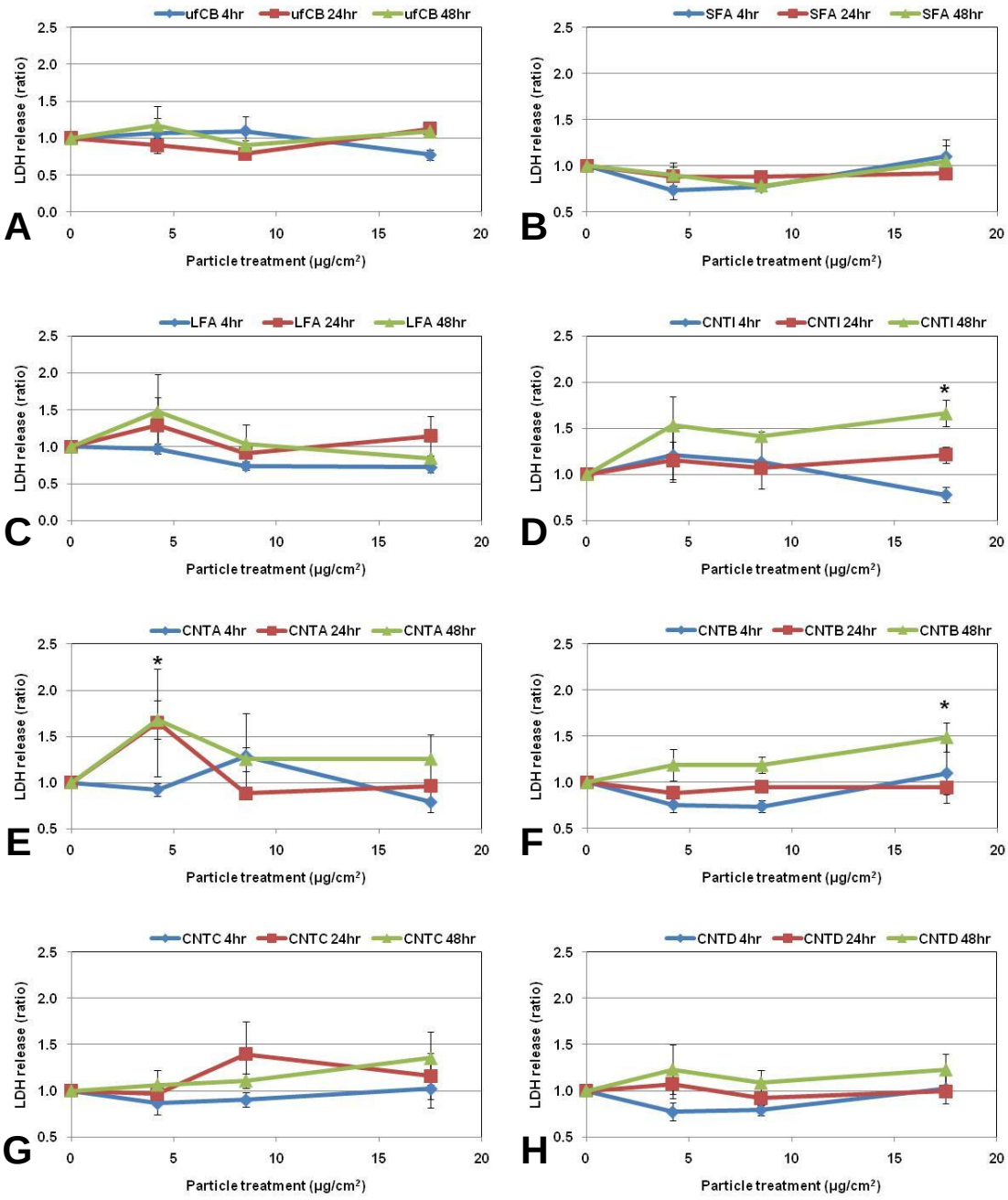

Figure 5.8 LDH release from MM6 cells after exposure to particle panel B. Cells were treated with medium-only, 4.2, 8.5, and 17.5 µg/cm^2 (A) ufCB, (B) SFA, (C) LFA, (D) CNTI, (E) CNTA, (F) CNTB, (G) CNTC, and (H) CNTD; for 4, 24, and 48 hours. Triton X-100 was used as a positive control. Results are expressed as a ratio compared to medium-only control, and each data point represents the mean ± SEM (n=3). Statistical significance is shown by * for 48-hour exposure, * = $p<0.05$, compared to control.

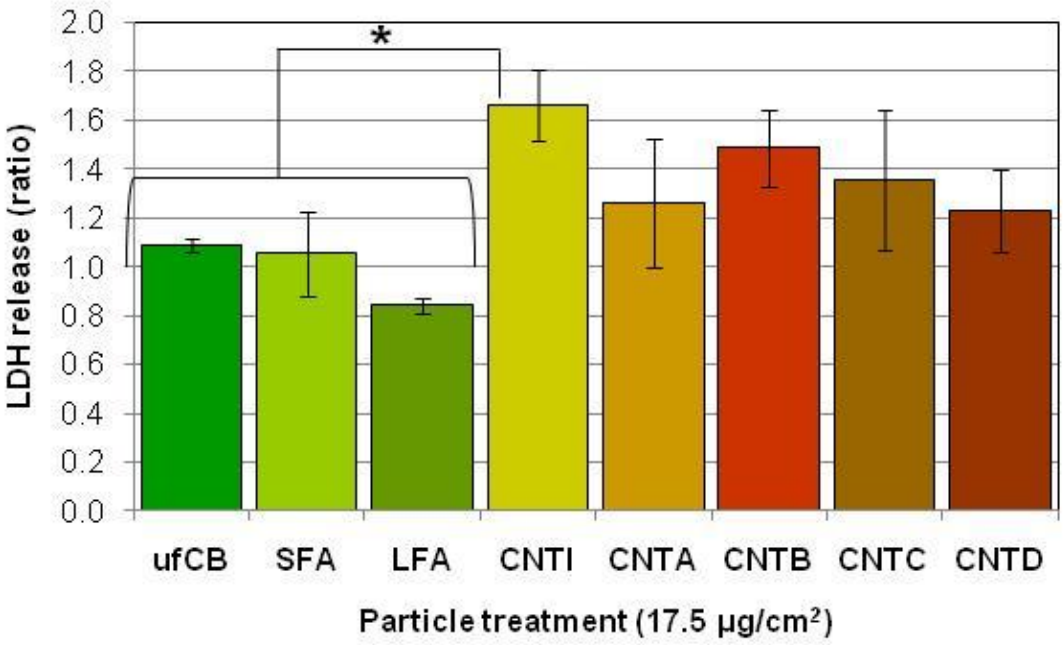

Figure 5.9 LDH release from MM6 cells after exposure to particle panel B. Summary graph. Cells were treated with 17.5 µg/cm^2 ufCB, SFA, LFA, CNTI, CNTA, CNTB, CNTC, and CNTD, for 48 hours. Results are expressed as a ratio compared to medium-only control, and each data point represents the mean ± SEM (n=3). Statistical significance is shown by * = $p<0.05$, compared to relative particle treatment.

5.2.1.3 Lactate dehydrogenase – J774A.1

The mouse macrophage cell line J774A.1 was also exposed to the full particle panel B range, for the same exposure periods of 4, 24, and 48 hours. The exposure dose was extended to concentrations of 1.1, 2.1, 4.2, 8.5, and 17.5µg/cm^2. Again, no significant cell death was found in response to the reference materials (figure 5.10 A, B, C), or to CNTA and CNTB (figure 5.10 E, F). CNTI and both long CNT (CNTC and CNTD) consistently caused significant cell death (figure 5.10 D, G, H) during the 48-hour exposure ($p<0.05$-0.001); and also during 24 hours exposure, but only in response to the highest concentration ($p<0.001$). The greatest response was induced by CNTC and CNTD during 24-hour exposure, with a 2-fold increase in LDH release, this, however, was only statistically significant in values for CNTC exposure, standard deviation of CNTD treatments appeared too high to achieve significance.

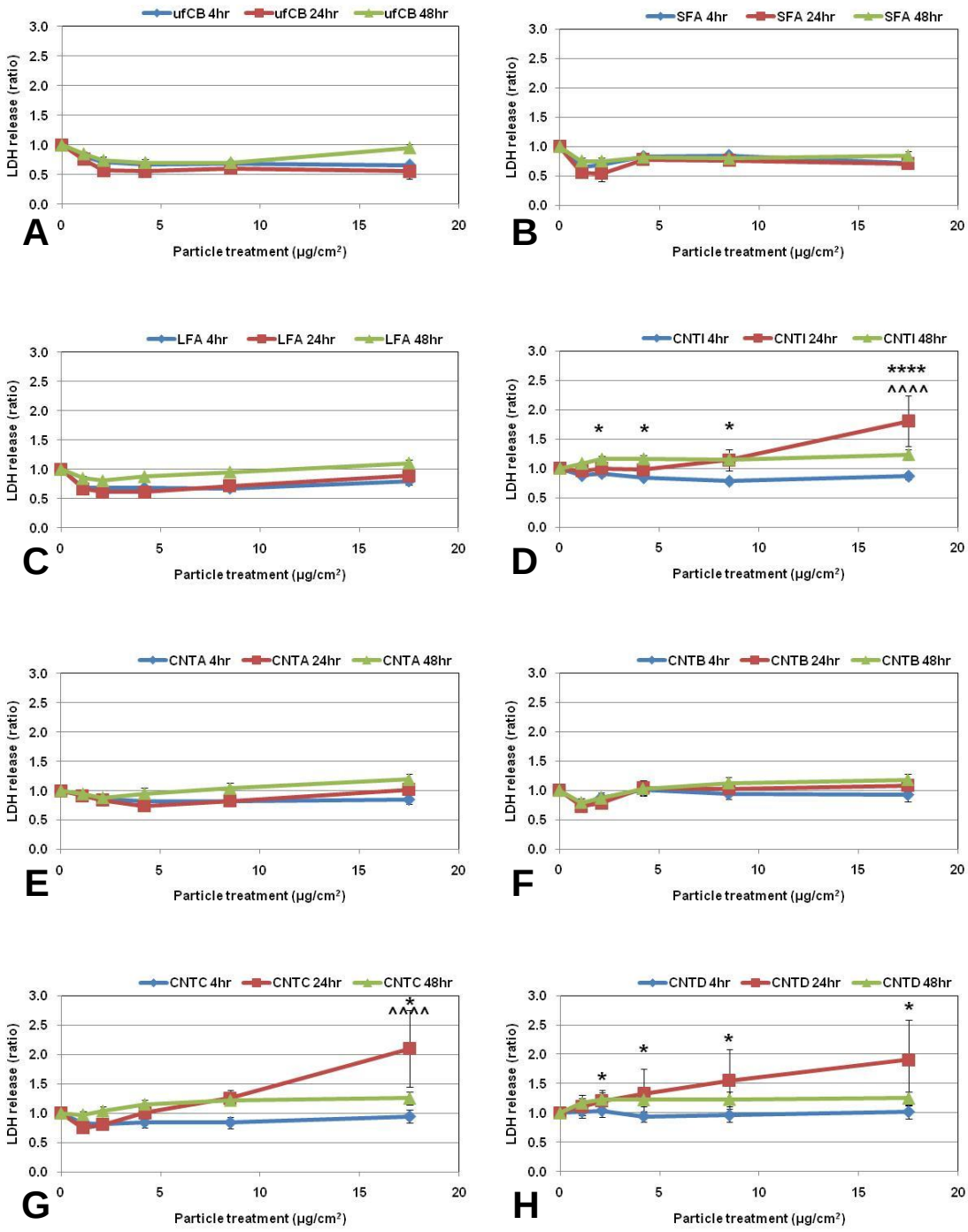

Figure 5.10 LDH release from J774A.1 cells after exposure to particle panel B. Cells were treated with medium only, 1.1, 2.1, 4.2, 8.5, and 17.5 µg/cm^2 (A) ufCB, (B) SFA, (C) LFA, (D) CNTI, (E) CNTA, (F) CNTB, (G) CNTC, and (H) CNTD for 4, 24, and 48 hours. Triton X-100 was used as a positive control. Results are expressed as a ratio compared to medium-only control, and each data point represents the mean ± SEM (n=4). Statistical significance is shown by * for 48-hour exposure, * = p<0.05, **** = p<0.001, compared to control; and ^ for 24-hour exposure, ^^^^ = p<0.001, compared to control.

The summary graph of particle panel B exposure on J774A.1 (figure 5.11) infers that all CNT were significantly more cytotoxic than NPCB and SFA ($p<0.05$-0.001); and that LFA was also significantly more cytotoxic than SFA ($p<0.01$).

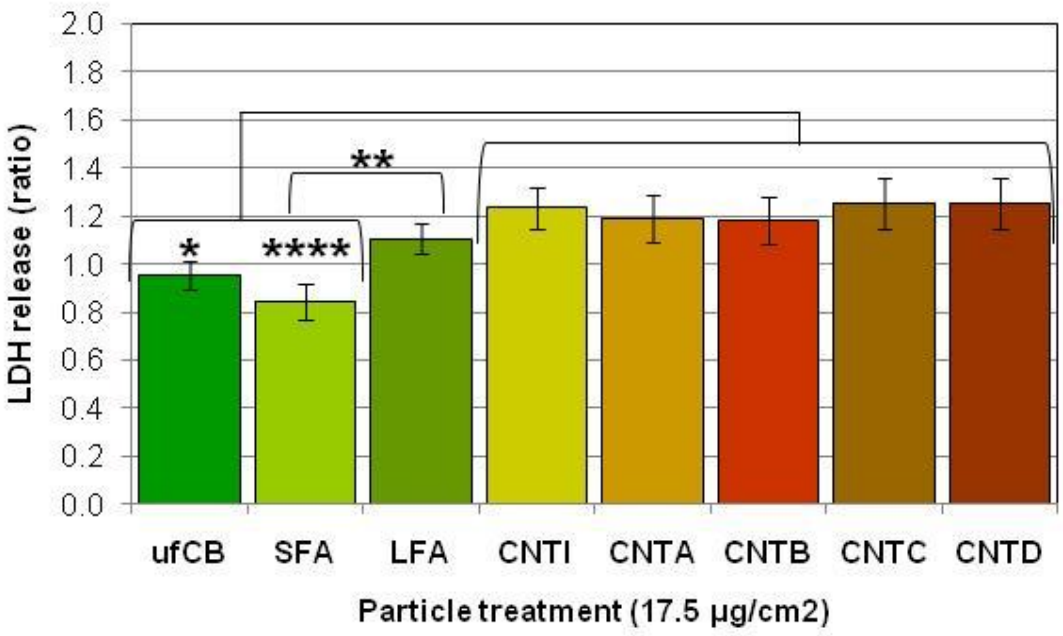

Figure 5.11 LDH release from J774A.1 cells after exposure to particle panel B. Summary graph. Cells were treated with 17.5 µg/cm^2 ufCB, SFA, LFA, CNTI, CNTA, CNTB, CNTC, and CNTD for 48 hours. Results are expressed as a ratio compared to medium-only control, and each data point represents the mean ± SEM (n=4). Statistical significance is shown by * = $p<0.05$, ** = $p<0.01$, *** = $p<0.005$, **** = $p<0.001$, compared to relative particle treatment.

5.2.1.4 WST-1 – monomac-6

The second marker of cytotoxicity investigated was a reduction in mitochondrial activity of a cell population in response to particle exposures. This was measured spectrophotometrically through the formation of formazan dye by mitochondrial dehydrogenases.

With the exposure of MM6 cells to 4.2, 8.5, and 17.5 μg/cm^2 of particle panel B (figure 5.12) the only reference material to cause any reduction in viability was NPCB, this was during 4-hours incubation, and only at the highest concentration ($p<0.05$) (figure 5.12 A). CNTI, CNTB and CNTC were all shown to significantly decrease viable cell populations. This was observed as early as 4 hours, but also after 48 hours, in response to CNTB exposure (figure 5.12 F). CNTI and CNTC were found to significantly reduce MM6 viability during both the 24 and 48 hour exposure periods; with highest cytotoxicity found in response to the long, high iron CNTC, with a reduction in viability of 30% ($p<0.01$) after treatment with highest concentration for 48 hours (figure 5.12 G). No changes in viable cell populations were found in response to CNTA or CNTD.

The summary graphs of inter-particle responses (figure 5.13) denotes that, although NPCB exposure caused a reduction in viability during the 4-hour exposure period in comparison to medium only controls, it did not significantly lower viability compared with any of the other particle treatments (figure 5.13 A). While both CNTI and CNTC were shown be significantly more cytotoxic than SFA after 24-hours (figure 5.13 B), and both asbestos samples after 48-hours (figure 5.13 C).

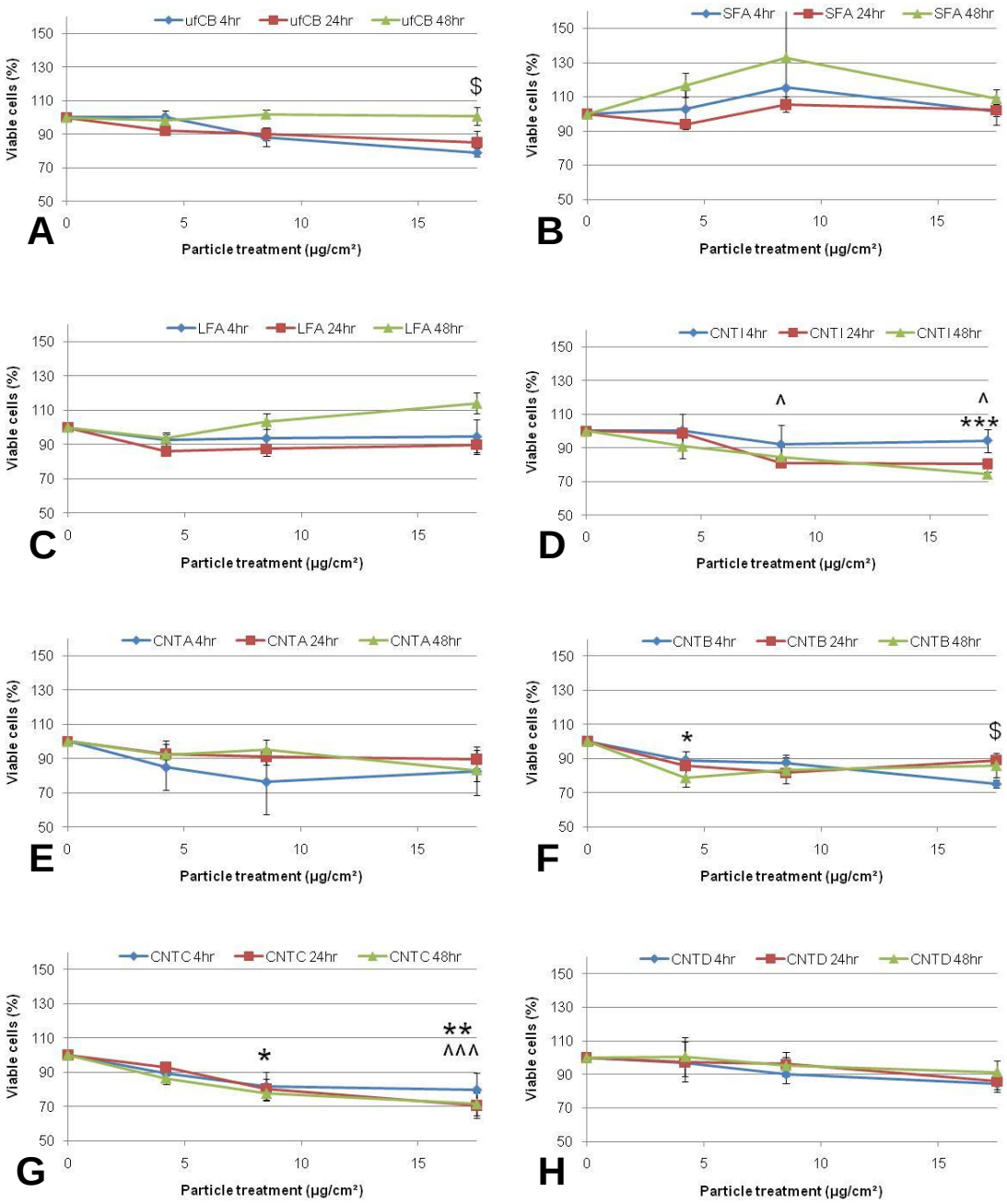

Figure 5.12 Mitochondrial function in MM6 cells after exposure to particle panel B. Cells were treated with medium only, 4.2, 8.5, and 17.5 µg/cm^2 (A) ufCB, (B) SFA, (C) LFA, (D) CNTI, (E) CNTA, (F) CNTB, (G) CNTC, and (H) CNTD for 4, 24, and 48 hours. Mitochondrial activity was measured using the WST-1 assay. Results are expressed as % viable cells, with medium-only control as 100%, and each data point represents the mean ± SEM (n=3). Statistical significance is shown by $ for 4-hour exposure ($ = $p<0.05$), compared to control; ^ for 24-hour exposure (^ = $p<0.05$, ^^^ = $p<0.005$), compared to control; and * for 48 hour exposure (* = $p<0.05$, ** = $p<0.01$, *** = $p<0.005$), compared to control.

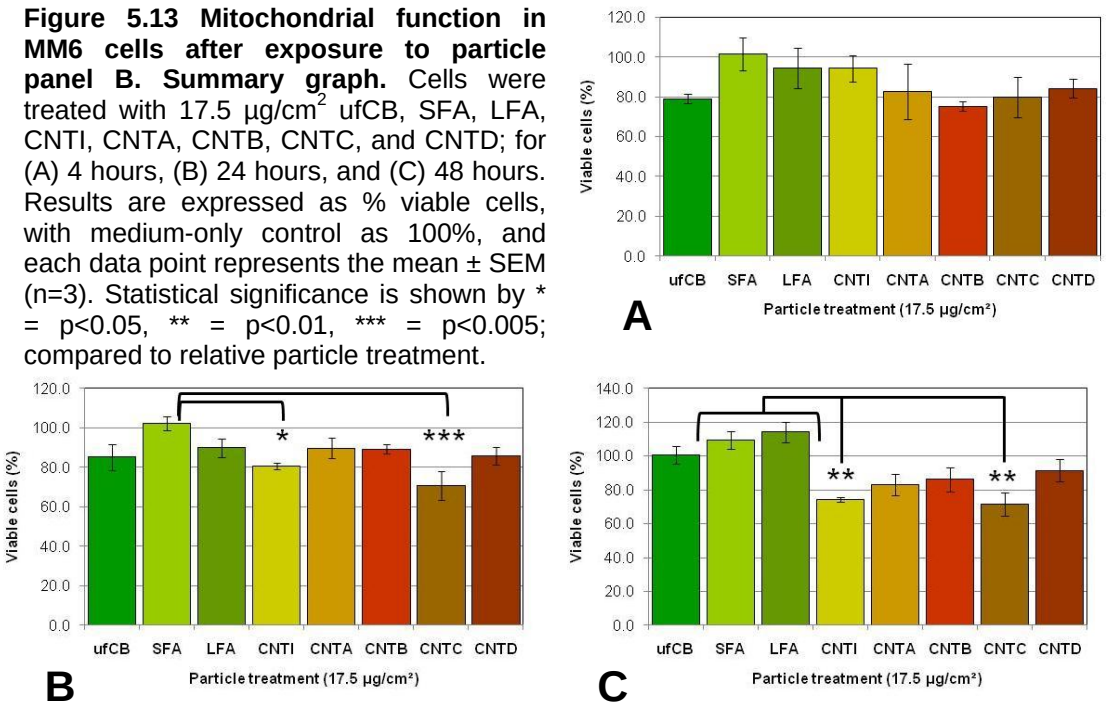

Figure 5.13 Mitochondrial function in MM6 cells after exposure to particle panel B. Summary graph. Cells were treated with 17.5 µg/cm^2 ufCB, SFA, LFA, CNTI, CNTA, CNTB, CNTC, and CNTD; for (A) 4 hours, (B) 24 hours, and (C) 48 hours. Results are expressed as % viable cells, with medium-only control as 100%, and each data point represents the mean ± SEM (n=3). Statistical significance is shown by * = p<0.05, ** = p<0.01, *** = p<0.005; compared to relative particle treatment.

5.2.1.5 WST-1 – J774A.1

Using exposure concentrations of 1.1-17.5µg/cm^2 both NPCB and SFA were found to reduce J774A.1 viability. This was observed only after 4-hour exposure to the highest concentration of SFA (p<0.05) (figure 5.14 B). Whereas, in response to NPCB, a significant reduction in viability was seen from numerous concentrations during 4- and 24-hour exposures; a full recovery, however, appeared to occur during the 48-hour exposure period (figure 5.14 A). There was no apparent cytotoxicity in response to LFA, CNTA or CNTB. CNTI and CNTD were both shown to reduce J774A.1 viability by over a third during the 48-hour exposure, at the highest concentration (figure 5.14 D and H), and in respect to CNTD, cytotoxic effects were also evident in response to additional exposure periods and concentrations (figure 5.14 H). The long, high iron CNTC demonstrated the greatest cytotoxic potential, with a reduced viable J774A.1 population of 50% in response to the highest dose and exposure time (figure 5.14 G), but mitochondrial function was also significantly reduced, to a lesser extent, with CNTC exposures of 8.5µg/cm^2 for 48 hours, and 2.1, 8.5, and 17.5µg/cm^2 with 24-hours.

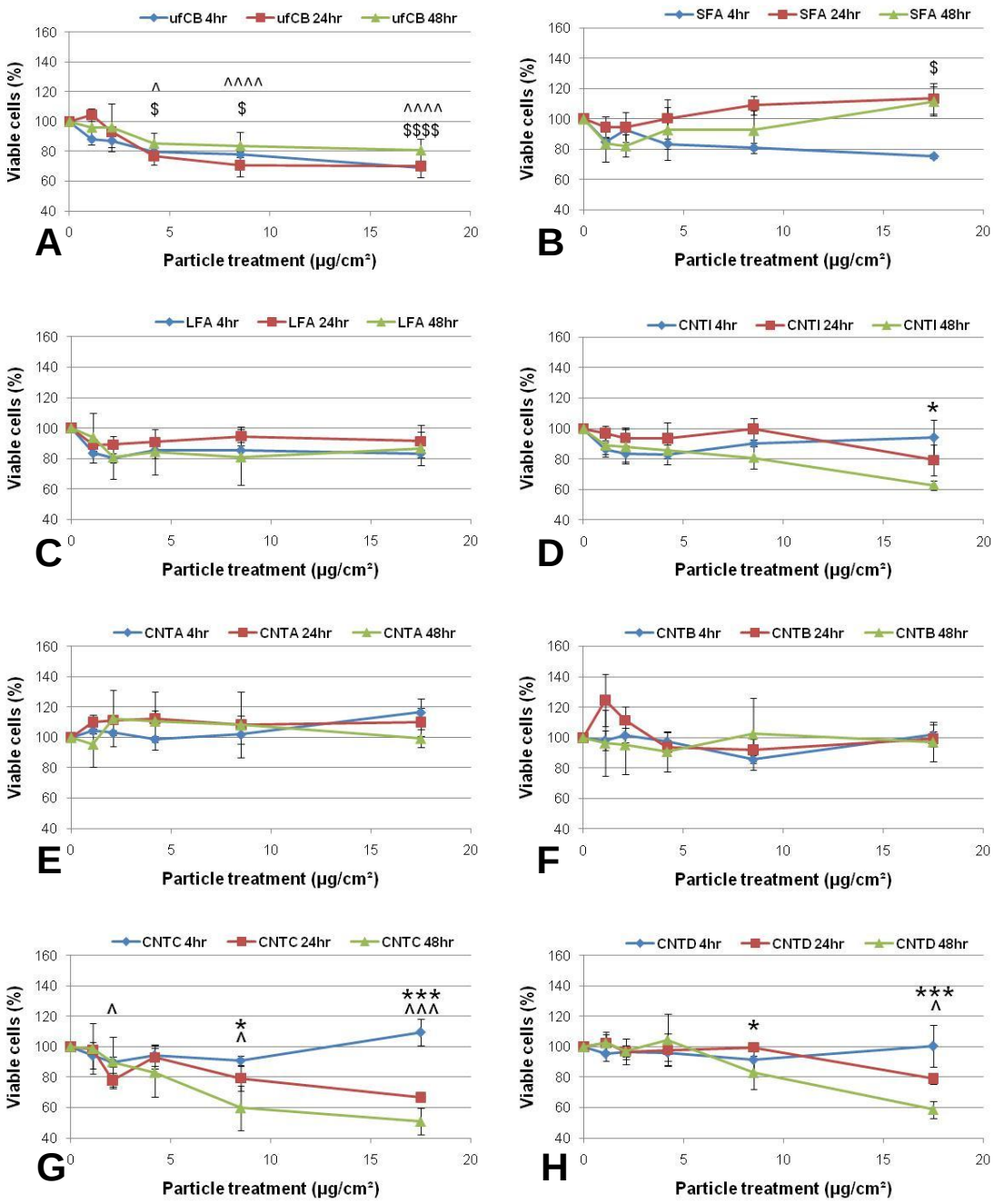

Figure 5.14 Mitochondrial function in J774A.1 cells after exposure to particle panel B. Cells were treated with medium-only, 1.1, 2.1, 4.2, 8.5, and 17.5 µg/cm^2 (A) ufCB, (B) SFA, (C) LFA, (D) CNTI, (E) CNTA, (F) CNTB, (G) CNTC, and (H) CNTD for 4, 24, and 48 hours. Mitochondrial activity was measured using the WST-1 assay. Results are expressed as % viable cells, with medium-only control as 100%, and each data point represents the mean ± SEM (n=3). Statistical significance is shown by $ for 4-hour exposure ($ = p<0.05, $$$$ = p<0.001), compared to control; ^ for 24-hour exposure (^ = p<0.05, ^^^ = p<0.005, ^^^^ = p<0.001), compared to control; and * for 48-hour exposure (* = p<0.05, *** = p<0.005), compared to control.

The reduced viability, compared to medium only controls, demonstrated during the 4-hour exposure to NPCB and SFA (figure 5.14), was also shown to translate as a significant reduction in cellular viability in comparison to all 4 purpose-grown CNT samples during 4-hours exposure (figure 5.15 A). The extension of this exposure period to 24- and 48 hours demonstrated a clear reversal. At 24 hours there were no significant differences between particle treatments; whereas, during 48 hours (figure 5.15 B) exposure to CNT samples, CNTI, CNTC, and CNTD are all shown to cause a significantly greater cytotoxic response than all other materials.

Prior to this data set, there have been no significant differences in CNT treatments, relative to length, iron content or production method.

Here, it was shown that during 24 hours exposure (figure 5.16 A), the long CNT (CNTC and CNTD) induced greater cell death than the short CNT (CNTA and CNTB), at numerous concentrations; and a greater reduction in viability is shown in response to the long, high iron CNTC, compared to the long, low iron CNTD ($p<0.05$). During 48 hours, the long CNT samples were again shown to significantly reduce J774A.1 cell viability, when compared to their short CNT counterparts (figure 5.16 B).

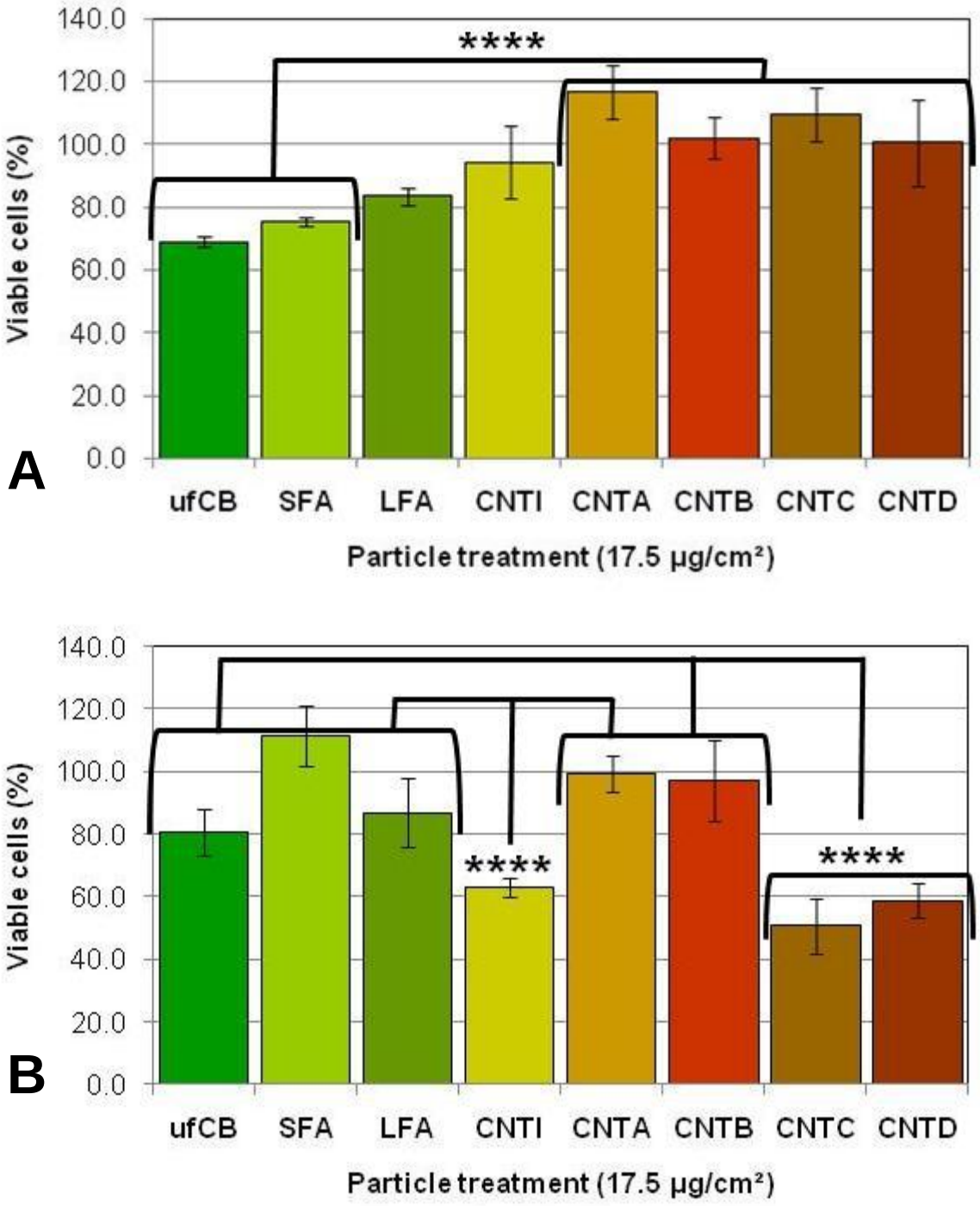

Figure 5.15 Mitochondrial function in J774A.1 cells after exposure to particle panel B. Summary graph. Cells were treated with 17.5 µg/cm^2 ufCB, SFA, LFA, CNTI, CNTA, CNTB, CNTC, and CNTD for (A) 4 hours, and (B) 48 hours. Results are expressed as % viable cells, with medium-only control as 100%; each data point represents the mean ± SEM (n=3). Statistical significance is shown by **** = p<0.001, compared to relative particle treatment.

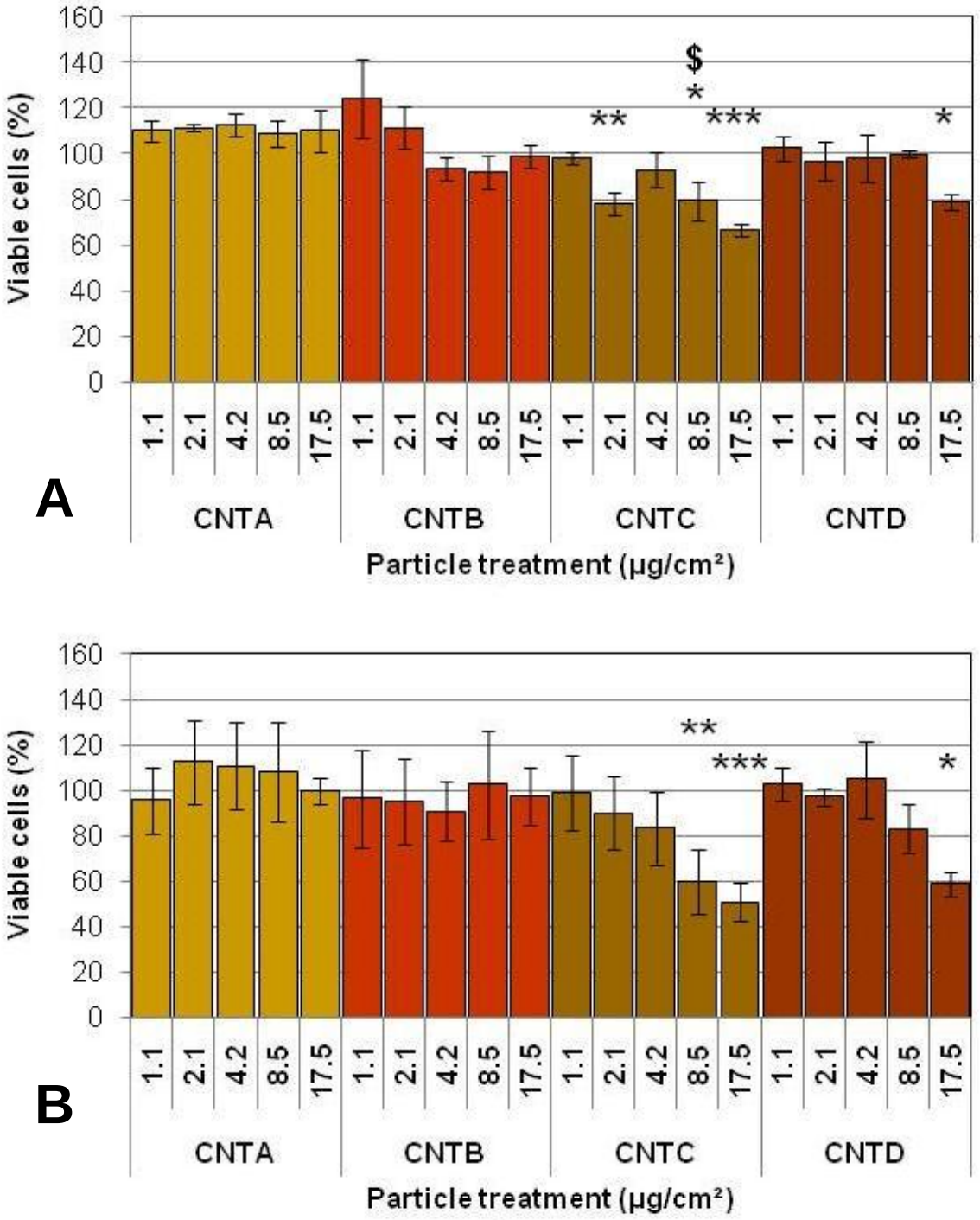

Figure 5.16 Mitochondrial function in J774A.1 cells after exposure to particle panel B. Summary graph. Cells were treated with 1.1, 2.1, 4.2, 8.5, and 17.5 µg/cm^2 CNTA, CNTB, CNTC, and CNTD for (A) 24 hours, and (B) 48 hours. Results are expressed as % viable cells, with medium only control as 100%, each data point represents the mean ± SEM (n=3). Statistical significance is shown by * = $p<0.05$, ** = $p<0.01$, *** = $p<0.005$, compared to short CNT at same dose; and $ = $p<0.05$, compared to CNT with depleted Fe content at same dose.

5.2.2 Cell signalling

5.2.2.1 Monomac-6

The treatment of MM6 cells with 4.2, 8.5, 17.5µg/cm^2 of particle panel B resulted in no discernible increase in release of GM-CSF, IL-6, IL-1α, IL-1β, or TNF-α when compared to medium-only treated cells. MM6 cells were, however, shown to secrete these cytokines, in response to LPS (figure 5.17).

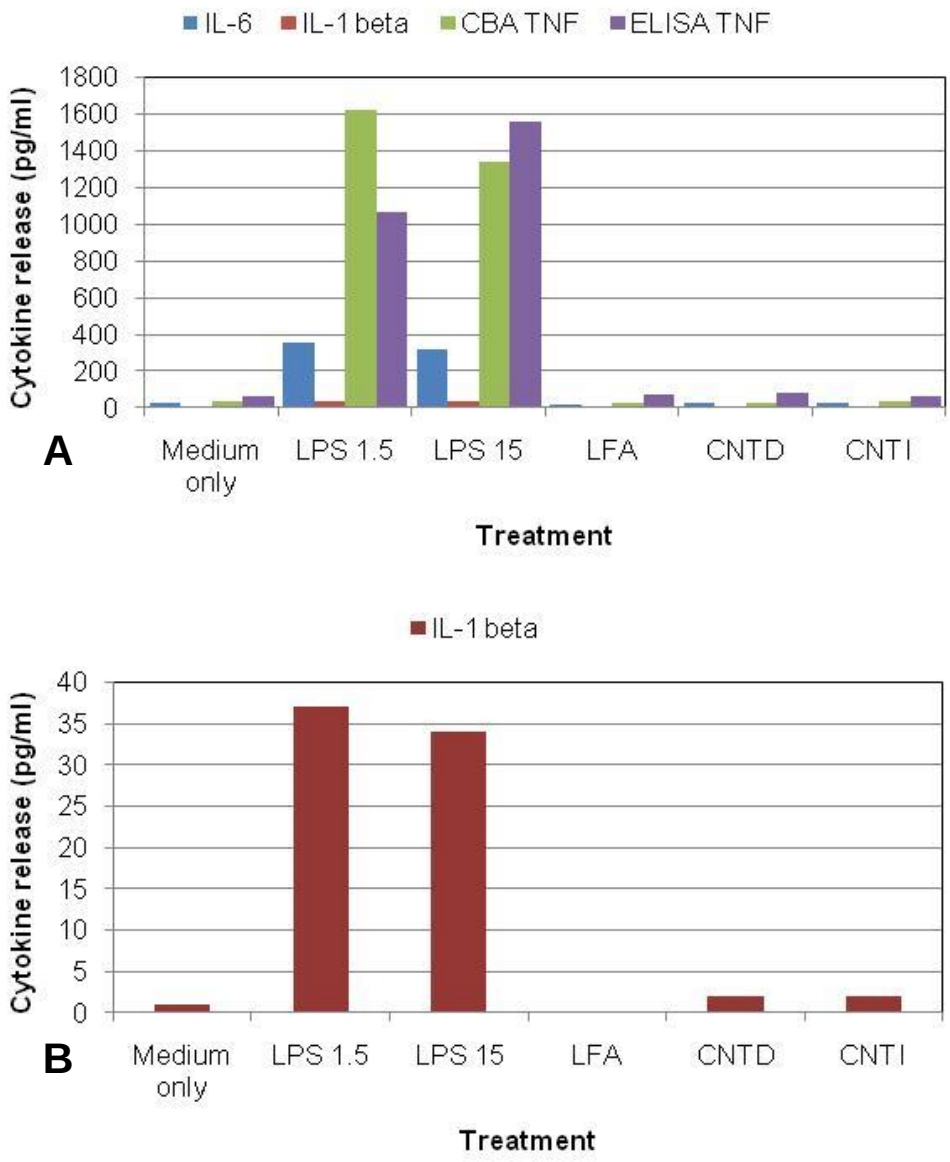

Figure 5.17 Cytokine release from MM6 cells in response to LPS, not seen in particle exposure. Cells were treated with medium-only, 1.5 and 15µg/ml LPS, or 8.5µg/cm^2 LFA, CNTI, and CNTD for 4 hours. Data is expressed as cytokine release (A) IL-6, IL-1β, TNF-α (the latter measured by CBA and ELISA), (B) IL-1β, shown alone(n=1).

Other signalling molecules, such as MCP-1, TGF-β1, and VEGF, were assayed, and induction of these markers in response to particle exposures was shown.

The reference materials were not found to induce secretion of the chemokine MCP-1 at any concentration or time point (figure 5.18 A-C). Neither was CNTA (figure 5.18 E) or CNTC (figure 5.18 G), the response to CNTC appeared elevated but was not statistically significant.

The industrial CNTI induced a significant increase in MCP-1 (figure 5.18 D) after 24 and 48 hours, at all concentrations ($p<0.05$-0.001). CNTB (figure 5.18 F) was also found to elevate MCP-1 production at all concentrations after 48-hour exposure ($p<0.05$-0.01), as was CNTD (figure 5.18 H). The MCP-1 secreted in response to CNTD was shown to be the greatest with over three times that of the medium-only control ($p<0.01$); it was, however only seen during exposure to the highest concentration.

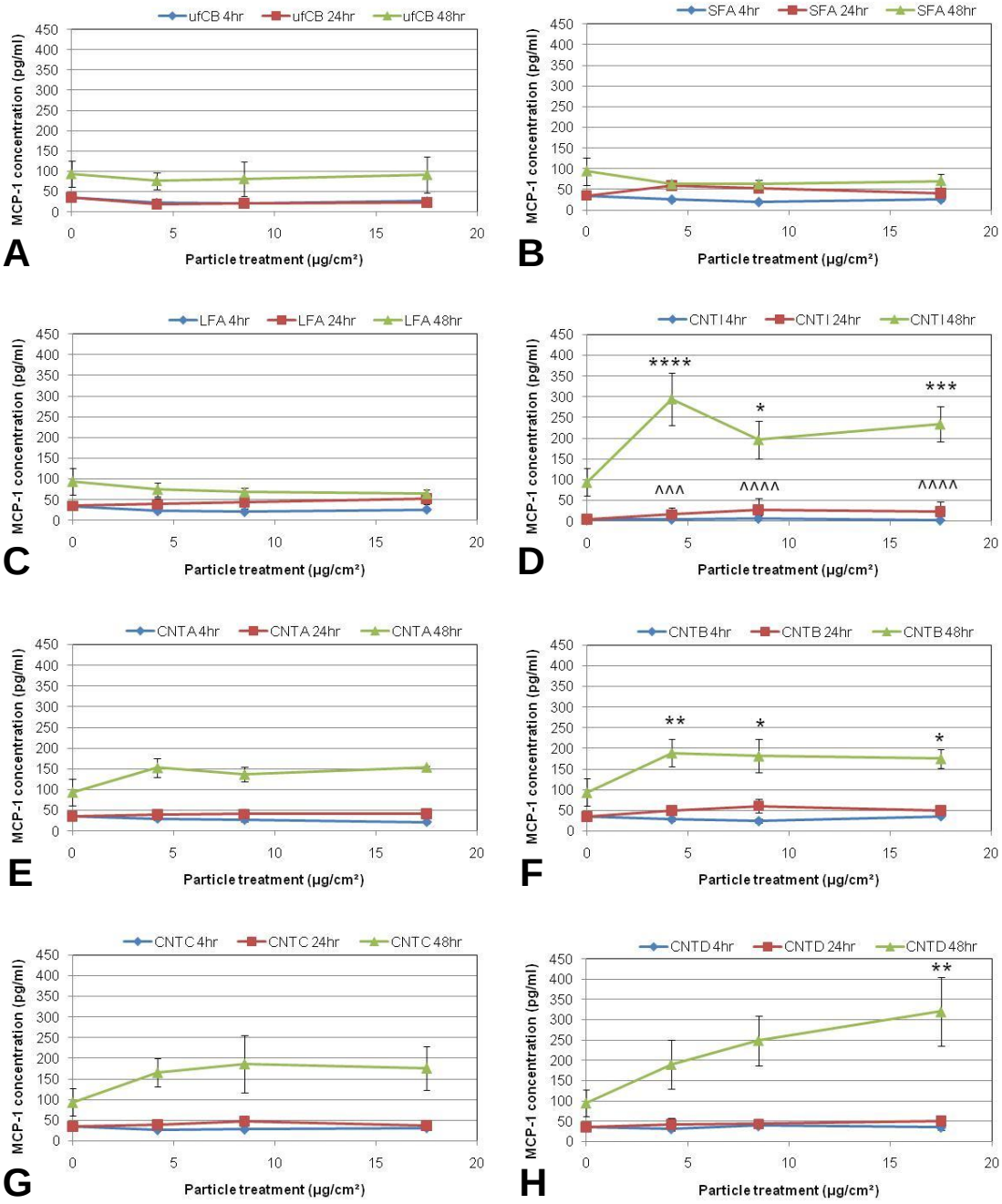

Figure 5.18 MCP-1 release from MM6 cells after exposure to particle panel B. Cells were treated with medium-only, 4.2, 8.5, and 17.5 µg/cm^2 (A) ufCB, (B) SFA, (C) LFA, (D) CNTI, (E) CNTA, (F) CNTB, (G) CNTC, and (H) CNTD for 4, 24, and 48 hours. Results are expressed as MCP-1 release, and each data point represents the mean ± SEM (n=3). Statistical significance is shown by ^ for 24-hour exposure (^^^ = p<0.005, ^^^^ = p<0.001), compared to control; and * for 48-hour exposure (* = p<0.05, ** = p<0.01, *** = p<0.005, **** = p<0.001), compared to control.

The particularly high increases in MCP-1 production in response to CNTI and CNTC provided, not only a greater release in comparison to medium only treated cells, but also in comparison to other particle treatments. The summary graphs shown in figure 5.19 demonstrate that, at the highest dose, CNTI generated more MCP-1 than all reference materials and the CNT samples of a lower crystalline structure ($p<0.001$), during 4-hours exposure (figure 5.19 A). After 24-hours, CNTI is significantly higher than all other materials ($p<0.001$) (figure 5.19 B), and after exposure for 48 hours CNTI is still inducing significantly more MCP-1 production than both asbestos samples ($p<0.05$) (figure 5.19 C).

At the longer exposure period of 48 hours, and in response to the highest exposure dose, the most pronounced change in MCP-1 production occurred with CNTD (figure 5.19 C). CNTD significantly increased MCP-1 production in MM6 cells, when compared to all the reference materials, for example, up to a 5-fold increase was shown in comparison to LFA.

The release of TGF-β1 from MM6 cells was not found to significantly increase in response to any of the particle treatments, when compared to medium-only controls (figure 5.20). However, TGF-β1 levels were particularly high when cells were exposed to CNTI, which translated as a significant increase compared to all other particles during 48-hour exposure to 8.5µg/cm^2 (figure 5.21).

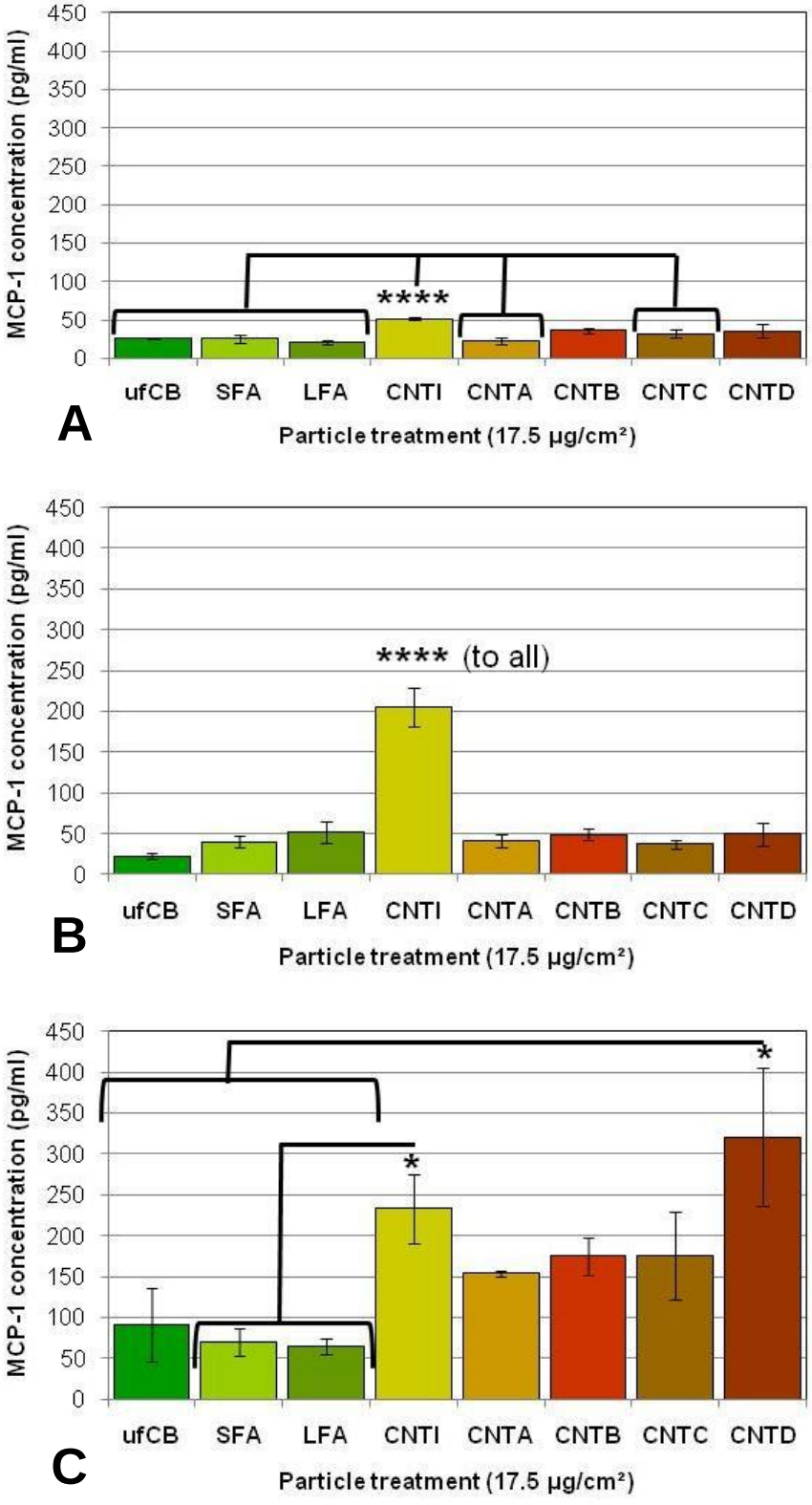

Figure 5.19 MCP-1 release from MM6 cells after exposure to particle panel B. Summary graph. Cells were treated with 17.5 µg/cm^2 ufCB, SFA, LFA, CNTI, CNTA, CNTB, CNTC, and CNTD for (A) 4 hours, (B) 24 hours, and (C) 48 hours. Results are expressed as MCP-1 release, each data point represents the mean ± SEM (n=3). Statistical significance is shown by **** = p<0.001, compared to relative particle treatment, at the same concentration.

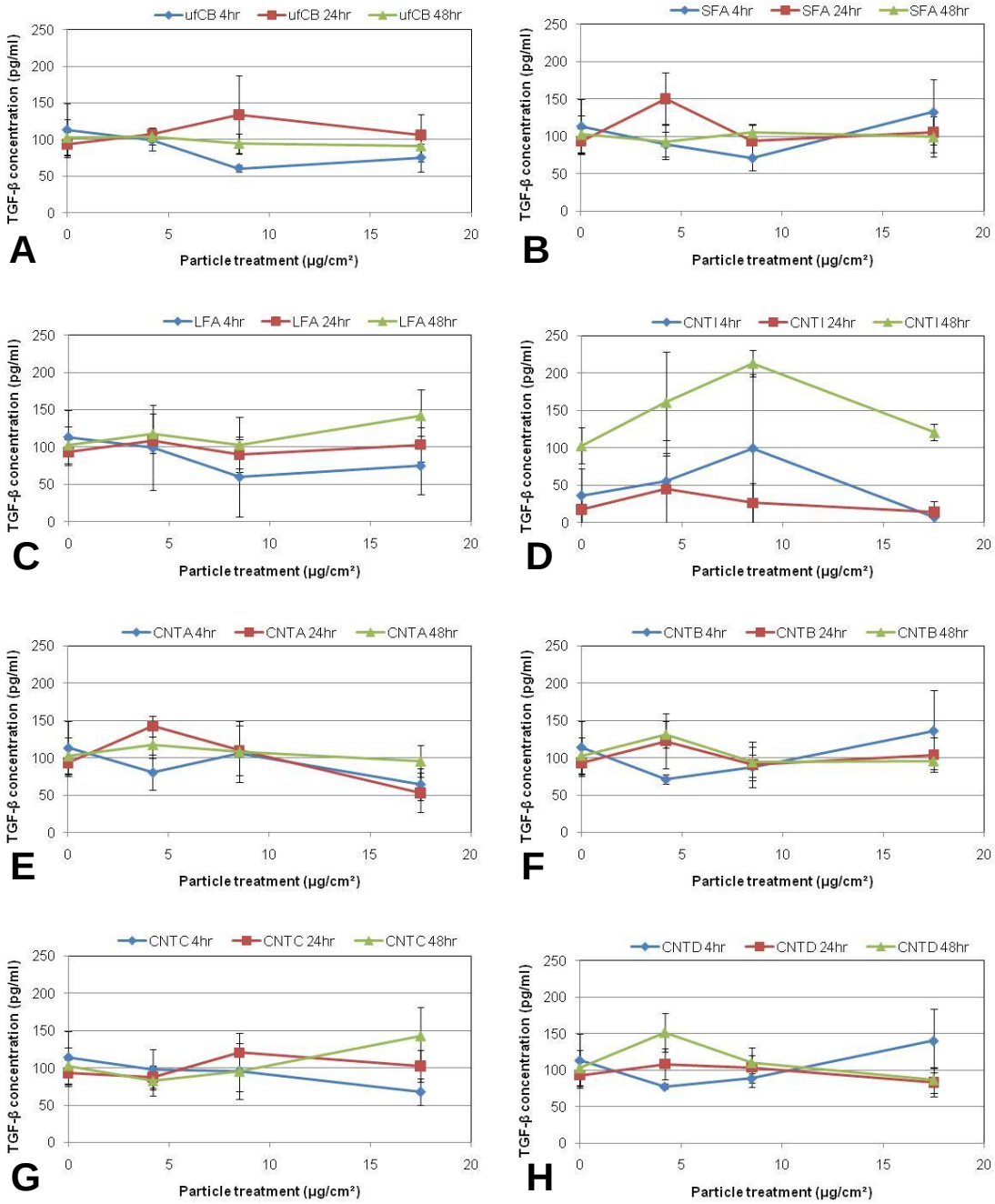

Figure 5.20 TGF-β1 release from MM6 cells after exposure to particle panel B. Cells were treated with medium-only, 4.2, 8.5, and 17.5 µg/cm^2 (A) ufCB, (B) SFA, (C) LFA, (D) CNTI, (E) CNTA, (F) CNTB, (G) CNTC, and (H) CNTD; for 4, 24, and 48 hours. Results are expressed as TGF-β release, and each data point represents the mean ± SEM (n=3).

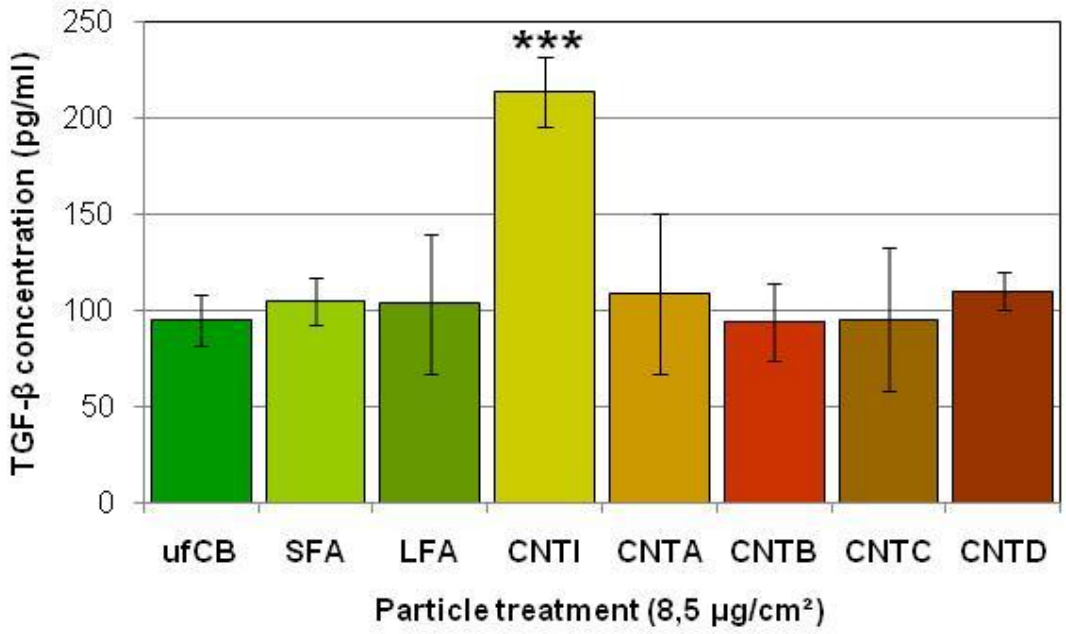

Figure 5.21 TGF-β release from MM6 cells after exposure to particle panel B. Summary graph. Cells were treated with 8.5 µg/cm^2 ufCB, SFA, LFA, CNTI, CNTA, CNTB, CNTC, and CNTD for 48 hours. Results are expressed as TGF-β release, and each data point represents the mean ± SEM (n=3). Statistical significance is shown by *** = p<0.005, compared to all other particle treatments.

Production of VEGF was shown to increase in response to a number of particles, but only during a 48-hour exposure period (figure 5.22). A relatively small, but significant, increase was seen in response to 8.5µg/cm^2 NPCB. A far greater increase was shown in response to 4.2µg/cm^2 treatments of CNTA, CNTB, and CNTC. The most pronounced secretion of VEGF was in response to CNTD (figure 5.22 H), this, however, was not found to be statistically significantly when compared to medium only controls.

When assessing the inter-particle differences, it was evident that all purpose-grown CNT (CNTA, CNTB, CNTC and CNTD) induced the production of significantly more VEGF than all reference materials during the 48-hour exposure to 4.2µg/cm^2 (figure 5.23).

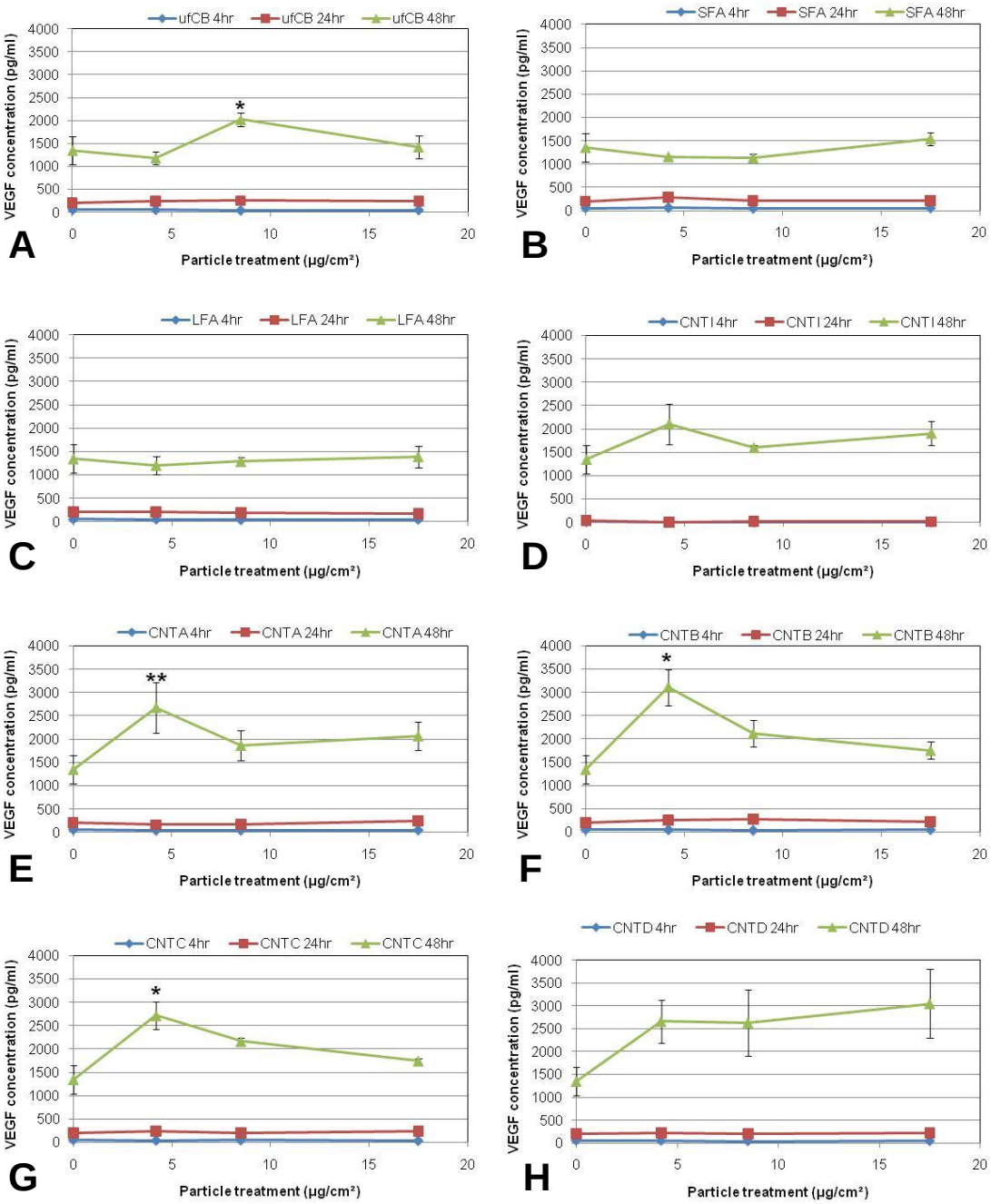

Figure 5.22 VEGF release from MM6 cells after exposure to particle panel B. Cells were treated with medium-only, 4.2, 8.5, and 17.5 µg/cm^2 (A) ufCB, (B) SFA, (C) LFA, (D) CNTI, (E) CNTA, (F) CNTB, (G) CNTC, and (H) CNTD for 4, 24, and 48 hours. Results are expressed as VEGF release, and each data point represents the mean ± SEM (n=3). Statistical significance is shown by * for 48-hour exposure (* = p<0.05, ** = p<0.01), compared to control.

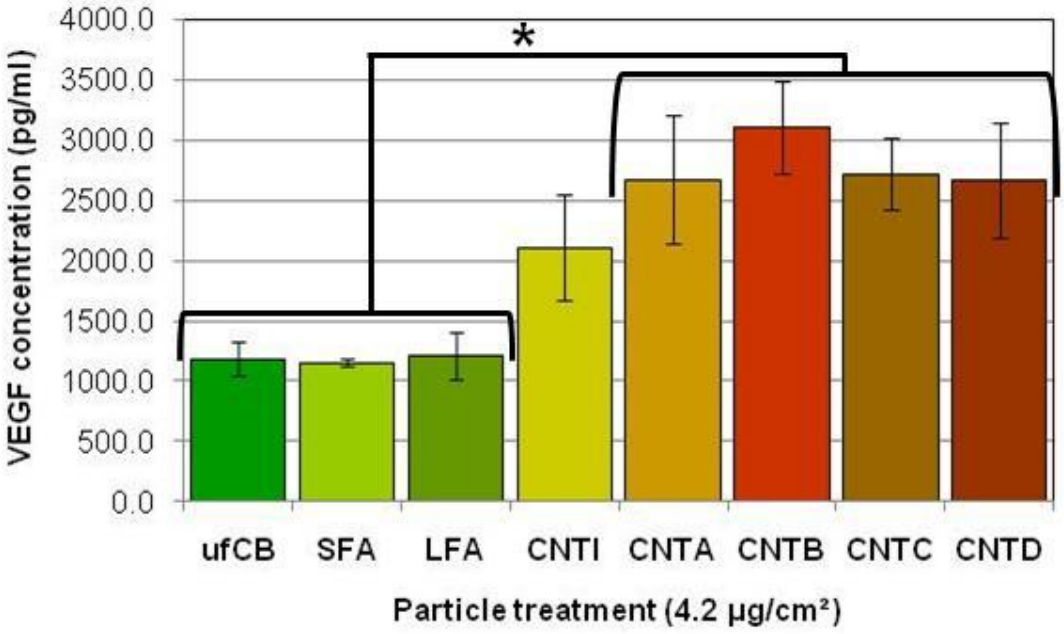

Figure 5.23 VEGF release from MM6 cells after exposure to particle panel B. Summary graph. Cells were treated with 4.2 µg/cm^2 ufCB, SFA, LFA, CNTI, CNTA, CNTB, CNTC, and CNTD for 48 hours. Results are expressed as VEGF release, and each data point represents the mean ± SEM (n=3). Statistical significance is shown by * = $p<0.05$, compared to relative particle treatment, of the same concentration.

5.2.2.2 J774A.1

The assessment of J774A.1 cell signalling was in response to 1.1–17.5µg/cm^2 of particle panel B (ufCB, SFA, LFA, CNTI, CNTA, CNTB, CNTC, and CNTD). Exposure periods were 4, 24, and 48 hours. Particle treatments induced no discernible differences in the release of IL-1β, IL-6, or IL-10, when compared to medium-only control cells. However, each cytokine was induced through J774A.1 exposure to LPS (figure 5.24).

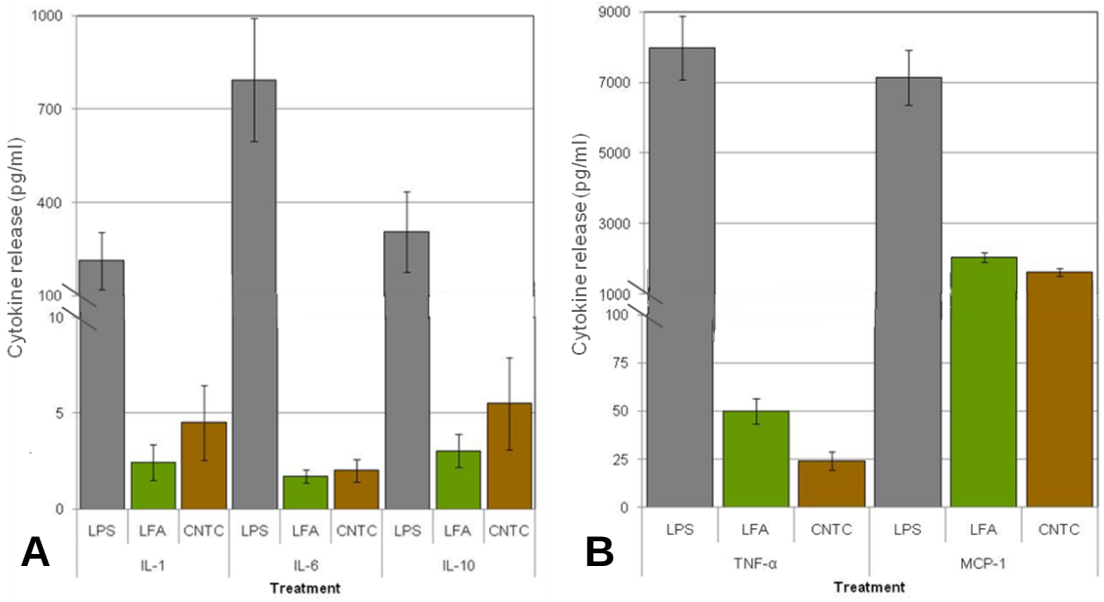

Figure 5.24 LPS induced cytokine release from J774A.1 cells in response to 1.5µg/ml LPS, or 17.5µg/cm^2 LFA, and CNTC, for 4 hours. Data is expressed as mean ± SEM, for cytokine release (A) IL-1, IL-6, and IL-10, and (B) TNF-α and MCP-1.

It was demonstrated that all particles within particle panel B can induce the release of MCP-1 from J774A.1 macrophage cells (figure 5.25).

NPCB induced a 1.6–fold increase in MCP-1 protein secretion compared to medium only control ($p<0.001$). This occurred during 48-hours of exposure to the highest concentration, and was considered the least responsive particle (figure 5.25 A). The induction of MCP-1 by SFA was slightly higher (figure 5.25 B), with a 2.7-fold increase ($p<0.001$), with increases found more frequently, in response to numerous concentrations and during both 24- and 48-hour exposures. LFA was also found to induce significant elevations of MCP-1 during the later time periods (figure 5.25 C), and with the highest response to LFA

being a 4.6-fold increase ($p<0.001$), it was considered the most response of the reference materials.

The MWCNT samples were shown to, not only induce a higher response than the reference materials, but to induce an increase of MCP-1 protein production at the lower exposure concentrations of 1.1 and 2.1µg/cm^2, not observed with exposure to the reference materials (figure 5.25). CNTI exposure resulted in an increase in MCP-1 after both 24- and 48-hour exposures (figure 5.25 D), with a highest response of 5.4-fold increase ($p<0.001$). Similarly, CNTA induced MCP-1 secretion during the 24- and 48-hour exposures (figure 5.25 E). CNTA was found to be slightly higher than treatments of CNTI, at the highest concentration, with a 6-fold induction compared to medium-only treated cells. CNTB was the least responsive of the CNT samples (figure 5.25 F), but still significantly induced MCP-1 release during both 24- and 48-hour exposure periods, with a highest response of a 3.9-fold increase after 48 hours at 17.5µg/cm^2 ($p<0.001$). Exposure to both CNTC (figure 5.25 G) and CNTD (figure 5.25 H) consistently resulted in significant MCP-1 secretions during the latter exposure periods, with 5.7 times that of medium-only control with CNTC exposure ($p<0.001$), and a 5.5-fold increase in response to CNTD ($p<0.001$).

Using the highest response, particle panel B can be placed in the following order, in respect to MCP-1 secretion: ufCB < SFA < CNTB < LFA < CNTI < CNTD < CNTC < CNTA. It is also worth noting that only CNT were able to induce a response at the lower concentrations.

When inter-particle differences were assessed, over the different concentrations, it was clearly the long, high iron CNTC that consistently induced a greater MCP-1 production. Over the 24-hour period (figure 5.26) CNTC exposure consistently resulted in a greater release of MCP-1 than other particles. During 48 hours exposure (figure 5.27) CNTC induced a greater response than all other particles at lower concentrations; at 8.5µg/cm^2 CNTC was still higher than both NPCB and SFA (figure 5.27 D). There were no differences found between particle treatments of 17.5µg/cm^2 at 24 or 48 hours (data not shown), and the high response to CNTC was not maintained, most likely this was due to the high cytotoxicity induced by CNTC at this dose.

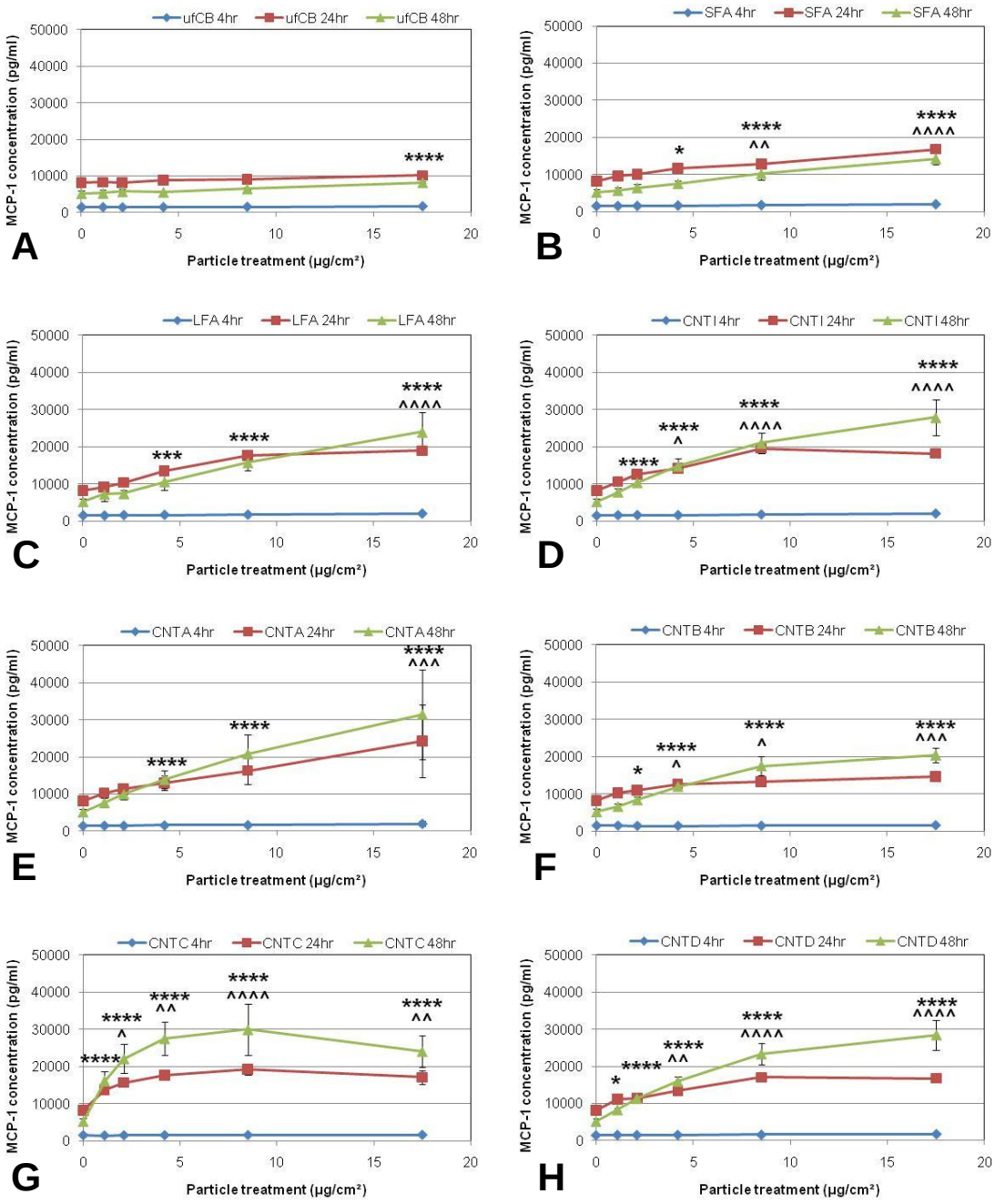

Figure 5.25 MCP-1 release from J774A.1 cells after exposure to particle panel B. Cells were treated with medium-only, 1.1, 2.1, 4.2, 8.5, and 17.5 µg/cm^2 (A) ufCB, (B) SFA, (C) LFA, (D) CNTI, (E) CNTA, (F) CNTB, (G) CNTC, and (H) CNTD for 4, 24, and 48 hours. Results are expressed as MCP-1 release, and each data point represents the mean ± SEM (n=3). Statistical significance is shown by ^ for 24-hour exposure (^ = p<0.05, ^^ = p<0.01, ^^^ = p<0.005, ^^^^ = p<0.001), compared to control; and * for 48-hour exposure (* = p<0.05, *** = p<0.005, **** = p<0.001), compared to control.

Figure 5.26 MCP-1 release from J774A.1 cells after exposure to particle panel B. Summary graph. Cells were treated with (A) 1.1, (B) 2.1, and (C) 8.5 μg/cm^2 ufCB, SFA, LFA, CNTI, CNTA, CNTB, CNTC, and CNTD for 24 hours. Results are expressed as MCP-1 release, and each data point represents the mean ± SEM (n=3). Statistical significance is shown by *** = p<0.005, **** = P<0.001,compared to relative particle treatment of the same concentration and

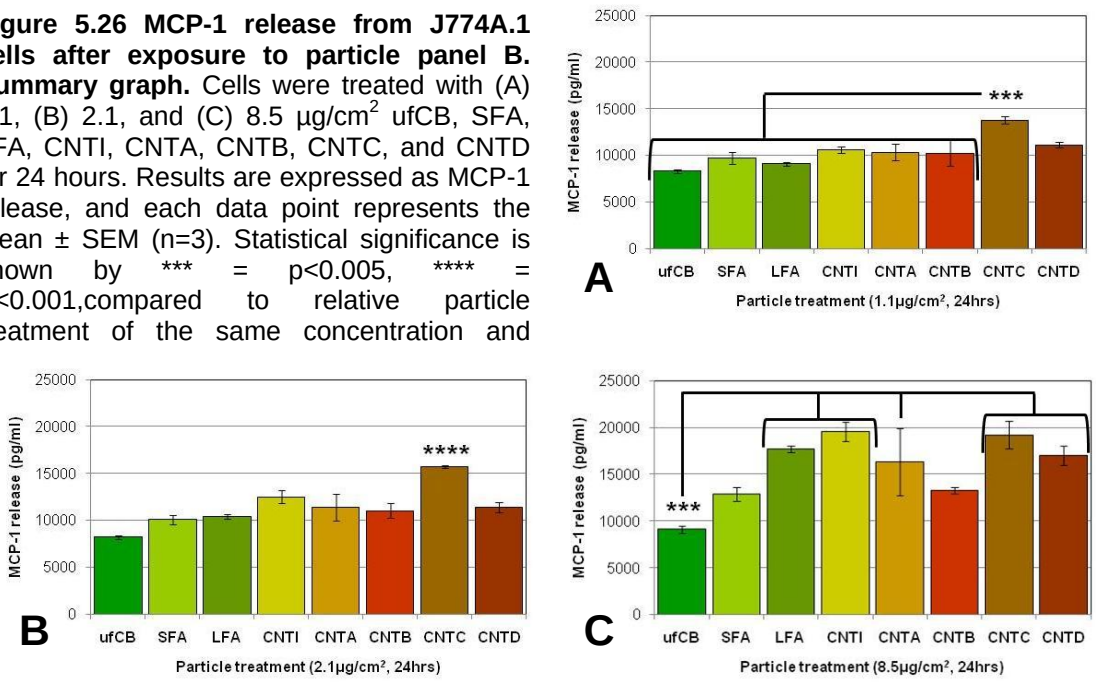

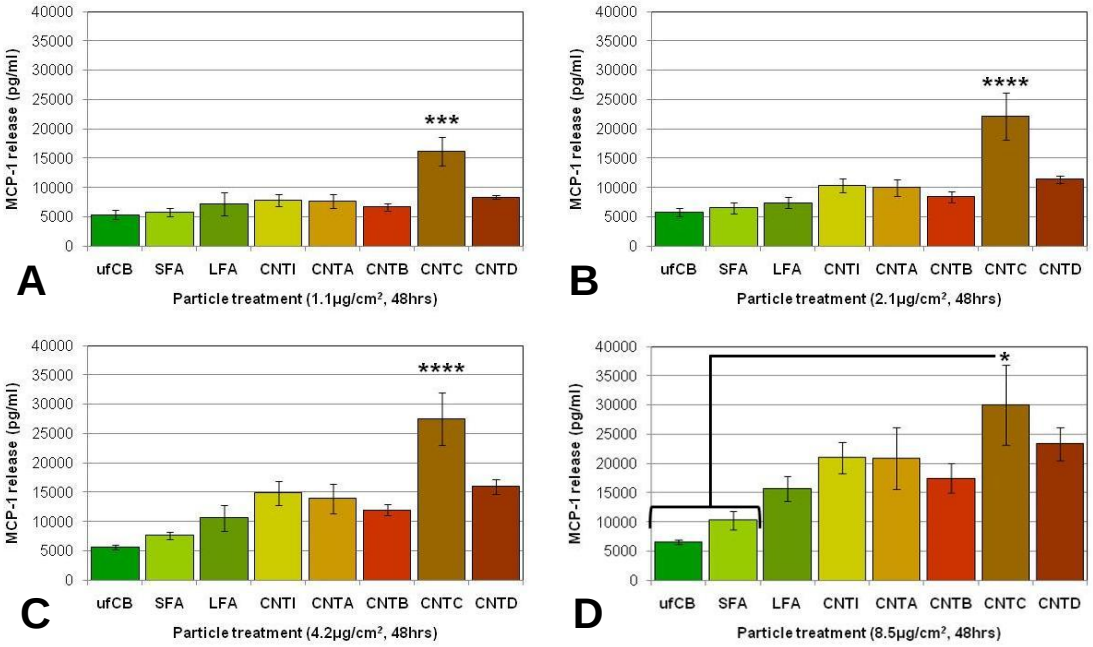

Figure 5.27 MCP-1 release from J774A.1 cells after exposure to particle panel B. Summary graph. Cells were treated with (A) 1.1, (B) 2.1, (C) 4.2, and (D) 8.5 μg/cm^2 ufCB, SFA, LFA, CNTI, CNTA, CNTB, CNTC, and CNTD for 48 hours. Results are expressed as MCP-1 release, and each data point represents the mean ± SEM (n=3). Statistical significance is shown by * = p<0.05, *** = p<0.005, **** = P<0.001, compared to relative particle treatment of the same concentration and exposure period.

The induction of TGF-β1 expression in J774A.1 cells (figure 5.28) was far clearer than that of MM6 cells. All particles were shown to stimulate a significant increase in TGF-β1 during the 48-hour exposure period, when compared to relative control cells. CNTA, CNTC, and CNTD also induced a significant increase after only 24-hour exposure to the highest particle concentration. The highest escalation in TGF-β1 was again with treatment of the long, high iron CNTC (figure 5.28 G). In this case a 3.2-fold increase was found in response to CNTC ($p<0.001$), compared to medium-only treated cells.

Comparing inter-particle responses (figure 5.29), the long, high iron CNTC was shown to have a greater ability to stimulate the production of TGF-β1, over 24 and 48 hours, than all reference materials and the short, low iron CNTB. The long, low iron CNTD was also able to induce a greater TGF-β1 production than all of the reference materials, except LFA. While the short, high iron CNTA was shown to induce a greater TGF-β1 release than its two length comparable counterparts (CNTI and CNTB), as well as all of the reference materials, during the 24-hour exposure period.

In respect to TGF-β1 secretion, it appears that both CNT length and iron content are influencing factors (figure 5.30). CNTB generated significantly less TGF-β1 than both the long CNT samples (with and without iron) during 24-hour exposure, at the highest concentration. Furthermore, during this exposure period CNTB generated significantly less TGF-β1 than its length comparable, high iron counterpart (CNTA) (figure 5.30 A). This pattern concerning CNTB was maintained during the 48-hour treatments; and additionally at this time period, lower concentrations of CNTC (4.2 and 8.5μg/cm^2) were shown to induce an increase in TGF-β1 protein secretion compared to their iron comparable counterpart, of shorter length, CNTA (figure 5.30 B).

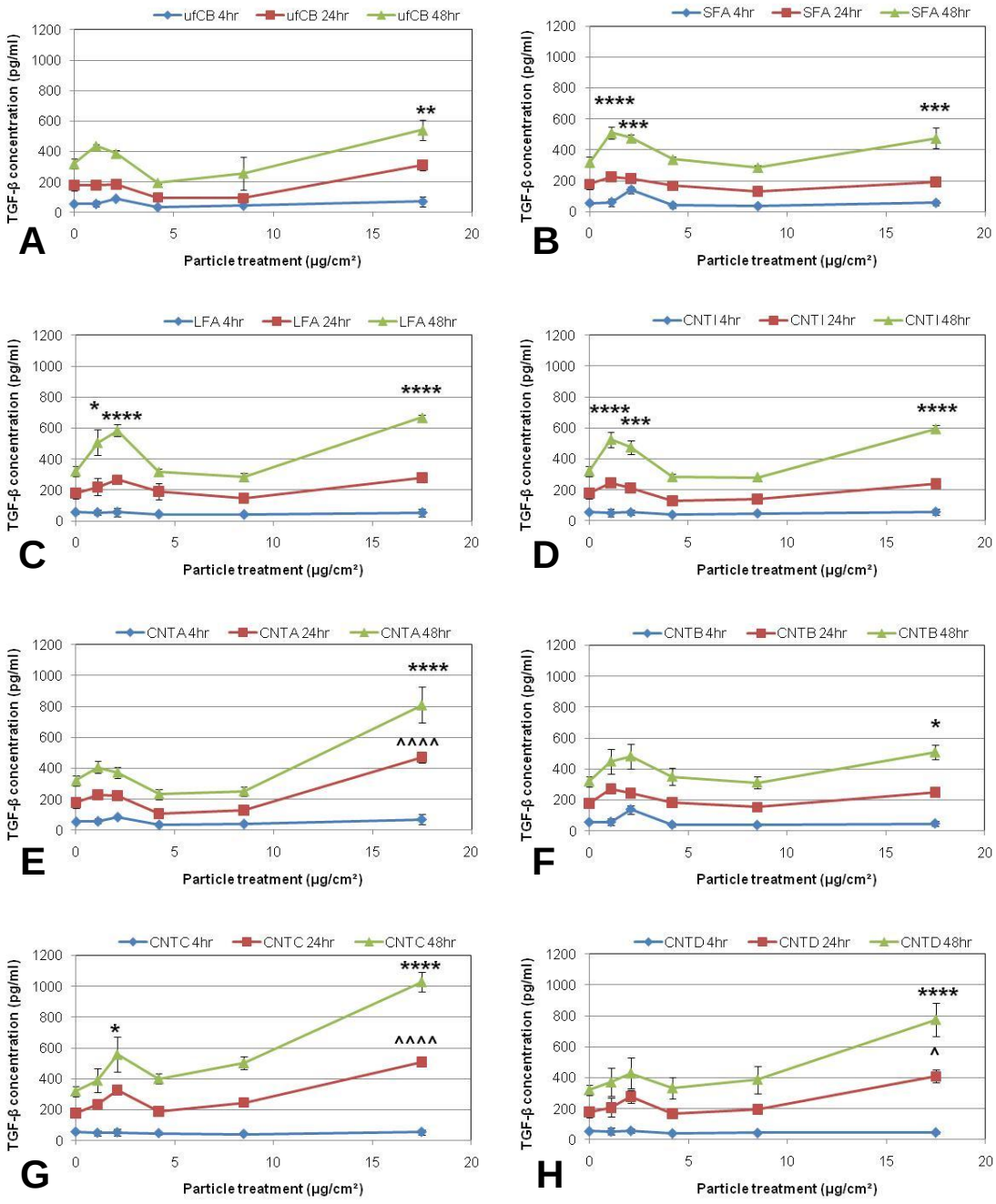

Figure 5.28 TGF-β release from J774A.1 cells after exposure to particle panel B. Cells were treated with medium-only, 1.1, 2.1, 4.2, 8.5, and 17.5 µg/cm^2 (A) ufCB, (B) SFA, (C) LFA, (D) CNTI, (E) CNTA, (F) CNTB, (G) CNTC, and (H) CNTD for 4, 24, and 48 hours. Results are expressed as TGF-β release, and each data point represents the mean ± SEM (n=3). Statistical significance is shown by ^ for 24-hour exposure (^ = p<0.05, ^^^^ = p<0.001), compared to control; and * for 48-hour exposure (* = p<0.05, ** = p<0.01, *** = p<0.005, **** = p<0.001), compared to control.

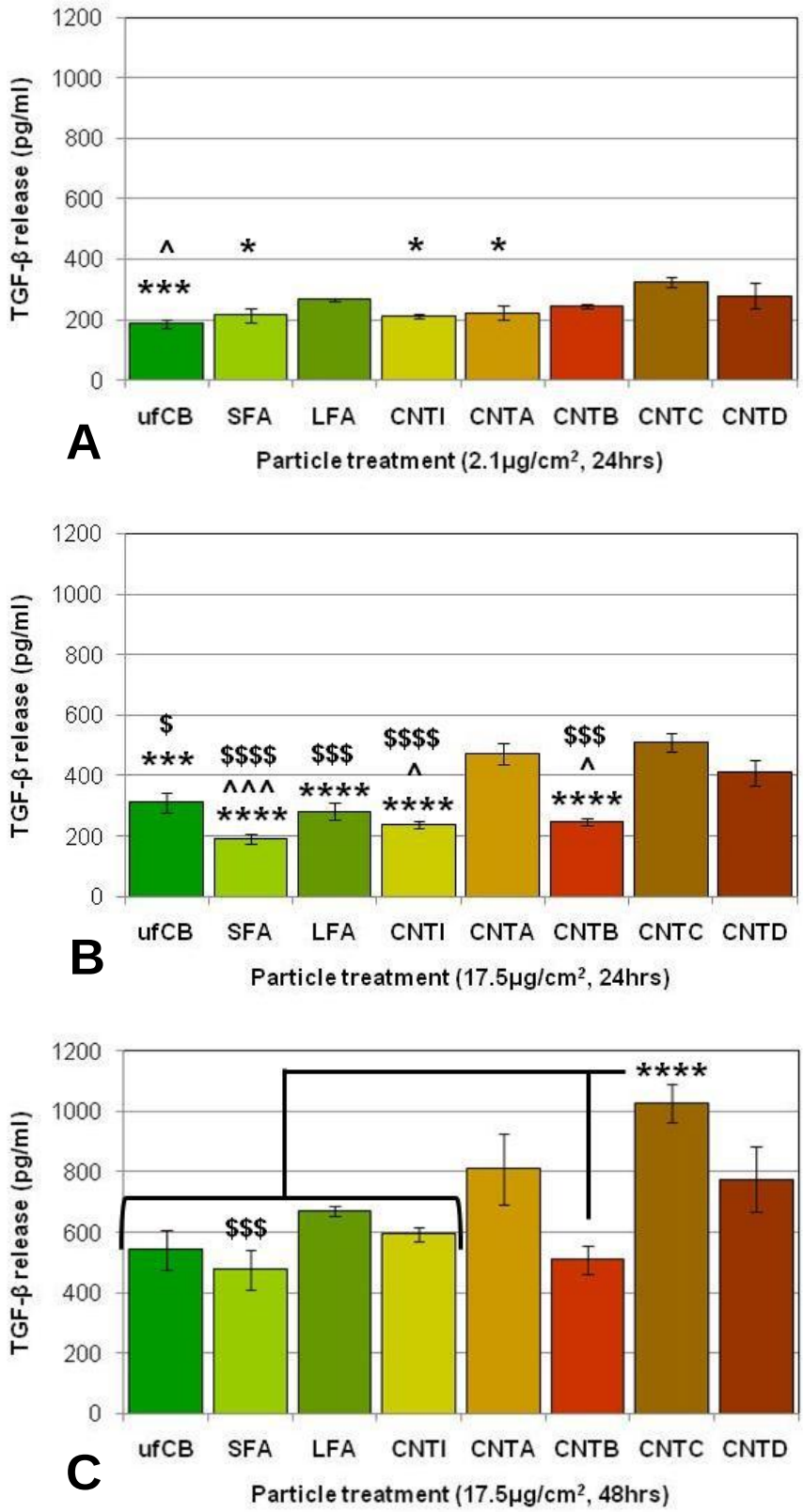

Figure 5.29 TGF-β release from J774.A1 cells after exposure to particle panel B. Summary graph. Cells were treated with (A) 2.1, 24 hours, (B) 17.5, 24 hours, and (C) 17.5 µg/cm^2, 48 hours; with ufCB, SFA, LFA, CNTI, CNTA, CNTB, CNTC, and CNTD. Results are expressed as TGF-β release, and each data point represents the mean ± SEM (n=3). Statistical significance is shown by * = p<0.05, *** = p<0.005, **** = P<0.001 compared to CNTC; ^ = p<0.05, ^^^ = p<0.005 compared to CNTD; and $ = p<0.05, $$$ = p<0.005, $$$$ = P<0.001 compared to CNTA same concentration and exposure period.

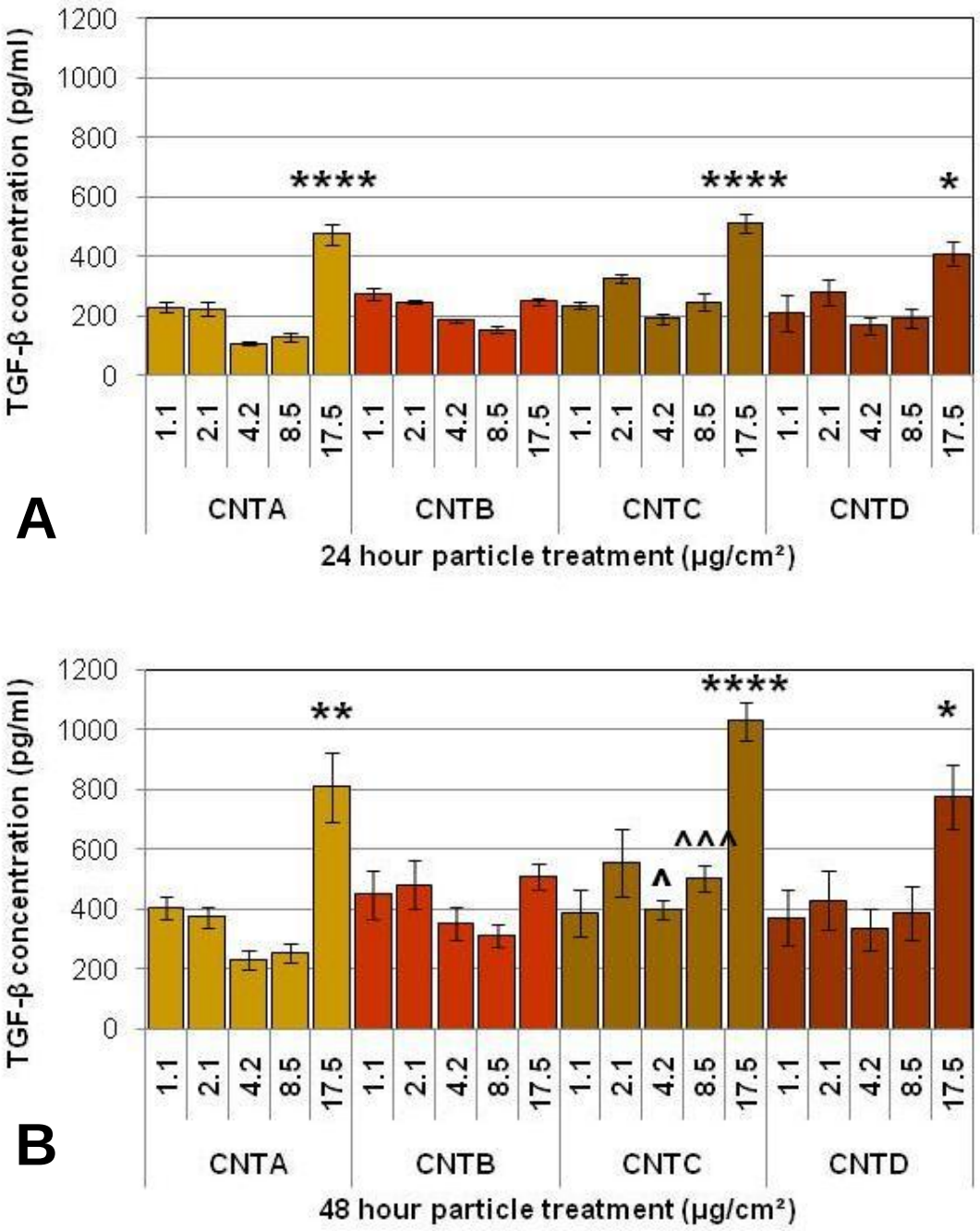

Figure 5.30 TGF-β release from J774A.1 cells after exposure to particle panel B. Summary graph. Cells were treated with 1.1, 2.1, 4.2, 8.5, and 17.5 µg/cm^2 CNTA, CNTB, CNTC, and CNTD for (A) 24 hours, and (B) 48 hours. Results are expressed as TGF-β release, each data point represents the mean ± SEM (n=3). Statistical significance is shown by * = $p<0.05$, ** = $p<0.01$, **** = $p<0.001$ compared to short/low iron CNTB at same time and dose; and ^ = $p<0.05$, ^^^ = $p<0.005$, compared to short/high iron CNTA at same time and dose.

During MM6 exposure the stimulation of TNF-α was only achieved in response to LPS, and not to any particle treatments. Here, with J774A.1 exposure, substantial TNF-α production was found in response to most particle treatments. The only particle not to induce any TNF-α production under these exposure conditions was NPCB (figure 5.31 A). SFA was shown to induce a significant response as early as 4 hours ($p<0.001$) (figure 5.31 B). Both SFA and LFA consistently induced TNF-α production during the later exposures ($p<0.001$). However, in comparison to CNT treatments, these reference materials generated relatively low levels of TNF-α protein, at highest a 3-fold increase was found in response to SFA, and a 5-fold to LFA.

CNT exposures induced a far greater response, and again it was only the CNT samples that induced a significant response at the lower concentrations. At the highest dose and longest exposure period, a 13-fold increase in TNF-α production was found in response to CNTI (figure 5.31 D). Moreover, CNTI stimulated a significant increase in TNF-α at the highest concentration from as early as 4 hours ($p<0.001$), and was found to be significantly higher than controls at numerous concentrations during 24- and 48-hour exposure periods. Of all the CNT, the short CNTA and CNTB were found to be the lowest inducers of TNF-α, but were still found to be significantly higher than controls at 8.5–17.5μg/cm^2 during 24- and 48-hours (figure 5.31 E and F). The long, high iron CNTC (figure 5.31 G) was shown to induce a significant TNF-α response with all exposure concentrations during 48 hours, and all except the lowest dose during 24 hours. The long, low iron CNTD (figure 5.31 H) also induced significant TNF-α release in response to numerous concentrations during both 24- and 48- hours.

Taking the top concentration as an example, the summary graphs (figure 5.32) demonstrate that the early induction of TNF-α caused by SFA was significantly higher than all other particle treatments (figure 5.32 A). However, as the exposure time increases it was the long (CNTC and CNTD) and industrial (CNTI) CNT samples that caused a greater TNF-α release compared to the reference materials, and the shorter CNT (figure 5.32 B and C). The graphs highlighting any differences in TNF-α production induced by CNT length or iron content (figure 5.33) identify CNT length as a factor that can significantly influence, with long CNT stimulating significantly greater responses than short.

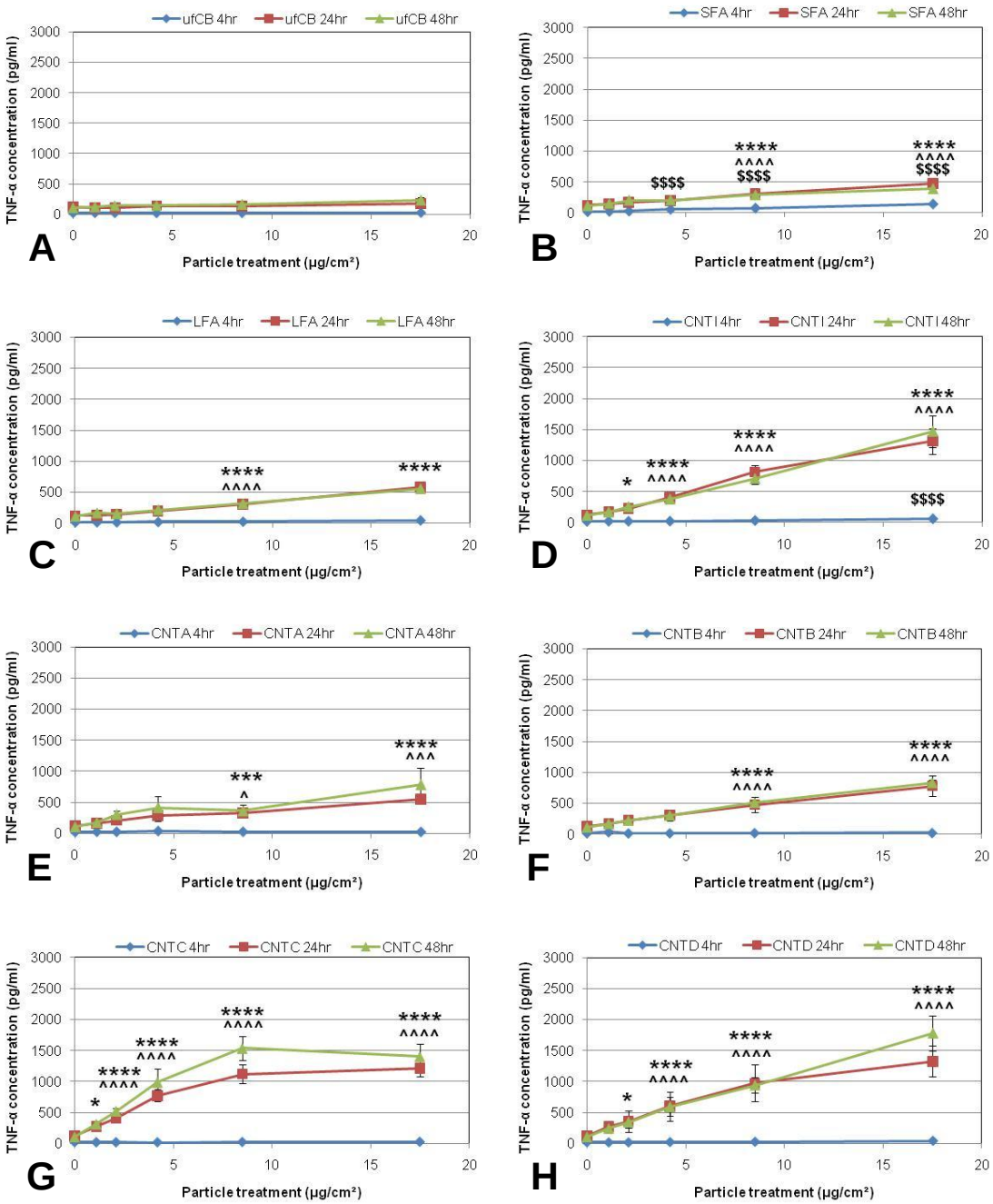

Figure 5.31 TNF-α release from J774.A1 cells after exposure to particle panel B. Cells were treated with medium-only, 1.1, 2.1, 4.2, 8.5, and 17.5 µg/cm^2 (A) ufCB, (B) SFA, (C) LFA, (D) CNTI, (E) CNTA, (F) CNTB, (G) CNTC, and (H) CNTD for 4, 24, and 48 hours. Results are expressed as TNF-α release, and each data point represents the mean ± SEM (n=4). Statistical significance is shown by $ for 4-hour exposure ($$$$ = p<0.001); ^ for 24-hour exposure (^^^ = p<0.005, ^^^^ = p<0.001), compared to control; and * for 48-hour exposure (* = p<0.05, **** = p<0.001), compared to control.

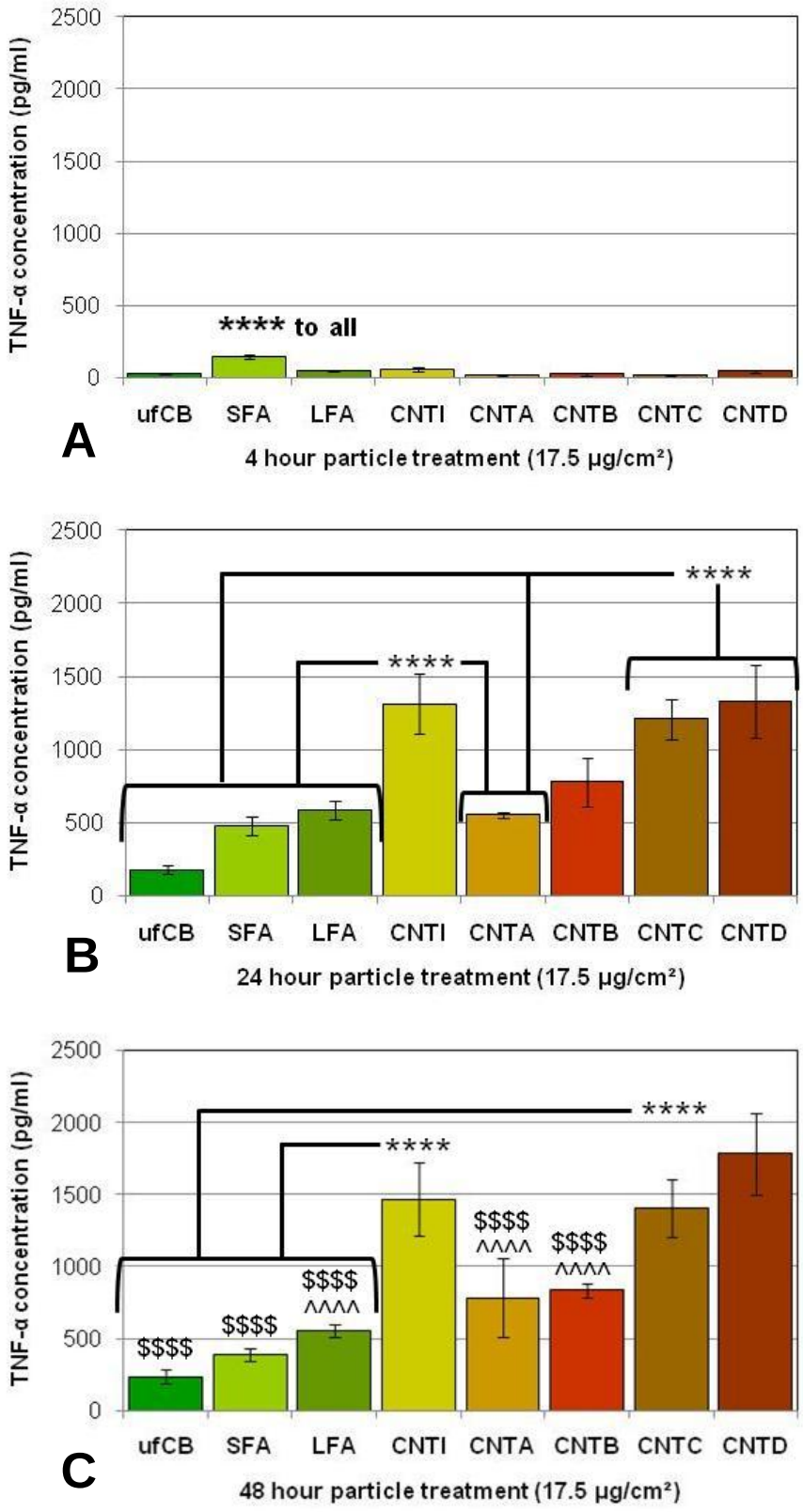

Figure 5.32 TNF-α release from J774.A1 cells after exposure to particle panel B. Summary graph. Cells were treated with 17.5 µg/cm^2 for (A) 4 hours, (B) 24 hours, and (C) 48 hours with ufCB, SFA, LFA, CNTI, CNTA, CNTB, CNTC, and CNTD. Results are expressed as TNF-α release, and each data point represents the mean ± SEM (n=4). Statistical significance is shown by **** = P<0.001 compared to relative particle treatment; ^^^^ = p<0.001, compared to ufCB; and $$$$ = P<0.001, compared to CNTD at same concentration and exposure period.

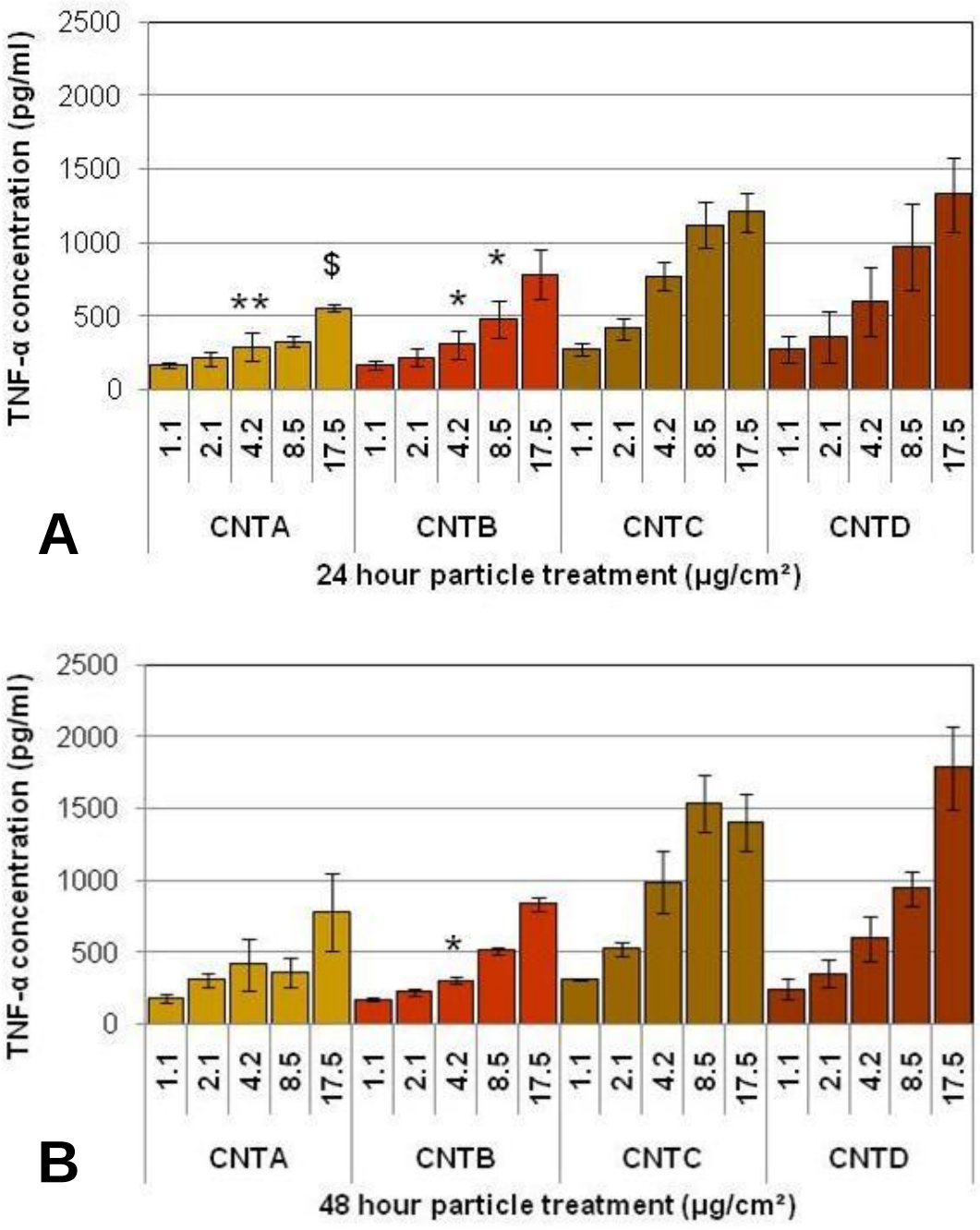

Figure 5.33 TNF-α release from J774A.1 cells after exposure to particle panel B. Summary graph. Cells were treated with 1.1, 2.1, 4.2, 8.5, and 17.5 µg/cm^2 CNTA, CNTB, CNTC, and CNTD for (A) 24 hours, and (B) 48 hours. Results are expressed as TNF-α release, each data point represents the mean ± SEM (n=4). Statistical significance is shown by * = $p<0.05$, ** = $p<0.01$, compared to long/high iron CNTC, at same time and dose; and $ = $p<0.05$, compared to long/low iron CNTD at same time and dose.

5.3 Discussion

The aim of this chapter was to evaluate the cytotoxicity of nanoparticle CB, SFA, LFA, CNTI, CNTA, CNTB, CNTC, and CNTD on exposure to macrophage cell lines MM6 and J774A.1; initially using measurements of fluorescently labelled DNA and apoptotic cell surface markers (PI and annexin-V), but later measurements of membrane permeability (LDH) and cellular respiration (WST-1). Both cell lines were also assessed for the production of inflammatory signalling proteins, using ELISA and CBA to measure release of GM-CSF, IL-1α, IL-1β, IL-6, MCP-1, TGF-β, TNF-α, and VEGF from MM6, and IL-1β, IL-6, IL-10, MCP-1, TGF-β, and TNF-α from J774A.1. The data obtained would be used to assess the inflammatory response and potential cytotoxicity of MWCNT, and relate any found to specific characteristics of the MWCNT used here, in particular CNT length, iron content, and crystallinity; but also relate any cytotoxic effect to a range of known pathogenic materials.

A number of cytokines were not induced by any particle treatment in this study. The release of GM-CSF, IL-6, IL-1α, IL-1β, or TNF-α were not found in particle exposures to MM6 cells; but IL-1, IL-6, and TNF-α were all induced during treatment with LPS. Particle exposure to J774A.1 cells provided no release of IL-1, IL-6, or IL-10, which again were all induced through LPS treatment. The lack of TNF-α release from MM6 cells in any particle treatment is particularly surprising, but not an isolated occurrence; no discernable release of TNF-α, IL-1β, IL-10, TGF-β was observed upon *in vitro* exposure of RAW 264.7 macrophages to SWCNT (Shvedova *et al.*, 2005); and Giorgio *et al.* (2011) were unable to induce TNF-α release from RAW 264.7 macrophage cells with treatments of either SWCNT or MWCNT at 10 and 50µg/ml up to 24 hours, but release was elicited through LPS stimulation. It is possible this may indicate a difference in particle-cell interactions occurring between the cell lines; or a cell sensitivity issue, for example MM6 cells have been shown to release MIP-1, IL-1β, IL-8, and TNF-α in response to household dust, while the same exposures do not induce MCP-1, IL-1α, or VEGF (Riechelmann *et al.*, 2007), and MWCNT have been shown to stimulate the production of IL-1α, IL-6, IL-8, VEGF (amongst others) with the *in vitro* exposure to bronchial epithelial cells, but not TGF-β (Hirano *et al.*, 2010). Co-stimulation of the cells, e.g. to LPS, could encourage TNF-α production. However, some macrophage studies using

preceding activation with LPS were not shown to increase their inflammatory response (TNF-α secretion) with secondary exposure to CNT, nanoparticle CB or quartz, with exposure concentrations up to 62.5μg/cm^2 (Pulskamp *et al.*, 2007a). Macrophages have been shown to release insignificant levels of IL-10 or IL-12 in response to short MWCNT and SWCNT (Murr, 2005). Similarly, epithelial cell exposure to CNT induced no IL-8 release, while nanoparticle CB and quartz at 62.5μg/cm^2 did (Pulskamp *et al.*, 2007a). In contrast, MWCNT were shown to cause the release of IL-8 in epithelial A549 cells when nanoparticle CB exposure did not (Han *et al.*, 2010).

As mentioned, the co-stimulation of cells with LPS and particles may, or may not, have encouraged the release of TNF- α from MM6 cells; but co-stimulatory effects on IL-1 secretion from both cell types should also be considered. There are differences in the signalling pathways that lead to secretion of TNF-α and mature IL-1, for TNF-α only one signal and one stimulus is needed for the release of a functional protein. Contrary to this, the eventual secretion of mature IL-1 requires two signals, one for the synthesis of pro-IL-1 and a second for mature IL-1 to be formed and secreted. It is the action of inflammasomes that are responsible for this secondary activity; initial TLR binding can be the stimuli for the first signal, for pro-IL-1 expression, with the maturation of IL-1 due to the inflammasome associated caspase-1 enzyme (Meunier *et al.*, 2011). In allergen induced lung inflammation, for example, the binding of TLR4 at the cell surface is found to be essential, but also so is the activation of the cytosolic nod-like receptor NLRP3, which upon activation forms a multiprotein complex containing activated caspase-1, called an inflammasome. This protein modulates inflammatory responses, such as the maturation of pro-IL-1 to IL-1, and IL-1 secretion (Besnard *et al.*, 2012), by cleaving the inactive pro-IL-1 precursor (Dostert *et al.*, 2008). The secretion of both IL-1α and IL-1β can be modulated in parallel by inflammasomes, with the simultaneous secretion of both. However, IL-1α secretion may also be independent of any inflammasome activity, such as through the activity of intracellular calcium and binding of foreign particles (Groß *et al.*, 2012). Incidentally, IL-1α release can be both independent of inflammasome activation, and in conjunction with inflammasome activation (Groß *et al.*, 2012). There is an emerging body of evidence that implicates the involvement of inflammasomes is numerous inflammatory

disorders, from allergic asthma (Besnard *et al.*, 2012) to CNT and particle induced inflammation (Dostert *et al.*, 2008, Meunier *et al.*, 2011), and links to fibrotic respiratory disorders such as silicosis (Cassel *et al.*, 2008, Hornung *et al.*, 2008) and asbestosis (Dostert *et al.*, 2008) have been proposed.

The mechanisms of inflammasome activation appear to be numerous, it may be through the action of ROS (Shvedova *et al.*, 2012) generated by particle phagocytosis associated NADPH oxidase complex activity (Shvedova *et al.*, 2012), or from cathepsin B enzyme activity and ROS released due to the disruption of lysosomes subsequent to particle internalisation (Hornung *et al.*, 2008, Shvedova *et al.*, 2012). Asbestos and silica induced IL-1β secretion has been shown to be dependent on the NLRP3 inflammasome. This, however, is not the case for all particles, as parallel exposures of DEP, for example, show no such secretion of mature IL-1β (Dostert *et al.*, 2008). In the case of asbestos it was shown that inflammasome activation was at least partially due to the ROS produced during active phagocytosis and the NADPH oxidase complex, and also ROS generated through the Fenton chemistry reactions involving iron housed upon the asbestos samples (Dostert *et al.*, 2008). These data were collected *in vitro*, but similar results were found *in vivo* when asbestos exposed NLRP3 deficient mice were reported to have a lesser inflammatory response than NLRP3$^{+/+}$ mice upon identical asbestos exposures (Dostert *et al.*, 2008).

Here it has been shown that MWCNT are actively phagocytosed, and that both long CNT and short CNT agglomerates cause frustrated phagocytosis and ROS release; however, in this study the release of mature IL-1 was not found. This is in disagreement with the statements of Dostert *et al.* (2008), that NLRP3 inflammasome activation may be through ROS produced during NADPH oxidase activity, but lends more to the theory that ROS induced activation is more likely through the complete internalisation of fibres, with subsequent lysosome disruption. This later theory is somewhat corroborated by Meunier *et al.* (2011) who demonstrated that the inflammasome associated maturation of IL-1 may be associated with the complete phagocytosis of the DWCNT used in their study. It is, however, also important to mention that Meunier *et al.* (2011) also demonstrated that a release of potassium from a loss of cell membrane integrity can also be implicated in NLRP3 inflammasome activation (Meunier *et al.*, 2011). Due to this, and the study by Dostert *et al.* (2008) - who implicated

the ROS generated during frustrated phagocytosis in inflammasome activation - CNT induced membrane impairment cannot be ruled out, and may be implicit in NLRP3 inflammasome activation. In fact, using TiO_2 nanospheres and nanobelts, a particle length dependency has been associated with NLRP3 inflammasome activation, with only TiO_2 nanobelts of a length to impede phagocytosis were found to elicit a response (Hamilton *et al.*, 2009). Other studies have implicated particle morphology in inflammasome activation. Palomäki et al. (2011) demonstrated that inflammasome activation was intrinsic in CNT induced IL-1 secretion, for long needle-like CNT and asbestos it was essential that the NLRP3 inflammasome was activated prior to IL-1β secretion by both these fibres. In the study by Palomäki *et al.* (2011) it was shown that IL-1α was released only in exposures of CNT and not asbestos, or other carbon NM, and that this secretion was dependent on NLRP3 inflammasome activation, but also on ROS production. However, with exposures of particles (nano sized titanium dioxide and silica) (Yazdi *et al.*, 2010), or UV radiation (Nasti and Timares, 2012), to keratinocytes it has been shown that inflammasome associated IL-1α and IL-1β secretion can occur independently of phagocytosis.

The lack of IL-1 secretion found here, from both cell types, may or may not be associated with the inflammasome signalling. It is possible that the ROS produced in response to MWCNT exposures, and the significant disruption to the cells' membrane integrity did not induce the formation and activation of the NLRP3 inflammasome; but it also possible that these events did induce inflammasome activation, and that it is the first signal that was missing, therefore no pro-IL-1 would have been produced. It was not done here, but one method to test this would have been to use the co-stimulation of these cells with LPS.

5.3.1 Inflammatory response by MWCNT

The function and implications of expression of the various cytokines and chemokines investigated in this study have been described in section 5.1.4; and the inhalation of NP and pathogenic fibres has for many years been seen to cause severe problems, such as lung inflammation, fibrosis, and tumourigenesis (Donaldson and Borm, 1998, Donaldson *et al.*, 2002, Mossman

and Churg, 1998, Wilson *et al.*, 2002). It is therefore important to establish what conditions may be stimulated in response to CNT.

The reference materials were shown to elicit varying degrees of pro-inflammatory and pro-fibrotic conditions, but were habitually surpassed by the signalling response to MWCNT. During the 4-hour exposure period of MM6 cells there was no increase in cytokine release from any treatment condition. In fact for the reference materials there was also no evidence of chemoattractant MCP-1 release during the whole exposure period of up to 48 hours. However, exposure of MM6 cells to CNTI, CNTB, and CNTD all resulted in MCP-1 protein secretion during the 48-hour exposure period, at all concentrations of CNTI and CNTB, and at 24 hours to all concentrations of CNTI. These CNT do not share many of the predetermined toxicity-inducing characteristics, only that they are all of a higher crystallinity. This does, however, start to indicate the inflammatory potential of MWCNT over the nanoparticle CB and asbestos samples used here. In fact, CNTI was shown to consistently and significantly induce higher MCP-1 release than the reference materials, and often when compared to the other CNT. If the influence that MCP-1 has on both fibrosis and potentially tumourigenesis are to be considered, discussed in the introduction to this chapter (section 5.1.4), this high level of MCP-1 release induced by CNT exposures is very significant.

It was also CNTI that stands out when observing release of TGF-β from MM6 cells. Compared to the control cells, incubated in medium alone, CNTI almost induced a significant increase in TGF-β protein release from MM6 cells with p-value = 0.056 at a concentration of 8.5μg/cm^2, while a comparison within particle exposures reveals that CNTI significantly caused approximately a 100% increase in expression of TGF-β in comparison to all other particles on this panel. CNTI is similar in length to CNTA and CNTB, and iron content and iron dissolution to CNTA and CNTC; the only clear discernible characteristic of CNTI is that it has a far greater graphite purity than the other samples.

The measure of VEGF secretion is the first time any of the reference materials provides an increase compared to MM6 control cells; with 48-hour exposure to nanoparticle CB at 8.5μg/cm^2 inducing a 50% increase in VEGF compared to control cells. During this exposure CNTA, CNTB, and CNTC also increased VEGF, but to a greater extent, with 98%, 131% and 102% increases,

respectively. CNTD induced consistently high VEGF expression, up to 126% increase compared to controls, but this was not found to be significant. However, CNTD, along with all other laboratory-produced CNT, was found to induce greater VEGF than all reference materials at the lowest dose in this study (4.2μg/cm^2). The results observed in MM6 cell exposures do not really provide any clear evidence of any single CNT characteristics being responsible for inducing the greatest response; the high crystallinity of the industrially produced sample appears significant in MCP-1 and TGF-β secretion, but this CNT has little effect on VEGF release, indicating that the possibility of differences in more discrete signalling may be occurring.

The J774A.1 cells were found to be more responsive than the MM6 cells. MCP-1 was found to increase, compared to medium-only controls, in response to all particles used here during the 24- and 48-hour exposures. The lowest response was by nanoparticle CB exposure with only a 57% increase; while again it was the full range of CNT that induced the greatest response with approximately 418% increases found at the highest dose of 17.5μg/ml. Also worth noting is the observation that most of the CNT have a somewhat linear relationship between exposure dose and MCP-1 release, while exposure to the long, high iron release CNTC resulted on a relatively high MCP-1 release at low doses with almost plateauing effect as the concentration increases. When comparisons are made within the particle exposures, this effect was found to be significant, and MCP-1 production from CNTC exposure continued to be statistically higher than all other material at the lower concentrations.

There was also a clear trend observed for secretion of the pro-fibrotic cytokine TGF-β. With exposure of J774A.1 cells to the two lowest concentrations (1.1 and 2.1μg/cm^2) (which incidentally were not used during MM6 experiments,) there was a clear initial rise which dipped with the following two concentrations and then finally peaked at 17.5μg/cm^2, and this was seen in practically all exposures. The measurements of TGF-β were found to be particularly similar across the whole of the particle panel. The lowest release, however, was found in response to both nanoparticle CB and, interestingly, the short low iron CNTB, while the highest TGF-β production was again seen in response to CNTC. It was also clear that within this group of material CNTC consistently induced a greater production of TGF-β compared to much of the panel.

The measurement of TNF-α in exposure supernatant follows the pattern that has been observed throughout this study. The least responsive were cells treated with nanoparticle CB which displayed no significant increases, all other material did, to varying degrees. MWCNT again induce the greatest response, particularly the industrial sample and the two long MWCNT samples. With a 1500% increase in response to 17.5μg/cm^2 after 48 hours. The same exposure conditions for nanoparticle CB, SFA, and LFA gave increases of only 115%, 252%, and 405%, respectively. This clearly demonstrates the scope of the inflammatory response occurring with exposure to long MWCNT, particularly as LFA is a known pathogenic fibre, causing malignancies in the mesothelium and lung tissue (Fisher *et al.*, 2000). The function of TGF-β as an anti-inflammatory mediator (discussed in section 5.1.4) may shed some light on the pattern of its secretion here, and using a comparison with the pro-inflammatory mediators there may be an insight into what is occurring with MWCNT exposure. The inflammatory response initiated by all particles during J774A.1 exposure was clear, with expression of both MCP-1 and TNF-α clearly present in response to the entire panel. The release of TGF-β, levels of which are found to be similar amongst the panel, should in some way stay this inflammatory response. However, the vast increases in MCP-1 and TNF-α in response to many of the CNT samples compared to the minor increases found in the other particles, particularly nanoparticle CB and SFA at the later time points, is an indication that the cells have some level of control over the exposure of nanoparticle CB and SFA, while response to the MWCNT increases unperturbed irrespective of the anti-inflammatory signalling, which may be indicative of frustrated phagocytosis.

5.3.2 Effect of MWCNT characteristics on inflammatory response

There is a clear difference in the response to MWCNT compared to the reference materials used here; CNT consistently induce elevated pro-inflammatory and pro-fibrotic conditions in comparison to the reference material. Observations within the different MWCNT samples indicate that there is little to discern them with respect to MM6 cell exposure, or through MCP-1 release from J774A.1 cells. However, observations of TGF-β and TNF-α make it clear that the long samples CNTC and CNTD induced the highest response, with the

short CNTA also promoting a greater pro-fibrotic response than its low iron counterpart, CNTB. This was also seen in other studies used to determine the effect of CNT length. Poland *et al.* (2008) observed an increase in granuloma formation and enhanced inflammatory response following injection of particularly high aspect ratio CNT into the peritoneal cavity, especially when compared to negative controls and shorter CNT samples, but also when compared to a long asbestos sample (LFA), displaying a clear correlation with results of this study in all respects. A significant release of TNF-α from THP-1 cells in response to exposure of long and short MWCNT for 4 hours has also previously been shown, with no significant increases in response to entangled CNT or CNF samples; and similarly to this study no increases were found from carbon nanoparticles at the 24-hour exposure period (Brown *et al.*, 2007b). The same long MWCNT used by Brown *et al.* (2007b), which incidentally are almost identical to CNTC used here, are shown to induce a significant inflammatory response with *in vivo* instillation into the rat lung, not seen in response to either a short or entangled CNT samples (Rothen-Rutishauser *et al.*, 2010). When a mouse macrophage cell line (RAW 264.7) was exposed to glass fibres of lengths that are either easily engulfed by the macrophages, or too long and therefore undergo frustrated phagocytosis, there is a clear length-dependent effect. Both induce a time- and dose-dependent release of TNF-α, but substantially more in response to the long fibres; this release was associated with oxidative stress and NF-κB activity (Ye *et al.*, 1999a). Any difference in response by iron content was limited, in measures of cytotoxicity. In inflammatory and fibrotic indicators an increase in bioavailable iron is shown to increase TNF-α expression, as long as the CNT is of a length that a phagocyte may easily engulf; however, Lam *et al.* (2004a) found granuloma formation irrespective of CNT sample iron content, again indicating that CNT morphology is more important than iron content.

5.3.3 Cytotoxic response to MWCNT

Similarly to the inflammatory response, observations of cytotoxicity induced by MWCNT on the different cell lines of this study clearly indicate certain patterns of toxicity, within the group of five MWCNT and when compared to the reference materials.

When assessing the deterioration of membrane stability by LDH release it is shown that, irrespective of cell type, there is no increase in LDH in response to the asbestos or nanoparticle CB, compared to a healthy population of cells, or from any of the particle panel over the initial 4-hour exposure period. This may in part be due to a 1–2 hour period it takes CNT suspensions to fully deposit on a cell monolayer (Hirano *et al.*, 2010). Measurements of mitochondrial function, however, appeared to be more discerning, which is understandable as the LDH release would only be from cells that have undergone primary or secondary necrosis, while a measure of cell population by its mitochondrial function would reveal cells undergoing necrosis or early and late apoptosis. At the early stages of these exposures nanoparticle CB (4 and 24 hours) and to a lesser extent SFA (only at top concentration of 17.5µg/ml), caused a decline in cell viability, illustrated by WST-1 reduction. This effect, however, disappeared by 48 hours when the cells demonstrated full recovery. The data for these reference materials in all cytotoxicity experiments in this study indicate the ability of both cell lines to consistently manage and control exposures of these materials (nanoparticle CB, SFA, and LFA) under these conditions. In some instances this is surprising as nanoparticle CB, chrysotile asbestos, and aggregated MWCNT have been shown to elicit the same levels of cytotoxicity in RAW 264.7, THP-1, and A549 cell lines, with as little as 5µg/ml for 48 hours (Soto *et al.*, 2008); crocidolite asbestos is shown to cause cell death, with exposure conditions relevant to this study, in A549 epithelial cells (Thurnherr *et al.*, 2010), fibroblasts (Cardinali *et al.*, 2006), mesothelial cells (Cardinali *et al.*, 2006, Jimenez *et al.*, 1997), and macrophages (Cardile *et al.*, 2004). Nanoparticle CB was also at times seen to demonstrate considerable cell death in alveolar macrophages (Pulskamp *et al.*, 2007a). There is also, however, clarifying and complimentary findings to the data presented here that show the doses used as sublethal concentrations are justified: crocidolite is shown to need 637µg/ml and 24-hour exposure to reach IC_{50} in J774A.1 cells (Hirano *et al.*, 2008), C_{60} displays no relative cytotoxicity in alveolar macrophages at 28.25µg/cm^2 (Jia *et al.*, 2005), and nanoparticle CB displays no cytotoxic response on epithelial cells *in vitro* at 100µg/ml, even though it was internalised (Tabet *et al.*, 2009).

At later time points all the MWCNT were shown to cause significant cytotoxicity when compared to a healthy control cell population, bearing in mind this is

looking at the two cell types (MM6 and J774A.1) as a whole. Typically it was the highest concentration of 17.5µg/cm^2 causing the most extensive cytotoxicity in both cell lines. The largest increase of LDH release from J774A.1 cells, approximately two-fold, was in response to 17.5µg/cm^2 CNTC; CNTI and CNTD exposures also displayed significant LDH leakage at the lower concentrations. In MM6 cells, however, it was the short CNTA and CNTB that induced significant membrane impairment; this response was not as notable, however, indicating J774A.1 cells to be far more susceptible to particle-induced cytotoxicity than MM6 cells, as was also shown in respect to an inflammatory reaction. All MWCNT, except CNTA, were found to reduce cell viability measured by mitochondrial function at the later time points, with particular emphasis on the long CNT samples (CNTC and CNTD), with CNTC exposure inducing a 50% and 30% reduction in viable J774A.1 and MM6 cells, respectively, after 48-hour exposure to 17.5µg/cm^2. This length-dependent cytotoxicity has been mirrored in other studies with 100µm SWCNT causing 30% reduction in THP-1 cell viability at 7.8µg/cm^2 (Kalbacova *et al.*, 2006), and MWCNT with varying length from 3–30µm shown to display considerable cytotoxicity to J774A.1 cells, reaching an IC_{50} after 32-hour exposure to 22µg/ml (Hirano *et al.*, 2008), and as previously mentioned, this response was much greater than their reference asbestos sample, as crocidolite needed 637µg/ml to reach IC_{50}. The cell death here was not associated with any oxidative stress or markers of apoptosis, and therefore was presumed to occur through direct membrane injury by the fibrous material (Hirano *et al.*, 2008).

A comparative look at cytotoxicity within the particle panel and not in respect to the negative control medium-only treated cells, further highlights the impact these MWCNT are having on these inflammatory cells. In J774A.1 at exposure concentrations of 17.5µg/cm^2, all the MWCNT samples demonstrate a greater cytotoxicity than nanoparticle CB and SFA, and in MM6 exposure CNTI is found to induce more LDH release than all of the reference materials. Incidentally, during J774A.1 exposure the LFA sample was shown to have a greater cytotoxicity than its shorter counterpart, SFA.

5.3.4 Effect of MWCNT characteristics on cytotoxicity

Much of the data presented here clearly demonstrates that the cytotoxic potential of these five MWCNT samples is considerable, and is greater than that of the reference materials, including that of the long fibre amosite asbestos. However, it is also important to assess the characteristics that are responsible for CNT cytotoxicity. It is not always clear which aspects were responsible for the cytotoxicity shown in this study. Certainly the greatest responses were found from treatment with the long CNT samples, but it was only with mitochondrial function assessment of J774A.1 cells that statistical differences were found between the CNT samples, and indeed the long MWCNT were shown to be considerably more cytotoxic than the short; and in one occasion the long high iron CNTC was found to reduce viability to a greater extent than its long low iron counterpart. This somewhat indicates that morphology is key, and an increase in fibre length greater than that which is easy to phagocytose increases cytotoxicity in CNT. This is not to say that iron content and crystallinity are not important, they may be, but this was less evident here. Much of the literature focussing on the *in vitro* assessment of macrophage exposure to CNT supports the findings here, that CNT morphology is the discerning factor in their ability to induce cell death.

In a study with a similar MWCNT and experimental conditions to this one human monocyte-derived macrophages (HMM) were exposed to MWCNT with an identical production method, and also with decreasing levels of iron. Both were at a length likely to cause frustrated phagocytosis, and both pristine and purified MWCNT caused a dose-dependent decrease in viable cell populations, mainly by necrosis, as the exposure increased from 0-20µg/ml during a 4-day exposure (Cheng *et al.*, 2009). Pulskamp et al. (2007b) have shown that reduction of A549 epithelial cell viability occurs in response to SWCNT exposure, irrespective of metal contaminant. It has been demonstrated by Kim *et al.* (2010b) that iron contaminants have little influence on MWCNT cytotoxicity, with high aspect ratio MWCNT often demonstrating a greater cytotoxicity than the low aspect ratio, and also that iron oxide displays no such cytotoxicity (Karlsson *et al.*, 2008, Kim *et al.*, 2010b); this was also shown by Cheng *et al.* (2009).

The lowest two concentrations used by Kim *et al.* (2010b) are similar to the highest doses used in the results given in this chapter, and much of the particle dose range used by Cheng *et al.* (2009) is comparable to this study also. When comparing the relevant aspects of these studies to the results given here for LDH release and WST-1 reduction, it is clear that they are very similar, permitting confidence in the data presented in this chapter, which indicates the potential cytotoxicity of MWCNT in general, and highlights that the main physiochemical factor of MWCNT associated cytotoxicity is morphology, particularly their length and high aspect ratio.

5.3.5 Concluding remarks

The results presented here are in line with much of the data published on fibre toxicity, and demonstrates the ability of MWCNT to generate pro-inflammatory and pro-fibrotic conditions, with clear cytotoxicity; importantly, this was shown under conditions that can be determined as non-cytotoxic for known pathogenic reference materials such as nanoparticle CB and asbestos. It is, however, unclear from the data obtained in this study if the cytotoxicity of the MWCNT is as a direct result of cell insult, or indirectly through a cascade of signalling in response to the elevated inflammatory response, such known apoptosis inducing agent TNF-α (Aubry *et al.*, 1999), or possibly to an increase in oxidative stress. It is possibly a combination of all.

The presence of TNF-α, VEGF, MCP-1, and TGF-β in the exposure supernatant found here does not imply that angiogenesis is occurring, but does infer that exposures of MWCNT have the ability to induce macrophage cells to encourage and maintain not only pro-inflammatory and pro-fibrotic conditions, but also to encourage new blood vessel formation if all other necessary constituents are present. The CNT exposures provided particularly enhanced responses when compared to the other material examined here, and characteristics such as CNT length, and to a lesser extent iron content and crystallinity, provided some separation between the inflammatory response produced by these MWCNT.

The initiation of potentially detrimental cell signalling in response to numerous MWCNT has been demonstrated here. The interaction of MWCNT with alveolar

macrophages and macrophage cell lines causing frustrated phagocytosis has been indicated in this chapter, and is later confirmed in chapter 6, with an inability of J774A.1 and rat BAL cells to adequately remove these fibres, and the oxidative potential of MWCNT is evident in chapter 4. The ensuing response generated from continued frustrated phagocytosis, and a rise in oxidant levels and inflammatory responses is likely to be significant and has been shown here to ultimately lead to cell death. This will only exacerbate the destructive conditions further and therefore needs serious consideration, as if this process of elevated immune secretions and continued cytotoxicity becomes chronic, the current literature of MWCNT exposure indicates that further disease progression is inevitable in such an environment.

Chapter 6

Particle uptake

6.1 Introduction

6.1.1 Uptake within the lung

There are three key aspects that this chapter will address with respect to particle uptake which have all been shown to have associated pathology. The first is particle uptake resulting in frustrated phagocytosis, which is often a fibre specific process. Frustrated phagocytosis and/or cell burden can lead to an inhibition of the cells' phagocytic ability, and so the second issue addressed is impaired phagocytosis, which can diminish the host defences but also result in "overload cancer" (Renwick *et al.*, 2001). The third area is oxidative burst generated during cell-particle interactions and the subsequent production of superoxide anions; this is particularly important when combined with frustrated phagocytosis.

There is a consumption of oxygen that is found during phagocytosis of exogenous material by leukocytes (Babior *et al.*, 1973), including macrophages (Johnston *et al.*, 1978), and a rapid release of superoxide (O_2^-) (Park, 2003). This is called the oxidative, respiratory or phagocytic burst. During an oxidative burst a membrane-bound NADPH enzyme complex acts as an electron donor in the reduction of oxygen to form a O_2^- (Park, 2003), which is primarily used in the intracellular destruction of engulfed microorganisms (Babior *et al.*, 1973, Ridley, 2001) through formation of hydrogen peroxide, hydroxyl radicals and singlet oxygen (Johnston *et al.*, 1975). Therefore O_2^- release into the surrounding media is not considered beneficial, and is normally abrupt and short-lived to ensure limited damage to the surrounding tissue (Ridley, 2001). Internalisation of material by cells is unaffected by the formation of these reactive oxygen metabolites (Babior *et al.*, 1973, Johnston *et al.*, 1975), the production of which will occur irrespective of whether the particles are fully incorporated into a phagosome or not.

Inhalation of pathogens and environmental particles, including asbestos and nanoparticle CB, will result in deposition throughout the respiratory tract, but also within the alveolar sacs. This occurrence is reviewed in chapter one. For particles that reach the alveolar region, it is phagocytosis by alveolar macrophages that is the key defensive mechanism vital for removal of this material. Phagocytosis involves a sequential process to internalise exogenenous material within membrane-bound vacuoles, to allow safe

destruction or removal. However, attempted and failed phagocytosis can lead to a state of frustrated phagocytosis, which is considered to be length dependent (Brown *et al.*, 2007b, Ye *et al.*, 1999a, Ye *et al.*, 2000). This frustrated phagocytosis causes additional tissue injury and an ensuing inflammatory response through the continued release of damaging reactive oxygen metabolites, which can initiate disease progression (Brown *et al.*, 2007b). There is a long standing association between asbestos lung burden, fibre length and risk of mesothelioma (Rogers *et al.*, 1994), and long fibre amosite asbestos has been shown to induce elevated inflammatory responses compared to short samples, in vivo, leading to fibrosis in response to the long sample only (Brown *et al.*, 1994a). This response to long fibres is known to escalate to a more advanced, severe prognosis, such as the development of pulmonary tumours and mesotheliomas (Davis *et al.*, 1986). It is the effect of this frustrated phagocytosis which is often considered a prominent factor in asbestos and other fibre pathogenicity (Donaldson and Tran, 2004, Goodglick and Kane, 1986). Any interference with normal phagocytic ability, through either frustrated phagocytosis or increased particle burden, may also impact on the ability of respiratory defensive mechanisms to control addition exposure to other pathogenic material (Brown *et al.*, 2007b, Renwick *et al.*, 2001). CNT induced frustrated phagocytosis has already been reported and was related to CNT morphology (Brown *et al.*, 2007b), but not specifically to length or metal content, and therefore form the basis of this study.

6.1.2 Aim and hypothesis

The aim of this study was to test the phagocytic ability of monocytic cells when confronted with particle panel B (nanoparticle CB, SFA, LFA, CNTI, CNTA, CNTB, CNTC and CNTD). The initial uptake was assessed by SEM observation of J774A.1 cells after a short exposure period. The same exposure conditions were used to establish BAL cell-particle interactions and attempted uptake and the generation of an oxidative burst. A number of techniques were undertaken to measure this oxidative burst including chemiluminescence of luminol and lucigenin, and reduction of cytochrome C. The impairment of host defensive mechanisms was also assessed by gauging the ability of J774A.1 cells to

remove organic bioparticles from their surrounding media that may represent a pathological hazard, subsequent to exposure of particle panel B.

During the short exposure time utilised for the phagocytic burst assay all particles are expected to generate some degree of respiratory burst associated ROS. However, long CNT are expected to induce frustrated phagocytosis, associated with an incomplete uptake of particles observed by SEM. In these cases of frustrated phagocytosis there will likely be a sustained release of ROS and an impairment of the cell's ability to internalise biological particles.

6.2 Results

6.2.1 Scanning electron microscopy

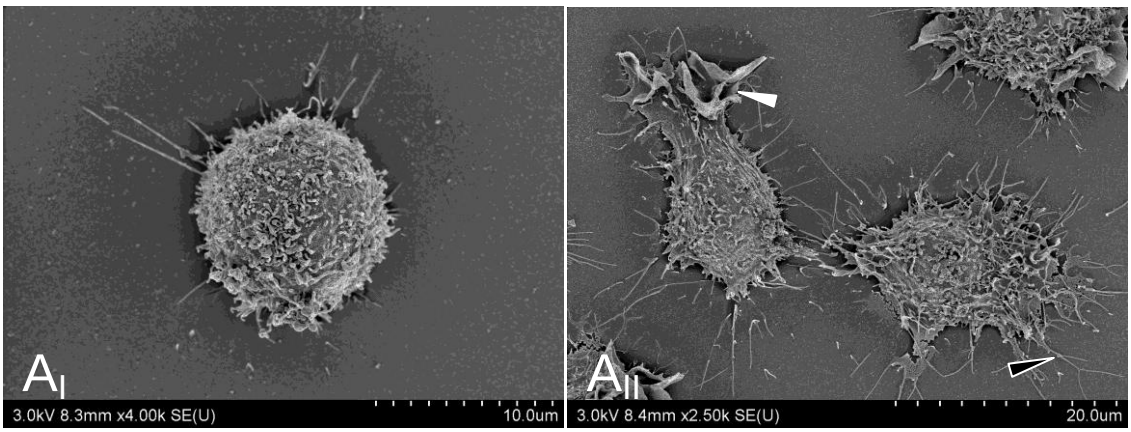

Figure 6.1 Scanning electron microscope analysis of untreated J774A.1 cell line. Cells were incubated in culture medium alone for 4 hours prior to SEM preparation, and imaged using a Hitachi S-4800 FEG SEM scanning electron microscope. A scale bar is shown at the bottom right corner of each image. White arrows: lamellipodia directional ruffling. Black arrows: spreading associated microvilli.

The exposure of J774A.1 macrophage cells to particle panel B was observed by SEM in order to investigate the interaction between the cells and the nanotubes as well as subsequent changes in cell morphology. The J774A.1 cells in figure 6.1 were grown in complete cell culture medium only; their appearance was often round (figure 6.1 A_I), or spread and flattened, with spreading sometimes leading to directional lamellipodia ruffles, distinctive of motility (figure 6.1 A_{II}). Ruffles elsewhere on cell membranes were few, with most of the cell having a microvillous surface of short microvilli, sometimes protruding further during cell spreading (figure 6.1 A_{II}). With the treatment of J774A.1 cells with 10µg/cm^2 nanoparticle CB (figure 6.2) there is less evidence of cells spreading: any flattening (lamellipodium) appears to be directional towards particle aggregates (figure 6.2 A_{IV}). There was the appearance of further ruffles that were not directional, and the appearance of further microvilli. Active acquisition of particulate matter by extending protrusions was evident, as well as the engulfing of those particles that have settled onto the cell surface (figure 6.2 A_{II} and A_{III}). J774A.1 cells exposed to SFA (figure 6.2 B) displayed a similar morphology as those exposed to nanoparticle CB. There was less spreading (figure 2 B_{II}) and a slight increase in surface ruffling (figure 6.2 B_{III} and B_{IV}), with the appearance of individual SFA fibres within the ruffles but also associating loosely with the microvillous membrane (figure 6.2 B_I and B_{IV}).

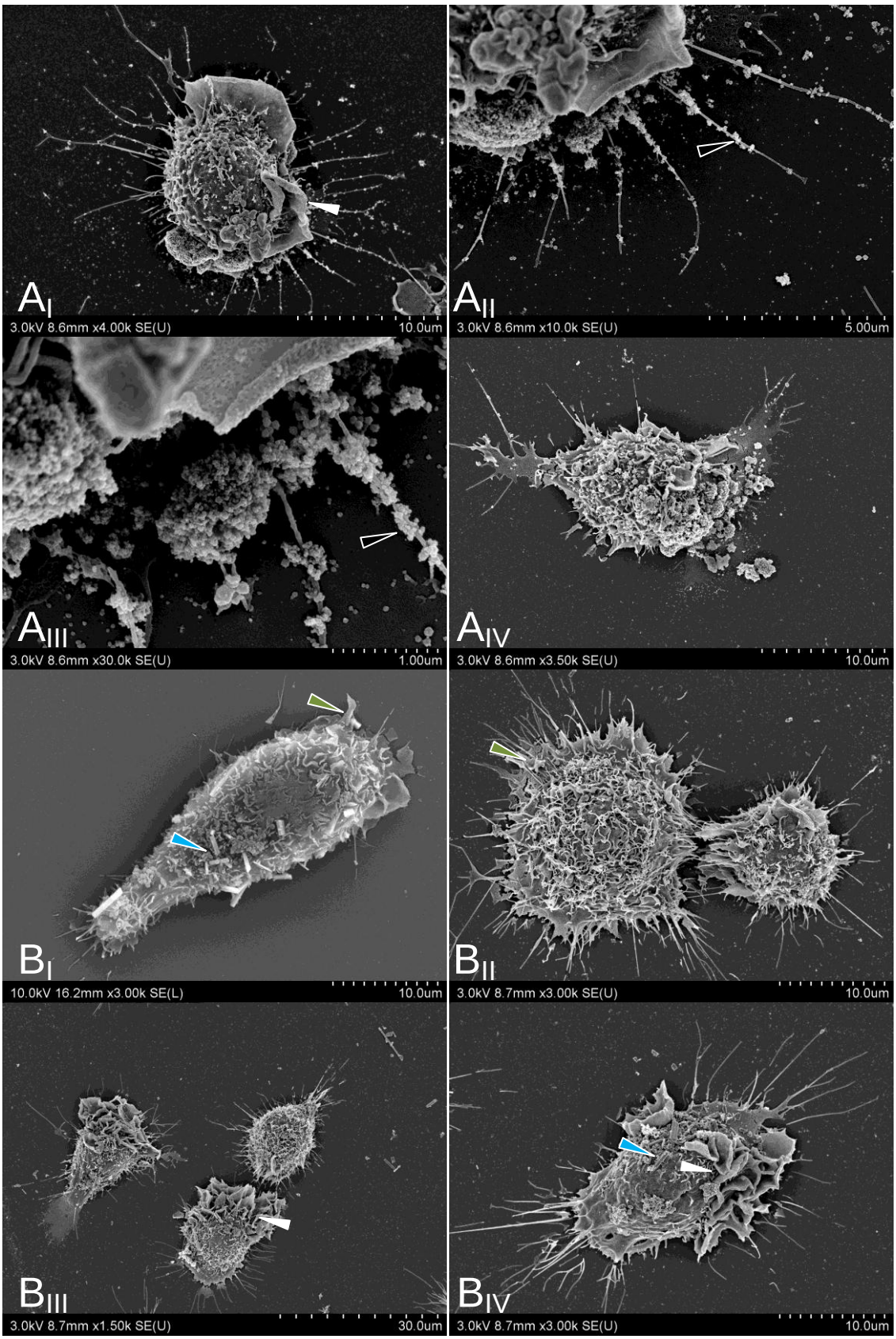

Figure 6.2 Scanning electron microscope analysis of (A) nanoparticle CB and (B) SFA-treated J774A.1 cells. Cells were exposed to 2.1µg/cm^2 for 4 hours prior to SEM preparation, and imaged using a Hitachi S-4800 FEG SEM scanning electron microscope. A scale bar is shown at the bottom right corner of each image. White arrows: non-directional surface ruffling. Black arrows: microvilli protrusions actively acquiring particles. Blue arrows: loosely associating SFA. Green arrows: SFA within membrane ruffling.

The exposure of cells to LFA (figure 6.3 A) results in considerably more phagocytosis-associated membrane ruffling, as well as lamellipodia from cells migrating towards and along fibres. These cells are seen to “spear” themselves along fibres that are too long for phagocytosis, and also attempt to phagocytose multiple LFA fibres simultaneously (figure 6.3 A_{III}).

For the CNTI sample, the first thing to notice is that the fibres are less well dispersed than for the LFA, with large agglomerates of particles in contact with the macrophage cells. The activation state of CNTI-treated cells (figure 6.3 B) is similar to that of LFA-treated cells, with significant membrane ruffling and particle attachments, and with multiple cells attaching to CNT agglomerates (figure 6.3 B_{I} and B_{II}). Large numbers of microvilli are associated with CNT the agglomerates; however, this needs close inspection as the two are often indistinguishable. In some cases MWCNT agglomerates are being drawn into the cell at different locations through different pseudopods simultaneously (figure 6.3 B_{III}), while other cells are attempting to phagocytose large agglomerates through one large pseudopod (figure 6.3 B_{IV}). Once semi-internalised there is often the appearance of outward stress being exerted by MWCNT agglomerates on the cell surfaces; CNTI agglomerates can be seen to enter the cell through a pseudopod and, while the cell appears to drag in the aggregate, the portion already within the cell is seen to noticeably press on the cell membrane from the inside outwards, evident by its outline (figure 6.3 B_{III}).

The J774A.1 cells exposed to the laboratory-designed short CNT samples displayed a range of activation states. There was often cell spreading, and with the attachment of almost single CNTA structures (figure 6.4 A), there is little surface ruffling indicative of phagocytosis, only at the sight of CNT attachment. There is, however, an increase in surface microvilli compared to untreated cells. At times the short CNT sample appeared to break the surface of the cell membrane with no pseudopod formation, as MWCNT were seen to enter the cell with no ruffling and exit at a different location (figure 6.4 A_{I}). J774A.1 cells exposed to CNTB displayed an increase in membrane ruffling and an increase in microvilli (figure 6.4 B), even when attached to a low number of CNT (figure 6.4 B_{III}); similarly to CNTI, J774A.1 exposure to CNTB agglomerates caused the formation of multiple pseudopodia (figure 6.4 B_{II}) during attempts to phagocytose of these agglomerates. As discussed in chapter three, it was

proposed that the annealing treatment of CNT to deplete the iron content would inadvertently increase the sample hydrophobicity, this is evident in these images as CNTB were shown to remain more agglomerated compared to CNTA.

With exposure of J774A.1 cells to the long CNT samples, CNTC (figure 6.5 A) and CNTD (figure 6.5 B), most of the cell membrane appears to consist of phagocytosis associated ruffling, indicating the extent of the phagocytic activity occurring. As with LFA, multiple cells are attempting phagocytosis of the same particle aggregates (figure 6.5 A_{III} and A_{IV}; and figure 6.5 B_{I}), and cells are attempting to internalise multiple fibres simultaneously (figure 6.5 A_{I} and A_{II}; and figure 6.5 B_{I} and B_{II}). The elongated morphology due to cell extensions along fibre lengths seen with LFA exposure was not evident in cells treated with long CNT. Instead J774A.1 cells exposed to long MWCNT appear to remain relatively rounded, and to draw the CNT into the formed pseudopods instead of displaying any motive action along the CNT, whether the nanotubes were agglomerated or individual. The active phagocytosis of long MWCNT and MWCNT agglomerates from numerous pseudopods in different locations (figure 6.5 B_{II}) was often observed to ultimately result in the appearance of large indentations at the source of these particle uptake locations (figure 6.5 B_{III} and B_{IV}).

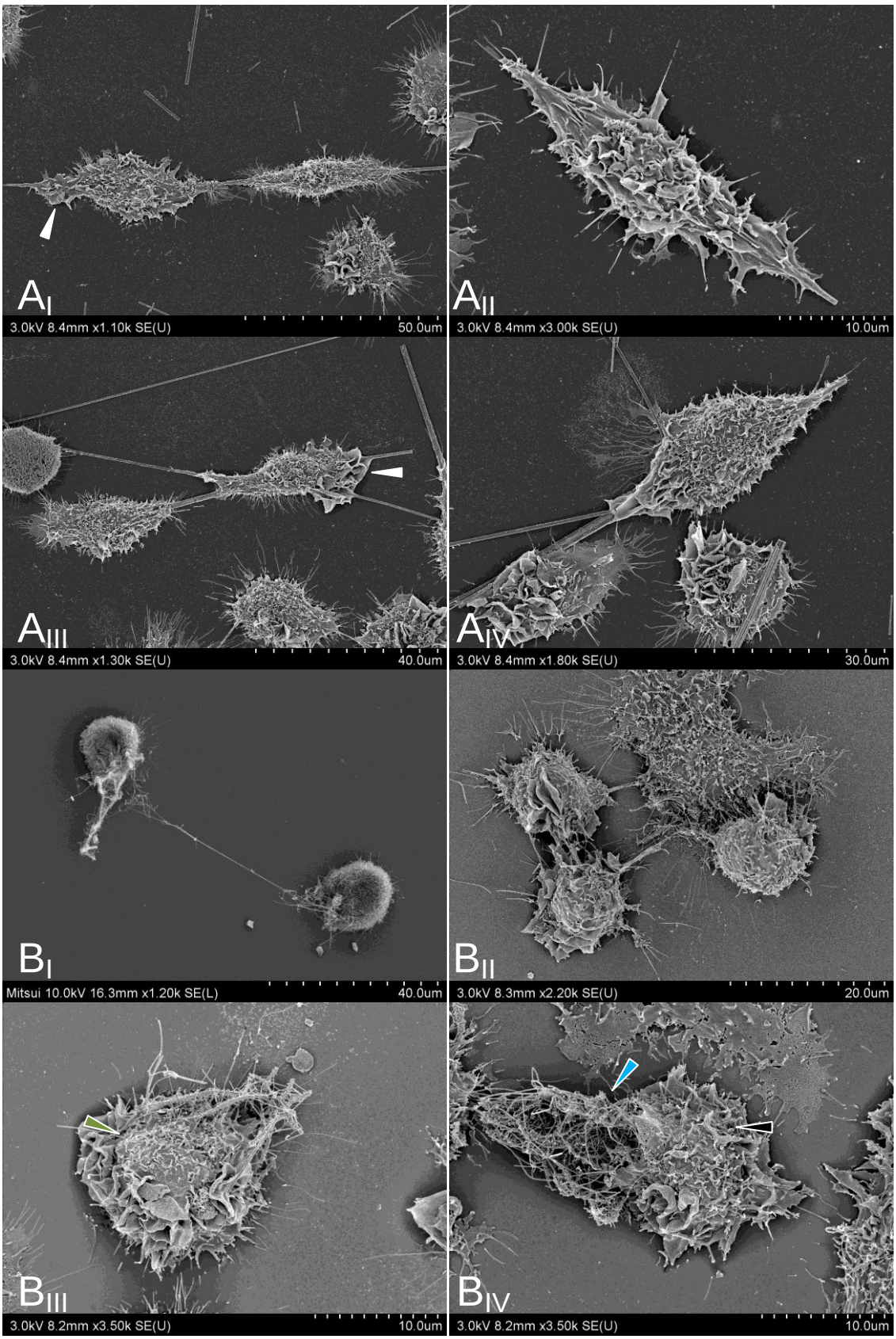

Figure 6.3 Scanning electron microscope images of (A) LFA- and (B) CNTI-treated J774A.1 cells. Cells were exposed to 2.1µg/cm^2 for 4 hours prior to SEM preparation, and imaged using a Hitachi S-4800 FEG SEM scanning electron microscope. A scale bar is shown at the bottom right corner of each image. White arrows: lamellipodia directional ruffling. Black arrows: increased surface ruffling. Blue arrows: attempt of phagocytosis of agglomerate. Green arrow: CNT protrusion after phagosome internalisation, risk of membrane piecing.

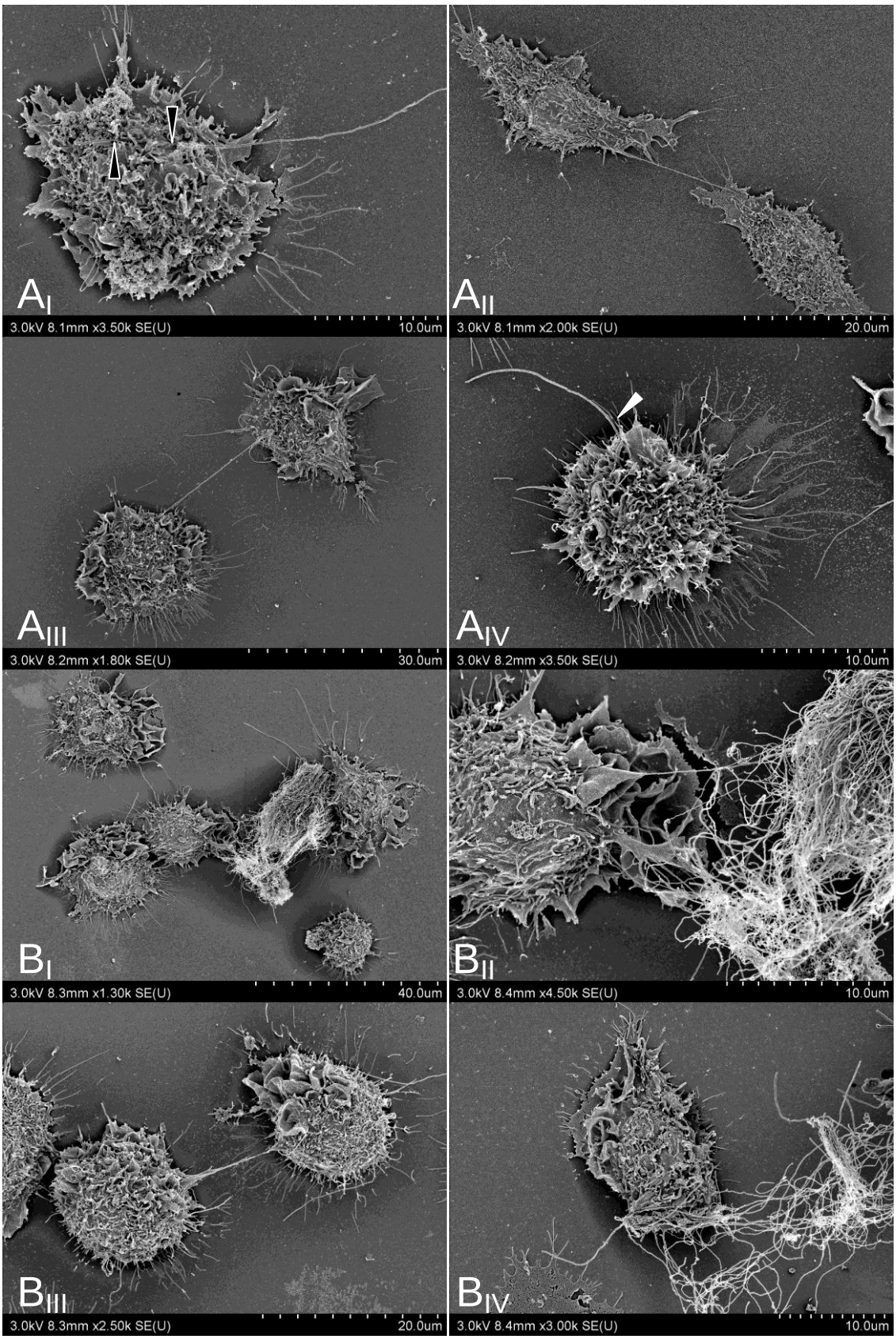

Figure 6.4 Scanning electron microscope images of (A) CNTA- and (B) CNTB-treated J774A.1 cells. Cells were exposed to 2.1µg/cm^2 for 4 hours prior to SEM preparation, and imaged using a Hitachi S-4800 FEG SEM scanning electron microscope. A scale bar is shown at the bottom right corner of each image. White arrows: attachment of single CNT. Black arrows: CNT piecing membrane with no associated pseudopod.

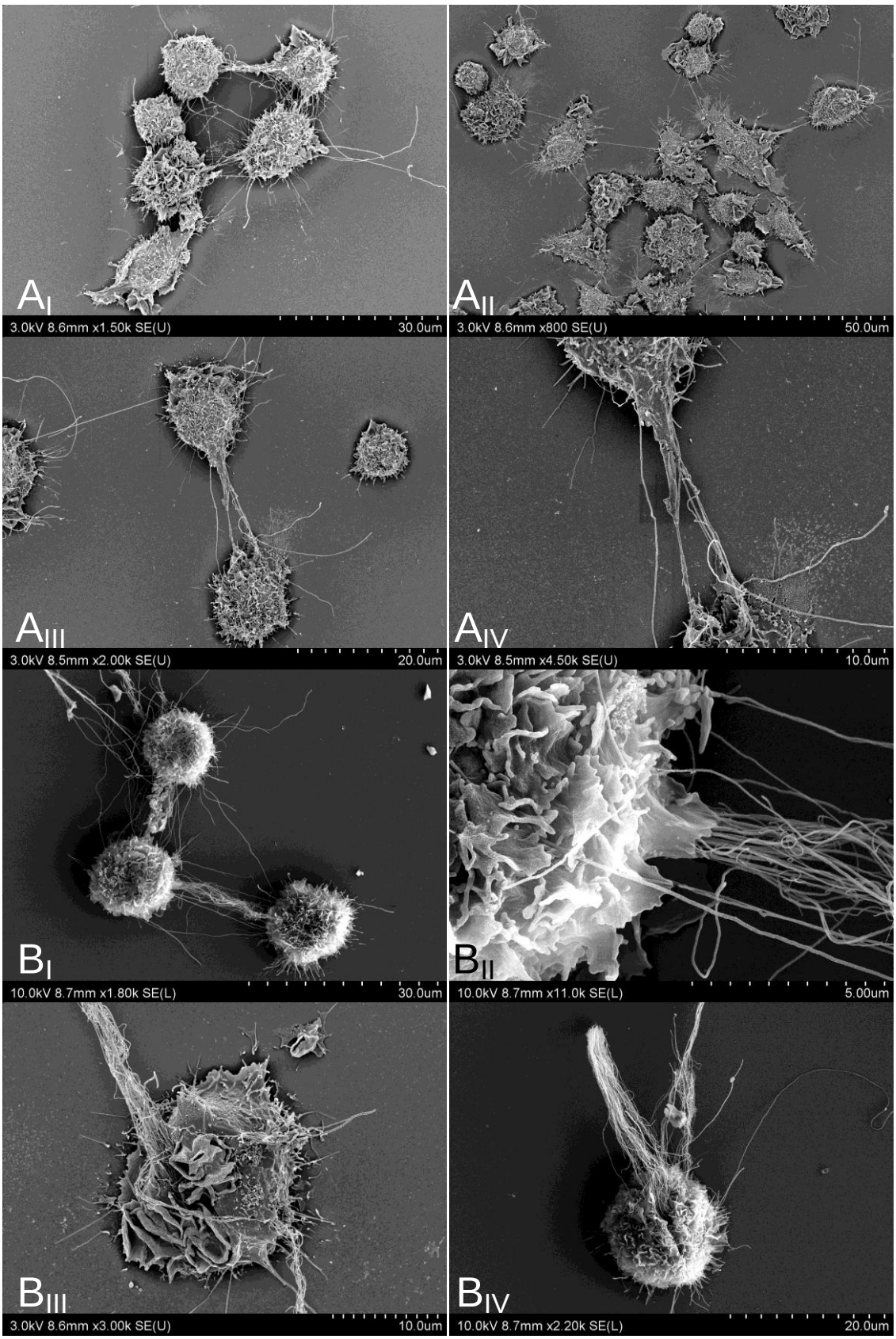

Figure 6.5 Scanning electron microscope images of (A) CNTC- and (B) CNTD-treated J774A.1 cells. Cells were exposed to 2.1µg/cm^2 for 4 hours prior to SEM preparation, and imaged using a Hitachi S-4800 FEG SEM scanning electron microscope. A scale bar is shown at the bottom right corner of each image.

6.2.2 Phagocytic burst – suitability of chemiluminescence

The respiratory burst generated through particle interaction with cell membrane receptors was initially investigated using the chemiluminescence of lucigenin and luminol. It is thought that lucigenin luminescence occurs specifically in response to superoxide production (Li *et al.*, 1999), while luminol luminescence is an indication of myeloperoxidase-mediated formation of hypochlorous acid from hydrogen peroxide (Hasegawa *et al.*, 1997a), or it is a direct measure of peroxynitrite, hydrogen peroxide, hydroxyl radicals and superoxide formation (Rinaldi *et al.*, 2007).

The initial investigation into chemiluminescence used both luminol and lucigenin. Exposure of BAL cells to medium alone, SOD negative control, PMA positive control, and 8µg/cm^2 of LFA and an unknown pharmaceutical compound (C2) provided a clear difference in luminol and lucigenin responses. The C2 compound was only used at this stage as the initial pilot analysis was undertaken in collaboration with other laboratory members, and was not used again. The intensity of luminol luminescence was considerably low (figure 6.6 A) and differences between controls and treatments were not clearly evident. The use of lucigenin, however, provides much higher detectable levels of light emission, and clear discernable differences between treatments and controls (figure 6.6 B).

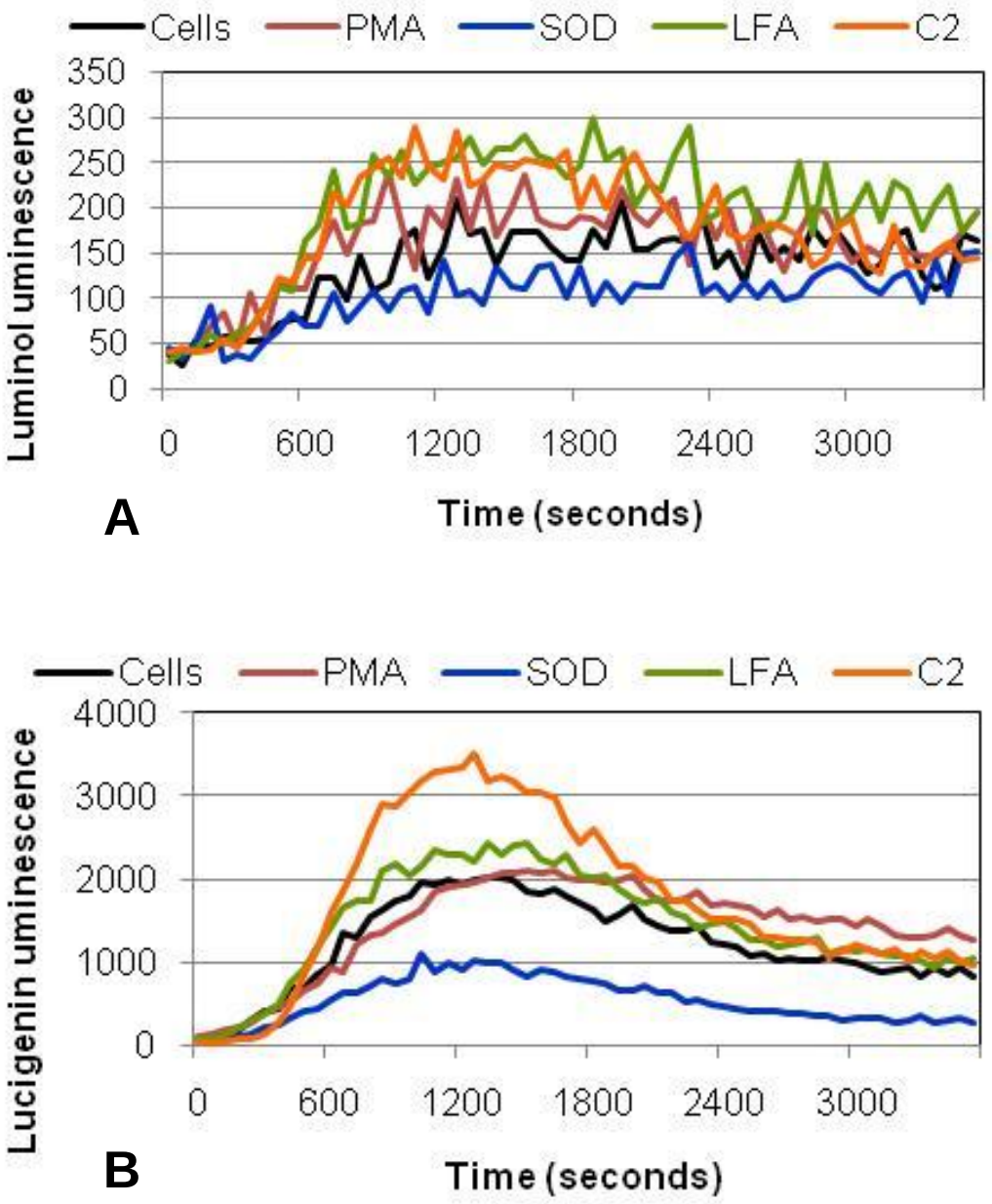

Figure 6.6 Chemiluminescence of (A) luminol and (B) lucigenin during phagocytic burst of BAL cells. Data is representative of light emissions during 1-hour exposure of cells to SOD, PMA and medium-only controls, and to LFA and C2 particle treatments. (n=1)

The use of the MM6 monocytic cell line for luminol chemiluminescence (figure 6.7 A) indicated a similar, low detectable level of light intensity that was seen from BAL cell exposure, providing further evidence to suggest this compound was not useful for future experiments. The assessment of lucigenin chemiluminescence in response to MM6 exposure to a sample of particle panel B (figure 6.7 B) provided a number of observations that indicate the unsuitability of the cell line use in this assay. The detectable light emissions are far below

that seen during BAL cell exposures, and the only discernible differences were found after treatment with the PMA positive control. The particle treatments appeared to have no effect on the chemiluminescence measured by lucigenin. This was confirmed when comparisons were made between particle-treated cells and cell-free systems, and no differences in chemiluminescence signals were found (figure 6.7 B). This may have been due to the exposure period employed or particle aggregation, therefore a longer pre-lucigenin particle exposure period was used with J774.A1 cells (figure 6.8) with the absence and presence of BSA to modify particle agglomeration. Additionally, different concentrations of lucigenin were examined. It was shown that a lucigenin concentration of 500µM is necessary as 13µM provides little light emission (figure 6.8 A). BSA was found to enhance the luminescence in response to PMA exposure (figure 6.8 B and C). J774A.1 cells provided a clear detectable increase in ROS-induced light emission compared to MM6 cells. This, however, was only in response to PMA positive controls and a good particle response was still not seen with treatment of cell lines.

Therefore, at this stage lucigenin was considered the most appropriate reagent to use, and with a clear particle response in BAL exposure it was decided BAL cells were the most appropriate cell type to use.

It was deemed necessary that with the use of primary BAL cells it was important to reduce the cell number used in this assay, to reduce the animal number. Therefore the chemiluminescence of lucigenin in response to varied BAL cell number was assessed (figure 6.9). A clear detectable particle and control response was still observed using $2.25x10^6$cells/ml, and therefore was the cell density chosen for subsequent analysis.

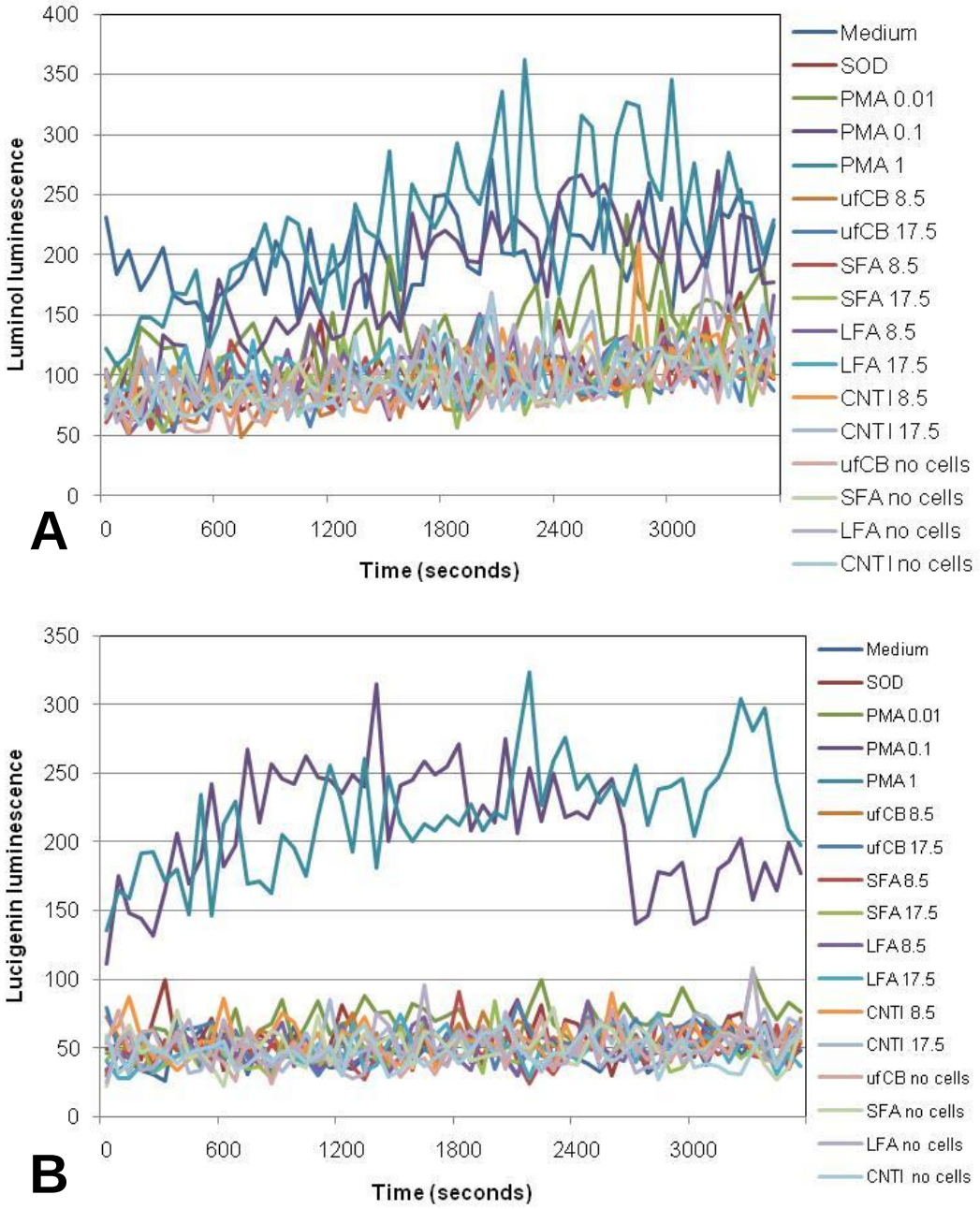

Figure 6.7 Chemiluminescence of (A) luminol and (B) lucigenin during phagocytic burst of MM6 cells. Data is representative of light emissions during 1-hour exposure of cells to SOD, PMA and medium-only controls, and to nanoparticle CB, SFA, LFA and CNTI particle treatments at 8.5 and 17.5µg/cm^2, and the light emitted during incubation of said particles in a cell free system. (n=1)

A

BSA: 1mg/ml

Lucigenin: 13µM

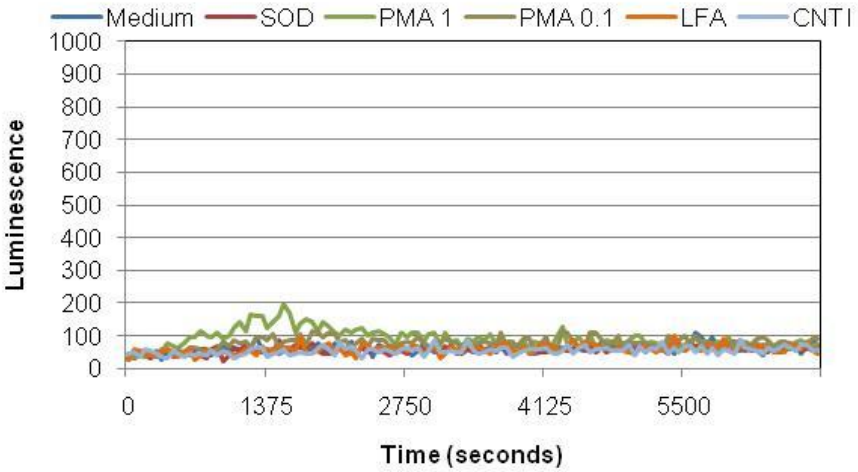

B

BSA: none

Lucigenin: 500µM

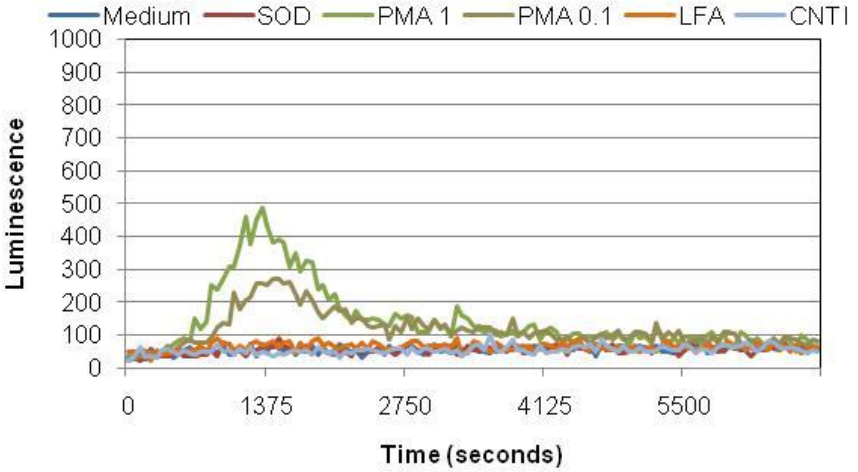

C

BSA: 1mg/ml

Lucigenin: 500µM

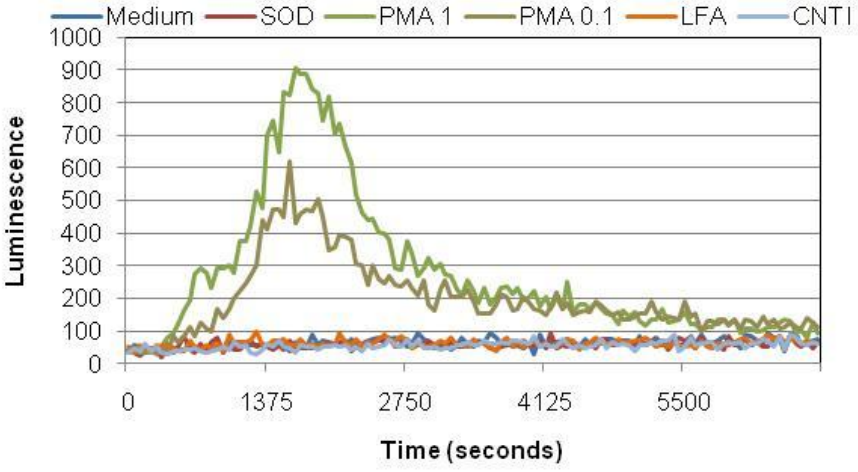

Figure 6.8 Chemiluminescence of lucigenin during phagocytic burst of J774A.1 cells. Cells were treated with medium only, SOD, 1µg/ml and 0.1µg/ml PMA, and 8.5µg/cm^2 LFA and CNTI, for 4 hours. Data is representative of light emissions with addition of lucigenin. Exposure medium varied with respect to BSA content and lucigenin. (n=1) Exposure medium either included (A) and (C), or excluded (B) 1mg/ml BSA; and lucigenin concentration was either (A) 13µM, or (B) and (C) 500µM. (n=1)

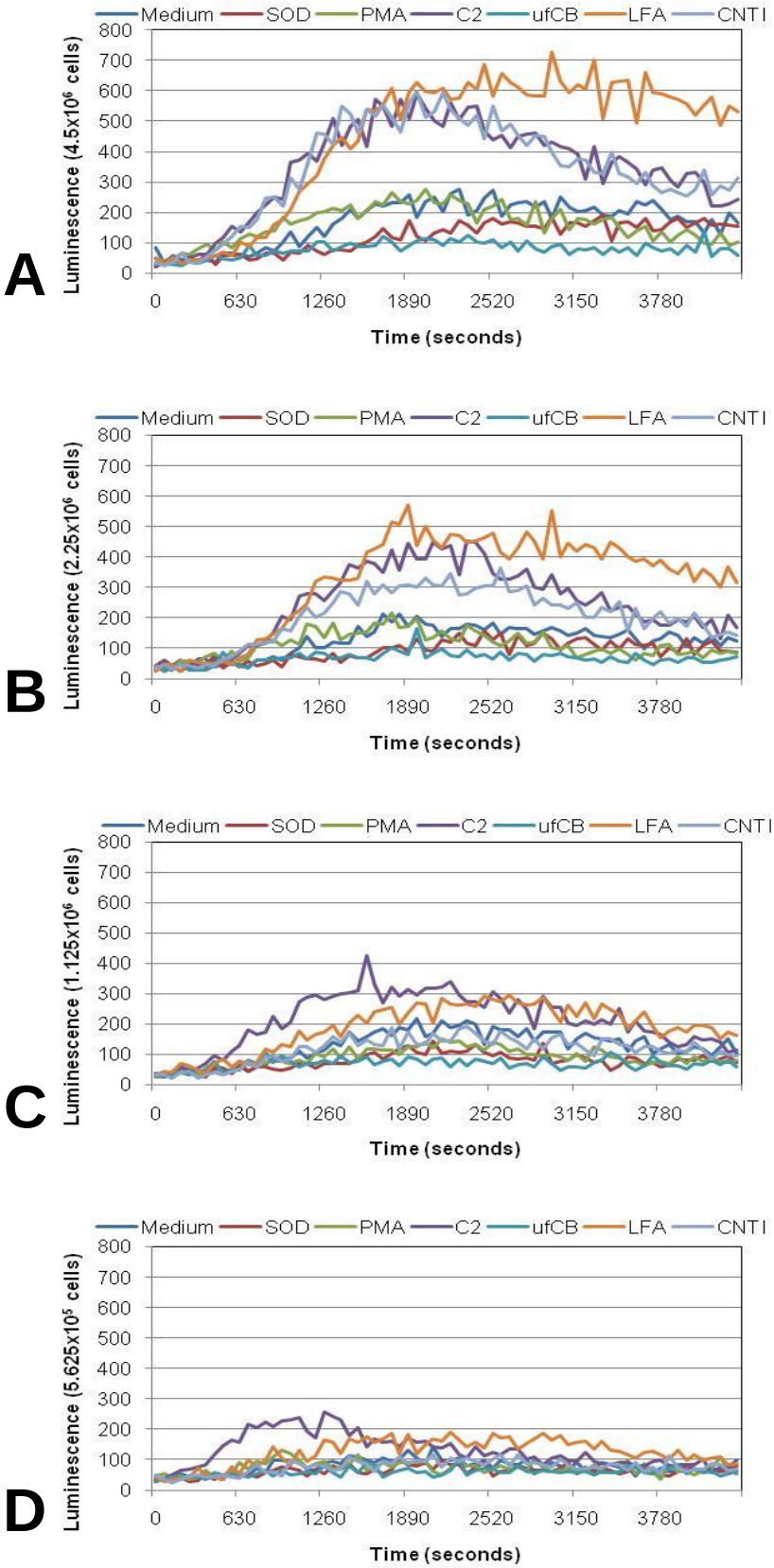

Figure 6.9 Effect of modifying cell density on the chemiluminescence of lucigenin during the phagocytic burst of BAL cells. BAL cells at different cell densities (A) $4.5x10^6$, (B) $2.25x10^6$, (C) $1.125x10^6$ and (D) $5.625x10^5$ cells/ml were treated with medium only, SOD, PMA, C2, nanoparticle CB, LFA and CNTI. Data is representative of light emitted during the 1.5 hour exposure period. (n=1)

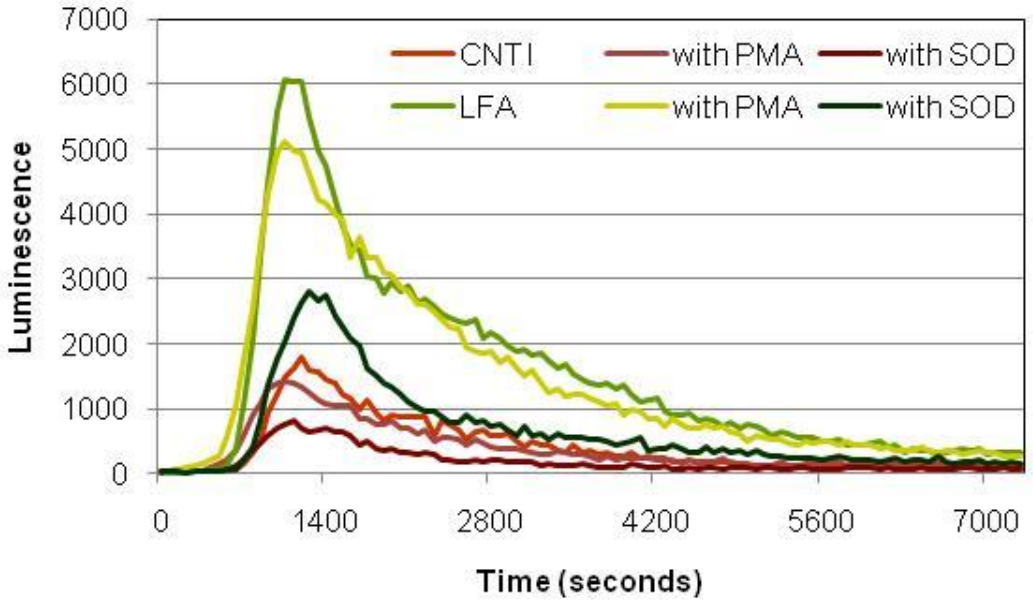

Figure 6.10 Chemiluminescence of lucigenin during phagocytic burst of BAL cells – test for luminescence quenching. Cells were treated with 8.5µg/cm^2 LFA and CNTI, for 2 hours, with additional treatments containing LFA (8.5µg/cm^2) and CNTI (8.5µg/cm^2) with either 0.1µg/ml PMA or 150IU/ml SOD. Data is representative of light emissions during 2-hour exposure period. (n=1)

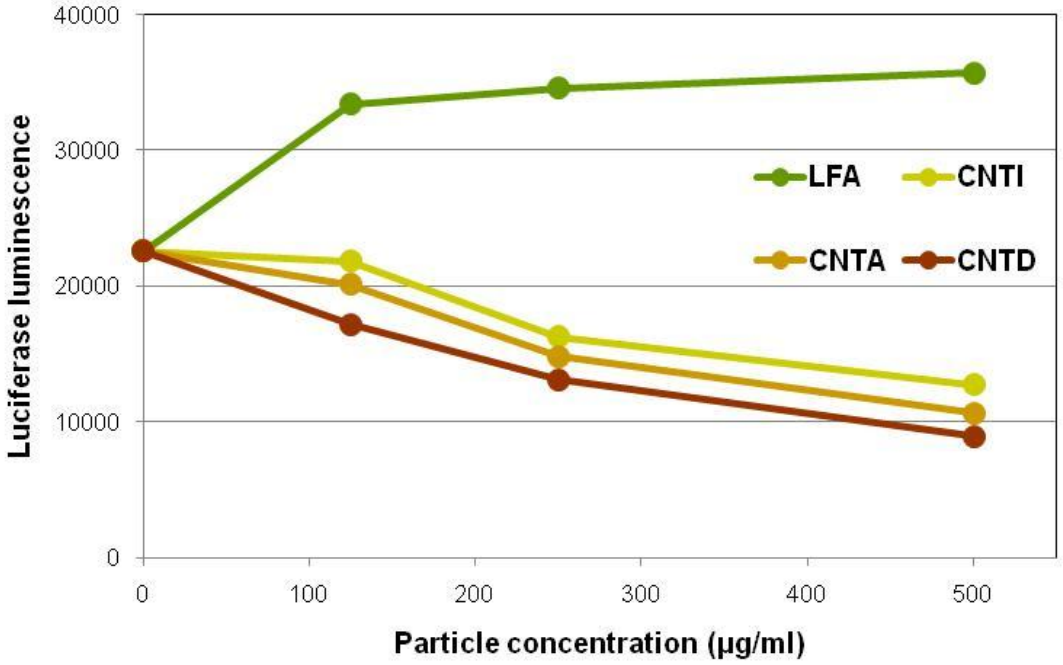

Figure 6.11 Cell free luciferase chemiluminescence – test for luminescence quenching. The enzyme induced chemiluminescence of luciferase was measured in the presence of different concentrations (0.4-1.6µg/cm^2) of LFA, CNTI, CNTA and CNTD, to test for any particle interference. (n=1)

With uptake of all CNT samples evident in SEM imaging, the phagocytic burst response of BAL cells to MWCNT was considered surprisingly low, therefore before proceeding it was thought best to ensure this response was accurate and not a result of particle interference. BAL cells were exposed to LFA and CNTI alone, and in the presence of PMA and SOD (figure 6.10). With no interference the CNTI plus PMA treatment should generate a similar light intensity as the LFA plus PMA; it did not, and was in fact much lower, suggesting a quenching of the luminescence occurring in the CNT containing wells. This particle interference was tested using a cell-free luciferase assay and quenching did seem evident (figure 6.11), with a clear dose-dependent decrease in luciferase enzyme-induced luminescence in response to relatively low concentrations of CNTI, CNTA and CNTD, which was not evident with inclusion of LFA.

Through observation of the data collected in the initial quenching assessment (figure 6.10) it appeared that the inclusion of SOD in particle exposures provided a baseline level of light emission that was comparable to any particle interference, and therefore relative to any particle-induced response. Particle-plus-SOD exposures were then used to transform data into a ratio response, with the aim of circumventing any issues of particle interference. The raw data of average luminescence intensity taken over 2 hours incubation of BAL cells with particle panel B (figure 6.12 A) further demonstrated the interference. The same data but transformed using the particle-plus-SOD controls (figure 6.12 B) potentially demonstrated alleviation of any interference, and indicated the only clear response was with treatment of LFA. However, at this point it was considered prudent to follow other methods of respiratory burst analysis that have less scope for false interpretation, primarily the reduction of cytochrome C, which involves the removal of particles not associated with cells prior to analysis.

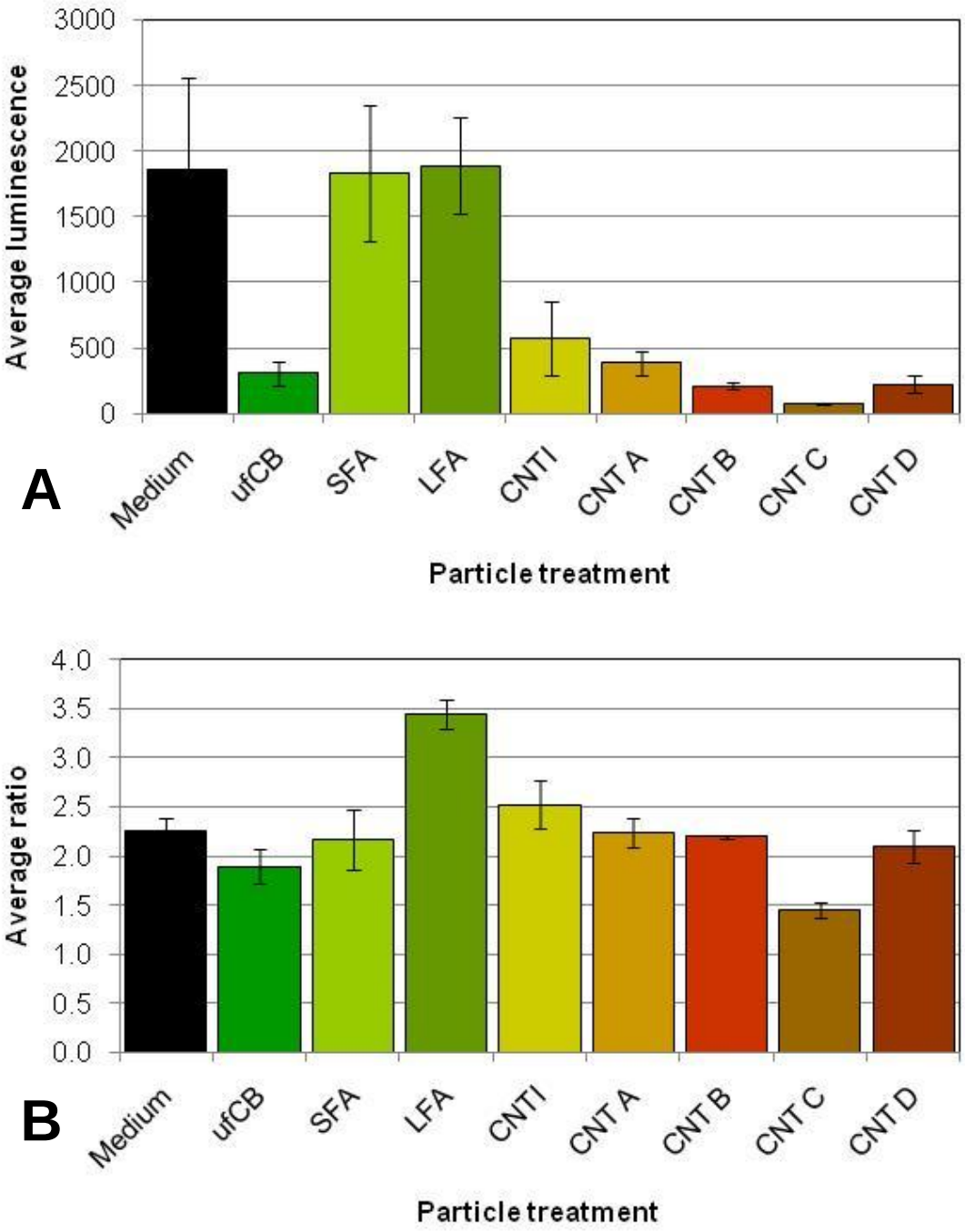

Figure 6.12 Chemiluminescence of lucigenin during phagocytic burst of BAL cells exposed to particle panel B. Cells were exposed to 8.5µg/cm^2 of full particle panel, with additional treatments of particle-plus-SOD. Data is expressed as (A) average luminescence and (B) ratio compared to relative particle-plus-SOD negative control. (n=3)

6.2.3 Phagocytic burst – cytochrome C reduction

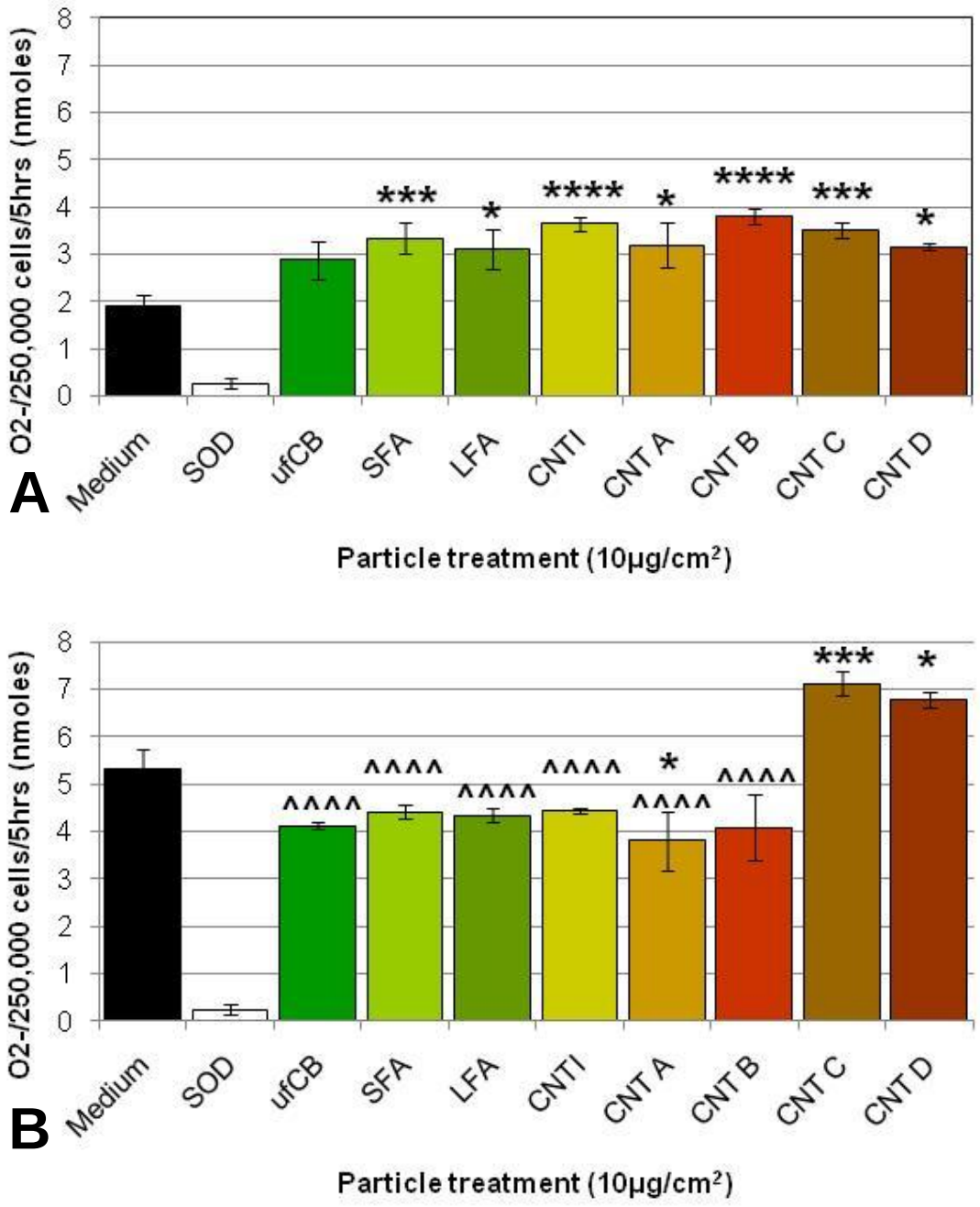

Figure 6.13 Phagocytic burst of BAL cells, measured by cytochrome C reduction. Cells were treated with 10µg/cm^2 medium only, ufCB, SFA, LFA, CNTI, CNTA, CNTB, CNTC and CNTD for 5 hours. With SOD as a negative control, and the (A) exclusion, or (B) inclusion of PMA 1 hour before the end of the measurement period. Data is expressed as superoxide anion release by 2.5x10^5 cells over 5 hours exposure, in nanomoles. Each data point represents mean ± SEM (n=6). Statistical significance is shown by * = $p<0.05$, and *** = $p<0.005$, compared to medium only control; and ^^^^ = $p<0.001$, compared to long CNTC and CNTD.

The oxidative burst generated by attachment of BAL cells to particle panel B was measured by the release of O_2^-; and expressed as nmoles O_2^- generated over 5 hours with exposure of particles to $2.5x10^5$ BAL cells.

In the absence of PMA (figure 6.13 A), cells cultured in growth medium alone generated 1.9nmoles O_2^-, this response was significantly removed with the inclusion of SOD in the reaction mixture, causing the O_2^- concentration to drop to 0.27nmoles. The application of particle panel B into this system resulted in an increase in supernatant O_2^- concentration in all cases. All treatments were significantly higher than that of the medium-only control cells except nanoparticle CB treatment, which although it raised the release of O_2^-, was not statistically significant (p-value = 0.15). The greatest response was from CNTB which generated a 99% increase compared to the medium-only control. Any particle interference resulting in over estimation in response was analysed by additional treatments of particles plus SOD (figure 6.14). It was shown that in all cases the presence of SOD substantially lowered the amount of O_2^- available for cytochrome C reduction, suggesting that interference in this assay by the particles was not present.

The addition of 0.1µg/ml PMA induced varied responses (figure 13 B). In the cells maintained in growth medium alone, there is a 178% increase in O_2^- release compared to the equivalent assay devoid of PMA. The O_2^- release in response to CNTC and CNTD treated cells was also particularly high. Other particle treatments were only stimulated slightly further in their release of O_2^- when compared to the equivalent assay devoid of PMA. In comparison to medium only PMA stimulated BAL cells, only CNTC and CNTD were found to significantly induce higher release of O_2^-, which incidentally were also higher than all other particles in particle panel B.

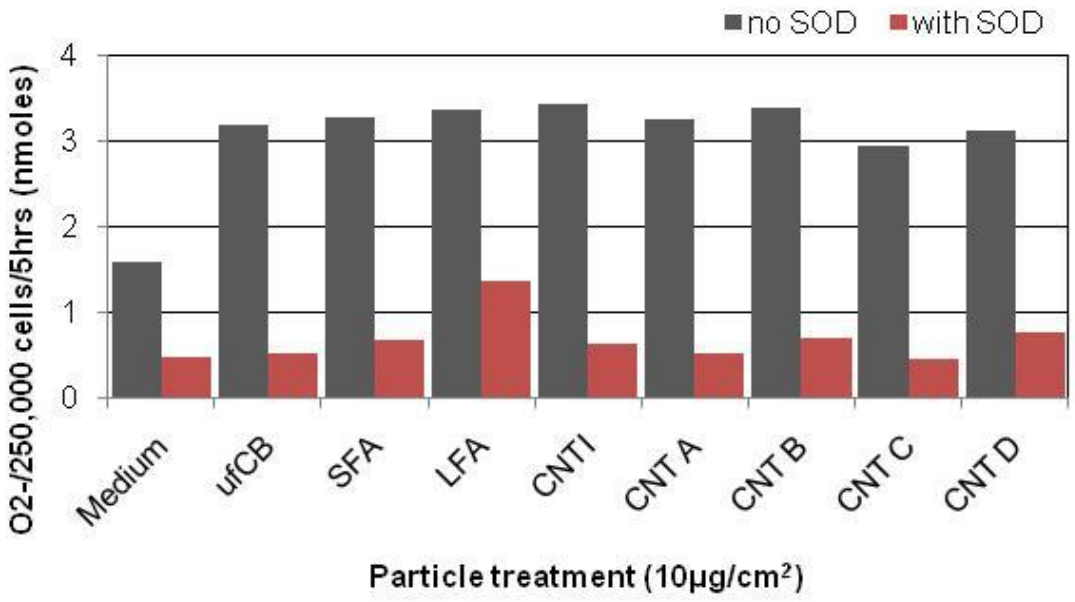

Figure 6.14 BAL cell superoxide anion production – test for particle interference. Cells were treated with 10µg/cm^2 of all particle panel B, with additional treatments of particles-plus-SOD. Data is expressed as nmoles O_2^-/250,000cells/5 hours. (n=1)

6.2.4 Light microscopy of BAL cell-particle interactions

The BAL cells were exposed to particle panel B at 10µg/cm^2 for 5 hours. The imaging suggested that cells often interacted with relatively large aggregates of nanoparticle CB, and it was not always clear how much had been internalised by the cells (figure 6.15 B). SFA was well dispersed, and clearly was readily taken up by BAL monocytic cells (figure 6.15 C), with some cells clearly laden. Observations of LFA exposure revealed multiple cells attempting phagocytosis of the same fibres, and cells attempting phagocytosis of multiple fibres, with clear membrane penetration also evident (figure 6.16 A). CNTI was found to be relatively well dispersed with the appearance of some large aggregates. Uptake of both aggregates and dispersed CNTI is evident, with possible interaction with the cell's nucleus, and clear indications of frustrated phagocytosis (figure 6.16 B). Both short CNT samples, CNTA (figure 6.16 C) and CNTB (figure 6.17 A), appear as both aggregated and mono-dispersed. The short MWCNT are clearly internalised by cells. However, both appeared to induce frustrated phagocytosis, particularly in response to aggregates, and both were observed to promote the formation of cellular aggregates to a greater extent than other

particle exposures. The interaction of the long MWCNT samples was harder to interpret. The sheer volume of CNT, although relatively well dispersed in CNTC exposure (figure 6.17 B), seems to create a lattice of CNT and cells, making individual interactions hard to distinguish; it does appear, however, that the MWCNT “net” is primarily surrounding the cells, implicating their association. The long CNTD sample was far less dispersed (figure 6.17 C), but was also believed to be actively acquired by BAL cells.

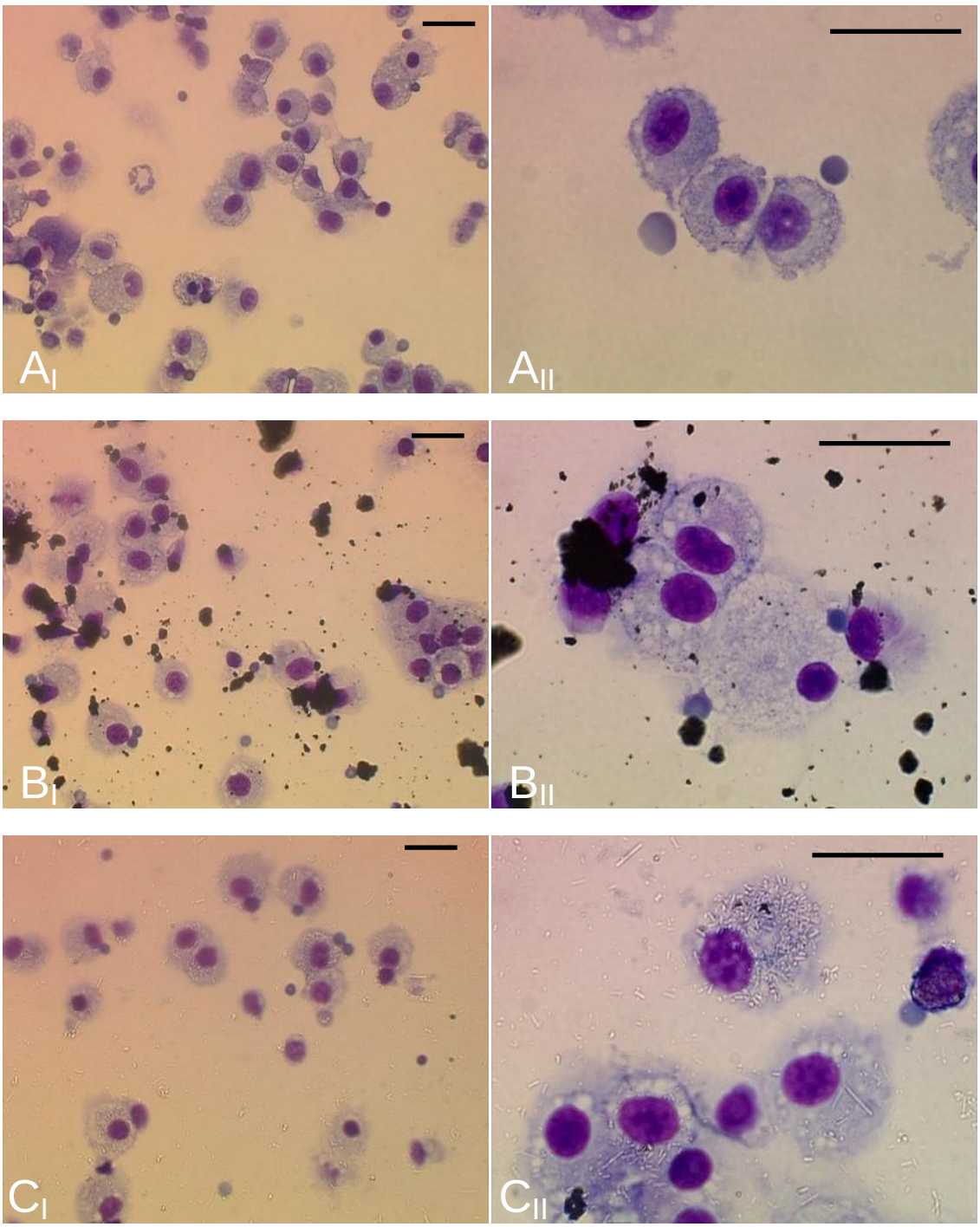

Figure 6.15 Light microscopy images of BAL cells; treated with (A) medium only, (B) ufCB, (C) SFA – in conditions representative of cytochrome C assay. Cells were treated with 10µg/cm^2 for 4 hours. Magnification is at x400 or x1000. Black bars indicate 20µm.

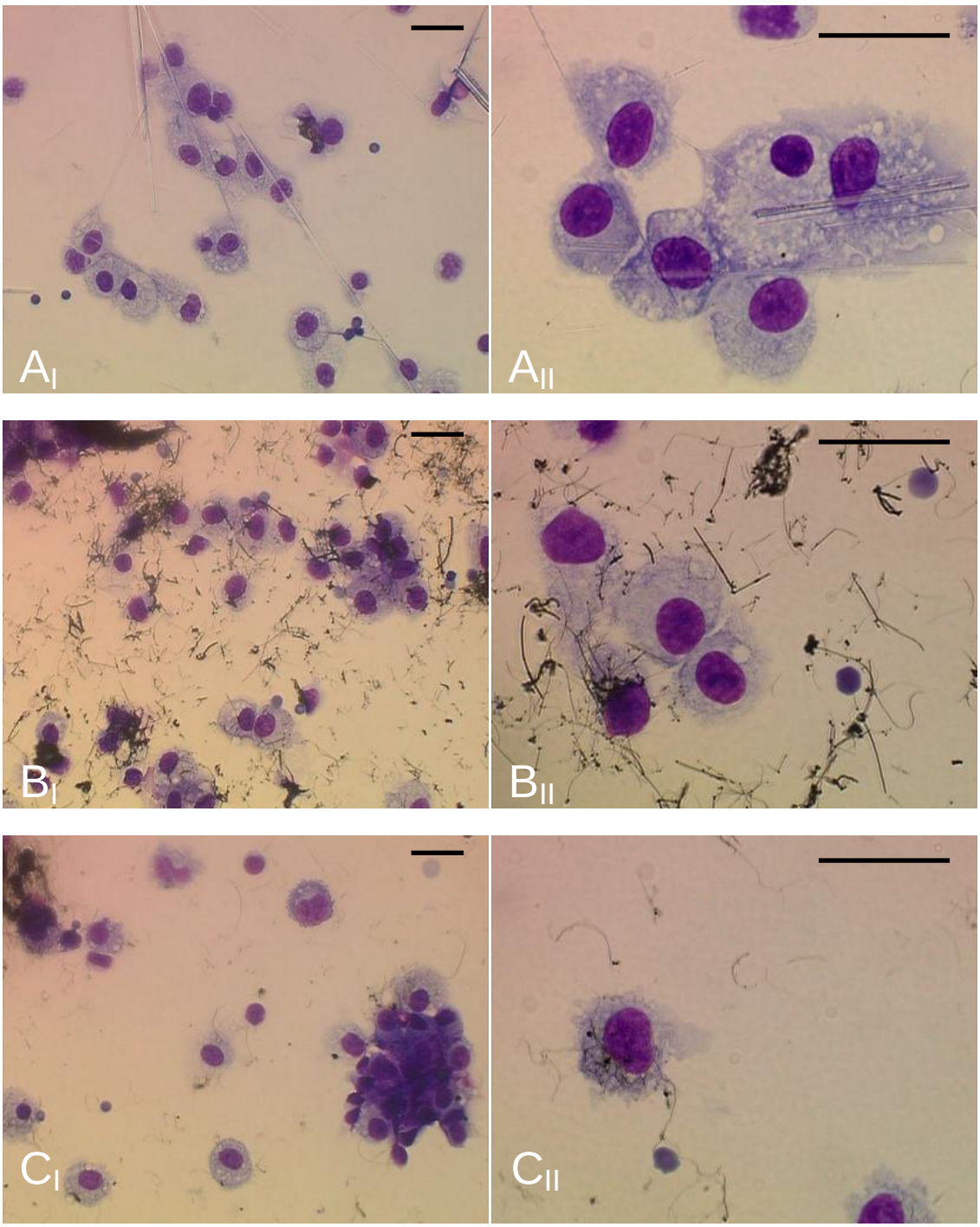

Figure 6.16 Light microscopy images of BAL cells; treated with (A) LFA, (B) CNTI, (C) CNTA – in conditions representative of cytochrome C assay. Cells were treated with 10µg/cm^2 for 4 hours. Magnification is at x400 or x1000. Black bars indicate 20µm.

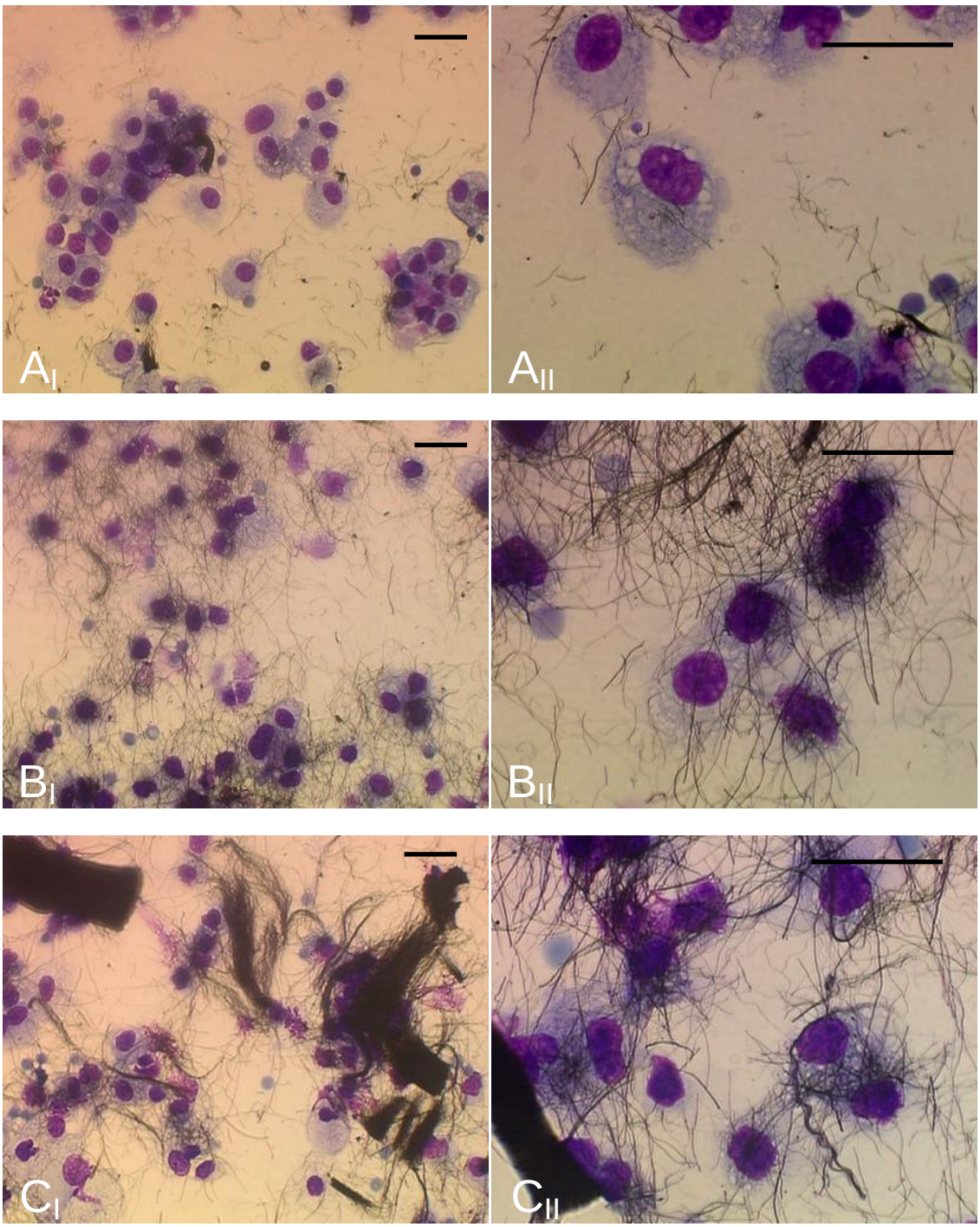

Figure 6.17 Light microscopy images of BAL cells; treated with (A) CNTB, (B) CNTC, and (C) CNTD – in conditions representative of cytochrome C assay. Cells were treated with 10µg/cm^2 for 4 hours. Magnification is at x400 or x1000. Black bars indicate 20µm.

6.2.5 Impairment of phagocytosis

The ability of J774A.1 cells to actively phagocytose potentially pathogenic bacteria after exposure to CNT was assessed using fluorescently labelled *Escherichia coli* bioparticles. With a pre-exposure of cells to all of particle panel B for 1 hour (figure 6.16 A), there is no significant difference in the amount of fluorescent *E. coli* phagocytosed by J774A.1 cells, compared to the 100% responsive medium-only positive control cells. After 4 hours pre-exposure to particles (figure 6.16 B) there is a 50% reduction in the uptake of *E. coli* particles induced with previous exposure of cells to the long CNTC sample; this was statistically significant compared to the positive uptake control, and to all other particle pre-treatments, excluding the other long CNT sample, CNTD. CNTD was the only other treatment to cause a reduction in *E. coli* phagocytosis; however, this result was not statistically significant.

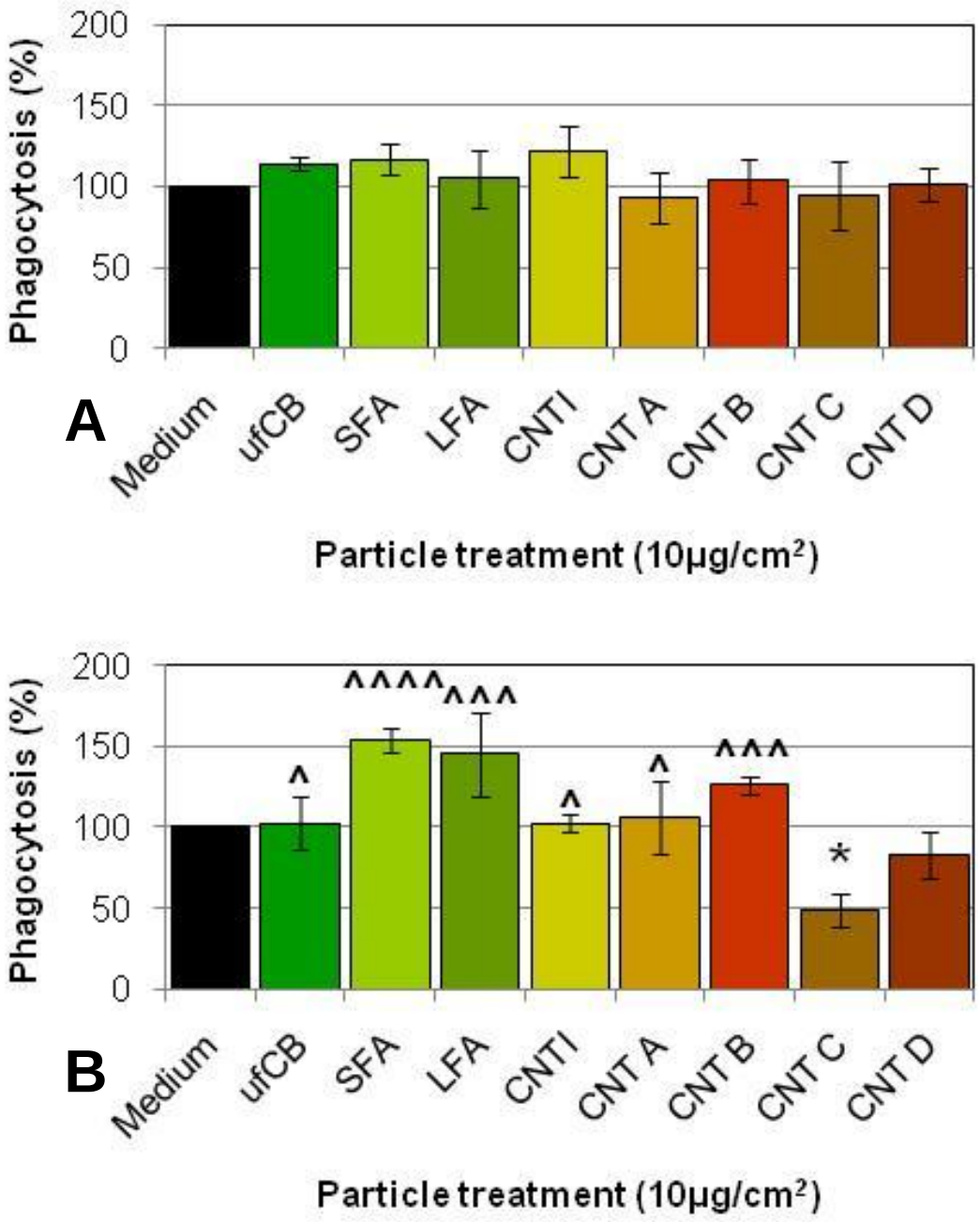

Figure 6.18 Inhibited phagocytosis of J774.A1 cells. Cells were pre-treated with 10µg/cm^2 medium only, ufCB, SFA, LFA, CNTI, CNTA, CNTB, CNTC and CNTD, for (A) 1 hour, and (B) 4 hours, prior to exposure to fluorescently labelled *E. Coli* for 1 hour. Data is expressed as percentage phagocytosis of *E. coli*, with medium-only pre-treatment as 100%. Each data point represents mean ± SEM (n=4). Statistical significance is shown by * = $p<0.05$, compared to medium-only control; and ^ = $p<0.05$, ^^^ = $p<0.005$, and ^^^^ = $p<0.001$, compared to long/high iron CNTC.

6.3 Discussion

The goal of this present study was to assess the initial interactions between CNT and monocytic cells, likely their first defensive encounter during the first few hours of exposure. Interactions and subsequent respiratory burst was assessed in BAL cells; morphological changes in a mouse macrophage-like cell line J774A.1 were observed by SEM, and any host immune impairment was assessed by the uptake of *E. coli* bioparticles by J774A.1 subsequent to particle exposure. All analysis was done in response to particle panel B: nanoparticle CB, SFA, LFA, CNTI, CNTA, CNTB, CNTC and CNTD.

6.3.1 Respiratory burst

The release of O_2^- is evident with exposure of alveolar macrophages to numerous particles. During asbestos exposure the release of ROS is shown to cause lipid peroxidation, tissue damage and ensue an inflammatory reaction, which is often considered to be the instigating factor of asbestos tumourigenesis (Hansen and Mossman, 1987), with greatest response often seen from fibrous material, when compared to non-fibrous equivalents (Hansen and Mossman, 1987, Hill *et al.*, 1995). Length, however, is not the only contributing factor in the extent of particle binding and respiratory burst. Without opsonisation of inhaled particles, fibrous or not, there may be limited cell-particle interaction, and limited O_2^- production. While opsonisation with IgG, for example, will amplify a particle response, but will do so to a higher degree in response to fibrous material (Hill *et al.*, 1995), the function and location of particle exposed cells may also influence their responsiveness and level of respiratory burst. Man-made vitreous fibres, with lengths that would encourage frustrated phagocytosis, are shown to induce considerable release of O_2^- from alveolar macrophages, while not in peritoneal macrophages (Dörger *et al.*, 2001). This raises an issue of the consequence of specific receptor binding and particle exposure conditions.

The respiratory burst measured here was assessed as the release of O_2^- during a 4-hour exposure to nanoparticle CB, SFA, LFA, CNTI, CNTA, CNTB, CNTC and CNTD. Without cell priming it was shown that all the exposure conditions generated an increase in O_2^- release compared to untreated cells. All particle treatments were statistically significant with the exception of nanoparticle CB.

All significant particle responses displayed an approximate 2-fold increase, with the highest response being a 2.1-fold increase in O_2^- release from CNTB exposed cells, therefore demonstrating that a clear particle/cellular interaction and attempted phagocytosis of most of particle panel B was occurring. There would not have been any nonspecific particle coating during this assay, as the "reaction mixture" is relatively simple in its composition, and therefore no opsonisation would occur. However, the addition of PMA to the experiment may give an indication of a more biologically relevant response, as within lung surfactant there would be considerable opportunity for macrophage activation and for particle coating and opsonisation. On occasion an extra stimulus is needed before binding or reaction to particles is achieved. Cells may become primed or activated with stimulation from PMA, chemokines or TNF-α; and internalisation may occur independently of any oxidative burst (Park, 2003). Activation of the enzyme that catalyses a respiratory burst (NADPH oxidase or respiratory burst oxidase) can be mediated through membrane receptor binding, or through stimulus by soluble compounds such as PMA. Upon activation of the oxidase system there is activation of components through phosphorylation, and translocation of components to the plasma membrane. Receptor-induced oxidase activation is short-lived and is restricted to the site of interaction, while activation via PMA may last considerably longer and can be used as a way to prime or activate a cell, which may enable its responsiveness (Chanock *et al.*, 1994).

Resident macrophages are considered relatively inactive in terms of respiratory burst, with cell priming allowing a more vigorous response, as well as potentially enhancing surface receptors and adhesion molecules (Halliwell and Gutteridge, 2007). With simultaneous cell activation and particle treatment there is a clear difference in respiratory burst, compared to the pattern seen in the un-stimulated analysis. The PMA-activated cells are shown to increase their release of O_2^- release 2.8-fold, compared to the untreated control, which was more than all reference materials and all of the short MWCNT. However, the two long MWCNT samples, following PMA stimulation, still induced a significantly larger respiratory burst ($p<0.05$ for CNTD and $p<0.005$ for CNTC) than the control PMA stimulated cells, but also considerably more pronounced ($p<0.001$) than all other particles, with PMA. It is unclear what this change in

response truly signifies, the response to nanoparticle CB, SFA, LFA, CNTI, CNTA and CNTB is still elevated with inclusion of PMA, but only slightly, which indicates that interference of particles with the function of PMA, by particle:PMA binding for example, is unlikely. It may be that less of the long, uncoated MWCNT were bound prior to PMA stimulation, and that addition of PMA simply triggered a response in the BAL cells that is more likely to be seen in biologically relevant conditions.

A change in exposure time may help to clarify what effect particle length and particle type might have on the phagocytic burst. Alveolar macrophages have been shown to not release significant levels of O_2^- until they have been exposed to chrysotile asbestos for 9 days, while NO can be measured at only 1 day, and neither was apparent in response to crocidolite (Mongan *et al.*, 2000). Shorter exposure times of 2 hours on unstimulated peripheral blood mononuclear (PMN) cells are shown to stimulate significant release of O_2^- in response to short CNT and CNF, not seen in response to other CNT, nanoparticle CB or LFA (Brown *et al.*, 2007b). PMA-primed PMN cells have been shown to be particularly responsive to treatment with both short and long fibre-like MWCNT with significantly high O_2^- release, while similarly to the results presented here, nanoparticle CB and LFA are again shown to stimulate no response compared to controls, with nanoparticle CB appearing to decrease the respiratory burst in these PMA-stimulated cells (Brown *et al.*, 2007b).

Kagan *et al*. (2006) and Shvedova *et al*. (2005) found no evidence of SWCNT-exposed macrophages initiating oxidative burst or production of nitric oxide (NO), or even attempting to actively phagocytose the fibres. Through the measure of nitrite concentrations it was also shown by Pulskamp *et al.* (2007a) that NO is not produced in response to SWCNT or MWCNT. Additionally it was shown that LPS-induced formation of NO is dampened with the inclusion of MWCNT, which seems to be occurring here in respect to PMA stimulation combined with many of particle panel B. Pulskamp *et al.* (2007a) believe this to be due to the binding of CNT to the protein inducible nitric oxide synthase (iNOS). This does not seem likely with respect to soluble PMA, but it does raise questions regarding the host's ability to react to inhaled pathogens with previous CNT exposure, which is discussed later. The binding of cells to the particles examined here is clear from the respiratory burst that is initiated and

the visualisation of BAL cell-particle interactions during this assay by light microscopy, with an indication that an elevated response to long MWCNT may occur in activated cells. This binding and internalisation was examined further with the use of SEM of J774A.1 cells treated with 4.2µg/cm^2 nanoparticle CB, SFA, LFA, CNTI, CNTA, CNTB, CNTC and CNTD for 4 hours. This assessment did not include the identification of specific receptor binding; however, as previously mentioned, the consequence of specific receptor binding upon particle exposure may have substantial impact of a cell's reaction, and therefore needs some consideration.

Macrophages have an array of surface receptors for different binding mechanisms to allow inherently and functionally different responses to the binding of different materials (Beamer and Holian, 2005). For example, antibody opsonised material generates a considerable inflammatory response which is achieved through Fc receptor binding, while the binding of phagocytes to apoptotic cells results in anti-inflammatory conditions, and a significant lack of inflammation is also seen from complement receptor binding (Aderem, 2003). Receptor mediated binding of MWCNT may be important in explaining the patterns of uptake and conditions induced with MWCNT exposure, and would certainly warrant future investigation, as recognition and designation of inhaled particles for removal is through recognition of certain surface proteins on pathogens, or by opsonisation by host proteins, such as antibodies, complement or surfactant components (Aderem, 2003).

The impact on toxicity seen from opsonisation of inorganic inhaled particles is likely to be significant, as lung surfactant contains high levels of IgG, but also numerous surfactant proteins. Therefore inhaled particles could be coated, uncoated or IgG-optimised once resident within the lungs, and the cellular (immune) response may differ accordingly. Specific receptor functionality, or particle opsonisation may influence the extent of cell-particle binding, and therefore particle uptake, but also may directly influence the formation of a respiratory burst (Brown *et al.*, 1997). A range of previously uncoated fibres (pathogenic and non-pathogenic) were shown to induce no or little O_2^- release; however, opsonisation using a coating with IgG causes the increased release in some – including LFA – but not all fibres, and O_2^- release is seen from both pathogenic and non-pathogenic fibres (Brown *et al.*, 1997). It is apparent that

the binding of certain receptors will drastically influence the pathogenicity of inhaled particles; one group of receptors, scavenger receptors (SR), are implicated in the removal of inhaled material by alveolar macrophages (Beamer and Holian, 2005). The functional response to adhered particles may also differ with SR attachment, dependent on which SR type is bound, and what is attaching to it. Interaction with class B SR CD36 is shown to cause the production of MCP-1, therefore a pro-inflammatory response when stimulated with β-amyloid (Moore *et al.*, 2002). However, CD36 is also seen to function in an anti-inflammatory capacity in the recognition and removal of apoptotic cells (Savill *et al.*, 1992). During CD36 initiated phagocytosis of *Plasmodium falciparum* (malaria parasite) (Serghides and Kain, 2001) or binding of atherosclerosis-associated oxidised low density lipoprotein by macrophage SR (Shackelford *et al.*, 1995) there is also the generation of anti-inflammatory conditions with a down regulation of TNF-α production. It is suggested that the SR are responsible for the interaction between cells and non-biological material, including crocidolite asbestos (Gilberti *et al.*, 2008, Resnick *et al.*, 1993). Antibody opsonised crystalline silica are rapidly phagocytosed by macrophages, likely through initial binding of Fc receptors; the uptake is rapid and results in little cytotoxicity. However, when uncoated or nonspecific protein-coated, crystalline silica is still phagocytosed, although at a slower rate, and will cause considerable cell death (Gilberti *et al.*, 2008). This increased uptake is mirrored in a faster oxidative burst stimulated by Fc receptor binding, which is also shown to occur more rapidly than class A SR binding (Jozefowski and Kobzik, 2004), but uptake will still occur (Gilberti *et al.*, 2008). If interaction with silica is via AM class A SR (CD204) there is promotion of pro-fibrotic conditions with an increase in cell death. Without CD204 present, which is apparently specific for silica (in terms of environmental particle inhalation), the silica particles are still taken in by cells – possibly through associating with other SR such as macrophage receptor with collagenous structure (MARCO) or CD36; however, the response is very different, with no evidence of fibrosis. Instead, less cytotoxicity and a considerable inflammatory response is produced (Beamer and Holian, 2005). MARCO are certainly considered to be instrumental in the binding and endocytosis of inhaled unopsonised particles (Arredouani *et al.*, 2005, Palecanda *et al.*, 1999), and may be involved in the binding of CNT (Hirano *et al.*, 2008). The binding and subsequent internalisation of titanium

dioxide nanospheres appeared to be governed by the macrophage MARCO receptor. In contrast, this receptor is not used in the phagocytosis of titanium dioxide with fibre-like dimensions (Hamilton *et al.*, 2009), indicating a morphological influence on binding to this receptor. However, MWCNT have been shown to selectively bind the class A SR, MARCO, enabling phagocytosis, which incidentally results in considerable membrane disregulation (Hirano *et al.*, 2008). The importance of SR MARCO binding during exposure to infectious microorganisms and to TiO_2 has clearly been shown by Arredouani *et al.* (2004) to influence host response. *Streptococcus pneumonia* exposed $MARCO^{-/-}$ mice will generate considerably more TNF-α, MIP-2, and recruit more PMN than $MARCO^{+/+}$ mice, while binding of TiO_2 to $MARCO^{+/+}$ mouse BAL cells is apparent and associated with an increase in TNF-α, not seen on exposure of $MARCO^{-/-}$ mice to TiO_2 (Arredouani *et al.*, 2004), which further implicates MARCO in non-organic particle phagocytosis.

6.3.2 Particle uptake

Professional phagocytes use phagocytosis as a method for removal of inhaled material and the destruction and removal of pathogens and dead cells. Internalisation by phagocytosis involves membrane binding of specific receptors, rearrangement of cytoskeleton (Park, 2003) through actin polymerisation (Aderem, 2003) to form and extend pseudopods, and finally intracellular enclosure within a phagosome (Park, 2003). Protruding filopodia will appear in response to both physical and chemical stimuli (Karp, 2002), and during cellular motility along a substrata there is a flattening of the cell in the direction of its intended movement. These projections are called lamellipodium, with the formation of a tail on the opposite side; the motion of these lamellipodia will often give the appearance of ruffles (Karp, 2002). With exposure of fibres to alveolar macrophages there is a rapid formation of lamellipodia directionally towards fibres (Luoto *et al.*, 1994). The appearance of ruffles extending outwards from any direction from a phagocytic cell, with no flattening, is likely to indicate phagocytosis and is the formation of pseudopods that will engulf what the cell has attached to and hold it within a phagosome (Alberts *et al.*, 2002). When contact is made cells will project pseudopods and cable-like microvilli to attach fibres and stabilise the cell (Luoto *et al.*, 1994). As exposure time

continues cells are likely to display a morphology expressive of pronounced phagocytosis, with an increase in ruffles indicative of an increase in phagocytosis (Warheit *et al.*, 1988). However, if the exposure conditions are particularly cytotoxic there is likely to be a reduction of membrane ruffles, the membrane will become granular, and initiation of blebbing will occur (Luoto *et al.*, 1994).

The inability of cells to fully engulf respirable fibres during phagocytosis results in a state of frustrated phagocytosis. One aspect of this – the continued release of ROS, due to phagocytosis associated binding of particles to the cell membrane triggering an oxidative burst and O_2^- release into the surrounding medium – is thought to initiate the progression of disease through continued injury to cells and surrounding tissue (Brown *et al.*, 2007b). The full implications of frustrated phagocytosis are numerous, and are discussed in chapter one. Briefly, with frustrated phagocytosis, in addition to the continued ROS release, there is likely to be a lack of lung clearance of cells and inhaled material, and a continued release pro-inflammatory mediators (Brown *et al.*, 2007b), contributing to any pathogenicity. The pathogenicity of crocidolite is linked to frustrated phagocytosis and the subsequent ROS release (Goodglick and Kane, 1986), which may damage surrounding tissues directly and also encourage inflammatory responses through transcription factor activation (Chanock *et al.*, 1994). A length dependency of frustrated phagocytosis is clear from exposure of alveolar macrophages to short (<5μm) and long (>15μm) titanium dioxide nanobelts, where the short are clearly shown to be isolated within lysosomes, while the long are seen to protrude through the cell membrane, are free within the cytoplasm, and not clearly held or associated within lysosomal structures within the cell (Hamilton *et al.*, 2009). The association between fibre length and enhancement of pro-inflammatory and oxidative conditions through frustrated phagocytosis have been clearly demonstrated with exposure of glass fibres (Ye *et al.*, 1999a, Ye *et al.*, 2000) and CNT (Brown *et al.*, 2007b) of different length.

SEM observations of J774A.1 cells exposed to particle panel B were used primarily to check for frustrated phagocytosis, and for the activation state of the cells. The appearance of control J774A.1 cells used here, cultured in growth-medium only, were typically inactive. They were often round or flattened due to

spreading, with evidence of filopodia during spread but only with occasional motility-associated lamellipodium ruffles.

The morphological response to the particle exposure conditions used here were generally as expected. With the exposure of cells to nanoparticle CB and SFA the extent of spreading is far less than those induced by other particle exposures, and any lamellipodium formation is directional towards particle aggregates, signifying cells actively searching for particulate matter, probably in response to chemical signals of other cells engaged with material. Additionally, in response to both nanoparticle CB and SFA the increase in sporadic membrane ruffles that are not directional but are associated with particles, and an increase in microvilli actively extending protrusions to obtain CB particulate matter, all indicate morphology indicative of active phagocytosis. There is also, however, the occasional loose association of SFA with the microvillous membrane, which may signify a lack of cell-particle binding.

The phagocytic response of J774A.1 cells to LFA was far more vigorous than to nanoparticle CB or SFA. LFA caused the directional lamellipodia associated with cells actively seeking and migrating towards particles; however, once found the cells migrate and extend along fibres, at which point the appearance of considerably more phagocytosis, associated membrane ruffling indicates the exertion and activation state the cells have reached. Fibres of a length greater than the limit of macrophage phagocytosis will often attract numerous cells to one fibre, and single cells will attach numerous fibres (Dika Nguea *et al.*, 2005). This is clearly a common occurrence in the 4-hour LFA exposure period used here, with cells attempting to phagocytose multiple LFA fibres simultaneously, and somewhat “spearing” themselves along fibres that are too long for phagocytosis. Over time this will cause cells and fibres to group and accumulate (Dika Nguea *et al.*, 2005). The length of fibres is considered the vital characteristic for frustrated phagocytosis, with man-made vitreous fibres used to show a clear cut-off point of approximately 20μm causing the incomplete phagocytosis of these fibres (Dörger *et al.*, 2001), while alveolar macrophages often struggle to fully internalise >15μm titanium dioxide nanobelts (Hamilton *et al.*, 2009); the human macrophage cell line U-937 is only capable of phagocytosing fibres of lengths up to 27μm (Dika Nguea *et al.*, 2005). The maximum length of LFA that J774A.1 seem capable of fully engulfing also

seems to be below 30µm; this can be seen in figure 3 A_{II}. It is clear though that any cell motility will be dramatically impaired with the cell extended to this limit, and therefore in a biologically relevant environment these exposure conditions would not be resolved.

The pattern of MWCNT uptake appears far less consistent. Significant membrane ruffling and particle attachments in response to CNTI are on a par with LFA-treated cells, indicating a similar activation state. Also similar to LFA, CNTI exposure results in multiple cells attaching to single CNT aggregates. However, the method of uptake appears far more arduous with CNTI exposure than LFA. Instead of extending over the CNT aggregates as was seen in LFA exposure, the J774A.1 cells remain relatively round and protrude large numbers of microvilli that become intertwined with the aggregates until the two are indistinguishable, and they then attempt to encompass the CNT aggregates within large pseudopods, or draw in separate aggregate sections at different membrane locations through different pseudopods simultaneously. The responses to LFA and CNTI are clearly morphologically distinct, but both are creating the condition of frustrated phagocytosis. The appearance of these large attempted vacuoles in CNTI treatment and the evident outward pressure on the plasma membrane exerted by internalised CNTI aggregates, are likely to accelerate any detrimental effects of MWCNT frustrated phagocytosis. The electron microscopy images suggest that the pressure exerted on the plasma membrane with exposure of cells to the short CNT samples results in obvious piecing of the surface of the cell membrane, where MWCNT are seen to enter the cell with no ruffling and exit at a different location; this alone is likely to induce cytotoxic conditions.

The actual phagocytic response of cells to the short laboratory-designed MWCNT samples appears to be largely dependent on aggregation, although in all cases there is an increase in cell surface microvilli. With small aggregates and cells associating with fewer CNT there is the appearance of ruffling, but only at the sight of CNT attachment, while large aggregates generate the same conditions seen in CNTI exposure.

The response to the long MWCNT samples is clearly the most detrimental. Phagocytosis-associated membrane ruffling appears consistently over the cell membrane. Similarly to LFA exposure seen here, and to MWCNT exposures

observed elsewhere (Asakura *et al.*, 2010), bridging of cells by MWCNT occurs from multiple cells attempting phagocytosis of the same single CNT or CNT aggregates, and single cells are attempting phagocytosis of numerous MWCNT simultaneously. However, unlike LFA exposure, but similarly to other MWCNT, the cells remain round and do not elongate themselves along fibres, but instead attempt to draw MWCNT within by actively phagocytosing CNT from many pseudopods in different locations. This continues to result in the appearance of large indentations at the source of these particle uptake locations, and is very likely to result in cell and cell membrane dysfunction. There is, however, no evidence of cell blebbing – an indicator of cell dysfunction and forthcoming cell death – in any of the cell cultures within this study. The appearance of RAW 264.7 macrophages exposed to SWCNT and MWCNT for longer periods of time, display a morphology more akin to cytotoxic responses, with a marked decrease in microvilli and membrane ruffles at 24 hours, and at 72 hours there is clear induction of apoptosis, with the appearance of blebbing (Giorgio *et al.*, 2011). However, 24-hour exposure of MDM cells with SWCNT have been reported to induce displays of an activated morphology, but not cytotoxicity, while the same exposure conditions using graphite displays clear membrane blebbing (Fiorito *et al.*, 2006).

The results presented here suggest that the MWCNT used in this study are internalised by J774A.1 cells. The rupturing of cells is likely through the direct piercing of plasma membrane but also through the continued frustrated phagocytosis caused by long MWCNT or CNT aggregates. Partial uptake of both MWCNT and chrysotile asbestos fibres has been shown on exposure of a hamster lung cell line (CHL/IU), where longer fibres are shown to penetrate the cell membrane partly entering the cytoplasm, with suggestions of this physical interference interrupting cytokinesis, causing genotoxicity (Asakura *et al.*, 2010). The passive entry through the cell membrane at times shown here has also been observed, with SWCNT physically penetrating human lymphocyte A3 cell membranes (Hu *et al.*, 2010), and in the treatment of human monocyte-derived macrophages (HMM) with long (>50μm) MWCNT, where they are found within the cytoplasm and inserted into the nucleus. This is believed to be through either membrane translocation or frustrated phagocytosis (Cheng *et al.*, 2009). However, due to CNT fibre-like morphology, it cannot be presumed that

dysfunction will not occur when cells fully and successfully internalise CNT. MWCNT material taken up within phagolysosomes may still cause damage to these membrane-bound structures resulting in release of MWCNT into the cytoplasm, also allowing interaction with the cell's nucleus (Giorgio *et al.*, 2011).

It has been shown here, and within the literature, that the accumulation of CNT within a cell is likely to be through both passive and active mechanisms. CNT may simultaneously be phagocytosed by HMM cells, ending up in lysosomes, and translocate across the plasma membrane (Porter *et al.*, 2007b), often altering membrane integrity causing ruptures (Hirano *et al.*, 2008), but certainly allowing free penetration within the cytoplasm and nucleus (Porter *et al.*, 2007b). This intracellular distribution, however, is not a CNT specific phenomenon, exposure of C_{60} to macrophage cells also results in particles found not only in lysosomes, but also in the cytoplasm and nucleus of the cells (Porter *et al.*, 2007a), with uptake presumed to be through phagocytosis and diffusion. This indicates that although the fibre-like morphology of CNT provides needle-like insertion into cells, particle size is also important in non-endocytotic mechanisms of particle uptake. In the presence of phagocytosis inhibitors pulmonary macrophages are still found to contain particles, this appears to be size dependent, where particles of 1μm are only engulfed via phagocytosis, while <200nm titanium dioxide (TiO_2) are found to enter both macrophages and RBC via diffusion or adhesion, with no association to any endocytic vesicle (Geiser *et al.*, 2005).

6.3.3 Inhibited immune response

The impairment of normal phagocytic cell function may be a consequence of frustrated phagocytosis, an increase in cell burden, or a combination of both. In the respiratory system any impairment in phagocytic function may have a number of effects, including the hampered clearance of both particles (Ferin *et al.*, 1992) and fibres (Mossman and Churg, 1998), and associated pathology originating from the chronic pro-inflammatory and pro-fibrotic conditions (Becker *et al.*, 1996, Mossman and Churg, 1998) created through a lack of respiratory clearance. Alternatively, there is an issue of an impairment of host respiratory defensive mechanisms with a decrease in clearance of infectious agents, such as bacteria (Shvedova *et al.*, 2005), in response to CNT as any lung burden

increases. The effect respirable particles will have on this is easily tested through the phagocytic ability of cells undergoing secondary exposure to alternative particles, preferably particles that would use alternative binding mechanisms, such as bacterial LPS.

Particle panel B was used here to expose J774A.1 cells for 1- and 4-hours to a particle dose of 10µg/cm^2, which was subsequently removed and replaced with fluorescently labelled *E. coli* bioparticles. The uptake of *E. coli* demonstrates normal phagocytic functioning. It is clear that with only a 1-hour pre-treatment with particles there was no decrease in the volume of *E. coli* bioparticles internalised by J774A.1. However, with 4 hours pre-treatment the phagocytic ability of J774A.1 was greatly impaired in response to both long MWCNT samples. This was only significant with the pre-treatment with CNTC, where *E. coli* bioparticle uptake was shown to drop to only 50% that of control untreated cells. The reduced ability of J774A.1 cells to remove *E. coli* particles from the media after pre-treatment with both long MWCNT samples, may be due to the sequestration of membrane receptors by the fibres, even if they are not fully engulfed, which certainly is evident by the O_2^- production from primed long-CNT treated cells. Alternatively, the clear and considerably destructive frustrated phagocytosis induced by these CNT would likely leave little functionality for secondary exposures. The phagocytic ability of AM is shown to be considerably impaired when incubated with chrysotile asbestos (Mongan *et al.*, 2000) and pre-treatment with SWCNT, MWCNT, C60 and quartz (Jia *et al.*, 2005), but not with identical exposures of crocidolite (Mongan *et al.*, 2000). The ability of THP-1 cells to phagocytose fluorescently labelled *E. coli* after pre-treatment with a range of particles is shown to be impeded in response to long and short CNT, nanoparticle CB and LFA, particularly at the higher dose of 62.5µg/ml (Brown *et al.*, 2007b), while a lower dose of nanoparticle CB, equivalent to the 17.5µg/cm^2 concentration used here, is shown to cause an approximately 40% reduction in *E. coli* particle uptake after a 4-hour pre-incubation; this response, however, is not shown to be significant (Wilson *et al.*, 2007). It also takes a higher exposure dose than those used here to impede phagocytic function of J774A.2 macrophage cells with exposure to nanoparticle CB. Renwick *et al.* (2001) demonstrated that the uptake of latex beads is unchanged with pre-treatment of

nanoparticle CB until a dose of 39µg/cm^2 is used, and 78µg/cm^2 for other particles, such as bulk CB, and fine and ultrafine titanium dioxide.

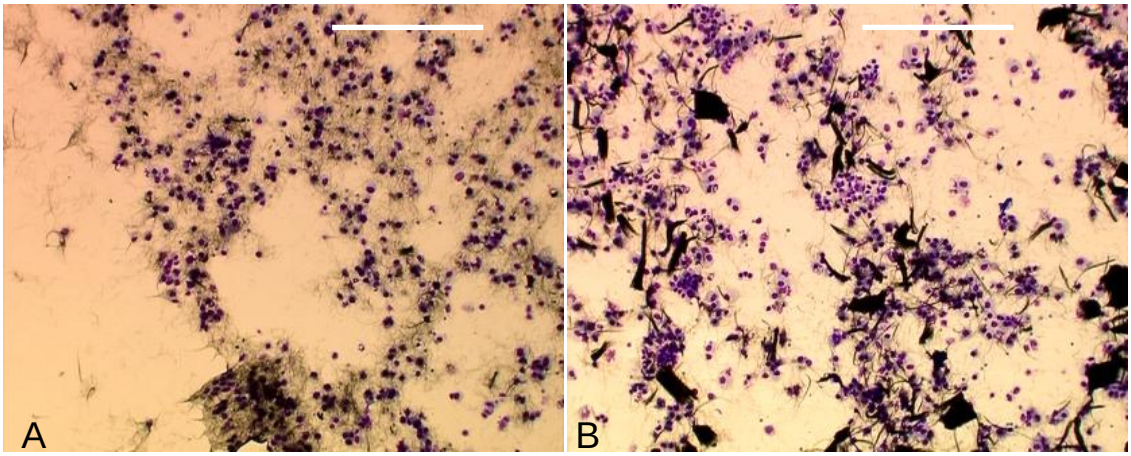

Figure 6.19 Light microscopy images of BAL cells treated with 10 µg/cm^2 (A) CNTC and (B) CNTD for 4 hours. Magnification x100. White bars indicate 200µm.

The reason for differences between CNTC and CNTD is less clear; structurally they are similar; however, light microscopy images of particle exposed BAL cells indicate the increased dispersion of CNTC compared to CNTD (figure 6.17). This increased dispersion has resulted in an observed increase CNTC sequestering by cells, creating a net-like structure, which may explain any further impairment in respect to CNTC. Incidentally, if internalisation of either long MWCNT were attempted by BAL cells under these conditions, it would surely result in frustrated phagocytosis.

6.3.4 Concluding remarks

There were three key aspects that this chapter had to address, all relating to particle uptake: (1) frustrated phagocytosis, (2) impaired phagocytosis of secondary microorganism exposure, and (3) the extent of respiratory burst caused by particle exposure.

Through SEM observations and the oxidative burst generated in response to all of particle panel B, it is evident that the binding and internalisation, at least attempted, was occurring with all particle treatments. However, the images obtained suggest that MWCNT translocation through the cell membrane may occur, that if true, would allow free interaction with cellular components. The

evident frustrated phagocytosis in response to both long MWCNT and MWCNT agglomerates clearly has the potential to enhance toxicity to the macrophages as well as to enhance pathogenicity *in vivo*, providing that the agglomerates are respirable. If exposure to MWCNT is to be likened to that of asbestos, then the consequence of these findings are substantial, and may lead to asbestos associated pathogenicity, which was discussed in chapter one.

Frustrated phagocytosis is caused by a number of the exposures in this study, while impaired phagocytic ability was only statistically significant in response to the long/high iron CNTC. This response was only evaluated at one concentration. However, as particle dose increases it is expected that the extent of impairment will also increase (Renwick *et al.*, 2001). *In vivo* numerous particle respiratory exposures can inhibit subsequent phagocytic ability, including fine and ultrafine titanium dioxide and CB, all dose-dependently, with the greatest impairment from the respective ultrafine particle (Renwick *et al.*, 2004). This indicates that any pathology related to the proposed lack of clearance and biopersistence of MWCNT would not only occur at lower level of particle exposure compared to other inhaled material, but would likely increase with increased dose. A reduction in infectious agent clearance is not the only impact of this frustrated phagocytosis-related phagocytosis impairment will have. Cheng *et al.* (2009) observed the appearance of cells undergoing secondary necrosis with MWCNT exposure, indicating not only cytotoxicity but also further impairment of macrophage phagocytic abilities, in their inability to remove sister cells undergoing apoptosis. Additionally, pulmonary defence protein sequestering by CNT, such as pulmonary surfactant proteins (SP-A and SP-D) which play a key role in the pulmonary defence against allergens and microorganisms, will hinder pulmonary defence systems (Salvador-Morales *et al.*, 2007, Shvedova *et al.*, 2007). The proteins would be unavailable for defence against pathogen infection, and phagocytosis of SP-A- and SP-D-coated CNT would be encouraged (Salvador-Morales *et al.*, 2007), with the outcome of further frustrated phagocytosis, biopersistence and enhanced, maintained inflammation.

It is worth noting that during measurements of respiratory burst, it is possible that there is an underestimation of the level of O_2^- release being stimulated by some of the particles used here. The pattern of Fe^{3+} release from a number of

the particle panel, to different degrees (demonstrated in chapter 3) indicated the bioavailability and possibly surface location of these iron molecules. With the ability of O_2^- to reduce Fe^{3+} removing it from a particles surface (Ghio *et al.*, 1994), consequently creating O_2, the release of O_2^- during phagocytosis may be underestimated in the case of SFA, LFA, CNTA and CNTC. Also noteworthy is the apparent inhibition of respiratory burst found with exposure to nanoparticle CB, SFA, LFA, CNTI, CNTA and CNTB, in the presence of PMA. This is unexplained, but its occurrence can be an indication of cell burden, but in this case it is not believed to be the cause as *E. coli* particle uptake demonstrated the phagocytic ability of cells is not impeded by these particle exposures, albeit in a different cell type. It is, however, worth bearing in mind that the inhibition is only in respect to other PMA treatments: the addition of PMA still stimulates an enhanced response compared to relative treatments in its absence. Additionally, this is not an isolated occurrence: the same response has been seen in other nanoparticle CB exposures (Brown *et al.*, 2007b).

Chapter 7

General discussion

7.1 Carbon nanotube characteristics

The aim of the research undertaken during this study was primarily to establish physiochemical factors responsible for MWCNT toxicity. This could then be combined and discussed with collaborators, in order to inform the safety of manufacturing methods and procedures. To attain this information, morphologically and compositionally distinct MWCNT were designed and manufactured, or donated. MWCNT samples were produced to allow comparisons of short (<20µm) vs. long (>20µm), low iron content vs. high iron content, and samples of high crystallinity vs. low crystallinity. The production process of these CNT and their characterisation, alongside that of the asbestos and amorphous carbon reference materials, was presented in depth in chapter three, and an overview table was given in chapter two. Here, a reminder of the classification of the five CNT samples of particle panel B is provided (this was also given in chapter five); to provide the following orders in which they sit in the aforementioned research criteria:

- Length: CNTC = CNTD > CNTI = CNTA = CNTB
- Crystallinity: CNTI > CNTD > CNTB > CNTA > CNTC
- Iron content – dry: CNTA > CNTB > CNTC > CNTI > CNTD
- Iron release – neutral pH: CNTI > CNTC > CNTD > CNTA > CNTB
- Iron release – acidic pH: CNTA > CNTC > CNTI > CNTD > CNTB

The reference materials have not been included, but there are a number of points that are important to mention. The two asbestos reference materials were chosen to be long fibrous (LFA) and short fibrous (SFA) materials, to identify if CNT effects are mirrored by these materials in any way. However, it is not only their lengths which are comparable; these asbestos samples also show a relatively high iron release in all environments tested, more so from SFA, which was equivalent to CNTA, while LFA was equivalent to CNTC. A relatively high amount of Fe^{++} was also found to leach from the third reference material, NPCB, but little Fe^{+++}.

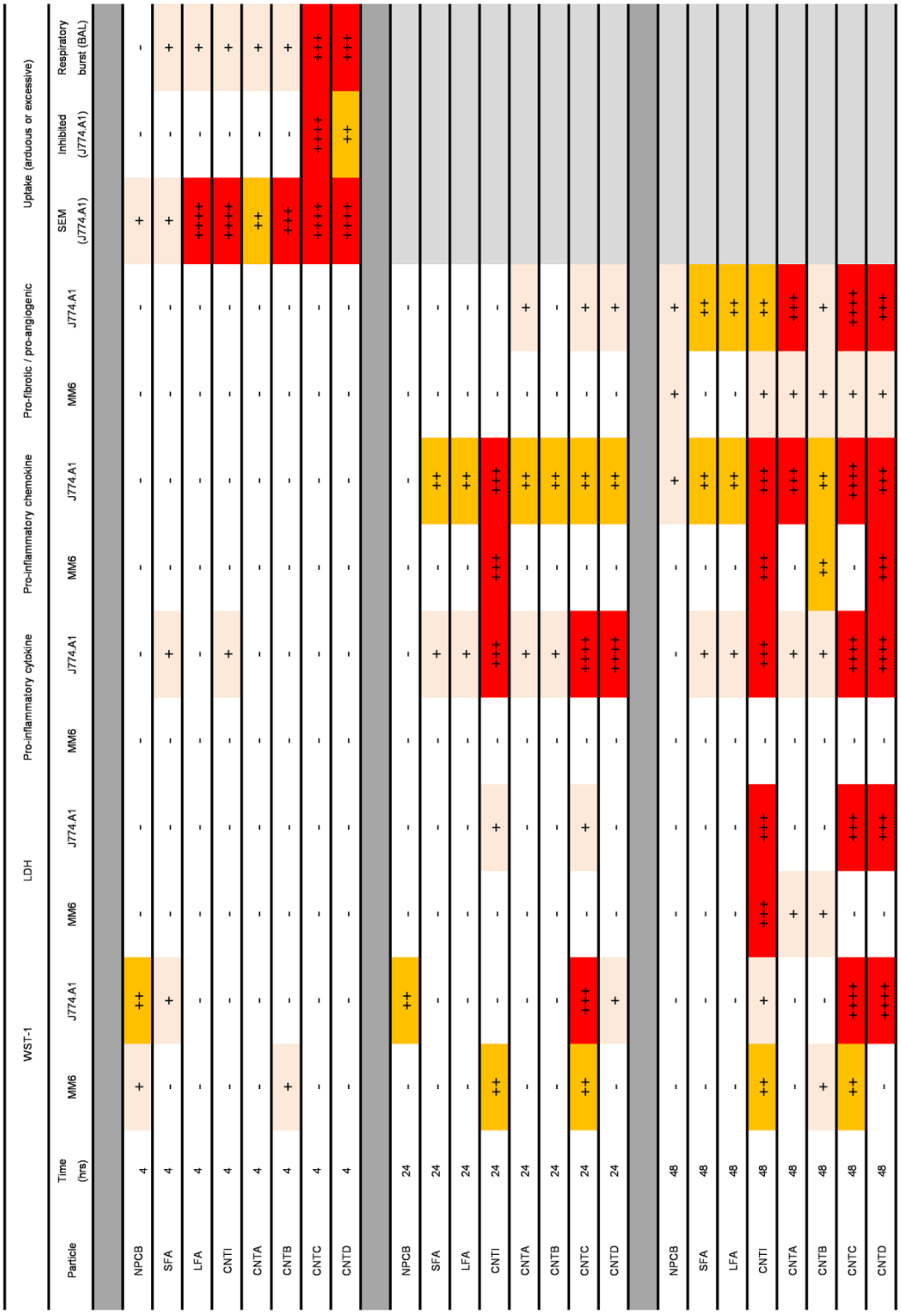

Table 7.1 Outline of particle panel B toxicity and comparison of cell responses. All time points are expressed, − (no colour) indicates no particle response, + (pale pink) indicates a weak particle response, increasing in relative response (orange through to red) until ++++, indicating the highest response. The designation of markers communicates the extent of response, the numerical of particle dose, and the comparison to other particles in the same assay.

7.2 Carbon nanotube toxicology

7.2.1 Brief overview of toxicological responses

Each individual chapter thus far has been used to analyse numerous endpoints and relate the observed effects to potential impacts that MWCNT may have. Chapter 3 highlights the production processes used and identifies characteristics that may influence these impacts. In chapter 4 the oxidative potential was examined, chapter 5 identified the potential for MWCNT to cause cell death and induce various signalling pathways, while chapter 6 highlighted problems associated with uptake, and frustrated phagocytosis. A general summary, and relatively subjective presentation of this data is shown in table 7.1. It is subjective as the designation of markers tries to highlight the most detrimental particles, the particles communicating the highest response across the full range of different particle concentrations, and the impact of one particle in relation to the rest of particle panel B from the same assay, and incorporates information taken from numerous cell types.

Using this table it is evident that during the first 4-hours of *in vitro* exposure there is little or no response to any particles tested, with respect to biochemical responses. Particle uptake was only evaluated at this 4-hour time point and, as hypothesised, it was shown that long MWCNT and LFA cause hampered and frustrated phagocytosis. The uptake of shorter MWCNT was also impeded, which is likely attributed to the agglomeration of both CNTI and CNTB, perceivably due to their proposed high hydrophobicity. In the case of CNTB the high hydrophobicity is an unintentional effect of the high temperature annealing used to remove catalytic iron particles from the sample (and to sample CNTD); it does, however, also generate a sample with a low defect, crystalline structure. The reduced dispersion of CNTI and CNTD in cell culture medium seen in chapter 3 figure 3.15 highlighted this feature. However, although visually it is apparent that much of the fibre-like material hampers phagocytosis, during the 4-hour exposure period only the two long MWCNT samples were shown to elicit impaired phagocytic abilities through particle burden and clear increases in respiratory burst. In hindsight it would have been interesting to continue the particle uptake assays over a greater length of time; this would clarify the effect of frustrated phagocytosis induced by all the fibrous material, but also would

help relate uptake to the biochemical analysis attained during the later time points.

During the later exposure periods employed throughout this study, the initial observations of frustrated phagocytosis were shown to escalate to potentially damaging inflammatory and cytotoxic conditions. Moreover, this escalation was observed to be considerably greater with respect to the MWCNT samples than is was with the exposure of macrophages to LFA. After 24 hours exposure a low level of cell death was shown to occur, but this was limited to only a few particles, the most pronounced being the long, high iron CNTC. The most significant finding of this exposure period was the induction of cell signalling responses. The long CNT (CNTC and CNTD) and CNTI, with a particularly high crystal structure, were shown to induce the secretion of cytokines and chemokines that are associated with conditions favourable for inflammation, fibrosis and angiogenesis.

The immunological responses found during 24 hours did not reside with the advancing exposure times, but were found to escalate. At this last stage of the experimental assessment all of the MWCNT were found to be able to produce a considerable immune response. The only CNT found to be slightly lacking in this respect was the short, low iron CNTB, which, nevertheless, was found to induce a response at least if not greater than the asbestos reference materials. The prolonged exposure period of 48 hours also proved sufficient in providing a clear pattern in cytotoxic behaviour, with CNTC, CNTD and CNTI inducing the greatest level of cell death.

7.2.2 Characteristics responsible of CNT toxicity

There are numerous characteristics that CNT can contain that may influence and impact upon the biological systems they are exposed to, with many factors potentially responsible for toxicity and therefore influencing CNT pathogenicity. A number have been studied during this doctoral thesis. In chapter 3 the production of purposefully-designed MWCNT was described, with the aim of trying to identify intrinsic factors in the toxicity of MWCNT. These included CNT length, iron content and crystal structure. The results obtained during this study do not often provide discernible differences between samples of different iron content or crystal structure, but do clearly demonstrate that CNT length (and at

times aggregation/agglomeration) is a characteristic with potential associated hazards and therefore needs addressing. This study has shown that under certain conditions MWCNT are certainly harmful and pose a clear hazard; there is a mounting body of literature that, albeit some in disagreement, predominantly supports this belief, and is extensively reviewed in chapter one. Much of the literature has also attempted to discern the factors responsible for CNT toxicity, including investigations into length, dispersion and sample purity. A common theory is that the presence of sample impurities such as iron may induce oxidative stress (Kagan *et al.*, 2006, Pulskamp *et al.*, 2007a, Shvedova *et al.*, 2008a). The association of length and fibre pathogenicity has been shown by Donaldson *et al.* (1989, 1992) and Ye *et al.* (1999a), and more specifically to CNT *in vitro* and *in vivo* by Brown *et al.* (2007b), Dörger *et al.* (2001), Kim *et al.* (2010a) and Poland *et al.* (2008). The dispersion of CNT samples is found to influence biological responses, where a good dispersion is shown to enhance the effect of both entangled and uniformly straight CNT samples (Brown *et al.*, 2007b, Rothen-Rutishauser *et al.*, 2010), and to induce a greater level of toxicity at a lower dose *in vivo* and *in vitro* (Sager *et al.*, 2007). However, effects can also be seen in response to both dispersed and aggregated CNT deposits (Muller *et al.*, 2005, Shvedova *et al.*, 2005). It therefore seems important to at least know the dispersal state of the material upon exposure. A study by Tian *et al.* (2006) has also attempted to elucidate which aspect is critical to carbon particle toxicity; the study is relatively comprehensive except that although they make an investigation into high aspect ratio NP, and include SWCNT and MWCNT with aspect ratios of 250 and 100, there is nothing over 1000. In this study Tian *et al.* (2006) highlight the importance of surface area, and in disagreement with much NP toxicology, find that a substantially lower surface area results in an increase in toxic effects, and a purification of the carbon material also results in a higher toxicity (Tian *et al.*, 2006). It is important to mention that the method used by Tian *et al.* (2006) for removal of catalytic metal content is an acid wash treatment, which differs from that used in this study. An acid wash will remove metal contaminants, but will also increase surface functional groups and therefore increase hydrophilicity and dispersion, while the method used in this study was high temperature annealing which will remove iron contaminants, but also remove surface imperfections, increase hydrophobicity and decrease dispersion.

7.2.2.1 Oxidative stress

In chapter 4 the formation of ROS by CNT is attributed to a number of different factors. In the assessment of independent ROS production it appears that it is a combination of a high surface area and proposed release of metal contaminants that can lead to an increase in ROS production. With the incubation of CNT with phagocytic cells, CNT with a high surface area and potentially high iron content that form relatively small (~10μm) bundles are adequately controlled, with only minimal and acute ROS release. Higher and prolonged responses appear to be induced through the frustrated phagocytosis of CNT by cells with greater individual or aggregated length, causing continued and sustained ROS production, potentially leading to oxidative stress, with significant *in vivo* inflammatory responses also found in response to these long MWCNT (Rothen-Rutishauser *et al.*, 2010). Incidentally, these longer MWCNT will also contain relatively high levels of bioavailable iron, which may be relevant as both length and release of bioavailable iron can be implicit in fibre-induced ROS production, subsequent oxidative stress and inflammatory responses (Brown *et al.*, 2010, Brown *et al.*, 2007b, Gilmour *et al.*, 1995, Kagan *et al.*, 2006, Kim *et al.*, 2010a, Muller *et al.*, 2008b).

The causes and consequences of oxidative stress are highlighted and related to various particles in sections 1.2.1, 1.4.3, 1.5.2, and 4.1.1, and its occurrence can be related to the changes in various antioxidant defence mechanisms. The investigation, described later in chapter four, into gene expression of these defence mechanisms and the expression of markers for oxidative DNA damage begin to potentiate the proposed oxidative stress, predicted in response to the clear ROS production demonstrated earlier in chapter 4. Any activity found was in response to MWCNT exposure with CNTB highlighted as causing a significant increase in HO-1 gene expression. These gene expression assays use CNT most similar to those that displayed a delayed response in section 4.2.2, therefore it is possible that, although some small effects were found, the chosen time points may have been unsuitable to observe further changes in gene expression. This seems particularly likely as the induction of antioxidant defence mechanisms has been demonstrated in response to MWCNT very similar to CNTC, in the form of expression of the enzyme haemoxygenase-1 (HO-1), which is accompanied with an increase in pro-inflammatory markers

such as IL-1β (Brown *et al.*, 2010). With the addition of antioxidant treatments it was possible to reduce IL-1β secretion and establish oxidative stress as the mechanism for this inflammatory enhancement (Brown *et al.*, 2010). This study also used an exposure period of 4 hours but with different cells (THP-1). No increase in the gene expression of oxidative stress markers were found in response to LFA by Brown *et al.* (2010), but an increase in HO-1 in response to NPCB was, although not significant. If essential time points have been missed in the treatment of MM6 here for the evaluation of redox gene activity it may have been useful to expand exposure conditions to include further time points and to confirm responses using additional cell types.

It has repeatedly been shown that the generation of ROS by fibres (Chen *et al.*, 1996, Fung *et al.*, 1997, Gilmour *et al.*, 1995) and NP (Brown *et al.*, 2004, Foucaud *et al.*, 2007, Li *et al.*, 2008, Stone *et al.*, 1998) can be implicit in their toxicity, by causing oxidative DNA damage (Gilmour *et al.*, 1995) or stimulating inflammatory responses (Brown *et al.*, 2004). Oxidative DNA damage was not confirmed in this study, as there was no increased expression of the enzyme OGG1, which is known for its role in the repair of oxidative-induced DNA damage. This, however, may not be the best representation of oxidative DNA damage; it certainly is used for the repair of oxidative induced lesions in DNA, but as described earlier, OGG1 may be expressed at much earlier time points, in response to the initial stimuli and the activation of Nrf2 (Dhénaut *et al.*, 2000). Other methods for the determination of oxidative DNA damage are available, such as FPG-modified comet assay, but were not used in this study. An inflammatory reaction to MWCNT has certainly been confirmed and is discussed later. The inference that the subsequent cellular responses found in response to CNT during this study, such as the release of inflammatory mediators, cannot be attributed to ROS production with any great assurance. To attain these assertions it would be essential to use methods of redox control, such as the inclusion of antioxidants, to diminish induction of oxidative stress, with further observations of whether this also results in a reduction in cell death per se, or limiting of mediator release.

The results of this study concerning ROS are largely in agreement with much of the current literature (Kagan *et al.*, 2006, Pulskamp *et al.*, 2007b, Shvedova *et al.*, 2007, Srivastava *et al.*, 2010, Thurnherr *et al.*, 2010), in that many

compositionally distinct MWCNT are capable of producing ROS *in vivo*, *in vitro* and independently; and that MWCNT mildly induce the expression of HO-1 in response to the formation of these oxidants. With the comparisons made in this study it can be, at this stage, tentatively proposed that an increase in ROS production is attributed to CNT length, or at least CNT aggregate size, and that MM6 cells will initiate antioxidant defensive mechanisms in response to MWCNT exposure.

ROS generated during the respiratory burst of cells attempting phagocytosis of particles was assessed in chapter six. All particle exposures were shown to cause an increase in ROS production associated with a respiratory burst, only NPCB was found not to be significantly higher than the control cells; this was to be expected as all particles should be actively phagocytosed. Only when cells were primed for a phagocytic response were other differences found. With the addition of PMA prior to particle treatment, long MWCNT alone were found to induce higher ROS production than the negative control cells and incidentally higher than all other particles. The phagocytic burst induced with cellular exposure to CNT (Pulskamp *et al.*, 2007b) was also demonstrated to be higher than that of asbestos by Thurnherr *et al*. (2010). The implication of these factors together is that it is not only MWCNT length that is responsible but also something distinguishable between asbestos and CNT that is causing this increase in ROS production. If left unresolved, due to frustrated phagocytosis per se, the pro-inflammatory conditions directly stimulated and intensified by CNT-induced ROS generation (Han *et al.*, 2010), as is seen with other NP (Brown *et al.*, 2004, Donaldson *et al.*, 2002, Wilson *et al.*, 2002), can lead to continued tissue injury, cell death and further ROS production (MacNee, 2001), potentially ending in the serious disease progressions which are typified in asbestos exposure.

Again the implication of this is that the greatest phagocytosis-associated ROS release is through exposure to MWCNT with the greatest length and highest aspect ratio; and with the implications of the relationship between CNT-induced ROS production and the induction of inflammation (Brown *et al.*, 2010, Han *et al.*, 2010), it is therefore necessary to clarify if it is also CNT length that has the greatest effect on inflammatory responses.

7.2.2.2 Inflammation

A release of pro-inflammatory mediators is found to both long and short CNT *in vitro* (Brown *et al.*, 2007b, Sato *et al.*, 2005). *In vivo* exposure to short CNT and small CNT agglomerates has been shown at times to cause no inflammation (Kobayashi *et al.*, 2010, Sato *et al.*, 2005, Tian *et al.*, 2006); however, at times a strong inflammatory response to CNT, when compared to negative control treatments, has also been demonstrated (Mercer *et al.*, 2008, Muller *et al.*, 2008b, Shvedova *et al.*, 2008a). When comparisons relating to CNT length are made the inflammatory response to particularly high aspect ratio CNT are often found to be greater than that of shorter fibres (Poland *et al.*, 2008). All particles used within this study are shown to induce some form of inflammatory response, but this is to be expected as the natural response of phagocytes is to initiate inflammation; the question is how high is the response and how long would it be maintained? The particularly high aspect ratio MWCNT in particle panel A are shown to induce a significant inflammatory response *in vivo*, which was not seen following exposures to short or entangled samples (Rothen-Rutishauser *et al.*, 2010). The *in vitro* investigation into inflammatory potential, using particle panel B, confirmed the importance of CNT length in inflammatory responses but also the amplified response to CNT in general over other known pathogenic material, albeit under the exposure conditions used here. Chapter 5 demonstrates the full extent of MWCNT-induced cell signalling where, although all particle exposures, reference and CNT are found to display at least some induction of chemical messaging, it is clear that the response to the MWCNT used here is far greater than that to any of the reference materials. This is in respect to all cell types, and regardless of whether the observations relate to the induction of pro-inflammatory, fibrotic, or angiogenic cytokines and chemokines.

In respect to differences between CNT samples the pattern is less clear. By observing the overview table 7.1, it is apparent that there is no rapid secretion of inflammatory proteins, shown in the 4-hour analysis. Perhaps PCR analysis of gene expression at this time point may have been more suitable. After 24 hours, in general, the highest protein secretion is found in response to the long laboratory-generated MWCNT and the industrial sample; this pattern is maintained during the 48-hour exposure period. At times the shorter CNT also induce cell signalling responses, but to a lesser extent than the long. This is,

however, a broad overview; taking a closer detailed look into the inflammatory response can at times (but only occasionally and not consistently) allow observations of discernable differences between other factors under investigation here, such as iron content and crystallinity. For example, MCP-1 release from MM6 cells is found to be particularly high in exposures to CNT with a higher crystalline structure; but these occurrences are rare, and rarer still is any discernable difference between the release of iron during the exposure periods. Therefore the emphasis is still firmly on CNT length as a discerning factor in their toxicity.

As described in previous chapters, the implications of such an accumulation of inflammatory proteins are certainly severe, and clearly warrant close control and monitoring of the production of MWCNT. The use of *in vitro* experiments of this nature only allow us to infer the subsequent impact these conditions will have; therefore the inevitable cell death of cells under frustrated phagocytosis of durable material and the secretion of proteins such as TNF-α, a known apoptotic stimulating agent (Aubry *et al.*, 1999), a next obvious step is to establish the cytotoxic effect CNT exposure will have.

7.2.2.3 Cytotoxicity

The potential for this particle panel to cause cell death clearly coincides with its ability to stimulate mechanisms of cell signalling and an inflammatory response. There is pronounced cell death in response to MWCNT, which may in fact be length dependent, which is not categorically seen with the exposure of the other reference particles. At later time points it is only MWCNT that cause any significant cell death, and is more pronounced in response to the long MWCNT and industrial MWCNT sample.

This cytotoxicity in response to long MWCNT has also been shown in the exposure of relatively low concentrations of SWCNT to other phagocytic cell lines, such as THP-1 cells (Kalbacova *et al.*, 2006), and the exposure of the J774A.1 cells to MWCNT of up to 30µm has considerable cytotoxicity at potentially low concentration of 22µg/ml (Hirano *et al.*, 2008). Hirano *et al.* (2008) found no evidence of associated oxidative stress, and there were no indicators of the activation of apoptotic pathways. This may imply that the damage caused and ensuing cell death was due to direct membrane injury by

this fibrous material; when observing the SEM images of MWCNT exposure in this study it seems that this is very likely also happening here. This is further highlighted when much shorter CNT, less than 1µm in length, are engulfed by macrophages, causing an acute but controlled inflammatory response, with no *in vivo* or *in vitro* cytotoxicity (Sato *et al.*, 2005), as was shown with the NPCB and short asbestos fibres used here. In a study exposing human monocyte-derived macrophages (HMM) to MWCNT similar in length and iron content as CNTC and CNTD, with an increase in necrotic cell death irrespective of iron content (Cheng *et al.*, 2009). This, again, may infer that the method of cell death presented in this thesis in response to MWCNT was indeed necrosis, and also confirm the impact that CNT length has and how ineffectual iron content is when a high aspect ratio is present. The presence or absence of metal contaminants has in fact been repeatedly shown to have little impact on cell viability in respect to CNT exposure (Cheng *et al.*, 2009, Karlsson *et al.*, 2008, Kim *et al.*, 2010b, Pulskamp *et al.*, 2007b), while an increase in aspect ratio does increase cytotoxicity (Kim *et al.*, 2010b). This is further underlined as the exposure of epithelial cells to short MWCNT at equivalent conditions does not cause substantial cell death (Srivastava *et al.*, 2010).

7.2.2.4 Frustrated phagocytosis

The preceding evaluation of the data collected during this doctoral research study has clearly implicated MWCNT length as the main causative factor in CNT toxicity, and the mechanism by which these effects occur is proposed to be through frustrated phagocytosis. The SEM observations of long MWCNT and their effect on phagocytic burst and macrophage phagocytic ability impairment post CNT exposure, all confirm frustrated phagocytosis is indeed occurring here, and this is perceivably responsible for the other observed responses. The inability of J774.A1 cells to phagocytose *Escherichia coli* K-12 Bioparticles after exposure to CNTC and CNTD not only confirms the frustrated and hampered phagocytosis but also reveals the potential for long CNT to impede a normally effective immune or phagocytic activity. The other (short) MWCNT visually appear to cause some level of frustrated phagocytosis; this is likely due to an increase in agglomerate size and strength, and not tube length. The reduced response at later time points to these shorter samples in the biochemical assay

signifies that cells were at least partially controlling these bundles. Incidentally, any visual difference in aggregation between the short MWCNT samples is likely due to their differences in water interaction, with CNTB having a higher hydrophobicity than its size-relative counterpart CNTA. The dissimilarity between visual uptake and biochemical measurement of phagocytic problems may be cleared up by proceeding with longer exposure times to fully elucidate if the shorter CNT forming bundled aggregates would be adequately constrained, as they had been shown to in the study presented in chapter 4 involving particle panel A (Rothen-Rutishauser *et al.*, 2010).

7.2.3 CNT toxicity in relation to reference materials

The purpose of the inclusion of the reference materials NPCB and asbestos was to ascertain if MWCNT are potentially more hazardous than known toxic materials. The data presented in figure 7.1 are a small representation of the patterns observed throughout this study, and clearly show that under the conditions of this study MWCNT are more reactive in all aspects than NPCB and asbestos, and therefore are potentially more hazardous. There was a particularly low response to exposures of NPCB, and little in response to either asbestos sample. A slight elevation in pro-inflammatory cytokines and the induction of a phagocytic burst in response to asbestos, and observation by SEM of all the reference materials, does demonstrate that cells are actively taking up these materials up. However, the acute controlled cytokine release and the lack of cytotoxicity show that the cells were adept at controlling and managing these materials, and were relatively unperturbed under the conditions used here. Studies using very similar materials to those used here have also shown enhanced inflammatory responses to high aspect ratio MWCNT compared to NPCB and to LFA (Brown *et al.*, 2007b, Murphy *et al.*, 2011, Poland *et al.*, 2008), therefore the results presented here are well founded, and relatively comparable to *in vivo* occurrences. At times the concentration of asbestos used to generate a clear response has been much greater (Palekar *et al.*, 1979) than that used here or that is generally used today in nanotube studies.

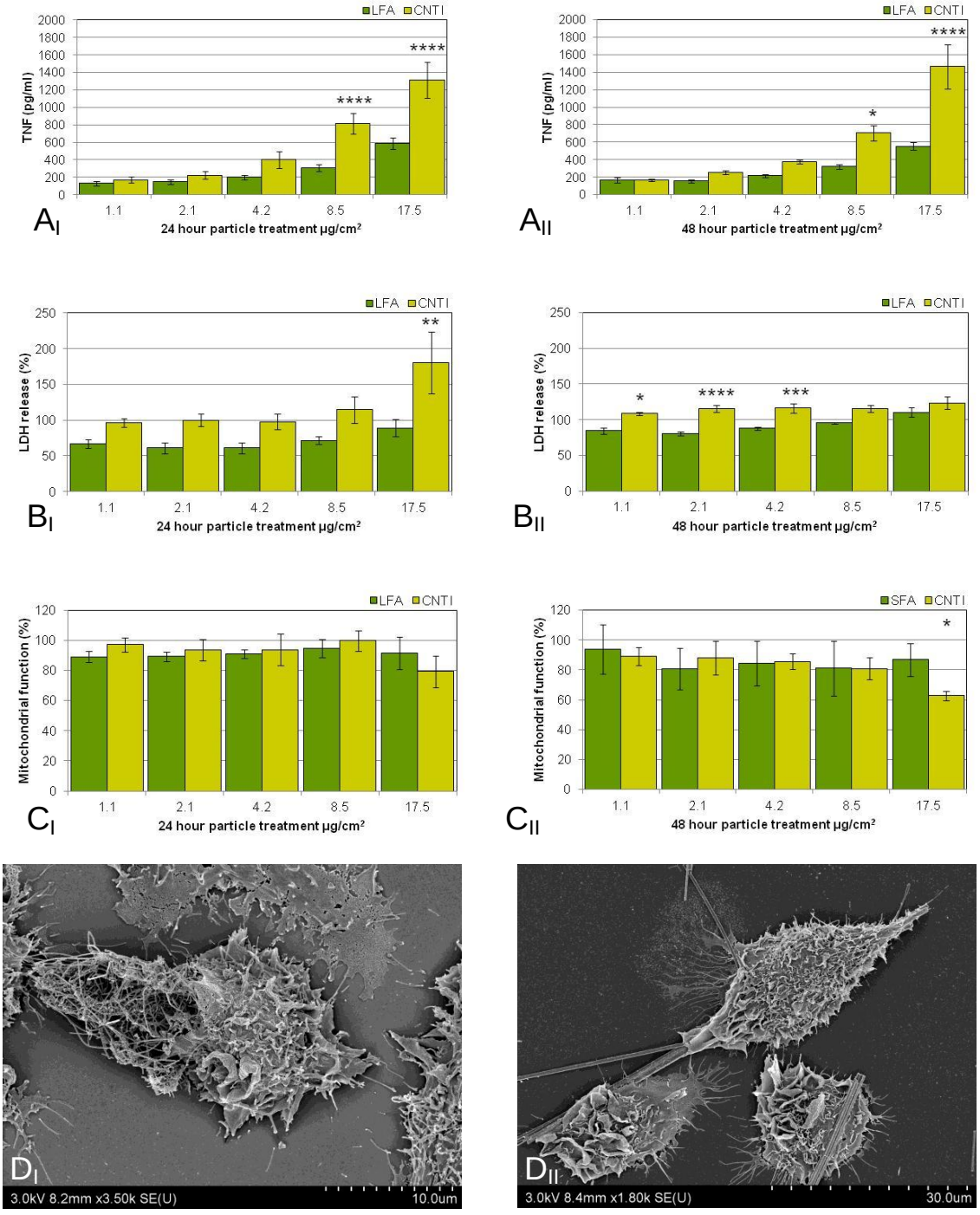

Figure 7.1 Comparison of MWCNT to LFA, assessed by (A) induction of pro-inflammatory conditions, (B) membrane impairment (C) mitochondrial function, and (D) frustrated phagocytosis of murine macrophages upon exposure of MWCNT (D_I) and LFA (D_{II}).

The increase in toxic potential of CNT compared to asbestos shown here is not an isolated occurrence, but is also not always agreed upon. Although asbestos is known for its toxic potential, amosite asbestos has at times been shown to have no cytotoxicity during short exposure periods of up to 100µg/cm^2 (Kinnula *et al.*, 1994). Crocidolite has been shown to be considerably less cytotoxic than

short MWCNT with a 5550% increase in crocidolite dose needed to reach the same IC_{50} value as MWCNT (Hirano *et al.*, 2010), and MWCNT aggregates are shown to have greater or at least equivalent cytotoxicity to crocidolite and chrysotile (Tabet *et al.*, 2009); and in respect to the other reference material used here, NPCB has also previously been shown to have no effect even when internalised (Tabet *et al.*, 2009). MWCNT, including one identical to CNTC used here, consistently cause a greater inflammatory response than LFA and NPCB (Brown *et al.*, 2010). The uptake of crocidolite by rat macrophage cells has at times shown no production of ROS when the same cells are induced into forming ROS with exposure to zymosan, although there is an increased expression of iNOS, with an increase in associated inflammatory markers (Guichard *et al.*, 2010).

In some publications the cellular response to various reference materials, and a comparison to CNT, are not quite as clear as presented in this study. NPCB and chrysotile asbestos can at times cause the same relative cell death as MWCNT at low concentrations in a number of cell lines (Soto *et al.*, 2008). However, this study does not really concern CNT length: the individual CNT are very short and aggregates are also potentially too small to hamper effective phagocytosis. Other studies implicate the involvement of metal contaminants, amorphous carbons (Pulskamp *et al.*, 2007a) and diameter (Cheng *et al.*, 2009, Porter *et al.*, 2007b) in CNT toxicity. NPCB are also shown to cause considerable cell death in alveolar macrophages (Pulskamp *et al.*, 2007a). The same level of cytotoxicity can be found with treatments of NPCB, chrysotile asbestos and aggregated MWCNT (Soto *et al.*, 2008). Asbestos can cause cell death and the induction of apoptosis at concentrations and time points similar to those used in this study (Cardinali *et al.*, 2006, Jimenez *et al.*, 1997), and can equal (Thurnherr *et al.*, 2010) or surpass (Asakura *et al.*, 2010) the cytotoxicity of MWCNT at relatively low doses, as can low doses of low aspect ratio carbon nanofibres and carbon NP (Magrez *et al.*, 2006). Using various phagocytic cells, graphite is shown to have a greater cytotoxicity than SWCNT (length unknown) (Fiorito *et al.*, 2006), and crocidolite and chrysotile can reduce cell viability at low doses and equivalent exposure times (Cardile *et al.*, 2004).

The same disparities can be found in *in vivo* experiments, where it has been shown that for a panel consisting of CNT, asbestos and NPCB, it is the CNT that again induce the greatest response. In this case the CNT were short SWCNT (dispersion/aggregation state unknown) which produced greater collagen and cytokine secretion, seconded by crocidolite asbestos, and then NPCB (Teeguarden *et al.*); however Teeguarden *et al.* (2011), as was done in this study, used equivalent mass as their method of dosing, this, as mentioned before may not always be the most appropriate method of dosimetry. Teeguarden *et al.* (2011) even mention the difference in surface area of their samples, where the SWCNT are 125 times greater than the asbestos sample while others have shown that the effect of chrysotile asbestos in terms of inflammation, cytotoxicity and fibrogenesis is equivalent to that of MWCNT (<6µm in length), and that NPCB induced a lower response than either MWCNT or chrysotile (Muller *et al.*, 2005).

7.2.4 Conclusions on carbon nanotube toxicology

With much of the literature in agreement with the results of this study it may be simple to say that the only factor responsible for CNT toxicity is length, when CNT or CNT aggregates of a length that would cause some degree of frustrated phagocytosis are the most hazardous, and that CNT are more hazardous than other well-known toxic agents such as NPCB and asbestos. This, however, is not a statement that can be wholeheartedly made as a proportion of the existing literature has found a slightly different result: for example, shorter SWCNT can induce greater cell death than longer MWCNT (Jia *et al.*, 2005). These materials, however, are in fact structurally and compositionally very different, therefore this comparison may not be wholly relied upon to compare length alone. The study presented in this thesis has made a great effort to control the individual aspects that may influence toxicity.

In the case of the laboratory-produced MWCNT used here it is evident that a clear characteristic responsible for toxic behaviour is length-induced frustrated phagocytosis, with additional effects prompted by agglomeration through difficulties in dispersion. The leaching of metal ions from MWCNT samples has been confirmed, but is not associated with any additional toxicology, neither are alterations to carbon structure and sample purity. No studies were undertaken

to observe the effects of metal ions alone on these cells but published work has shown that where toxic behaviour, such as reduced viability and increased DNA damage is observed in response to MWCNT, the same does not occur in parallel experiments using relative concentrations of soluble metal ions (Karlsson *et al.*, 2008).

The industrially produced CNT sample often exerts a response similar to that of the long MWCNT samples, but it is unclear to what the cause is. CNTI contains relatively high levels of bioavailable iron, but no more than CNTA (particularly in acidic environments), its length is in relation to those shorter MWCNT, with only a small percentage over 20µm. One clear difference, and possible responsible factor, is the relative sample purity: it has a very high crystalline structure. This may in fact infer a certain durability, as CNT with increased functional groups are far more likely to be broken down in response to pH, or enzyme degradation (Schönfelder *et al.*, 2012); or may infer that the increased hydrophobicity is allowing for far more stable aggregation of CNTI, and less dispersion. A study using controlled treatments to isolate CNT catalyst and carbonaceous content, and to influence aggregation has shown that the impact of metal catalyst is indeed minimal in respect to proliferation and cell activity, and that an increase in dispersion lowers any toxic effects (Wick *et al.*, 2007). However, perceptions of dispersal effect are far from in agreement. Grinding of short (6µm) to shorter (0.7µm) MWCNT can result in a better dispersion and better deposition upon intratracheal instillation, which was accompanied by a greater level of cell death and far greater inflammatory response; however, the level of fibrogenesis appears to be equal (Muller *et al.*, 2005); these effects may be in response to the increased structural surface modifications that are known to be introduced with CNT grinding (Fenoglio *et al.*, 2008). While a study by Rotoli *et al.* (2009), using both MWCNT and SWCNT of equivalent lengths as Muller *et al.* (2005) of 5-9µm and 0.5-2µm, found that the longer fibres, both MWCNT and SWCNT, will disrupt the tight junctions formed during culture of primary epithelial cells, while neither of the shorter will (Rotoli *et al.*, 2009).

A lack of dispersion may also lie parallel with the dosimetry of this study. Using the SEM observations it is apparent that cells attempting phagocytosis of CNT are attempting to phagocytose much larger numbers than they are for LFA, for example. This is resulting in a clear struggle, as each cell is attempting to clear

a greater number of CNT than they are asbestos fibres. This, plus the high aspect ratio or increased size of aggregates, is causing most of the observed responses found in this study. Therefore if the particles were better dispersed the same effect is likely in respect to the long CNT, while the short are likely to be adequately controlled. If the exposure had been done using particle number per cell instead of mass per square cm the results may be very different, and the LFA would likely cause far more effects than were seen here. There is of course also a question concerning the respirability of MWCNT agglomerates, but since such agglomerates can be of relatively small overall size, and of a low density, their aerodynamic diameter is likely to be sufficiently low and allow inhalation. Moreover, as the aerodynamic diameter is largely unaffected by length and is generally determined by diameter, CNT which are particularly small diameter would be easily respired (Donaldson *et al.*, 2006).

If an overview of the data collected during this research is taken it is clear that, according to the exposure conditions used in this study, MWCNT have a high, detrimental impact on phagocytic cell lines. The use of known toxic reference materials has shown that MWCNT may have a greater impact than materials such as asbestos. There was a clear lack of response to even the long fibre amosite sample, which was indeed included to provide a positive control in respect to high aspect ratio-based conclusions. The lack of response to this positive control, however, is not a shortcoming of the experimental work presented here, but instead highlights the sensitivity of cell systems to relatively low doses of MWCNT when exposed at equal mass doses.

So in terms of this study and those that have made considerable effort to highlight numerous factors, it does appear that when CNT have a high aspect ratio it is this factor alone that is capable of causing extensive stress and potential hazardous environments.

The potential pathological hazard posed by CNT has been demonstrated in this thesis and throughout much of the current literature, however although many responses are found to be determined by specific CNT characteristics such as morphology and composition, these detrimental responses are not always defined by the same characteristics, and in some cases contradictions have been shown in respect to CNT characteristics display the greatest toxicity.

Therefore there are many unanswered questions, and many issues that need elucidating, and certainly more research is needed on the potential pathogenicity of MWCNT. As the use of CNT is increasing globally, and more and more products are becoming available, it may be practical to tailor future toxicity studies to these new products, therefore providing an assessment of existing products and the breakdown of these products. However, for the assessment of specific characteristics, it is proposed here that the four CNT samples that were generated in a controlled fashion would be very suitable for future use in MWCNT toxicological studies; they provide a clear way to evaluate important toxic components such as fibre length, transition metal contamination, and crystal structure. However, to allow a fully transferable evaluation of data obtained using these CNT it is recommended that steps are taken to allow greater dispersion of samples, allowing a clearer determination of length dependent effects that are not influenced by particle agglomeration. Secondly, it is recommended that the respirability of these CNT samples is also addressed.

There is no clear guidance regarding the handling of CNT, and with much of the literature concerning CNT toxicity being inconclusive, and as, due to the youth of this material, there are no true chronic exposure studies, or epidemiological assessments, it is difficult to assign a clear path that should be taken by individuals or industries upon cases of CNT exposure. Therefore, in figure 7.2 a suggestion of the type of questions that may arise, and the potential decisions that should be made, is provided. This diagram is based on the findings of this research, but also a selection of papers that have highlighted potentially hazardous CNT characteristics (Brown *et al.*, 2007b, Kagan *et al.*, 2006, Migliore *et al.*, 2010, Muller *et al.*, 2008b, Murphy *et al.*, 2011, Poland *et al.*, 2008, Pulskamp *et al.*, 2007a).

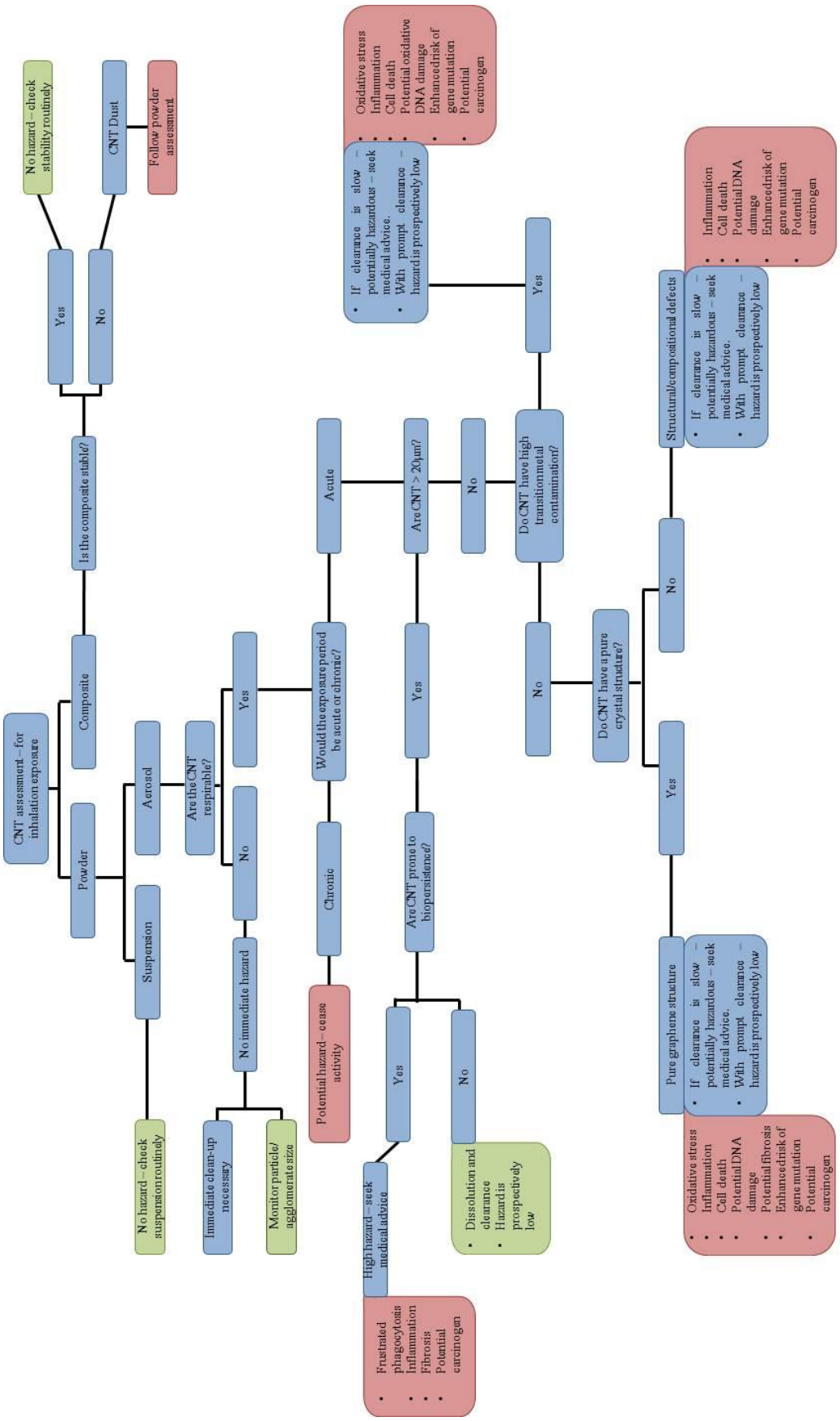

Figure 7.2 A proposed decision tree for the assessment of CNT exposure scenarios. Based on this study, and the current literature, this is a proposed hazard assessment to CNT exposure.

7.3 Assay suitability and comparability of cell types and endpoints

There was a disparity between some cell type responses, and an apparent particle interference issue dependent on assay endpoint. For example, two cell lines with similar functions were used to measure cell signalling; both were stimulated into pro-inflammatory conditions, but increases were found in different cytokines. One in particular, TNFα, is often key in this form of investigation and was found to be lacking in response by MM6 (which may cause an underestimation of inflammatory response), but substantially present in the response from J774.A1; indicating that the J774.A1 cell line may be a better model for this design of study. However, the use of immortalised cell lines in the assays measuring respiratory burst appeared not to have the sensitivity needed to provide any discernible differences, while the use of primary rat BAL cells were incredibly responsive in all assays. Particle interference was found to occur in two assays, in both cases resulting in false negative results for the CNT samples, which may have been perceived as a lack of toxicity if such interference had not been recognised. These, and similar, aspects are discussed in the subsequent section.

7.3.1 Unsuitable assay selection

During this study it has been highlighted on a number of occasions that not all assays are suitable for all particles and all cell types in toxicological studies. The exploration into cell death using flow cytometry and cellular component staining with annexin-V and propidium iodide is the first item that under scrutiny was found to be unsuitable. The assay itself is extremely useful, and is widely used in many research areas as it allows the user to discern between three cell populations: healthy, necrotic, and early and late apoptotic (Aubry *et al.*, 1999, Moreau *et al.*, 2007, Prasad *et al.*, 1998, Riccardi and Nicoletti, 2006), and has even been used for the analysis of CNT, albeit a sample of a comparatively small size (Markovic *et al.*, 2011). The issues found here are not related to the functioning of the assay; problems were related to either mechanical impedance of the sample injection port (SIP), or by formation of large cell clusters around particle exposures. Mechanical impedance would occur with all high aspect ratio CNT and asbestos samples and these fibres would consistently cause what was believed to be a mesh-like structure blocking flow into the FACS

apparatus. For FACS analysis it is crucial for cells to be monodispersed, therefore the formation of larger cell structures would not be addressed during FACS analysis. It is these points that are addressed in chapter five, relating the reasons for assay unsuitability for CNT analysis to the formation of giant cell bodies and apparatus obstruction.

The use of the luminescence assay for respiratory burst assessment in chapter six, with real-time measurement during the exposure period, was also found to be unsuitable, due, in this case, to the attempted analysis of particularly dense dark material. It is not the actual use of a luminescent signal per se, but the structure of the experimental procedure that is found to produce complications. This assay relies on the measure of ROS formation during exposure due to the short-lived luminescent signal; therefore it is necessary for particles to remain in the experimental wells resulting in the absorption or blocking of light signal. This was avoided by using an assay of cytochrome C reduction. The change in light absorption with a change in the oxidative state of cytochrome C is relatively stable; this allows the removal of particles prior to measurements, circumventing any interference.

Two issues relating to the sensitivity of assays were uncovered, both in relation to ROS production. During the chemiluminescence assessment of phagocytic burst, and related to cell source selection. With the use of cell lines described in chapter six, in this case MM6 (figure 6.7) and J774A.1 (figure 6.8), the ROS produced during phagocytosis of all particles was not sufficient enough to generate clear detectable luminescence. Henceforth, the assay was continued with rat BAL cells, which were shown to be perfectly capable of inducing a clear signal. Secondly, it has previously been shown that when considering the independent generation of ROS by NP in a cell free system, it is helpful and sometimes necessary to use a peroxidase to aid detection in DCFH assays. In chapter four it was shown that this addition of HRP did little to allow distinction between particle treatments, but did appear to impede the detection of differences between medium only controls and suspensions of CNT.

It therefore seems reasonable to recommend that appropriate controls are always included to allow for recognition of these types of issues and that results are confirmed using different cells types, where possible and applicable, and

that HRP is not used when using DCFH to assess independent ROS production by CNT.

7.3.2 Comparison of viability assays

In the previous section the inappropriateness of flow cytometry for assessment of these particles was discussed. Comparison of the flow cytometry Annexin V/PI technique with the detection of LDH released from non-viable cells demonstrated different results for the same particles and the same cells. This clarifies the need to use numerous assays, mechanistically different but for the same endpoint. Once it was established that the FACS analysis was unsuitable, further cytotoxicity experiments were employed that involved the measure of membrane impairment (LDH) and of mitochondrial activity (WST-1). In figure 7.3 a representative dataset of the cytotoxicity following exposure of particles to the MM6 cell line, and in figure 7.4 a dataset from J774.A1 exposures are presented. These can be used to assess if these methods of cell death analysis are comparable.

In both cell types there appears to be a good continuity across analysis methods; there is often a clear dose response found, and significant particle induced effects are often matched in each assay type. This allows some form of confidence in the data collected. One observation that was not explored was a slight disparity between these cytotoxicity endpoints at the later time points. It often appeared that there was a far greater reduction in cell viability (WST-1) than there was membrane impairment (LDH release). This may be explained by the stability, or rather instability of LDH. The method of supernatant cold storage used here (-80°C) would not have altered LDH activity, as it has been shown that LDH is relatively stable at these temperatures for months (Shain *et al.*, 1983), and is stable at room temperature for numerous days (Boyanton and Blick, 2002). However, during the long exposure periods of 48 hours, where cultures were kept at 37°C, it is possible that LDH was somewhat denatured and inactivated. Although 37°C is approximately the optimal temperature for LDH catalytic activity (Coquelle *et al.*, 2007), this enzyme has been shown to be unstable when maintained at temperatures of 30°C (Ono *et al.*, 1981) and 35°C (Tanner *et al.*, 2008) for periods of 8 or 24 hours. Taking this into consideration, the level of cell death demonstrated through LDH release may in fact be an underestimation.

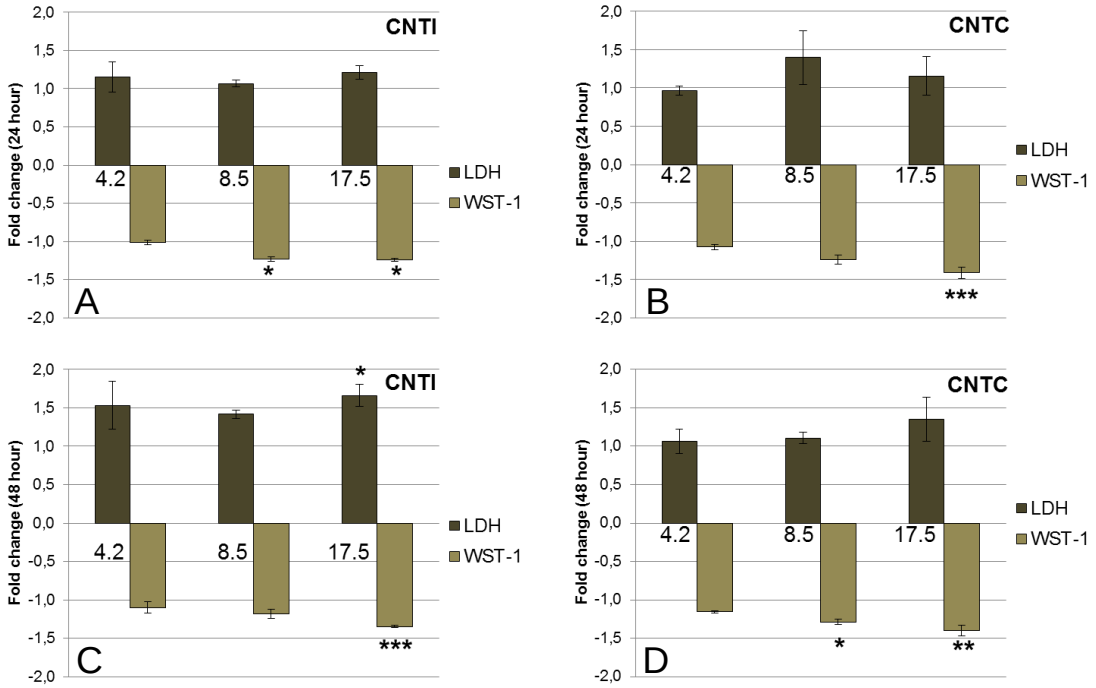

Figure 7.3 Comparison of cytotoxicity assays in MM6 exposure. Data is expressed as a fold increase (LDH release) or fold decrease (mitochondrial function) to assess the continuity in using functionally different cytotoxicity assays, using a selection of particle treatments including 24 hour exposure to (A) CNTI and (B) CNTC, and 48 hour exposure to (C) CNTI and (D) CNTC. Data points represents the mean ± SEM (n=3). Statistical significance is shown by * = p<0.05, ** = p<0.01, and *** = p<0.005; compared to medium-only treatments.

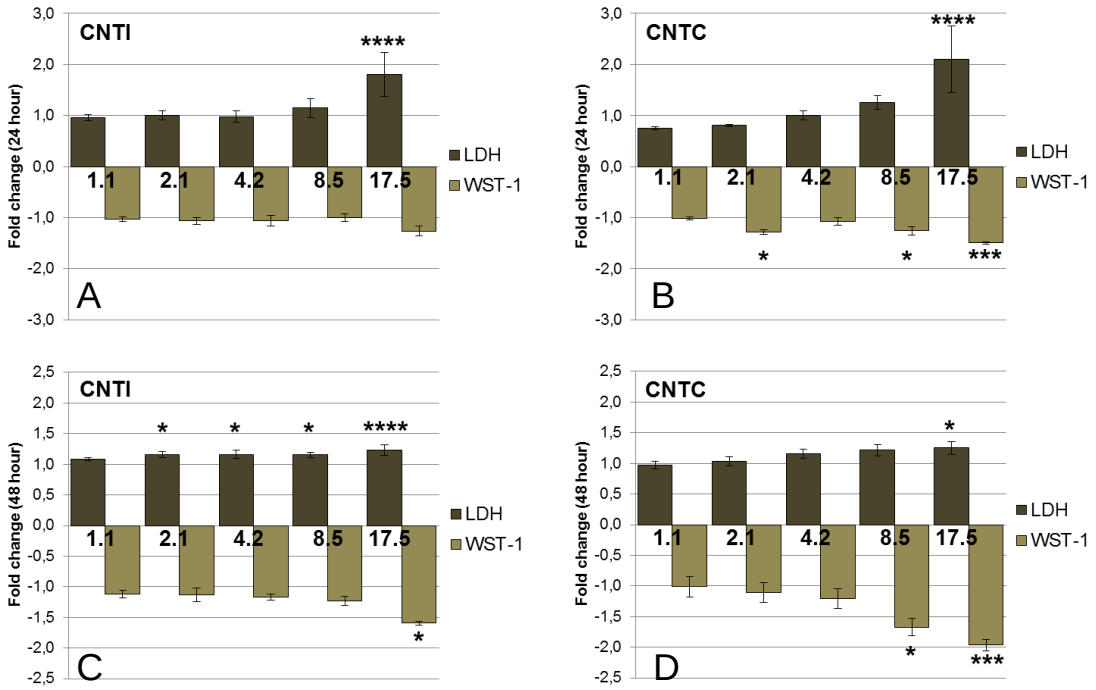

Figure 7.4 Comparison of cytotoxicity assays in J774.A1 exposure. Data is expressed as a fold increase (LDH release) or fold decrease (mitochondrial function) to assess the continuity in using functionally different cytotoxicity assays, using a selection of particle treatments including 24 hour exposure to (A) CNTI and (B) CNTC, and 48 hour exposure to (C) CNTI and (D) CNTC. Data points represents the mean ± SEM (n=3). Statistical significance is shown by * = p<0.05, *** = p<0.005, and **** = p<0.001; compared to medium-only treatments.

7.3.3 Comparison of cell lines

The use of various cells was done at times out of necessity, for example the use of rat BAL cells in the analysis of respiratory burst was due to the cell lines not generating a high enough signal to provide adequate readings. In other instances, such as the assessment of cytotoxicity and inflammatory responses, the use of different cell types was to evaluate if particles would affect different sourced macrophages in a similar fashion. As discussed in the following sections, the MM6 and J774A.1 cell lines used here were found to behave similarly in how they resist or succumb to cell death, but were considerably different in their protein secretions in response to particle treatments.

Variations in cell responses may occur through differences in the interaction with particles by different cell types of the same lineage, different locations therefore potentially playing discretely different roles of cells of the same lineage, or maybe through a difference in their source (as in sourced from different laboratories). The response of the same mesothelial cell line to glass wool and rock wool is found to be considerably different dependent on the research group, with no mortality found in one, to either material (Cardinali *et al.*, 2006), and considerable mortality found in response to glass wool by another (Pelin *et al.*, 1992), both using comparative doses and exposure periods.

Depending on location, macrophages are shown to be phenotypically distinct (Dijkstra *et al.*, 1985, Gjomarkaj *et al.*, 1999). This tissue specificity is known to influence the response of macrophages and the capacity for response (Dörger *et al.*, 2001). Man-made vitreous fibres (MMVF) are shown to illicit a far more pronounced respiratory burst in alveolar macrophages than in peritoneal macrophages, and are shown to fully phagocytose fibres of a greater length (Dörger *et al.*, 2001). Autologous rat pleural, peritoneal and alveolar phagocytes are found to differ in their phagocytic capabilities, their abilities in bacterial eradication and their function as accessory cells (Gjomarkaj *et al.*, 1999), likely due to discrete differences of their role in any given environment or tissue. Additionally, the differences in observed responses from the treatment of different phagocytes that was found during this study may be due to the cells' size. This could be determined by either differentiation state, or by species. For example, the volume and surface area of a differentiated macrophage is known

to be considerably greater than that of a monocyte (Sokol *et al.*, 1987). This phenomenon is an unlikely causal factor here, as it is the J774.A1 macrophages that appear more sensitive than the monocytic MM6 cell line. However, it has been shown that human alveolar macrophages are of a greater size than rat alveolar macrophages, and that this increase in size translated to an accomplished phagocytosis of glass fibres by human alveolar macrophages, while the smaller rat macrophages underwent frustrated phagocytosis and continued elevated toxicity (Zeidler-Erdely *et al.*, 2006). This is a possible explanation of the perceived sensitivity of the J774.A1 cells, and it may in fact simply be due to the more accomplished phagocytosis of the MM6 due to their species determined larger size. However, the phagocytic ability of MM6 cells was not assessed, and therefore this is only conjecture.

A comparison of cell lines and primary cells has shown that at times the inflammatory response to fibres can be similar (Fisher *et al.*, 2000), as can the inflammatory and oxidative response of primary alveolar macrophages from different species to airborne respirable particles (Becker *et al.*, 1996), but these responses can also differ. A pathogenic silicon fibre can consistently induce a high secretion of TNF-α in numerous primary and stable cell types, while exposure of cells to another pathogenic fibre (LFA) results in TNF-α secretion from the THP-1 cell line and primary rat alveolar macrophages, but none from human peripheral blood monocytes or the J774.A1 cell line (Fisher *et al.*, 2000). Inversely, CNT and reference materials similar to those used in this study have not been shown to induce the release of TNF-α, MCP-1 or IL-6 from THP-1 cells, but have been shown to induce the secretion of significant levels of IL-1β and GM-CSF when exposed to structurally and compositionally different CNT (Brown *et al.*, 2010).

7.3.3.1 Assessment of cytotoxicity data

In figures 7.5 and 7.6 a comparison between the two cell lines MM6 and J774.A1 is made in terms of reduction in mitochondrial function (figure 7.5) and membrane impairment (figure 7.6) in response to CNTI and CNTC. Here the statistical analysis was done between cell lines for each respective treatment scenario. It appeared that the J774.A1 cell line was slightly more sensitive to particle exposures than MM6 cells. However, in this comparison there was only

one statistically significant difference found between these cell lines, and it can therefore be assumed that in terms of cytotoxicity these cell lines have responded principally in the same way.

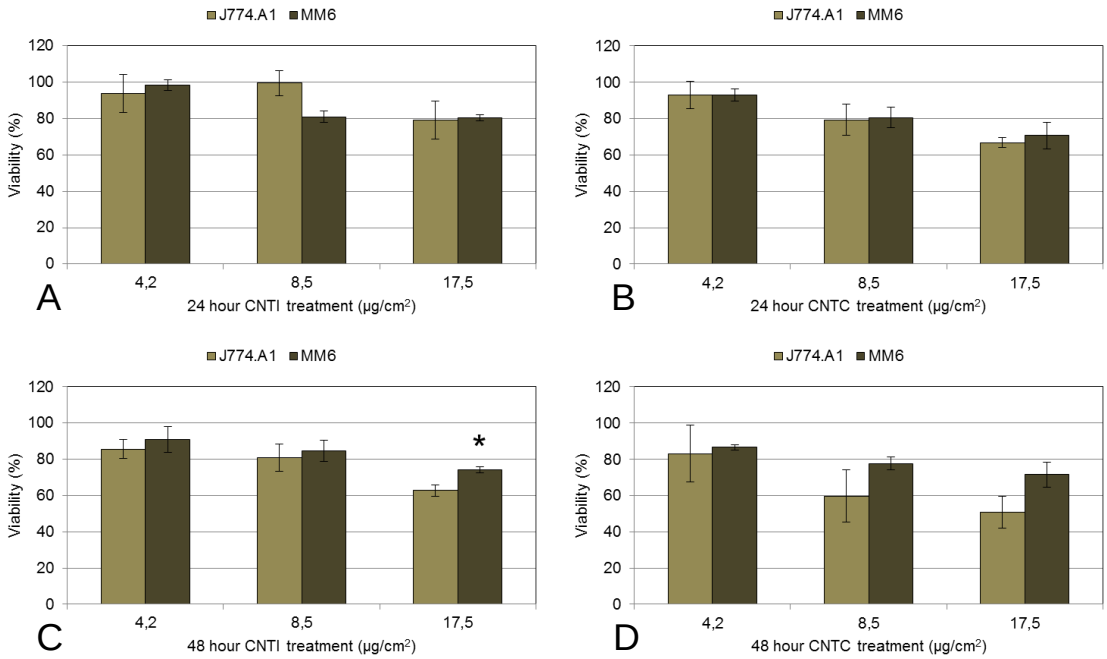

Figure 7.5 Comparison of cell lines – mitochondrial function. Data is expressed as % viability compared to medium only treatments and is used to assess the continuity of functionally similar cell lines (J774.A1 and MM6) used in cytotoxicity assays, using a selection of particle treatments including 24-hour exposure to (A) CNTI and (B) CNTC, and 48-hour exposure to (C) CNTI and (D) CNTC. Data points represents the mean ± SEM (n=3). Statistical significance is shown by * = $p<0.05$; compared to relative cell type.

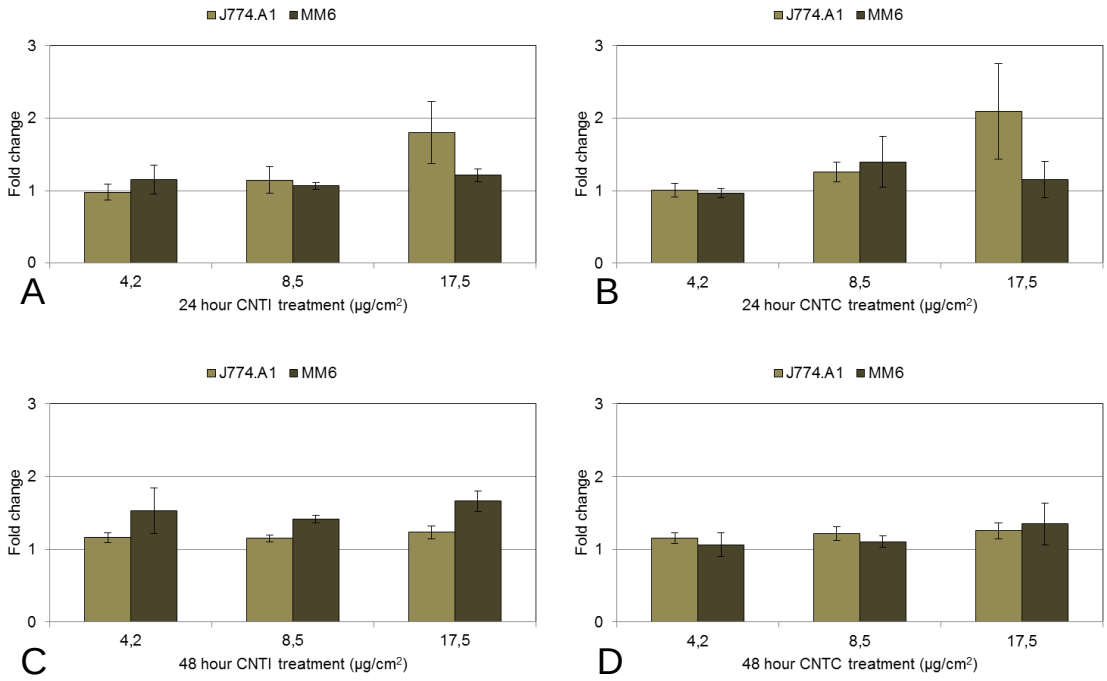

Figure 7.6 Comparison of cell lines – LDH release. Data is expressed as fold change compared to medium only treatments, and is used to assess the continuity of functionally similar cell lines (J774.A1 and MM6) used in cytotoxicity assays, using a selection of particle treatments including 24-hour exposure to (A) CNTI and (B) CNTC, and 48-hour exposure to (C) CNTI and (D) CNTC. Data points represents the mean ± SEM (n=3).

7.3.3.2 Assessment of functionality

An overview of MM6 and J774.A1 signalling responses to particle exposures is shown in table 7.1. It is clear that cell line inflammatory responses are very different, and that again J774.A1 cells appear more sensitive. MM6 cells did not secrete significant TNF-α in response to particle exposures, but neither did they secrete IL-1 or GM-CSF, but they did generate significant amounts of MCP-1 in response to some CNT exposures. J774.A1 cells secreted significant TNF-α in response all material except NPCB, and significant levels of MCP-1 to all particle treatments, but were devoid in their release of some other inflammatory markers such as IL-6. There clearly are differences in the inflammatory responses of these two cell lines, but they are, however, both responding in an inflammatory manner. The fact that the use of LPS controls, shown in figures 5.17 (MM6) and 5.24 (J774.A1), has demonstrated that all inflammatory markers can be induced, and therefore these cells are clearly capable of producing all markers of inflammation that were examined, inferring that differences found are in fact mechanistically relevant responses.

NF-κB is responsive to oxidative stress and is responsible for transcription of genes for TNF-α, MIP-2, and IL-8 (Driscoll *et al.*, 1997); here MM6 cells were assessed for markers of oxidative stress and it was shown that only CNTB exposure induced a significant expression of antioxidant defensive genes, which may give an indication to the non-detectable levels of TNF-α release. The presence of high TNF-α release from J774.A1 cells may imply that oxidative stress had occurred. In chapter two it was demonstrated that J774A.1 cells treated with CNT will generate ROS capable of the oxidation of DCFH with as little as 30 minutes exposure; and a notable correlation between GSH depletion in J774A.1 cells and DCFH oxidation by MM6 cells, in response to NPCB, was shown by Wilson *et al.* (2002). These patterns indicate that in some aspects these two cell types can respond similarly. Incidentally, TNF-α is a known apoptotic stimulating agent (Aubry *et al.*, 1999) which may give a reason to the increased sensitivity of J774.A1 cells shown in the cytotoxicity assessment.

The intracellular signalling mechanism involving cytosolic calcium has been shown to be comparable and reproducible in J774A.1 (Clift *et al.*, 2010b), MM6 cells (Brown *et al.*, 2000) and rat alveolar macrophages (Brown *et al.*, 2004) in response to NPCB; further highlighting the behavioural similarities between these two cell lines, but also their similarity to primary cell responses can put the responses found during this study in context of real exposure scenarios, and therefore potentially a good marker of alveolar macrophage responses.

However, these mechanistic factors were largely not addressed and therefore these statements are only speculative. Mechanisms of cell activation, e.g. transcription factor activation or membrane binding, have not been assessed. If done so this may have given some indication to the reasons for these different cellular responses found during this study.

7.3.4 Conclusions on assay and cell suitability

It is clear that adequate controls need to be incorporated into all assays to ensure that the results interpreted are a true account of what the treatments have induced, this can be in the form of assays that measure interference, or the addition of functionally different assays that measure the same endpoint.

It appears that measurements of cytotoxicity are much more reproducible across cell types than measurements of functionality or inflammatory protein release, and that J774.A1 cells are more sensitive and expressive than MM6 cells, and may be a more suitable model for toxicity assessment, although species determined cell size cannot be eliminated as a causal factor here. Additionally, neither J774.A1 nor MM6 were as responsive as primary cell cultures.

7.4 General conclusions of this study

The potential hazard posed by the MWCNT used in this study far surpassed that of known toxic agents such as NPCB and asbestos. This, in part, may be attributed to CNT, or CNT agglomerate, length induced frustrated phagocytosis. The effort made to control and characterise CNT size and composition in this study results in a relatively high assurance being placed on this observation. Additional iron leaching did not appear to play much of an additional role in the toxic responses found here, and there was only a slight indication that a high purity graphene structure may play some role in toxic potential. This graphene purity may play it's role through encouragement of particle agglomeration when in suspension, from an increased hydrophobicity, and may also enhance sample durability. The detrimental impact in response to MWCNT that has been shown in this study, in relation to the fibres themselves but also when compared to materials such as asbestos, clearly indicates the potential pathological hazard posed by CNT. However, the global advantage that may come from using this material highlights the need to continue to find answers to the unanswered questions, and determine how the CNT pathogenicity can be avoided, to enable the handling and use of this material safe.

Consequently, at this moment in time, it is not possible to put a blanket evaluation on “carbon nanotubes”, but that every parameter needs to be explored, and any conclusions can only be made in relation to specific samples. It is evident that risk associated characteristics should be identified to allow the safe and sustainable production of CNT, and that during the handling of raw CNT material there is the need for precautions to be put in place that would prevent undue exposure.

Chapter 8

Appendices

8.1 Appendix I – Angiogenesis

During the course of this research there were a number of findings highlighting a high release of certain signalling proteins relating to angiogenic potential. These are presented in chapter 5 and led to the initiation of parallel studies into the potential for MWCNT to indirectly induce angiogenesis. This studies was not anticipated and therefore was not in the original proposed aims, but it was thought that an investigation into CNT induced angiogenesis was justified and could highlight interesting and important findings. This area of CNT research is still relatively new but an investigation into this mechanism could give an insight into the proposed pathogenicity of CNT; as at times CNT exposure has been shown to induce markers of disease progression that are potentially inherent of future cancer formation (Shvedova *et al.*, 2005, Shvedova *et al.*, 2007), and more so, CNT have been shown to induce the transformation of lung epithelial cells, with potential to induce tumourigenesis when implanted (Wang *et al.*, 2011).

In chapter 5, it was demonstrated that MWCNT can encourage the release of pro-inflammatory and pro-fibrotic mediators such as TNF-α, VEGF, MCP-1, and TGF-β, during the exposure of macrophages. These factors are also known to be implicit in the promotion of angiogenesis. It was stated that the accumulation of these cytokines, although not an observable example of the carcinogenic potential of MWCNT, could be perceived as a potential to encourage the development of new blood vessel growth, in addition to the maintenance of pro-inflammatory and pro-fibrotic conditions. All of which are factors important in cancer development.

To my knowledge, there is not any literature identifying the indirect effect (through generation of conditioned media, or the co-culture techniques) of CNT on angiogenesis. The direct exposure of CNT to endothelial cells has been shown to induce a disruption in the cell's ability to form tubular structures *in vitro*, this was shown to be through the direct interaction with cytoskeleton actin and the disruption of tight junction formation between cells (Walker *et al.*, 2009). It has also been shown that CNT can disrupt the tube formation of HAEC *in vitro* (Chaudhuri *et al.*, 2009). These results, however, are evaluating direct exposure, here it was proposed that any angiogenesis induced would be

through the extracellular signalling molecules released by other cell types. A review by Sunderkötter et al. (1994) highlights the role and importance of macrophage activity in tumour instigated angiogenesis, and therefore it was justifiable to assess the effects of the MWCNT stimulated conditioned medium, from macrophages, on angiogenesis.

For reasons discussed during this section, it was not possible to make any clear conclusions concerning the potential of CNT to induce angiogenesis, and this body of work remains largely unfinished. For this reason, and as this avenue of research does not follow the original line of research with complete continuity, it was not included in the main results chapters. However, this potential phenomenon certainly is an important component of the proposed CNT pathogenicity, and the results of this pilot study have highlighted some important assay considerations, as well as providing a speculative blood vessel growth in response to CNT, therefore has been included in this appendix chapter.

8.1 Angiogenesis

The action of angiogenesis is essential during numerous embryo developmental processes, and also during the repair of damaged tissue. Angiogenesis is, however, also found to occur during the progression of numerous diseases, including cancer (Sunderkötter *et al.*, 1994). There is a long and complicated procedure involved in successful tumour growth, and a complex signalling response is needed for malignancies to be maintained, part of which involves the development of new blood vessels. Before the blood can flow, a complicated procedure is needed involving cellular migration and proliferation, basement membrane degradation, matrix reconstruction, and the assembly of cells into a lumen (Ma *et al.*, 2007). The complicated process of angiogenesis involves many contributing factors, and a full review of this process is unnecessary for this addition to the appendices. However, for the sake of this section it is important to highlight the impact of certain extracellular signalling molecules that were found to be over expressed in response to treatment of macrophages with MWCNT, particularly MCP-1, TGF-β and VEGF. More information can be found in numerous extensive reviews (Conway *et al.*, 2001, Griffioen and Molema, 2000).

MCP-1 is a chemokine that is found to be prevalent during tumour formation (Salcedo *et al.*, 2000). Additionally to its role in inflammatory responses, where it recruits lymphocytes, MCP-1 plays a critical role in angiogenesis. *In vitro* MCP-1 has been shown to directly cause the migration of endothelial cells, and *in vivo* and *ex vivo*, to induce blood vessel formation during chick embryo development, in matrigel plug assays in mice, and during rat aortic ring assays (Salcedo *et al.*, 2000). MCP-1, VEGF and TGF-β can in fact all encourage the recruitment, migration and proliferation of endothelial cells and smooth muscle cells to sites where angiogenesis is necessary (Ma *et al.*, 2007), and MCP-1 may be essential in the control of TGF-β induced angiogenesis (Ma *et al.*, 2007).

The role of TGF-β is commonly found during embryo development (Ma *et al.*, 2007) and wound healing, and when in excess its activity can promote fibrosis (Branton and Kopp, 1999, Sime *et al.*, 1997). It is also implicated in tumourigenesis, as a growth factor for cell differentiation and proliferation; and, like MCP-1, TGF-β is prevalent in many cancers (Kloen *et al.*, 1997, Marzo *et al.*, 1997). The role of TGF-β in angiogenesis is shown to aid endothelial cell growth and to assist the anchoring of vessels, but also to encourage communication between vessel component cells, such as endothelial cells and smooth muscle cells (Ma *et al.*, 2007). This is potentially achieved through the promotion of secretion of other angiogenic mediators, such as VEGF (Alfranca *et al.*, 2008, Lee *et al.*, 2002, Ma *et al.*, 2007, Park *et al.*, 2002).

VEGF is also found to be prevalent in pleural malignancies, and other tumours. (Cacciotti *et al.*, 2002, Ferrara and Davis-Smyth, 1997, Marzo *et al.*, 1997), and is found to be at high levels during periods of tumour development (Katsabeki-Katsafli *et al.*, 2008). VEGF is thought to be important for this cellular migration and proliferation of both endothelial cells and immune cells such as monocytes and macrophages (Kerber *et al.*, 2008, Ma *et al.*, 2007), and for lumen formation (Ma *et al.*, 2007); in fact, patient survival rate in cases of pleural mesotheliomas is often correlated with the abundance of VEGF and its angiogenic properties (Cacciotti *et al.*, 2002).

8.1.2 Methodology

Conditioned media

To assay the ability of MWCNT to induce angiogenesis a conditioned medium system was used, where the supernatant of particle exposed macrophages were collected, and were to be used as culture medium for both *in vitro* assays using endothelial cells (EA.hy926) and *ex vivo* studies using isolated rat aortic tissue.

MM6 cells were seeded in 75cm^2 cell culture flasks at a density of 1.7x10^5 cells/cm^2. Cells were then treated with 4.2, 8.5 and 17.5µg/cm^2 CNTD for 48 hours, after this period the cell suspensions were centrifuged and the supernatant removed and frozen at -80°C.

In vitro capillary tubular network formation

This *in vitro* investigation was adapted from Montesano *et al.* (1983) The immortalised endothelial cell line EA.hy926 was used in. This cell type represents cells of large vessel endothelium and was created by the hybridisation of HUVEC with lung epithelial carcinoma cells (A549) (Edgell *et al.*, 1983).

A collagen gel matrix (consisting of rat tail collagen type I) or a commercially available basement membrane matrix (BD Bioscience, Matrigel) were used to coat the bottom of 24 well plates prior to cell seeding.

Various combinations were tested using collagen sourced from BD Biosciences, Sigma and SERVA Electrophoresis, with different pH and different component concentrations tested, to aid the polymerisation of the gel. Many of the combinations did not fully polymerise (not shown), some did, and were used to investigate optimal cell growth conditions and angiogenic potential. The combinations that provided adequate polymerisation included:

- 10% 10xPBS, 50% SERVA collagen, 2.4% 1M NaOH, 37.6% RPMI 1640, with FCS
- 10% 10xPBS, 50% SERVA collagen, 4.8% 1M NaOH, 35.2% RPMI 1640, with FCS
- 10% 10xPBS, 50% SERVA collagen, 2.4% 1M NaOH, 37.6% dH_2O
- 10% 10xPBS, 50% SERVA collagen, 1% 4M NaOH, 39% dH_2O

EA.hy926 cells were seeded at $4x10^4$ cells/well on top of the aforementioned collagen gels, left to proliferate for up to 5 days at 37°C, 5% CO_2, and imaged periodically. On day 5 VEGF (50ng/ml) was added to test for morphological changes. Subsequently, when no clear chemotaxis and morphological changes could be induced, various treatment combinations were examined, such as varying cell density, changing the initial exposure time to VEGF, or the inclusion of VEGF in the gel matrix. Ultimately, clear tubular formation was not obtained with the SERVA collagen and so matrigel was used as a matrix, with cells again seeded at a density of $4x10^4$ cells/well.

Ex vivo rat aortic ring assay for angiogenesis

The *ex vivo* investigation of particle induced angiogenesis was based on the protocol described by Masson *et al.* (2002), rat aortic tissue was isolated from 3-month-old Sprague-Dawley (SD) rats. The animals were euthanised using a 2ml single intraperitoneal injection of Euthatal (sodium pentobarbital), and then bled by cardiac puncture to clear vessels of blood, prior to tissue extraction. The aortic tissue was excised at the aortic arc of the thoracic aorta, transferred to cold DMEM, containing 100IU/ml penicillin and 100µg/ml streptomycin, where it was cleaned of fibroadipose tissue and sectioned into 1mm ring segments. At this stage the samples could be kept for up to two hours. During this time gels and media were prepared.

Gels:

- An agarose gel (Type VII, Low Gelling Temperature, Sigma) was prepared by dissolving agarose powder (1.5g) in 100ml dH_2O. After initial cooling, 30ml of gel was transferred to a 10cm petri dish, where it was allowed to polymerise. Rings, with a diameter of approximately 2cm and with an internal, hollow ring of 1cm, were punched and excised, and positioned in a 6cm dish.
- Collagen gels were prepared containing 75% 2mg/ml rat tail collagen type I, 10% minimum essential medium (MEM), 15% 186mM sodium bicarbonate ($NaHCO_3$), and 0.1% 1M NaOH.

Media:

- MCDB131 medium, supplemented with 25mM $NaHCO_3$, 2.5% rat serum, 2mM L-glutamine, 100µg/ml streptomycin and 100IU/ml penicillin.
- MCDB131 medium, supplemented with 25mM $NaHCO_3$, 2.5% rat serum, 2mM L-glutamine, 100µg/ml streptomycin, 100IU/ml penicillin and 20ng/ml VEGF.
- RPMI 1640, supplemented with 25mM $NaHCO_3$, 2.5% rat serum, 2mM L-glutamine, 100µg/ml streptomycin and 100IU/ml penicillin.
- RPMI 1640, supplemented with 25mM $NaHCO_3$, 2.5% rat serum, 2mM L-glutamine, 100µg/ml streptomycin, 100IU/ml penicillin and 20ng/ml VEGF.
- VEGF (50ng/ml) in MM6 cell culture medium.
- Conditioned media (CM) from MM6 cells treated with 17.5µg/cm^2 CNTD, diluted 1:10 in MM6 cell culture medium.
- CM from MM6 cells treated with 4.2, 8.5 and 17.5µg/cm^2, diluted 1:2 in MM6 cell culture medium, or not diluted.

Three agarose gel rings were laid within one 6cm petri dish, and rat aorta slices were embedded in collagen gels, within the agarose rings. Collagen gel (100µl) was pipetted inside the agarose gel ring and allowed to polymerase at 37°C for 30 minutes. After polymerisation one aortic segment was positioned on to each collagen gel, with the lumen parallel to the bottom of the plate, covered with another 200µl of collagen gel, which was also allowed to polymerise. After which, 5.85ml of respective medium was added to the plates, and cultures were incubated at 37°C, 5% CO_2 for designated time periods, and imaged periodically.

At times, the collagen gel would not fully polymerise, and it was thought that this could affect either the passage of growth factors through towards the aortic tissue, or would affect the new tissue growth outwards through the gel. Therefore, different conditions were tested, including different sources of type I collagen (BD and SERVA), alternative matrices, e.g. matrigel, and different concentration of NaOH (for good polymerisation a slightly alkaline conditions were needed, and the collagen is received dissolved in acetic acid). It was ultimately deemed necessary to use the commercial complete matrix called

matrigel. Matrices such as these are purchased in a complete state and therefore need no additional controlling, such as pH adjustments, which may have been the cause of the initial gels not fully polymerising. In this case a growth factor reduced basement membrane matrix (BD Biosciences) was used.

Fluorescent labelling of endothelial cells

After a period of five days aortic ring incubation the stimulation medium was removed and replaced with 10µg/ml (in RPMI) Acetylated Low Density Lipoprotein, labeled with 1,1\'-dioctadecyl–3,3,3\',3\'-tetramethyl-indocarbocyanine perchlorate (DiI-Ac-LDL), and incubated at 37°C, 5% CO_2 for 4 hours. The uptake of acetylated low density lipoproteins (acLDL) is functional phenotype of only endothelial cells and macrophages (Bouïs *et al.*, 2001) and therefore was used here to identify, and potentially quantify, the presence of endothelial cells.

After this period attempts were made to image stained cells using a Zeiss LSM 510 Meta confocal imaging system, with an inverted Zeiss microscope, with excitation/emission wavelengths of 549/565 nm.

For EA.hy926 staining, the cells were cultured on chamber slides and stained with 5-10µg/ml Dil-Ac-LDL for 4 hours, washed three times with PBS, fixed with 3% paraformaldehyde for 20 minutes at room temperature. After fixation cells were washed again with PBS, the chambers removed and slides were mounted on glass coverslips using mowiol. After an overnight incubation the cell cultures were examined, again using a Zeiss LSM 510 Meta confocal imaging system, with an inverted Zeiss microscope, with excitation/emission wavelengths of 549/565 nm.

8.1.3 Results

8.1.3.1 *In vitro*

Growth matrix test

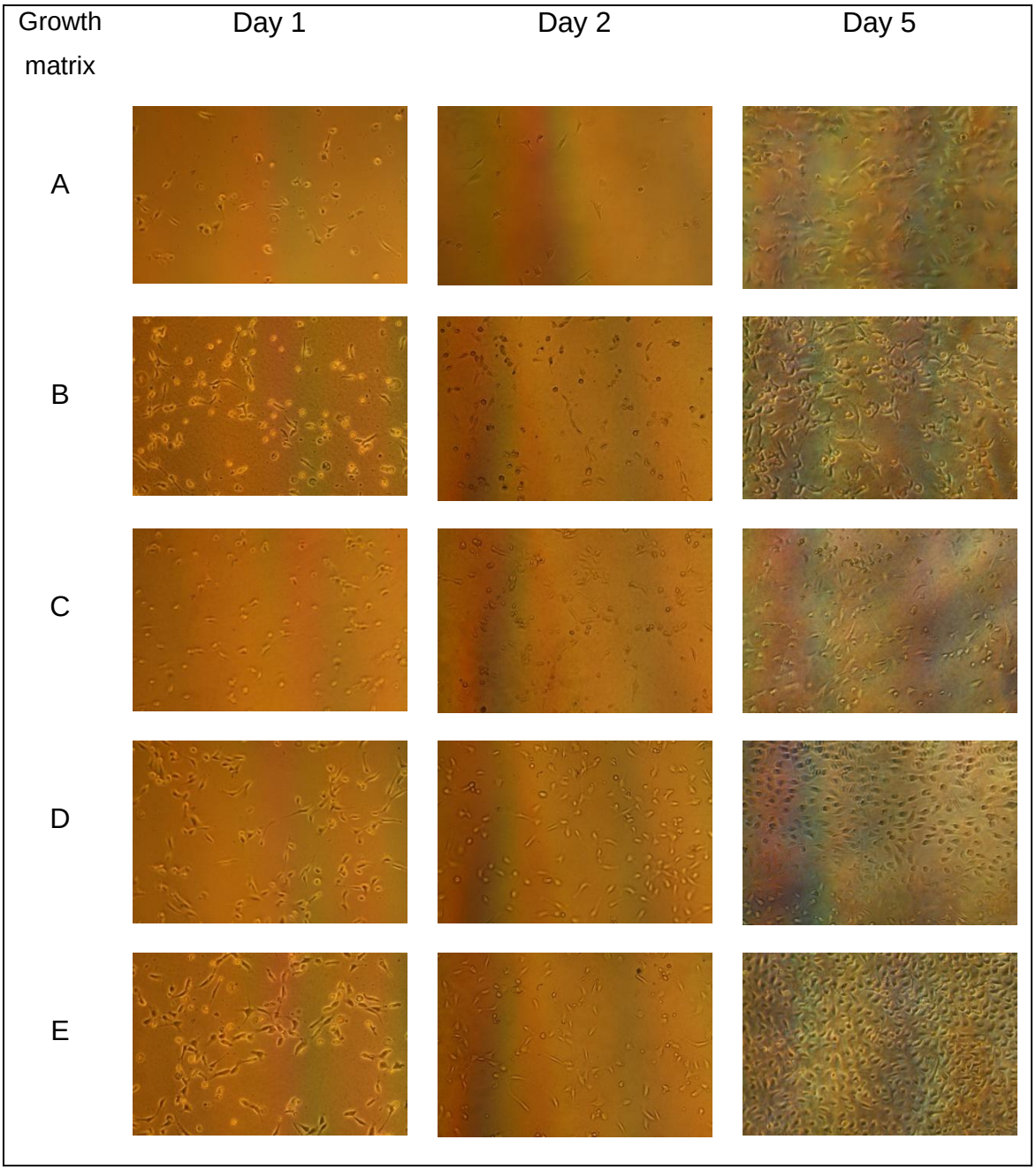

Figure 8.1 Collagen gel for *in vitro* angiogenesis - pilot. EA.hy926 cells grown with different gel matrices: (A) medium only, (B) 10% 10xPBS, 50% SERVA collagen, 2.4% 1M NaOH, 37.6% RPMI 1640, with FCS, (C) 10% 10xPBS, 50% SERVA collagen, 4.8% 1M NaOH, 35.2% RPMI 1640, with FCS, (D) 10% 10xPBS, 50% SERVA collagen, 2.4% 1M NaOH, 37.6% dH2O, and (E) 10% 10xPBS, 50% SERVA collagen, 1% 4M NaOH, 39% dH2O. Cells were incubated for 5days prior to VEGF addition.

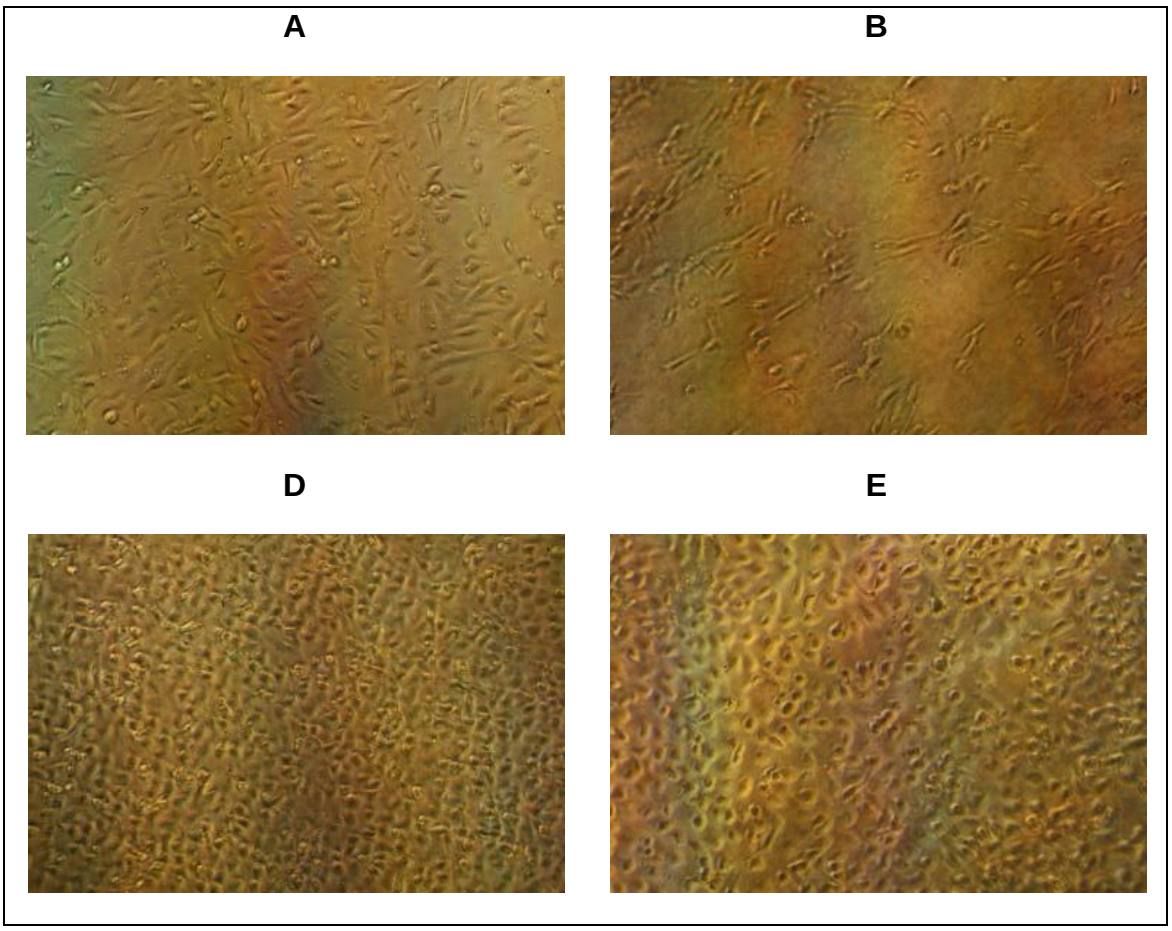

Figure 8.2 VEGF induction of endothelial cell tubular structures - pilot. After 5 days incubation of EA.hy926 cells under conditions shown in figure 8.1 cells were exposed to 50ng/ml VEGF for 24 hours. Growth matrices were the same as for figure 8.1, gel C was not stable and therefore was not photographed.

Over a five day period cells grew adequately well on all surfaces (figure 8.1), including the uncoated cell culture plate (figure 8.1 A). The highest level of proliferation on day five was shown to be in cells incubated on both gel matrices containing dH_2O (figure 8.1 D and E), when compared to those cells grown on matrices containing RPMI (figure 8.1 B and C), or those cultured in cell culture medium alone. During this period no tubular formation was observed.

When VEGF was added to these cultures (figure 8.2), matrix C did not remain stable, and only the cells grown on matrix B (10% 10xPBS, 50% SERVA collagen, 2.4% 1M NaOH, 37.6% RPMI 1640, with FCS) displayed any chemotaxis or morphological changes. Other cells cultures appeared to continue to proliferate. Images in figures 8.1 and 8.2 are of 250µl of gel, 500µl was also used, with similar results (not shown).

Conditioned media test

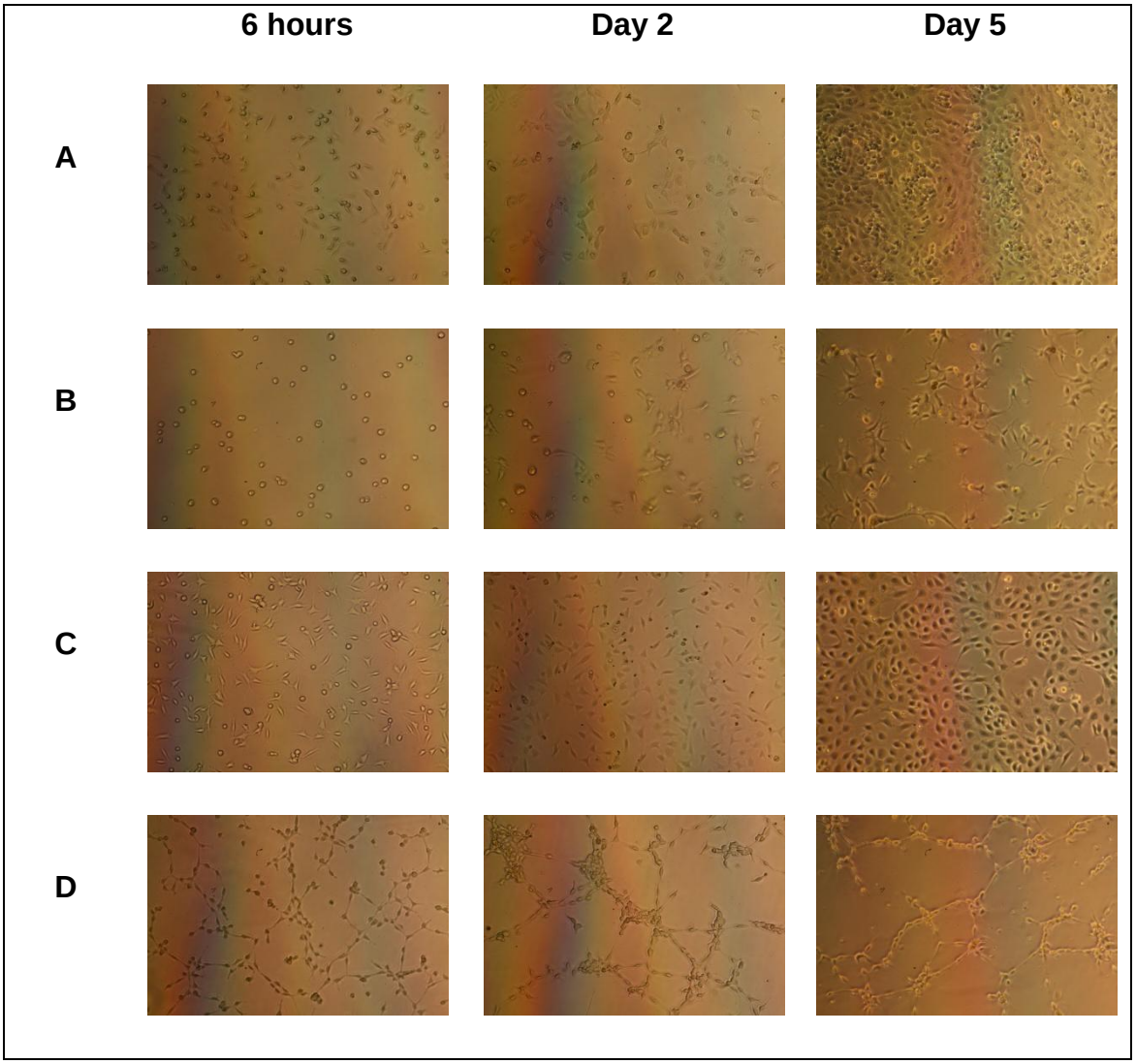

Figure 8.3a Conditioned medium induction of endothelial cell tubular structures - pilot. EA.hy926 cells grown using different stimulation media and on different volumes of growth factor reduced matrigel: (A) CNTD 17.5 µg/cm^2 CM on 50µl matrigel, (B) CNTD 17.5 µg/cm^2 CM on 100µl matrigel, (C) RPMI1640 on 50µl matrigel, and (D) RPMI1640 on 100µl matrigel.

The first pilot study looking into the *in vitro* angiogenesis induced in response to conditioned media obtained by particle exposures of MM6 cells. This study involved a five day incubation of EA.hy926 endothelial cells with either conditioned medium (from the treatment with CNTD 17.5 µg/cm^2), VEGF (50ng/ml), RPMI 1640, or RPMI 1640 supplemented with FCS.

The appearance of cell cultures on Day 1 (not shown) were similar to those at 6 hours. During the further five day exposure period EA.hy926 cells cultured on 50µl matrigel (figures 8.3a A,C and 8.3b E,G) exhibited a proliferation rate that was much faster than those cells cultured on 100µl matrigel (figures 8.3a B,D

and 8.3b F,H), resulting in complete confluence on day 5 when cells were grown on 50µl matrigel.

As for the formation of tubular structures, only the cells incubated with normal RPMI 1640 when cultured on 100µl of matrigel displayed any clear migration and morphological changes, which started to appear as early as 6 hours after seeding (figure 8.3a D). The other treatments (CM, VEGF or RPMI 1640 with FCS) induced only slight changes in cell morphology with evidence of minor elongation (figure 8.3 a/b).

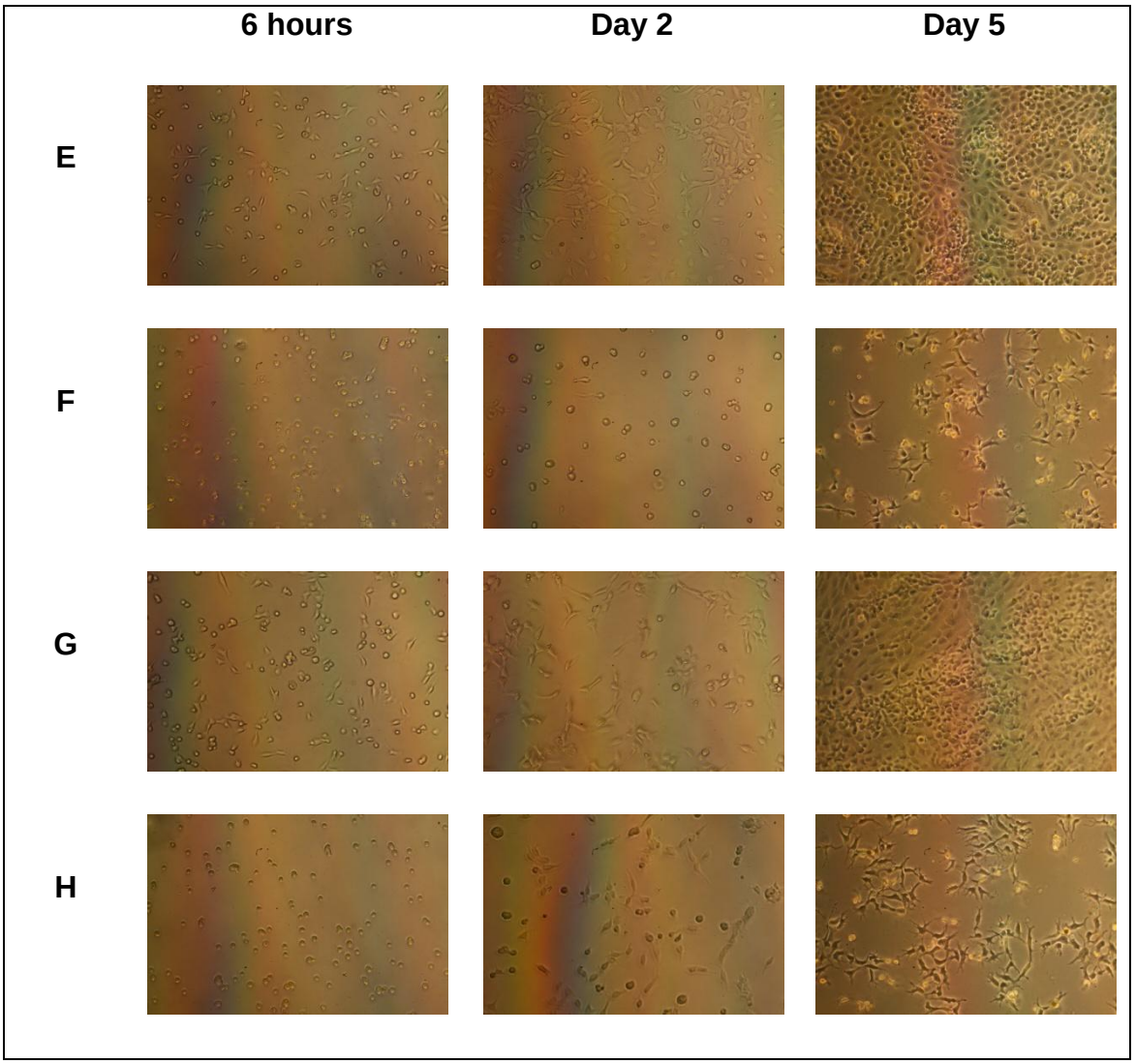

Figure 8.3b Conditioned medium induction of endothelial cell tubular structures - pilot. EA.hy926 cells grown using different stimulation media and on different volumes of growth factor reduced matrigel: (E) RPMI1640 with FCS on 50µl matrigel, (F) RPMI1640 with FCS on 100µl matrigel, (G) RPMI1640 with VEGF on 50µl matrigel, and (H) RPMI1640 with VEGF on 100µl matrigel.

8.1.3.2 *Ex vivo*

Growth matrix test

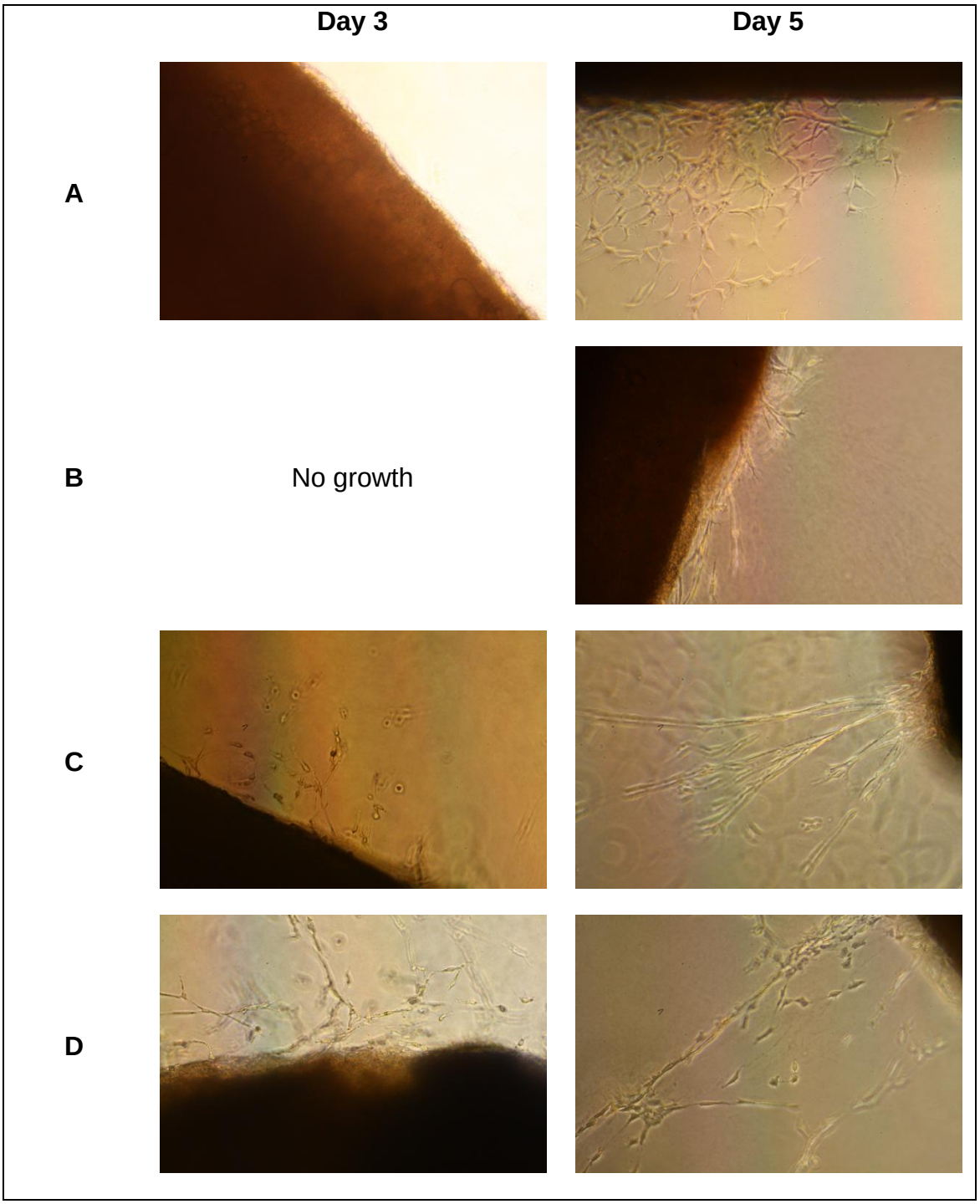

Figure 8.4 Rat aortic tissue cultured in different stimulation media - collagen gel pilot. Rat aortic rings were embedded within collagen type I gels, held within agarose gels and stimulated with different growth media: (A) MCDB131 medium, (B) MCDB131 medium with 50ng/ml VEGF, (C) RPMI1640, and (D) RPMI1640 with 50ng/ml VEGF.

During the assessment of rat aortic tissue embedded in collagen gels (figure 8.4), it was evident that cellular proliferation and growth occurred with all stimulation media, but was faster and more pronounced with RPMI 1640 than MCDB131. The inclusion of VEGF did not appear to stimulate any cell proliferation or morphological changes that were different to those observed for the medium only treatments. Although not observable in these images these gels appeared not to be fully polymerised.

Conditioned media test

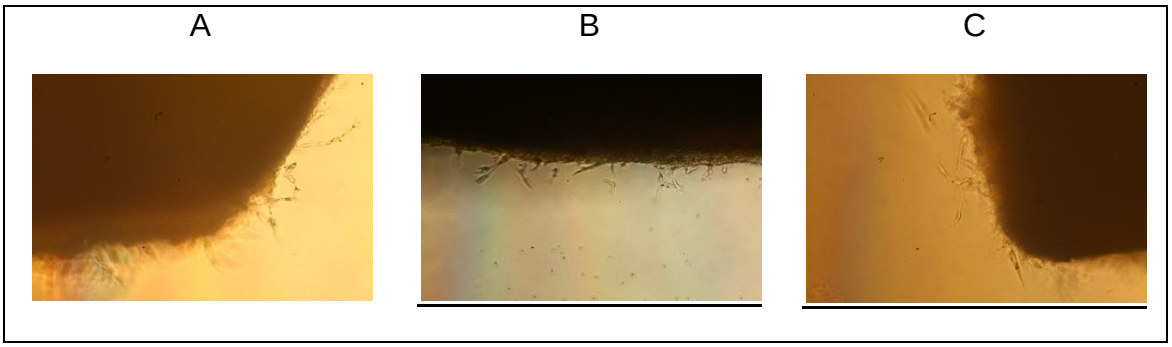

Figure 8.5a Rat aortic tissue cultured in growth factor reduced matrigel with different stimulation media – conditioned media pilot. Rat aortic tissue was embedded within matrigel and incubated with (A) RPMI1640, (B) CM from MM6 exposed to 17.5µg/cm^2 CNTD, and (C) RPMI1640 with 50ng/ml VEGF, for 2 days prior to imaging.

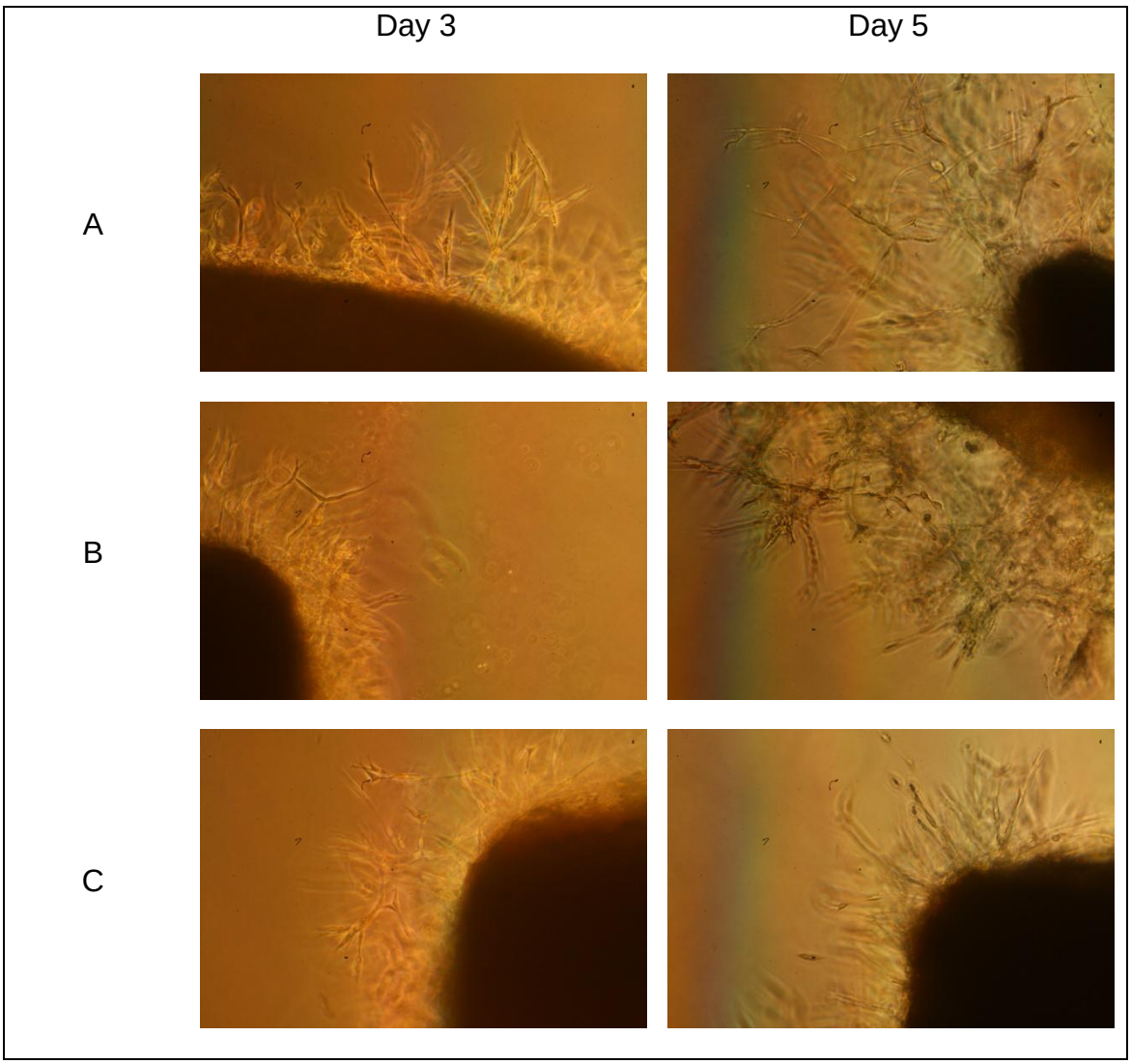

Figure 8.5b Rat aortic tissue cultured in growth factor reduced matrigel with different stimulation media – conditioned media pilot. Rat aortic tissue was embedded within matrigel and incubated with (A) RPMI1640, (B) CM from MM6 exposed to 17.5µg/cm^2 CNTD, and (C) RPMI1640 with 50ng/ml VEGF, for 3-5 days prior to imaging.

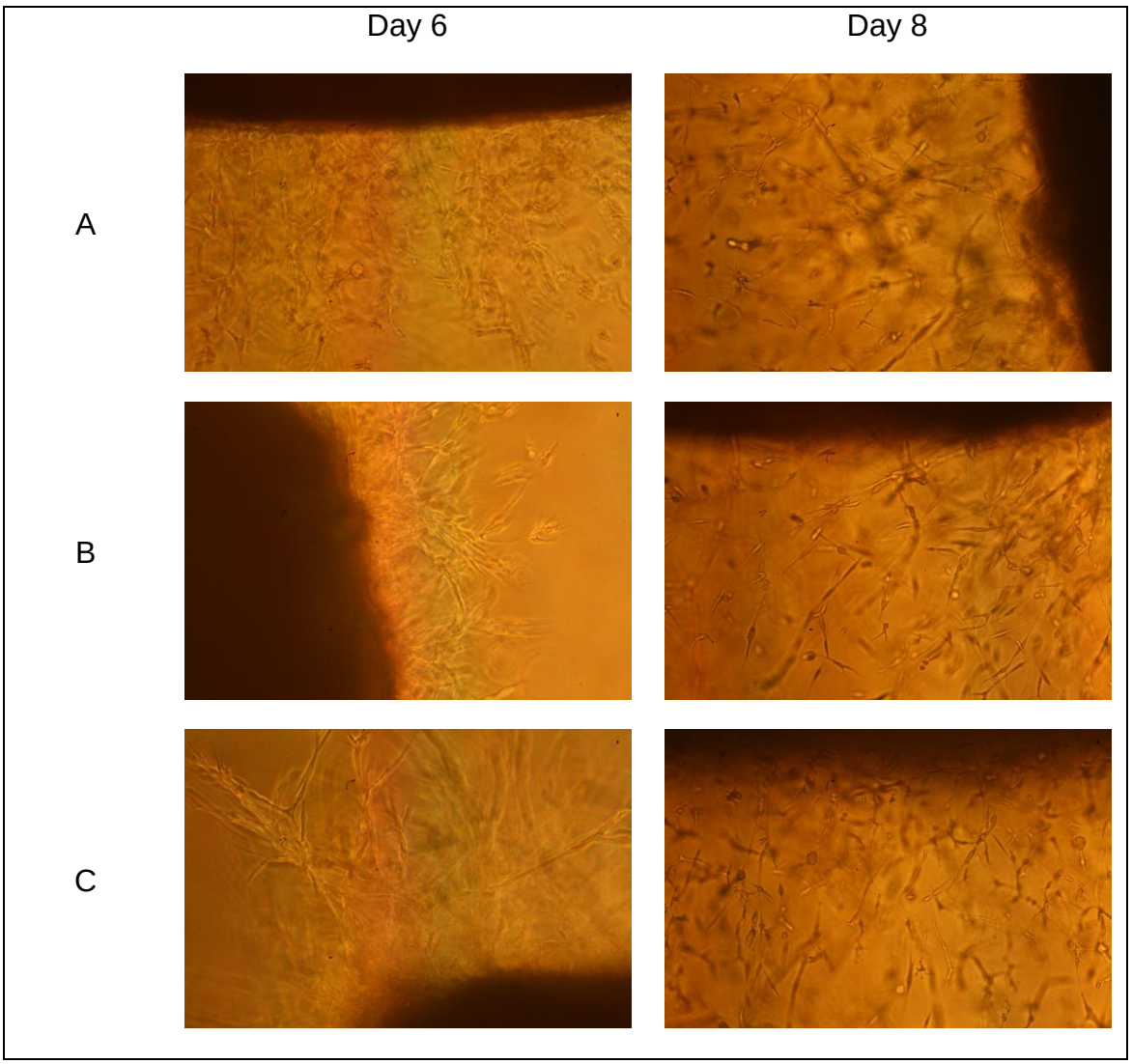

Figure 8.5c Rat aortic tissue cultured in growth factor reduced matrigel with different stimulation media – conditioned media pilot. Rat aortic tissue was embedded within matrigel and incubated with (A) RPMI1640, (B) CM from MM6 exposed to 17.5µg/cm^2 CNTD, and (C) RPMI1640 with 50ng/ml VEGF, for 6-8 days prior to imaging.

When rat aortic tissue was exposed to CM obtained from MM6 cells exposed to 17.5µg/cm^2 CNTD (figure 8.5), the generation of new blood vessel outgrowths was clearly evident during the exposure period of 8 days, as it was with treatments of 50ng/ml VEGF. However, these were observed to be no greater than the outgrowths in response to RPMI 1640 medium alone.

Matrigel test

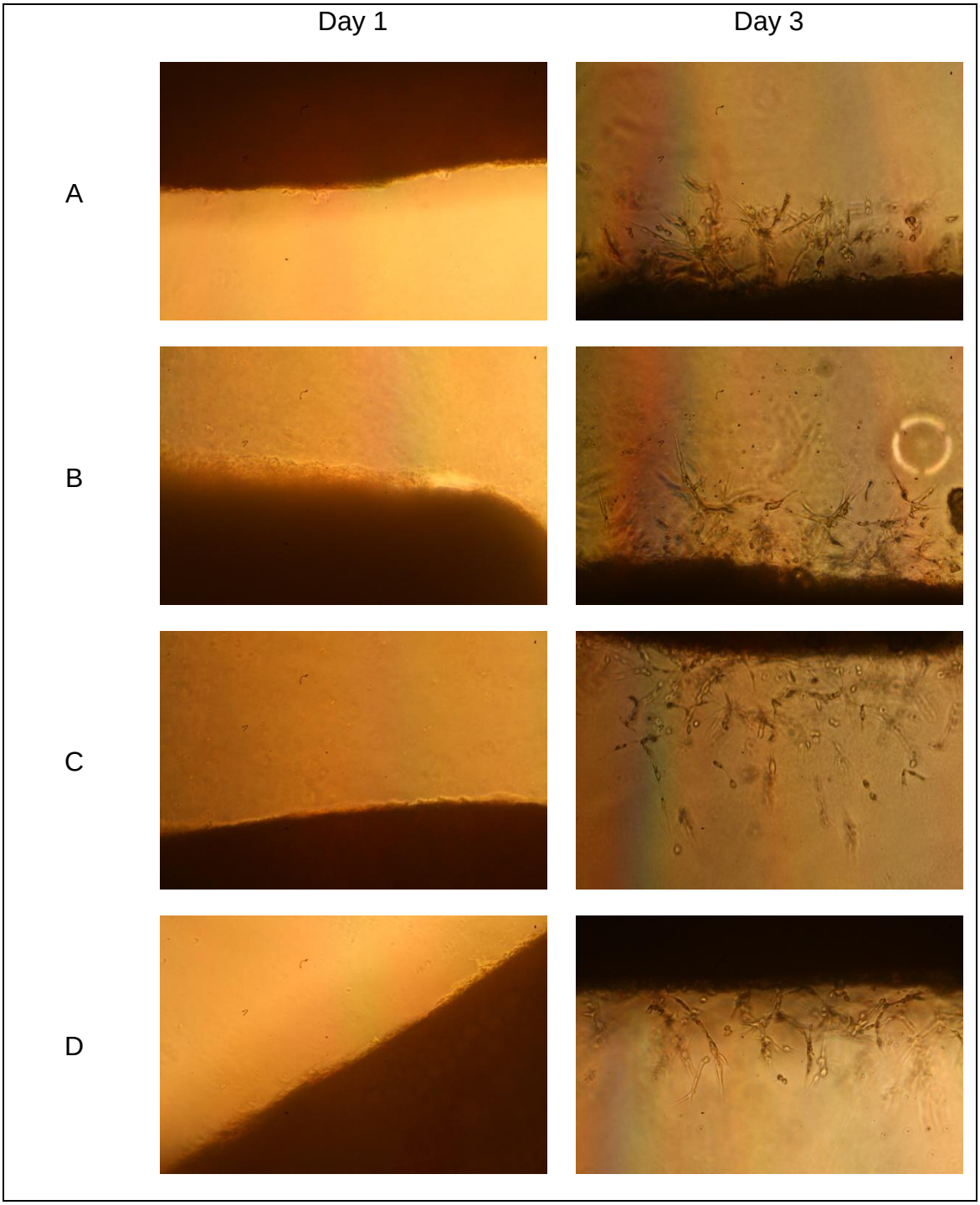

Figure 8.6 Rat aortic tissue cultured in growth factor reduced matrigel with different stimulation media – matrigel dilution. Rat aortic tissue was embedded within matrigel and incubated with (A) RPMI1640, (B) CM from MM6 exposed to 17.5µg/cm2 CNTD, (C) RPMI1640 with 50ng/ml VEGF and matrigel diluted 1:1 with DMEM, and (D) RPMI1640 with 50ng/ml VEGF, for 1-3 days prior to imaging.

When matrigel was used instead of the collagen gels (figure 8.6), again, there appeared to be no discernible differences between tissue exposed to medium only and tissue exposed to medium supplemented with VEGF. This was also

the case when tissue was exposed to conditioned media obtained from MM6 cells exposed to 17.5µg/cm^2 CNTD (figure 8.6 B), which also appeared to generate similar angiogenic potential as medium only treatments (figure 8.6 A).

With the inclusion of conditioned media obtained through the exposure of MM6 cells to slightly lower concentrations of CNTD, 4.2 µg/cm^2 (figure 8.7 B) and 8.5 µg/cm^2 (figure 8.7 C), it appeared that there was potentially an increase in angiogenesis when compared to either the medium only treated aortic tissue (figure 8.7 A), or that of the tissue treated with 17.5 µg/cm^2 CNTD (figure 8.7 D), at the later stages of a 7 day exposure period.

MWCNT concentration test

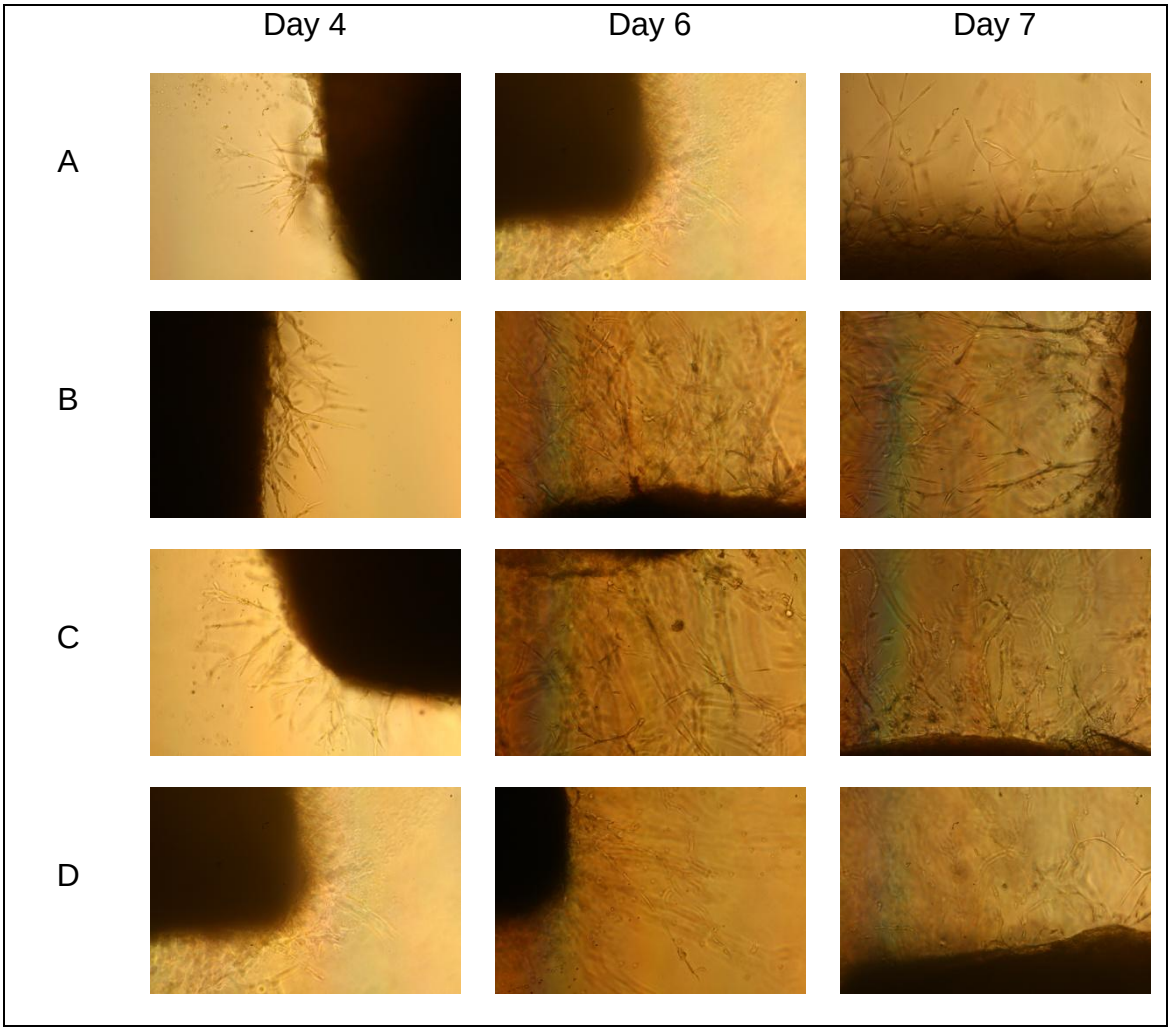

Figure 8.7 Rat aortic tissue cultured in growth factor reduced matrigel with different stimulation media – MWCNT dilution pilot. Rat aortic tissue was embedded within matrigel and incubated with (A) RPMI1640, (B) CM from MM6 exposed to 4.2µg/cm^2 CNTD, (C) CM from MM6 exposed to 8.5µg/cm^2 CNTD, and (D) CM from MM6 exposed to 17.5µg/cm^2 CNTD, for 1-7 days prior to imaging.

DiI-Ac-LDL staining of EA.hy926 cells

It was shown that during a four hour incubation period EA.hy926 cells readily internalised the DiI-Ac-LDL fluorescent marker (figure 8.8). Similar uptake studies, using this fluorescently labelled LDL involving rat aortic tissue embedded in matrigel and stimulated with various growth factors, did not produce any clear cellular uptake (not shown).

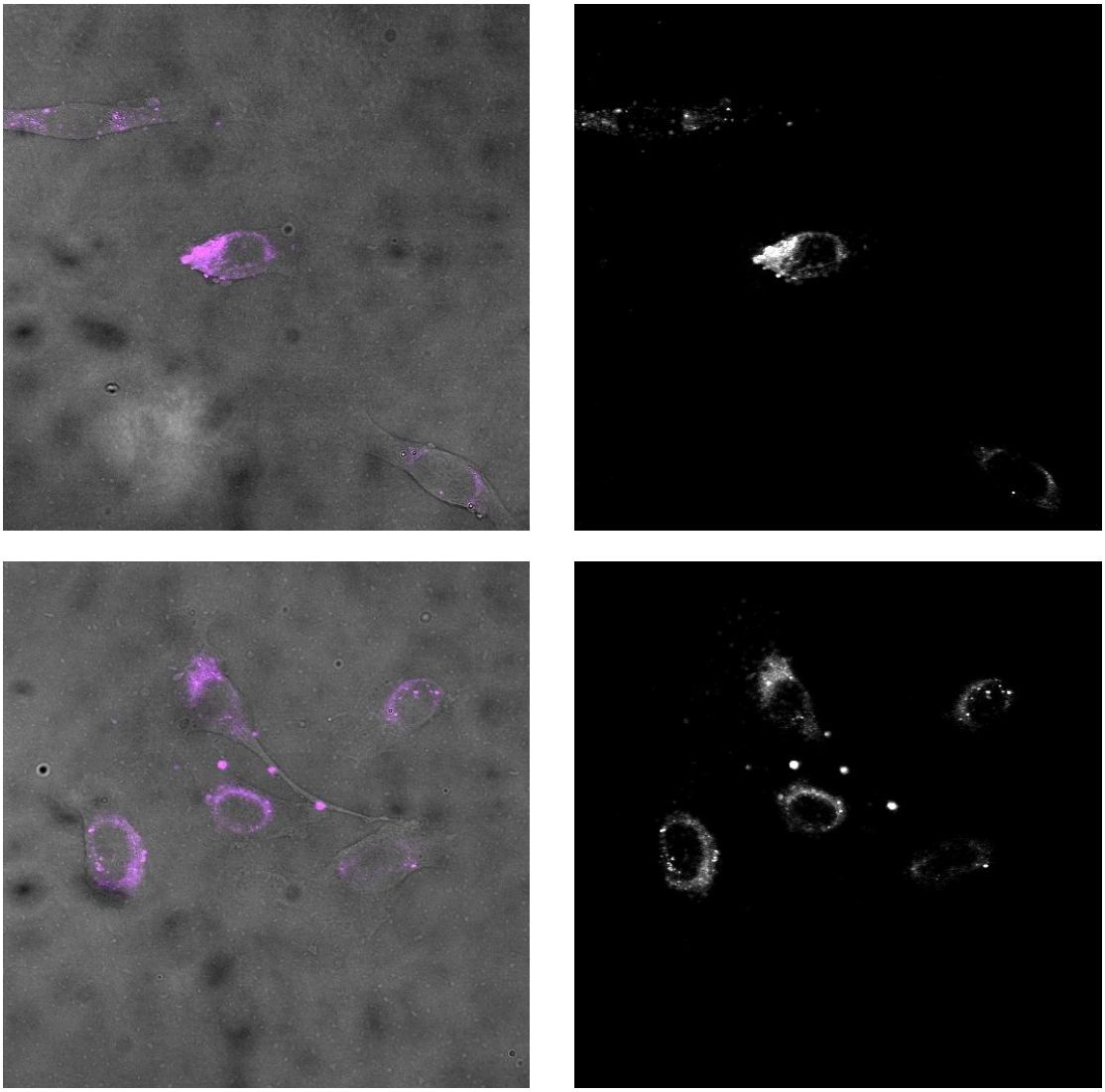

Figure 8.8 Cellular staining of endothelial cells. EA.hy926 cells were stained with 10µg/ml DiI-Ac-LDL for 4 hours, fixed, and observed by confocal and bright field microscopy. Images on right are of fluorescent channel only, on left is the overlay of the bright field and fluorescent images.

8.1.4 Conclusions

There are numerous methods used for the evaluation of angiogenesis, including *in vitro*, *ex vivo* and *in vivo* techniques, which vary in their complexity. Staton *et al.* (2009) provide a comprehensive review of current methods to assay angiogenesis. Here, it was planned to assess angiogenic potential using the capillary-like tube formation in immortalised endothelial cells, and also using the rat aortic ring *ex vivo* method. The work presented in this section remains largely incomplete, there was much assay optimisation needed and before the analysis of particle induced angiogenesis could be accurately investigated the study had to be abandoned. This was due to requests for an alternative direction in the research by project collaborators, and later to time constraints at the end of the project. There are, however, a number of conclusions that can be made from this pilot study.

In vitro

Capillary tube formation

During the initial stages of this study it was not possible to induce the clear tube formation that is evident in much of the literature, and has been shown when cells were cultured on collagen gels (Montesano *et al.*, 1983, Pepper *et al.*, 1998) or upon matrigel (Jones *et al.*, 1998). When this formation occurs it is possible to take numerous measurements to quantify the effects, including counting the tubular branching points, lengths, areas and number (Staton *et al.*, 2009). None of these methods could be utilised here as only ever a slight indication of tube formation occurred. There appeared to be slight morphological changes in all treatments when the cells were not too densely cultured, and the only cultures to form any clear tubular structures were in treatment of medium only, with cells grown on the growth factor reduced matrigel. This is surprising, as the greatest effects would have been expected from treatment with VEGF, as has been clearly demonstrated in the literature, using similar exposure conditions (Nör *et al.*, 1999, Pepper *et al.*, 1998). Other studies have clearly shown this tubular formation of endothelial cells, using isolated primary rat endothelial cells (Jones *et al.*, 1999), HUVEC cells (Raikwar *et al.*, 2005), EA.hy926 cells (Iwai *et al.*, 2004, Jones *et al.*, 1998), and even

EA.hy926 cells cultured on matrigel supplemented with conditioned media from cultures of T-cells (Vacca *et al.*, 1998).

One explanation for the problems, or the lack of response to expected stimuli may involve the choice of matrix, as when collagen I or III is used tubule formation is limited, while the use of collagen IV and V promotes tubule formation (Staton *et al.*, 2009); here collagen I was used. Another is that the cultured cells may need to be serum-starved just prior to the initiation of the experiment (Jones *et al.*, 1998, Jones *et al.*, 1999). Or potentially, as was demonstrated by Vacca *et al.* (1998), the stimulus may need to be incorporated within the gel, and not in the medium alone.

Proliferation

The migration and differentiation of endothelial cells to form tube structures attempted here is representative of late stage angiogenesis (Staton *et al.*, 2009); in hindsight it may have been wise to first perform a more basic analysis of angiogenic potential that would provide an early stage assessment. In this case a basic assessment of endothelial cell proliferation in response to macrophage conditioned media may have provided an early indicator of angiogenesis, as would the measure of cellular chemotaxis in either 3D or 2D models (Staton *et al.*, 2009).

Proliferation was not quantified during this study, but observations of the images taken can clearly identify some aspects that influence the proliferation rate of EA.hy926 endothelial cells.

When the initial collagen gels were used it was clear that there was an increase in EA.hy926 proliferation when the gels are formed using dH_2O instead of RPMI 1640 supplemented with FCS. This may be due to an observed improvement of polymerisation when gels are formed using dH_2O, which is potentially owing to the buffering capacity of cell culture medium. NaOH is added as a component of the gel to change the pH of the solution, enabling good polymerisation, if the gels are buffered (through the presence of cell culture medium) the gels would not become basic and therefore not fully polymerise. This may hinder any studies looking into proliferation as all cultures would become confluent too

quickly, and this would certainly hinder the tube network formation as a confluent plate allows no space for rearrangements and chemotaxis. Therefore gel composition is an important consideration when assessing angiogenesis by these techniques. Another factor that appeared to heavily influence the rate of proliferation was the thickness of the gel matrix. Cells seeded in a 24 well plate on 100µl matrigel proliferated at a far slower rate than those EA.hy926 cells seeded onto 50µl matrigel; therefore to allow the opportunity to distinguish between treatments, 100µl matrigel cultures would be more suitable to use. This infers that, not only matrix composition is important, but for this format of angiogenesis assay the actual height (volume) of matrix is critical.

Aortic ring

It was clear that in all cases of the aortic ring assays, some level of new blood vessel formation did occur. It was evident that the use of RPMI 1640 encouraged more growth than MCDB131, and that the inclusion of VEGF in these assays did not enhance the angiogenic effect in either case. In these cases the collagen gels were identified as not suitable due to a lack of polymerisation, and it is unknown whether this had an effect on the ability of the protein to diffuse through the gel and stimulate the tissue. In other studies however, a clear effect has been shown, not only in collagen gel matrices, but also with stimulation using VEGF (Nicosia *et al.*, 1994, Zhu and Nicosia, 2002). In these studies the appearance of medium only control cultures do appear to display slightly less sprouting than those shown here, therefore greater control over this here may help to elucidate responses.

When the matrix was exchanged for the commercially available matrigel the growth was certainly more pronounced. However, this was again the case for all treatments, and in most cases it was difficult to distinguish between medium only stimulated tissue and either the VEGF or the CM stimulated tissue. With the inclusion of further CNT dilutions during the generation of CM it did appear that there was a distinguishable difference in new vessel growth with the treatment with CM generated from 4.2µg/cm^2 and 8.5µg/cm^2 CNTD exposures. This effect was seen in comparison to medium only exposed tissue, and to tissue exposed to CM generated from MM6 exposures to 17.5µg/cm^2 CNTD,

which had consistently shown no greater effect than the medium only treatments.

The inhibition (Gerhardt *et al.*, 2003, Kruger *et al.*, 2000, Raikwar *et al.*, 2005), and stimulation (Blacher *et al.*, 2001, Zhu and Nicosia, 2002) of blood vessel formation from isolated aortic tissue has often been shown to provide relatively clear results. Here, as most of the exposures demonstrated indistinguishable generation of new cells and vessel formation it was decided that a more quantifiable method of endothelial cell presence was required, as from the aortic tissue it is possible to have various cell types, including endothelial cells, smooth muscle cells and fibroblasts (Masson *et al.*, 2002, Voyta *et al.*, 1984, Zhu and Nicosia, 2002).

Endothelial cell staining

There are a number of endothelial characteristics that can be used to identify them from other cell types, such as aspects of their phenotype: the presence of Weibel–Palade-bodies or von Willebrand Factor; or their function, with the uptake of acetylated low density lipoproteins (acLDL), or the activity of angiotensin-converting enzyme (Bouïs *et al.*, 2001).

Here, a fluorescently labelled acLDL molecule: DiI-Ac-LDL was used to clarify that endothelial cells were forming, and that the outgrowths were not consisting of numerous different cell types. The uptake of DiI-Ac-LDL should be predominately by endothelial cells or macrophages, and not by other cell types that may be present.

It was shown that this staining procedure was accurate and that endothelial cells do internalise DiI-Ac-LDL, using EA.hy926 cells. However, when this method was used for the aortic rings embedded within gels no staining was detected, and it was believed that either the incubation period was not long enough for the stain to move through the gel and enter the cells, the DiI-Ac-LDL concentration was not high enough, or the gel would need to be sectioned prior to visualisation.

As previously mentioned, the continuation of this study was not possible. However, there were indications that if continued this study may have given

some interesting results. Issues concerning gels in the *in vitro* studies were identified and therefore this aspect could certainly be continued; the potential for increased blood vessel formation was evident when the original particle treatments generating the CM for the *ex vivo* experiments were altered; and the proposed method for distinguishing between endothelial cells and smooth muscle cells in the *ex vivo* experiments may have allowed clearer elucidation between responses to different treatments.

8.2 Appendix II – Publications

Clift, M. J. D., Boyles, M. S. P., Brown, D. M. & Stone, V. (2010) An investigation into the potential for different surface-coated quantum dots to cause oxidative stress and affect macrophage cell signalling in vitro. Nanotoxicology, 4, 139-149. (N.B. The work produced for this paper, on my part, was done during a Carnegie funded research fellowship, and that was started prior to this PhD)

Gaiser, B. and Clift, M. and Johnston, H. and Boyles, M. and Fernandes, T.. (2011). Human and natural environment effects of nanomaterials. In: Sattler, K. *Handbook of nanophysics - nanomedicine and nanorobotics*. 7th ed. Florida: Taylor & Francis Group. 14.1-14.24.

Rothen-Rutishauser, B., Brown, D. M., Piallier-Boyles, M., Kinloch, I. A., Windle, A. H., Gehr, P. & Stone, V. (2010) Relating the physicochemical characteristics and dispersion of multiwalled carbon nanotubes in different suspension media to their oxidative reactivity in vitro and inflammation in vivo. Nanotoxicology, 4, 331-342.

References

Aam, B. B. & Fonnum, F. (2007) ROS scavenging effects of organic extract of diesel exhaust particles on human neutrophil granulocytes and rat alveolar macrophages. *Toxicology,* **230,** 207-218.

Abarrategi, A., Gutiérrez, M. C., Moreno-Vicente, C., Hortigüela, M. J., Ramos, V., López-Lacomba, J. L., Ferrer, M. L. & del Monte, F. (2008) Multiwall carbon nanotube scaffolds for tissue engineering purposes. *Biomaterials,* **29,** 94-102.

Acworth, I. N., McCabe, D. R. & Mayer, T. M. (1997) *Oxidants, antioxidants, and free radicals,* Washington, Taylor & Francis.

Aderem, A. (2003) Phagocytosis and the Inflammatory Response. *Journal of Infectious Diseases,* **187,** S340-345.

Aitken, R. J., Chaudhry, M. Q., Boxall, A. B. A. & Hull, M. (2006) Manufacture and use of nanomaterials: current status in the UK and global trends. *Occup Med (Lond),* **56,** 300-306.

Al-Ali, M. K. & Howarth, P. H. (1998) Nitric oxide and the respiratory system in health and disease. *Respiratory medicine,* **92,** 701-715.

Alazzam, A., Mfoumou, E., Stiharu, I., Kassab, A., Darnel, A., Yasmeen, A., Sivakumar, N., Bhat, R. & Moustafa, A.-E. A. (2010) Identification of deregulated genes by single wall carbon-nanotubes in human normal bronchial epithelial cells. *Nanomedicine: Nanotechnology, Biology and Medicine,* **6,** 563-569.

Alberts, B., Johnson, A., Lewis, J., Raff, M., Roberts, K. & Walter, P. (2002) Molecular Biology of the Cell (4th Ed.). *Garland Science – Taylor and Francis Group, New York*.

Albrecht, C., Knaapen, A., Becker, A., Hohr, D., Haberzettl, P., van Schooten, F., Borm, P. & Schins, R. (2005) The crucial role of particle surface reactivity in respirable quartz-induced reactive oxygen/nitrogen species formation and APE/Ref-1 induction in rat lung. *Respiratory Research,* **6,** 129.

Alfranca, A., Lopez-Oliva, J. M., Genis, L., Lopez-Maderuelo, D., Mirones, I., Salvado, D., Quesada, A. J., Arroyo, A. G. & Redondo, J. M. (2008) PGE2 induces angiogenesis via MT1-MMPâ€“mediated activation of the TGFÎ²/Alk5 signaling pathway. *Blood,* **112,** 1120-1128.

Andrews, R., Jacques, D., Rao, A. M., Derbyshire, F., Qian, D., Fan, X., Dickey, E. C. & Chen, J. (1999) Continuous production of aligned carbon nanotubes: a step closer to commercial realization. *Chemical Physics Letters,* **303,** 467-474.

Antoniades, H. N., Neville-Golden, J., Galanopoulos, T., Kradin, R. L., Valente, A. J. & Graves, D. T. (1992) Expression of monocyte chemoattractant protein 1 mRNA in human idiopathic pulmonary fibrosis. *Proceedings of the National Academy of Sciences,* **89,** 5371-5375.

Arenberg, D. A., Keane, M. P., DiGiovine, B., Kunkel, S. L., Strom, S. R. B., Burdick, M. D., Iannettoni, M. D. & Strieter, R. M. (2000) Macrophage infiltration in human non-small-cell lung cancer: the role of CC chemokines. *Cancer Immunology, Immunotherapy,* **49,** 63-70.

Arepalli, S., Nikolaev, P., Gorelik, O., Hadjiev, V. G., Holmes, W., Files, B. & Yowell, L. (2004) Protocol for the characterization of single-wall carbon nanotube material quality. *Carbon,* **42,** 1783-1791.

Arepalli, S. & Scott, C. D. (1999) Spectral measurements in production of single-wall carbon nanotubes by laser ablation. *Chemical Physics Letters,* **302,** 139-145.

Arredouani, M., Yang, Z., Ning, Y., Qin, G., Soininen, R., Tryggvason, K. & Kobzik, L. (2004) The Scavenger Receptor MARCO Is Required for Lung Defense against Pneumococcal Pneumonia and Inhaled Particles. *The Journal of Experimental Medicine,* **200,** 267-272.

Arredouani, M. S., Palecanda, A., Koziel, H., Huang, Y.-C., Imrich, A., Sulahian, T. H., Ning, Y. Y., Yang, Z., Pikkarainen, T., Sankala, M., Vargas, S. O., Takeya, M., Tryggvason, K. & Kobzik, L. (2005) MARCO Is the Major Binding Receptor for Unopsonized Particles and Bacteria on Human Alveolar Macrophages. *The Journal of Immunology,* **175,** 6058-6064.

Asakura, M., Sasaki, T., Sugiyama, T., Takaya, M., Koda, S., Nagano, K., Arito, H. & Fukushima, S. (2010) Genotoxicity and cytotoxicity of multi-wall carbon nanotubes in cultured Chinese hamster lung cells in comparison with chrysotile A fibers. *Journal of Occupational Health,* **52,** 155-166.

Ashrafi, M. H., Kiumarsi, A., Khajavi, R. & Parvinzadeh, M. (2007) Microscopic Characterization of Silk Fibers Coated with ZnO Nanoparticles. *AIP Conference Proceedings,* **929,** 220-223.

Aubry, J.-P., Blaecke, A., Lecoanet-Henchoz, S., Jeannin, P., Herbault, N., Caron, G., Moine, V. & Bonnefoy, J.-Y. (1999) Annexin V used for measuring apoptosis in the early events of cellular cytotoxicity. *Cytometry,* **37,** 197-204.

Azarmi, S., Roa, W. H. & Löbenberg, R. (2008) Targeted delivery of nanoparticles for the treatment of lung diseases. *Advanced Drug Delivery Reviews,* **60,** 863-875.

Babior, B. M. (2000) Phagocytes and oxidative stress. *The American journal of medicine,* **109,** 33-44.

Babior, B. M., Kipnes, R. S. & Curnutte, J. T. (1973) Biological Defense Mechanisms. The production by leukocytes of superoxide, a potential bactericidal agent. *The Journal of Clinical Investigation,* **52,** 741-744.

Baldys, A. & Aust, A. E. (2005) Role of Iron in Inactivation of Epidermal Growth Factor Receptor after Asbestos Treatment of Human Lung and Pleural Target Cells. *Am. J. Respir. Cell Mol. Biol.,* **32,** 436-442.

Baltog, I., Baibarac, M., Lefrant, S. & Mevellec, J. Y. (2008) Raman and FTIR studies on electro-reduction of single-walled carbon nanotube films in the presence of Li salts. *Diamond and Related Materials,* **17,** 1558-1564.

Bandow, S., Asaka, S., Saito, Y., Rao, A. M., Grigorian, L., Richter, E. & Eklund, P. C. (1998) Effect of the Growth Temperature on the Diameter Distribution and Chirality of Single-Wall Carbon Nanotubes. *Physical Review Letters,* **80,** 3779.

Bang, J. J., Guerrero, P. A., Lopez, D. A., Murr, L. E. & Esquivel, E. V. (2004) Carbon nanotubes and other fullerene nanocrystals in domestic propane and natural gas combustion streams. *J Nanosci Nanotechnol,* **4,** 716-718.

Bao, G. & Suresh, S. (2003) Cell and molecular mechanisms of biological materials. *Nature Materials,* **2,** 715-725.

Barlow, P. G., Clouter-Baker, A., Donaldson, K., MacCallum, J. & Stone, V. (2005a) Carbon black nanoparticles induce type II epithelial cells to release chemotaxins for alveolar macrophages. BioMed Central Ltd.

Barlow, P. G., Donaldson, K., MacCallum, J., Clouter, A. & Stone, V. (2005b) Serum exposed to nanoparticle carbon black displays increased potential to induce macrophage migration. *Toxicology Letters,* **155,** 397-401.

Baud, V. & Karin, M. (2001) Signal transduction by tumor necrosis factor and its relatives. *Trends in Cell Biology,* **11,** 372-377.

Bauer, L. A., Birenbaum, N. S. & Meyer, G. J. (2004) Biological applications of high aspect ratio nanoparticles. *Journal of Materials Chemistry,* **14,** 517-526.

Beamer, C. A. & Holian, A. (2005) Scavenger receptor class A type I/II (CD204) null mice fail to develop fibrosis following silica exposure. *American Journal of Physiology - Lung Cellular and Molecular Physiology,* **289,** L186-L195.

Becker, S., Soukup, J. M., Gilmour, M. I. & Devlin, R. B. (1996) Stimulation of Human and Rat Alveolar Macrophages by Urban Air Particulates: Effects on Oxidant Radical Generation and Cytokine Production. *Toxicology and Applied Pharmacology,* **141,** 637-648.

Belin, T. & Epron, F. (2005) Characterization methods of carbon nanotubes: a review. *Materials Science and Engineering B,* **119,** 105-118.

Bergamaschi, E. (2009) Aggregated carbon nanotubes increase the permeability across human airway epithelium: a pathway for translocation? *NanoImpactNet International Conference, Lausanne,* **Unpublished data**.

Bernstein, D., Castranova, V., Donaldson, K., Fubini, B., Hadley, J., Hesterberg, T., Kane, A., Lai, D., McConnell, E. E., Muhle, H., Oberdorster, G., Olin, S. & Warheit, D. B. (2005) Testing of Fibrous Particles: Short-Term Assays and Strategies. *Inhalation Toxicology,* **17,** 497-537.

Berry, C. C., Charles, S., Wells, S., Dalby, M. J. & Curtis, A. S. G. (2004) The influence of transferrin stabilised magnetic nanoparticles on human dermal fibroblasts in culture. *International Journal of Pharmaceutics,* **269,** 211-225.

Besnard, A.-G., Togbe, D., Couillin, I., Tan, Z., Zheng, S. G., Erard, F., Le Bert, M., Quesniaux, V. & Ryffel, B. (2012) Inflammasome–IL-1–Th17 response in allergic lung inflammation. *Journal of Molecular Cell Biology,* **4,** 3-10.

Bhushan, B. (2007) Nanotechnology: a Boon or Bane? *AIP Conference Proceedings,* **929,** 250-254.

Bilski, P., Belanger, A. G. & Chignell, C. F. (2002) Photosensitized oxidation of 2',7'-dichlorofluorescin: singlet oxygen does not contribute to the formation of fluorescent oxidation product 2',7'-dichlorofluorescein. *Free Radical Biology and Medicine,* **33,** 938-946.

Blacher, S., Devy, L., Burbridge, M., Roland, G., Tucker, G., Noël, A. & Foidart, J.-M. (2001) Improved quantification of angiogenesis in the rat aortic ring assay. *Angiogenesis,* **4,** 133-142.

Bolton, R. E., Davis, J. M. G., Donaldson, K. & Wright, A. (1982) Variations in the Carcinogenicity of Mineral Fibres. *Annals of Occupational Hygiene,* **26,** 569-582.

Bootz, A., Vogel, V., Schubert, D. & Kreuter, J. (2004) Comparison of scanning electron microscopy, dynamic light scattering and analytical ultracentrifugation for the sizing of poly(butyl cyanoacrylate) nanoparticles. *European Journal of Pharmaceutics and Biopharmaceutics,* **57,** 369-375.

Borm, P., Robbins, D., Haubold, S., Kuhlbusch, T., Fissan, H., Donaldson, K., Schins, R., Stone, V., Kreyling, W., Lademann, J., Krutmann, J., Warheit, D. & Oberdorster, E. (2006) The potential risks of nanomaterials: a review carried out for ECETOC. *Particle and Fibre Toxicology,* **3,** 11.

Bottini, M., Bruckner, S., Nika, K., Bottini, N., Bellucci, S., Magrini, A., Bergamaschi, A. & Mustelin, T. (2006) Multi-walled carbon nanotubes induce T lymphocyte apoptosis. *Toxicology Letters,* **160,** 121-126.

Bouïs, D., Hospers, G., Meijer, C., Molema, G. & Mulder, N. (2001) Endothelium in vitro: A review of human vascular endothelial cell lines for blood vessel-related research. *Angiogenesis,* **4,** 91-102.

Boyanton, B. L. & Blick, K. E. (2002) Stability Studies of Twenty-Four Analytes in Human Plasma and Serum. *Clinical Chemistry,* **48,** 2242-2247.

Boylan, A. M., Sanan, D. A., Sheppard, D. & Broaddus, V. C. (1995) Vitronectin enhances internalization of crocidolite asbestos by rabbit pleural mesothelial cells via the integrin alpha v beta 5. *The Journal of Clinical Investigation,* **96,** 1987-2001.

Brady-Estévez, A. S., Kang, S. & Elimelech, M. (2008) A Single-Walled-Carbon-Nanotube Filter for Removal of Viral and Bacterial Pathogens. *Small,* **4,** 481-484.

Branca, C., Magazù, V. & Mangione, A. (2005) Determination of MWNTs length-to-diameter ratio by static and dynamic light scattering. *Diamond and Related Materials,* **14,** 846-849.

Branton, M. H. & Kopp, J. B. (1999) TGF-[beta] and fibrosis. *Microbes and Infection,* **1,** 1349-1365.

Bräuner, E. V., Forchhammer, L., Møller, P., Simonsen, J., Glasius, M., Wåhlin, P., Raaschou-Nielsen, O. & Loft, S. (2007) Exposure to Ultrafine Particles from Ambient Air and Oxidative Stress-Induced DNA Damage. *Environmental Health Perspectives,* **115,** 1177-1182.

Brody, A., Hill, L., Adkins, B. J. & O'Connor, R. (1981) Chrysotile asbestos inhalation in rats: deposition pattern and reaction of alveolar epithelium and pulmonary macrophages. *The American Review of Respiratory Disease,* **123,** 670-679.

Broekelmann, T. J., Limper, A. H., Colby, T. V. & McDonald, J. A. (1991) Transforming growth factor beta 1 is present at sites of extracellular matrix gene expression in human pulmonary fibrosis. *Proceedings of the National Academy of Sciences,* **88,** 6642-6646.

Brown, D., Donaldson, K., Borm, P. J., Schins, R. P. F., Dehnhardt, M., Gilmour, P. S., Jimenez, L. A. & Stone, V. (2004) Calcium and ROS-mediated activation of transcription factors and TNF-Î± cytokine gene expression in macrophages exposed to ultrafine particles. *American Journal of Physiology. Lung Cellular and Molecular Physiology.,* **286,** L344-L353.

Brown, D., Donaldson, K. & Stone, V. (2010) Nuclear Translocation of Nrf2 and Expression of Antioxidant Defence Genes in THP-1 Cells Exposed to Carbon Nanotubes. *Journal of Biomedical Nanotechnology,* **6,** 224-233.

Brown, D. M., Donaldson, K. & Stone, V. (2002) Role of Calcium in the Induction of TNFα Expression by Macrophages on Exposure to Ultrafine Particles. *Annals of Occupational Hygiene,* **46,** 219-222.

Brown, D. M., Hutchison, L., Donaldson, K., MacKenzie, S. J., Dick, C. A. J. & Stone, V. (2007a) The effect of oxidative stress on macrophages and lung epithelial cells: The role of phosphodiesterases 1 and 4. *Toxicology Letters,* **168,** 1-6.

Brown, D. M., Kinloch, I. A., Bangert, U., Windle, A. H., Walter, D. M., Walker, G. S., Scotchford, C. A., Donaldson, K. & Stone, V. (2007b) An in vitro study of the potential of carbon nanotubes and nanofibres to induce inflammatory mediators and frustrated phagocytosis. *Carbon,* **45,** 1743-1756.

Brown, D. M., Roberts, N. K. & Donaldson, K. (1997) Effect of Coating with Lung Lining Fluid on the Ability of Fibres to Produce a Respiratory Burst in Rat Alveolar Macrophages. *Toxicology in Vitro,* **12,** 15-24.

Brown, D. M., Stone, V., Findlay, P., MacNee, W. & Donaldson, K. (2000) Increased inflammation and intracellular calcium caused by ultrafine carbon black is independent of transition metals or other soluble components. *Occupational and Environmental Medicine,* **57,** 685-691.

Brown, D. M., Wilson, M. R., MacNee, W., Stone, V. & Donaldson, K. (2001) Size-Dependent Proinflammatory Effects of Ultrafine Polystyrene Particles: A Role for Surface Area and Oxidative Stress in the Enhanced Activity of Ultrafines. *Toxicology and Applied Pharmacology,* **175,** 191-199.

Brown, G. M., Brown, D. M., Li, X.-Y. & Donaldson, K. (1994a) Inflammatory Responses in the Lungs of Rats Exposed to Amosite Asbestos. *Annals of Occupational Hygiene,* **38,** 683-691.

Brown, R. C., Sara, E. A., Hoskins, J. A. & Houghton, C. E. (1994b) Interaction Between Mineral Fibres and Cell Surface Receptors Studied with Amosite and Surface Derivatized Amosite Asbestos. *Annals of Occupational Hygiene,* **38,** 587-593.

BSI (2007) Terminology for nanomaterials. PAS 136:2007. BSI, London, UK.

Cacciotti, P., Strizzi, L., Vianale, G., Iaccheri, L., Libener, R., Porta, C., Tognon, M., Gaudino, G. & Mutti, L. (2002) The Presence of Simian-Virus 40 Sequences in Mesothelioma and Mesothelial Cells Is Associated with High Levels of Vascular Endothelial Growth Factor. *Am. J. Respir. Cell Mol. Biol.,* **26,** 189-193.

Cai, D., Mataraza, J. M., Qin, Z. H., Huang, Z., Huang, J., Chiles, T. C., Carnahan, D., Kempa, K. & Ren, Z. (2005) Highly efficient molecular delivery into mammalian cells using carbon nanotube spearing. *Nat Methods,* **2,** 449-454.

Cardile, V., Renis, M., Scifo, C., Lombardo, L., Gulino, R., Mancari, B. & Panico, A. (2004) Behaviour of the new asbestos amphibole fluoro-edenite in different lung cell systems. *The International Journal of Biochemistry & Cell Biology,* **36,** 849-860.

Cardinali, G., Kovacs, D., Maresca, V., Flori, E., Dell'Anna, M. L., Campopiano, A., Casciardi, S., Spagnoli, G., Torrisi, M. R. & Picardo, M. (2006) Differential in vitro cellular response induced by exposure to synthetic vitreous fibers (SVFs) and asbestos crocidolite fibers. *Experimental and Molecular Pathology,* **81,** 31-41.

Casey, A., Davoren, M., Herzog, E., Lyng, F. M., Byrne, H. J. & Chambers, G. (2007) Probing the interaction of single walled carbon nanotubes within cell culture medium as a precursor to toxicity testing. *Carbon,* **45,** 34-40.

Casey, A., Herzog, E., Lyng, F. M., Byrne, H. J., Chambers, G. & Davoren, M. (2008) Single walled carbon nanotubes induce indirect cytotoxicity by medium depletion in A549 lung cells. *Toxicology Letters,* **179,** 78-84.

Cassel, S. L., Eisenbarth, S. C., Iyer, S. S., Sadler, J. J., Colegio, O. R., Tephly, L. A., Carter, A. B., Rothman, P. B., Flavell, R. A. & Sutterwala, F. S. (2008) The Nalp3 inflammasome is essential for the development of

silicosis. *Proceedings of the National Academy of Sciences,* **105,** 9035-9040.

Cassell, A. M., Raymakers, J. A., Kong, J. & Dai, H. (1999) Large Scale CVD Synthesis of Single-Walled Carbon Nanotubes. *The Journal of Physical Chemistry B,* **103,** 6484-6492.

Cesta, M. F., Ryman-Rasmussen, J. P., Wallace, D. G., Masinde, T., Hurlburt, G., Taylor, A. J. & Bonner, J. C. (2010) Bacterial Lipopolysaccharide Enhances PDGF Signaling and Pulmonary Fibrosis in Rats Exposed to Carbon Nanotubes. *Am. J. Respir. Cell Mol. Biol.,* **43,** 142-151.

Chanock, S. J., el Benna, J., Smith, R. M. & Babior, B. M. (1994) The respiratory burst oxidase. *Journal of Biological Chemistry,* **269,** 24519-24522.

Chaudhuri, P., Harfouche, R., Soni, S., Hentschel, D. M. & Sengupta, S. (2009) Shape Effect of Carbon Nanovectors on Angiogenesis. *ACS Nano,* **4,** 574-582.

Chen, Q., Marsh, J., Ames, B. & Mossman, B. (1996) Detection of 8-oxo-2'-deoxyguanosine, a marker of oxidative DNA damage, in culture medium from human mesothelial cells exposed to crocidolite asbestos. *Carcinogenesis,* **17,** 2525-2527.

Cheng, C., Müller, K. H., Koziol, K. K. K., Skepper, J. N., Midgley, P. A., Welland, M. E. & Porter, A. E. (2009) Toxicity and imaging of multi-walled carbon nanotubes in human macrophage cells. *Biomaterials,* **30,** 4152-4160.

Chiang, I. W., Brinson, B. E., Smalley, R. E., Margrave, J. L. & Hauge, R. H. (2001) Purification and Characterization of Single-Wall Carbon Nanotubes. *The Journal of Physical Chemistry B,* **105,** 1157-1161.

Cho, H. G., Kim, S. W., Lim, H. J., Yun, C. H., Lee, H. S. & Park, C. R. (2009) A simple and highly effective process for the purification of single-walled carbon nanotubes synthesized with arc-discharge. *Carbon,* **47,** 3544-3549.

Choe, N., Tanaka, S., Xia, W., Hemenway, D. R., Roggli, V. L. & Kagan, E. (1997) Pleural Macrophage Recruitment and Activation in Asbestos-Induced Pleural Injury. *Environmental Health Perspectives,* **105,** 1257-1260.

Chou, S. G., Ribeiro, H. B., Barros, E. B., Santos, A. P., Nezich, D., Samsonidze, G. G., Fantini, C., Pimenta, M. A., Jorio, A., Filho, F. P., Dresselhaus, M. S., Dresselhaus, G., Saito, R., Zheng, M., Onoa, G. B., Semke, E. D., Swan, A. K., Ünlü, M. S. & Goldberg, B. B. (2004) Optical characterization of DNA-wrapped carbon nanotube hybrids. *Chemical Physics Letters,* **397,** 296-301.

Clift, M. J. D., Bhattacharjee, S., Brown, D. M. & Stone, V. (2010a) The effects of serum on the toxicity of manufactured nanoparticles. *Toxicology Letters,* **198,** 358-365.

Clift, M. J. D., Boyles, M. S. P., Brown, D. M. & Stone, V. (2010b) An investigation into the potential for different surface-coated quantum dots to cause oxidative stress and affect macrophage cell signalling in vitro. *Nanotoxicology,* **4,** 139-149.

Coker, R. K. & Laurent, G. J. (1998) Pulmonary fibrosis: cytokines in the balance. *European Respiratory Journal,* **11,** 1218-1221.

Conway, E. M., Collen, D. & Carmeliet, P. (2001) Molecular mechanisms of blood vessel growth. *Cardiovascular Research,* **49,** 507-521.

Coquelle, N., Fioravanti, E., Weik, M., Vellieux, F. & Madern, D. (2007) Activity, Stability and Structural Studies of Lactate Dehydrogenases Adapted to Extreme Thermal Environments. *Journal of Molecular Biology,* **374,** 547-562.

Crouzier, D., Follot, S., Gentilhomme, E., Flahaut, E., Arnaud, R., Dabouis, V., Castellarin, C. & Debouzy, J. C. (2010) Carbon nanotubes induce inflammation but decrease the production of reactive oxygen species in lung. *Toxicology,* **272,** 39-45.

Cveticanin, J., Joksic, G., Leskovac, A., Petrovic, S., Sobot, A. V. & Neskovic, O. (2010) Using carbon nanotubes to induce micronuclei and double strand breaks of the DNA in human cells. *Nanotechnology,* **21,** 015102.

Dale, D. C., Boxer, L. & Liles, W. C. (2008) The phagocytes: neutrophils and monocytes. *Blood,* **112,** 935-945.

Davis, J. M. (1994) The role of clearance and dissolution in determining the durability or biopersistence of mineral fibers. *Environmental Health Perspectives,* **102 Suppl 5,** 113-117.

Davis, J. M., Addison, J., Bolton, R. E., Donaldson, K., Jones, A. D. & Smith, T. (1986) The pathogenicity of long versus short fibre samples of amosite asbestos administered to rats by inhalation and intraperitoneal injection. *British journal of experimental pathology,* **67,** 415-430.

Davis, J. M. G. & Cowie, H. A. (1990) The Relationship between Fibrosis and Cancer in Experimental Animals Exposed to Asbestos and Other Fibers. *Environmental Health Perspectives,* **88,** 305-309.

Davoren, M., Herzog, E., Casey, A., Cottineau, B., Chambers, G., Byrne, H. J. & Lyng, F. M. (2007) In vitro toxicity evaluation of single walled carbon nanotubes on human A549 lung cells. *Toxicology in Vitro,* **21,** 438-448.

De Saint-Hubert, M., Prinsen, K., Mortelmans, L., Verbruggen, A. & Mottaghy, F. M. (2009) Molecular imaging of cell death. *Methods,* **48,** 178-187.

Dement, J. M., Harris, R. L., Symons, M. J. & Shy, C. (1982) Estimates of dose-response for respiratory cancer among chrysotile asbestos textile workers. *The Annals of occupational hygiene,* **26,** 869-887.

Deng, X., Jia, G., Wang, H., Sun, H., Wang, X., Yang, S., Wang, T. & Liu, Y. (2007) Translocation and fate of multi-walled carbon nanotubes in vivo. *Carbon,* **45,** 1419-1424.

Dhénaut, A., Boiteux, S. & Radicella, J. P. (2000) Characterization of the hOGG1 promoter and its expression during the cell cycle. *Mutation Research/DNA Repair,* **461,** 109-118.

Dick, C. A. J., Brown, D. M., Donaldson, K. & Stone, V. (2003) The Role of Free Radicals in the Toxic and Inflammatory Effects of Four Different Ultrafine Particle Types. *Inhalation Toxicology,* **15,** 39-52.

Dijkstra, C. D., Döpp, E. A., Joling, P. & Kraal, G. (1985) The heterogeneity of mononuclear phagocytes in lymphoid organs: distinct macrophage subpopulations in the rat recognized by monoclonal antibodies ED1, ED2 and ED3. *Immunology,* **54,** 589-599.

Dika Nguea, H., Rihn, B., Mahon, D., Bernard, J.-L., Reydellet, A. & Le Faou, A. (2005) Effects of various man-made mineral fibers on cell apoptosis and viability. *Archives of Toxicology,* **79,** 487-492.

Doak, S. H., Griffiths, S. M., Manshian, B., Singh, N., Williams, P. M., Brown, A. P. & Jenkins, G. J. S. (2009) Confounding experimental considerations in nanogenotoxicology. *Mutagenesis,* **24,** 285-293.

Dockery, D. W., Pope, C. A., Xu, X., Spengler, J. D., Ware, J. H., Fay, M. E., Ferris, B. G. & Speizer, F. E. (1993) An Association between Air Pollution

and Mortality in Six U.S. Cities. *New England Journal of Medicine,* **329,** 1753-1759.

Dogra, S. & Donaldson, K. (1995) Effect of long and short fibre amosite asbestos on in vitro TNF production by rat alveolar macrophages: the modifying effect of lipopolysaccharide. *Industrial Health,* **33,** 131-141.

Donaldson, K., Aitken, R., Tran, L., Stone, V., Duffin, R., Forrest, G. & Alexander, A. (2006) Carbon Nanotubes: A Review of Their Properties in Relation to Pulmonary Toxicology and Workplace Safety. *Toxicological Sciences,* **92,** 5-22.

Donaldson, K. & Borm, P. J. A. (1998) The Quartz Hazard: A Variable Entity. *Ann Occup Hyg,* **42,** 287-294.

Donaldson, K., Brown, D., Clouter, A., Duffin, R., MacNee, W., Renwick, L., Tran, L. & Stone, V. (2002) The pulmonary toxicology of ultrafine particles. *J Aerosol Med,* **15,** 213-220.

Donaldson, K., Brown, G. M., Brown, D. M., Bolton, R. E. & Davis, J. M. (1989) Inflammation generating potential of long and short fibre amosite asbestos samples. *British Journal of Industrial Medicine,* **46,** 271-276.

Donaldson, K., Li, X. Y., Dogra, S., Miller, B. G. & Brown, G. M. (1992) Asbestos-stimulated tumour necrosis factor release from alveolar macrophages depends on fibre length and opsonization. *The Journal of Pathology,* **168,** 243-248.

Donaldson, K., Poland, C. A. & Schins, R. P. F. (2010) Possible genotoxic mechanisms of nanoparticles: Criteria for improved test strategies. *Nanotoxicology,* **4,** 414-420.

Donaldson, K. & Stone, V. (2003) Current hypotheses on the mechanisms of toxicity of ultrafine particles. *Ann Ist Super Sanita,* **39,** 405-410.

Donaldson, K., Stone, V., Tran, C. L., Kreyling, W. & Borm, P. J. A. (2004) Nanotoxicology. *Occup Environ Med,* **61,** 727-728.

Donaldson, K., Szymaniec, S., Li, X. Y., Brown, D. M. & Brown, G. M. (1991) Inflammation and immunomodulation caused by short and long amosite asbestos samples. *Mechanisms in Fiber Carcinogenesis: Plenum Press, New York***,** 287–307.

Donaldson, K. & Tran, C. L. (2004) An introduction to the short-term toxicology of respirable industrial fibres. *Mutation Research/Fundamental and Molecular Mechanisms of Mutagenesis,* **553,** 5-9.

Donaldson, K., Tran, L., Jimenez, L., Duffin, R., Newby, D. E., Mills, N., MacNee, W. & Stone, V. (2005) Combustion-derived nanoparticles: A review of their toxicology following inhalation exposure. BioMed Central Ltd.

Dörger, M., Münzing, S., Allmeling, A.-M., Messmer, K. & Krombach, F. (2001) Differential Responses of Rat Alveolar and Peritoneal Macrophages to Man-Made Vitreous Fibers in Vitro. *Environmental Research,* **85,** 207-214.

Dostert, C., Petrilli, V., Van Bruggen, R., Steele, C., Mossman, B. T. & Tschopp, J. (2008) Innate Immune Activation Through Nalp3 Inflammasome Sensing of Asbestos and Silica. *Science,* **320,** 674-677.

Dresselhaus, M. S., Dresselhaus, G. & Hofmann, M. (2007) The big picture of Raman scattering in carbon nanotubes. *Vibrational Spectroscopy,* **45,** 71-81.

Dresselhaus, M. S., Jorio, A., Hofmann, M., Dresselhaus, G. & Saito, R. (2010) Perspectives on Carbon Nanotubes and Graphene Raman Spectroscopy. *Nano Letters,* **10,** 751-758.

Driscoll, K., Carter, J., Hassenbein, D. & Howard, B. (1997) Cytokines and particle-induced inflammatory cell recruitment. *Environ Health Perspect,* **105,** 1159-1164.

Driscoll, K. E. (2000) TNF[alpha] and MIP-2: role in particle-induced inflammation and regulation by oxidative stress. *Toxicology Letters,* **112-113,** 177-183.

Duffin, R., Tran, C. L., Clouter, A., Brown, D. M., MacNee, W., Stone, V. & Donaldson, K. (2002) The Importance of Surface Area and Specific Reactivity in the Acute Pulmonary Inflammatory Response to Particles. *Annals of Occupational Hygiene,* **46,** 242-245.

Dumortier, H., Lacotte, S., Pastorin, G., Marega, R., Wu, W., Bonifazi, D., Briand, J. P., Prato, M., Muller, S. & Bianco, A. (2006) Functionalized Carbon Nanotubes Are Non-Cytotoxic and Preserve the Functionality of Primary Immune Cells. *Nano Lett.,* **6,** 1522-1528.

Eck, J., Sans, J. L. & Balat-Pichelin, M. (2011) Experimental study of carbon materials behavior under high temperature and VUV radiation: Application to Solar Probe+ heat shield. *Applied Surface Science,* **257,** 3196-3204.

Edgell, C. J., McDonald, C. C. & Graham, J. B. (1983) Permanent cell line expressing human factor VIII-related antigen established by hybridization. *Proceedings of the National Academy of Sciences,* **80,** 3734-3737.

Edinger, A. L. & Thompson, C. B. (2004) Death by design: apoptosis, necrosis and autophagy. *Current Opinion in Cell Biology,* **16,** 663-669.

Edwards, S. L., Church, J. S., Werkmeister, J. A. & Ramshaw, J. A. M. (2009) Tubular micro-scale multiwalled carbon nanotube-based scaffolds for tissue engineering. *Biomaterials,* **30,** 1725-1731.

El-Hag, A., Ul-Haq, S., Jayaram, S. & Cherney, E. (2007) Improving the Erosion Resistance of Electrical Insulating Materials Using Nano Fillers. *AIP Conference Proceedings,* **929,** 209-215.

Elmore, S. (2007) Apoptosis: A Review of Programmed Cell Death. *Toxicologic Pathology,* **35,** 495-516.

Emad, A. & Emad, V. (2007) Elevated levels of MCP-1, MIP-α and MIP-1β in the bronchoalveolar lavage (BAL) fluid of patients with mustard gas-induced pulmonary fibrosis. *Toxicology,* **240,** 60-69.

Endo, M. (2010) Carbon nanotubes: State-of-the-art technology and safety for success. *Indian Journal of Engineering & Materials Sciences,* **17,** 317-320.

Endo, M., Kim, Y. A., Hayashi, T., Nishimura, K., Matusita, T., Miyashita, K. & Dresselhaus, M. S. (2001) Vapor-grown carbon fibers (VGCFs): Basic properties and their battery applications. *Carbon,* **39,** 1287-1297.

Esquivel, E. V. & Murr, L. E. (2004) A TEM analysis of nanoparticulates in a Polar ice core. *Materials Characterization,* **52,** 15-25.

Evans, M. J., Cabral, L. J., Stephens, R. J. & Freeman, G. (1973) Cell division of alveolar macrophages in rat lung following exposure to NO2. *The American journal of pathology,* **70,** 199-208.

Fan, Z.-J., Wang, Y., Luo, G.-H., Li, Z.-F. & Wei, F. (2008) The synergetic effect of carbon nanotubes and carbon black in a rubber system. *Carbon,* **46,** 3.

Faux, S. P., Houghton, C. E., Hubbard, A. & Patrick, G. (2000) Increased expression of epidermal growth factor receptor in rat pleural mesothelial cells correlates with carcinogenicity of mineral fibres. *Carcinogenesis,* **21,** 2275-2280.

Fenoglio, I., Greco, G., Tomatis, M., Muller, J., Raymundo-PinÌƒero, E., BeÌ• guin, F. o., Fonseca, A., Nagy, J. B., Lison, D. & Fubini, B. (2008) Structural Defects Play a Major Role in the Acute Lung Toxicity of Multiwall Carbon Nanotubes: Physicochemical Aspects. *Chemical Research in Toxicology,* **21,** 1690-1697.

Ferin, J., Oberdörster, G. & Penney, D. P. (1992) Pulmonary retention of ultrafine and fine particles in rats. *Am J Respir Cell Mol Biol,* **6,** 535-542.

Ferrara, N. & Davis-Smyth, T. (1997) The Biology of Vascular Endothelial Growth Factor. *Endocr Rev,* **18,** 4-25.

Fialkow, L., Wang, Y. & Downey, G. P. (2007) Reactive oxygen and nitrogen species as signaling molecules regulating neutrophil function. *Free Radical Biology and Medicine,* **42,** 153-164.

Fiorito, S., Serafino, A., Andreola, F. & Bernier, P. (2006) Effects of fullerenes and single-wall carbon nanotubes on murine and human macrophages. *Carbon,* **44,** 1100-1105.

Fisher, C. E., G. Rossi, A., Shaw, J., Beswick, P. H. & Donaldson, K. (2000) Release of TNF[alpha] in response to SiC fibres: differential effects in rodent and human primary macrophages, and in macrophage-like cell lines. *Toxicology in Vitro,* **14,** 25-31.

Folkmann, J., Risom, L., Jacobsen, N., Wallin, H., Loft, S. & Møller, P. (2009) Oxidatively damaged DNA in rats exposed by oral gavage to C60 fullerenes and single-walled carbon nanotubes. *Environ Health Perspect.,* **117,** 703-708.

Foucaud, L., Wilson, M. R., Brown, D. M. & Stone, V. (2007) Measurement of reactive species production by nanoparticles prepared in biologically relevant media. *Toxicology Letters,* **174,** 1-9.

Fubini, B. & Otero Arean, C. (1999) Chemical aspects of the toxicity of inhaled mineral dusts. *Chemical Society Reviews,* **28**.

Fung, H., Kow, Y. W., Van Houten, B. & Mossman, B. T. (1997) Patterns of 8-hydroxydeoxyguanosine formation in DNA and indications of oxidative stress in rat and human pleural mesothelial cells after exposure to crocidolite asbestos. *Carcinogenesis,* **18,** 825-832.

Gao, N., Keane, M. J., Ong, T., Ye, J., Miller, W. E. & Wallace, W. E. (2001) Effects of Phospholipid Surfactant on Apoptosis Induction by Respirable Quartz and Kaolin in NR8383 Rat Pulmonary Macrophages. *Toxicology and Applied Pharmacology,* **175,** 217-225.

Gardiner, K., Hale, K. A., Calvert, I. A., Rice, C. & Harrington, J. M. (1992) The suitability of the urinary metabolite 1-hydroxypyrene as an index of poly nuclear aromatic hydrocarbon bioavailability from workers exposed to carbon black. *Annals of Occupational Hygiene,* **36,** 681-688.

Gardiner, K., Tongeren, M. v. & Harrington, M. (2001) Respiratory health effects from exposure to carbon black: results of the phase 2 and 3 cross sectional studies in the European carbon black manufacturing industry. *Occup Environ Med.,* **58,** 496–503.

Gauldie, J., Jordana, M. & Cox, G. (1993) Cytokines and pulmonary fibrosis. *Thorax,* **48,** 931-935.

Geiser, M., Rothen-Rutishauser, B., Kapp, N., Schurch, S., Kreyling, W., Schulz, H., Semmler, M., Hof, V. I., Heyder, J. & Gehr, P. (2005) Ultrafine Particles Cross Cellular Membranes by Nonphagocytic Mechanisms in Lungs and in Cultured Cells. National Institute of Environmental Health Sciences.

Gerhardt, H., Golding, M., Fruttiger, M., Ruhrberg, C., Lundkvist, A., Abramsson, A., Jeltsch, M., Mitchell, C., Alitalo, K., Shima, D. & Betsholtz, C. (2003) VEGF guides angiogenic sprouting utilizing endothelial tip cell filopodia. *The Journal of Cell Biology,* **161,** 1163-1177.

Germano, G., Allavena, P. & Mantovani, A. (2008) Cytokines as a key component of cancer-related inflammation. *Cytokine,* **43,** 374-379.

Gerritsen, J. (2000) Series: Basic Sciences: Host defence mechanisms of the respiratory system. *Paediatric Respiratory Reviews,* **1,** 128-134.

Ghilardi, G., Biondi, M. L., La Torre, A., Battaglioli, L. & Scorza, R. (2005) Breast Cancer Progression and Host Polymorphisms in the Chemokine System: Role of the Macrophage Chemoattractant Protein-1 (MCP-1) −2518 G Allele. *Clinical Chemistry,* **51,** 452-455.

Ghio, A. J., Stonehuerner, J., Steele, M. P. & Crumbliss, A. L. (1994) Phagocyte-Generated Superoxide Reduces Fe3+ to Displace It from the Surface of Asbestos. *Archives of Biochemistry and Biophysics,* **315,** 219-225.

Gilberti, R. M., Joshi, G. N. & Knecht, D. A. (2008) The Phagocytosis of Crystalline Silica Particles by Macrophages. *Am J Respir Cell Mol Biol,* **39,** 619–627.

Gilmour, P., Brown, D. M., Beswick, P. H., MacNee, W., Rahman, I. & K., D. (1997) Free radical activity of industrial fibers: role of iron in oxidative stress and activation of transcription factors. *Environ Health Perspect,* **105,** 1313-1317.

Gilmour, P., Ziesenis, A., Morrison, E., Vickers, M., Drost, E., Ford, I., Karg, E., Mossa, C., Schroeppel, A., Ferron, G., Heyder, J., Greaves, M., MacNee, W. & Donaldson, K. (2004) Pulmonary and systemic effects of short-term inhalation exposure to ultrafine carbon black particles. *Toxicol Appl Pharmacol,* **195,** 35-44.

Gilmour, P. S., Beswick, P. H., Brown, D. M. & Donaldson, K. (1995) Detection of surface free radical activity of respirable industrial fibres using supercoiled Ï†X174 RF1 plasmid DNA. *Carcinogenesis,* **16,** 2973-2979.

Giorgio, M. L. D., Di Bucchianico, S., Ragnelli, A. M., Aimola, P., Santucci, S. & Poma, A. (2011) Effects of single- and multi-walled carbon nanotubes on macrophages: cytotoxicity, genotoxicity and ultrastructural damage. *Mutation Research/Genetic Toxicology and Environmental Mutagenesis,* **In Press, Accepted Manuscript**.

Gjomarkaj, M., Pace, E., Melis, M., Spatafora, M., Profita, M., Vignola, A. M., Bonsignore, G. & Toews, G. B. (1999) Phenotypic and Functional Characterization of Normal Rat Pleural Macrophages in Comparison with Autologous Peritoneal and Alveolar Macrophages. *Am. J. Respir. Cell Mol. Biol.,* **20,** 135-142.

Goodglick, L. & Kane, A. (1986) Role of reactive oxygen metabolites in crocidolite asbestos toxicity to mouse macrophages. *Cancer Res,* **46,** 5558-5566.

Graham, A., Higinbotham, J., Allan, D., Donaldson, K. & Beswick, P. H. (1999) Chemical differences between long and short amosite asbestos: differences in oxidation state and coordination sites of iron, detected by infrared spectroscopy. *Occupational & Environmental Medicine,* **56,** 606-611.

Gretzer, C., Gisselfält, K., Liljensten, E., Rydén, L. & Thomsen, P. (2003) Adhesion, apoptosis and cytokine release of human mononuclear cells

cultured on degradable poly(urethane urea), polystyrene and titanium in vitro. *Biomaterials,* **24,** 2843-2852.

Griffioen, A. W. & Molema, G. (2000) Angiogenesis: Potentials for Pharmacologic Intervention in the Treatment of Cancer, Cardiovascular Diseases, and Chronic Inflammation. *Pharmacological Reviews,* **52,** 237-268.

Griffith, D. E., Miller, E. J., Gray, L. D., Idell, S. & Johnson, A. R. (1994) Interleukin-1-mediated release of interleukin-8 by asbestos-stimulated human pleural mesothelial cells. *Am. J. Respir. Cell Mol. Biol.,* **10,** 245-252.

Groß, O., Yazdi, Amir S., Thomas, Christina J., Masin, M., Heinz, Leonhard X., Guarda, G., Quadroni, M., Drexler, Stefan K. & Tschopp, J. (2012) Inflammasome Activators Induce Interleukin-1α Secretion via Distinct Pathways with Differential Requirement for the Protease Function of Caspase-1. *Immunity,* **36,** 388-400.

Guichard, Y., Gaté, L., Darne, C., Bottin, M.-C., Langlais, C., Micillino, J.-C., Goutet, M., Julien, S. & Stephane, B. (2010) In Vitro Study of Mutagenesis Induced by Crocidolite-Exposed Alveolar Macrophages NR8383 in Cocultured Big Blue Rat2 Embryonic Fibroblasts. *Journal of Toxicology***,** 1-11.

Guo, L., Morris, D. G., Liu, X., Vaslet, C., Hurt, R. H. & Kane, A. B. (2007a) Iron Bioavailability and Redox Activity in Diverse Carbon Nanotube Samples. *Chemistry of Materials,* **19,** 3472-3478.

Guo, L., Morris, D. G., Liu, X., Vaslet, C., Hurt, R. H. & Kane, A. B. (2007b) Iron Bioavailability and Redox Activity in Diverse Carbon Nanotube Samples. *Chem. Mater.,* **19,** 3472-3478.

Haegens, A., van der Vliet, A., Butnor, K. J., Heintz, N., Taatjes, D., Hemenway, D., Vacek, P., Freeman, B. A., Hazen, S. L., Brennan, M. L. & Mossman, B. T. (2005) Asbestos-Induced Lung Inflammation and Epithelial Cell Proliferation Are Altered in Myeloperoxidase-Null Mice. *Cancer Research,* **65,** 9670-9677.

Halliwell, B. & Gutteridge, J. M. C. (2007) *Free radicals in biology and medicine,* New York, Oxford University Press.

Hamilton, R., Wu, N., Porter, D., Buford, M., Wolfarth, M. & Holian, A. (2009) Particle length-dependent titanium dioxide nanomaterials toxicity and bioactivity. *Particle and Fibre Toxicology,* **6,** 35.

Hampton, M. B., Kettle, A. J. & Winterbourn, C. C. (1998) Inside the Neutrophil Phagosome: Oxidants, Myeloperoxidase, and Bacterial Killing. *Blood,* **92,** 3007-3017.

Han, M., Ye, S., Wen, W. & Zhang, Q. (2010) Oxidative stress-mediated pro-inflammatory responses in lung epithelial cells exposed to multiwalled carbon nanotubes. *Bioinformatics and Biomedical Engineering (iCBBE), 2010 4th International Conference***,** 1-4.

Hansen, K. & Mossman, B. (1987) Generation of superoxide (O2-.) from alveolar macrophages exposed to asbestiform and nonfibrous particles. *Cancer Res,* **47,** 1681-1686.

Hasegawa, Sato & Takehara (1999) Augmented production of chemokines (monocyte chemotactic protein-1 (MCP-1), macrophage inflammatory protein-1α (MIP-1α) and MIP-1β) in patients with systemic sclerosis: MCP-1 and MIP-1α may be involved in the development of pulmonary fibrosis. *Clinical & Experimental Immunology,* **117,** 159-165.

Hasegawa, H., Suzuki, K., Nakaji, S. & Sugawara, K. (1997a) Analysis and assessment of the capacity of neutrophils to produce reactive oxygen species in a 96-well microplate format using lucigenin- and luminol-dependent chemiluminescence. *Journal of Immunological Methods,* **210,** 1-10.

Hasegawa, T., Sorensen, L., Dohi, M., Rao, N. V., Hoidal, J. R. & Marshall, B. C. (1997b) Induction of urokinase-type plasminogen activator receptor by IL-1 beta. *Am. J. Respir. Cell Mol. Biol.,* **16,** 683-692.

Heinrich, U., Fuhst, R., Rittinghausen, S., Creutzenberg, O., Bellmann, B., Koch, W. & Levsen, K. (1995) Chronic Inhalation Exposure of Wistar Rats and two Different Strains of Mice to Diesel Engine Exhaust, Carbon Black, and Titanium Dioxide. *Inhalation Toxicology,* **7,** 533-556.

Hemraj-Benny, T., Bandosz, T. J. & Wong, S. S. (2008) Effect of ozonolysis on the pore structure, surface chemistry, and bundling of single-walled carbon nanotubes. *Journal of Colloid and Interface Science,* **317,** 375-382.

Hill, I. M., Beswick, P. H. & Donaldson, K. (1995) Differential release of superoxide anions by macrophages treated with long and short fibre amosite asbestos is a consequence of differential affinity for opsonin. *Occupational and Environmental Medicine,* **52,** 92-96.

Hirano, S., Fujitani, Y., Furuyama, A. & Kanno, S. (2010) Uptake and cytotoxic effects of multi-walled carbon nanotubes in human bronchial epithelial cells. *Toxicology and Applied Pharmacology,* **249,** 8-15.

Hirano, S., Kanno, S. & Furuyama, A. (2008) Multi-walled carbon nanotubes injure the plasma membrane of macrophages. *Toxicology and Applied Pharmacology,* **232,** 244-251.

Hornung, V., Bauernfeind, F., Halle, A., Samstad, E. O., Kono, H., Rock, K. L., Fitzgerald, K. A. & Latz, E. (2008) Silica crystals and aluminum salts activate the NALP3 inflammasome through phagosomal destabilization. *Nat Immunol,* **9,** 847-856.

Hu, X., Cook, S., Wang, P., Hwang, H.-m., Liu, X. & Williams, Q. L. (2010) In vitro evaluation of cytotoxicity of engineered carbon nanotubes in selected human cell lines. *Science of The Total Environment,* **408,** 1812-1817.

Huang, H., Kajiura, H., Yamada, A. & Ata, M. (2002) Purification and alignment of arc-synthesis single-walled carbon nanotube bundles. *Chemical Physics Letters,* **356,** 567-572.

Iijima, S. (1991) Helical microtubules of graphitic carbon. *Nature Materials,* **354,** 56-58.

Ischiropoulos, H., Zhu, L. & Beckman, J. S. (1992) Peroxynitrite formation from macrophage-derived nitric oxide. *Archives of Biochemistry and Biophysics,* **298,** 446-451.

Ishiyama, M., Tominaga, H., Shiga, M., Sasamoto, K., Ohkura, Y., Ueno, K. & Watanabe, M. (1995) Novel cell proliferation and cytotoxicity assays using a tetrazolium salt that produces a water-soluble formazan dye. *In vitro toxicology,* **8,** 187-190.

Ito, T., Ikeda, M., Yamasaki, H., Sagai, M. & Tomita, T. (2000) Peroxynitrite formation by diesel exhaust particles in alveolar cells: Links to pulmonary inflammation. *Environmental Toxicology and Pharmacology,* **9,** 1-8.

Iwai, K., Adachi, S., Takahashi, M., Möller, L., Udagawa, T., Mizuno, S. & Sugawara, I. (2000) Early Oxidative DNA Damages and Late

Development of Lung Cancer in Diesel Exhaust-Exposed Rats. *Environmental Research,* **84,** 255-264.

Iwai, K., Hirata, K.-i., Ishida, T., Takeuchi, S., Hirase, T., Rikitake, Y., Kojima, Y., Inoue, N., Kawashima, S. & Yokoyama, M. (2004) An anti-proliferative gene BTG1 regulates angiogenesis in vitro. *Biochemical and Biophysical Research Communications,* **316,** 628-635.

Jacobsen, N., Moller, P., Jensen, K., Vogel, U., Ladefoged, O., Loft, S. & Wallin, H. (2009) Lung inflammation and genotoxicity following pulmonary exposure to nanoparticles in ApoE-/- mice. *Particle and Fibre Toxicology,* **6,** 2.

Jahanshahi, M., Sanati, M. H., Minuchehr, Z., Hajizadeh, S. & Babaei, Z. (2007) Controlled Fabrication of Gelatin Nanoparticles as Drug Carriers. *AIP Conference Proceedings,* **929,** 228-232.

Jain, K. (2005) Nanotechnology in clinical laboratory diagnostics. *Clinica Chimica Acta,* **358,** 37-54.

Janssen, Y. M., Barchowsky, A., Treadwell, M., Driscoll, K. E. & Mossman, B. T. (1995) Asbestos induces nuclear factor kappa B (NF-kappa B) DNA-binding activity and NF-kappa B-dependent gene expression in tracheal epithelial cells. *Proceedings of the National Academy of Sciences of the United States of America,* **92,** 8458-8462.

Jaurand, M. C., Gaudichet, A., Halpern, S. & Bignon, J. (1984) In vitro biodegradation of chrysotile fibres by alveolar macrophages and mesothelial cells in culture: comparison with a pH effect. *British Journal of Industrial Medicine,* **41,** 389-395.

Jeong, T., Kim, W.-Y. & Hahn, Y.-B. (2001) A new purification method of single-wall carbon nanotubes using H2S and O2 mixture gas. *Chemical Physics Letters,* **344,** 18-22.

Jia, G., Wang, H., Yan, L., Wang, X., Pei, R., Yan, T., Zhao, Y. & Guo, X. (2005) Cytotoxicity of Carbon Nanomaterials: Single-Wall Nanotube, Multi-Wall Nanotube, and Fullerene. *Environmental Science and Technology,* **39,** 1378 - 1383.

Jiang, J., Oberdörster, G. & Biswas, P. (2009) Characterization of size, surface charge, and agglomeration state of nanoparticle dispersions for toxicological studies. *Journal of Nanoparticle Research,* **11,** 77-89.

Jimenez, L. A., Zanella, C., Fung, H., Janssen, Y. M. W., Vacek, P., Charland, C., Goldberg, J. & Mossman, B. T. (1997) Role of extracellular signal-regulated protein kinases in apoptosis by asbestos and H2O2. *American Journal of Physiology - Lung Cellular and Molecular Physiology,* **273,** L1029-L1035.

Johnston, J. R. B., Godzik, C. A. & Cohn, Z. A. (1978) Increased superoxide anion production by immunologically activated and chemically elicited macrophages. *The Journal of Experimental Medicine,* **148,** 115-129.

Johnston, R. B., Keele, B. B., Misra, H. P., Lehmeyer, J. E., Webb, L. S., Baehner, R. L. & RaJagopalan, K. V. (1975) The role of superoxide anion generation in phagocytic bactericidal activity. Studies with normal and chronic granulomatous disease leukocytes. *The Journal of Clinical Investigation,* **55,** 1357-1372.

Jones, M. K., Sarfeh, I. J. & Tarnawski, A. S. (1998) Induction ofin VitroAngiogenesis in the Endothelial-Derived Cell Line, EA hy926, by Ethanol Is Mediated through PKC and MAPK. *Biochemical and Biophysical Research Communications,* **249,** 118-123.

Jones, M. K., Wang, H., Peskar, B. M., Levin, E., Itani, R. M., Sarfeh, I. J. & Tarnawski, A. S. (1999) Inhibition of angiogenesis by nonsteroidal anti-inflammatory drugs: insight into mechanisms and implications for cancer growth and ulcer healing. *Nature medicine,* **5,** 1418-1423.

Jozefowski, S. & Kobzik, L. (2004) Scavenger receptor A mediates H2O2 production and suppression of IL-12 release in murine macrophages. *Journal of Leukocyte Biology,* **76,** 1066-1074.

Jugan, M.-L., Barillet, S., Simon-Deckers, A., Herlin-Boime, N., Sauvaigo, S., Douki, T. & Carriere, M. (2011) Titanium dioxide nanoparticles exhibit genotoxicity and impair DNA repair activity in A549 cells. *Nanotoxicology,* **0,** 1-13.

Kagan, V. E., Konduru, N. V., Feng, W., Allen, B. L., Conroy, J., Volkov, Y., Vlasova, I. I., Belikova, N. A., Yanamala, N., Kapralov, A., Tyurina, Y. Y., Shi, J., Kisin, E. R., Murray, A. R., Franks, J., Stolz, D., Gou, P., Klein-Seetharaman, J., Fadeel, B., Star, A. & Shvedova, A. A. (2010) Carbon nanotubes degraded by neutrophil myeloperoxidase induce less pulmonary inflammation. *Nat Nano,* **5,** 354-359.

Kagan, V. E., Tyurina, Y. Y., Tyurin, V. A., Konduru, N. V., Potapovich, A. I., Osipov, A. N., Kisin, E. R., Schwegler-Berry, D., Mercer, R., Castranova, V. & Shvedova, A. A. (2006) Direct and indirect effects of single walled carbon nanotubes on RAW 264.7 macrophages: Role of iron. *Toxicology Letters,* **165,** 88-100.

Kalbacova, M., Kalbac, M., Dunsch, L., Kataura, H. & Hempel, U. (2006) The study of the interaction of human mesenchymal stem cells and monocytes/macrophages with single-walled carbon nanotube films. *physica status solidi (b),* **243,** 3514-3518.

Kam, N. W. S., O'Connell, M., Wisdom, J. A. & Dai, H. (2005) Carbon Nanotubes as multifunctional biological transporters and near-infrared agents for selective cancer cell destruction. *Proceedings of the National Academies of Science,* **102,** 11600 - 11605.

Kamp, D. W. & Weitzman, S. A. (1999) The molecular basis of asbestos induced lung injury. *Thorax,* **54,** 638-652.

Kannan, K. & Jain, S. K. (2000) Oxidative stress and apoptosis. *Pathophysiology,* **7,** 153-163.

Karlsson, H. L., Cronholm, P., Gustafsson, J. & Moller, L. (2008) Copper Oxide Nanoparticles Are Highly Toxic: A Comparison between Metal Oxide Nanoparticles and Carbon Nanotubes. *Chemical Research in Toxicology,* **21,** 1726-1732.

Karp, G. (2002) Cell and Molecular Biology Concepts and Experiments (3rd Ed.). *John Wiley & Sons, Inc., New York*.

Kastner, J., Pichler, T., Kuzmany, H., Curran, S., Blau, W., Weldon, D. N., Delamesiere, M., Draper, S. & Zandbergen, H. (1994) Resonance Raman and infrared spectroscopy of carbon nanotubes. *Chemical Physics Letters,* **221,** 53-58.

Katsabeki-Katsafli, A., Kerenidi, T., Kostikas, K., Dalaveris, E., Kiropoulos, T. S., Gogou, E., Papaioannou, A. I. & Gourgoulianis, K. I. (2008) Serum vascular endothelial growth factor is related to systemic oxidative stress in patients with lung cancer. *Lung cancer (Amsterdam, Netherlands),* **60,** 271-276.

Kelly, F. J. (1999) Gluthathione: in Defence of the Lung. *Food and Chemical Toxicology,* **37,** 963-966.

Kerber, M., Reiss, Y., Wickersheim, A., Jugold, M., Kiessling, F., Heil, M., Tchaikovski, V., Waltenberger, J., Shibuya, M., Plate, K. H. & Machein, M. R. (2008) Flt-1 Signaling in Macrophages Promotes Glioma Growth In vivo. *Cancer Research,* **68,** 7342-7351.

Keston, A. S. & Brandt, R. (1965) The fluorometric analysis of ultramicro quantities of hydrogen peroxide. *Analytical Biochemistry,* **11,** 1-5.

Kim, H.-N., Morimoto, Y., Tsuda, T., Ootsuyama, Y., Hirohashi, M., Hirano, T., Tanaka, I., Lim, Y., Yun, I.-G. & Kasai, H. (2001) Changes in DNA 8-hydroxyguanine levels, 8-hydroxyguanine repair activity, and hOGG1 and hMTH1 mRNA expression in human lung alveolar epithelial cells induced by crocidolite asbestos. *Carcinogenesis,* **22,** 265-269.

Kim, J.-E., Lim, H.-T., Minai-Tehrani, A., Kwon, J.-T., Shin, J.-Y., Woo, C.-G., Choi, M., Baek, J., Jeong, D. H., Ha, Y.-C., Chae, C.-H., Song, K.-S., Ahn, K.-H., Lee, J.-H., Sung, H.-J., Yu, I.-J., Beck, G. R. & Cho, M.-H. (2010a) Toxicity and Clearance of Intratracheally Administered Multiwalled Carbon Nanotubes from Murine Lung. *Journal of Toxicology and Environmental Health, Part A: Current Issues,* **73,** 1530 - 1543.

Kim, J. S., Song, K. S., Joo, H. J., Lee, J. H. & Yu, I. J. (2010b) Determination of Cytotoxicity Attributed to Multiwall Carbon Nanotubes (MWCNT) in Normal Human Embryonic Lung Cell (WI-38) Line. *Journal of Toxicology and Environmental Health, Part A: Current Issues,* **73,** 1521 - 1529.

Kingma, P. S. & Whitsett, J. A. (2006) In defense of the lung: surfactant protein A and surfactant protein D. *Current Opinion in Pharmacology,* **6,** 277-283.

Kinloch, I. A., Chen, G. Z., Howes, J., Boothroyd, C., Singh, C., Fray, D. J. & Windle, A. H. (2003) Electrolytic, TEM and Raman studies on the production of carbon nanotubes in molten NaCl. *Carbon,* **41,** 1127-1141.

Kinnula, V. L., Aalto, K., Raivio, K. O., Walles, S. & Linnainmaa, K. (1994) Cytotoxicity of oxidants and asbestos fibers in cultured human mesothelial cells. *Free Radical Biology and Medicine,* **16,** 169-176.

Kinnula, V. L., Linnala, A., Viitala, E., Linnainmaa, K. & Virtanen, I. (1998) Tenascin and Fibronectin Expression in Human Mesothelial Cells and Pleural Mesothelioma Cell-Line Cells. *Am. J. Respir. Cell Mol. Biol.,* **19,** 445-452.

Kisin, E. R., Murray, A. R., Keane, M. J., Shi, X.-C., Schwegler-Berry, D., Gorelik, O., Arepalli, S., Castranova, V., Wallace, W. E., Kagan, V. E. & Shvedova, A. A. (2007) Single-walled Carbon Nanotubes: Geno- and Cytotoxic Effects in Lung Fibroblast V79 Cells. *Journal of Toxicology and Environmental Health, Part A,* **70,** 2071-2079.

Kloen, P., Gebhardt, M. C., Perez-Atayde, A., Rosenberg, A. E., Springfield, D. S., Gold, L. I. & Mankin, H. J. (1997) Expression of transforming growth factor-β (TGF-β) isoforms in osteosarcomas. *Cancer,* **80,** 2230-2239.

Kobayashi, N., Naya, M., Ema, M., Endoh, S., Maru, J., Mizuno, K. & Nakanishi, J. (2010) Biological response and morphological assessment of individually dispersed multi-wall carbon nanotubes in the lung after intratracheal instillation in rats. *Toxicology,* **276,** 143-153.

Koo, O. M., Rubinstein, I. & Onyuksel, H. (2005) Role of nanotechnology in targeted drug delivery and imaging: a concise review. *Nanomedicine: Nanotechnology, Biology and Medicine,* **1,** 193-212.

Koziol, K., Vilatela, J., Moisala, A., Motta, M., Cunniff, P., Sennett, M. & Windle, A. (2007) High-Performance Carbon Nanotube Fiber. *Science,* **318,** 1892-1895.

Kreyling, W. G., Semmler, M., Erbe, F., Mayer, P., Takenaka, S., Schulz, H., Oberdorster, G. & Ziesenis, A. (2002) Translocation of ultrafine insoluble iridium particles from lung epithelium to extrapulmonary organs is size dependent but very low. *J Toxicol Environ Health A,* **65,** 1513-1530.

Kruger, E. A., Duray, P. H., Tsokos, M. G., Venzon, D. J., Libutti, S. K., Dixon, S. C., Rudek, M. A., Pluda, J., Allegra, C. & Figg, W. D. (2000) Endostatin Inhibits Microvessel Formation in the ex Vivo Rat Aortic Ring Angiogenesis Assay. *Biochemical and Biophysical Research Communications,* **268,** 183-191.

Kusaba, M. & Tsunawaki, Y. (2006) Production of single-wall carbon nanotubes by a XeCl excimer laser ablation. *Thin Solid Films,* **506-507,** 255-258.

Kutty, R. K., Kutty, G., Nagineni, C. N., Hooks, J. J., Chader, G. J. & Wiggert, B. (1994) RT-PCR Assay for Heme Oxygenase-1 and Heme Oxygenase-2: A Sensitive Method to Estimate Cellular Oxidative Damage. *Annals of the New York Academy of Sciences,* **738,** 427-430.

Kwon, J. T., Hwang, S. K., Jin, H., Kim, D. S., Minai-Tehrani, A., Yoon, H. J., Choi, M., Yoon, T. J., Han, D. Y., Kang, Y. W., Yoon, B. I., Lee, J. K. & Cho, M. H. (2008) Body distribution of inhaled fluorescent magnetic nanoparticles in the mice. *J Occup Health,* **50,** 1-6.

Kwong, K. Y., Niang, S., Literat, A., Zhu, N. L., Ramanathan, R., Jones, C. A. & Minoo, P. (2006) Expression of transforming growth factor beta (TGF-b1) by human preterm lung inflammatory cells. *Life Sciences,* **79,** 2349-2356.

Lakin, N. D. & Jackson, S. P. (1999) Regulation of p53 in response to DNA damage. *Oncogene,* **18,** 7644-7655.

Lam, C. W., James, J. T., McCluskey, R., Arepalli, S. & Hunter, R. L. (2006) A Review of Carbon Nanotube Toxicity and Assessment of Potential Occupational and Environmental Health Risks. *Critical Reviews in Toxicology,* **36,** 189 - 217.

Lam, C. W., James, J. T., McCluskey, R. & Hunter, R. L. (2004a) Pulmonary toxicity of single-wall carbon nanotubes in mice 7 and 90 days after intratracheal instillation. *Toxicol Sci,* **77,** 126-134.

Lam, C. W., James, J. T., McCluskey, R. & Hunter, R. L. (2004b) Pulmonary toxicity of single-wall carbon nanotubes in mice 7 and 90 days after intratracheal instillation. *Toxicol Sci,* **77,** 126-134.

Lawrence, D. A. (2001) Latent-TGF-β: An overview. *Molecular and Cellular Biochemistry,* **219,** 163-170.

Lee, B. I., Qi, L. & Copeland, T. (2005) Nanoparticles for materials design: present & future. *Journal of Ceramic Processing Research,* **6,** 31-40.

Lee, W. L., Harrison, R. E. & Grinstein, S. (2003) Phagocytosis by neutrophils. *Microbes and Infection,* **5,** 1299-1306.

Lee, Y. C. G., Melkerneker, D. E. E., Thompson, P. J., Light, R. W. & Lane, K. B. (2002) Transforming Growth Factor beta Induces Vascular Endothelial Growth Factor Elaboration from Pleural Mesothelial Cells in Vivo and in Vitro. *Am. J. Respir. Crit. Care Med.,* **165,** 88-94.

LeVine, A. M. & Whitsett, J. A. (2001) Pulmonary collectins and innate host defense of the lung. *Microbes and Infection,* **3,** 161-166.

Li, N., Xia, T. & Nel, A. E. (2008) The role of oxidative stress in ambient particulate matter-induced lung diseases and its implications in the toxicity of engineered nanoparticles. *Free Radical Biology and Medicine,* **44,** 1689-1699.

Li, X., Peng, Y., Ren, J. & Qu, X. (2006) Carboxyl-modified single-walled carbon nanotubes selectively induce human telomeric i-motif formation. *Proceedings of the National Academy of Sciences,* **103,** 19658-19663.

Li, Y.-H., Wang, S., Cao, A., Zhao, D., Zhang, X., Xu, C., Luan, Z., Ruan, D., Liang, J., Wu, D. & Wei, B. (2001) Adsorption of fluoride from water by amorphous alumina supported on carbon nanotubes. *Chemical Physics Letters,* **350,** 412-416.

Li, Y.-L., Kinloch, I. A., Shaffer, M. S. P., Geng, J., Johnson, B. & Windle, A. H. (2004a) Synthesis of single-walled carbon nanotubes by a fluidized-bed method. *Chemical Physics Letters,* **384,** 98-102.

Li, Y.-L., Kinloch, I. A. & Windle, A. H. (2004b) Direct Spinning of Carbon Nanotube Fibers from Chemical Vapor Deposition Synthesis. *Science,* **304,** 276-278.

Li, Y., Stansbury, K. H., Zhu, H. & Trush, M. A. (1999) Biochemical Characterization of Lucigenin (Bis-N-methylacridinium) as a Chemiluminescent Probe for Detecting Intramitochondrial Superoxide Anion Radical Production. *Biochemical and Biophysical Research Communications,* **262,** 80-87.

Li, Z., Hulderman, T., Salmen, R., Chapman, R., Leonard, S. S., Young, S. H., Shvedova, A., Luster, M. I. & Simeonova, P. P. (2007) Cardiovascular effects of pulmonary exposure to single-wall carbon nanotubes. *Environ Health Perspect,* **115,** 377-382.

Light, W. G. & Wei, E. T. (1977) Surface charge and asbestos toxicity. *Nature,* **265,** 537-539.

Lin, W.-W. & Karin, M. (2007) A cytokine-mediated link between innate immunity, inflammation, and cancer. *The Journal of Clinical Investigation,* **117,** 1175-1183.

Lindberg, H. K., Falck, G. C. M., Suhonen, S., Vippola, M., Vanhala, E., Catalán, J., Savolainen, K. & Norppa, H. (2009) Genotoxicity of nanomaterials: DNA damage and micronuclei induced by carbon nanotubes and graphite nanofibres in human bronchial epithelial cells in vitro. *Toxicology Letters,* **186,** 166-173.

Liu, X., Hurt, R. H. & Kane, A. B. (2010) Biodurability of single-walled carbon nanotubes depends on surface functionalization. *Carbon,* **48,** 1961-1969.

Liu, Y. & Gao, L. (2005) A study of the electrical properties of carbon nanotube-NiFe2O4 composites: Effect of the surface treatment of the carbon nanotubes. *Carbon,* **43,** 47-52.

Liu, Y., Wu, D. C., Zhang, W. D., Jiang, X., He, C. B., Chung, T. S., Goh, S. H. & Leong, K. W. (2005) Polyethylenimine-grafted multiwalled carbon nanotubes for secure noncovalent immobilization and efficient delivery of DNA. *Angew Chem Int Ed Engl,* **44,** 4782-4785.

Lu, Y., Cai, Z., Galson, D. L., Xiao, G., Liu, Y., George, D. E., Melhem, M. F., Yao, Z. & Zhang, J. (2006) Monocyte chemotactic protein-1 (MCP-1) acts as a paracrine and autocrine factor for prostate cancer growth and invasion. *The Prostate,* **66,** 1311-1318.

Luoto, K., Holopainen, M. & Savolainen, K. (1994) Scanning Electron Microscopic Study on the Changes in the Cell Surface Morphology of Rat Alveolar Macrophages After Their Exposure to Man-Made Vitreous Fibers. *Environmental Research,* **66,** 198-207.

Luster, M. I. & Simeonova, P. P. (1998) Asbestos induces inflammatory cytokines in the lung through redox sensitive transcription factors. *Toxicology Letters,* **102-103,** 271-275.

Ma-Hock, L., Treumann, S., Strauss, V., Brill, S., Luizi, F., Mertler, M., Wiench, K., Gamer, A. O., van Ravenzwaay, B. & Landsiedel, R. (2009) Inhalation Toxicity of Multiwall Carbon Nanotubes in Rats Exposed for 3 Months. *Toxicological Sciences,* **112,** 468-481.

Ma, J., Wang, Q., Fei, T., Han, J. D. & Chen, Y. G. (2007) MCP-1 mediates TGF-beta-induced angiogenesis by stimulating vascular smooth muscle cell migration. *Blood,* **109,** 987-994.

MacNee, W. (2001) Oxidative stress and lung inflammation in airways disease. *European Journal of Pharmacology,* **429,** 195-207.

Magrez, A., Kasas, S., Salicio, V., Pasquier, N., Seo, J. W., Celio, M., Catsicas, S., Schwaller, B. & Forro, L. (2006) Cellular Toxicity of Carbon-Based Nanomaterials. *Nano Letters,* **6,** 1121-1125.

Mamalis, A. G. (2007) Recent advances in nanotechnology. *Journal of Materials Processing Technology,* **181,** 52-58.

Mangum, J., Turpin, E., Antao-Menezes, A., Cesta, M., Bermudez, E. & Bonner, J. (2006) Single-Walled Carbon Nanotube (SWCNT)-induced interstitial fibrosis in the lungs of rats is associated with increased levels of PDGF mRNA and the formation of unique intercellular carbon structures that bridge alveolar macrophages In Situ. *Particle and Fibre Toxicology,* **3,** 15.

Manning, C. B., Vallyathan, V. & Mossman, B. T. (2002) Diseases caused by asbestos: mechanisms of injury and disease development. *International Immunopharmacology,* **2,** 191-200.

Marchesi, E., Rota, C., Fann, Y. C., Chignell, C. F. & Mason, R. P. (1999) Photoreduction of the fluorescent dye 2'-7'-dichlorofluorescein: a spin trapping and direct electron spin resonance study with implications for oxidative stress measurements. *Free Radical Biology and Medicine,* **26,** 148-161.

Markovic, Z. M., Harhaji-Trajkovic, L. M., Todorovic-Markovic, B. M., Kepic, D. P., Arsikin, K. M., Jovanovic, S. P., Pantovic, A. C., Dramicanin, M. D. & Trajkovic, V. S. (2011) In vitro comparison of the photothermal anticancer activity of graphene nanoparticles and carbon nanotubes. *Biomaterials,* **32,** 1121-1129.

Martínez, C., Monsó, E. & Quero, A. (2004) Emerging Pleuropulmonary Diseases Associated With Asbestos Inhalation. *Archivos de Bronconeumologia,* **40,** 166-177.

Marzo, A. L., Fitzpatrick, D. R., Robinson, B. W. S. & Scott, B. (1997) Antisense Oligonucleotides Specific for Transforming Growth Factor Î²2 Inhibit the Growth of Malignant Mesothelioma Both in Vitro and in Vivo. *Cancer Research,* **57,** 3200-3207.

Masson, V., Devy, L., Grignet-Debrus, C., Bernt, S., Bajou, K., Blacher, S., Roland, G., Chang, Y., Fong, T., Carmeliet, P., Foidart, J.-M. & Noël, A. (2002) Mouse aortic ring assay: A new approach of the molecular genetics of angiogenesis. *Biological Procedures Online,* **4,** 24-31.

Mercer, R., Hubbs, A., Scabilloni, J., Wang, L., Battelli, L., Schwegler-Berry, D., Castranova, V. & Porter, D. (2010) Distribution and persistence of pleural penetrations by multi-walled carbon nanotubes. *Particle and Fibre Toxicology,* **7,** 28.

Mercer, R. R., Scabilloni, J., Wang, L., Kisin, E., Murray, A. R., Schwegler-Berry, D., Shvedova, A. A. & Castranova, V. (2008) Alteration of deposition pattern and pulmonary response as a result of improved

dispersion of aspirated single-walled carbon nanotubes in a mouse model. *Am J Physiol Lung Cell Mol Physiol,* **294,** L87-97.
Meunier, E., Coste, A., Olagnier, D., Authier, H., Lefèvre, L., Dardenne, C., Bernad, J., Béraud, M., Flahaut, E. & Pipy, B. (2011) Double-walled carbon nanotubes trigger IL-1β release in human monocytes through Nlrp3 inflammasome activation. *Nanomedicine: Nanotechnology, Biology and Medicine*.
Mevorach, D., Trahtemberg, U., Krispin, A., Attalah, M., Zazoun, J., Tabib, A., Grau, A. & Verbovetski-Reiner, I. (2010) What do we mean when we write "senescence,""apoptosis,""necrosis," or "clearance of dying cells"? *Annals of the New York Academy of Sciences,* **1209,** 1-9.
Migliore, L., Saracino, D., Bonelli, A., Colognato, R., D'Errico, M. R., Magrini, A., Bergamaschi, A. & Bergamaschi, E. (2010) Carbon nanotubes induce oxidative DNA damage in RAW 264.7 cells. *Environmental and Molecular Mutagenesis,* **51,** 294-303.
Miller, B. G., Searl, A., Davis, J. M. G., Donaldson, K., Cullen, R. T., Bolton, R. E., Buchanan, D. & Soutar, C. A. (1999) Influence of fibre length, dissolution and biopersistence on the production of mesothelioma in the rat peritoneal cavity. *Annals of Occupational Hygiene,* **43,** 155-166.
Misra, A., Tyagi, P. K., Singh, M. K. & Misra, D. S. (2006) FTIR studies of nitrogen doped carbon nanotubes. *Diamond and Related Materials,* **15,** 385-388.
Mitchell, L. A., Gao, J., Vander Wal, R., Gigliotti, A., Burchiel, S. W. & McDonald, J. D. (2007) Pulmonary and Systemic Immune Response to Inhaled Multiwalled Carbon Nanotubes. *Toxicol. Sci.,* **100,** 203-214.
Moisala, A., Nasibulin, A. G. & Kauppinen, E. I. (2004) The Role of Metal Nanoparticles in the Catalytic Production of Single-Walled Carbon Nanotubes — A Review. *ChemInform,* **35,** no-no.
Mongan, L. C., Jones, T. & Patrick, G. (2000) Cytokine and free radical responses of alveolar macrophages in vitro to asbestos fibres. *Cytokine,* **12,** 1243-1247.
Monteiro-Riviere, N. A., Nemanich, R. J., Inman, A. O., Wang, Y. Y. & Riviere, J. E. (2005) Multi-walled carbon nanotube interactions with human epidermal keratinocytes. *Toxicology Letters,* **155,** 377-384.
Montesano, R., Orci, L. & Vassalli, P. (1983) In vitro rapid organization of endothelial cells into capillary-like networks is promoted by collagen matrices. *The Journal of Cell Biology,* **97,** 1648-1652.
Moore, K. J., El Khoury, J., Medeiros, L. A., Terada, K., Geula, C., Luster, A. D. & Freeman, M. W. (2002) A CD36-initiated Signaling Cascade Mediates Inflammatory Effects of Î²-Amyloid. *Journal of Biological Chemistry,* **277,** 47373-47379.
Moreau, M. F., Guillet, C., Massin, P., Chevalier, S., Gascan, H., Baslé, M. F. & Chappard, D. (2007) Comparative effects of five bisphosphonates on apoptosis of macrophage cells in vitro. *Biochemical Pharmacology,* **73,** 718-723.
Morris, R. H. K., Price, A. J., Tonks, A., Jackson, S. K. & Jones, K. P. (2000) Prostaglandin E2 and tumour necrosis factor-[alpha] release by monocytes are modulated by phospholipids. *Cytokine,* **12,** 1717-1719.
Mossman, B., Borm, P., Castranova, V., Costa, D., Donaldson, K. & Kleeberger, S. (2007) Mechanisms of action of inhaled fibers, particles and nanoparticles in lung and cardiovascular diseases. *Particle and Fibre Toxicology,* **4,** 4.

Mossman, B. T., Bignon, J., Corn, M., Seaton, A. & Gee, J. B. (1990) Asbestos: scientific developments and implications for public policy. *Science,* **247,** 294-301.

Mossman, Brooke T. & Churg, A. (1998) Mechanisms in the Pathogenesis of Asbestosis and Silicosis. *Am. J. Respir. Crit. Care Med.,* **157,** 1666-1680.

Mossman, B. T., Faux, S., Janssen, Y., Jimenez, L. A., Timblin, C., Zanella, C., Goldberg, J., Walsh, E., Barchowsky, A. & Driscoll, K. (1997) Cell signaling pathways elicited by asbestos. *Environ Health Perspect,* **105,** 1121-1125.

Motta, M., Li, Kinloch, I. & Windle, A. (2005) Mechanical Properties of Continuously Spun Fibers of Carbon Nanotubes. *Nano Letters,* **5,** 1529-1533.

Muhle, H., Bellmann, B. & Pott, F. (1991) Durability of various mineral fibres in rat lungs. *Mechanisms in Fiber Carcinogenesis: Plenum Press, New York***,** 181-187.

Muller, J., Decordier, I., Hoet, P. H., Lombaert, N., Thomassen, L., Huaux, F., Lison, D. & Kirsch-Volders, M. (2008a) Clastogenic and aneugenic effects of multi-wall carbon nanotubes in epithelial cells. *Carcinogenesis,* **29,** 427-433.

Muller, J., Huaux, F., Moreau, N., Misson, P., Heilier, J.-F., Delos, M., Arras, M., Fonseca, A., Nagy, J. B. & Lison, D. (2005) Respiratory toxicity of multi-wall carbon nanotubes. *Toxicology and Applied Pharmacology,* **207,** 221-231.

Muller, J., Huaux, F. o., Fonseca, A., Nagy, J. B., Moreau, N., Delos, M., Raymundo-PinÌƒero, E., BeÌ• guin, F. o., Kirsch-Volders, M., Fenoglio, I., Fubini, B. & Lison, D. (2008b) Structural Defects Play a Major Role in the Acute Lung Toxicity of Multiwall Carbon Nanotubes: Toxicological Aspects. *Chemical Research in Toxicology,* **21,** 1698-1705.

Murphy, F. A., Poland, C. A., Duffin, R., Al-Jamal, K. T., Ali-Boucetta, H., Nunes, A., Byrne, F., Prina-Mello, A., Volkov, Y., Li, S., Mather, S. J., Bianco, A., Prato, M., MacNee, W., Wallace, W. A., Kostarelos, K. & Donaldson, K. (2011) Length-Dependent Retention of Carbon Nanotubes in the Pleural Space of Mice Initiates Sustained Inflammation and Progressive Fibrosis on the Parietal Pleura. *The American Journal of Pathology,* **178,** 2587-2600.

Murr, L. E. & Bang, J. J. (2003) Electron microscope comparisons of fine and ultra-fine carbonaceous and non-carbonaceous, airborne particulates. *Atmospheric Environment,* **37,** 4795-4806.

Murr, L. E., Bang, J. J., Esquivel, E. V., Guerrero, P. A. & Lopez, D. A. (2004a) Carbon Nanotubes, Nanocrystal Forms, and Complex Nanoparticle Aggregates in common fuel-gas combustion sources and the ambient air. *Journal of Nanoparticle Research,* **6,** 241-251.

Murr, L. E., Garza, K. M., Soto, K. F., Carrasco, A., Powell, T. G., Ramirez, D. A., Guerrero, P. A., Lopez, D. A. & Venzor, J., 3rd (2005) Cytotoxicity assessment of some carbon nanotubes and related carbon nanoparticle aggregates and the implications for anthropogenic carbon nanotube aggregates in the environment. *Int J Environ Res Public Health,* **2,** 31-42.

Murr, L. E., Garza, K. M., Soto, K. F., Carrasco, A., Powell, T. G., Ramirez, D. A., Guerrero, P. A., Lopez, D. A. & Venzor, J., 3rd (2005) Cytotoxicity assessment of some carbon nanotubes and related carbon nanoparticle aggregates and the implications for anthropogenic carbon nanotube aggregates in the environment. *Int J Environ Res Public Health,* **2,** 31-42.

Murr, L. E., Soto, K., Esquivel, E., Bang, J., Guerrero, P., Lopez, D. & Ramirez, D. (2004b) Carbon nanotubes and other fullerene-related nanocrystals in the environment: A TEM study. *JOM Journal of the Minerals, Metals and Materials Society,* **56,** 28-31.

Murray, L. A., Chen, Q., Kramer, M. S., Hesson, D. P., Argentieri, R. L., Peng, X., Gulati, M., Homer, R. J., Russell, T., van Rooijen, N., Elias, J. A., Hogaboam, C. M. & Herzog, E. L. (2011) TGF-beta driven lung fibrosis is macrophage dependent and blocked by Serum amyloid P. *The International Journal of Biochemistry & Cell Biology,* **43,** 154-162.

Myhre, O., Andersen, J. M., Aarnes, H. & Fonnum, F. (2003) Evaluation of the probes 2',7'-dichlorofluorescin diacetate, luminol, and lucigenin as indicators of reactive species formation. *Biochemical Pharmacology,* **65,** 1575-1582.

Myrvik, Q. N., Knox, E. A., Gordon, M. & Shirley, P. S. (1985) Effects of Asbestos on the Random Migration of Rabbit Alveolar Macrophages. *Environmental Health Perspectives,* **60,** 387-393.

Nasti, T. H. & Timares, L. (2012) Inflammasome activation of IL-1 family mediators in response to cutaneous photodamage. *Photochemistry and Photobiology,* **In print**.

Negus, R. P., Stamp, G. W., Relf, M. G., Burke, F., Malik, S. T., Bernasconi, S., Allavena, P., Sozzani, S., Mantovani, A. & Balkwill, F. R. (1995) The detection and localization of monocyte chemoattractant protein-1 (MCP-1) in human ovarian cancer. *The Journal of clinical investigation,* **95,** 2391-2396.

Nel, A., Xia, T., Madler, L. & Li, N. (2006) Toxic Potential of Materials at the Nanolevel. *Science,* **311,** 622-627.

Nemmar, A., Hoet, P. H. M., Vanquickenborne, B., Dinsdale, D., Thomeer, M., Hoylaerts, M. F., Vanbilloen, H., Mortelmans, L. & Nemery, B. (2002) Passage of Inhaled Particles Into the Blood Circulation in Humans. *Circulation,* **105,** 411-414.

Nicosia, R. F., Nicosia, S. V. & Smith, M. (1994) Vascular endothelial growth factor, platelet-derived growth factor, and insulin-like growth factor-1 promote rat aortic angiogenesis in vitro. *The American journal of pathology,* **145,** 1023-1029.

Nör, J. E., Christensen, J., Mooney, D. J. & Polverini, P. J. (1999) Vascular Endothelial Growth Factor (VEGF)-Mediated Angiogenesis Is Associated with Enhanced Endothelial Cell Survival and Induction of Bcl-2 Expression. *The American journal of pathology,* **154,** 375-384.

Norbury, C. J. & Zhivotovsky, B. (2004) DNA damage-induced apoptosis. *Oncogene,* **23,** 2797-2808.

Novoselov, K. S., Geim, A. K., Morozov, S. V., Jiang, D., Zhang, Y., Dubonos, S. V., Grigorieva, I. V. & Firsov, A. A. (2004) Electric Field Effect in Atomically Thin Carbon Films. *Science,* **306,** 666-669.

Nymark, P., Lindholm, P., Korpela, M., Lahti, L., Ruosaari, S., Kaski, S., Hollmen, J., Anttila, S., Kinnula, V. & Knuutila, S. (2007) Gene expression profiles in asbestos-exposed epithelial and mesothelial lung cell lines. *BMC Genomics,* **8,** 62.

Oberdorster, G., Oberdorster, E. & Oberdorster, J. (2005) Nanotoxicology: an emerging discipline evolving from studies of ultrafine particles. *Environmental Health Perspectives,* **113,** 823 - 839.

Oberdörster, G., Oberdörster, E. & Oberdörster, J. (2005) Nanotoxicology: an emerging discipline evolving from studies of ultrafine particles. *Environ Health Perspect,* **113,** 823-839.

Oberdörster, G., Sharp, Z., Atudorei, V., Elder, A., Gelein, R., Kreyling, W. & Cox, C. (2004) Translocation of Inhaled Ultrafine Particles to the Brain. *Inhalation Toxicology,* **16,** 437 - 445.

Oberdörster, G., Sharp, Z., Atudorei, V., Elder, A., Gelein, R., Lunts, A., Kreyling, W. & Cox, C. (2002) Extrapulmonary translocation of ultrafine carbon particles following whole-body inhalation exposure of rats. *Journal of Toxicology and Environmental Health, Part A,* **65,** 1531-1543.

Oberdorster, G., Stone, V. & Donaldson, K. (2007) Toxicology of nanoparticles: a historical perspective. *Nanotoxicology,* **1,** 2-25.

Oberdörster, G., Stone, V. & Donaldson, K. (2007) Toxicology of nanoparticles: a historical perspective. *Nanotoxicology,* **1,** 2-25.

Ohmer-Schrock, D., Schlatterer, C., Plattner, H. & Schlepper-Schafer, J. (1995) Lung surfactant protein A (SP-A) activates a phosphoinositide/calcium signaling pathway in alveolar macrophages. *J Cell Sci,* **108,** 3695-3702.

Ono, T., Kitaguchi, K., Takehara, M., Shiiba, M. & Hayami, K. (1981) Serum-constituents analyses: effect of duration and temperature of storage of clotted blood. *Clinical Chemistry,* **27,** 35-38.

Orozco, L. D., Kapturczak, M. H., Barajas, B., Wang, X., Weinstein, M. M., Wong, J., Deshane, J., Bolisetty, S., Shaposhnik, Z., Shih, D. M., Agarwal, A., Lusis, A. J. & Araujo, J. A. (2007) Heme Oxygenase-1 Expression in Macrophages Plays a Beneficial Role in Atherosclerosis. *Circulation Research,* **100,** 1703-1711.

Ouyang, Y., Cong, L. M., Chen, L., Liu, Q. X. & Fang, Y. (2008) Raman study on single-walled carbon nanotubes and multi-walled carbon nanotubes with different laser excitation energies. *Physica E: Low-dimensional Systems and Nanostructures,* **40,** 2386-2389.

Palecanda, A., Paulauskis, J., Al-Mutairi, E., Imrich, A., Qin, G., Suzuki, H., Kodama, T., Tryggvason, K., Koziel, H. & Kobzik, L. (1999) Role of the Scavenger Receptor MARCO in Alveolar Macrophage Binding of Unopsonized Environmental Particles. *The Journal of Experimental Medicine,* **189,** 1497-1506.

Palekar, L. D., Spooner, C. M. & Coffin, D. L. (1979) Influence of crystallization habit of minerals on In vitro cytotoxicity. *Annals of the New York Academy of Sciences,* **330,** 673-686.

Palomäki, J., Välimäki, E., Sund, J., Vippola, M., Clausen, P. A., Jensen, K. A., Savolainen, K., Matikainen, S. & Alenius, H. (2011) Long, Needle-like Carbon Nanotubes and Asbestos Activate the NLRP3 Inflammasome through a Similar Mechanism. *ACS Nano,* **5,** 6861-6870.

Panduri, V., Surapureddi, S., Soberanes, S., Weitzman, S. A., Chandel, N. & Kamp, D. W. (2006) P53 Mediates Amosite Asbestos-Induced Alveolar Epithelial Cell Mitochondria-Regulated Apoptosis. *Am. J. Respir. Cell Mol. Biol.,* **34,** 443-452.

Panduri, V., Weitzman, S. A., Chandel, N. & Kamp, D. W. (2003) The Mitochondria-Regulated Death Pathway Mediates Asbestos-Induced Alveolar Epithelial Cell Apoptosis. *Am. J. Respir. Cell Mol. Biol.,* **28,** 241-248.

Pantarotto, D., Briand, J. P., Prato, M. & Bianco, A. (2004a) Translocation of bioactive peptides across cell membranes by carbon nanotubes. *Chem Commun (Camb)***,** 16-17.

Pantarotto, D., Singh, R., McCarthy, D., Erhardt, M., Briand, J. P., Prato, M., Kostarelos, K. & Bianco, A. (2004b) Functionalized carbon nanotubes for plasmid DNA gene delivery. *Angew Chem Int Ed Engl,* **43,** 5242-5246.

Papanikolaou, G. & Pantopoulos, K. (2005) Iron metabolism and toxicity. *Toxicology and Applied Pharmacology,* **202,** 199-211.

Paradise, M. & Goswami, T. (2007) Carbon nanotubes - Production and industrial applications. *Materials & Design,* **28,** 1477-1489.

Park, C., Kim, W.-S., Choi, Y., Kim, H. & Park, K. (2002) Effects of transforming growth factor β (TGF-β) receptor on lung carcinogenesis. *Lung cancer (Amsterdam, Netherlands),* **38,** 143-147.

Park, J. B. (2003) Phagocytosis induces superoxide formation and apoptosis in macrophages. *Exp Mol Med,* **35,** 325-335.

Parvinzadeh, M. & Hajiraissi, R. (2007) Physical Properties of Polyester Fabrics Treated with Nano, Micro and Macro Emulsion Silicones. *AIP Conference Proceedings,* **929,** 216-219.

Pathan, A. K., Bond, J. & Gaskin, R. E. (2010) Sample preparation for SEM of plant surfaces. *Materials Today,* **12,** 32-43.

Peebles, R. S. (2009) The intelectins: a new link between the immune response to parasitic infections and allergic inflammation? *American Journal of Physiology - Lung Cellular and Molecular Physiology,* **298,** L288-L289.

Pelin, K., Husgafvel-Pursiainen, K., Vallas, M., Vanhala, E. & Linnainmaa, K. (1992) Cytotoxicity and anaphase aberrations induced by mineral fibres in cultured human mesothelial cells. *Toxicology in Vitro,* **6,** 445-450.

Pepper, M. S., Mandriota, S. J., Jeltsch, M., Kumar, V. & Alitalo, K. (1998) Vascular endothelial growth factor (VEGF)-C synergizes with basic fibroblast growth factor and VEGF in the induction of angiogenesis in vitro and alters endothelial cell extracellular proteolytic activity. *Journal of Cellular Physiology,* **177,** 439-452.

Perkins, R. C., Courtney Broaddus, V., Shetty, S., Hamilton, S. & Idell, S. (1999) Asbestos Upregulates Expression of the Urokinase-Type Plasminogen Activator Receptor on Mesothelial Cells. *Am. J. Respir. Cell Mol. Biol.,* **21,** 637-646.

Peters, A., Dockery, D. W., Muller, J. E. & Mittleman, M. A. (2001) Increased Particulate Air Pollution and the Triggering of Myocardial Infarction. *Circulation,* **103,** 2810-2815.

Peters, A., Wichmann, E., Tuch, T., Heinrich, J. & Heyder, J. (1997) Respiratory effects are associated with the number of ultrafine particles. *Am j respir crit care med,* **155,** 1376-1383.

Pfeffer, K. (2003) Biological functions of tumor necrosis factor cytokines and their receptors. *Cytokine & Growth Factor Reviews,* **14,** 185-191.

Pison, U., Welte, T., Giersig, M. & Groneberg, D. A. (2006) Nanomedicine for respiratory diseases. *European Journal of Pharmacology,* **533,** 341-350.

Poland, C. A., Duffin, R., Kinloch, I., Maynard, A., Wallace, W. A. H., Seaton, A., Stone, V., Brown, S., MacNee, W. & Donaldson, K. (2008) Carbon nanotubes introduced into the abdominal cavity of mice show asbestos-like pathogenicity in a pilot study. *Nat Nano,* **3,** 423-428.

Popat, K. C., Eltgroth, M., LaTempa, T. J., Grimes, C. A. & Desai, T. A. (2007) Decreased Staphylococcus epidermis adhesion and increased osteoblast functionality on antibiotic-loaded titania nanotubes. *Biomaterials,* **28,** 4880-4888.

Popov, V. N. (2004) Carbon nanotubes: properties and application. *Materials Science and Engineering: R: Reports,* **43,** 61-102.

Porter, A. E., Gass, M., Muller, K., Skepper, J. N., Midgley, P. & Welland, M. (2007a) Visualizing the Uptake of C60 to the Cytoplasm and Nucleus of Human Monocyte-Derived Macrophage Cells Using Energy-Filtered Transmission Electron Microscopy and Electron Tomography. *Environmental Science & Technology,* **41,** 3012-3017.

Porter, A. E., Gass, M., Muller, K., Skepper, J. N., Midgley, P. A. & Welland, M. (2007b) Direct imaging of single-walled carbon nanotubes in cells. *Nat Nano,* **2,** 713-717.

Porter, D., Sriram, K., Wolfarth, M., Jefferson, A., Schwegler-Berry, D., Andrew, M. E. & Castranova, V. (2008) A biocompatible medium for nanoparticle dispersion. *Nanotoxicology,* **2,** 144-154.

Possel, H., Noack, H., Augustin, W., Keilhoff, G. & Wolf, G. (1997) 2,7-Dihydrodichlorofluorescein diacetate as a fluorescent marker for peroxynitrite formation. *FEBS Letters,* **416,** 175-178.

Potts, R. J., Watkin, R. D. & Hart, B. A. (2003) Cadmium exposure down-regulates 8-oxoguanine DNA glycosylase expression in rat lung and alveolar epithelial cells. *Toxicology,* **184,** 189-202.

Prasad, N. K. A., Papoff, G., Zeuner, A., Bonnin, E., Kazatchkine, M. D., Ruberti, G. & Kaveri, S. V. (1998) Therapeutic Preparations of Normal Polyspecific IgG (IVIg) Induce Apoptosis in Human Lymphocytes and Monocytes: A Novel Mechanism of Action of IVIg Involving the Fas Apoptotic Pathway. *The Journal of Immunology,* **161,** 3781-3790.

Proskuryakov, S. Y., Konoplyannikov, A. G. & Gabai, V. L. (2003) Necrosis: a specific form of programmed cell death? *Experimental Cell Research,* **283,** 1-16.

Pulskamp, K., Diabaté, S. & Krug, H. F. (2007a) Carbon nanotubes show no sign of acute toxicity but induce intracellular reactive oxygen species in dependence on contaminants. *Toxicology Letters,* **168,** 58-74.

Pulskamp, K., Wörle-Knirsch, J. M., Hennrich, F., Kern, K. & Krug, H. F. (2007b) Human lung epithelial cells show biphasic oxidative burst after single-walled carbon nanotube contact. *Carbon,* **45,** 2241-2249.

Pumera, M. (2007) Nanobiomaterials for Electrochemical Biosensors. *AIP Conference Proceedings,* **929,** 191-194.

Qiu, J., Chen, G., Li, Z. & Zhao, Z. (2010) Preparation of double-walled carbon nanotubes from fullerene waste soot by arc-discharge. *Carbon,* **48,** 1312-1315.

Raffray, M. & Cohen, G. M. (1997) Apoptosis and necrosis in toxicology: A continuum or distinct modes of cell death? *Pharmacology & Therapeutics,* **75,** 153-177.

Rahman, I. (2002) Oxidative stress, transcription factors and chromatin remodelling in lung inflammation. *Biochemical Pharmacology,* **64,** 935-942.

Raikwar, S. P., Temm, C. J., Raikwar, N. S., Kao, C., Molitoris, B. A. & Gardner, T. A. (2005) Adenoviral Vectors Expressing Human Endostatin-Angiostatin and Soluble Tie2: Enhanced Suppression of Tumor Growth and Antiangiogenic Effects in a Prostate Tumor Model. *Mol Ther,* **12,** 1091-1100.

Ravichandran, P., Periyakaruppan, A., Sadanandan, B., Ramesh, V., Hall, J. C., Jejelowo, O. & Ramesh, G. T. (2009) Induction of apoptosis in rat lung epithelial cells by multiwalled carbon nanotubes. *Journal of Biochemical and Molecular Toxicology,* **23,** 333-344.

Renwick, L. C., Brown, D., Clouter, A. & Donaldson, K. (2004) Increased inflammation and altered macrophage chemotactic responses caused by two ultrafine particle types. *Occupational and Environmental Medicine,* **61,** 442-447.

Renwick, L. C., Donaldson, K. & Clouter, A. (2001) Impairment of Alveolar Macrophage Phagocytosis by Ultrafine Particles. *Toxicology and Applied Pharmacology,* **172,** 119-127.

Resnick, D., Freedman, N. J., Xu, S. & Krieger, M. (1993) Secreted extracellular domains of macrophage scavenger receptors form elongated trimers which specifically bind crocidolite asbestos. *Journal of Biological Chemistry,* **268,** 3538-3545.

Riccardi, C. & Nicoletti, I. (2006) Analysis of apoptosis by propidium iodide staining and flow cytometry. *Nat. Protocols,* **1,** 1458-1461.

Ridley, A. J. (2001) Rho family proteins: coordinating cell responses. *Trends in Cell Biology,* **11,** 471-477.

Riechelmann, H., Deutschle, T., Grabow, A., Heinzow, B., Butte, W. & Reiter, R. (2007) Differential Response of Mono Mac 6, BEAS-2B, and Jurkat Cells to Indoor Dust. *Environmental Health Perspectives,* **115,** 1325-1332.

Rinaldi, M., Moroni, P., Paape, M. J. & Bannerman, D. D. (2007) Evaluation of assays for the measurement of bovine neutrophil reactive oxygen species. *Veterinary Immunology and Immunopathology,* **115,** 107-125.

Risom, L., Dybdahl, M., Bornholdt, J., Vogel, U., Wallin, H., Møller, P. & Loft, S. (2003a) Oxidative DNA damage and defence gene expression in the mouse lung after short-term exposure to diesel exhaust particles by inhalation. *Carcinogenesis,* **24,** 1847-1852.

Risom, L., Møller, P. & Loft, S. (2005) Oxidative stress-induced DNA damage by particulate air pollution. *Mutation Research/Fundamental and Molecular Mechanisms of Mutagenesis,* **592,** 119-137.

Risom, L., Møller, P., Vogel, U., Kristjansen, P. E. & Loft, S. (2003b) X-ray-induced oxidative stress: DNA damage and gene expression of HO-1, ERCC1 and OGG1 in mouse lung. *Free radical research,* **37,** 957-966.

Robledo, R. & Mossman, B. (1999) Cellular and molecular mechanisms of asbestos-induced fibrosis. *Journal of Cellular Physiology,* **180,** 158-166.

Rogers, A. J., Leigh, J., Berry, G., Ferguson, D. A., Mulder, H. B., Ackad, M. & Morgan, G. G. (1994) Dose-Response Relationship Between Airborne and Lung Asbestos Fibre Type, Length and Concentration, and the Relative Risk of Mesothelioma. *Annals of Occupational Hygiene,* **38,** 631-638.

Roos, W. P. & Kaina, B. (2006) DNA damage-induced cell death by apoptosis. *Trends in Molecular Medicine,* **12,** 440-450.

Rota, C., Chignell, C. F. & Mason, R. P. (1999a) Evidence for free radical formation during the oxidation of 2'-7'-dichlorofluorescin to the fluorescent dye 2'-7'-dichlorofluorescein by horseradish peroxidase: Possible implications for oxidative stress measurements. *Free Radical Biology and Medicine,* **27,** 873-881.

Rota, C., Fann, Y. C. & Mason, R. P. (1999b) Phenoxyl Free Radical Formation during the Oxidation of the Fluorescent Dye 2,7-Dichlorofluorescein by Horseradish Peroxidase. *Journal of Biological Chemistry,* **274,** 28161-28168.

Rothen-Rutishauser, B., Brown, D. M., Piallier-Boyles, M., Kinloch, I. A., Windle, A. H., Gehr, P. & Stone, V. (2010) Relating the physicochemical characteristics and dispersion of multiwalled carbon nanotubes in

different suspension media to their oxidative reactivity in vitro and inflammation in vivo. *Nanotoxicology,* **4,** 331-342.
Rotoli, B., Bussolati, O., Barilli, A., Zanello, P., Bianchi, M., Magrini, A., Pietroiusti, A., Bergamaschi, A. & Bergamaschi, E. (2009) Airway barrier dysfunction induced by exposure to carbon nanotubes in vitro: which role for fiber length? *Human & Experimental Toxicology,* **28,** 361-368.
Roy, I., Ohulchanskyy, T. Y., Pudavar, H. E., Bergey, E. J., Oseroff, A. R., Morgan, J., Dougherty, T. J. & Prasad, P. N. (2003) Ceramic-Based Nanoparticles Entrapping Water-Insoluble Photosensitizing Anticancer Drugs: A Novel Drug-Carrier System for Photodynamic Therapy. *J. Am. Chem. Soc.,* **125,** 7860-7865.
Ryman-Rasmussen, J. P., Cesta, M. F., Brody, A. R., Shipley-Phillips, J. K., Everitt, J. I., Tewksbury, E. W., Moss, O. R., Wong, B. A., Dodd, D. E., Andersen, M. E. & Bonner, J. C. (2009a) Inhaled carbon nanotubes reach the subpleural tissue in mice. *Nat Nano,* **4,** 747-751.
Ryman-Rasmussen, J. P., Tewksbury, E. W., Moss, O. R., Cesta, M. F., Wong, B. A. & Bonner, J. C. (2009b) Inhaled Multiwalled Carbon Nanotubes Potentiate Airway Fibrosis in Murine Allergic Asthma. *Am. J. Respir. Cell Mol. Biol.,* **40,** 349-358.
Sager, T. M., Porter, D. W., Robinson, V. A., Lindsley, W. G., Schwegler-Berry, D. E. & Castranova, V. (2007) Improved method to disperse nanoparticles for in vitro and in vivo investigation of toxicity. *Nanotoxicology,* **1,** 118-129.
Salcedo, R., Ponce, M. L., Young, H. A., Wasserman, K., Ward, J. M., Kleinman, H. K., Oppenheim, J. J. & Murphy, W. J. (2000) Human endothelial cells express CCR2 and respond to MCP-1: direct role of MCP-1 in angiogenesis and tumor progression. *Blood,* **96,** 34-40.
Salvador-Morales, C., Townsend, P., Flahaut, E., Vénien-Bryan, C., Vlandas, A., Green, M. L. H. & Sim, R. B. (2007) Binding of pulmonary surfactant proteins to carbon nanotubes; potential for damage to lung immune defense mechanisms. *Carbon,* **45,** 607-617.
Salvetat-Delmotte, J.-P. & Rubio, A. (2002) Mechanical properties of carbon nanotubes: a fiber digest for beginners. *Carbon,* **40,** 1729-1734.
Sato, Y., Yokoyama, A., Shibata, K.-i., Akimoto, Y., Ogino, S.-i., Nodasaka, Y., Kohgo, T., Tamura, K., Akasaka, T., Uo, M., Motomiya, K., Jeyadevan, B., Ishiguro, M., Hatakeyama, R., Watari, F. & Tohji, K. (2005) Influence of length on cytotoxicity of multi-walled carbon nanotubes against human acute monocytic leukemia cell line THP-1 in vitro and subcutaneous tissue of rats in vivo. *Molecular BioSystems,* **1,** 176-182.
Savill, J., Hogg, N., Ren, Y. & Haslett, C. (1992) Thrombospondin cooperates with CD36 and the vitronectin receptor in macrophage recognition of neutrophils undergoing apoptosis. *J Clin Invest,* **90,** 1513-1522.
Schadler, L. S., Giannaris, S. C. & Ajayan, P. M. (1998) Load transfer in carbon nanotube epoxy composites. *Applied Physics Letters,* **73,** 3842-3844.
Schlesinger, R. B. (1985) Clearance from the respiratory tract. *Fundamental and Applied Toxicology,* **5,** 435-450.
Schönfelder, R., Avilés, F., Bachmatiuk, A., Cauich-Rodriguez, J., Knupfer, M., Büchner, B. & Rümmeli, M. (2012) On the merits of Raman spectroscopy and thermogravimetric analysis to asses carbon nanotube structural modifications. *Applied Physics A: Materials Science & Processing,* **106,** 843-852.

Schwartz, J. (1994) What Are People Dying of on High Air Pollution Days? *Environmental Research,* **64,** 26-35.

Schwartz, J. & Morris, R. (1995) Air Pollution and Hospital Admissions for Cardiovascular Disease in Detroit, Michigan. *American Journal of Epidemiology,* **142,** 23-35.

Scott, C. D., Arepalli, S., Nikolaev, P. & Smalley, R. E. (2001) Growth mechanisms for single-wall carbon nanotubes in a laser-ablation process. *Applied Physics A: Materials Science & Processing,* **72,** 573-580.

Sen, C. K., Roy, S. & Packer, L. (1996) Involvement of intracellular Ca2+ in oxidant-induced NF-[kappa]B activation. *FEBS Letters,* **385,** 58-62.

Serghides, L. & Kain, K. C. (2001) Peroxisome Proliferator-Activated Receptor Î³-Retinoid X Receptor Agonists Increase CD36-Dependent Phagocytosis of Plasmodium falciparum-Parasitized Erythrocytes and Decrease Malaria-Induced TNF-Î± Secretion by Monocytes/Macrophages. *The Journal of Immunology,* **166,** 6742-6748.

Shackelford, R. E., Misra, U. K., Florine-Casteel, K., Thai, S.-F., Pizzo, S. V. & Adams, D. O. (1995) Oxidized Low Density Lipoprotein Suppresses Activation of NFB in Macrophages via a Pertussis Toxin-sensitive Signaling Mechanism. *Journal of Biological Chemistry,* **270,** 3475-3478.

Shain, S. A., Boesel, R. W., Klipper, R. W. & Lancaster, C. M. (1983) Creatine kinase and lactate dehydrogenase: stability of isoenzymes and their activity in stored human plasma and prostatic tissue extracts and effect of sample dilution. *Clinical Chemistry,* **29,** 832-835.

Shanley, T. P., Vasi, N. & Denenberg, A. (2000) Regulation of chemokine expression by IL-10 in lung inflammation. *Cytokine,* **12,** 1054-1064.

Shaw, R. J. (1991) The role of lung macrophages at the interface between chronic inflammation and fibrosis. *Respiratory medicine,* **85,** 267-273.

Showa_Denko http://www.sdk.co.jp/english/products/137/139.html. *Accessed 15.02.2012*.

Shukla, A., Gulumian, M., Hei, T. K., Kamp, D., Rahman, Q. & Mossman, B. T. (2003a) Multiple roles of oxidants in the pathogenesis of asbestos-induced diseases. *Free Radical Biology and Medicine,* **34,** 1117-1129.

Shukla, A., Ramos-Nino, M. & Mossman, B. (2003b) Cell signaling and transcription factor activation by asbestos in lung injury and disease. *The International Journal of Biochemistry & Cell Biology,* **35,** 1198-1209.

Shvedova, A. A., Castranova, V., Kisin, E. R., Schwegler-Berry, D., Murray, A. R., Gandelsman, V. Z., Maynard, A. & Baron, P. (2003) Exposure to carbon nanotube material: assessment of nanotube cytotoxicity using human keratinocyte cells. *J Toxicol Environ Health A,* **66,** 1909-1926.

Shvedova, A. A., Kisin, E., Murray, A. R., Johnson, V. J., Gorelik, O., Arepalli, S., Hubbs, A. F., Mercer, R. R., Keohavong, P., Sussman, N., Jin, J., Yin, J., Stone, S., Chen, B. T., Deye, G., Maynard, A., Castranova, V., Baron, P. A. & Kagan, V. E. (2008a) Inhalation vs. aspiration of single-walled carbon nanotubes in C57BL/6 mice: inflammation, fibrosis, oxidative stress, and mutagenesis. American Physiological Society.

Shvedova, A. A., Kisin, E. R., Mercer, R., Murray, A. R., Johnson, V. J., Potapovich, A. I., Tyurina, Y. Y., Gorelik, O., Arepalli, S., Schwegler-Berry, D., Hubbs, A. F., Antonini, J., Evans, D. E., Ku, B.-K., Ramsey, D., Maynard, A., Kagan, V. E., Castranova, V. & Baron, P. (2005) Unusual inflammatory and fibrogenic pulmonary responses to single-walled

carbon nanotubes in mice. *Am J Physiol Lung Cell Mol Physiol,* **289,** L698-708.

Shvedova, A. A., Kisin, E. R., Murray, A. R., Gorelik, O., Arepalli, S., Castranova, V., Young, S.-H., Gao, F., Tyurina, Y. Y., Oury, T. D. & Kagan, V. E. (2007) Vitamin E deficiency enhances pulmonary inflammatory response and oxidative stress induced by single-walled carbon nanotubes in C57BL/6 mice. *Toxicology and Applied Pharmacology,* **221,** 339-348.

Shvedova, A. A., Kisin, E. R., Murray, A. R., Kommineni, C., Castranova, V., Fadeel, B. & Kagan, V. E. (2008b) Increased accumulation of neutrophils and decreased fibrosis in the lung of NADPH oxidase-deficient C57BL/6 mice exposed to carbon nanotubes. *Toxicology and Applied Pharmacology,* **231,** 235-240.

Shvedova, A. A., Pietroiusti, A., Fadeel, B. & Kagan, V. E. (2012) Mechanisms of carbon nanotube-induced toxicity: Focus on oxidative stress. *Toxicology and Applied Pharmacology,* **261,** 121-133.

Sime, P. J., Xing, Z., Graham, F. L., Csaky, K. G. & Gauldie, J. (1997) Adenovector-mediated gene transfer of active transforming growth factor-beta1 induces prolonged severe fibrosis in rat lung. *The Journal of Clinical Investigation,* **100,** 768-776.

Singh, C., Quested, T., Boothroyd, C. B., Thomas, P., Kinloch, I. A., Abou-Kandil, A. I. & Windle, A. H. (2002) Synthesis and Characterization of Carbon Nanofibers Produced by the Floating Catalyst Method. *The Journal of Physical Chemistry B,* **106,** 10915-10922.

Singh, C., Shaffer, M. S. P., Koziol, K. K. K., Kinloch, I. A. & Windle, A. H. (2003a) Towards the production of large-scale aligned carbon nanotubes. *Chemical Physics Letters,* **372,** 860-865.

Singh, C., Shaffer, M. S. P. & Windle, A. H. (2003b) Production of controlled architectures of aligned carbon nanotubes by an injection chemical vapour deposition method. *Carbon,* **41,** 359-368.

Singh, R., Pantarotto, D., Lacerda, L., Pastorin, G., Klumpp, C. d., Prato, M., Bianco, A. & Kostarelos, K. (2006) Tissue biodistribution and blood clearance rates of intravenously administered carbon nanotube radiotracers. *Proceedings of the National Academy of Sciences of the United States of America,* **103,** 3357-3362.

Sinha, N. & Yeow, J. T. (2005) Carbon nanotubes for biomedical applications. *IEEE Trans Nanobioscience,* **4,** 180-195.

Snyderman, R., Pike, M. C., Fischer, D. G. & Koren, H. S. (1977) Biologic and Biochemical Activities of Continuous Macrophage Cell Lines P388D1 and J774.1. *The Journal of Immunology,* **119,** 2060-2066.

Sokol, R. J., Hudson, G., James, N. T., Frost, I. J. & Wales, J. (1987) Human macrophage development: a morphometric study. *Journal of anatomy,* **151,** 27-35.

Soto, K. F., Garza, K. M., Shi, Y. & Murr, L. E. (2008) Direct contact cytotoxicity assays for filter-collected, carbonaceous (soot) nanoparticulate material and observations of lung cell response. *Atmospheric Environment,* **42,** 1970-1982.

Sotowa, C., Origi, G., Takeuchi, M., Nishimura, Y., Takeuchi, K., Jang, I. Y., Kim, Y. J., Hayashi, T., Kim, Y. A., Endo, M. & Dresselhaus, M. S. (2008) The Reinforcing Effect of Combined Carbon Nanotubes and Acetylene Blacks on the Positive Electrode of Lithium-Ion Batteries. *ChemSusChem,* **1,** 911-915.

Srivastava, R. K., Pant, A. B., Kashyap, M. P., Kumar, V., Lohani, M., Jonas, L. & Rahman, Q. (2010) Multi-walled carbon nanotubes induce oxidative stress and apoptosis in human lung cancer cell line-A549. *Nanotoxicology,* **0,** 1-13.

Srivastava, R. K., Pant, A. B., Kashyap, M. P., Kumar, V., Lohani, M., Jonas, L. & Rahman, Q. (2011) Multi-walled carbon nanotubes induce oxidative stress and apoptosis in human lung cancer cell line-A549. *Nanotoxicology,* **5,** 195-207.

Staton, C. A., Reed, M. W. R. & Brown, N. J. (2009) A critical analysis of current in vitro and in vivo angiogenesis assays. *International Journal of Experimental Pathology,* **90,** 195-221.

Stayner, L. T., Dankovic, D. A. & Lemen, R. A. (1996) Occupational exposure to chrysotile asbestos and cancer risk: a review of the amphibole hypothesis. *Am J Public Health,* **86,** 179-186.

Steplewska, A. & Borowiak-Palen, E. (2009) Resonance Raman studt on carbon nanotubes formation. *Acta Physica polonica A,* **116,** 93-95.

Stobinski, L., Lesiak, B., Kövér, L., Tóth, J., Biniak, S., Trykowski, G. & Judek, J. (2010) Multiwall carbon nanotubes purification and oxidation by nitric acid studied by the FTIR and electron spectroscopy methods. *Journal of Alloys and Compounds,* **501,** 77-84.

Stone, V., Johnston, H. & Clift, M. J. (2007) Air pollution, ultrafine and nanoparticle toxicology: cellular and molecular interactions. *IEEE transactions on nanobioscience,* **6,** 331-340.

Stone, V., Shaw, J., Brown, D. M., MacNee, W., Faux, S. P. & Donaldson, K. (1998) The role of oxidative stress in the prolonged inhibitory effect of ultrafine carbon black on epithelial cell function. *Toxicology in Vitro,* **12,** 649-659.

Stone, V., Tuinman, M., Vamvakopoulos, J., Shaw, J., Brown, D., Petterson, S., Faux, S., Borm, P., MacNee, W., Michaelangeli, F. & Donaldson, K. (2000) Increased calcium influx in a monocytic cell line on exposure to ultrafine carbon black. *European Respiratory Journal,* **15,** 297-303.

Stone, V., Wilson, M., Lightbody, J. & Donaldson, K. (2003) Investigating the potential for interaction between the components of PM<sub>10</sub&gt. *Environmental Health and Preventive Medicine,* **7,** 246-253.

Stopford, W., Turner, J., Cappellini, D. & Brock, T. (2003) Bioaccessibility testing of cobalt compounds. *Journal of Environmental Monitoring,* **5,** 675-680.

Sunderkötter, C., Steinbrink, K., Goebeler, M., Bhardwaj, R. & Sorg, C. (1994) Macrophages and angiogenesis. *Journal of Leukocyte Biology,* **55,** 410-422.

Szpaderska, A. M., Zuckerman, J. D. & DiPietro, L. A. (2003) Differential Injury Responses in Oral Mucosal and Cutaneous Wounds. *Journal of Dental Research,* **82,** 621-626.

Tabet, L., Bussy, C., Amara, N., Setyan, A., Grodet, A., Rossi, M. J., Pairon, J.-C., Boczkowski, J. & Lanone, S. (2009) Adverse Effects of Industrial Multiwalled Carbon Nanotubes on Human Pulmonary Cells. *Journal of Toxicology and Environmental Health, Part A: Current Issues,* **72,** 60 - 73.

Taeri, B. & Eliasi, M. (2007) Recent Results on Topological Indices of Nanotubes. *AIP Conference Proceedings,* **929,** 243-249.

Tan, K. S., Qian, L., Rosado, R., Flood, P. M. & Cooper, L. F. (2006) The role of titanium surface topography on J774A.1 macrophage inflammatory cytokines and nitric oxide production. *Biomaterials,* **27,** 5170-5177.

Tanner, M., Kent, N., Smith, B., Fletcher, S. & Lewer, M. (2008) Stability of common biochemical analytes in serum gel tubes subjected to various storage temperatures and times pre-centrifugation. *Annals of clinical biochemistry,* **45,** 375-379.

Teeguarden, J. G., Webb-Robertson, B.-J., Waters, K. M., Murray, A. R., Kisin, E. R., Varnum, S. M., Jacobs, J. M., Pounds, J. G., Zanger, R. C. & Shvedova, A. A. Comparative Proteomics and Pulmonary Toxicity of Instilled Single-Walled Carbon Nanotubes, Crocidolite Asbestos, and Ultrafine Carbon Black in Mice. *Toxicological Sciences,* **120,** 123-135.

Teeguarden, J. G., Webb-Robertson, B.-J., Waters, K. M., Murray, A. R., Kisin, E. R., Varnum, S. M., Jacobs, J. M., Pounds, J. G., Zanger, R. C. & Shvedova, A. A. (2011) Comparative Proteomics and Pulmonary Toxicity of Instilled Single-Walled Carbon Nanotubes, Crocidolite Asbestos, and Ultrafine Carbon Black in Mice. *Toxicological Sciences,* **120,** 123-135.

Thess, A., Lee, R., Nikolaev, P., Hongjie, D., Petit, P., Robert, J., Chunhui, X., Young Hee, L., Seong Gon, K., Rinzler, A. G., Colbert, D. T., Scuseria, G. E., Tomanek, D., Fischer, J. E. & Smalley, R. E. (1996) Crystalline ropes of metallic carbon nanotubes. *Science,* **v273,** p483(485).

Thurnherr, T., Brandenberger, C., Fischer, K., Diener, L., Manser, P., Maeder-Althaus, X., Kaiser, J.-P., Krug, H. F., Rothen-Rutishauser, B. & Wick, P. (2010) A comparison of acute and long-term effects of industrial multiwalled carbon nanotubes on human lung and immune cells in vitro. *Toxicology Letters,* **200,** 176-186.

Tian, F., Cui, D., Schwarz, H., Estrada, G. G. & Kobayashi, H. (2006) Cytotoxicity of single-wall carbon nanotubes on human fibroblasts. *Toxicology in Vitro,* **20,** 1202-1212.

Tilkes, F. & Beck, E. G. (1983) Macrophage functions after exposure to mineral fibers. *Environmental Health Perspectives,* **51,** 67-72.

Tonks, A., Morris, R. H. K., Price, A. J., Thomas, A. W., Jones, K. P. & Jackson, S. K. (2001) Dipalmitoylphosphatidylcholine modulates inflammatory functions of monocytic cells independently of mitogen activated protein kinases. *Clinical & Experimental Immunology,* **124,** 86-94.

Tran, C. L., Hankin, S. M., Ross, B., Aitken, R. J., Jones, A. D., Donaldson, K., Stone, V. & Trantra, R. (2008) An outline scoping study to determine whether high aspect ratio nanoparticles (harn) should raise the same concerns as do asbestos fibres. *Report on project CB0406 2008 [http://www.safenano.org/Portals/3/SN_Content/Documents/HARN.pdf].*

Tsurudome, Y., Hirano, T., Yamato, H., Tanaka, I., Sagai, M., Hirano, H., Nagata, N., Itoh, H. & Kasai, H. (1999) Changes in levels of 8-hydroxyguanine in DNA, its repair and OGG1 mRNA in rat lungs after intratracheal administration of diesel exhaust particles. *Carcinogenesis,* **20,** 1573-1576.

Unfried, K., Schürkes, C. & Abel, J. (2002) Distinct Spectrum of Mutations Induced by Crocidolite Asbestos. *Cancer Research,* **62,** 99-104.

Vacca, A., Ribatti, D., Iurlaro, M., Albini, A., Minischetti, M., Bussolino, F., Pellegrino, A., Ria, R., Rusnati, M., Presta, M., Vincenti, V., Persico, M. & Dammacco, F. (1998) Human lymphoblastoid cells produce extracellular matrix-degrading enzymes and induce endothelial cell proliferation,

migration, morphogenesis, and angiogenesis. *International Journal of Clinical & Laboratory Research,* **28,** 55-68.
Valberg, P. A. & Watson, A. Y. (1996) Lung Cancer Rates in Carbon-Black Workers Are Discordant with Predictions from Rat Bioassay Data. *Regulatory Toxicology and Pharmacology,* **24,** 155-170.
Valdivia-Arenas, M. A., Amer, A., Henning, L. N., Wewers, M. D. & Schlesinger, L. S. (2007) Lung infections and innate host defense. *Drug Discovery Today: Disease Mechanisms,* **4,** 73-81.
Valko, M., Leibfritz, D., Moncol, J., Cronin, M. T. D., Mazur, M. & Telser, J. (2007) Free radicals and antioxidants in normal physiological functions and human disease. *The International Journal of Biochemistry & Cell Biology,* **39,** 44-84.
Valko, M., Morris, H. & Cronin, M. T. D. (2005) Metals, Toxicity and Oxidative Stress. *Current Medicinal Chemistry,* **12,** 1161-1208.
Valko, M., Rhodes, C. J., Moncol, J., Izakovic, M. & Mazur, M. (2006) Free radicals, metals and antioxidants in oxidative stress-induced cancer. *Chemico-Biological Interactions,* **160,** 1-40.
van Tongeren, M. J. A., Gardiner, K., Rossiter, C. E., Beach, J., Harber, P. & Harrington, M. J. (2002) Longitudinal analyses of chest radiographs from the European Carbon Black Respiratory Morbidity Study. *European Respiratory Journal,* **20,** 417-425.
Vazquez, E., Georgakilas, V. & Prato, M. (2002) Microwave-assisted purification of HIPCO carbon nanotubes. *Chemical Communications***,** 2308-2309.
Venugopal, R. & Jaiswal, A. K. (1998) Nrf2 and Nrf1 in association with Jun proteins regulate antioxidant response element-mediated expression and coordinated induction of genes encoding detoxifying enzymes. *Oncogene,* **17,** 3145-3156.
Voyta, J. C., Via, D. P., Butterfield, C. E. & Zetter, B. R. (1984) Identification and isolation of endothelial cells based on their increased uptake of acetylated-low density lipoprotein. *The Journal of Cell Biology,* **99,** 2034-2040.
Wagner, J. C., Pooley, F. D., Berry, G., Seal, R. M. E., Munday, D. E., Morgan, J. & Clark, N. J. (1982) A pathological and mineralogical study of asbestos-related deaths in the United Kingdom in 1977. *Annals of Occupational Hygiene,* **26,** 423-431.
Wali, A., Morin, P. J., Hough, C. D., Lonardo, F., Seya, T., Carbone, M. & Pass, H. I. (2005) Identification of intelectin overexpression in malignant pleural mesothelioma by serial analysis of gene expression (SAGE). *Lung Cancer,* **48,** 19-29.
Walker, V. G., Li, Z., Hulderman, T., Schwegler-Berry, D., Kashon, M. L. & Simeonova, P. P. (2009) Potential in vitro effects of carbon nanotubes on human aortic endothelial cells. *Toxicology and Applied Pharmacology,* **236,** 319-328.
Wang, B., Ma, Y., Wu, Y., Li, N., Huang, Y. & Chen, Y. (2009) Direct and large scale electric arc discharge synthesis of boron and nitrogen doped single-walled carbon nanotubes and their electronic properties. *Carbon,* **47,** 2112-2115.
Wang, H. & Joseph, J. A. (1999) Quantifying cellular oxidative stress by dichlorofluorescein assay using microplate reader. *Free Radical Biology and Medicine,* **27,** 612-616.

Wang, H., Wang, J., Deng, X., Sun, H., Shi, Z., Gu, Z., Liu, Y. & Zhao, Y. (2004) Biodistribution of carbon single-wall carbon nanotubes in mice. *J Nanosci Nanotechnol,* **4,** 1019-1024.

Wang, J., Sun, P., Bao, Y., Liu, J. & An, L. (2010a) Cytotoxicity of single-walled carbon nanotubes on PC12 cells. *Toxicology in Vitro,* **25,** 242-250.

Wang, L., Castranova, V., Mishra, A., Chen, B., Mercer, R., Schwegler-Berry, D. & Rojanasakul, Y. (2010b) Dispersion of single-walled carbon nanotubes by a natural lung surfactant for pulmonary in vitro and in vivo toxicity studies. *Particle and Fibre Toxicology,* **7,** 31.

Wang, L., Luanpitpong, S., Castranova, V., Tse, W., Lu, Y., Pongrakhananon, V. & Rojanasakul, Y. (2011) Carbon Nanotubes Induce Malignant Transformation and Tumorigenesis of Human Lung Epithelial Cells. *Nano Letters,* **11,** 2796-2803.

Warheit, D. B., Hartsky, M. A. & Stefaniak, M. S. (1988) Comparative physiology of rodent pulmonary macrophages: in vitro functional responses. *Journal of Applied Physiology,* **64,** 1953-1959.

Warheit, D. B., Laurence, B. R., Reed, K. L., Roach, D. H., Reynolds, G. A. M. & Webb, T. R. (2004) Comparative Pulmonary Toxicity Assessment of Single-wall Carbon Nanotubes in Rats. *Toxicological Sciences,* **77,** 117-125.

Wei, W., Sethuraman, A., Jin, C., Monteiro-Riviere, N. A. & Narayan, R. J. (2007) Biological properties of carbon nanotubes. *J Nanosci Nanotechnol,* **7,** 1284-1297.

Wick, P., Manser, P., Limbach, L. K., Dettlaff-Weglikowska, U., Krumeich, F., Roth, S., Stark, W. J. & Bruinink, A. (2007) The degree and kind of agglomeration affect carbon nanotube cytotoxicity. *Toxicology Letters,* **168,** 121-131.

Wieder, M. E., Hone, D. C., Cook, M. J., Handsley, M. M., Gavrilovic, J. & Russell, D. A. (2006) Intracellular photodynamic therapy with photosensitizer-nanoparticle conjugates: cancer therapy using a 'Trojan horse'. *Photochem Photobiol Sci,* **5,** 727-734.

Wieder, M. E., Hone, D. C., Cook, M. J., Handsley, M. M., Gavrilovic, J. & Russell, D. A. (2006) Intracellular photodynamic therapy with photosensitizer-nanoparticle conjugates: cancer therapy using a 'Trojan horse'. *Photochem Photobiol Sci,* **5,** 727-734.

Wilson, M. R., Foucaud, L., Barlow, P. G., Hutchison, G. R., Sales, J., Simpson, R. J. & Stone, V. (2007) Nanoparticle interactions with zinc and iron: Implications for toxicology and inflammation. *Toxicology and Applied Pharmacology,* **225,** 80-89.

Wilson, M. R., Lightbody, J. H., Donaldson, K., Sales, J. & Stone, V. (2002) Interactions between Ultrafine Particles and Transition Metals in Vivo and in Vitro. *Toxicology and Applied Pharmacology,* **184,** 172-179.

Winterbourn, C. C. (2002) Biological reactivity and biomarkers of the neutrophil oxidant, hypochlorous acid. *Toxicology,* **181–182,** 223-227.

Worle-Knirsch, J. M., Pulskamp, K. & Krug, H. F. (2006) Oops they did it again! Carbon nanotubes hoax scientists in viability assays. *Nano Letters,* **6,** 1261 - 1268.

Wu, W., Wieckowski, S., Pastorin, G., Benincasa, M., Klumpp, C., Briand, J. P., Gennaro, R., Prato, M. & Bianco, A. (2005) Targeted delivery of amphotericin B to cells by using functionalized carbon nanotubes. *Angew Chem Int Ed Engl,* **44,** 6358-6362.

Yazdi, A. S., Guarda, G., Riteau, N., Drexler, S. K., Tardivel, A., Couillin, I. & Tschopp, J. (2010) Nanoparticles activate the NLR pyrin domain containing 3 (Nlrp3) inflammasome and cause pulmonary inflammation through release of IL-1α and IL-1β. *Proceedings of the National Academy of Sciences,* **107,** 19449-19454.

Ye, J., Shi, X., Jones, W., Rojanasakul, Y., Cheng, N., Schwegler-Berry, D., Baron, P., Deye, G. J., Li, C. & Castranova, V. (1999a) Critical role of glass fiber length in TNF-alpha production and transcription factor activation in macrophages. *Am J Physiol,* **276,** L426-434.

Ye, J., Shi, X., Jones, W., Rojanasakul, Y., Cheng, N., Schwegler-Berry, D., Baron, P., Deye, G. J., Li, C. & Castranova, V. (1999b) Critical role of glass fiber length in TNF-alpha production and transcription factor activation in macrophages. *Am J Physiol,* **276,** L426-434.

Ye, J., Shi, X., Jones, W., Rojanasakul, Y., Cheng, N., Schwegler-Berry, D., Baron, P., Deye, G. J., Li, C. & Castranova, V. (1999c) Critical role of glass fiber length in TNF-Î± production and transcription factor activation in macrophages. *American Journal of Physiology - Lung Cellular and Molecular Physiology,* **276,** L426-L434.

Ye, J., Zeidler, P., Young, S., Martinez, T., Robinson, V. A., Jones, W., Baron, P., Shi, X. & Castranova, V. (2000) Activation of MAP Kinase p38 and ERK is Involved in Glass Fiber-induced TNF-alpha Production in Macrophages. *Journal of Biological Chemistry,* **276,** 5360-5367.

Yuan, Z., Taatjes, D. J., Mossman, B. T. & Heintz, N. H. (2004) The Duration of Nuclear Extracellular Signal-Regulated Kinase 1 and 2 Signaling during Cell Cycle Reentry Distinguishes Proliferation from Apoptosis in Response to Asbestos. *Cancer Research,* **64,** 6530-6536.

Zeidler-Erdely, P., Calhoun, W., Ameredes, B., Clark, M., Deye, G., Baron, P., Jones, W., Blake, T. & Castranova, V. (2006) In vitro cytotoxicity of Manville Code 100 glass fibers: Effect of fiber length on human alveolar macrophages. *Particle and Fibre Toxicology,* **3,** 5.

Zeni, O., Palumbo, R., Bernini, R., Zeni, L., Sarti, M. & Scarfi, M. R. (2008) Cytotoxicity investigation on cultured human blood cells treated with single-walled carbon nanotubes. *Sensors,* **8,** 488-499.

Zhu, L., Chang, D. W., Dai, L. & Hong, Y. (2007) DNA Damage Induced by Multiwalled Carbon Nanotubes in Mouse Embryonic Stem Cells. *Nano Letters,* **7,** 3592-3597.

Zhu, W.-H. & Nicosia, R. (2002) The thin prep rat aortic ring assay: A modified method for the characterization of angiogenesis in whole mounts. *Angiogenesis,* **5,** 81-86.

Ziegler-Heitbroc, H. W. L., Thiel, E., Futterer, A., Herzog, V., Wirtz, A. & Riethmüller, G. (1988) Establishment of a human cell line (mono mac 6) with characteristics of mature monocytes. *International Journal of Cancer,* **41,** 456-461.

Zimmermann, K. C., Bonzon, C. & Green, D. R. (2001) The machinery of programmed cell death. *Pharmacology & Therapeutics,* **92,** 57-70.

Zong, W.-X., Ditsworth, D., Bauer, D. E., Wang, Z.-Q. & Thompson, C. B. (2004) Alkylating DNA damage stimulates a regulated form of necrotic cell death. *Genes & Development,* **18,** 1272-1282.